

**THE MINERALOGY AND MAJOR ELEMENT GEOCHEMISTRY  
OF FERROMANGANESE CRUSTS AND NODULES  
FROM THE NORTHEASTERN EQUATORIAL  
PACIFIC OCEAN**

By

LOWELL WADE

A THESIS SUBMITTED IN PARTIAL FULFILLMENT OF  
THE REQUIREMENTS FOR THE DEGREE OF  
MASTER OF SCIENCE

in

THE FACULTY OF GRADUATE STUDIES  
(Department of Oceanography)

We accept this thesis as conforming  
to the required standard

THE UNIVERSITY OF BRITISH COLUMBIA

April 1991

© Lowell Wade, 1991

In presenting this thesis in partial fulfilment of the requirements for an advanced degree at the University of British Columbia, I agree that the Library shall make it freely available for reference and study. I further agree that permission for extensive copying of this thesis for scholarly purposes may be granted by the head of my department or by his or her representatives. It is understood that copying or publication of this thesis for financial gain shall not be allowed without my written permission.

Department of OCEANOGRAPHY

The University of British Columbia  
Vancouver, Canada

Date April 10, 1991

## ABSTRACT

A study of the mineralogy and major element geochemistry of ferromanganese crusts and nodules from the northeastern equatorial Pacific Ocean involved three inter-related projects: (1) the major element geochemistry of crusts and nodules from two study areas, (2) the development of a selective sequential extraction scheme (SSES) and a differential X-ray diffraction technique (DXRD) for the study of the mineralogy of the deposits, and (3) the application of the SSES and DXRD to a small population of crusts and nodules from the two study areas. The objectives of the first project were to relate the composition of the crust and nodule samples to the environment of formation as well as to the mineralogy which could be identified from a bulk powdered sample. The SSES was developed to determine the partitioning of Cu, Ni, and Co concentrations between the Mn and Fe oxides present in crusts and nodules. In developing a SSES, two goals had to be attained: (1) since crust and nodule samples are finite in size and numerous different analyses are to be preformed on a single sample, a SSES should be developed which uses as small amount of sample as feasible, and (2) develop a SSES which is as time efficient as possible. The development of the DXRD in conjunction with the SSES identified which Mn and Fe oxide mineral phase was responsible for hosting Cu, Ni, and Co. In developing the DXRD procedure two other goals had to be attained: (1) use of small leached samples, and (2) recovery of the sample after XRD analysis. The purpose of the third project was to test the two analytical procedures on a group of crust and nodule samples which have a wide range in compositions and oxide phase mineralogies.

One group of hydrothermal nodules, from Survey Region B, was found to be enriched in Mn and depleted in Fe and Si. The Mn-rich mineral phases were identified as todorokite and birnessite. The second group of hydrothermal nodules, from Survey Region B, was found to be enriched in Fe and Si and depleted in Mn. The Fe-Si rich mineral phase was identified as iron-rich nontronite. Both groups of hydrothermal nodules were depleted in Co, Cu, and Ni. Dymond *et al.* (1984) and Chen & Owen (1989) identified one group of hydrothermal nodules located close to the East Pacific Rise (EPR) as being enriched in Fe but depleted in Mn, Cu, Ni, and Co. This composition agrees with the Fe-Si rich hydrothermal nodules identified in Survey Region B. Both Dymond *et al.* (1984) and Chen & Owen (1989), however, interpreted a second group of nodules, close to the EPR, which were enriched in Mn but depleted in Cu, Ni, and Co as suboxic diagenetic deposits. This group of nodules is the Mn-rich end-member composition of hydrothermal nodules identified in this study.

The composition of nodules from Survey Region B indicates there is a correlation between Co abundance and the proximity of the nodules to the hydrothermal discharge from the EPR. Nodules that are Co-enriched are found farthest away from hydrothermal activity. In contrast, cobalt-depleted nodules coincide with known areas of hydrothermal activity.

The SSES and DXRD was applied to a small population of crusts and nodules from the two Survey Regions. The DXRD patterns from the second stage of leaching on the crusts and nodules showed that the iron phase mineralogy in marine crusts and nodules is either akaganéite or ferrihydrite. The DXRD patterns from the second stage of leaching on the Mn-rich hydrothermal crusts and nodules, from Survey Region B, identified the Mn-bearing mineral hausmannite.

## TABLE OF CONTENTS

	Page
Title Page .....	i
Abstract .....	ii
Table of Contents .....	iii
List of Figures.....	x
Lists of Tables.....	xx
<b>CHAPTER 1 THE GEOCHEMISTRY OF FERROMANGANESE CRUSTS AND NODULES FROM THE CENTRAL AND EASTERN NORTH EQUATORIAL PACIFIC .....</b>	<b>1</b>
1.1 INTRODUCTION.....	2
1.1.1 PREVIOUS WORK.....	2
1.1.2 STATEMENT OF THE PROBLEM .....	4
1.2 SELECTION OF STUDY AREAS .....	5
1.2.1 SELECTION OF SAMPLES .....	5
1.2.2 REGIONAL SETTING .....	10
1.2.2.1 Line Island Archipelago .....	10
1.2.2.2 East Pacific Rise .....	14
1.2.2.3 Abyssal Seafloor Between the CCFZ.....	14
1.2.3 MORPHOLOGY AND TEXTURE.....	16
1.3 ANALYTICAL METHODS.....	18
1.3.1 GEOCHEMISTRY .....	18
1.3.1.1 Sample Preparation.....	18
1.3.1.2 Calibration.....	20
1.3.1.3 Experimental Conditions.....	20
1.3.1.4 Precision and Accuracy.....	21
1.3.2 MINERALOGY.....	26
1.3.2.1 Sample Preparation.....	26



1.3.2.2 Experimental Conditions.....	27
1.3.2.3 Precision.....	28
1.4 RESULTS AND DISCUSSION .....	30
1.4.1 SURVEY REGION A .....	30
1.4.1.1 Crusts.....	30
1.4.1.1.1 Mineralogy.....	30
1.4.1.1.2 Bulk Composition.....	33
1.4.1.1.3 Interelement Associations.....	33
1.4.1.1.3.1 Correlations with Aluminium .....	33
1.4.1.1.3.2 Phosphorite .....	38
1.4.1.1.3.3 Correlations with Manganese and Iron.....	41
1.4.1.1.4 Variations with Depth.....	48
1.4.1.1.4.1 Correlations with Manganese and Iron.....	48
1.4.1.1.4.2 Correlations with Manganese Phase Mineralogy .....	58
1.4.1.1.5 Correlations with Latitude .....	61
1.4.1.2 Nodules .....	62
1.4.1.2.1 Mineralogy.....	62
1.4.1.2.2 Bulk Composition.....	62
1.4.1.2.3 Interelement Associations.....	66
1.4.1.2.3.1 Correlations with Aluminium .....	66
1.4.1.2.3.2 Phosphorite .....	70
1.4.1.2.3.3 Correlations with Manganese and Iron.....	75
1.4.1.2.3.3.1 Complex Correlations Between Cobalt with Manganese and Iron.....	86
1.4.1.2.3.3.2 Correlations of Copper with Nickel.....	89
1.4.2 SURVEY REGION B.....	92
1.4.2.1 Crusts.....	92

1.4.2.1.1 Mineralogy.....	92
1.4.2.1.2 Bulk Compostion.....	92
1.4.2.1.3 Interelement Associations.....	96
1.4.2.1.3.1 Correlations with Aluminium .....	96
1.4.2.1.3.2 Correlations with Calcium.....	100
1.4.2.1.3.3 Correlations with Manganese.....	107
1.4.2.1.3.4 Correlations with Iron.....	113
1.4.2.1.4 Correlation Between Cobalt Abundance and Distance from the EPR .....	113
1.4.2.2 Nodules .....	117
1.4.2.2.1 Mineralogy.....	117
1.4.2.2.2 Bulk Compostion.....	120
1.4.2.2.3 Interelement Associations.....	122
1.4.2.2.3.1 Correlations with Aluminium .....	122
1.4.2.2.3.2 Phosphorite .....	127
1.4.2.2.3.3 Correlations with Manganese.....	127
1.4.2.2.3.4 Correlations with Iron.....	136
1.4.2.2.3.5 Identification of the Two Groups of Hydrothermal Nodules.....	145
1.4.2.2.4 Variations with Depth.....	147
1.4.2.2.4.1 Behaviour of Manganese and Iron .....	147
1.4.2.2.4.2 Behaviour of Cobalt.....	154
1.5 REFERENCES .....	156
1.6 APPENDIX A THE LOCATION OF CRUST AND NODULE SAMPLES FROM SURVEY REGION A.....	166
1.7 APPENDIX B THE LOCATION OF CRUST AND NODULE SAMPLES FROM SURVEY REGION B.....	170
1.8 APPENDIX C THE CONCENTRATIONS OF THE MAJOR ELEMENTS AND THE TODOROKITE/ $\delta\text{MnO}_2$ RATIOS FOR CRUST AND NODULE SAMPLES FROM SURVEY REGION A.....	175

1.9 APPENDIX D THE CONCENTRATIONS OF THE MAJOR ELEMENTS AND THE TODOROKITE/ $\delta\text{MnO}_2$ RATIOS FOR CRUST AND NODULE SAMPLES FROM SURVEY REGION B .....	186
CHAPTER 2 DEVELOPMENT OF A SELECTIVE SEQUENTIAL EXTRACTION SCHEME AND A DIFFERENTIAL X-RAY DIFFRACTION TECHNIQUE TO DETERMINE THE CHEMICAL PARTITIONING OF Mn, Fe, Cu, Ni, AND Co BETWEEN THE MANGANESE AND IRON OXIDE PHASE MINERALOGY IN FERROMANGANESE CRUSTS AND NODULES.....	201
2.1 INTRODUCTION .....	202
2.1.1 REVIEW OF PREVIOUS WORK .....	202
2.1.1.1 Selective Dissolution of Manganese and Iron Oxides in Soils and Sediments.....	202
2.1.1.2 Selective Sequential Extraction Schemes for Soils and Sediments .....	203
2.1.1.3 Selective Dissolution of Manganese and Iron Oxides in Crusts and Nodules .....	204
2.1.1.4 Differential X-Ray Diffraction .....	209
2.1.2 STATEMENT OF PROBLEM .....	211
2.2 ANALYTICAL METHODS AND RESULTS.....	212
2.2.1 EFFECTIVENESS OF SELECTED REAGENTS.....	212
2.2.1.1 Reagents Used .....	212
2.2.1.2 Experimental Conditions.....	213
2.2.2 ANALYSIS OF THE LEACHATES.....	216
2.2.2.1 Calibration.....	216
2.2.2.2 Sample Preparation.....	216
2.2.2.3 Determining the Effectiveness of Each Reagent.....	222
2.2.3 DEVELOPMENT OF THE TWO STAGE LEACHING PROCEDURE.....	223
2.2.3.1 First Stage of the Selective Sequential Extraction Scheme .....	223

2.2.3.2 Second Stage of the Selective Sequential Extraction Scheme .....	226
2.2.3.3 Analysis of the Leachates .....	226
2.2.3.4 Precision and Accuracy .....	228
2.2.4 DEVELOPMENT OF DIFFERENTIAL X-RAY DIFFRACTION TECHNIQUE .....	233
2.2.4.1 Sample Preparation .....	233
2.2.4.2 Experimental Conditions .....	234
2.2.4.3 Production of a DXRD Diffractogram .....	235
2.2.4.3.1 Smoothing the Data .....	235
2.2.4.3.2 Equation of DXRD Pattern .....	236
2.2.4.3.3 Plotting the Tracing .....	239
2.2.4.4 Description of the DXRD Results .....	239
2.3 DISSCUSION AND CONCLUSIONS .....	262
2.4 REFERENCES .....	264
2.5 APPENDIX A <b>THE WEIGHT PERCENT Mn, Fe, Cu, Ni, AND Co IN THE LABORATORY STANDARD CRUST AS DETERMINED FROM THE LEACHATES</b> .....	268
2.6 APPENDIX B <b>PERCENT Mn, Fe, Cu, Ni, AND Co REMOVED FROM THE LABORATORY STANDARD CRUST</b> .....	273
2.7 APPENDIX C <b>THE SAVITZKY &amp; GOLAY (1964) SMOOTHING PROGRAM TRANSLATED INTO GW BASIC</b> .....	278
CHAPTER 3 <b>THE APPLICATION OF THE SELECTIVE SEQUENTIAL EXTRACTION SCHEME AND THE DIFFERENTIAL X-RAY DIFFRACTION TECHNIQUE TO A SMALL POPULATION OF CRUSTS AND NODULES FROM THE NORTHEAST EQUATORIAL PACIFIC OCEAN</b> .....	282
3.1 INTRODUCTION .....	283
3.1.1 PREVIEW .....	283
3.1.2 STATEMENT OF THE PROBLEM .....	283

3.2 SELECTION OF SAMPLES .....	284
3.3 ANALYTICAL METHODS.....	287
3.4 RESULTS.....	287
3.4.1 BACKGROUND GEOCHEMISTRY AND MINERALOGY .....	287
3.4.1.1 Survey Region A.....	290
3.4.1.1.1 Crusts.....	290
3.4.1.1.2 Nodules .....	290
3.4.1.2 Survey Region B .....	302
3.4.1.2.1 Crusts.....	302
3.4.1.2.2 Nodules .....	323
3.4.2 SELECTIVE SEQUENTIAL EXTRACTION AND DXRD.....	333
3.4.2.1 Survey Region A.....	333
3.4.2.1.1 First Stage of the Selective Sequential Extraction Scheme and DXRD .....	339
3.4.2.1.2 Second Stage of the Selective Sequential Extraction Scheme and DXRD .....	352
3.4.2.2 Survey Region B .....	365
3.4.2.2.1 First Stage of the Selective Sequential Extraction Scheme and DXRD.....	365
3.4.2.2.2 Second Stage of the Selective Sequential Extraction Scheme and DXRD .....	376
3.5 DISCUSSION .....	401
3.5.1 MANGANESE OXIDES IDENTIFIED IN CRUSTS AND NODULES.....	401
3.5.1.1 Todorokite.....	408
3.5.1.2 Birnessite .....	409
3.5.1.3 $\delta\text{MnO}_2$ .....	412
3.5.1.4 Hausmannite .....	417

3.5.2 IRON OXIDES IDENTIFIED IN CRUSTS AND NODULES .....	420
3.5.2.1 Akaganéite.....	421
3.5.2.2 Ferrihydrite.....	424
3.6 REFERENCES .....	428
<b>CHAPTER 4 SUMMARY OF PRINCIPAL RESULTS .....</b>	<b>432</b>
4.1 RESULTS FROM CHAPTER 1.....	433
4.1.1 REGIONAL VARIATIONS IN THE GEOCHEMISTRY OF CRUSTS AND NODULES .....	433
4.1.1.1 Survey Region A.....	433
4.1.1.2 Survey Region B .....	439
4.2 RESULTS FROM CHAPTER 2.....	442
4.2.1 SELECTIVE SEQUENTIAL EXTRACTION SCHEME .....	442
4.2.2 DIFFERENTIAL X-RAY DIFFRACTION TECHNIQUE.....	444
4.3 RESULTS FROM CHAPTER 3.....	448
4.4 REFERENCES .....	451

## LIST OF FIGURES

	Page
Figure 1-1. The location of the two Survey Regions within the northeastern equatorial Pacific Ocean (modified from Glasby <i>et al.</i> , 1987).....	6
Figure 1-2. Location of crust and nodule samples from within Survey Region A (modified from Chase <i>et al.</i> , 1970).....	8
Figure 1-3. Location of crust and nodule samples from within Survey Region B (modified from Chase <i>et al.</i> , 1970).....	11
Figure 1-4. A typical XRD pattern of a crust from Survey Region A. ....	31
Figure 1-5. The relationship between Al and other major elements. The open circles = samples from the Hawaiian Island Archipelago, the filled circles = samples from the Line Island Archipelago.....	35
Figure 1-6. The correlation between Ca and P. The open circles = samples from the Hawaiian Island Archipelago, the filled circles = samples from the Line Island Archipelago. ....	39
Figure 1-7. The association of major elements with Mn/Fe. The open circles = samples from the Hawaiian Island Archipelago, the filled circles = samples from the Line Island Archipelago.....	42
Figure 1-8. The correlation between Mn and those elements that are associated with Mn and water depth. The open circles = samples from the Hawaiian Island Archipelago, the filled circles = samples from the Line Island Archipelago.....	49

Figure 1-9. The correlation between Fe and those elements that are associated with Fe and water depth. The open circles = samples from the Hawaiian Island Archipelago, the filled circles = samples from the Line Island Archipelago.....	53
Figure 1-10. The profile of the O <sub>2</sub> concentration in seawater at Geosecs Station 235. ....	56
Figure 1-11. Correlation between manganese phase mineralogy and water depth. The open circles = samples from the Hawaiian Island Archipelago, the filled circles = samples from the Line Island Archipelago.....	59
Figure 1-12. A typical XRD pattern of a nodule from Survey Region A.....	63
Figure 1-13. The relationship between Al and other major elements. The open circles = diagenetic nodules, the filled circles = hydrogenous nodules.....	67
Figure 1-14. The correlation between Ca and P. The open circles = diagenetic nodules, the filled circles = hydrogenous nodules.....	71
Figure 1-15. An XRD pattern of a nodule with high Ca and P concentraions. ....	73
Figure 1-16. The association of major elements with Mn/Fe. The open circles = diagenetic nodules, the filled circles = hydrogenous nodules. ....	76
Figure 1-17. Correlation between manganese phase mineralogy and Mn/Fe. The open circles = diagenetic nodules, the filled circles = hydrogenous nodules.....	80
Figure 1-18. The crystal structure of todorokite. (Turner <i>et al.</i> , 1982). ....	83
Figure 1-19. Complex association of Co with Mn and Fe. The open circles = diagenetic nodules, the filled circles = hydrogenous nodules. ....	87



Figure 1-20. Correlation between Cu/Ni and Mn/Fe. The open circles = diagenetic nodules, the filled circles = hydrogenous nodules.....	90
Figure 1-21. A typical XRD pattern of a crust from Survey Region B. ....	93
Figure 1-22. The relationship between Al and other major elements. The open circles = hydrogenetic crusts, the filled circles = Mn-enriched hydrothermal crusts, the filled triangles = Mn-depleted hydrothermal crusts. ....	97
Figure 1-23. An XRD pattern of a crust with high concentrations of Fe and Si and low concentrations of trace elements.....	101
Figure 1-24. The relationship between Ca and other major elements. The open circles = hydrogenetic crusts, the filled circles = Mn-enriched hydrothermal crusts, the filled triangles = Mn-depleted hydrothermal crusts. ....	103
Figure 1-25. A typical XRD pattern of a crust with high concentrations of Ca, Si, and Mg. ....	105
Figure 1-26. The relationship between Mn and other major elements. The open circles = hydrogenetic crusts, the filled circles = Mn-enriched hydrothermal crusts, the filled triangles = Mn-depleted hydrothermal crusts. ....	108
Figure 1-27. An XRD pattern of a crust which is enriched in Mn ( > 30 weight per cent).....	111
Figure 1-28. The relationship between Fe and other major elements. The open circles = hydrogenetic crusts, the filled circles = Mn-enriched hydrothermal crusts, the filled triangles = Mn-depleted hydrothermal crusts. ....	114
Figure 1-29. A typical XRD pattern of a nodule from Survey Region B. ....	118

Figure 1-30. The relationship between Al and other major elements. The open circles = hydrogenous and diagenetic nodules, the filled circles = Mn-enriched hydrothermal nodules, the filled triangles = Mn-depleted hydrothermal nodules.....	123
Figure 1-31. The correlation between Ca and P. The open circles = hydrogenous and diagenetic nodules, the filled circles = Mn-enriched hydrothermal nodules, the filled triangles = Mn-depleted hydrothermal nodules.....	128
Figure 1-32. An XRD pattern of a nodule with high Ca and P concentraions.....	130
Figure 1-33. The relationship between Mn and other major elements. The open circles = hydrogenous and diagenetic nodules, the filled circles = Mn-enriched hydrothermal nodules, the filled triangles = Mn-depleted hydrothermal nodules.....	132
Figure 1-34. An XRD pattern of a nodule which is enriched in Mn ( > 30 weight per cent).....	137
Figure 1-35. The relationship between Fe and other major elements. The open circles = hydrogenous and diagenetic nodules, the filled circles = Mn-enriched hydrothermal nodules, the filled triangles = Mn-depleted hydrothermal nodules.....	139
Figure 1-36. An XRD pattern of a nodule with high concentrations of Fe and Si and low concentrations of trace elements.....	143
Figure 1-37. The correlation between Mn and those elements that are associated with Mn and water depth. The open circles = hydrogenous and diagenetic nodules, the filled circles = Mn-enriched hydrothermal nodules, the filled triangles = Mn-depleted hydrothermal nodules.....	148

Figure 1-38. The profile of the O <sub>2</sub> concentration in seawater at Geosecs Station 343. ....	152
Figure 2-1. Calibration curves of the elements Mn, Fe, Cu, Ni, and Co in various reagents. The open circles = Mn, the filled circles = Fe, the open triangles = Cu, the filled triangles = Ni, the open squares = Co. ....	218
Figure 2-2. The XRD diffraction pattern of the laboratory standard crust DODO 14 DZ.....	240
Figure 2-3. The XRD diffraction pattern of the laboratory standard nodule Mn 191 6-8. ....	242
Figure 2-4. The XRD diffraction pattern of the laboratory standard crust DODO 14 DZ after the first stage of the sequential extraction scheme. ....	244
Figure 2-5. The XRD diffraction pattern of the laboratory standard nodule Mn 191 6-8 after the first stage of the sequential extraction scheme. ....	246
Figure 2-6. The DXRD pattern obtained after the first stage of leaching of the sequential extraction scheme on the laboratory standard crust DODO 14 DZ.....	248
Figure 2-7. The DXRD pattern obtained after the first stage of leaching of the sequential extraction scheme on the laboratory standard nodule Mn 191 6-8. ....	251
Figure 2-8. The XRD diffraction pattern of the laboratory standard crust DODO 14 DZ after the second stage of the sequential extraction scheme. ....	253
Figure 2-9. The XRD diffraction pattern of the laboratory standard nodule Mn 191 6-8 after the second stage of the sequential extraction scheme. ....	255

Figure 2-10. The DXRD pattern obtained after the second stage of leaching of the sequential extraction scheme on the laboratory standard crust DODO 14 DZ. ....	257
Figure 2-11. The DXRD pattern obtained after the second stage of leaching of the sequential extraction scheme on the laboratory standard nodule Mn 191 6-8. ....	259
Figure 3-1. The association of Cu, Ni, and Co with Mn/Fe in hydrogenetic crusts from Survey Region A. ....	291
Figure 3-2. The XRD patterns of hydrogenetic crusts selected for the two stage selective sequential extraction scheme. ....	294
Figure 3-3. The association of Cu, Ni with Mn/Fe. The open circles = diagenetic nodules, the filled circles = hydrogenous nodules. ....	297
Figure 3-4. The complex association of Co with Mn/Fe. The open circles = diagenetic nodules, the filled circles = hydrogenous nodules. ....	300
Figure 3-5. The XRD patterns of hydrogenous nodules selected for the two stage selective sequential extraction scheme. ....	303
Figure 3-6. The XRD patterns of diagenetic nodules selected for the two stage selective sequential extraction scheme. ....	306
Figure 3-7. The relationship between Mn with Cu, Ni, and Co. The open circles = hydrogenetic crusts, the filled circles = Mn-enriched hydrothermal crusts, the filled triangles = Mn-depleted hydrothermal crusts. ....	309
Figure 3-8. The XRD patterns of hydrogenetic crusts selected for the two stage selective sequential extraction scheme. ....	312

Figure 3-9. The XRD patterns of Mn-enriched hydrothermal crusts selected for the two stage selective sequential extraction scheme. ....	316
Figure 3-10. The XRD pattern of a Mn-depleted hydrothermal crust enriched in Fe and Si. ....	319
Figure 3-11. The relationship between Fe and Co. The open circles = hydrogenetic crusts, the filled circles = Mn-enriched hydrothermal crusts, the filled triangles = Mn-depleted hydrothermal crusts. ....	321
Figure 3-12. The relationship between Mn with Cu, Ni, and Co. The open circles = hydrogenous and diagenetic nodules, the filled circles = Mn-enriched hydrothermal nodules, the filled triangles = Mn-depleted hydrothermal nodules.....	324
Figure 3-13. The XRD patterns of the hydrogenous and diagenetic nodules selected for the two stage selective sequential extraction scheme. ....	327
Figure 3-14. The XRD patterns of the Mn-enriched hydrothermal nodules selected for the two stage selective sequential extraction scheme. ....	330
Figure 3-15. The XRD patterns of the Mn-depleted hydrothermal nodules selected for the two stage selective sequential extraction scheme. ....	334
Figure 3-16. The weight per cent of Mn, Fe, Cu, Ni, and Co associated with the manganese phase mineralogy which was removed during the first stage of the selective extraction scheme. The open circles = hydrogenetic crusts, the filled circles = hydrogenous nodules, the open triangles = diagenetic nodules.....	340
Figure 3-17. The DXRD pattern obtained after the first stage of leaching of the sequential extraction scheme on the hydrogenetic crusts. ....	343

Figure 3-18. The DXRD pattern obtained after the first stage of leaching of the sequential extraction scheme on the hydrogenous nodules.....	346
Figure 3-19. The DXRD pattern obtained after the first stage of leaching of the sequential extraction scheme on the diagenetic nodules. ....	349
Figure 3-20. The weight per cent of Mn, Fe, Cu, Ni, and Co associated with the iron phase mineralogy which was removed during the second stage of the selective extraction scheme. The open circles = hydrogenetic crusts, the filled circles = hydrogenous nodules, the open triangles = diagenetic nodules. ....	353
Figure 3-21. The DXRD pattern obtained after the second stage of leaching of the sequential extraction scheme on the hydrogenetic crusts. ....	356
Figure 3-22. The DXRD pattern obtained after the second stage of leaching of the sequential extraction scheme on the hydrogenous nodules.....	359
Figure 3-23. The DXRD pattern obtained after the second stage of leaching of the sequential extraction scheme on the diagenetic nodules. ....	362
Figure 3-24. The weight per cent of Mn, Fe, Cu, Ni, and Co associated with the manganese phase mineralogy which was removed during the first stage of the selective extraction scheme. The open circles = hydrogenetic crusts, the filled circles = Mn-enriched hydrothermal crusts, the open triangles = hydrogenous and diagenetic nodules, the filled triangles = Mn-enriched hydrothermal nodules, the open squares = Mn depleted hydrothermal nodules.....	370
Figure 3-25. The DXRD pattern obtained after the filled first stage of leaching of the sequential extraction scheme on the hydrogenetic crusts. ....	373

Figure 3-26. The DXRD pattern obtained after the first stage of leaching of the sequential extraction scheme on the Mn-enriched hydrothermal crusts.....	377
Figure 3-27. The DXRD pattern obtained after the first stage of leaching of the sequential extraction scheme on the Mn-enriched hydrothermal nodules.....	380
Figure 3-28. The DXRD pattern obtained after the first stage of leaching of the sequential extraction scheme on the Mn-depleted hydrothermal nodules.....	383
Figure 3-29. The DXRD pattern obtained after the first stage of leaching of the sequential extraction scheme on the hydrogenous and diagenetic nodules.....	386
Figure 3-30. The weight per cent of Mn, Fe, Cu, Ni, and Co associated with the iron phase mineralogy which was removed during the second stage of the selective extraction scheme. The open circles = hydrogenetic crusts, the filled circles = Mn-enriched hydrothermal crusts, the open triangles = hydrogenous and diagenetic nodules, the filled triangles = Mn-enriched hydrothermal nodules, the open squares = Mn depleted hydrothermal nodules.....	389
Figure 3-31. The DXRD pattern obtained after the second stage of leaching of the sequential extraction scheme on the hydrogenetic crusts. ....	392
Figure 3-32. The DXRD pattern obtained after the second stage of leaching of the sequential extraction scheme on the Mn-enriched hydrothermal crusts. ....	395

Figure 3-33. The DXRD pattern obtained after the second stage of leaching of the sequential extraction scheme on the hydrogenous and diagenetic nodules.....	398
Figure 3-34. The DXRD pattern obtained after the second stage of leaching of the sequential extraction scheme on the Mn-enriched hydrothermal nodules.....	402
Figure 3-35. The DXRD pattern obtained after the second stage of leaching of the sequential extraction scheme on the Mn-depleted hydrothermal nodules.....	405
Figure 3-36. The crystal structure of todorokite (Turner <i>et al.</i> , 1982). ....	410
Figure 3-37. The crystal structure of birnessite (Giovanoli & Brüttsch, 1979). ....	413
Figure 3-38. The crystal structure of $\delta\text{MnO}_2$ (modified from Giovanoli <i>et al.</i> , 1965). ....	415
Figure 3-39. The crystal structure of hausmannite (Murray, 1979).....	418
Figure 3-40. The crystal structure of akaganéite. 1 = Mn, 2 = oxygen, 3 = Ba, K, Pb, Na, or $\text{H}_2\text{O}$ (Murray, 1979).....	422
Figure 3-41. The crystal structure of ferrihydrite (modified from Eggleton & Fitzpatrick, 1988). ....	425



## LIST OF TABLES

	Page
Table 1-1a. Precision of the method of analysis between samples.....	22
Table 1-1b. Precision of the XRF .....	23
Table 1-2. Comparison of analytical results with best estimates of two ferromanganese nodule reference standards. Results are given as weight percentages. ....	25
Table 1-3a. Precision of the method of analysis between sample. ....	29
Table 1-3b. Precision of the XRD .....	29
Table 1-4. Mean concentrations of major elements in crusts from Survey Region A. Concentrations are given in weight per cent.....	34
Table 1-5. Comparison of the composition of aluminosilicates in crusts to Average Pacific Pelagic Clay and Tholeiitic Lavas from the Hawaiian Islands.....	37
Table 1-6. Mean concentrations of major elements in nodules from Survey Region A. Concentrations are given in weight per cent.....	65
Table 1-7. Comparison of the composition of aluminosilicates in nodules to Average Pacific Pelagic Clay and Tholeiitic Lavas from the Hawaiian Islands.....	69
Table 1-8. Mean concentrations of major elements in crusts from Survey Region B. Concentrations are given in weight per cent.....	95
Table 1-9. Comparison of the composition of aluminosilicates in crusts to Average Pacific Pelagic Clay and Mid-Ocean Ridge Basalts.....	99

Table 1-10. Mean concentrations of major elements in nodules from Survey Region B. Concentrations are given in weight per cent.....	121
Table 1-11. Comparison of the composition of aluminosilicates in nodules to Average Pacific Pelagic Clay and Mid-Ocean Ridge Basalts.....	126
Table 2-1. The mean composition of the laboratory standard crust DODO 14DZ. Mean concentrations are given as weight per cents.....	214
Table 2-2. Instrumental setting for analysis of the five metals on the atomic absorption spectrophotometer. ....	217
Table 2-3. The effectiveness of 0.25M $\text{NH}_2\text{OH}\cdot\text{HCl}$ in 0.01M $\text{HNO}_3$ and 0.175M Ammonium Oxalate in 0.1M Oxalic Acid. Results are listed as the per cent of Mn and Fe removed from the laboratory standard crust DODO14DZ. ....	224
Table 2-4. The mean composition of the laboratory standard nodule Mn191 6-8. Mean concentraions are given as weight per cents.....	225
Table 2-5a. Concentrations of Mn, Fe, Cu, Ni, and Co in the leachates from the first stage of the two stage selective sequential extraction scheme. Results are given as weight per cents.....	227
Table 2-5b. Concentrations of Mn, Fe, Cu, Ni, and Co in the leachates from the second stage of the two stage selective sequential extraction scheme. Results are given as weight per cents and have been adjusted to be comparable to the first stage of leaching.....	227
Table 2-6a. Precision of the method of analysis for the first stage of the two stage selective sequential extraction scheme. Replicate samples are from the laboratory standard crust DODO 14DZ. Concentrations are given as weight per cents.....	229

Table 2-6b. Precision of the method of analysis for the second stage of the two stage selective sequential extraction scheme. Replicate samples are from the laboratory standard crust DODO 14DZ. Concentrations are given as weight per cents.....	229
Table 2-6c. Precision of the Atomic Absorbtion Spectrometer as determined by the absorbances of the standard 5ppm.....	230
Table 2-7. Comparison of the total amount of Mn, Fe, Cu, Ni, and Co removed from the laboratory standard crust and nodule by the two stage selective sequential extraction scheme compared to the XRF results used to determine precision of the XRF. Results are given as weight per cents. ....	232
Table 2-8. Comparison of the d-spacings (Å) of the two iron oxides identified in this study to those listed in the JCPDS card index.....	261
Table 3-1a. Location and depth of crust and nodule samples selected from Survey Region A for analysis. The location and depth of these samples are also shown in Figure 1-2 in Chapter 1.....	285
Table 3-1b. Location and depth of crust and nodule samples selected from Survey Region B for analysis. The location and depth of these samples are also shown in Figure 1-3 in Chapter 1.....	286
Table 3-2a. The major element composition of the bulk crust and nodule samples selected from Survey Region A. Results are listed as weight per cent.....	288

Table 3-2b. The major element composition of the bulk crust and nodule samples selected from Survey Region B. Results are listed as weight per cent.....	289
Table 3-3a. The concentrations of Mn, Fe, Cu, Ni, and Co in the leachates from the first stage of leaching for samples from Survey Region A. Results are listed as weight per cent.....	337
Table 3-3b. The mineral phase(s) removed during the first stage of the selective sequential extraction scheme and identified by DXRD.....	337
Table 3-4a. The concentrations of Mn, Fe, Cu, Ni, and Co in the leachates from the second stage of leaching for samples from Survey Region A. Results are listed as weight per cent.....	338
Table 3-4b. The mineral phase(s) removed during the second stage of the selective sequential extraction scheme and identified by DXRD.....	338
Table 3-5a. The concentrations of Mn, Fe, Cu, Ni and Co in the leachates from the first stage of leaching for samples from Survey Region B. Results are listed as weight per cent.....	366
Table 3-5b. The mineral phase(s) removed during the first stage of the selective sequential extraction scheme and identified by DXRD.....	367
Table 3-6a. The concentrations of Mn, Fe, Cu, Ni and Co in the leachates from the second stage of leaching for samples from Survey Region B. Results are listed as weight per cent.....	368
Table 3-6b. The mineral phase(s) removed during the second stage of the selective sequential extraction scheme and identified by DXRD.....	369

## **CHAPTER 1**

# **THE GEOCHEMISTRY OF FERROMANGANESE CRUSTS AND NODULES FROM THE CENTRAL AND EASTERN NORTH EQUATORIAL PACIFIC**

## 1.1 INTRODUCTION

### 1.1.1 PREVIOUS WORK

Ferromanganese crusts and nodules from the Central and Eastern North Equatorial Pacific have been studied to a greater extent than those from any other ocean. Initial interests within this area were focused on abyssal ferromanganese nodules (hereafter called nodules) from the Eastern Equatorial Pacific. The first systematic study of nodules from this area were recovered from the WAHINE Survey Region (1965) (Moore & Heath, 1966). This was later followed by the International Decade of Ocean Exploration (IDOE) during which three projects were conducted. These are the MANOP (1974-1975) (Margolis & Burns, 1976), DOMES (1975-1976), (Sorem *et al.*, 1979), and the International Cooperative Investigations of Manganese Nodule Environments (I.C.M.E) Project (1978) (Friedrich *et al.*, 1983). Also during this time West Germany investigated a number of small survey regions within this area. These survey regions include: P (1971), VA-04 (1972) (Roonwal & Friedrich, 1980), VA-05/1 (1973), VA-08/1 (1974) (Friedrich *et al.*, 1977), VA-13/1 and VA-13/2 (1976) (Marchig & Gundlach, 1979; Glasby *et al.*, 1982), and VA-18 (1978) (von Stackelberg, 1982).

The first ferromanganese crusts (hereafter called crusts) sampled from the Central North Equatorial Pacific were recovered from the Hawaiian Archelago by Moore (1965). Attention was later drawn to these crusts as potential resources of strategic metals, specifically cobalt, when in 1978 the Shaba Province of Zaire (formerly Katanga in the Belgian Congo) was invaded by Angola and Zambia. This caused the price of cobalt to peak and reflects the fact that Zaire (Shaba province) is the world's largest producer of cobalt. Unlike the mining of abyssal nodules, which is complicated by their location in international waters, most of the cobalt-rich crusts

occur within the exclusive economic zone of the United States and other nations (Manheim, 1986). Since then a number of cruises have collected crusts from the Hawaiian Archipelago, the Line Island Archipelago, and the Mid Pacific Mountains. The first detailed and systematic study was that of the German MIDPAC-1 Expedition (1981) (Halbach & Manheim, 1984). This was followed by the U.S. Geological Survey R/V "S.P. LEE" Expedition (1983) (Hein *et al.*, 1985a) and again by the German MIDPAC-2 Expedition (1984) (Mangini *et al.*, 1987). A number of shorter cruises have also examined crusts from this region. These include cruises by the U.S Geological Survey to Johnston Island (1986) and by the University of Hawaii to the Hawaiian Archipelago (1984) and to the Line Island Archipelago (1986 and 1987) (Hein *et al.*, in press a).

Examination of the results of these cruises shows that crusts and nodules have wide compositional variations throughout the Central and Eastern North Equatorial Pacific. This variable geochemistry is related to a combination of factors which include the availability and chemical behaviour of elements in the marine environment, the adsorptive and crystallo-chemical properties of the authigenic mineral phases, and their rate of formation (Cronan, 1980). Environmental parameters also control crust and nodule geochemistry. These environmental parameters are: 1) The form of the deposit, either as a crust or nodule; 2) The environment of deposition, either on top of a seamount or on the abyssal sea floor; 3) The lithology of the substrate; and 4) The water depth. It should be noted that these environmental parameters do not act independently of one another (Frazer & Fisk, 1981).

Three sources of metals contribute to the formation of crusts and nodules. This means that there is a continuous range in composition from an hydrogenetic end member to a diagenetic end member. Crusts located on the tops of seamounts and other topographic highs grow only in contact with ambient seawater. Crusts,

therefore, form by the direct precipitation of ferromanganese oxyhydroxide colloids from seawater (Lyle *et al.*, 1977). They, therefore, represent the purely hydrogenetic end member (Aplin & Cronan, 1985a). In basin regions, at a distinct distance from seamounts, two types of nodules coexist. Smaller nodules that are embedded in the uppermost "peneliquid" layer of the sediment. These nodules are formed by diagenetic remobilization of elements within the sediment column. They represent the purely diagenetic end member (Aplin & Cronan, 1985b). Larger nodules, with a distinct equatorial zone which divides the nodules into two distinct sections, are formed by hydrogenetic and diagenetic processes (Halbach *et al.*, 1980; 1981a,b). These nodules have been termed hydrogenous by Hein *et al.* (In Press b). As noted by Moore & Vogt (1976) and by Elderfield & Greaves (1981), the rate of formation of crusts and nodules associated with mid-ocean ridge crests is too rapid to be explained by hydrogenetic precipitation. Since ridge crest sediments are oxidizing throughout the sedimentary column, it is also unlikely that they are formed by diagenetic processes (Lyle, 1976). Crusts and nodules closely associated with mid-ocean ridge crests therefore represent the purely hydrothermal end member (Bonatti *et al.*, 1972).

### 1.1.2 STATEMENT OF THE PROBLEM

In this paper we examine a suite of crust and nodule samples recovered from the Central and North Equatorial Pacific Ocean. Calvert & Price (1977a) and Halbach *et al.* (1981b) have shown that crusts and nodules from different topographic provinces within the Central and Eastern Equatorial Pacific Ocean have varied and distinct compositions. This varied and distinct geochemistry is probably controlled by different mechanisms of formation, availability of constituent elements, and the adsorptive and crystallo-chemical properties of the authigenic mineral



phases. It is also probably controlled by the environmental parameters. The major element geochemistry and manganese phase mineralogy the suite of crust and nodule samples has been determined and will be compared and contrasted with work previously done within this region of the Pacific Ocean. Although the two survey regions discussed here are much larger than those of other authors, a comparison between this work and similar studies within the same survey regions will be attempted.

## 1.2 SELECTION OF STUDY AREAS

### 1.2.1 SELECTION OF SAMPLES

The crust and nodule samples used in this study were obtained from the collections at the Scripps Institution of Oceanography (SIO). From this collection, 167 samples were selected. Based on sample density, the Central and Equatorial North Pacific Ocean was divided into two survey regions (Figure 1-1). Survey Region A extends from the Hawaiian Island Archipelago at 21°N to the Equator and from the Line Island Archipelago at 170°W to 140°W. Samples from this region include nodules recovered from the abyssal sea floor located between the CCFZ and crusts from the Line Island Archipelago. The bathymetry and the location of crust and nodule samples within Survey Region A are shown in Figure 1-2. The precise location and depth of samples recovered from this area are listed in Appendix A.

Survey Region B is the larger of the two survey areas. It extends from 26°N to 5°N and from the eastern edge of Survey Region A at 140°W to the crest of the East Pacific Rise at 100°W. Samples from this region include nodules recovered from the abyssal seafloor North and South of the Clarion Fracture Zone as well as crusts

**Figure 1-1. The location of the two Survey Regions within the northeastern equatorial Pacific Ocean (modified from Glasby *et al.*, 1987).**

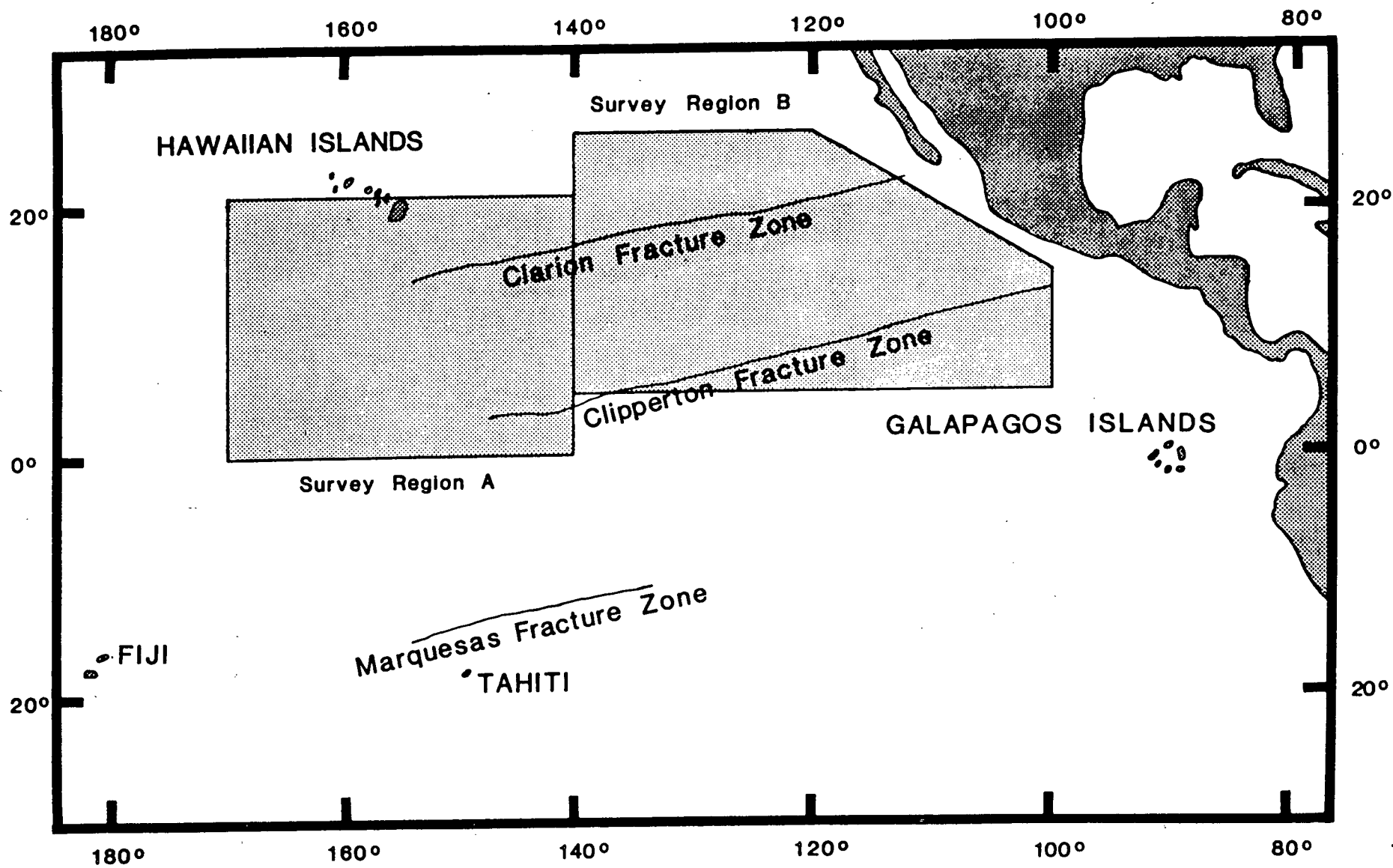


Figure 1-2. Location of crust and nodule samples from within Survey Region A  
(modified from Chase *et al.*, 1970).



recovered from the East Pacific Rise, Henderson Seamount, and the Suitcase Seamounts. The bathymetry and the location of crust and nodule samples within Survey Region B are shown in Figure 1-3. The precise location and depth of samples recovered from this area are listed in Appendix B.

## 1.2.2 REGIONAL SETTING

### 1.2.2.1 Line Island Archipelago

The origin of the Line Island Archipelago and the Mid Pacific Mountains is genetically related to basaltic volcanism during the Late Cretaceous (Halbach & Puteanus, 1984a). Clague (1981) stated that the first basaltic eruption in this area probably occurred 100 to 106Ma. Jackson & Schlanger (1976) proposed that the entire region underwent synchronous volcanism which uplifted the pre-existing shields into shallow water prior to 80 to 85Ma. The islands were covered by shallow water carbonate sediments before about 70 to 80Ma. Between 50 to 60Ma the islands probably began to submerge and the epoch of intense volcanism ended (Halbach & Puteanus, 1984a).

The former islands continued to subside through the remainder of the Cretaceous and Tertiary with the deposition of pelagic calcareous ooze. From the Middle Miocene to the Late Pliocene (about 12Ma), a period of non-deposition or erosion took place as a result of increased bottom current activity (Nishimura, 1981). This event is related to the development of a large ice cap on Antarctic and the resulting flow of Antarctic bottom water (AABW) (van Andel *et al.*, 1975). From the Late Pliocene onwards, siliceous clay sediments were deposited within the Central Equatorial North Pacific Basin along with calcareous ooze on seamounts above the CCD (Halbach *et al.*, 1982).

Figure 1-3. Location of crust and nodule samples from within Survey Region B  
(modified from Chase *et al.*, 1970).





The bathymetry of the Line Island Archipelago is characterized by high relief seamounts and seamount chains (Mangini *et al.*, 1987). The water depth varies between 1100 to 4900m and the CCD varies from 4700m in the south to 4200m in the north (Halbach & Puteanus, 1984b). The tops of the seamounts are often flat (guyots), which resulted from subsiding post-volcanic marine or subaerial conditions. Typical cliff-and-terrace structures exist on the flanks of the seamounts.

Crusts are common on seamount slopes and summit plateaus between 3000 to 1000m water depth. Crusts accumulate on unsedimented surfaces of seamount regions of the Line Island Archipelago and the Hawaiian Archipelago. Crusts precipitate primarily on nuclei or substrates of alkali basalt and its alteration products which consist of montmorillonite and phillipsite; hyaloclastites with fragments of highly vesicular basaltic rock; yellowish-green smectitic rocks; indurated phosphorite, formed by replacement of calcareous ooze; and occasionally claystone. Other clay minerals such as illite or kaolinite often make up a significant fraction of the substrate. While basaltic volcanics contribute minor amounts of olivine, magnetite and/or maghemite, ilmenite (?), and hematite (?) to the bulk composition of crusts, quartz is probably contributed by eolian transport from continental land masses (Frank *et al.*, 1976). On plateaus and flat terraces, nodules lie on top of partly consolidated calcareous sediments. Broken crusts and rock fragments in these regions provide nuclei for the formation of nodules. The AABW or other deep-water currents are sufficiently strong to prevent accumulation of pelagic material and promote hydrogenetic nucleation of crusts on substrate rocks.

### 1.2.2.2 East Pacific Rise

The East Pacific Rise (EPR) stands about 2 to 4km above the adjacent ocean bottom and varies from 2000 to 4000km in width. The EPR shows less bathymetric relief than other spreading ridges and has no prominent median valley along its crest, due to its rapid spreading rate of 6 to 10cm per year (Kennett, 1982). Hydrothermal solutions resulting from the convective circulation of seawater through newly emplaced basaltic crust (Corliss, 1971) supply dissolved metals to bottom seawater (Boström & Peterson, 1966). Upon mixing with cold oxygenated seawater the  $\text{Fe}^{2+}$  and  $\text{Mn}^{2+}$  present in the hydrothermal fluids oxidize and precipitate to form the Mn-Fe-rich sediments associated with mid-ocean spreading ridges (Skornyakova, 1964; Boström & Peterson, 1966; Bonatti *et al.*, 1972). The sediments associated with the EPR have been described as brown, X-ray amorphous metal oxide precipitates. Rather than being coatings or impregnations of other mineral grains, they are separate, very finely-disseminated or loosely aggregated materials (Boström & Peterson, 1966).

### 1.2.2.3 Abyssal Seafloor Between the CCFZ

The tectonic history and bathymetric relief of the abyssal seafloor between the CCFZ is directly related to seafloor spreading from the EPR (Craig, 1979). The age of the oceanic crust increases from the EPR to 20Ma at 115°W and to 75Ma at 150°W. A shift of the spreading centre from the Mathematicians Ridge to the EPR appears to have occurred sometime between 14 to 3Ma (van Andel & Heath, 1973). The bathymetry of this region is dominated by abyssal hills which are 50 to 200m in height (Andrews & Friedrich, 1979). These small scale features are generally elongated parallel to the crest of the EPR (Andrews *et al.*, 1977). The formation of

these features is a result of a combination of tensional, block faulting, and volcanic activity during the generation of oceanic crust at the EPR (Luyendyk, 1970). Andrews (1971) and van Andel *et al.* (1973) recognized variations in structural alignment and microtopographic relief on these abyssal hills and suggested that tectonic activity continues to modify these features at distances away from the EPR. The CCFZ originated as transform faults offsetting the EPR and are typically complex zones of ridges, basins, and seamounts on the order of 100km in width (Craig & Andrews, 1978). Subsidence of the cooling oceanic crust, formed at the EPR, has led to generally increasing regional water depths from 4000m at the western flank of the Mathematicians Ridge to about 5000m in the western part of the CCFZ (von Stackelberg, 1988). The CCD within the CCFZ ranges in depth from 4800m in the south to 4400m in the north (Berger *et al.*, 1976; Heath *et al.*, 1977; Piper *et al.*, 1979).

From the Cretaceous to the Early Oligocene, sedimentation within the CCFZ was governed mainly by the circumequatorial circulation through both the Atlantic and Pacific Oceans (Keller & Barron, 1983). The opening of the Drake Passage towards the end of the Oligocene to Early Miocene (25-20Ma) and the closing of the passage of Central America near the Early Middle Miocene (16-15Ma) resulted in the interruption of the circumequatorial circulation and the introduction of AABW. This caused a switch in deposition of silica from the Atlantic to the Pacific Ocean and in stronger deep sea erosion (von Stackelberg, 1988).

Various factors influence the distribution of sediment facies within the CCFZ. These have been listed by von Stackelberg (1988) as being: 1) the biogenic productivity zone parallel to the equator; 2) the CCFZ downthrown to the north; 3) the overall inclination of the seafloor to the west and the N-S orientation of the abyssal hills; and 4) the deflection to the south of the AABW by these abyssal hills. The distance of the CCFZ from the equatorial productivity zone and its increasing

water depth, which lies below the CCD, causes increasing dissolution of calcareous tests and results in a decreasing biogenic input to the sediments within the CCFZ (von Stackelberg, 1988). This, combined with the intensified AABW which passes northeastwards through the Line Island Archipelago and spreads over the abyssal seafloor within the CCFZ (Gordon & Gerard, 1970) has resulted in low sedimentation rates of 1-4mm/Ka (Theyer, 1977; Meyer, 1977). The main sediment facies of the CCFZ is, therefore, older outcropping siliceous oozes interfingered with pelagic clays. These sediment facies sometimes underlie a thin veneer of Pliocene-Quaternary sediments (von Stackelberg, 1988).

### 1.2.3 MORPHOLOGY AND TEXTURE

The samples used in this study were classified as either crusts or nodules based on their morphology, location, and depth. When the samples were selected from the SIO collections, a description of the sample's morphology was briefly noted. The morphological classification follows that of Raab & Meylan (1977) which divides ferromanganese deposits into four categories. These categories are: 1) stains, 2) agglutinations, 3) nodules, and 4) crusts. Stains are very thin deposits on some solid object such as a volcanic rock fragment or outcropping rock. Agglutinations are clusters of discrete nuclei united by a thin encrustation, generally less than 1mm thick. Nodules are thicker encrustations surrounding a single or multiple discrete nuclei. Crusts are relatively thick deposits on submarine rock outcrops or large boulders or volcanic slabs. There is one problem with this classification. No accepted distinction between objects that are stained or very thinly encrusted and objects that may be called nodules has been defined. Samples selected from the SIO collections were chosen so that there would be no doubt as to their being either a crust or a nodule. Nodules were further classified based on their surface texture as

described by Raab (1972), namely, smooth, gritty, "goose bumps", and pisolitic or knobby. Nodules with a smooth surface texture show essentially no visible pattern. Often these smooth surfaces develop black lustrous patches. Nodules with a gritty surface texture appear to be composed of sand-sized and finer particles which are loosely cemented to the nodule. These particles are often associated with a surface texture which is best described as being composed of "goose bumps". A surface which can be described as being composed of "goose bumps" is characterized by many small welts. These welts may represent internal growth structures. Pisolitic or knobby nodules have developed a distinct equatorial zone characterized by a knobby surface texture. This zone appears to be composed of fused grains larger than 2mm, hence the name pisolitic.

Further refinement of the classification was based on their location and water depth. Crusts occur on hard substrates on the flanks of seamounts, islands, plateaus, and other topographically positive areas in the Pacific (Hein *et al.*, 1987). The distribution of crusts within the Central and Eastern Equatorial North Pacific can, therefore, be related to two tectonic settings: they can occur on the flanks of seamounts, plateaus, and islands (mid-plate volcanic chains) such as those of the Line Island Archipelago, at depths less than 2500m and along oceanic spreading axes such as the East Pacific Rise (Hein *et al.*, 1987; Hein *et al.*, in press a). Nodules occur on unconsolidated sediments in abyssal water depths from 4000-5000m (Calvert, 1978; Exon, 1983). The distribution of nodules within the Central and Eastern Equatorial North Pacific is, therefore, confined to an east-west belt on the abyssal seafloor confined by the CCFZ (Halbach *et al.*, 1981b).

## 1.3 ANALYTICAL METHODS

### 1.3.1 GEOCHEMISTRY

The wide range in compositional variability of crusts and nodules makes routine analysis far from straightforward. In addition, in order to understand the mechanisms leading to the formation of crusts and nodules, multielement analysis of a relatively large number of samples is required. Thus X-ray fluorescence spectrometry (XRF) was selected as the analytical method to determine the major element geochemistry of the crust and nodule samples. X-Ray fluorescence is capable of routinely and precisely determining a wide range of elements in a large number of samples in relatively short time periods (Calvert *et al.*, 1985).

#### 1.3.1.1 Sample Preparation

As demonstrated by Harvey *et al.* (1973), sample preparation of geological materials using fusion methods involving a relatively high dilution and addition of a heavy absorber as a means of matrix correction offer the best means of achieving a high degree of accuracy and precision in XRF analyses. Samples prepared by this method, unlike undiluted powdered samples, do not suffer the problems of absorption and enhancement effects that require empirical matrix corrections. To determine the major element geochemistry of crusts and nodules, Calvert *et al.* (1985) describes a modification of the method developed by Harvey *et al.* (1973).

The powdered samples are diluted with a flux, having the following composition  $\text{Li}_2\text{B}_4\text{O}_7$  47.03%,  $\text{LiCO}_3$  36.63%,  $\text{La}_2\text{O}_3$  16.34%. The lanthanum, in the flux, is used as a heavy adsorber of X-rays and as a means of matrix correction (Norrish & Hutton, 1969). The flux used is commercially available as Spectroflux®

105 (Johnson and Matthey, Ltd). Crusts and nodules contain low concentrations of silica and alumina, which prevents a stable glass being formed on fusion. The addition of a known weight of Specpure® SiO<sub>2</sub> (Johnson and Matthey, Ltd) to the crust and nodule samples results in the production of stable glass beads.

The powdered sample (0.3000g), Specpure® SiO<sub>2</sub> (0.1000g), and Spectroflux® 105 (3.6000g) are sequentially weighed into a Pt-Au crucible and heated in an electric muffle furnace at 1100°C for 15 minutes. After the crucible has been removed from the furnace, it is allowed to cool to room temperature in an aluminum cooling block. The weight loss on fusion is made up by adding dried Li<sub>2</sub>B<sub>4</sub>O<sub>7</sub> (Spectroflux® 100). This compensates for the variable weight loss of individual samples and maintains the same degree of dilution of the sample and the same ratio to La to the major elements in the sample. After reweighing, the crucible containing the cooled glass and added tetraborate is placed over a Meeker® burner in a fume hood and the mixture remelted. The melt is quickly poured into an aluminium platten on a hot-plate maintained at 250°C and a brass plunger, at the same temperature, is brought down over the melt for a few seconds to form a flat bead. After removing the plunger, the platten with its bead is moved to the side of the hot-plate, covered with an inverted evaporating dish and the bead allowed to anneal for at least 10 minutes. The bead is finally cooled by moving the platten to a heat-resistant surface, after which it readily comes away from the platten. The bead is labelled on the bottom surface and stored in a plastic bag together with the excess glass fragments which are trimmed from the edges using a cleaned pair of needle-nose pliers. The fragments are retained for re-casting should the bead crack or break.

### 1.3.1.2 Calibration

The use of well-analyzed standards for the analysis of crusts and nodules is not possible because no such samples are available. Abbey (1983) has listed a few oxide ore and laterite standards but none has been analyzed for a full range of elements. A trustworthy consensus of values for their constituent elements, therefore, has not been obtained. This problem with the lack of standards which can be used for the analysis of crusts and nodules was solved by Calvert *et al.* (1985). They developed a series of synthetic calibration standards for the XRF.

The standards were made by preparing mixtures of Specpure® oxides, or appropriate salts, and a well-characterized aluminosilicate. The aluminosilicate selected as the diluent was the standard granite NIM-G which is listed in Abbey (1983). A 50:50 mixture of  $\text{MnO}_2$  and  $\text{Fe}_2\text{O}_3$  was first prepared. Half of this mixture was then doped with accurately weighed amounts of all other elements of interest and the mixture homogenized by shaking with methyl acrylate mixing balls on a mechanical blender. Thirteen standards were then produced by mixing weighed portions of the  $\text{MnO}_2$ - $\text{Fe}_2\text{O}_3$  mixture and NIM-G with the doped oxide mixture. Sub-samples of the standards were then made into glass beads for major element calibration of the XRF. The compositions of the standards are listed in Calvert *et al.* (1985).

### 1.3.1.3 Experimental Conditions

The crust and nodule samples along with the thirteen standards were analyzed by a Philips® PW 1400 wavelength-dispersive sequential automatic spectrometer. The operating conditions and relevant count-rate data are listed in Calvert *et al.* (1985). A Rh-target X-ray tube was used for analysis of all major elements. The



measurement of backgrounds in samples having high dilution and an added heavy adsorber is commonly not done (Norrish & Hutton, 1969). There was, however, sufficient variations in the background over the full range of compositions measured to make background measurements necessary for all major elements. Fixed time counting and the ratio method were also employed. The ratio method uses a sample of intermediate composition (one of the calibration standards) as a reference against which all measurements are ratioed to correct for instrument drift. The choice of crystals was made with regard to convenience and speed of the analytical program, problems of interferences, crystal fluorescence, and peak resolution. Finally, the appropriate pulse-analyzer settings were determined for each element determined.

The spectrometer was controlled by a DEC® PDT-11 microcomputer and up to 72 samples loaded at a time on an automatic sample changer. After setting up all measurement and control parameters in the PW 1400 microprocessor through the PDT-11 microcomputer, element calibrations were determined on the calibration standards and stored on floppy disc. Major element intensities and final concentrations were then available immediately after an individual sample was run.

#### 1.3.1.4 Precision and Accuracy

The precision of the methods for the determination of the major elements was obtained by analyzing the laboratory crust and nodule standards DODO 14DZ and Mn 191 6-8. Five sub-samples were prepared from each well mixed bulk sample. The sample precision includes errors due to the inherent inhomogeneity of the samples, sample handling and weighing, and the manufacture of the glass beads. In addition one of the calibration standards, chosen randomly, was analyzed five times in order to determine an estimate of the instrumental precision. The results are shown in Table 1-1a and b. The sample precision was found to vary from 0.00% up



Table 1-1b. Precision of the XRF.

XRF Standard #1 (See Calvert et al., 1985)

Element Repeat Analysis.

	1	2	3	4	5	Mean	S.D.	C.V.(%)
Si	5.90	5.77	5.96	5.91	5.74	5.86	0.01	1.70
Ti	0.70	0.70	0.71	0.70	0.69	0.70	0.01	1.43
Al	2.24	2.24	2.29	2.26	2.27	2.26	0.02	1.43
Fe	22.15	22.24	22.24	22.15	22.15	22.19	0.05	0.23
Mn	21.74	21.66	21.74	21.81	22.05	21.80	0.15	0.69
Mg	1.32	1.34	1.31	1.30	1.23	1.30	0.04	3.08
Ca	2.21	2.18	2.16	2.17	2.06	2.16	0.06	2.78
Na	0.55	0.42	0.55	0.60	0.50	0.52	0.07	13.46
K	0.73	0.75	0.72	0.70	0.68	0.72	0.03	4.17
P	0.09	0.09	0.09	0.09	0.10	0.09	0.00	0.00
Co	1.06	1.09	1.15	1.16	1.26	1.16	0.06	5.17
Ni	1.12	1.09	1.15	1.16	1.26	1.16	0.06	5.17
Cu	0.88	0.83	0.85	0.90	0.97	0.89	0.05	5.62
Zn	0.11	0.10	0.09	0.11	0.11	0.10	0.01	10.00
Ba	0.29	0.31	0.27	0.27	0.31	0.29	0.02	6.89

to 85.17% (coefficient of variation). In most cases the sample precision is greater than the instrumental precision. The coefficient of variation (C.V.) is a measure of the standard deviation which is independent of the sample mean. This allows for the comparison of the same element between sample and instrumental precision or to compare the precision between different elements (Snedecor & Cochran, 1956; Zar, 1974). Those elements with poorer precision are the result of the inherently lower count rates of the long-wavelength radiations or because of the relatively low concentrations of the particular analytes (Calvert *et al.*, 1985). This can be demonstrated by comparing the C.V. for the same element between the two laboratory standards. In the laboratory nodule standard the abundance of Cu is much higher than in the laboratory crust standard. Even though the standard deviation (S.D.) for the standard crust is significantly lower than for the standard nodule the C.V. for the standard crust (C.V.=16.67) is much higher than for the standard nodule (C.V.=7.30). As noted by Calvert *et al.* (1985) despite the wide ranging calibrations, no further matrix corrections were attempted.

The accuracy of the methods used in determining the major element composition was checked by comparing the analytical results with the best estimates of the composition of two nodule reference standards (Table 1-2). The values of best estimates have been adjusted by the amount of  $\text{H}_2\text{O}^-$  reported in Tables 30 and 31 of Flanagan & Gottfried (1980) in order to make them directly comparable with the procedure used here. This comparison does show that the calibrations obtained here provide reasonable values over a wide range of compositions.

Table 1-2. Comparison of analytical results with best estimates of two ferromanganese nodule reference standards. Results are given as weight percentages.

ELEMENT	Nod-A-1		Nod-P-1	
	XRF	Flanagan and Gottfried (1980)	XRF	Flanagan and Gottfried (1980)
Si	2.31	1.53	6.34	6.07
Ti	0.23	0.28	0.25	0.28
Al	1.77	1.77	2.25	2.38
Fe	10.15	9.43	5.62	5.38
Mn	16.32	15.99	27.16	27.17
Mg	2.73	2.47	1.86	1.85
Ca	9.88	9.51	2.03	2.04
Na	0.54	0.66	1.27	1.53
K	0.40	0.43	0.91	0.98
P	0.48	0.52	0.19	0.19
Co	0.26	0.27	0.19	0.21
Ni	0.57	0.55	1.26	1.25
Cu	0.09	0.09	1.06	1.07
Zn	0.05	0.05	0.16	0.15
Ba	0.12	0.14	0.24	0.32

### 1.3.2 MINERALOGY

The mineralogy of crusts and nodules determines most of their physical and chemical properties. The constituent minerals not only control the authigenesis, growth, and structure of the nodule but they also influence the uptake of certain elements. Crusts and nodules consist of a complex mixture of different mineral crystallites both detrital and authigenic, organic and colloidal matter, and altered igneous and metamorphic rock fragments (Burns & Burns, 1977). The mineralogy of crusts and nodules is difficult to determine because of the small size of the crystallites, intimate intergrowth of authigenic phases, and the presence of amorphous material (Calvert, 1978).

#### 1.3.2.1 Sample Preparation

Sample preparation for mineral analysis is not as involved as that for geochemical analysis. The only prerequisite is that the prepared sample consist ideally of crystalline particles in completely random orientation. When the orientation of the crystalline particles in the prepared sample is truly random, all possible diffractions take place simultaneously (Hurlbut & Klein, 1977). The powdered sample is pressed into a rigid disc which is held in an aluminum sample holder. The sample is then ready for analysis by powder X-ray diffraction (XRD), after which the sample is recovered.

### 1.3.2.2 Experimental Conditions

The prepared samples were loaded into a Philips® PW 1775 sample changer to be analyzed by a Philips X-ray diffractometer powered by a Philips® PW 1729 constant potential generator. Diffraction data were obtained using Cu K $\alpha$  radiation (40kV, 20mA) with a graphite monochromator and a Philips® PW 1050/70 vertical goniometer equipped with a diffracted beam graphite monochromator, an automated divergence slit, 0.1mm receiving slit, 1° scatter slit, and a gas proportional counter. Although identification of low intensity peaks is made difficult by the high background due to the fluorescent Mn and Fe radiation, Glasby (1972) found that an iron tube was only slightly superior to the copper tube. Work was therefore completed using a copper tube. The diffractometer was controlled by a Philips® PW 1710/00 diffraction control unit. Measurement and control parameters were set up in the PW 1710/00 microprocessor through a Zenith® Z-150 personal computer using MS-DOS Kermit (Gianone *et al.*, 1988).

The XRD was used for complete scans of some samples to correlate the sample geochemistry with mineralogy as well as to determine the relative abundances of todorokite to  $\delta\text{MnO}_2$  in all samples. Samples selected for mineral analysis were step scanned from 5° to 71°2 $\theta$  in 0.005°2 $\theta$  increments, using a counting time of 5 seconds per increment. Diffractograms were recorded using a rate full scale of 100 counts per second, a rate time constant of 5 seconds, and a chart speed of 5mm/°2 $\theta$ .

The relative abundances of todorokite to  $\delta\text{MnO}_2$  was estimated by measuring the net intensity of the 9.80Å peak for todorokite and the 1.40Å peak for  $\delta\text{MnO}_2$ . The value obtained for todorokite was then divided by the value obtained for  $\delta\text{MnO}_2$ . The net intensity of a peak was determined by collecting the total number of counts under a peak profile, in a scan. This value is divided by the total time and

the resulting total intensity is given in counts per second. The background is then measured at one point on each side of the peak for a preset time. This value for the background is then subtracted from the total intensity to give the net intensity of the peak. Since all calculations are done on an intensity scale, the resulting net intensity can be taken as the area of a peak above the line connecting the two background points. For todorokite, the net intensity of the  $9.80\text{\AA}$  peak was determined by step scanning from  $8^\circ$  to  $10.6^\circ 2\theta$  in  $0.005^\circ 2\theta$  increments. The background was measured at  $8^\circ$  and  $10.6^\circ 2\theta$  respectively for 10 seconds each. For  $\delta\text{MnO}_2$ , the net intensity of the  $1.40\text{\AA}$  peak was determined by step scanning from  $63.4^\circ$  to  $69^\circ 2\theta$  in  $0.005^\circ 2\theta$  increments. The background was measured at  $63.4^\circ$  and  $69^\circ 2\theta$  respectively for 10 seconds each.

### 1.3.2.3 Precision

The precision of the methods for the determination of the todorokite/ $\delta\text{MnO}_2$  ratio was obtained by analyzing a laboratory nodule standard. Ten sub-samples were prepared from a well mixed bulk sample. In addition, one of the replicates, chosen randomly, was analyzed ten times in order to provide an estimate of instrumental precision. The sample precision includes errors due to the inherent inhomogeneity of the sample, sample handling, manufacture of the pressed powder discs, poor crystallinity of the manganese mineral phases, and fortuitous orientation of the mineral crystallites. The sample precision was found to be 6.98% (coefficient of variation). The instrument precision was found to be similar to the sample precision (6.87% coefficient of variation). The results are listed in Table 1-3a and b.



Table 1-3a. Precision of the method of analysis between sample.

Replicate No.	Todorokite/ $\delta\text{MnO}_2$
1	1.65
2	1.76
3	1.87
4	1.73
5	1.74
6	1.80
7	1.48
8	1.67
9	1.88
10	1.62
Sample Mean	1.72
Standard Deviation	0.12
Coefficient of Variation	6.98

Table 1-3b. Precision of the XRD.

Repeat Analysis	Todorokite/ $\delta\text{MnO}_2$
1	1.71
2	1.72
3	1.49
4	1.57
5	1.60
6	1.54
7	1.43
8	1.58
9	1.60
10	1.80
Sample Mean	1.60
Standard Deviation	0.11
Coefficient of Variation	6.87

## 1.4 RESULTS AND DISCUSSION

### 1.4.1 SURVEY REGION A

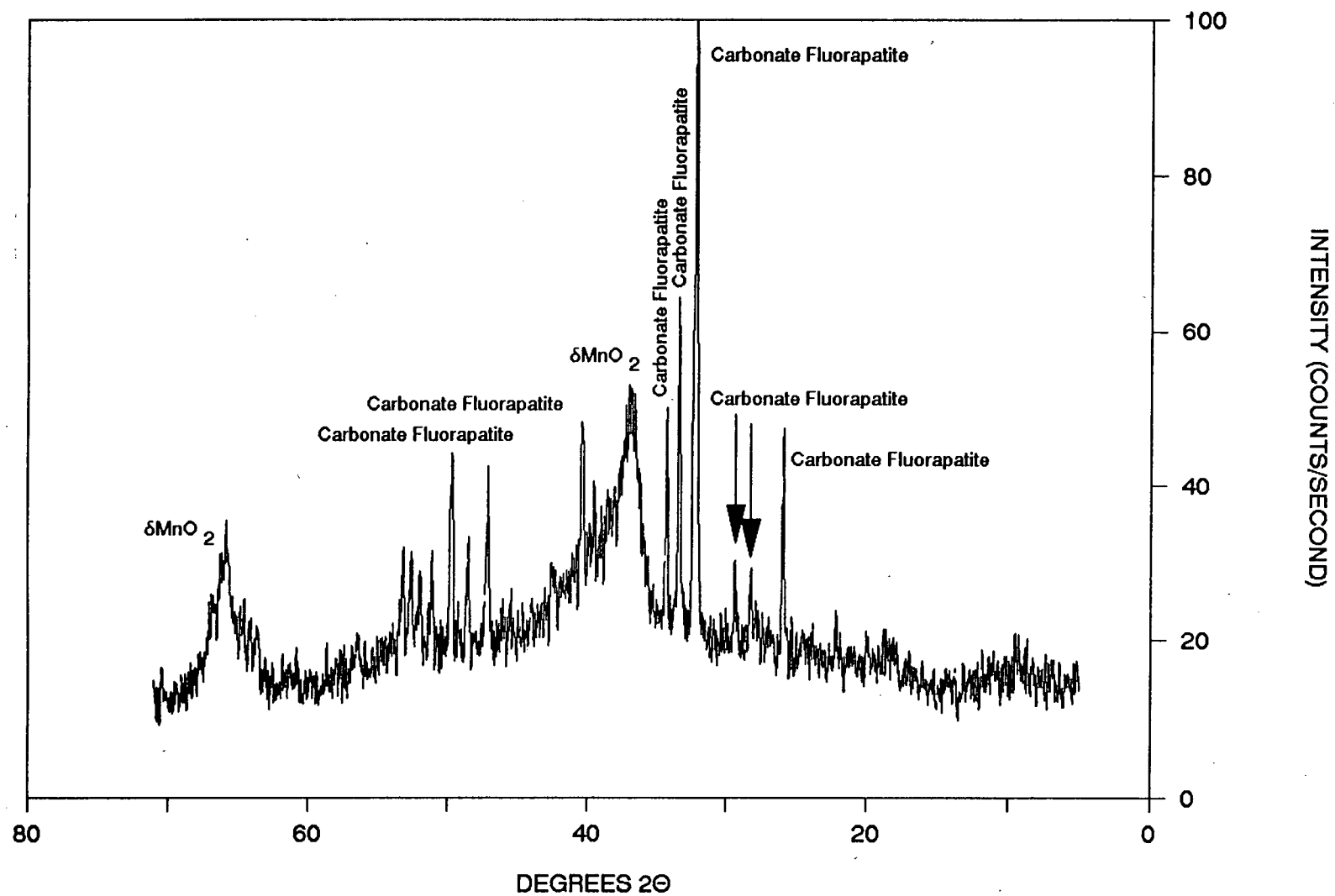
#### 1.4.1.1 Crusts

##### 1.4.1.1.1 Mineralogy

A general idea of the average mineralogical composition of crusts from this region can be obtained by examining an XRD diffractogram of a randomly selected crust (Figure 1-4). As shown by Figure 1-4, crusts from this region are composed of  $\delta\text{MnO}_2$ , aluminosilicates, mostly quartz and feldspar, and carbonate fluorapatite. The todorokite to  $\delta\text{MnO}_2$  ratio for crusts from this region varies from 0.00 to 0.91 with a mean of 0.09. This further supports the XRD evidence that the dominant manganese oxide in these crusts is  $\delta\text{MnO}_2$ . The X-ray powder diffractogram, shown in Figure 1-4 shows the presence of a fine-grained, poorly crystalline material, which contributes a considerable amount of background noise on which are superimposed the sharp peaks of the aluminosilicates and carbonate fluorapatite. The poorly crystalline material has been identified as being cryptocrystalline or amorphous hydrated iron oxides (Glasby, 1972; Crerar & Barns, 1974). Mössbauer spectroscopic studies by Herzenberg & Riley (1969), Gager (1968), Johnson & Glasby (1969), and Carpenter & Wakeman (1973) have also led to the suggestion that the iron-bearing phase can be regarded as an amorphous ferric hydroxide or oxide-hydroxide gel ( $\text{FeOOH} \times \text{H}_2\text{O}$ ) with a particle size less than  $200\text{\AA}$ . The identity of this phase is discussed in greater detail in chapters 2 and 3.

Figure 1-4. A typical XRD pattern of a crust from Survey Region A.

# DODO 7 D-2



#### 1.4.1.1.2 Bulk Composition

The major element composition and manganese phase mineralogy data for crusts recovered from Survey Region A are listed in Appendix C. This compositional data can be used to estimate the relative proportions of the iron and manganese oxides and other phases in the crusts and help interpret inter-element associations which will be discussed later.

The mean composition of crusts from this region is listed in Table 1-4 together with the average compositions of crusts from two other studies within the same area. Except for Mn and Fe, the mean composition of crusts from Survey Region A is similar to those of the other two studies. The concentrations of Mn and Fe, however, are considerably lower than those reported by Hein *et al*, (1987) and by Hablach & Manheim (1984). The Mn/Fe ratio of the crusts from Survey Region A is also lower than those reported for the two other studies.

#### 1.4.1.1.3 Interelement Associations

##### 1.4.1.1.3.1 Correlations with Aluminium

The nature of the aluminosilicates in the crusts is shown by the relationships between Al and other major elements (Figure 1-5). From the XRD diffractogram, these correlations with Al could be explained by the presence of quartz and feldspar. By using Si/Al and K/Al element ratios, the origin of the aluminosilicate fraction of the crusts can be identified. The average Si/Al and K/Al ratios of crusts from this region are found to be 3.18 and 0.38, respectively (Table 1-5). Both element ratios are consistently higher than those for "Average Pacific Pelagic Clay" (Bischoff *et al*., 1979) and for "Average Tholeiitic Lavas from the Hawaiian Islands" (Best, 1982).

Table 1-4. Mean concentrations of major elements in crusts from Survey Region A. Concentrations are given in weight per cent.

Mean Composition of Crusts from Survey Region A		Average central Pacific crusts (Hein et al., 1987)		Mean composition of all seamount oxide samples (Halbach & Manheim, 1984)	
Element	Concen.	Element	Concen.	Element	Concen.
Si	5.15	Si	3.69		
Ti	0.89	Ti	1.10	Ti	0.96
Al	1.62				
Fe	11.20	Fe	15.00	Fe	14.50
Mn	14.95	Mn	22.00	Mn	24.60
Mg	1.26				
Ca	5.06			Ca	4.24
Na	1.55				
K	0.61				
P	1.40	P	0.65	P	1.24
Co	0.46	Co	0.78	Co	0.79
Ni	0.36	Ni	0.44	Ni	0.49
Cu	0.07	Cu	0.08	Cu	0.07
Zn	0.04			Zn	0.07
Ba	0.18				
Mn/Fe	1.33	Mn/Fe	1.47	Mn/Fe	1.70

Figure 1-5. The relationship between Al and other major elements. The open circles = samples from the Hawaiian Island Archipelago, the filled circles = samples from the Line Island Archipelago.

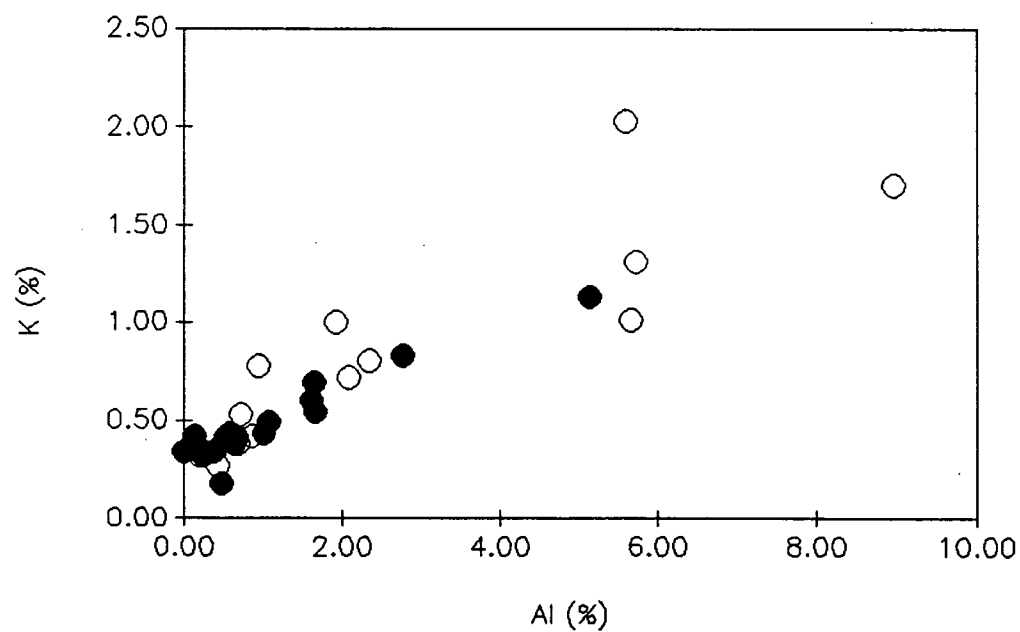
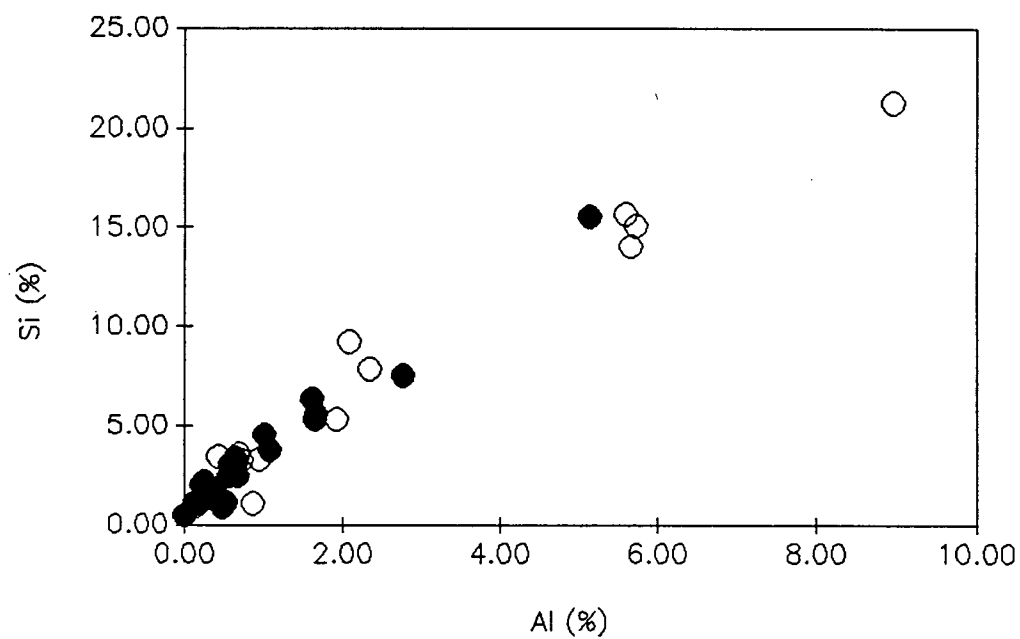




Table 1-5. Comparison of the composition of aluminosilicates in crusts to Average Pacific Pelagic Clay and Tholeiitic Lavas from the Hawaiian Islands.

	Element Ratios	
	Si/Al	K/Al
Crusts from Survey Region A (This Study)	3.18	0.38
Average Pacific Pelagic Clay (Bischoff et al., 1979)	2.92	0.25
Average Tholeiitic Lavas from the Hawaiian Islands (Best, 1982)	3.13	0.04

This seems to indicate that there are several sources contributing to the aluminosilicate fraction in the crusts. Quartz and some of the plagioclase and K-feldspar are eolian in origin and reflect the position of the crust-coated seamount relative to atmospheric wind belts (Hein *et al.*, 1985). The rest of the plagioclase, as well as K-feldspar and other aluminosilicates, are derived from the substrate, probably by resuspension of weathered material (Hein *et al.*, 1987).

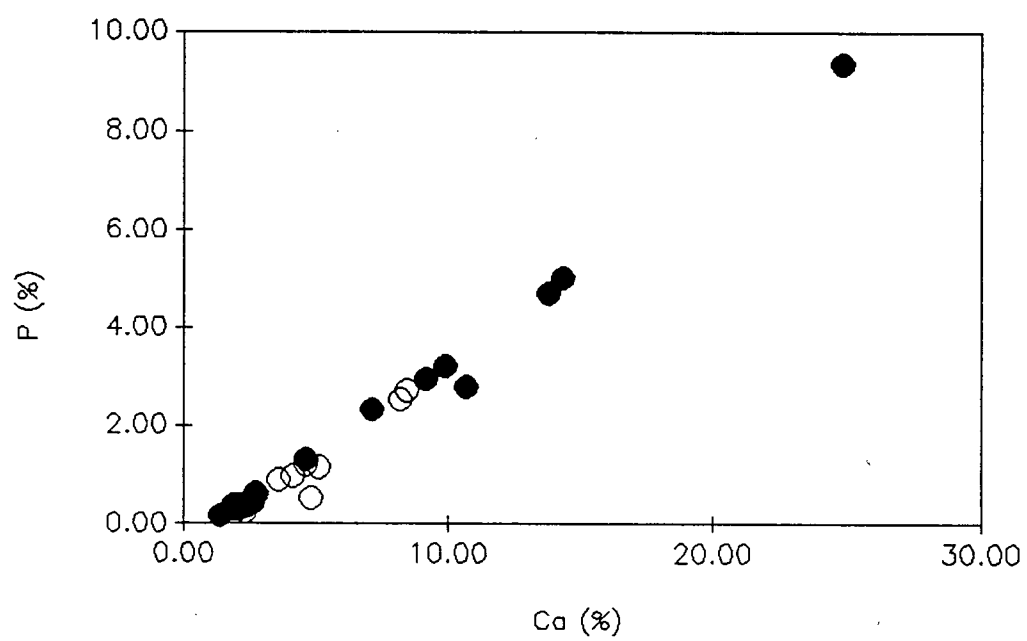
Calvert & Price (1977a) estimated the total amount of aluminosilicate impurity in their nodules from the Al contents, assuming that this fraction had the same composition as that in the associated sediments. Due to the lack of a sediment substrate and the multiple sources contributing to the aluminosilicate fraction in crusts, determining the aluminosilicate content of crusts from Survey Region A is not possible.

#### 1.4.1.1.3.2 Phosphorite

Some of the crusts have high concentrations of Ca and P, and for all crusts there is a strong positive correlation between these two elements (Figure 1-6). This is due to the presence of carbonate fluorapatite  $\{(Ca,Mg,Na,K)_{10}[(P,C)O_4]_6(F,OH)_2\}$ . The presence of carbonate fluorapatite is shown in the XRD diffractogram of the randomly selected crust (Figure 1-4).

As discussed in Halbach & Puteanus (1984a), crusts from the Line Island and the Hawaiian Archipelagoes are characterized by two generations of growth. Between the two crust generations is a period of phosphorite deposition during which formation of massive carbonate fluorapatite and impregnation of the older crust generation has taken place. Based on the results of age determinations by Halbach *et al.* (1983), the younger crust layer should not be older than 10Ma. The period of formation of the younger crust generation corresponds with the increasing

Figure 1-6. The correlation between Ca and P. The open circles = samples from the Hawaiian Island Archipelago, the filled circles = samples from the Line Island Archipelago.



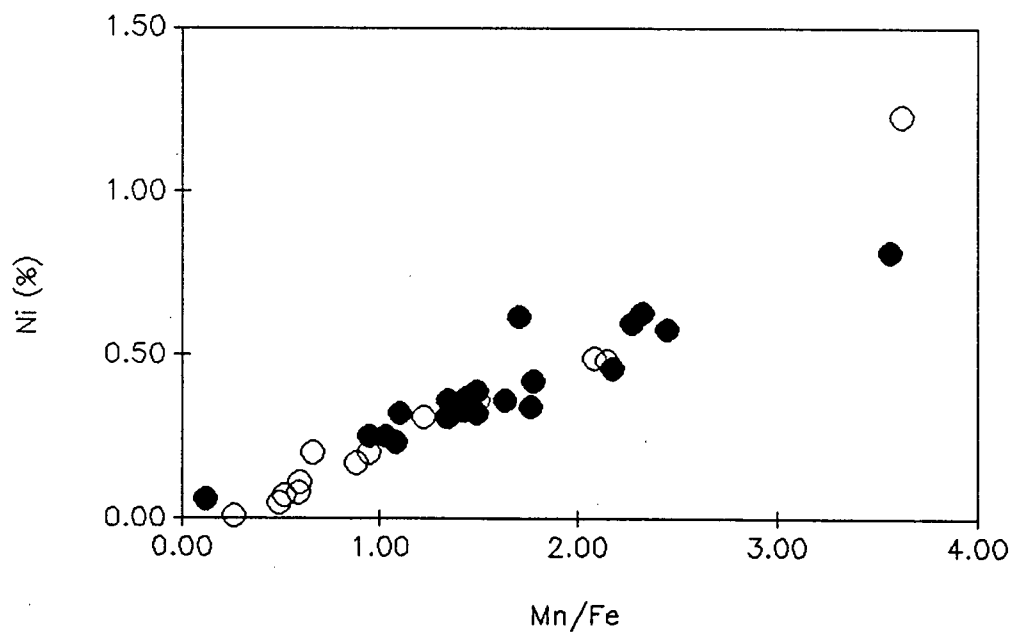
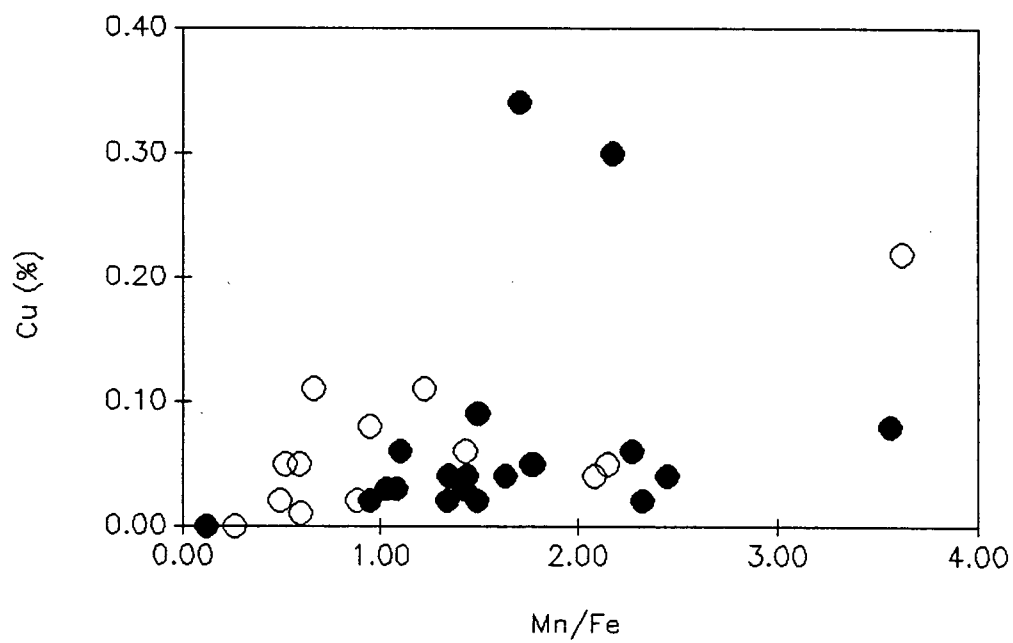
current activity of the AABW initiated by a major global cooling since the middle Miocene (Kennett *et al.*, 1975). The period of formation the older crust layer might have been during the Eocene to early Oligocene, when the first development of Antarctic glaciation at sea level and a marked stratification in the deep water, causing enhanced deep-sea erosion, took place (van Andel *et al.*, 1975).

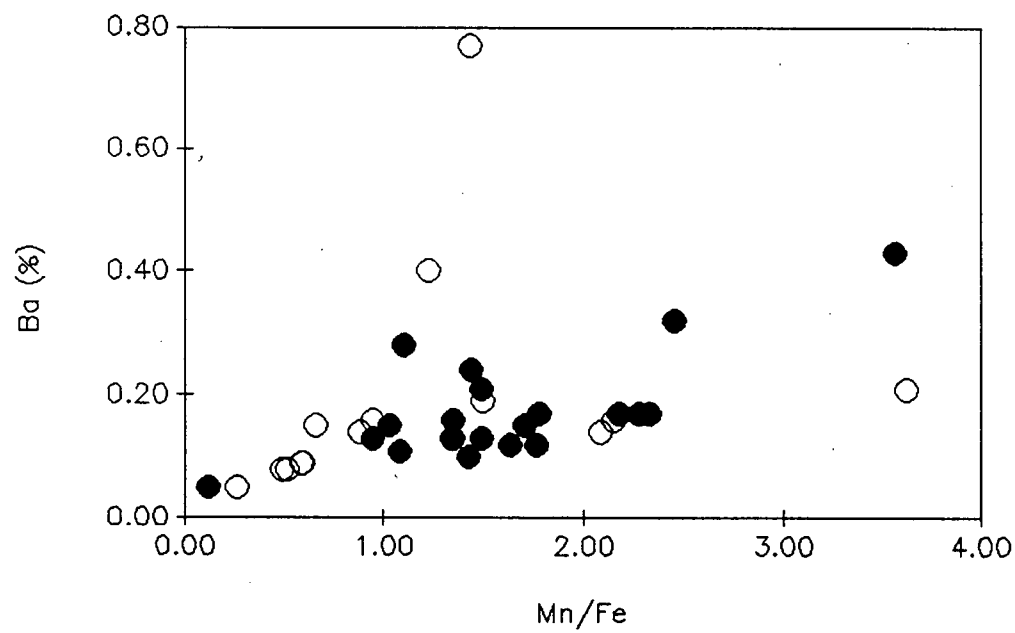
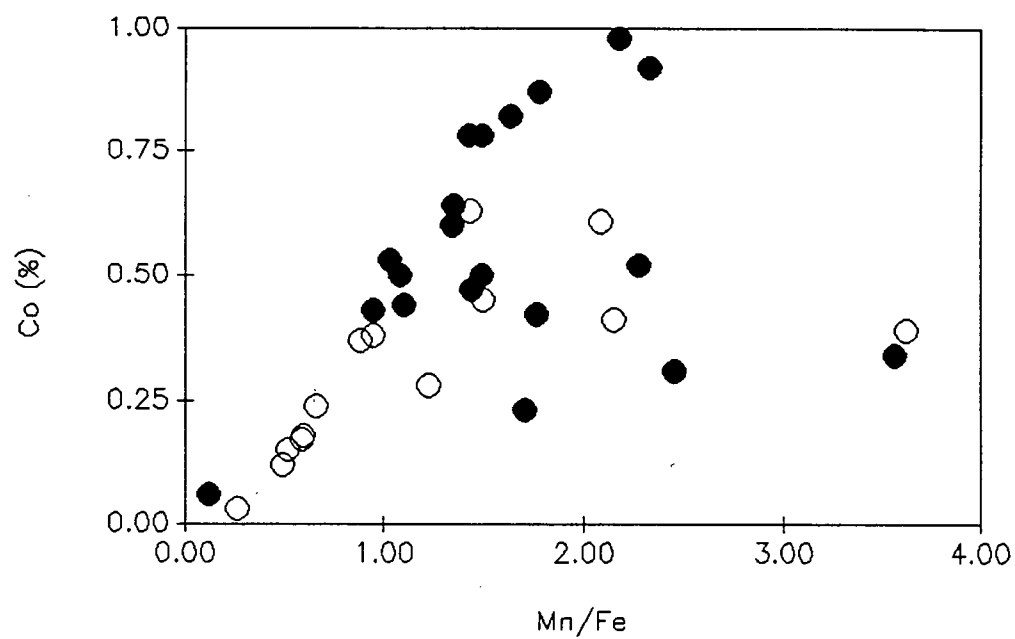
The massive phosphorite is thought to have formed mainly by carbonate replacement between the two periods of crust growth. From Oligocene to early Miocene, sedimentation in the central Pacific was characterized by carbonate deposition (van Andel *et al.*, 1975). The phosphorite formation probably took place between the periods of carbonate accumulation and the younger period of crust growth (Halbach *et al.*, 1983; Halbach & Puteanus, 1984b).

#### 1.4.1.1.3.3 Correlations with Manganese and Iron

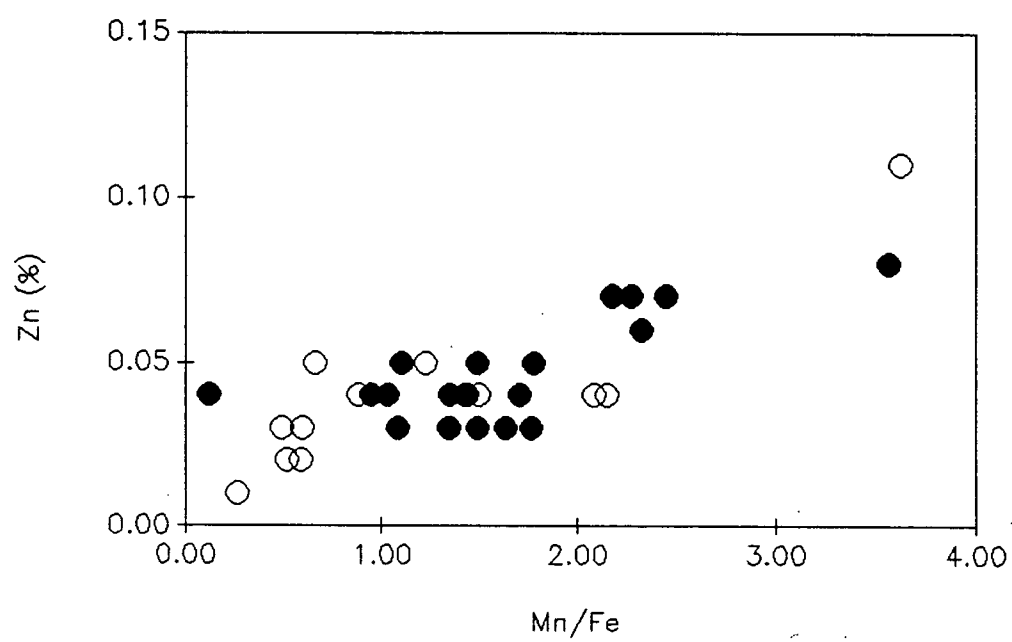
To examine the regional compositional variations with respect to Mn and Fe, the effects of the dilutant aluminosilicates and carbonate fluorapatite material must be removed (Calvert, 1978). Price & Calvert (1970) solved the problem by using element ratios instead of absolute abundances of elements to represent geochemical variations. Using the elemental ratio of Mn/Fe, the association of the major elements with either of the major oxide phases will become more apparent. Elements correlated with the manganese phase mineralogy will show a positive linear correlation with the Mn/Fe ratio. In the present case, these include Ba, Ni, Zn, and Co. Elements associated with the unidentified iron phase mineralogy show a negative correlation with the Mn/Fe ratio; these elements include Ti and Na (Figure 1-7). Hein *et al.* (in press a) identified the same correlations in crusts from the central Pacific. They noted that the degree of the correlations vary from area to

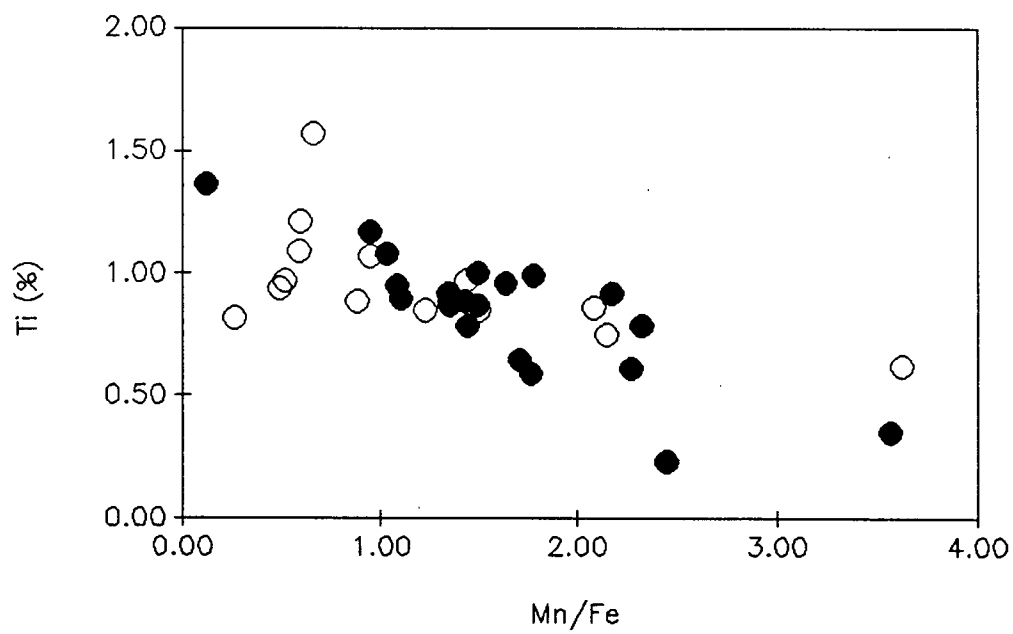
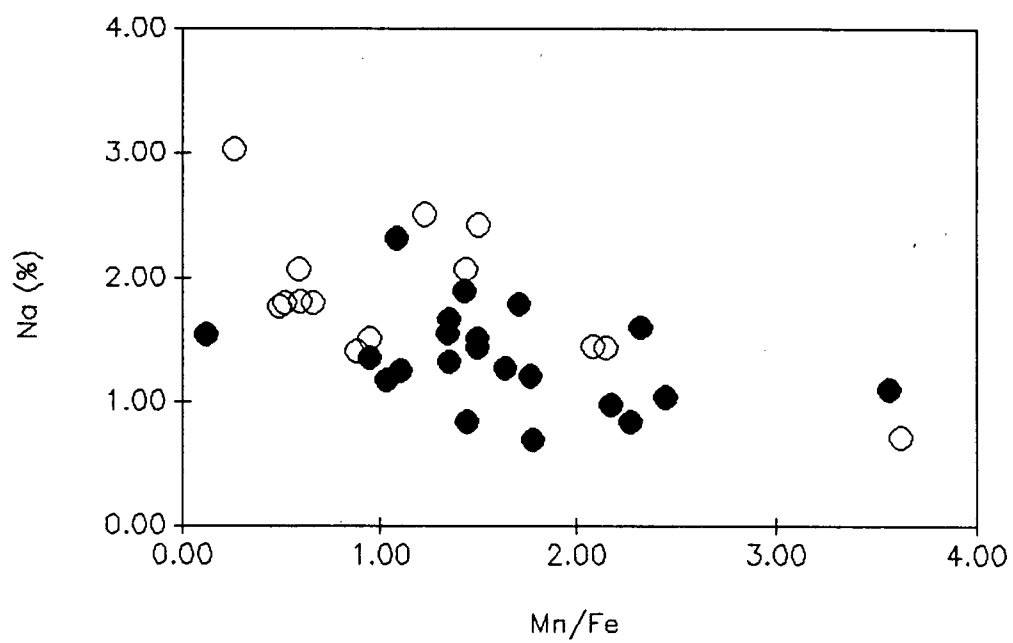
Figure 1-7. The association of major elements with Mn/Fe. The open circles = samples from the Hawaiian Island Archipelago, the filled circles = samples from the Line Island Archipelago.











area, but three correlations remained consistent. These were Mn with Co, Si with Al, and Ca with P.

The association of Si with Al and Ca with P has been explained previously. The reason for the association of Mn with Co has yet to be identified. Cobalt along with Ba, Ni, and Zn are fixed by lattice substitution for  $\text{Mn}^{4+}$  in the  $\text{MnO}_2$  or by coprecipitation of  $\text{CoO}_2$  with manganese oxide (Hem, 1978). The reason that Co is enriched in  $\delta\text{MnO}_2$  to a greater degree than are Ni, Zn, and Ba is because  $\text{Co}^{2+}$  is oxidized to  $\text{Co}^{3+}$  on the surface of the  $\text{MnO}_2$ . Cobalt (III) is less soluble and therefore more stable in the marine environment (Goldberg, 1954; Dillard *et al.*, 1982; Halbach *et al.*, 1983; Aplin & Cronan, 1985a).

As noted by Aplin & Cronan (1985a) in their work on crusts from the Line Island Archipelago, the chemical composition of crusts makes it unlikely that halmyrolytic, hydrothermal, or diagenetic processes influence the composition of the crusts. First, halmyrolysis is considered to be unimportant in supplying metals to the deposits in view of the lack of compositional similarity between the crusts and the substrate type. Secondly, the deposits exhibit none of the characteristics of hydrothermal crusts as described by Toth (1980). These characteristics include: low concentrations of Cu, Ni, and Co; extreme fractionation of Mn from Fe; and the presence of birnessite in Mn-rich hydrothermal crusts and amorphous hydrated iron oxides and silica in Fe-rich hydrothermal crusts. Thirdly, the compositional and mineralogical similarity of crusts of varying thickness indicates that both these parameters are fixed at the point of oxide accretion and that subsequent diagenesis is unimportant.

Crusts derive most of their metal content from dissolved and particulate matter in ambient bottom water, in proportions modified by the variable scavenging efficiency of the manganese and iron oxide phase mineralogy for susceptible ions (Manheim & Lane-Bostwick, 1988). This model is supported by the striking

resemblance between the crust/seawater trace metal enrichment sequence and laboratory determined oxide-trace metal selectivity sequences (Aplin & Cronan, 1985a).

#### 1.4.1.1.4 Variations with Depth

##### 1.4.1.1.4.1 Correlations with Manganese and Iron

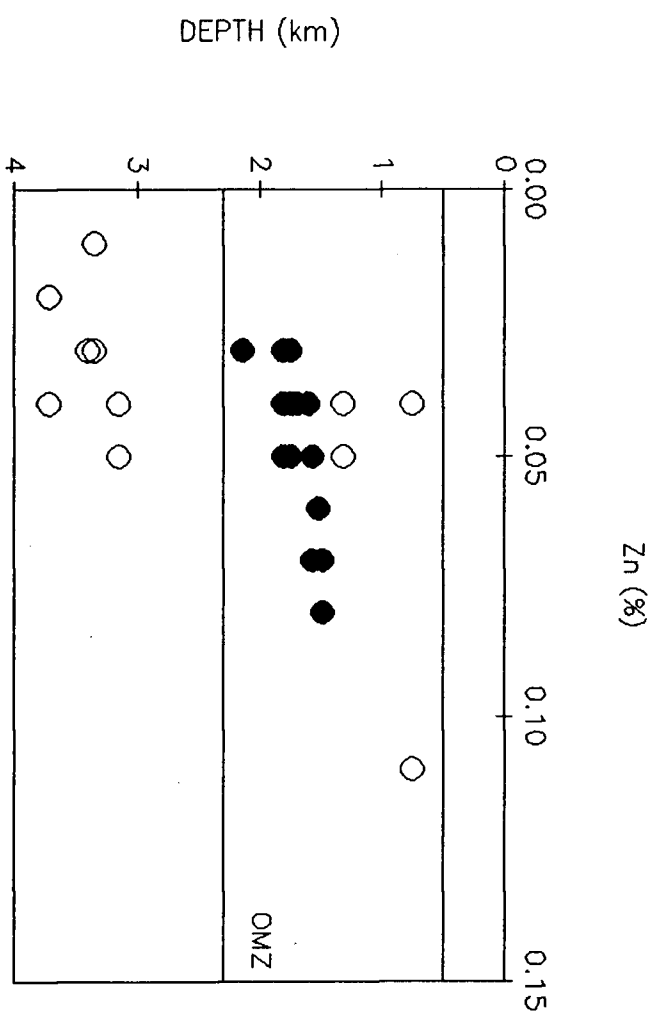
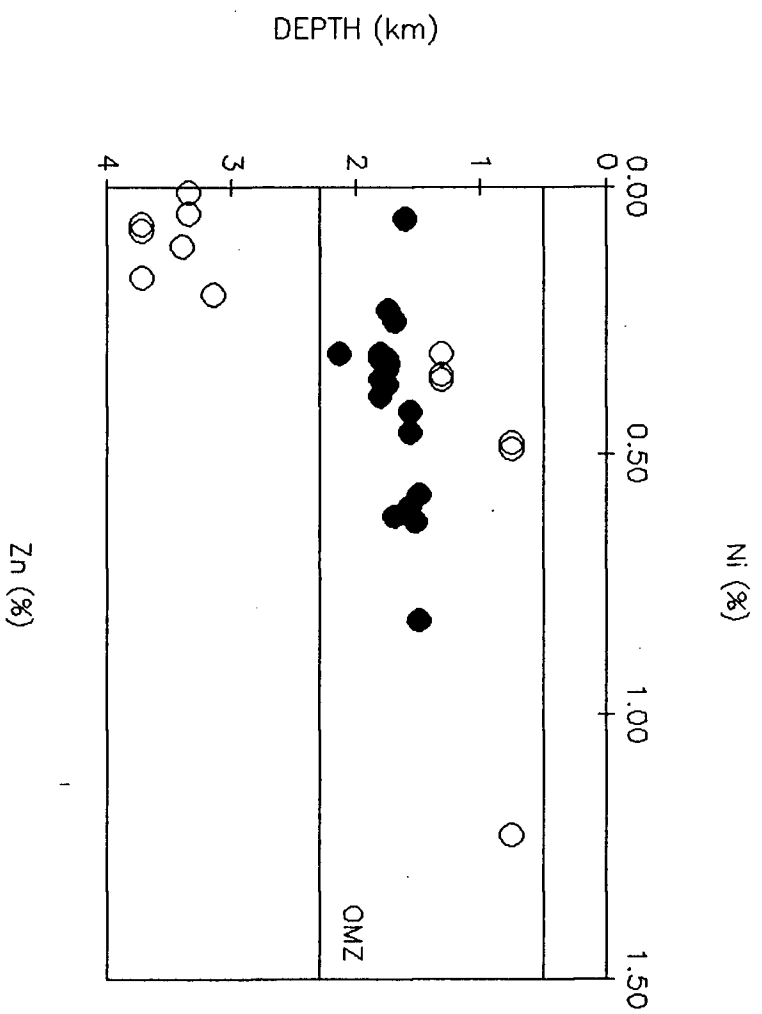
Not only does there exist interelement associations in crusts from this region, but for crusts from the Hawaiian Archipelago there also exists a correlation between the major element contents and water depth. Manganese and those minor metals that are correlated with manganese (Zn, Ba, Co, Ni, and Cu) all show a decrease in concentration with increasing water depth (Figure 1-8), while those elements that show a correlation with iron (Na, and Ti) all show an increase in concentration with increasing water depth (Figure 1-9).

To understand the correlation between crust geochemistry and water depth, the source of constituent elements must be identified. Halbach & Puteanus (1984b) have proposed that the main Fe source for hydrogenetic crusts of this region is colloidal Fe-hydroxide particles that are released in the water column from the dissolution of carbonate plankton skeletons. On the other hand, the source of Mn to hydrogenetic crusts evidently cannot be derived solely from this same source. They concluded that a further source of Mn enrichment following carbonate dissolution is necessary, and this is supplied via the Oxygen Minimum Zone (OMZ).

The extent of the OMZ in the central equatorial Pacific and the depletion of oxygen within this zone are, shown in Figure 1-10. Geosecs Station 235 is located within Survey Region A between the Hawaiian and Line Island Archipelagoes at 16°47.3'N and 161°22.9'W. Based on the oxygen profile at this site, the OMZ within

Figure 1-8. The correlation between Mn and those elements that are associated with Mn and water depth. The open circles = samples from the Hawaiian Island Archipelago, the filled circles = samples from the Line Island Archipelago.





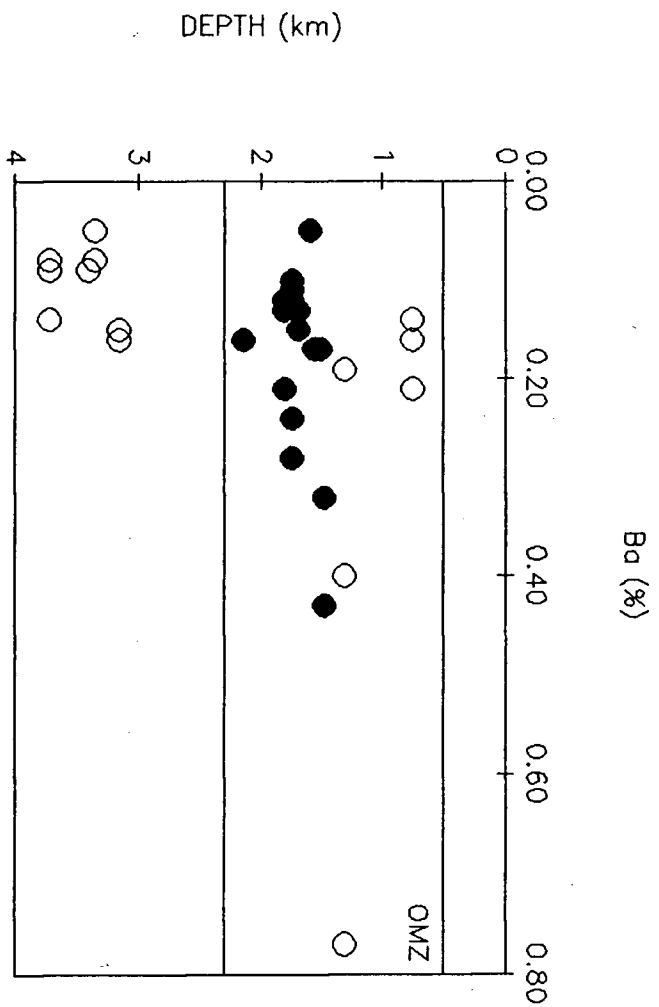
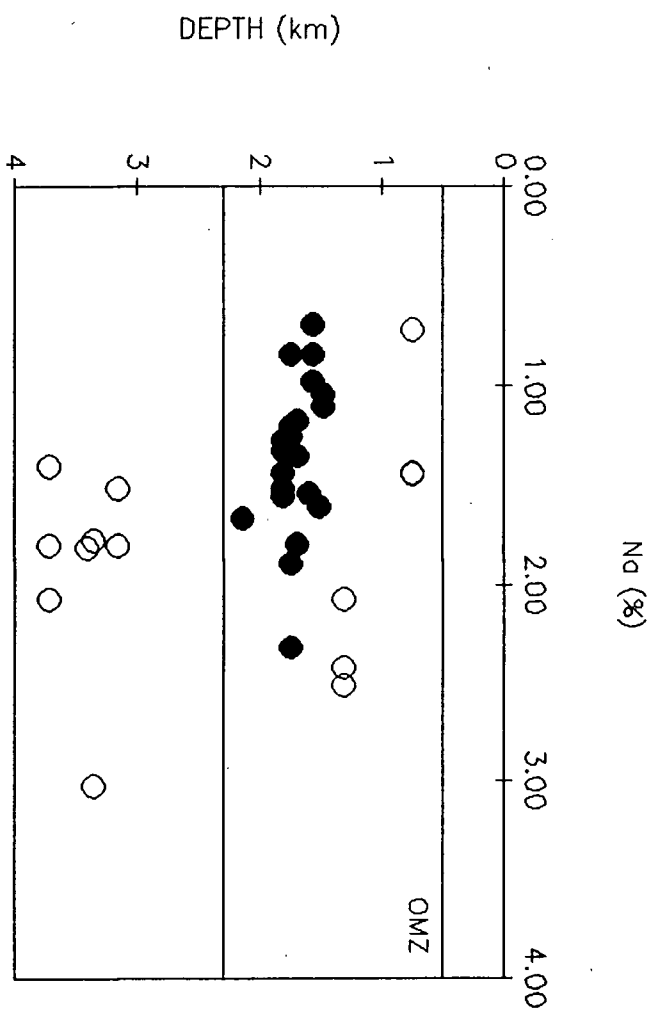
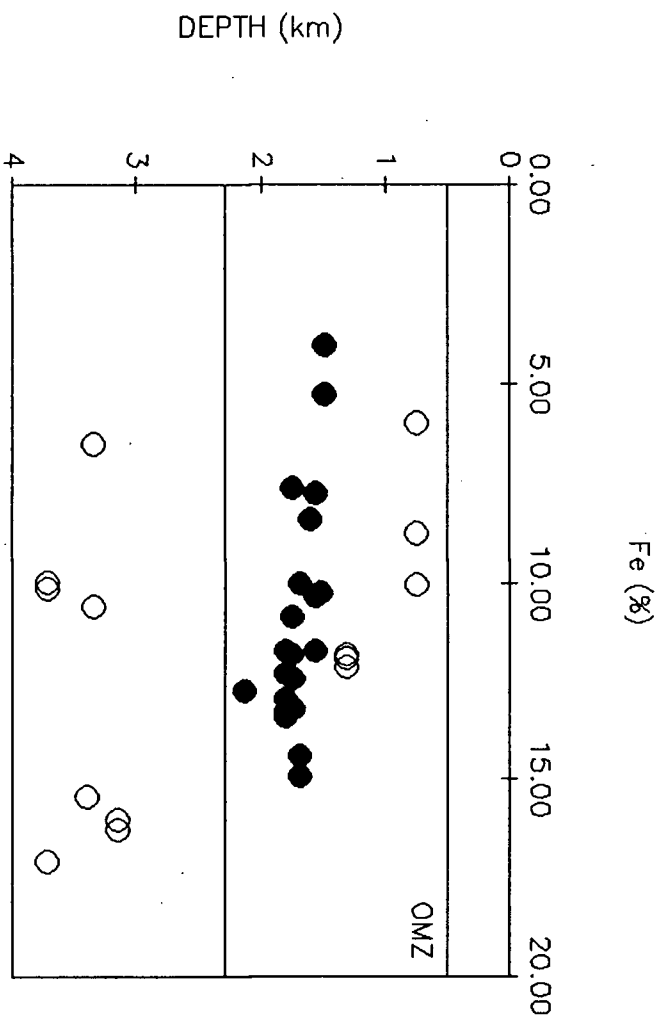




Figure 1-9. The correlation between Fe and those elements that are associated with Fe and water depth. The open circles = samples from the Hawaiian Island Archipelago, the filled circles = samples from the Line Island Archipelago.



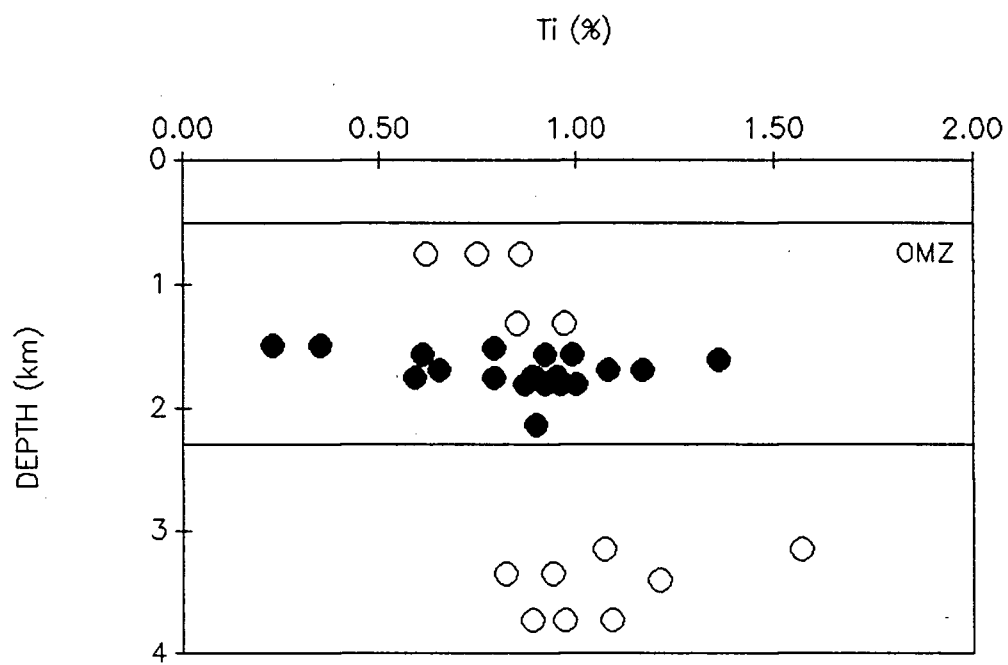
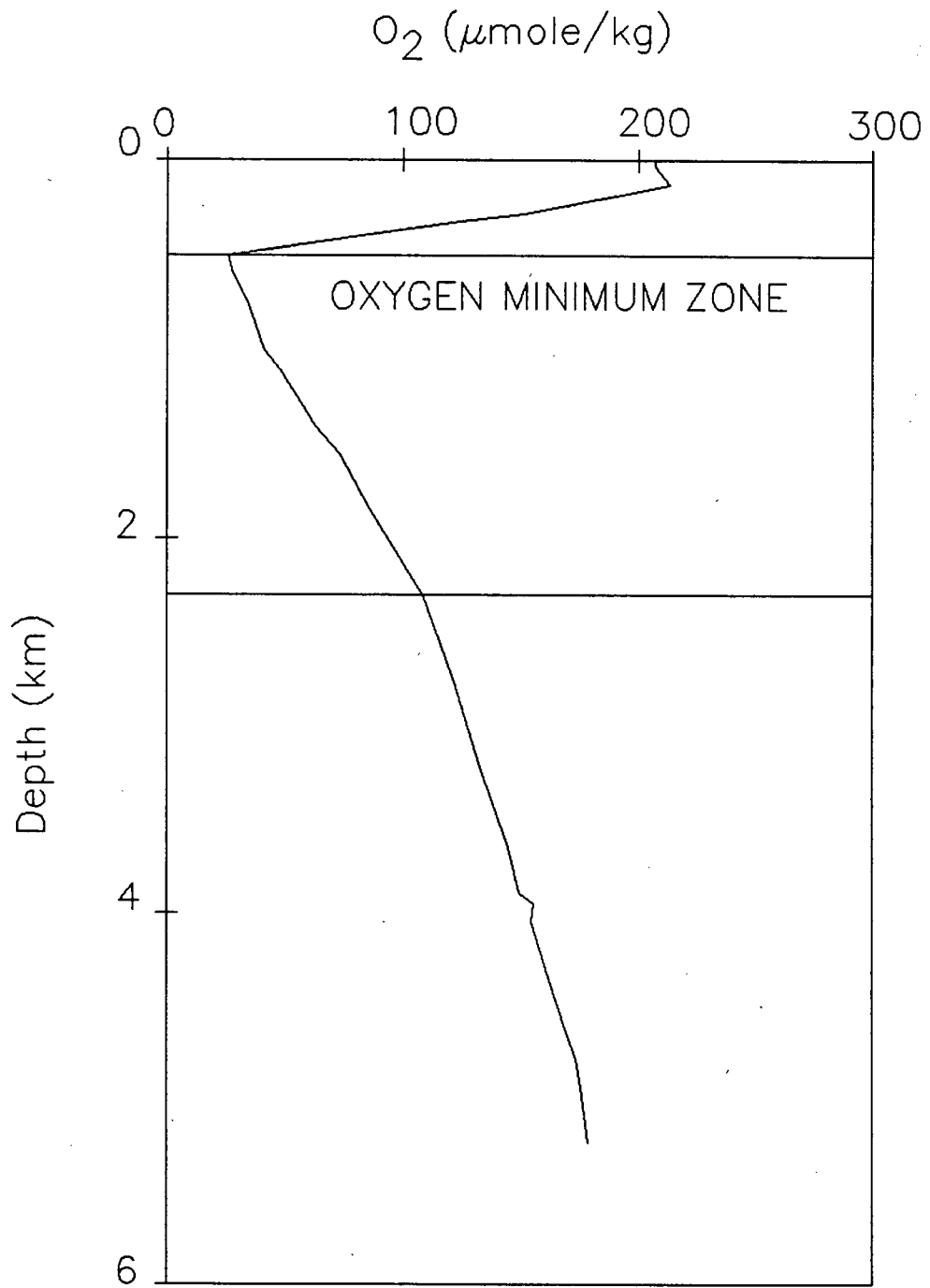


Figure 1-10. The profile of the O<sub>2</sub> concentration in seawater at Geosecs Station 235.



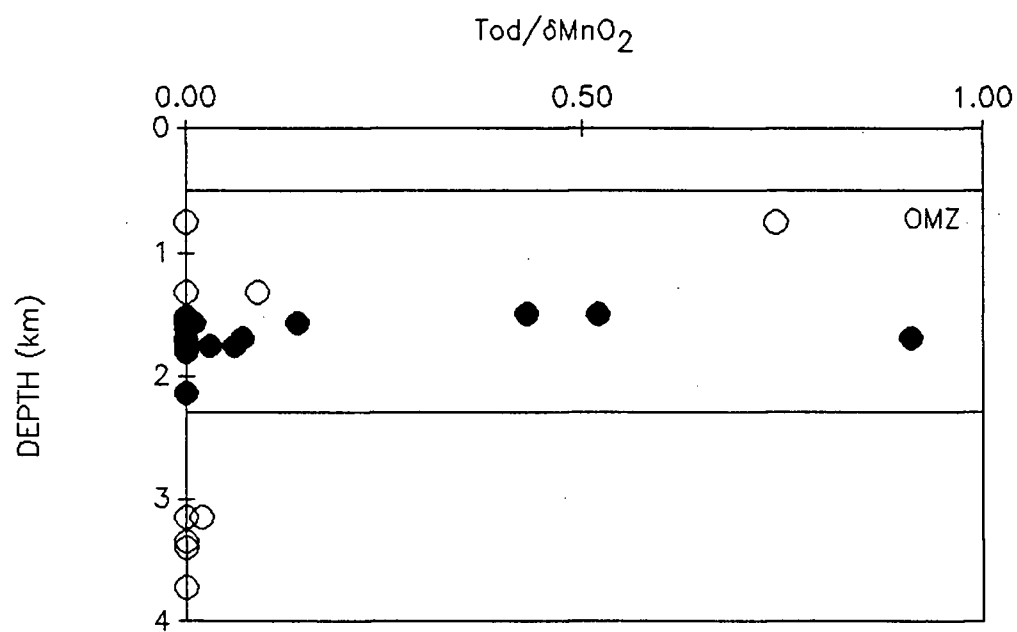
Survey Region A lies at water depths of between 503 and 2296m, and the minimum dissolved oxygen concentration is  $26\mu\text{mole/kg}$ .

Within the OMZ there is a high concentration of dissolved Mn as a result of the *in situ* decomposition of organic matter along with the *in situ* reduction of Mn-bearing solid phases (Klinkhammer & Bender, 1980; Landing & Bruland, 1980). This zone of maximum concentration of  $\text{Mn}^{2+}$  produces a flux of  $\text{Mn}^{2+}$  by diffusion and turbulent mixing into shallower and deeper waters which have an increased oxygen content. This causes oxidation of the  $\text{Mn}^{2+}$  and results in the formation of hydrated  $\text{MnO}_2$  particles which are incorporated into the crusts (Halbach *et al.*, 1988). As noted by Halbach *et al.* (1983), an increasing supply of Fe and its associated trace metals from the dissolution of calcite skeletons has a diluting effect on the concentration of Mn and its associated trace metals, that is the concentration of Mn and its associated trace metals should decrease with increasing water depth down to the CCD. This trend has also been observed by Halbach *et al.* (1983), Aplin & Cronan, (1985a), and by Hein *et al.* (in press b).

#### 1.4.1.1.4.2 Correlations with Manganese Phase Mineralogy

The XRD diffractogram shown in Figure 1-4 indicates that the manganese phase mineralogy in crusts from this region is dominated by  $\delta\text{MnO}_2$ . Although this is the most common manganese mineral present, todorokite also occurs in low abundances. The relative abundances of todorokite and  $\delta\text{MnO}_2$  in crusts from this region also appear to show a variation with water depth (Figure 1-11). Todorokite is more abundant in crusts located within the OMZ. As discussed by Glasby (1972), the redox potential in the environment of formation of ferromanganese deposits controls the manganese phase mineralogy. The depletion of oxygen in the OMZ to values of around  $26\mu\text{mole/kg}$  results in an environment with a lower redox potential. These

Figure 1-11. Correlation between manganese phase mineralogy and water depth.  
The open circles = samples from the Hawaiian Island Archipelago, the  
filled circles = samples from the Line Island Archipelago.





lower redox potentials combined with the high  $\text{Mn}^{2+}$  concentrations will result in manganese oxyhydroxides being precipitated as todorokite, where the  $\text{Mn}^{2+}(\text{OH})_2 \times 2\text{H}_2\text{O}$  layers bind successive  $[\text{Mn}^{4+}\text{O}_6]$  octahedra together. Below the OMZ, oxygen is more plentiful, this results in higher redox potentials, and combined with the low concentration of  $\text{Mn}^{2+}$  the layers of linked  $[\text{Mn}^{4+}\text{O}_6]$  octahedra are randomly oriented and constitute the  $\delta\text{MnO}_2$  phase (Burns & Burns, 1979).

#### 1.4.1.1.5 Correlations with Latitude

Although there appears to be a general correlation between crust geochemistry and water depth, crusts from the Line Island Archipelago show a very wide range in composition over a very small range in water depth (Figures 1-8 and 1-9). This variability is related to location; the concentrations of Mn, Ni, Zn, Cu, Co, and Ba decrease from the Equator towards the northwest along the Line Island Archipelago, while the concentrations of Fe, Ti, and Na increase with distance away from the Equator in the same direction.

This variation in the regional geochemistry of crusts from the Line Island Archipelago has also been observed by Halbach *et al.* (1982) and by Halbach & Puteanus (1984b). They proposed that although this correlation is not well understood, the processes likely to control these regional trends include deep and intermediate-depth current systems, biological productivity, differences in the position of the CCD, and the degree of depletion of oxygen in and the vertical extent of the OMZ zone.

### 1.4.1.2 Nodules

#### 1.4.1.2.1 Mineralogy

In contrast to the crusts, nodules from region A are composed mainly of todorokite and aluminosilicates, mostly quartz and feldspar (Figure 1-12). The todorokite to  $\delta\text{MnO}_2$  ratio for nodules from this region varies from 0.00 to 2.45 with a mean of 0.74 (Appendix C). This further supports the XRD evidence that the dominant manganese oxide in these nodules is todorokite. The XRD pattern also shows the presence of a fine-grained, poorly crystalline material, which contributes a considerable amount of background noise. Once again, the poorly crystalline material has been identified as being cryptocrystalline or amorphous hydrated iron oxides (Glasby, 1972; Crerar & Barnes, 1974). The identity of this phase will be discussed in greater detail in chapters 2 and 3.

#### 1.4.1.2.2 Bulk Composition

The major element data for nodules recovered from Survey Region A are listed in Appendix C. Again, these compositional data will be used to estimate the relative proportions of the iron and manganese oxides and other phases in the nodules and help interpret inter-element associations which will be discussed later.

The mean composition of nodules from this region is listed in Table 1-6 together with the average compositions of nodules from two other studies from within the same area. Except for Fe, the average composition of nodules from Survey Region A is similar to the average composition of nodules from the other two studies. The concentration of Fe, however, is considerably lower than those reported by Cronan & Tooms (1969) and Usui & Moritani (in press). Thus, the average

Figure 1-12. A typical XRD pattern of a nodule from Survey Region A.

# MN 39

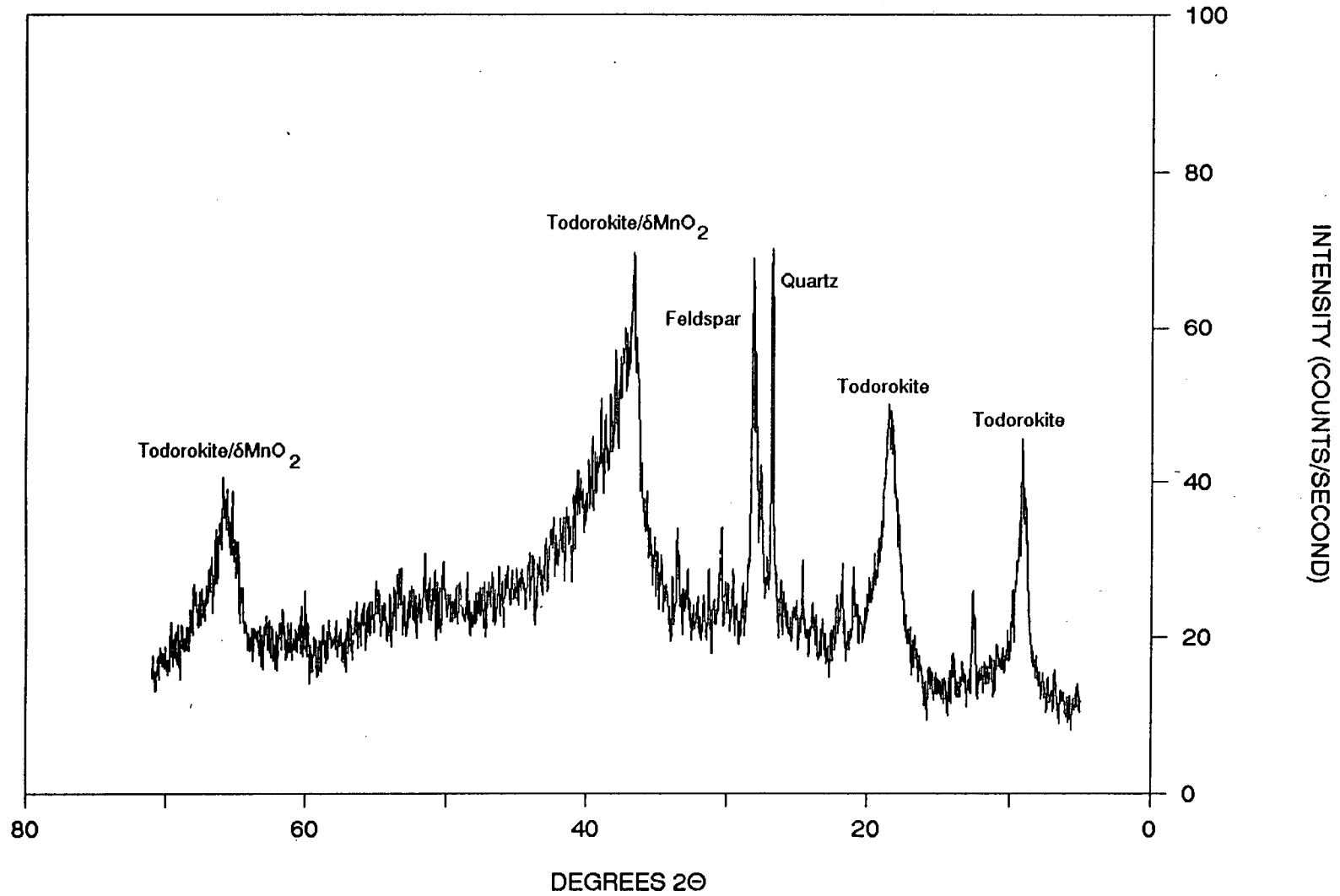


Table 1-6. Mean concentrations of major elements in nodules from Survey Region A. Concentrations are given in weight per cent.

Mean Composition of Nodules from Survey Region A		Average central Pacific nodules (Cronan & Tooms, 1969)		Mean composition of all nodule samples from the Central Pacific (Usui & Moritani, in press)	
Element	Concen.	Element	Concen.	Element	Concen.
Si	7.21			Si	6.91
Ti	0.63	Ti	0.81		
Al	2.45			Al	2.59
Fe	8.78	Fe	13.30	Fe	11.60
Mn	19.45	Mn	16.87	Mn	22.50
Mg	1.72				
Ca	2.03				
Na	1.52				
K	0.86				
P	0.32				
Co	0.22	Co	0.40	Co	0.25
Ni	0.74	Ni	0.56	Ni	0.89
Cu	0.60	Cu	0.39	Cu	0.75
Zn	0.08			Zn	0.09
Ba	0.15	Ba	0.15		
Mn/Fe	2.22	Mn/Fe	1.27	Mn/Fe	1.94

Mn/Fe ratio of nodules from this region is higher than those reported for the other two studies.

#### 1.4.1.2.3 Interelement Associations

##### 1.4.1.2.3.1 Correlations with Aluminium

As shown by the crusts, the nature of the aluminosilicates in the nodules is shown by the relationship between Al and other major elements. For the nodules, aluminum shows a strong positive correlation with Si and K (Figure 1-13). From the X-ray diffractogram (Figure 1-12), these correlations with Al could be explained by the presence of quartz and feldspar. By using the Si/Al and K/Al element ratios, the origin of the aluminosilicate fraction of the nodules can be identified. As shown in Table 1-7, the Si/Al and K/Al ratios are 2.94 and 0.35, respectively. The Si/Al of the nodules is closely similar to that of Average Pacific Pelagic Clay as determined by Bischoff *et al.* (1979), rather than Average Tholeiitic Lavas from the Hawaiian Islands as determined by Best (1982). The K/Al ratio, however, is much greater than either of the ratios determined by Bischoff *et al.* (1979) and Best (1982). This seems to indicate, just like the crusts, that there are several sources contributing to the aluminosilicate fraction in the nodules. Due to the proximity of the nodules to the crusts, the sources of aluminosilicates to the nodules should be the same as those contributing to the crusts. Almost all of the quartz and a minor proportion of the feldspars are incorporated into the nodules from the associated sediments as indicated by the Si/Al ratio of the nodules being almost identical to Average Pacific Pelagic Clay. The feldspars and the rest of the quartz are eolian in origin, and their abundance reflects the position of the nodules relative to the atmospheric wind belts (Hein *et al.*, 1985).

Figure 1-13. The relationship between Al and other major elements. The open circles = diagenetic nodules, the filled circles = hydrogenous nodules.

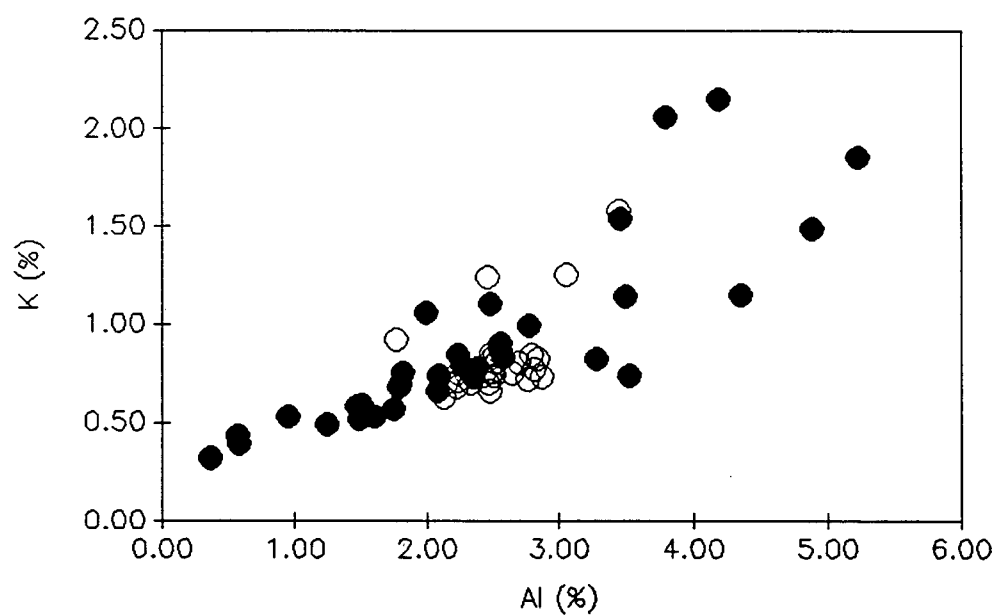
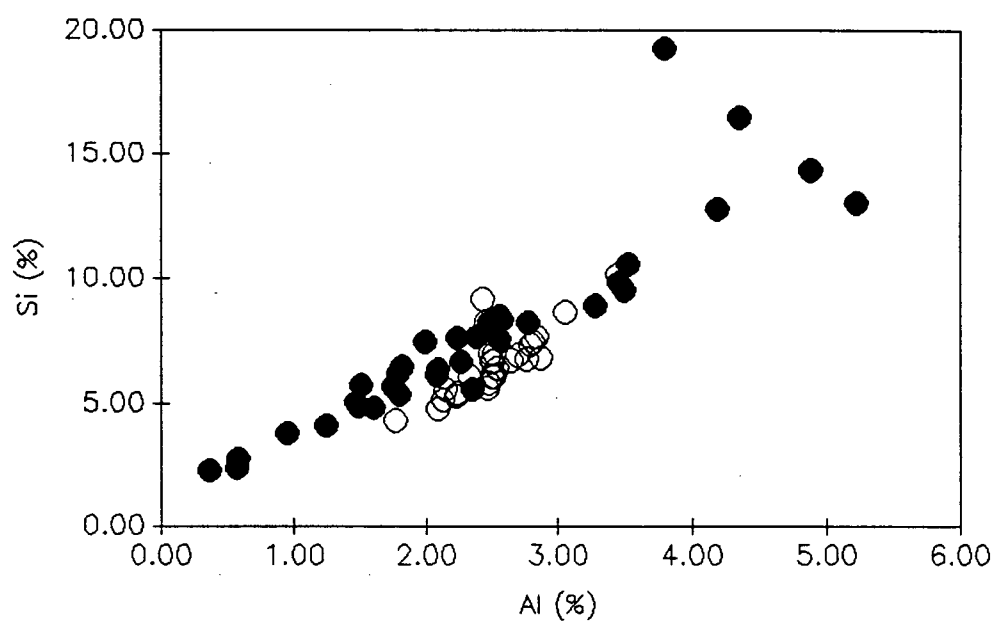




Table 1-7. Comparison of the composition of aluminosilicates in nodules to Average Pacific Pelagic Clay and Tholeiitic Lavas from the Hawaiian Islands.

	Element Ratios	
	Si/Al	K/Al
Nodules from Survey Region A (This Study)	2.94	0.35
Average Pacific Pelagic Clay (Bischoff et al., 1979)	2.92	0.25
Average Tholeiitic Lavas from the Hawaiian Islands (Best, 1982)	3.13	0.04

Calvert & Price (1977a) estimated the total amount of aluminosilicate impurity in their nodules based on the Al contents, assuming that this fraction had the same composition as that in the associated sediments. Even though there are associated sediments, they only contribute a portion of the total amount of the aluminosilicate fraction in nodules. Eolian deposition of quartz and feldspar into the ocean contributes the rest of the aluminosilicate fraction to the nodules. Because of these multiple sources of aluminosilicates in nodules, determining the aluminosilicate content of the nodules is not possible.

#### 1.4.1.2.3.2 Phosphorite

Some of the nodules are found to have high concentrations of Ca and P. Furthermore, there is a strong positive correlation between these two elements in all nodules (Figure 1-14). An XRD tracing of a nodule with high Ca and P concentrations shows that this correlation is due to the presence of carbonate fluorapatite  $\{(Ca,Mg,Na,K)_{10}[(P,C)O_4]_6(F,OH)_2\}$  (Figure 1-15).

The formation of carbonate fluorapatite has already been discussed to explain the correlation of P with Ca in crusts from this same region. The presence of carbonate fluorapatite in nodules is possibly due to the erosion of carbonate fluorapatite from the neighbouring seamounts and its incorporation into the nodules as nuclei.

Figure 1-14. The correlation between Ca and P. The open circles = diagenetic nodules, the filled circles = hydrogenous nodules.

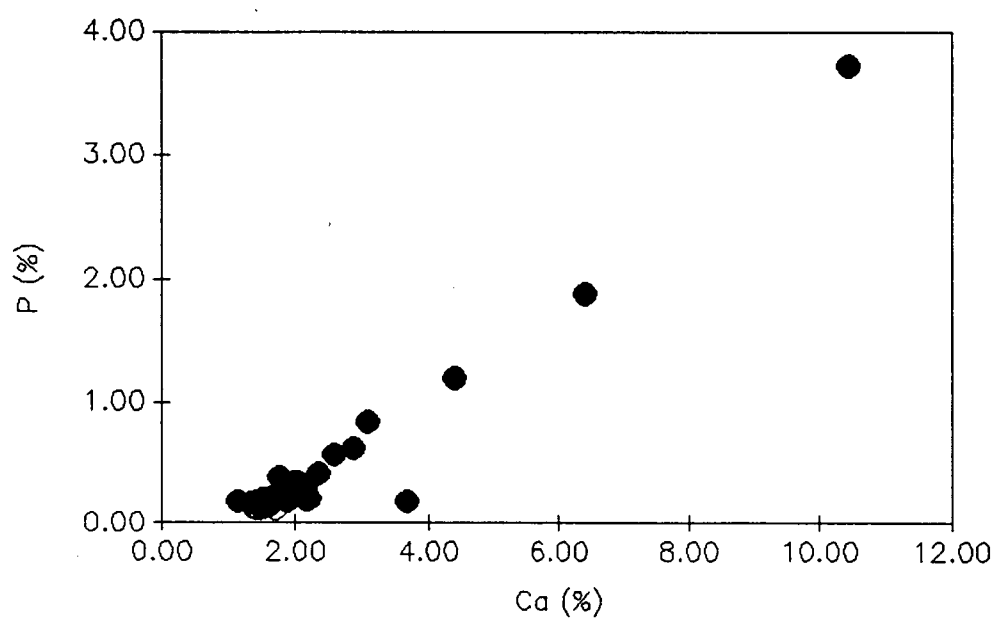
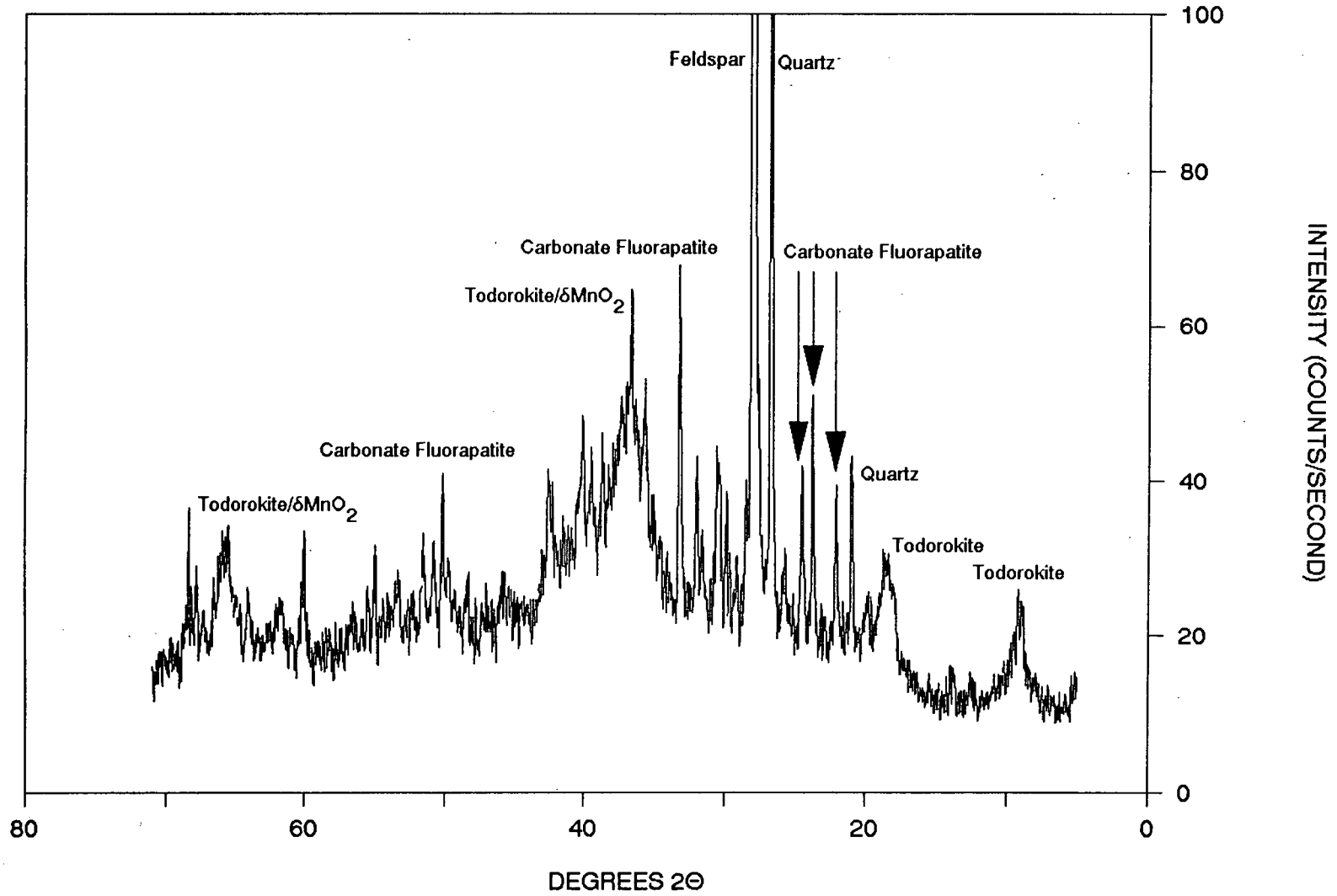


Figure 1-15. An XRD pattern of a nodule with high Ca and P concentraions.

# Mn 86



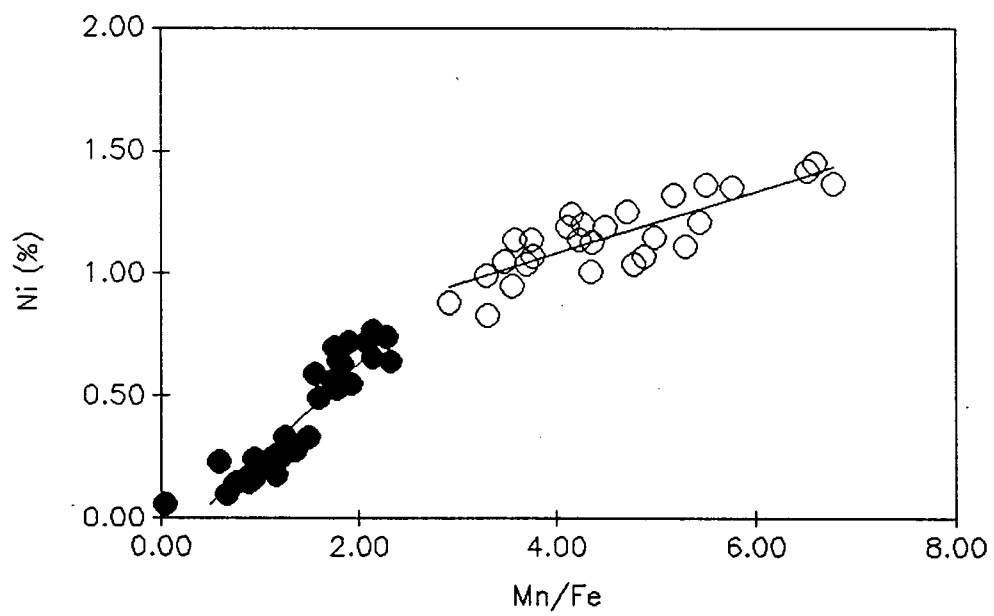
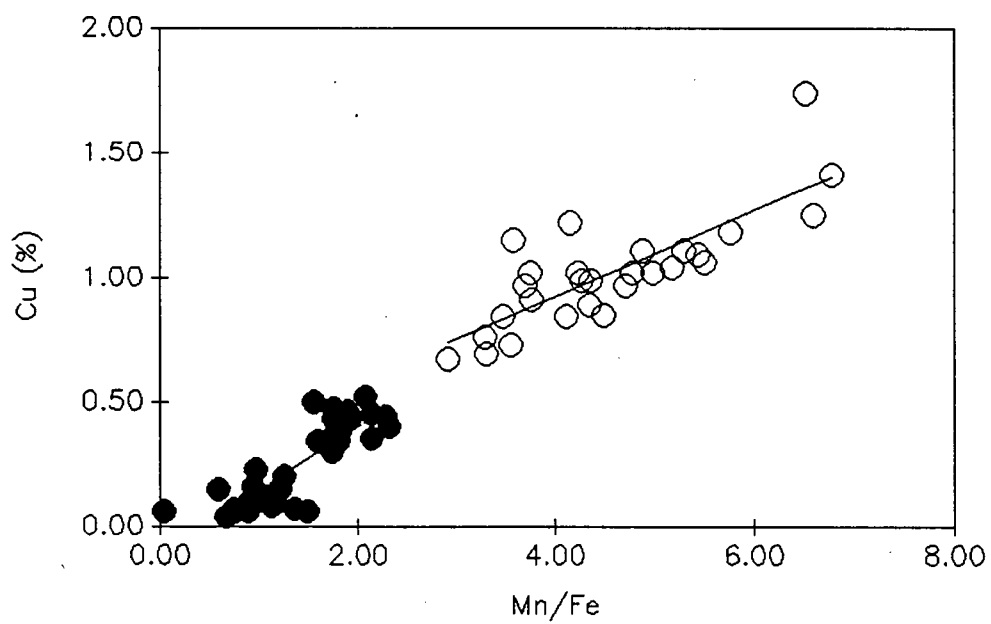
#### 1.4.1.2.3.3 Correlations with Manganese and Iron

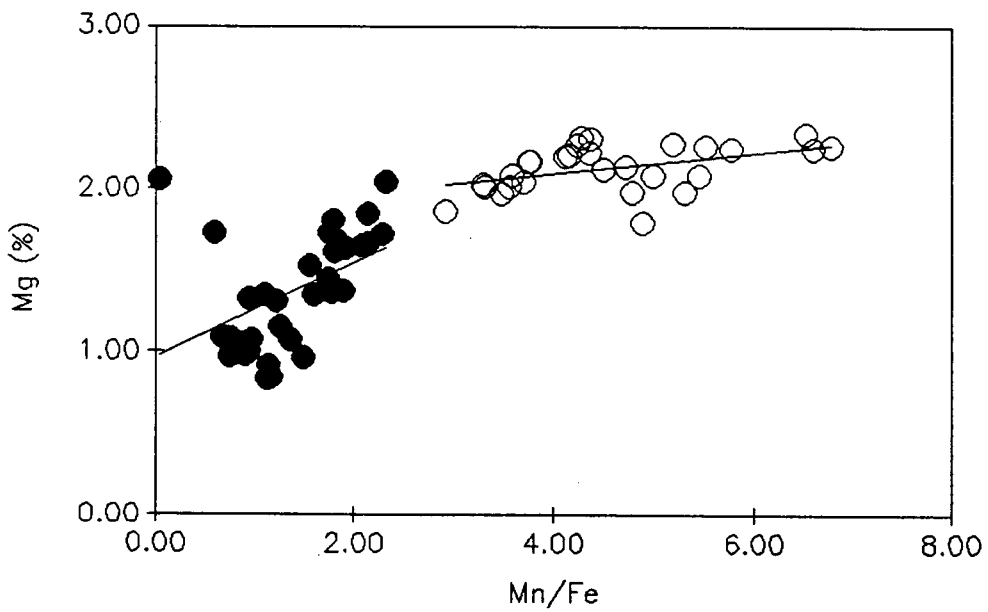
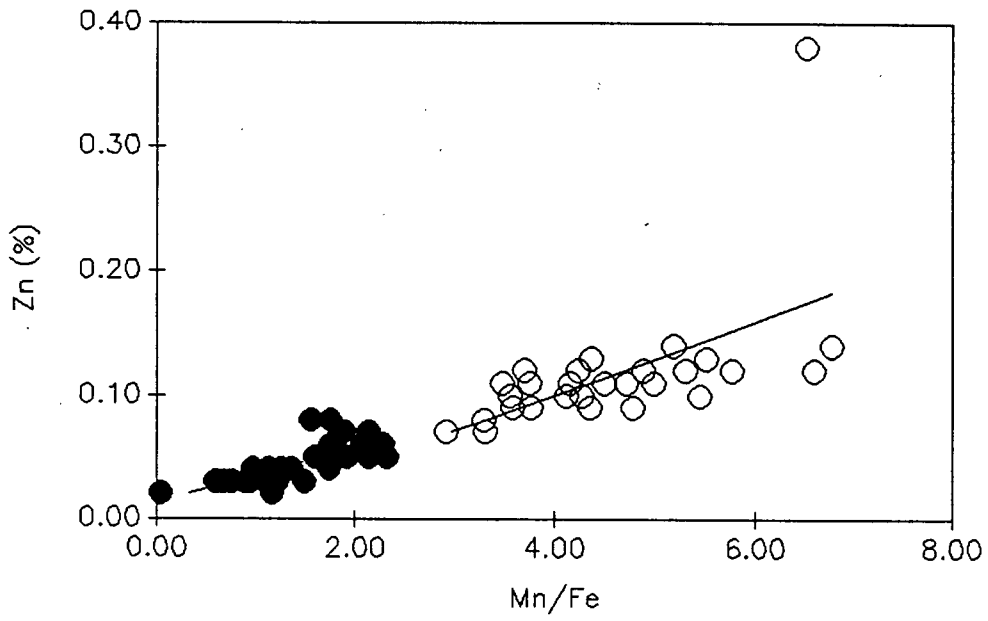
Although not the first, Halbach & Özkara (1979) used the Mn/Fe ratio as a criterion for distinguishing between different types of nodules from a small study area located within Survey Region A. They suggested that nodules with an Mn/Fe ratio less than 2.5 were predominantly hydrogenous in origin, while nodules with an Mn/Fe ratio above 2.5 were mainly diagenetic in origin. Nodules from Survey Region A can also be divided into these two groups, and there is a marked compositional distinction between them. As shown in Figure 1-16, hydrogenous nodules are depleted in Mn, Cu, Ni, Zn, Mg, and Ba compared to the diagenetic nodules whereas hydrogenous nodules are enriched in Fe and Ti compared to the diagenetic nodules. It can therefore be stated that the abundances of Cu, Ni, Zn, Mg, and Ba are correlated with Mn and that the abundance of Ti is correlated with Fe.

It is interesting to note in Figure 1-16 that there is a sharp break in slope of a first order regression line drawn through the hydrogenous nodules compared to one drawn through the diagenetic nodules. For those elements that are associated with Mn (apart from Co and Zn), the slope of the regression line for the hydrogenous nodules is greater than that of the diagenetic nodules. Since inter-element correlations with manganese are related to the manganese oxides present in the nodule, a similar association should be apparent when the todorokite to  $\delta\text{MnO}_2$  ratios are plotted against the Mn/Fe ratios (Figure 1-17). This shows that todorokite is more abundant than  $\delta\text{MnO}_2$  in diagenetic nodules compared to hydrogenous nodules. Even though the same change in the slopes of the first order regression lines is seen, almost all of the nodules contain some todorokite as indicated by the non zero values of the todorokite/ $\delta\text{MnO}_2$  ratios. In order to understand why there is

Figure 1-16. The association of major elements with Mn/Fe. The open circles = diagenetic nodules, the filled circles = hydrogenous nodules.







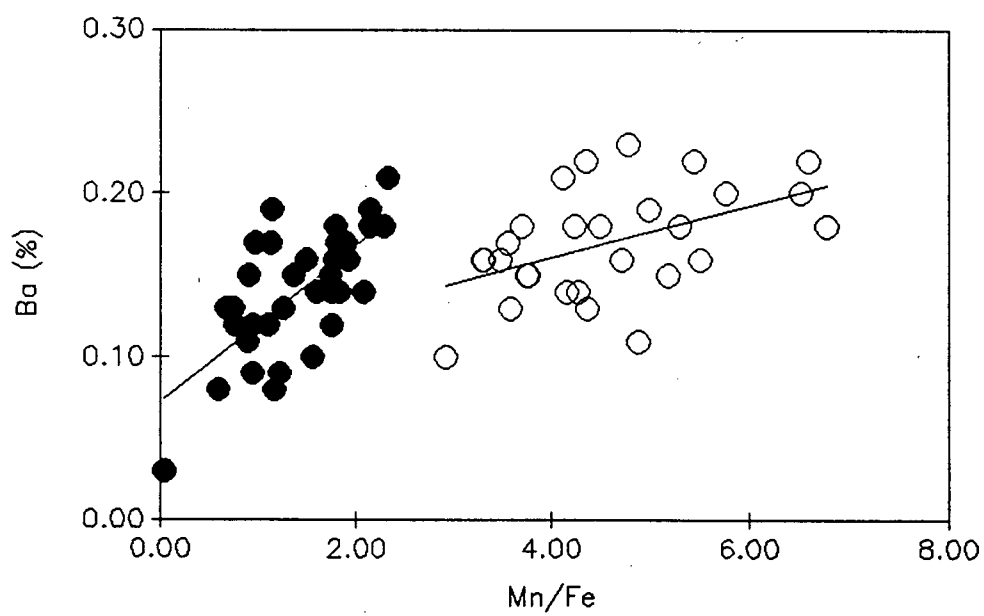
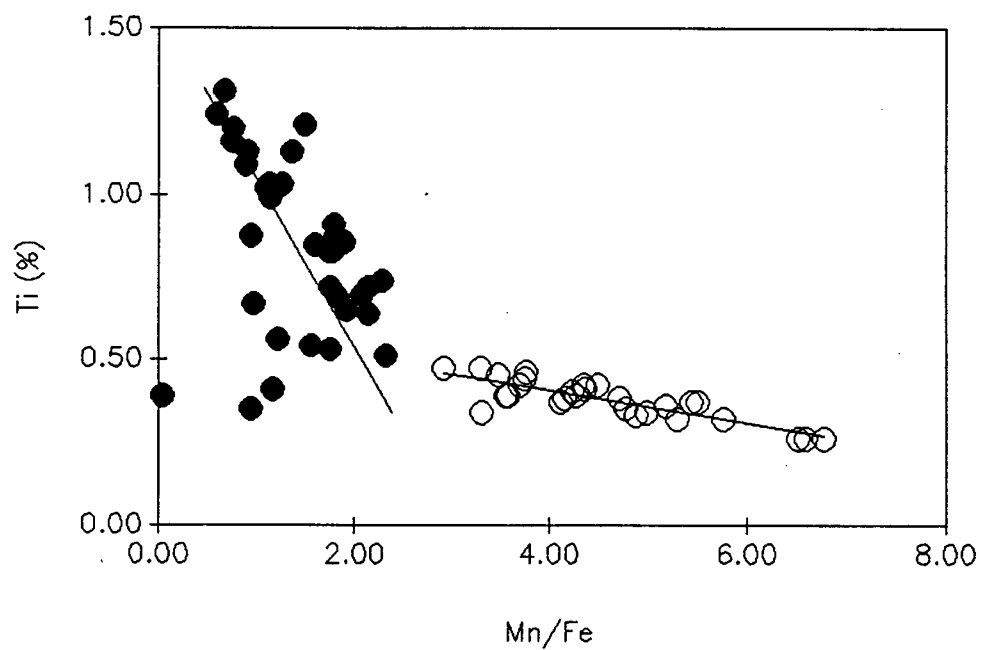


Figure 1-17. Correlation between manganese phase mineralogy and Mn/Fe. The open circles = diagenetic nodules, the filled circles = hydrogenous nodules.



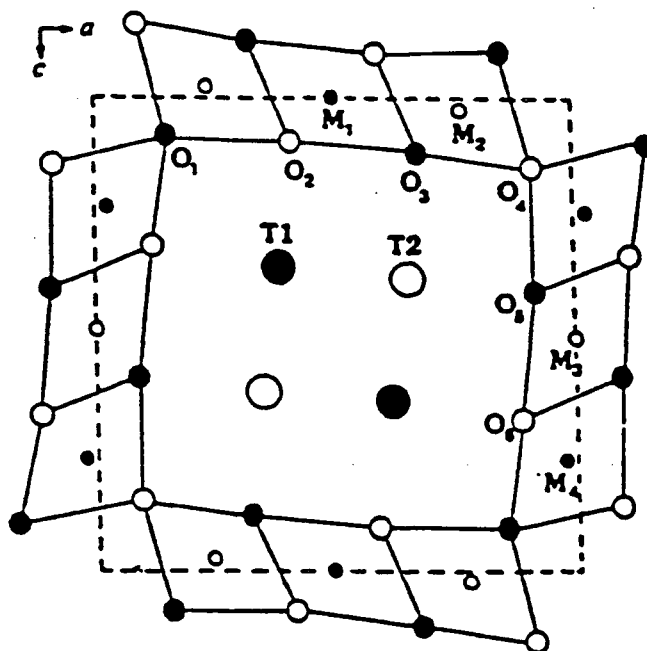
a change in the slopes of a first order regression lines shown in Figure 1-17 a better understanding of the crystal structure of todorokite is needed.

Todorokite is a tecktomanganate possessing a tunnel structure running parallel to the b axis. The tunnels are composed of "walls" of triple chains of edge-shared  $[\text{MnO}_6]$  octahedra containing  $\text{Mn}^{4+}$  ions in the M1 positions and  $\text{Mn}^{2+}$  ions in the M2 positions. "Floors" and "ceilings" of these tunnels consist of edge-shared  $[\text{MnO}_6]$  octahedra, most commonly three octahedra wide with  $\text{Mn}^{4+}$  ions in the M3 and M4 positions (Figure 1-18) (Burns *et al.*, 1983). These predominant  $[3 \times 3]$  tunnels are often intergrown with other tunnels ranging in dimension from  $[3 \times 2]$  to  $[3 \times 8]$  and higher (Burns *et al.*, 1985). The very wide tunnels, obtaining dimensions of  $[3 \times \infty]$ , produce the layered structure postulated for busserite (Burns *et al.*, 1983).

In the "ceilings" of the todorokite tunnels are cation vacancies within the bands of edge-shared  $[\text{Mn}^{4+}\text{O}_6]$  octahedra which become more prevalent with wider "ceiling" dimensions. These cation vacancies not only nucleate faults, kinks, and twinning observed in the HRTEM micrographs of todorokite fibres (Turner *et al.*, 1982), but they also influence the crystal chemistry and site occupancy of the tunnels. As a result, three types of atomic substitution contribute to the crystal chemistry of todorokite: (1) substitution of  $\text{Mn}^{4+}$  cations by other cations of smaller ionic radii in the "ceilings", such as low spin  $\text{Co}^{3+}$  ions (Burns, 1976); (2) substitution of divalent  $\text{Mn}^{2+}$  ions in the "walls" by  $\text{Mg}^{2+}$ ,  $\text{Ni}^{2+}$ ,  $\text{Cu}^{2+}$ ,  $\text{Zn}^{2+}$ , and other cations; and (3) constituents of the tunnels (T1 and T2 positions) consist of large cations such as  $\text{K}^+$ ,  $\text{Ba}^{2+}$ ,  $\text{Ag}^{2+}$ ,  $\text{Ca}^{2+}$ ,  $\text{Pb}^{2+}$ ,  $\text{Na}^{2+}$ , and  $\text{H}_2\text{O}$  molecules (Burns *et al.*, 1983).

A non-linear correlation between Ni and Cu versus the Mn/Fe ratio has also been observed by Halbach *et al.* (1981b) in nodules from the Northeast Pacific nodule belt and by Usui & Mita (1987) in nodules from the three survey areas of SONNE Cruise SO-25 in the Northeast equatorial Pacific. Halbach *et al.* (1981b)

Figure 1-18. The crystal structure of todorokite. (Turner *et al.*, 1982).



- ● Manganese
- ● Oxygen
- ● Tunnel cations or water molecules



concluded that their non-linear regressions describe the natural saturation of divalent cations in the lattice of todorokite. The decrease in the slope of the first order regression lines from the hydrogenous nodules to the diagenetic nodules recovered from Survey Region A can therefore be attributed to the saturation of the todorokite crystal lattice by manganese and associated divalent cations. The relationship between Zn and Mn/Fe does not show the same behaviour as the other elements associated with manganese. The reason for this is probably because of the low concentration of zinc in the nodules from this region compared to the other elements. Zinc, therefore, does not become saturated in the todorokite lattice structure.

It has already been shown that the abundance of Ti is correlated with the presence of Fe. When Ti is plotted against Mn/Fe there is a sharp break in the slope of the first order regression line drawn through the hydrogenous nodules compared to one drawn through the diagenetic nodules, the slope for the hydrogenous nodules being greater than that for the diagenetic nodules. Since Ti is correlated with Fe, this change in the slope of the first order regression lines is the inverse of that displayed by those elements (except Co and Zn) that correlate with Mn. Just like the saturation of the todorokite crystal lattice with Mn and its associated divalent cations, the change in the slopes of the first order regression lines from the hydrogenous nodules to the diagenetic nodules can be interpreted as the saturation of the crystal lattice of the unidentified iron oxyhydroxide with Ti.

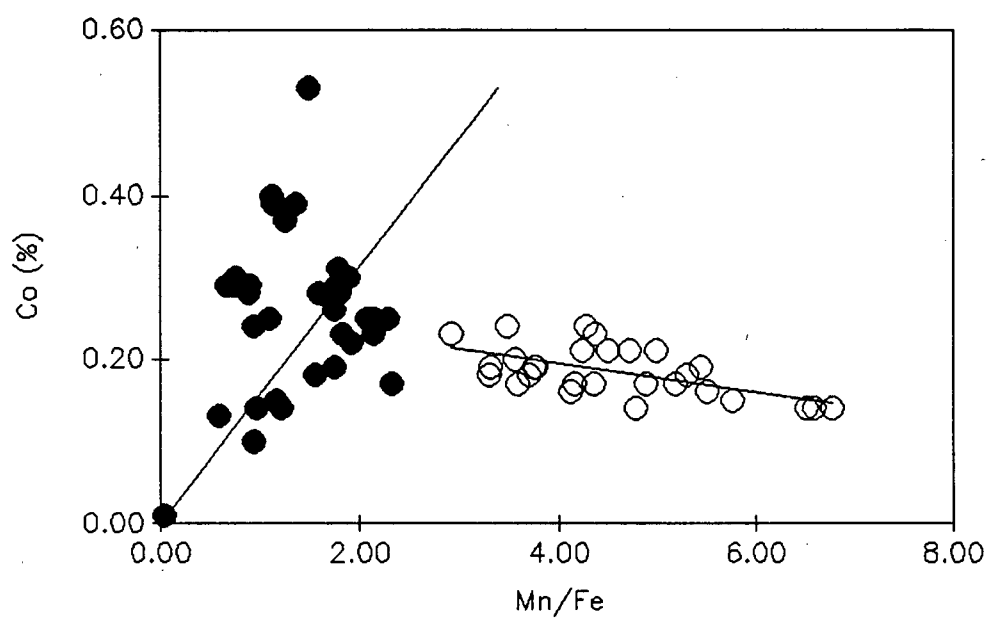
These interelement associations and the coexistence of hydrogenous and diagenetic nodules within the same survey area have also been observed in samples collected from smaller survey areas located within Survey Region A. These include: DOMES Site A (Calvert & Piper, 1984), WAHINE (Calvert *et al.*, 1978), Valdivia Sites VA 08-1 A1 and A2 (Friedrich & Plüger, 1974; Friedrich *et al.*, 1977), Valdivia Site 13/1 (Glasby *et al.*, 1982), and Valdivia Site 13/2 (Halbach & Özkara, 1979).

#### 1.4.1.2.3.3.1 Complex Correlations Between Cobalt with Manganese and Iron

Cobalt shows a complex association with Mn and Fe, which is unlike that of the other minor elements (Figure 1-19). In hydrogenous nodules, Co is positively correlated with Mn, whereas in diagenetic nodules Co is positively correlated with Fe. The complex association of Co with the manganese and iron oxide phases have been previously observed by Cronan & Tooms (1969), Price & Calvert (1970) and by Halbach *et al.* (1983).

Price & Calvert (1970) suggested that this observed complex behaviour of Co in nodules is due to  $\text{Co}^{3+}$  substituting for  $\text{Mn}^{4+}$  in nodules containing  $\delta\text{MnO}_2$  as well as  $\text{Fe}^{3+}$  in the iron oxyhydroxide phases. Cobalt (III) ( $d^6$ ) is stable when in the low spin state with octahedral coordination and has an ionic radius almost identical to that of  $\text{Fe}^{3+}$  or  $\text{Mn}^{4+}$ . Cobalt (III) will therefore preferentially substitute for both  $\text{Fe}^{3+}$  in the  $\text{FeOOH} \times n\text{H}_2\text{O}$  phase (Burns, 1965) and  $\text{Mn}^{4+}$  in the  $\delta\text{MnO}_2$  phase (Glasby & Thijessen, 1982a; Halbach *et al.*, 1981a). As noted previously,  $\text{Co}^{3+}$  will also substitute for  $\text{Mn}^{4+}$  in the "ceilings" of todorokite (Burns, 1976). Since hydrogenous nodules contain both  $\delta\text{MnO}_2$  and todorokite, this would explain the positive association of Co with Mn. Diagenetic nodules, on the other hand, contain mostly todorokite. Although the substitution of  $\text{Co}^{3+}$  for  $\text{Mn}^{4+}$  in the "ceilings" of todorokite probably occurs, the substitution of  $\text{Co}^{3+}$  for  $\text{Fe}^{3+}$  in the  $\text{FeOOH} \times n\text{H}_2\text{O}$  phase appears to be more dominant as seen by the correlation of Co with Fe in these nodules.

Figure 1-19. Complex association of Co with Mn and Fe. The open circles = diagenetic nodules, the filled circles = hydrogenous nodules.

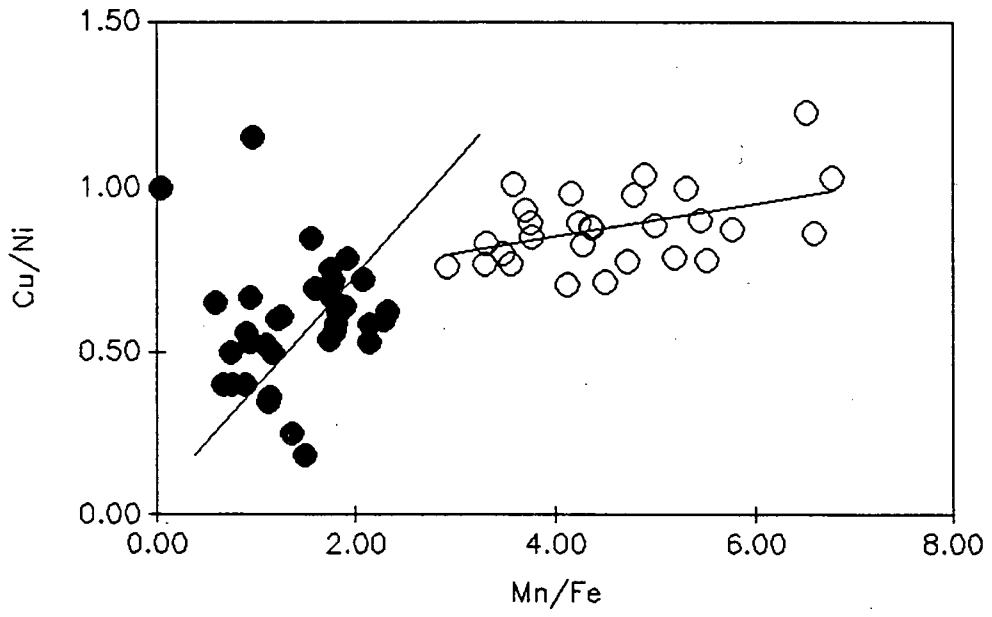


#### 1.4.1.2.3.3.2 Correlation of Copper with Nickel

The Cu/Ni ratio shows a strong positive correlation with the Mn/Fe ratio (Figure 1-20). Hydrogenous nodules are found to have generally lower Cu/Ni ratios than diagenetic nodules. This relationship has also been observed by Raab (1972), Calvert & Price (1977a), and Calvert *et al.* (1978). As noted by Seigel (1981) and Calvert & Piper (1984), nodules with higher Cu/Ni ratios contain more crystalline todorokite rather than  $\delta\text{MnO}_2$ . This trend is also seen for the nodules recovered from Survey Region A when comparing figure 1-20 with Figure 1-17.

The reason for this correlation can be explained by examining the behaviour of Cu and Ni during diagenesis. Work on the trace metal geochemistry of pelagic sediment pore waters by Klinkhammer (1980), Callender & Bowser (1980), and by Klinkhammer *et al.* (1982) has shown that Cu and Ni behave quite differently during diagenesis in marine sediments. During diagenesis, Ni follows Mn, apparently being taken up by solid Mn phases close to the sediment surface and is released to the pore water along with Mn at depth. In contrast, Cu is released to the pore water very close to the sediment surface where it can diffuse both into the bottom water and into the sediment. These different behaviours are consistent with the Cu-enrichment in the most markedly diagenetic nodules at Survey Region A.

Figure 1-20. Correlation between Cu/Ni and Mn/Fe. The open circles = diagenetic nodules, the filled circles = hydrogenous nodules.



## 1.4.2 SURVEY REGION B

### 1.4.2.1 Crusts

#### 1.4.2.1.1 Mineralogy

A typical XRD pattern of a crust from Survey Region B, shows that the mineralogy of crusts from this region is dominated by todorokite, birnessite, and minor amounts of  $\delta\text{MnO}_2$  (Figure 1-21). The todorokite to  $\delta\text{MnO}_2$  ratios range from 0.00 to 2.82 with an mean of 0.45. Also shown in Figure 1-21 is the presence of calcite. Once again the XRD pattern shows the presence of a fine-grained, poorly crystalline material which has been previously identified as being cryptocrystalline or amorphous hydrated iron oxides (Glasby, 1972; Crerar & Barnes, 1974). A more detailed study on the iron oxide phase mineralogy of crusts and nodules will be discussed in Chapter 2 and Chapter 3.

#### 1.4.2.1.2 Bulk Composition

The major element data for crusts recovered from Survey Region B are listed in Appendix D. As for samples recovered from Survey Region A, this compositional data will be used to estimate the relative proportions of the iron and manganese oxides and other phases in the crusts, and help interpret inter-element associations which will be discussed later.

The mean composition of crusts from this region is listed in Table 1-8, together with the average compositions of crusts and nodules from four other studies from within the same area. From Table 1-8, the two average compositions of the crusts show a very wide range in Mn, Fe, Cu, Ni, and Co concentrations while the two



Figure 1-21. A typical XRD pattern of a crust from Survey Region B.

# RISE III 3 D-1

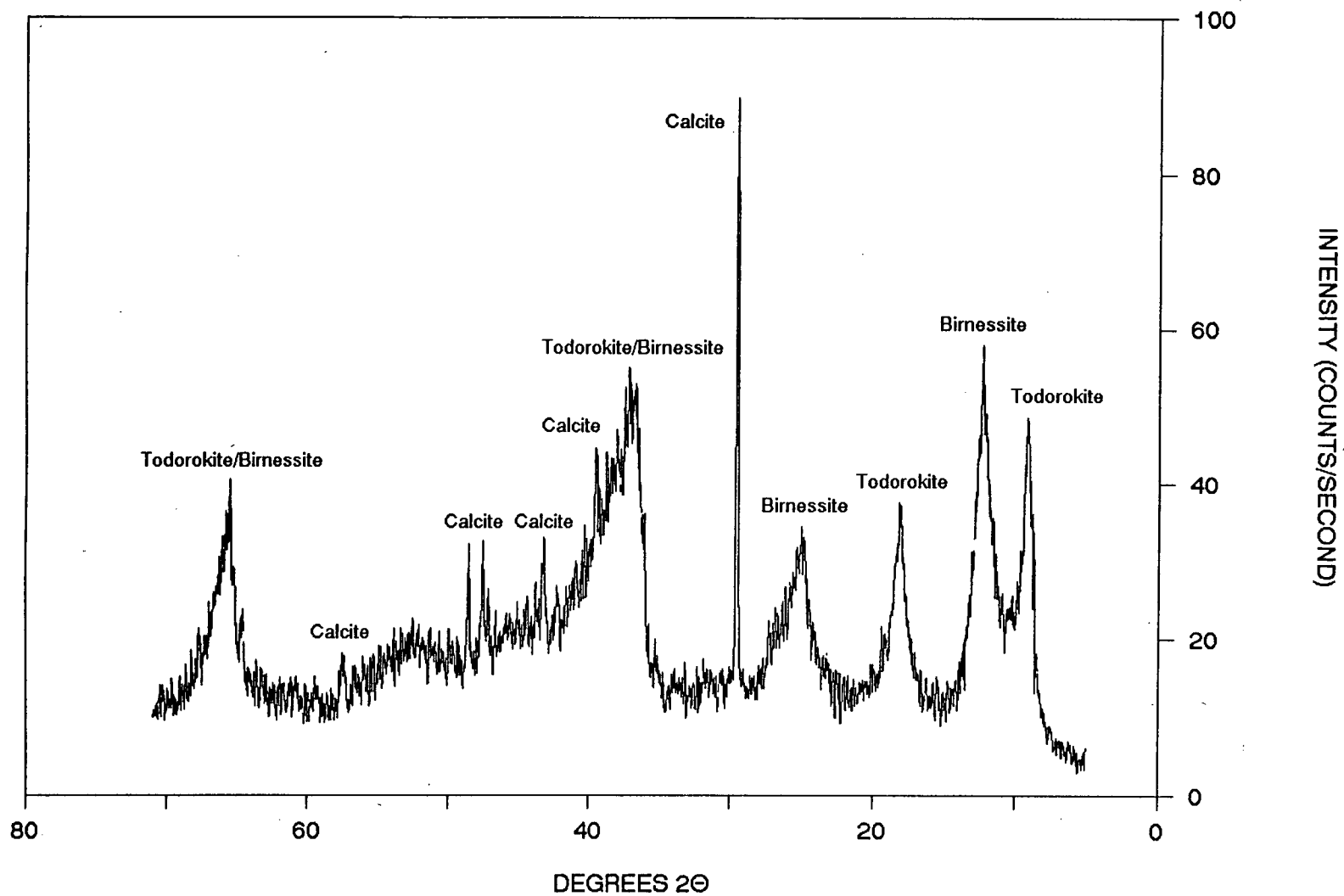


Table 1-8. Mean concentrations of major elements in crusts from Survey Region B.  
Concentrations are given in weight per cent.

Mean Composition of Crusts from Survey Region B		Average of two Eastern Pacific crusts (Lonsdale et al., 1980)		Representative hydrothermal crust from the E.P.R. (Bonatti et al., 1972)	
Element	Concen.	Element	Concen.	Element	Concen.
Si	9.44			Si	5.80
Ti	0.42				
Al	2.51			Al	<0.5
Fe	14.02	Fe	4.40	Fe	31.10
Mn	12.67	Mn	39.28	Mn	0.58
Mg	1.71				
Ca	2.63				
Na	1.84				
K	0.65				
P	0.27				
Co	0.06	Co	0.10	Co	0.00
Ni	0.19	Ni	0.24	Ni	0.01
Cu	0.08	Cu	0.08	Cu	0.01
Zn	0.04	Zn	0.11		
Ba	0.22				
Mn/Fe	0.90	Mn/Fe	8.93	Mn/Fe	0.02

average compositions of the nodules are similar. The mean concentrations of Mn, Cu, Ni, and Co in crusts from this study are significantly lower than the concentration of these elements in the average compositions of the nodules reported by Cronan & Tooms (1969) and by Skornyakova (1979), while the mean concentration of Fe in crusts from this study is significantly higher than the concentration of this element reported in the nodules. The average composition of the crusts from this study is also significantly different from the average composition of the crusts reported by Lonsdale *et al.* (1980) and by Bonatti *et al.* (1972). The average concentrations of Mn, Fe, Cu, Ni, and Co in the crusts from this study fall between the two extreme concentrations of these elements found by Lonsdale *et al.* (1980) and by Bonatti *et al.* (1972). The same is true for the average Mn/Fe ratios. The mean Mn/Fe ratio for the crusts from this study is 0.90. This is significantly lower than the mean Mn/Fe ratios of the nodules and between the two extreme Mn/Fe ratios of the crusts.

#### 1.4.2.1.3 Interelement Associations

##### 1.4.2.1.3.1 Correlations with Aluminium

Aluminium shows a strong positive correlation with Si and a weak correlation with Ti (Figure 1-22). An explanation for these correlations is not apparent when examining the XRD diffractogram shown in Figure 1-21, since this XRD pattern does not show the presence of aluminosilicates. Furthermore, when comparing the Si/Al and Ti/Al ratios of the crusts with those for the Average Pacific Pelagic Clay and for the Mid-Ocean-Ridge-Basalts (MORB) from the EPR, the Si/Al ratio for the crusts is considerably higher while the Ti/Al ratio for the crusts is relatively close to that of the Average Pacific Pelagic Clay (Table 1-9). Just like the crusts and nodules from Survey Region A, this suggests that several sources of Si contribute to the crusts

Figure 1-22. The relationship between Al and other major elements. The open circles = hydrogenetic crusts, the filled circles = Mn-enriched hydrothermal crusts, the filled triangles = Mn-depleted hydrothermal crusts.

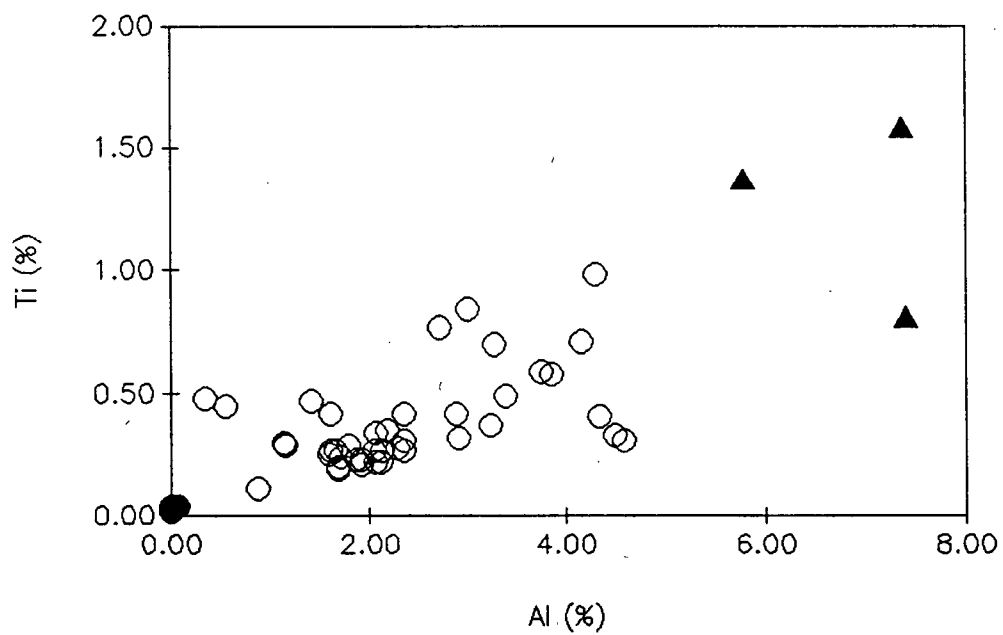
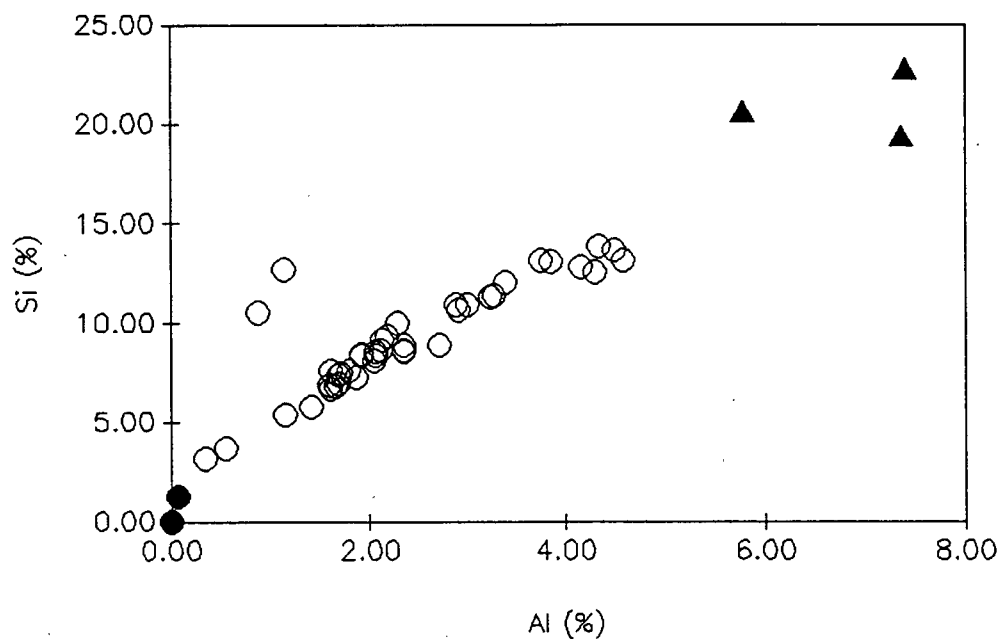


Table 1-9. Comparison of the composition of aluminosilicates in crusts to Average Pacific Pelagic Clay and Mid-Ocean Ridge Basalts.

	Element Ratios	
	Si/Al	Ti/Al
Crusts from Survey Region B (This Study)	3.76	0.17
Average Pacific Pelagic Clay (Bischoff et al., 1979)	2.92	0.06
Average Mid-Ocean-Ridge Basalts from the E.P.R. (Melson et al., 1976)	2.99	0.13

from this region. In crusts located close to the EPR, the abundance of silicon is determined by two sources: (1) incorporation of detrital aluminosilicates which are composed of eolian debris and volcanogenic debris eroded from submarine outcrops by bottom currents (Hein *et al.*, in press a); (2) an additional source of Si precipitated from hydrothermal sources (Toth, 1980). According to Toth (1980), iron- and silica-rich hydrothermal crusts are composed of iron-rich nontronite or amorphous hydrated iron oxides and silica, with very low trace-metal contents. An X-ray diffractogram of a crust with high concentrations of Fe and Si and low concentrations of trace elements (Figure 1-23) shows that an amorphous material is the dominant phase present. Some sharp diffraction peaks also occur in the diffractogram, but they are few in number and of such low intensity that it is impossible to identify which mineral(s) these peaks belong to.

#### 1.4.2.1.3.2 Correlations with Calcium

Calcium shows positive correlations with Si and Mg (Figure 1-24). The presence of Ca in crusts from this region can partly be attributed to the presence of calcite, as shown in Figure 1-21. However, the correlation of Ca with Si and Mg can not be so easily explained. In samples containing high concentrations of Ca, Si, and Mg, XRD analysis shows that the dominant mineral phase is the clinopyroxene manganoan diopside (Figure 1-25). The presence of this mineral would explain the correlation of Ca to Si and Mg since it has the chemical formula  $(\text{Ca},\text{Mn})(\text{Mg},\text{Fe},\text{Mn})\text{Si}_2\text{O}_6$ .



Figure 1-23. An XRD pattern of a crust with high concentrations of Fe and Si and low concentrations of trace elements.

# SOTW 9 32 D-1

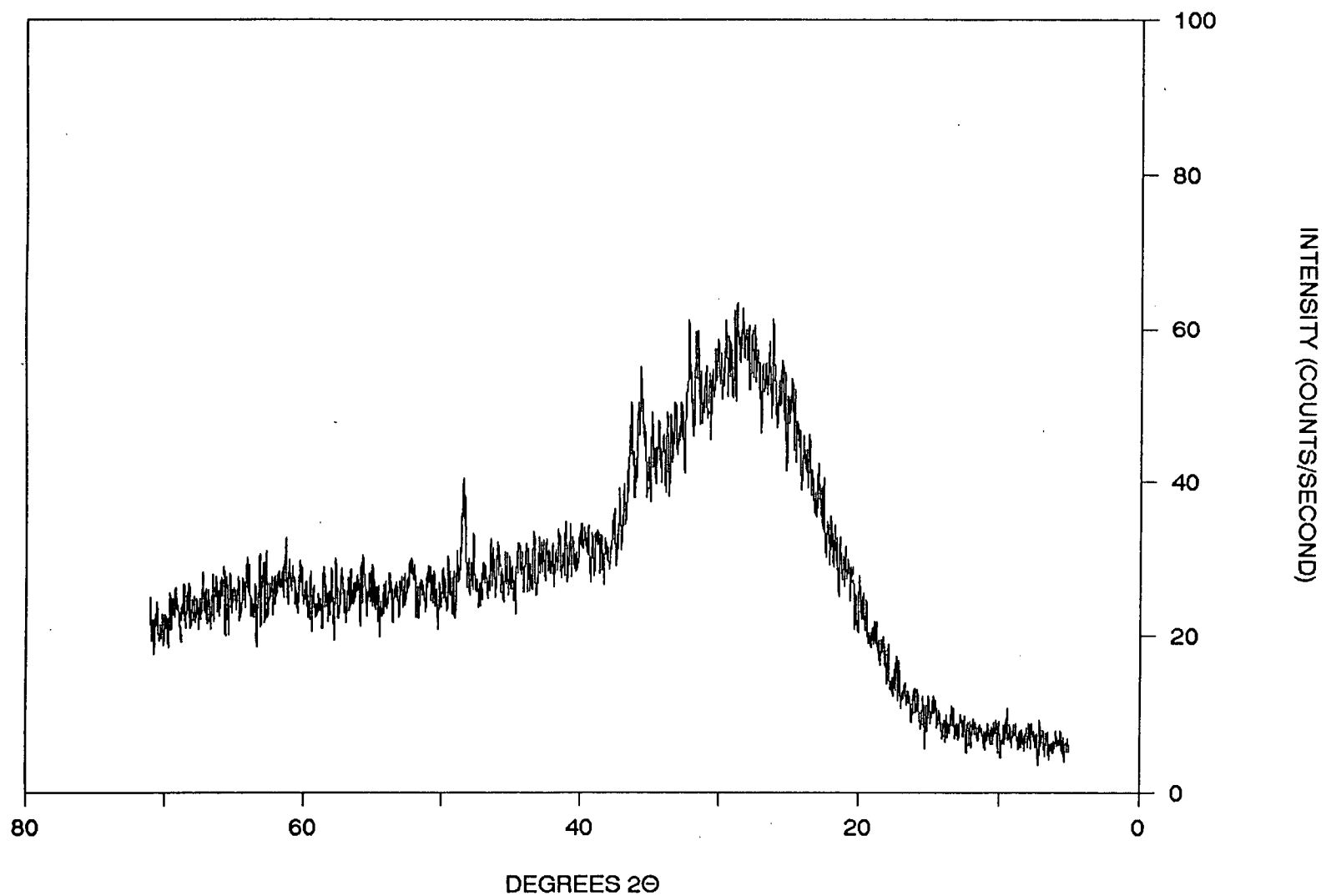


Figure 1-24. The relationship between Ca and other major elements. The open circles = hydrogenetic crusts, the filled circles = Mn-enriched hydrothermal crusts, the filled triangles = Mn-depleted hydrothermal crusts.

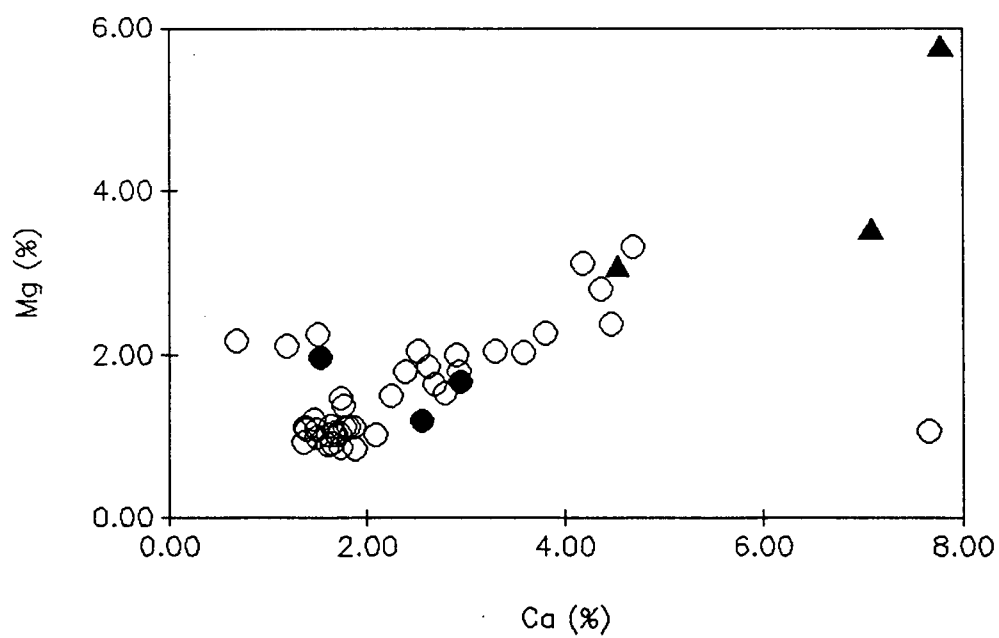
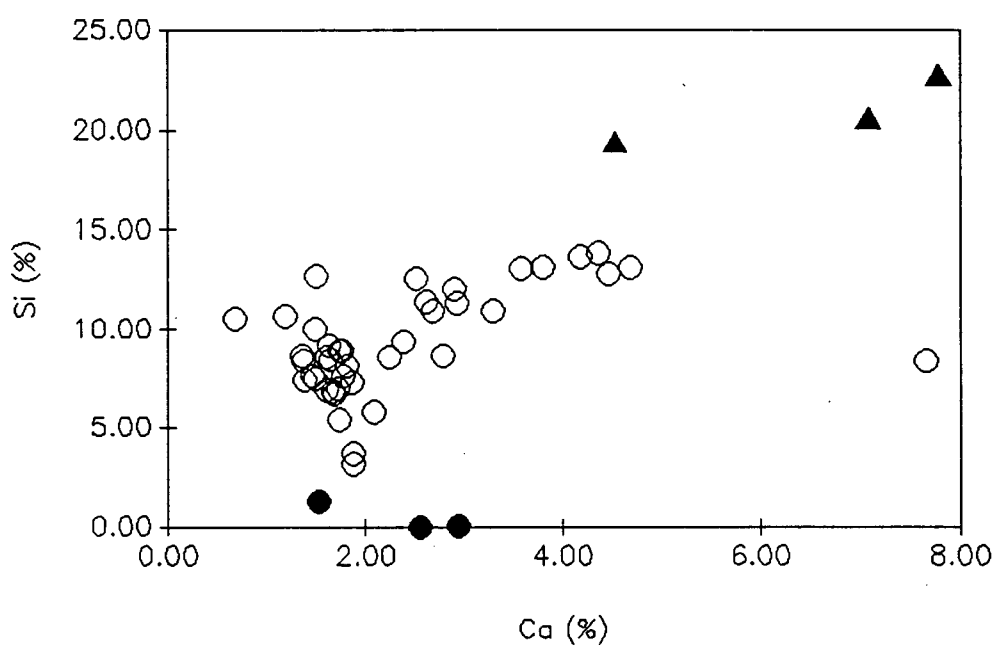
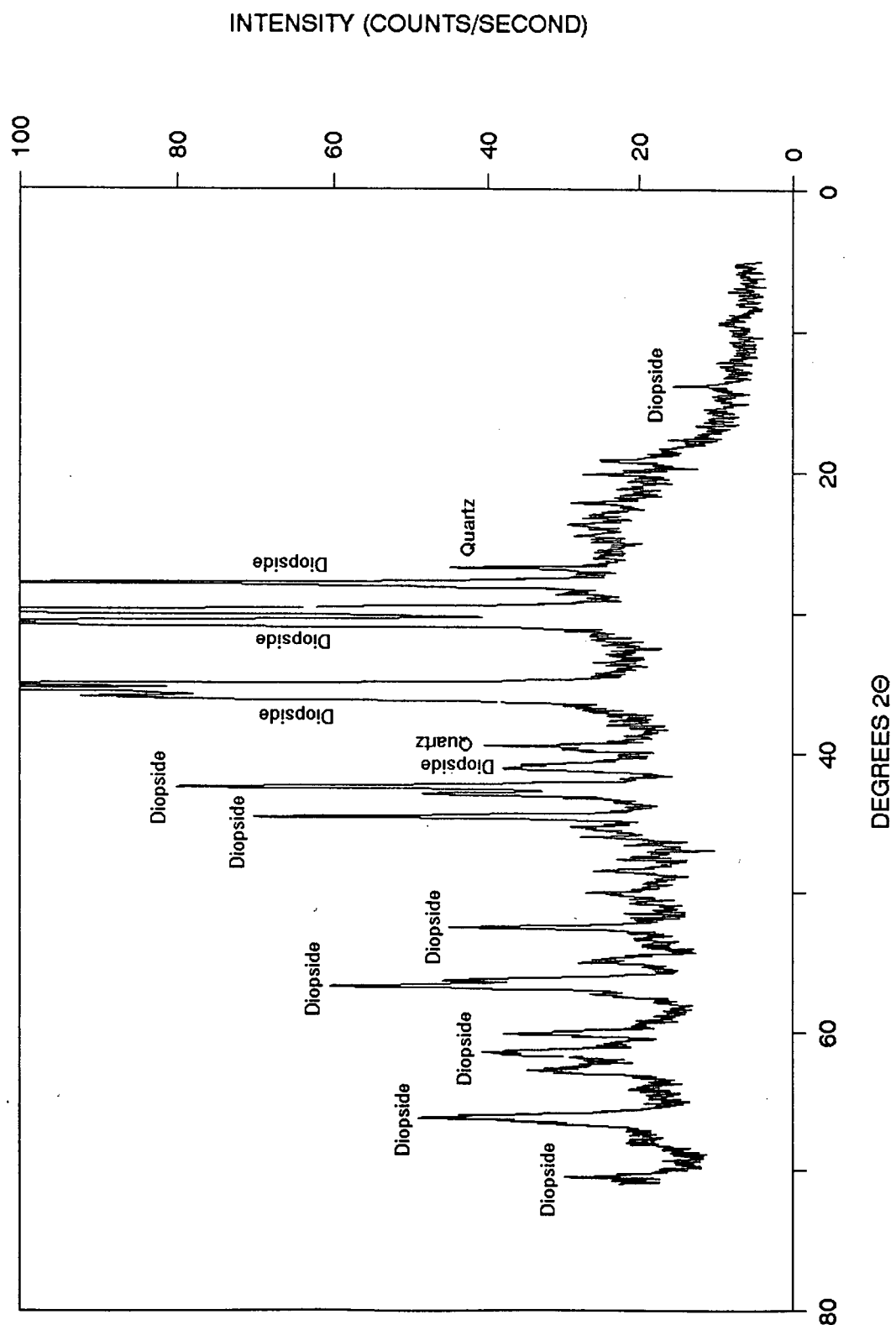


Figure 1-25. A typical XRD pattern of a crust with high concentrations of Ca, Si, and Mg.

**QBR 7(B) D-2**



#### 1.4.2.1.3.3 Correlations with Manganese

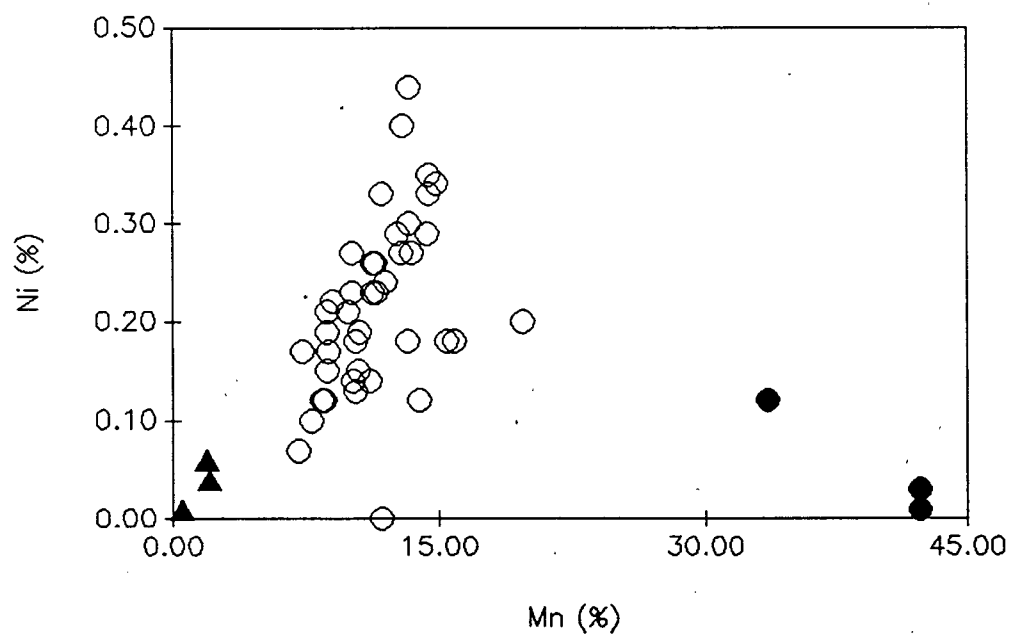
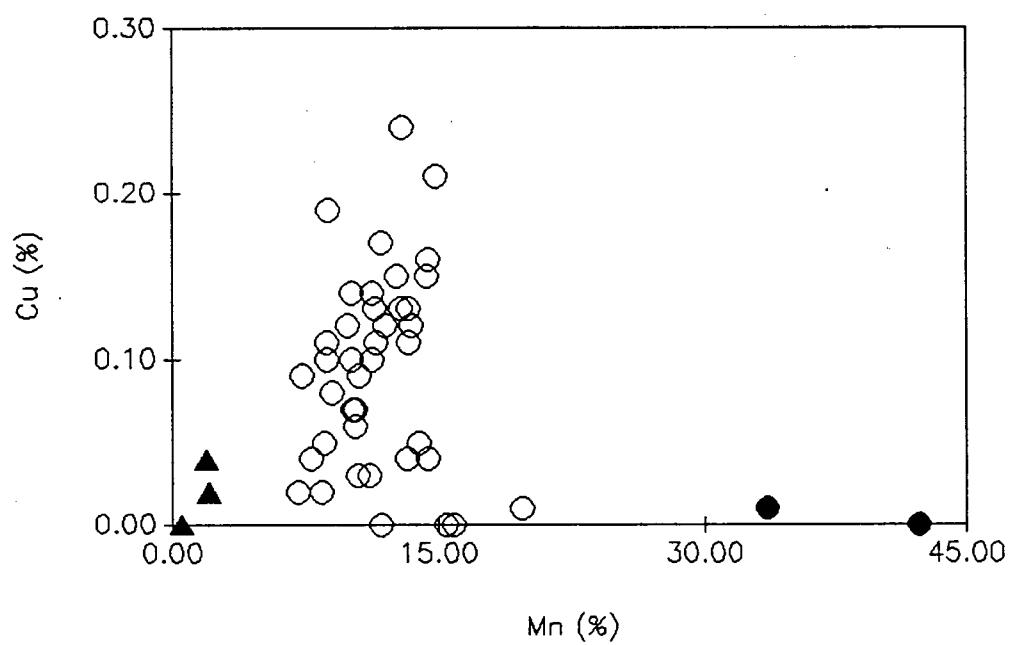
Although the crusts from Survey Region B have an average Mn/Fe ratio of 0.90 (Table 1-8), the range is extremely wide (0.06 to 222.68). Consequently, there is a high degree of fractionation of these two major elements in the crusts from this region.

The relationships between Mn and the minor elements indicate that there are three distinct groups of crusts that can be distinguished within Survey Region B. The largest group of crusts has Mn concentrations ranging from 7 to 20 weight per cent, Mn/Fe ratios ranging from 0.41 to 1.56, and show strong positive linear correlations between Mn and Co, Cu, and Ni (Figure 1-26). Like the crusts from Survey Region A, this group of crusts is of hydrogenetic origin, since the Mn/Fe ratios are less than 2.5.

The two remaining groups of crusts are characterized by their distinctively different concentrations of Mn. One group is highly enriched in Mn ( > 30 weight per cent) and has Mn/Fe ratios ranging from 7.04 to 222.68. XRD analysis shows that birnessite together with a minor amount of todorokite, is present (Figure 1-27). As noted by Toth (1980), hydrothermal crusts consist of nearly pure, well-crystallized birnessite, identified by its intense peaks at 7.0-7.2Å, and 3.5-3.6Å, and todorokite with its most intense peaks at 9.65Å, 4.82Å (Burns & Burns, 1977). The second group is depleted in Mn ( < 3 weight per cent), and has Mn/Fe ratios ranging from 0.06 to 0.21. Both groups of crusts are depleted Co, Cu, and Ni compared to the hydrogenetic crusts. These two groups of crusts show the same fractionation of Mn and Fe and low concentrations of trace elements as the two groups of hydrothermal crusts identified by Toth (1980)

Figure 1-26. The relationship between Mn and other major elements. The open circles = hydrogenetic crusts, the filled circles = Mn-enriched hydrothermal crusts, the filled triangles = Mn-depleted hydrothermal crusts.





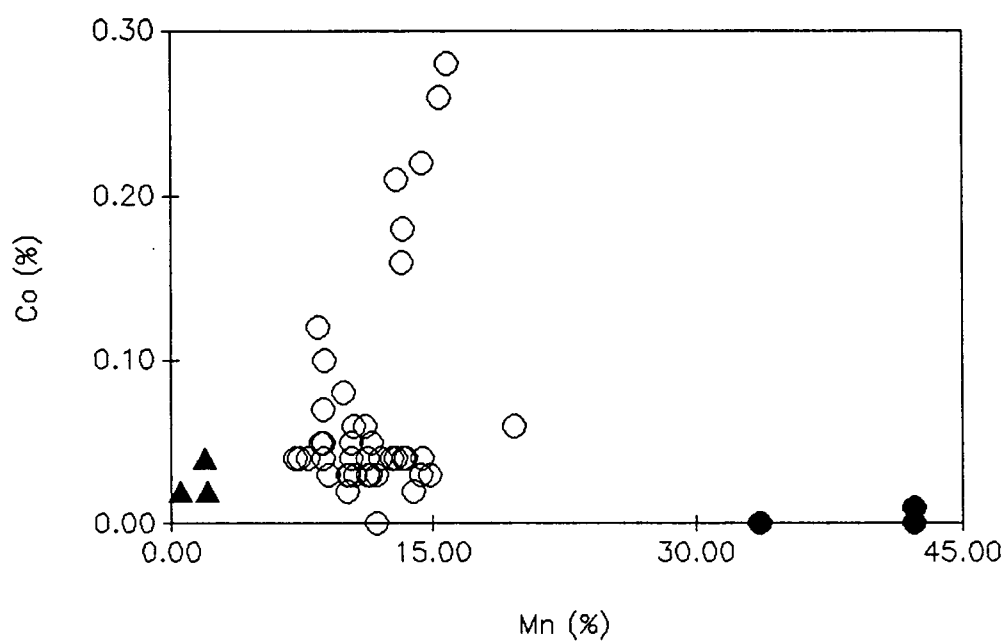
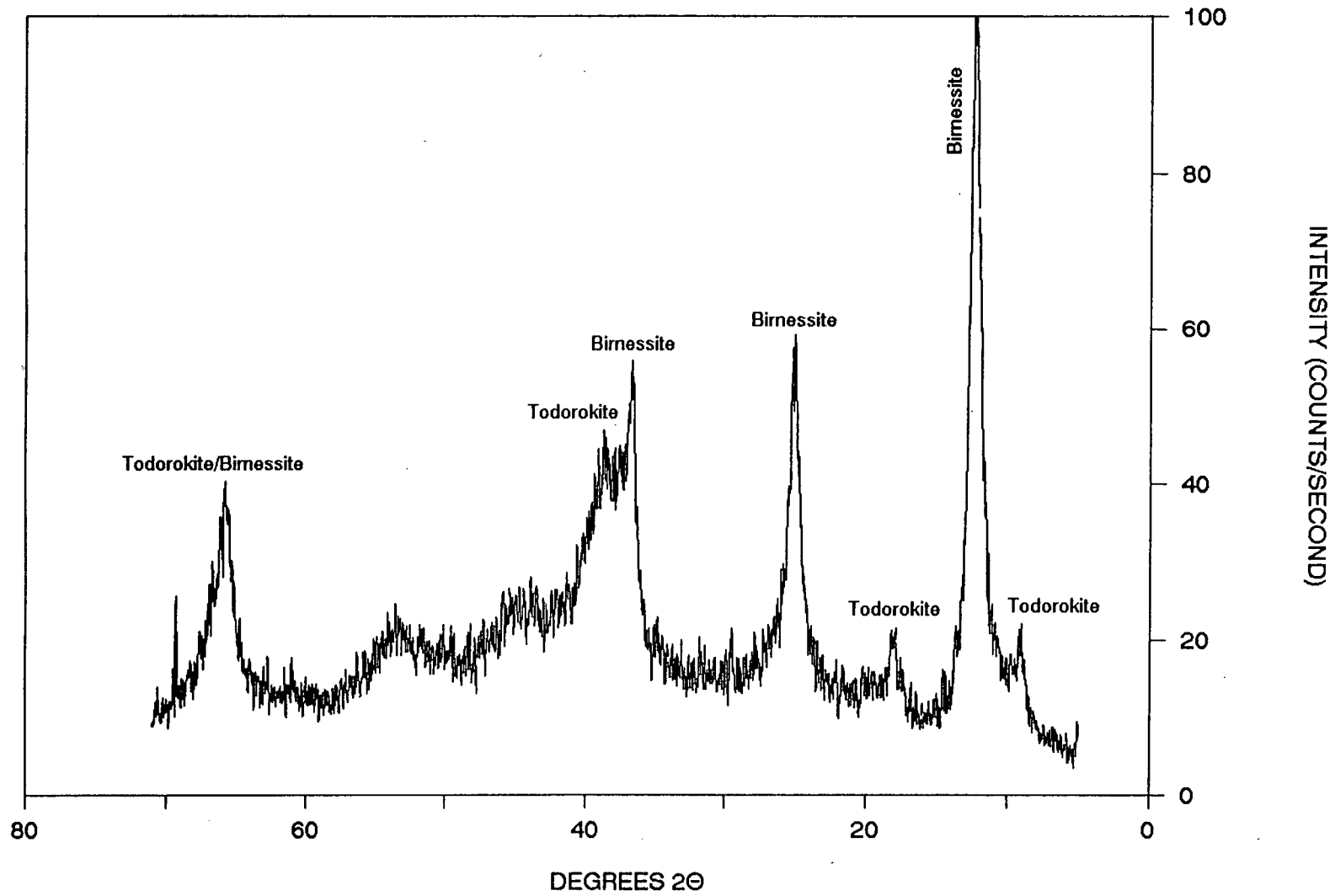


Figure 1-27. An XRD pattern of a crust which is enriched in Mn ( > 30 weight per cent).

# QBR 22 D-1



#### 1.4.2.1.3.4 Correlations with Iron

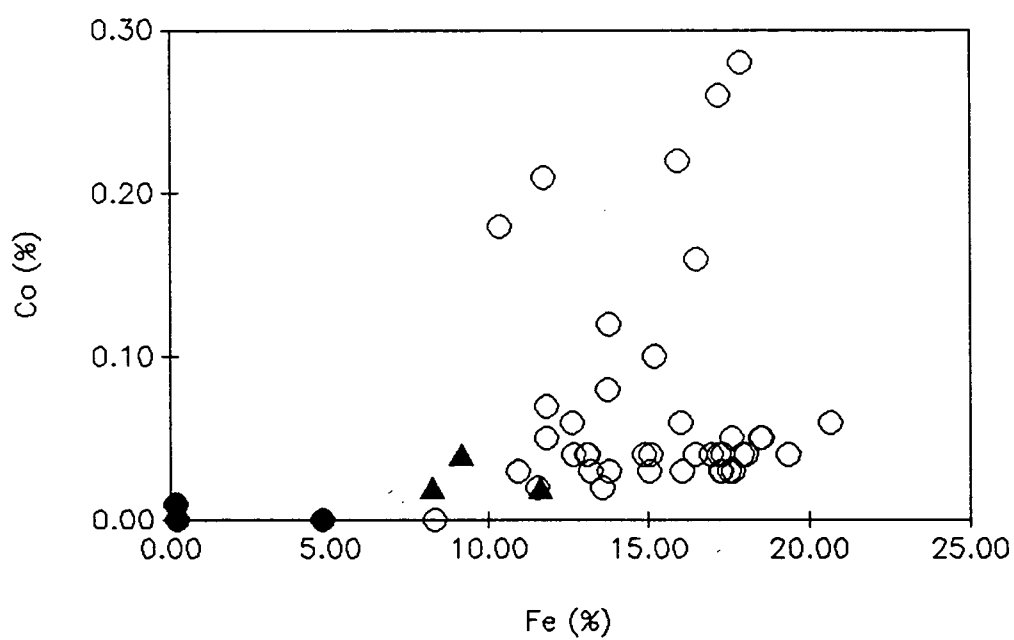
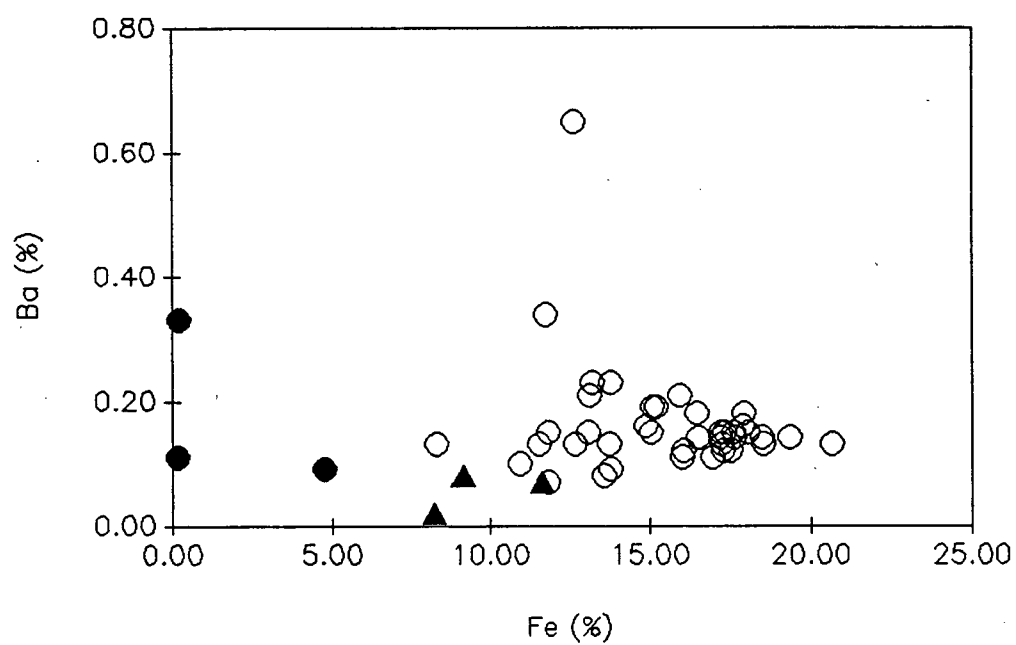
The concentrations of the elements that correlate positively with Fe (Ba, Co, P, and Zn) do not show the same marked difference between the three groups of crusts from this region (Figure 1-28).

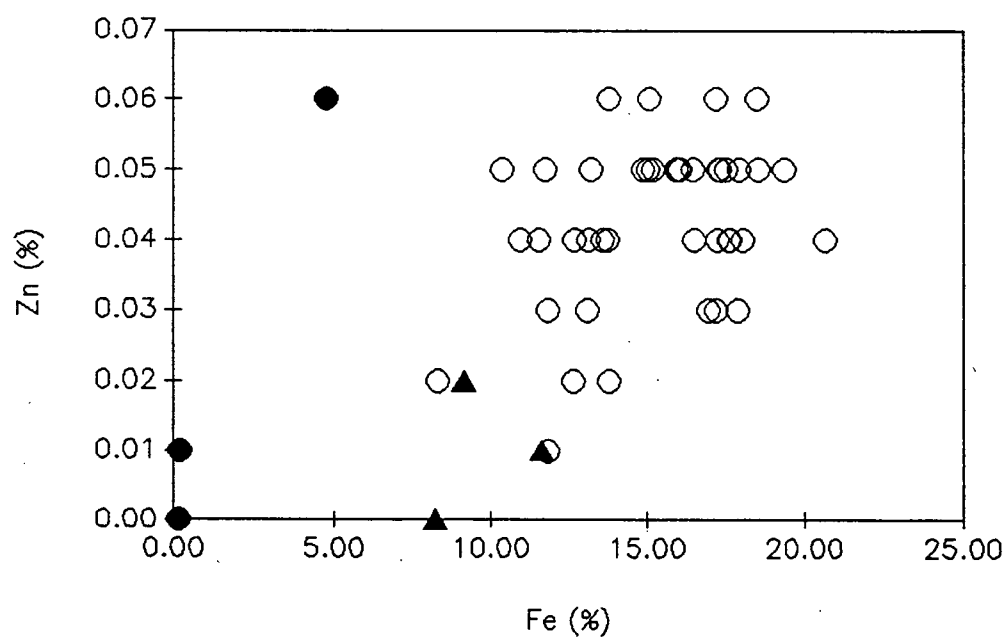
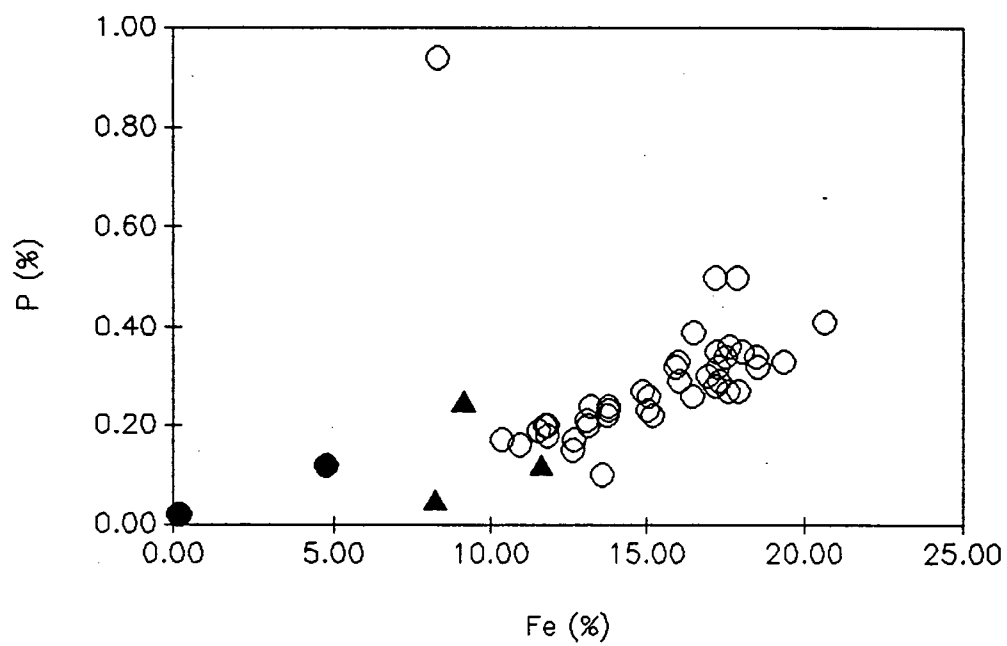
The high degree of correlation between P and Fe has not been observed previously in oceanic ferromanganese crusts. A correlation between Fe and P was first noted in oceanic ferromanganese nodules by Calvert & Price (1977a). A marked enrichment of P in the Fe phase of many shallow marine and lacustrine nodules has also been described by Sevast'yanov & Volkov (1966), Winterhalter (1966), Winterhalter & Siivola (1967), and Calvert & Price (1970; 1977b). This association has been attributed to the adsorption of P by hydrous ferric oxides (Winterhalter & Siivola, 1967) or to the formation of a ferric phosphate phase (Sevast'yanov & Volkov, 1966). The enrichment of P in the iron-rich sediments accumulating on the EPR has been explained in a similar way by Berner (1973). Since the P concentrations at equivalent Fe concentrations in hydrothermal crusts are consistent with those from the hydrogenous crusts, it is possible that either the adsorption of P by hydrous ferric oxides or the formation of a ferric phosphate phase can explain this observed association.

#### 1.4.2.1.4 Correlation Between Cobalt Abundance and Distance from the EPR

The concentration of Co in the hydrogenetic crusts from this region is significantly lower than that in the hydrogenetic crusts from Survey Region A. This trend in the depletion of Co in crusts with increasing proximity to the EPR is in agreement with the results of Manheim & Lane-Bostwick (1988). They concluded

Figure 1-28. The relationship between Fe and other major elements. The open circles = hydrogenetic crusts, the filled circles = Mn-enriched hydrothermal crusts, the filled triangles = Mn-depleted hydrothermal crusts.







that the depletion of Co in crusts is a reflection of the location and intensity of submarine hydrothermal discharge. Hydrothermal vent waters are greatly enriched in Fe and Mn with respect to normal waters, but Co:Mn and Co:Mn+Fe ratios for both vent fluids and marine hydrothermal oxides are two orders of magnitude lower than in normal ocean waters. Cobalt in crusts, therefore, is concentrated in inverse proportion to the regional influence of discharging hydrothermal fluids. The largest depletion of Co will be found in crusts recovered from the EPR. Higher Co concentrations are found in crusts farther removed from the hydrothermal discharge of the EPR with the highest Co concentrations found in the central parts of the Pacific Ocean.

Although the concentrations of Cu, Ni, and Zn are also depleted in hydrothermal crusts compared to hydrogenetic crusts recovered from Survey Region B, these elements do not show the same increase in concentration in crusts which are far removed from the hydrothermal influence of the EPR. It appears that no other major element shows such a trend in concentration with proximity to the EPR in this study.

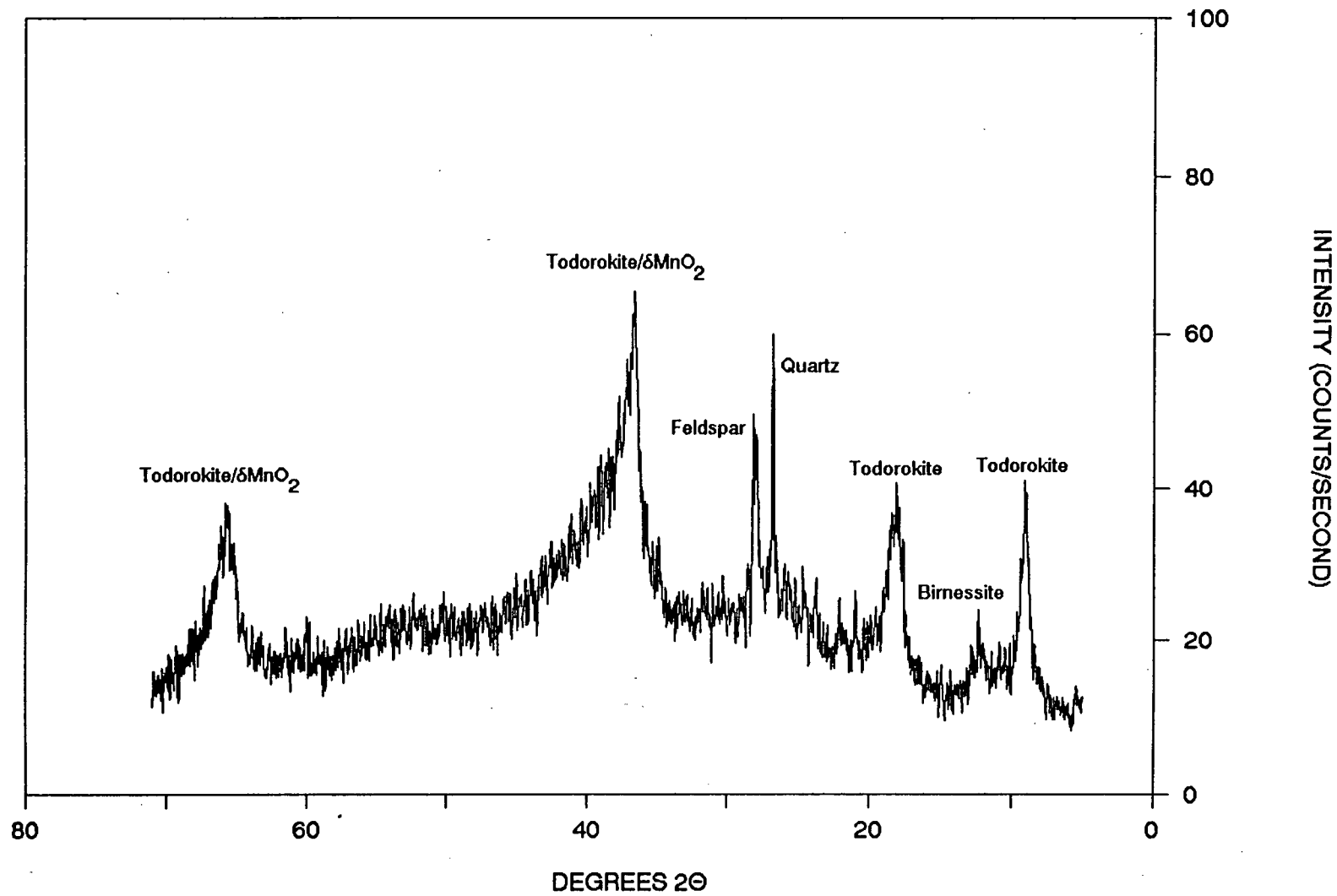
#### 1.4.2.2 Nodules

##### 1.4.2.2.1 Mineralogy

A typical XRD pattern of a nodule from Survey Region B, shows that the mineralogy of nodules from this region is dominated by todorokite, with minor amounts of birnessite and  $\delta\text{MnO}_2$  (Figure 1-29). The todorokite/ $\delta\text{MnO}_2$  ratios range from 0.00 to 2.68 with an mean of 1.12. Also shown in Figure 1-29 is the presence of quartz and feldspar. Once again, the XRD pattern shows the presence of a fine-grained, poorly crystalline material which has been previously identified as

**Figure 1-29. A typical XRD pattern of a nodule from Survey Region B.**

# B 104



being cryptocrystalline or amorphous hydrated iron oxides (Glasby, 1972; Crerar & Barnes, 1974). A more detailed study on the iron oxide phase mineralogy of crusts and nodules will be discussed in Chapter 2 and Chapter 3.

#### 1.4.2.2.2 Bulk Composition

The major element data for nodules recovered from Survey Region B are listed in Appendix D. As for samples recovered from Survey Region A, this compositional data will be used to estimate the relative proportions of the iron and manganese oxides and other phases in the crusts, and help interpret inter-element associations which will be discussed later.

The mean composition of nodules from this region is listed in Table 1-10, together with the average compositions of crusts and nodules from four other studies from within the same area. From Table 1-10, the compositions of the crusts show a very wide range in Mn, Fe, Cu, Ni, and Co concentrations, while the two average compositions of the nodules are similar. The mean concentrations of Cu, Ni, and Co in nodules from this study are significantly lower than the averages of the nodules reported by Cronan & Tooms (1969) and Skornyakova (1979), but are consistently higher than the average composition of the crusts reported by Lonsdale *et al.* (1980) and Bonatti *et al.* (1972). The mean concentration of Mn and Fe in nodules from this study is similar to those reported by Cronan & Tooms (1969) and Skornyakova (1979), but falls between the two extreme concentrations in the crusts. The average Mn/Fe ratio for the nodules from this study is 2.74 which is similar to the Mn/Fe ratio of the average composition of the nodules studied by Cronan & Tooms (1969) and by Skornyakova (1979) but falls between the two extreme Mn/Fe ratios of the crusts.

Table 1-10. Mean concentrations of major elements in nodules from Survey Region B. Concentrations are given in weight per cent.

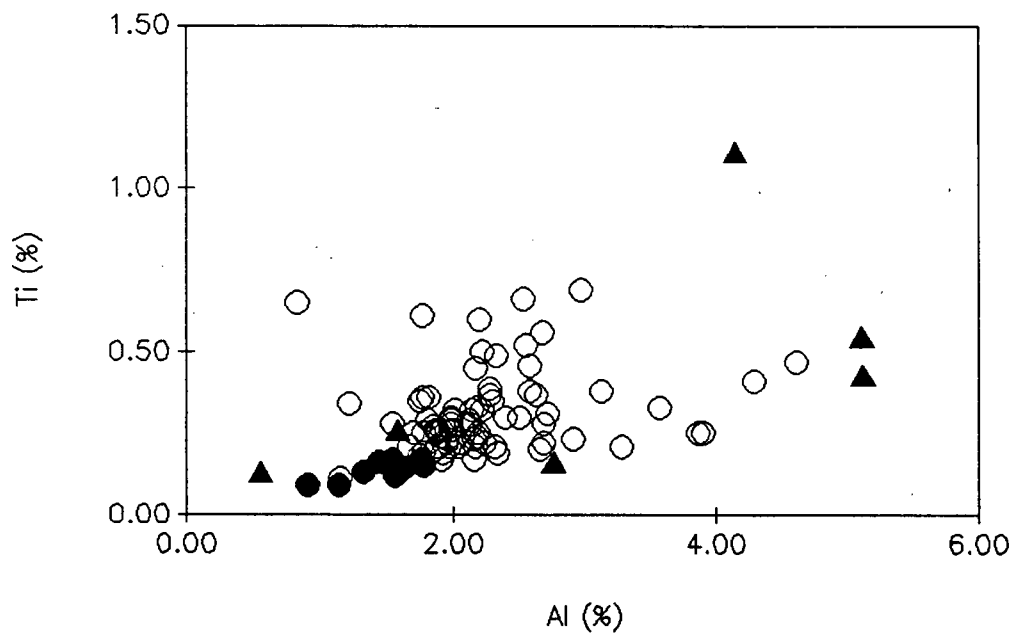
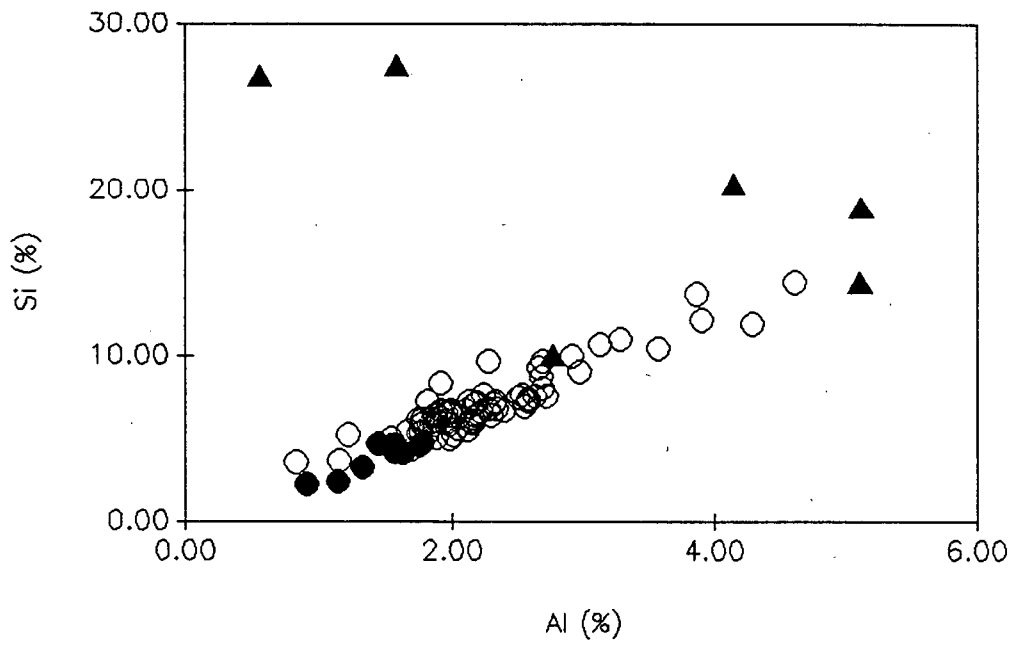
Mean Composition of nodules from Survey region B.		Average composition of nodules from the N.E. Pacific Ocean (Cronan & Tooms, 1969)		Average composition of nodules from the equatorial Pacific (Skornyakova, 1979)	
Element	Concen.	Element	Concen.	Element	Concen.
Si	7.55				
Ti	0.30	Ti	0.43	Ti	0.60
Al	2.23				
Fe	7.97	Fe	9.44	Fe	7.98
Mn	21.81	Mn	22.33	Mn	23.10
Mg	1.74				
Ca	1.79				
Na	1.61				
K	0.91				
P	0.31				
Co	0.12	Co	0.19	Co	0.18
Ni	0.71	Ni	1.08	Ni	1.10
Cu	0.46	Cu	0.63	Cu	0.89
Zn	0.09	Zn	0.11	Zn	0.11
Ba	0.24	Ba	0.38		
Mn/Fe	2.74	Mn/Fe	2.37	Mn/Fe	2.89

### 1.4.2.2.3 Interelement Associations

#### 1.4.2.2.3.1 Correlations with Aluminium

The nature of the aluminosilicates in the nodules is shown by the relationship between Al and other major elements. For the nodules, aluminium shows a strong positive correlation with Si, Ti, and K (Figure 1-30). From the X-ray diffractogram (Figure 1-29), these correlations with Al could be explained by the presence of quartz and feldspar. By using the Si/Al, Ti/Al, and K/Al element ratios, the origin of the aluminosilicate fraction of the nodules can be identified. As shown in Table 1-11, the Si/Al, Ti/Al, and K/Al ratios are 3.39, 0.13, and 0.09 respectively. The Si/Al ratio for the nodules is considerably higher than those for the Average Pacific Pelagic Clay and for the MORB from the EPR, while the Ti/Al and the K/Al ratios for the nodules are relatively close to that of the MORB. Although the Ti/Al and K/Al ratios may indicate that the aluminosilicate fraction of the nodules originates from MORB from the EPR, the Si/Al ratio suggests that several sources of Si contribute to the nodules from this region. In nodules located close to the EPR, the abundance of silicon is determined by two sources: (1) incorporation of detrital aluminosilicates which are composed of eolian debris and volcanogenic debris eroded from submarine outcrops by bottom currents (Hein *et al.*, in press a); (2) an additional source of Si precipitated from hydrothermal sources (Toth, 1980). According to Toth (1980), iron- and silica rich hydrothermal crusts are composed of iron-rich nontronite or amorphous hydrated iron oxides and silica, with very low trace-metal contents.

Figure 1-30. The relationship between Al and other major elements. The open circles = hydrogenous and diagenetic nodules, the filled circles = Mn-enriched hydrothermal nodules, the filled triangles = Mn-depleted hydrothermal nodules.





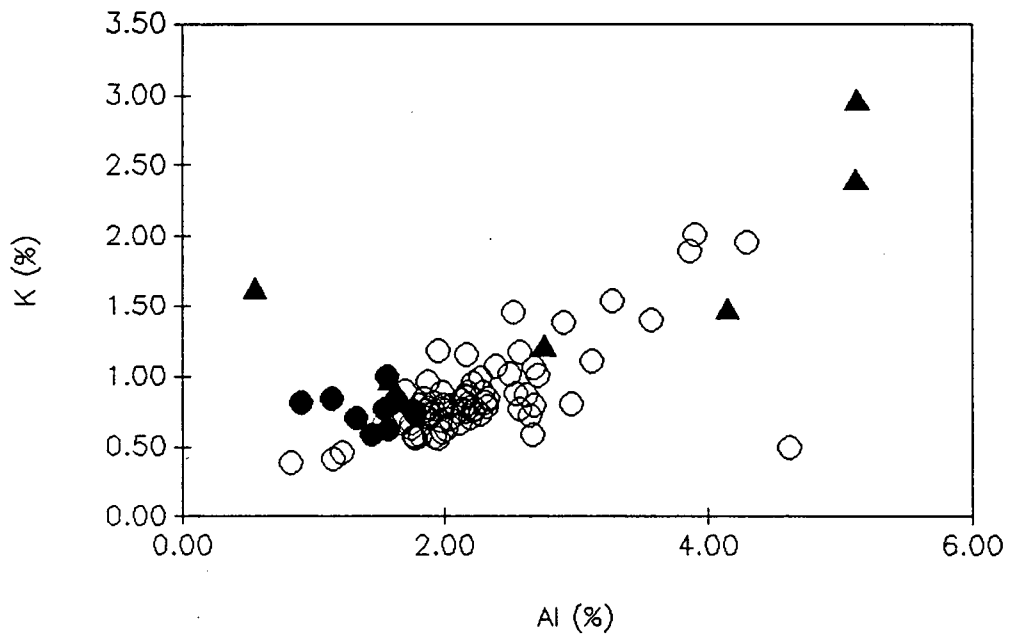


Table 1-11. Comparison of the composition of aluminosilicates in nodules to Average Pacific Pelagic Clay and Mid-Ocean Ridge Basalts.

	Element Ratios		
	Si/Al	Ti/Al	K/Al
Nodules from Survey Region B (This Study)	3.39	0.13	0.09
Average Pacific Pelagic Clay (Bischoff et al., 1979)	2.92	0.06	0.25
Average Mid-Ocean-Ridge Basalts from the E.P.R. (Melson et al., 1976)	2.99	0.13	0.02

#### 1.4.2.2.3.2 Phosphorite

Although the concentrations of Ca and P in the nodules from this region are considerably lower than those in the nodules from Survey Region A, they do show a positive correlation (Figure 1-31). An XRD tracing of a nodule with high Ca and P concentrations shows that this correlation is due to the presence of carbonate fluorapatite  $\{(Ca,Mg,Na,K)_{10}[(P,C)O_4]_6(F,OH)_2\}$  (Figure 1-32).

The presence of carbonate fluorapatite has already been used to explain the correlation of P with Ca in crusts from this same region. The presence of carbonate fluorapatite in nodules is possibly due to the erosion of carbonate fluorapatite from the neighbouring seamounts and its incorporation into the nodules as a nuclei.

#### 1.4.2.2.3.3 Correlations with Manganese

Although the nodules from Survey Region B have an average Mn/Fe ratio of 2.74 (Table 1-10), the range is extremely wide (0.63 to 23.93). Consequently, there is a high degree of fractionation of these two major elements in the nodules from this region. Although the range of Mn/Fe ratios for the nodules is not as extreme as for the crusts ( $0.06 \leq \text{Mn/Fe} \leq 222.68$ ), element correlations will be considered with respect to Mn concentrations to provide a comparison with the crusts from this same region.

The relationships between Mn and the minor elements indicate that three distinct groups of nodules can be distinguished within Survey Region B. The largest group of nodules has Mn concentrations ranging from 10 to 30 weight per cent, Mn/Fe ratios between 0.75 and 7.70, and show strong positive linear correlations between Mn and Co, Cu, Ni, Zn, Mg, and Ba (Figure 1-33). Unlike nodules from Survey Region A, this group of nodules does not show a distinct division between

Figure 1-31. The correlation between Ca and P. The open circles = hydrogenous and diagenetic nodules, the filled circles = Mn-enriched hydrothermal nodules, the filled triangles = Mn-depleted hydrothermal nodules.

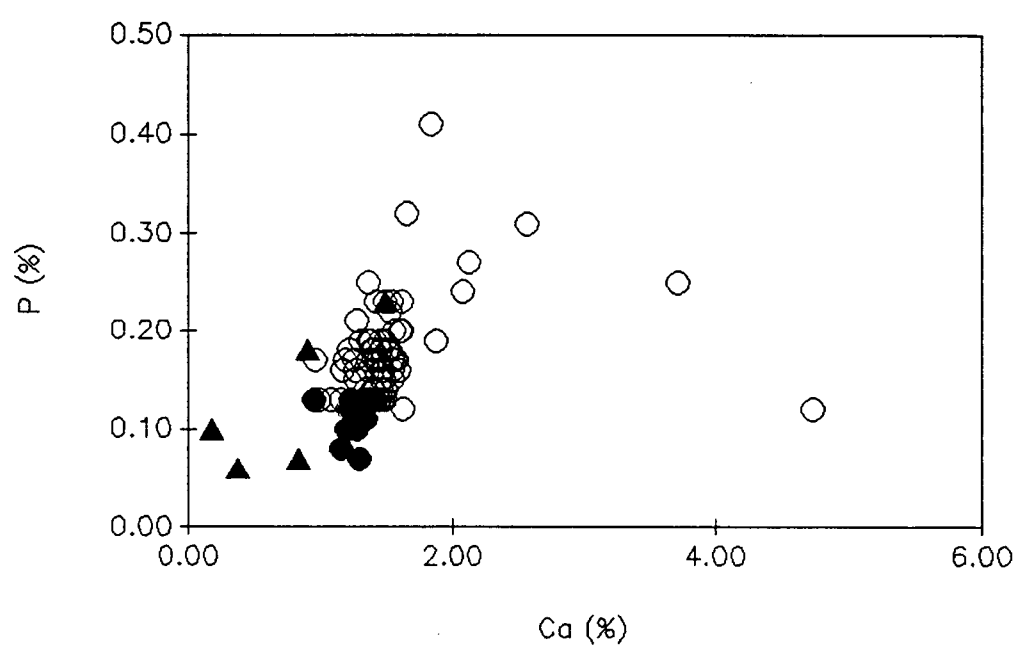


Figure 1-32. An XRD pattern of a nodule with high Ca and P concentraions.

# Mn 26

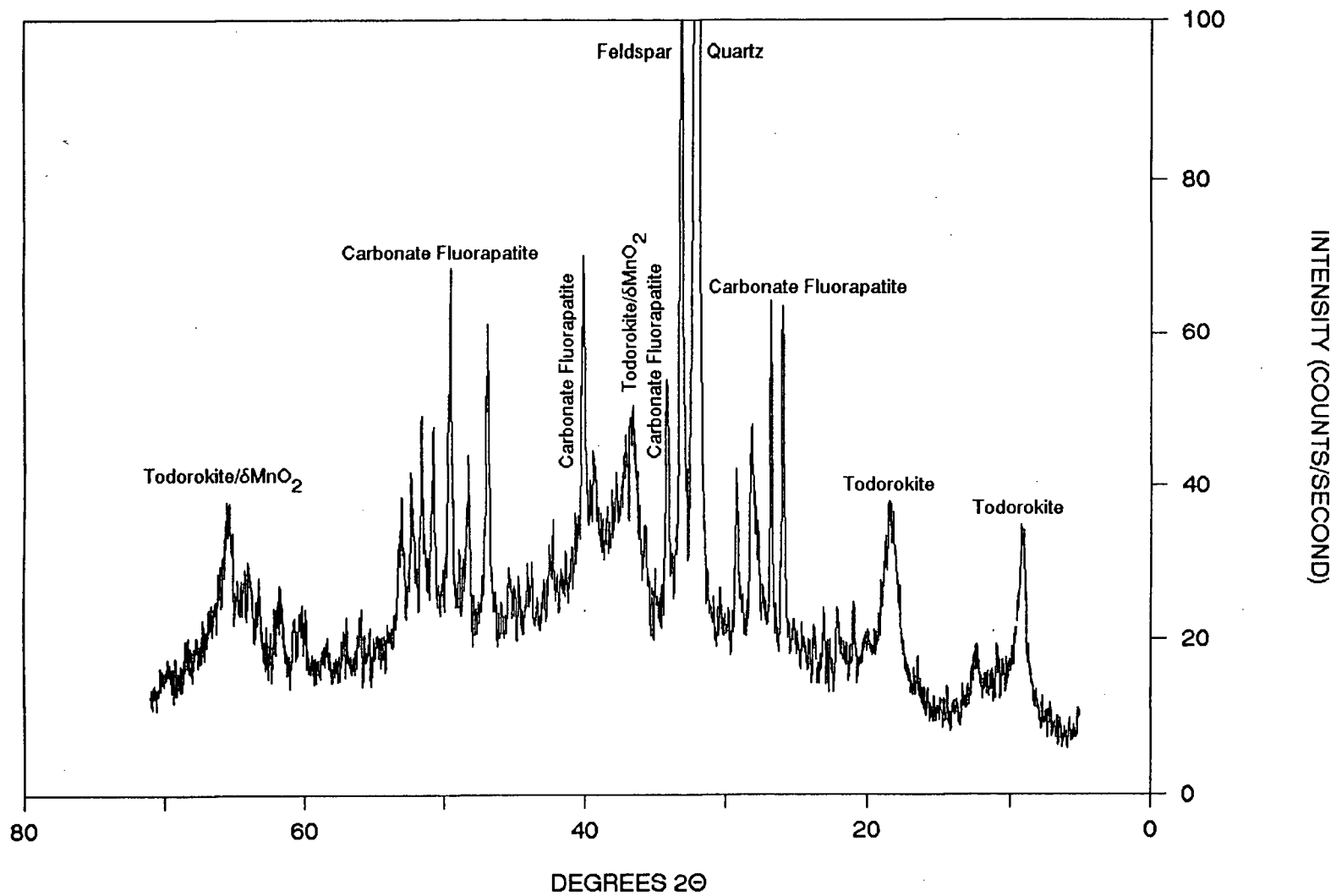
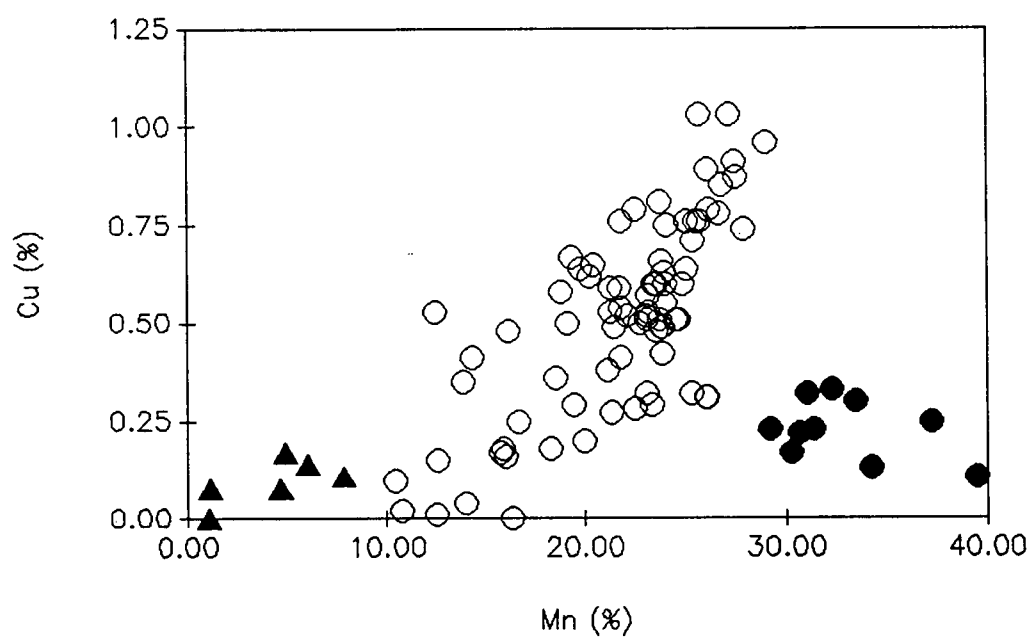
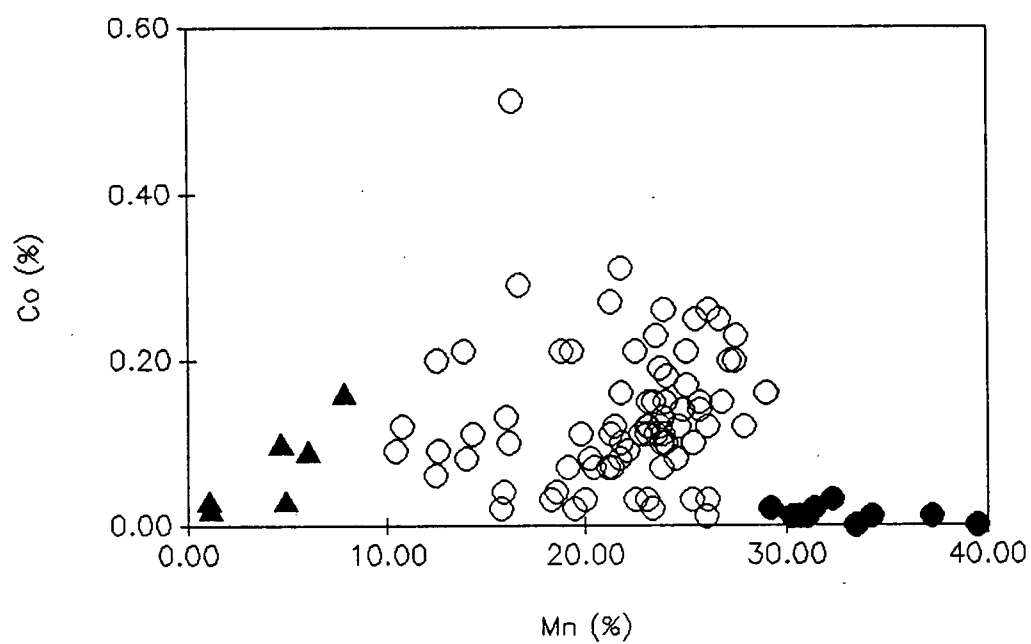
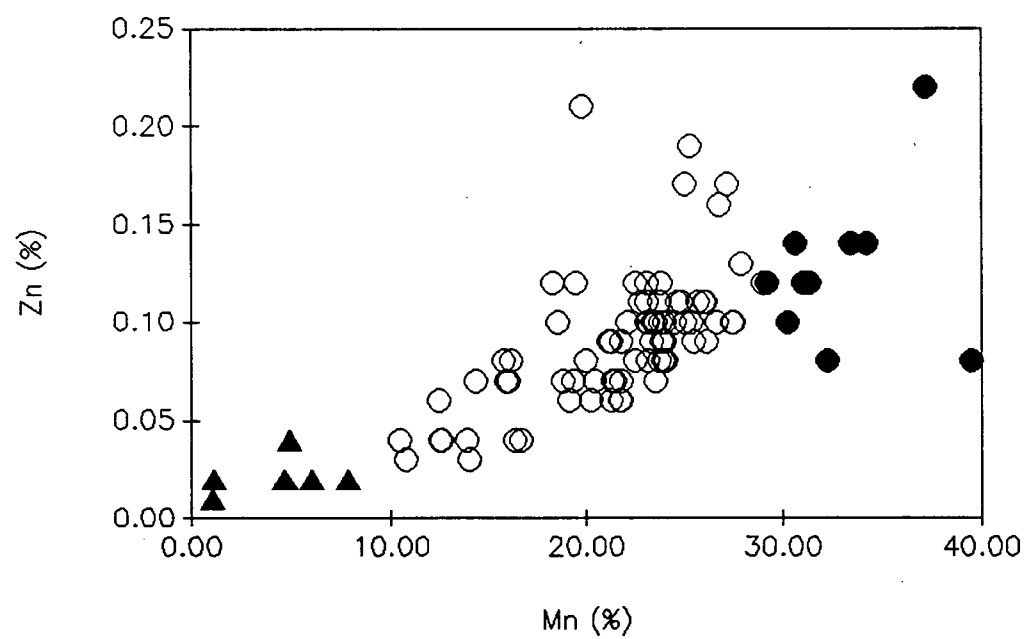
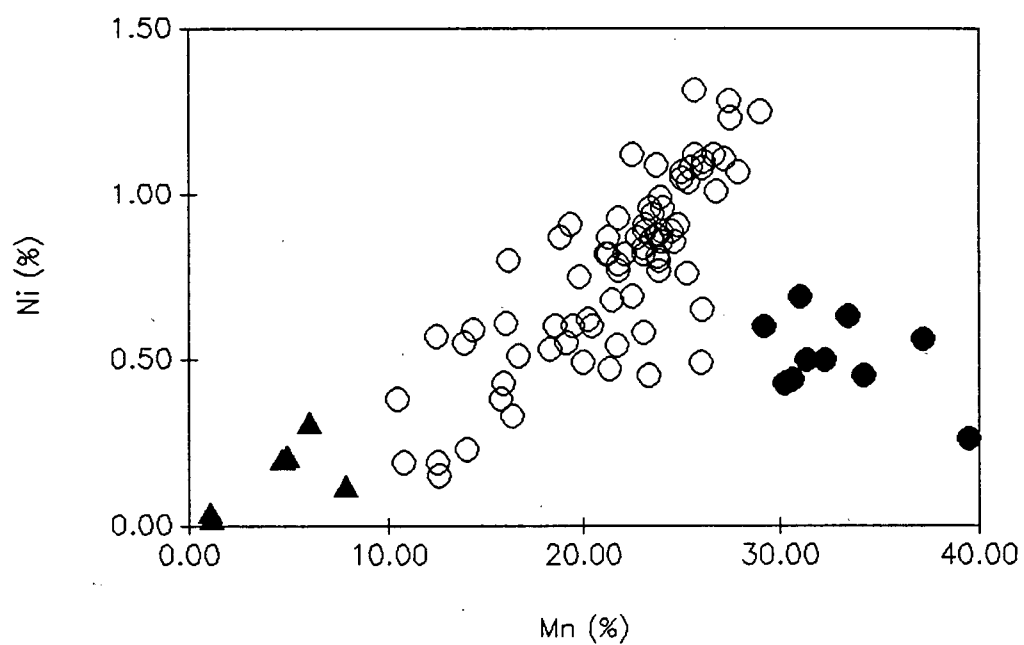
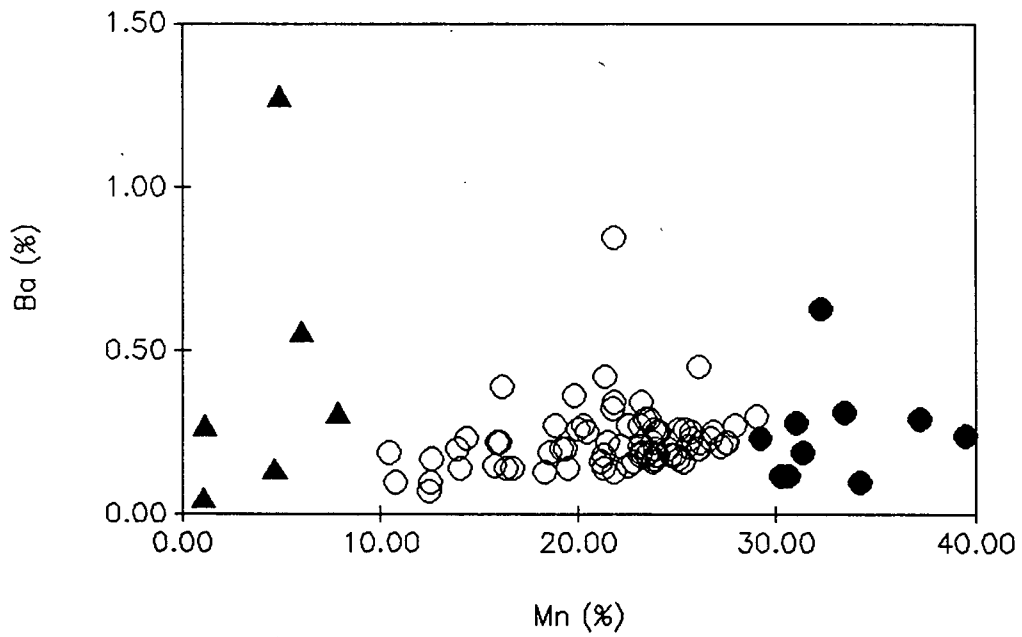
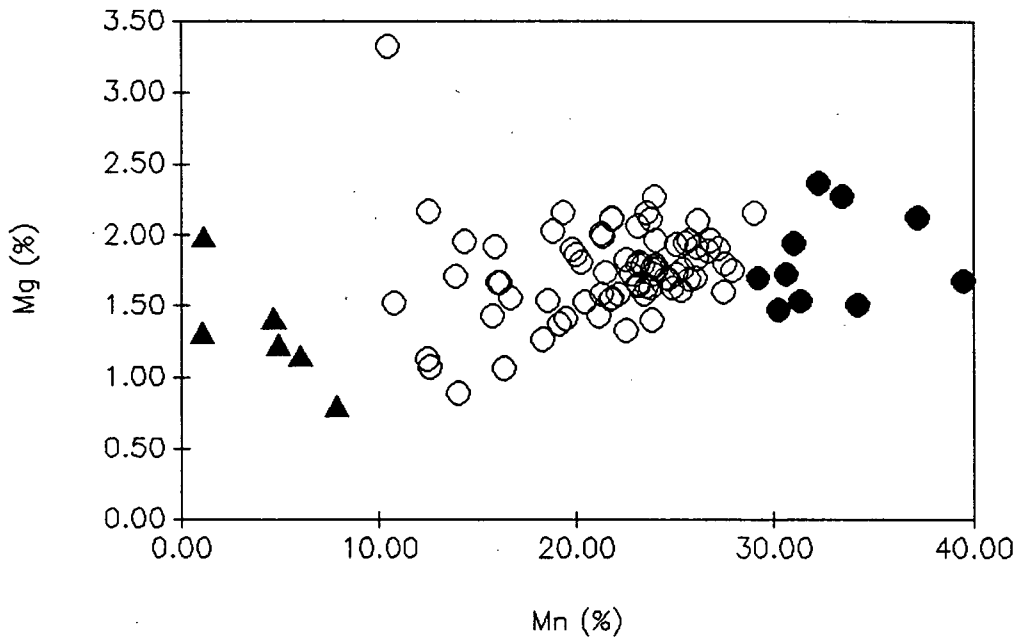


Figure 1-33. The relationship between Mn and other major elements. The open circles = hydrogenous and diagenetic nodules, the filled circles = Mn-enriched hydrothermal nodules, the filled triangles = Mn-depleted hydrothermal nodules.









hydrogenous nodules ( $\text{Mn/Fe} < 2.5$ ) and diagenetic nodules ( $\text{Mn/Fe} > 2.5$ ). Although the range of Mn/Fe ratios shows that these two types of nodules are present, the two groups do not show the same variation in interelement correlations as seen in Survey Region A. For identification purposes, this large group of nodules will be called hydrogenous nodules.

The two remaining groups of nodules are characterized by their distinctively different concentrations of Mn. One group is highly enriched in Mn ( $> 30$  weight per cent), has Mn/Fe ratios ranging from 4.96 to 23.93 and low concentrations of Cu, Ni, and Co compared with the hydrogenous group. XRD analysis shows that todorokite, together with minor birnessite, is present (Figure 1-34). As noted by Toth (1980), hydrothermal crusts consist of nearly pure, well-crystallized birnessite, identified by its intense peaks at  $7.0\text{-}7.2\text{\AA}$ , and  $3.5\text{-}3.6\text{\AA}$ , and todorokite, with its most intense peaks at  $9.65\text{\AA}$ ,  $4.82\text{\AA}$  (Burns & Burns, 1977). The second group of nodules is depleted in Mn ( $< 10$  weight per cent), and has Mn/Fe ratios ranging from 0.06 to 0.96. This group also has low concentrations of Cu, Ni, Co and Zn, as would be explained for the low Mn and todorokite contents.

#### 1.4.2.2.3.4 Correlations with Iron

The concentrations of the elements that correlate positively with Fe, (P, Ti and Si), do not show the same marked difference between the three groups of nodules from this region (Figure 1-35). A correlation between Fe and P was also noted in oceanic ferromanganese nodules by Calvert & Price (1977a). A marked enrichment of P in the Fe phase of many shallow marine and lacustrine nodules has also been described by Sevast'yanov & Volkov (1966), Winterhalter (1966), Winterhalter & Siivola (1967), and Calvert & Price (1970; 1977b). This association has been attributed to the adsorption of P by hydrous ferric oxides (Winterhalter &

Figure 1-34. An XRD pattern of a nodule which is enriched in Mn  
( > 30 weight per cent).

# CERS 21 D-3

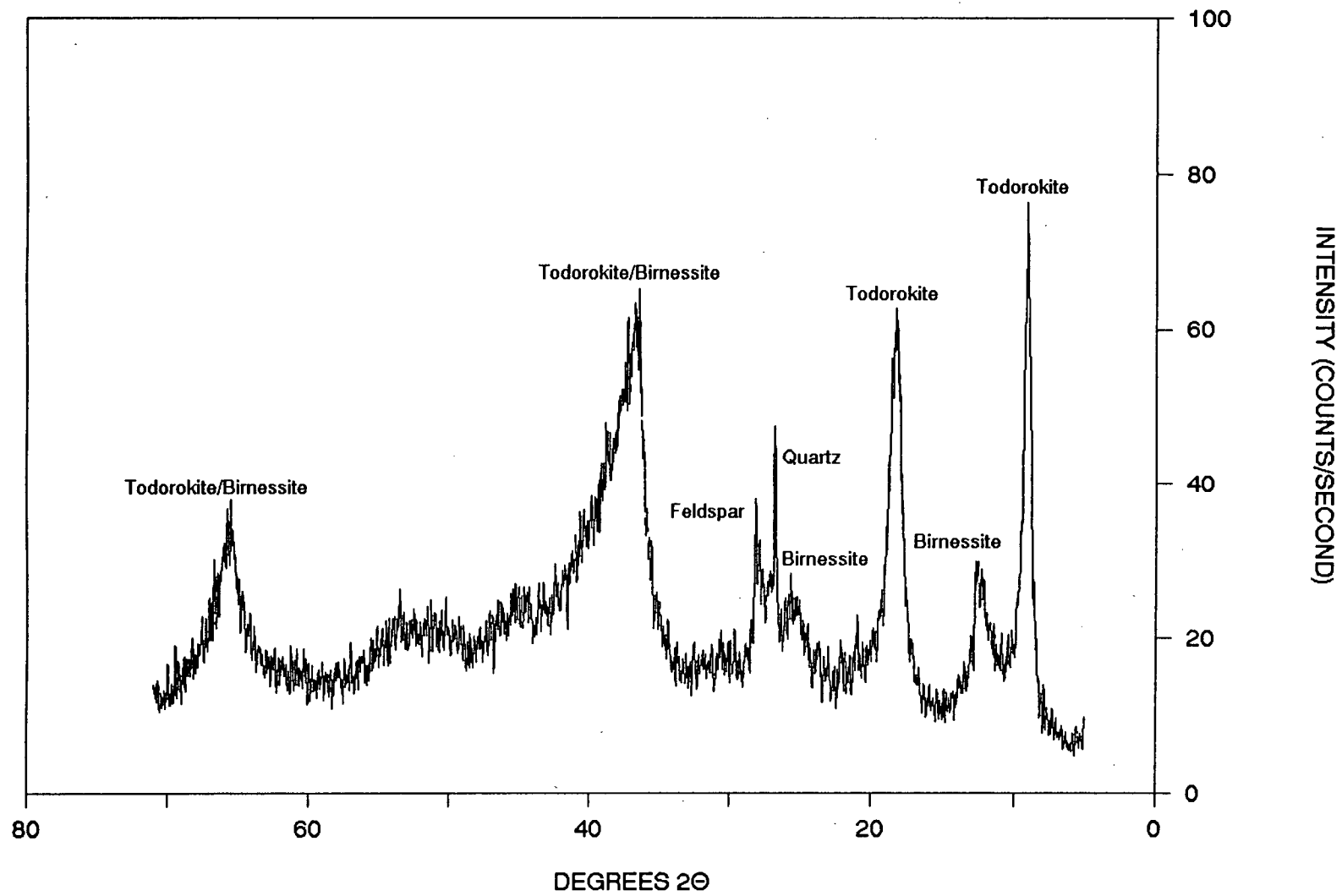
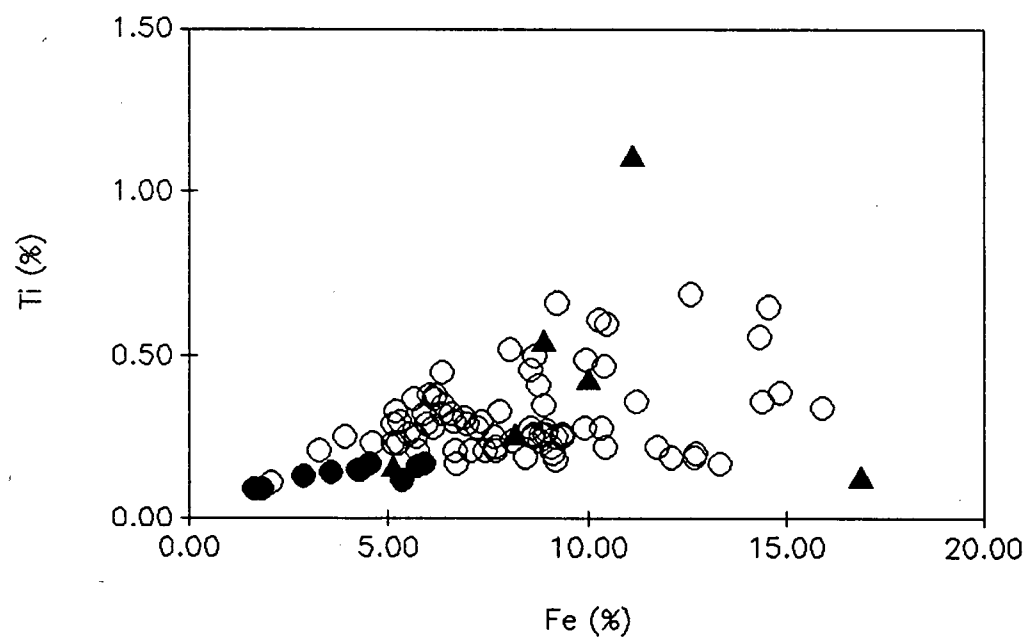
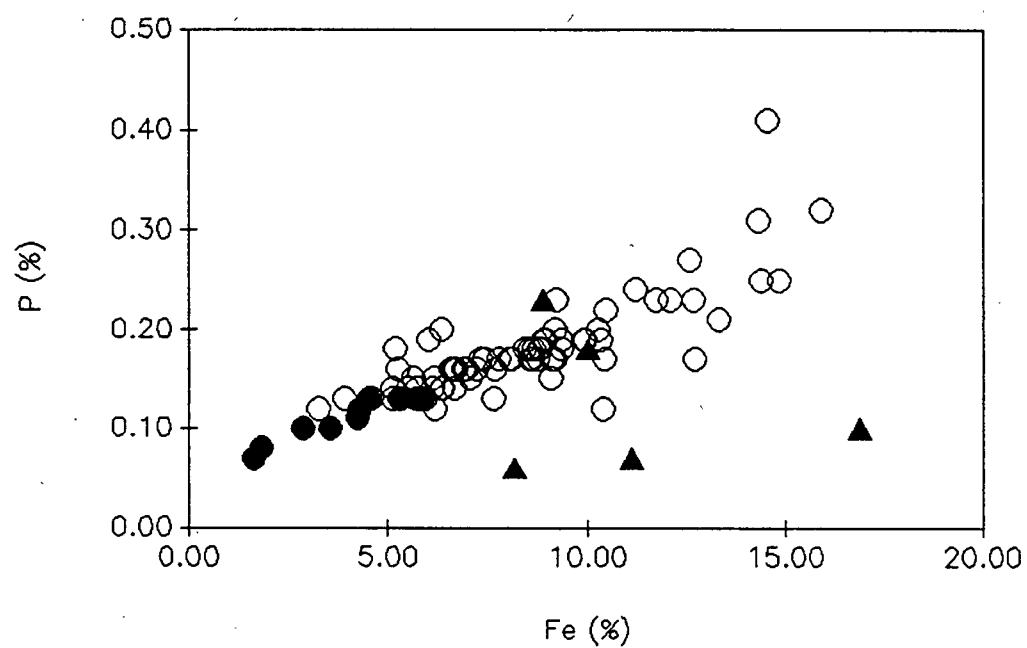


Figure 1-35. The relationship between Fe and other major elements. The open circles = hydrogenous and diagenetic nodules, the filled circles = Mn-enriched hydrothermal nodules, the filled triangles = Mn-depleted hydrothermal nodules.







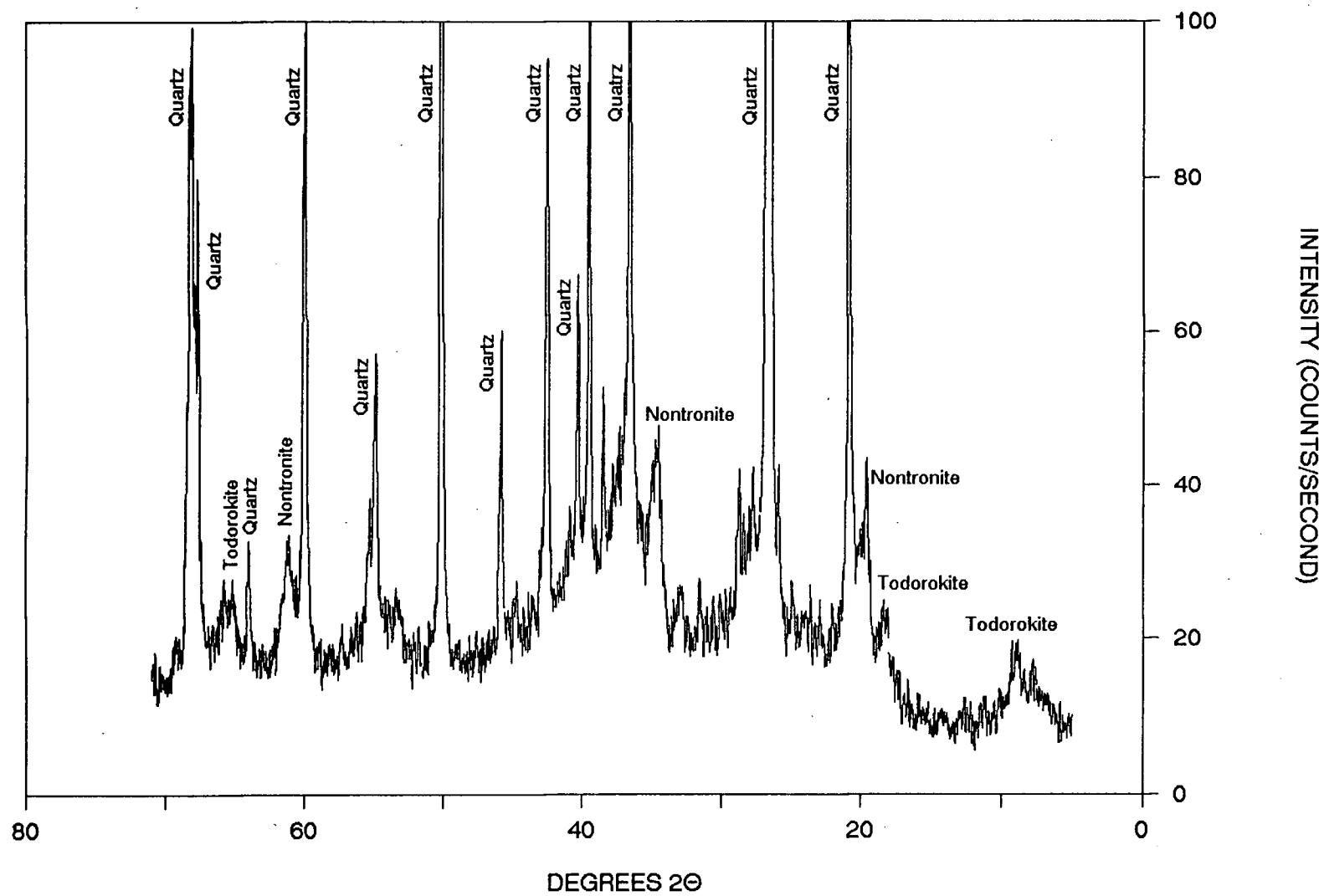
Siivola, 1967) or to the formation of a ferric phosphate phase (Sevast'yanov & Volkov, 1966). The enrichment of P in the iron rich sediments accumulating on the EPR has been explained in a similar way by Berner (1973). Except for three of the Fe-rich hydrothermal nodules, the P concentrations at equivalent Fe concentrations in hydrothermal crusts are similar to those from the hydrogenous crusts, it is possible that either the adsorption of P by hydrous ferric oxides or the formation of a ferric phosphate phase can explain this observed association.

For nodules located close to the EPR, the abundance of silicon is determined by two sources: (1) incorporation of detrital aluminosilicates which are composed of eolian debris and volcanogenic debris eroded from submarine outcrops by bottom currents (Hein *et al.*, in press a); (2) an additional source of Si precipitated from hydrothermal sources (Toth, 1980). According to Toth (1980), iron- and silica rich hydrothermal crusts are composed of iron-rich nontronite or amorphous hydrated iron oxides and silica, with very low trace-metal contents. An X-ray diffractogram of a nodule with high concentrations of Fe and Si and low concentrations of trace elements (Figure 1-36) shows that nontronite and quartz are the dominant iron- and silica rich phases present.

The correlation between Fe and Ti has also been noted in the crusts studied by Manheim & Lane-Bostwick (1989) and in nodules studied by Goldberg (1954), Burns & Fuerstenau (1966), Cronan (1967), and by Arrhenius *et al.* (1979). Manheim & Lane-Bostwick (1989) reported that the behavior of the Fe-Ti relationship is still poorly understood and much of the scatter is probably due to admixture in the detrital component.

**Figure 1-36. An XRD pattern of a nodule with high concentrations of Fe and Si and low concentrations of trace elements.**

# DWBD 1-2



#### 1.4.2.2.3.5 Identification of the Two Groups of Hydrothermal

##### Nodules

Because of the different geochemical behavior of Fe and Mn, fractionation of the two elements is common in hydrothermal solutions (Lyle, 1981). This results in the formation of two distinct end member deposits: (1) Well-crystallized birnessite and todorokite crusts with generally very low trace metal content, and (2) Iron- and silica-rich crusts composed of iron-rich nontronite or amorphous hydrated iron oxides and silica, also with very low trace metal contents. The fractionation of Fe and Mn occurs as a result of the lower solubility of iron species as both Fe and Mn undergo oxidation (Krauskopf, 1957) by mixing of the reduced hydrothermal fluid with oxygenated bottom water. The association of Si with Fe may result from coprecipitation or adsorption of dissolved  $\text{SiO}_2$  onto hydrated iron-oxide colloids. The low content of minor elements in these deposits results from: (1) the low concentrations of these elements relative to Fe and Mn in hydrothermal solutions, and (2) the rapid deposition of the deposits which minimizes adsorption of elements from seawater (Toth, 1980).

These two groups of crusts with distinct end-member compositions and mineralogy were identified in the crusts from Survey Region B. One group of hydrothermal crusts was found to be enriched in Mn and depleted in Fe and Si. The Mn-rich mineral phase was identified to be todorokite and birnessite. The second group of hydrothermal crusts was found to be enriched in Fe and Si and depleted in Mn. The Fe-Si rich mineral phase was identified as amorphous hydrated iron oxides and silica. Both groups of hydrothermal crusts were depleted in Co, Cu, and Ni.

Unlike crusts, nodules do not form by the direct precipitation of hydrothermal fluids, however, two groups of nodules, from Survey Region B, showed identical trends in composition and mineralogy as the two groups of hydrothermal crusts. One

group of hydrothermal nodules were found to be enriched in Mn and depleted in Fe and Si. The Mn-rich mineral phase was identified to be todorokite and birnessite. The second group of hydrothermal nodules was found to be enriched in Fe and Si and depleted in Mn. The Fe-Si rich mineral phase was identified as iron-rich nontronite. Both groups of hydrothermal nodules were depleted in Co, Cu, and Ni.

The two groups of hydrothermal nodules with this distinct end-member compositions and mineralogy have also been identified by Dymond *et al.* (1984) and by Chen & Owen (1989) in nodules from the eastern equatorial Pacific. In their study of nodules from the north equatorial Pacific, Dymond *et al.* (1984) proposed that the chemical composition of nodules from the three nodule-bearing MANOP sites in the Pacific can be accounted for in a qualitative way by variable contributions of distinct accretionary processes. They proposed that these accretionary modes are: (1) hydrogenous, the direct precipitation or accumulation of colloidal metal oxides in seawater; (2) oxic diagenesis, the variety of ferromanganese accretion processes occurring in oxic sediments; and (3) suboxic diagenesis, the reduction of  $\text{Mn}^{4+}$  by oxidation of organic matter in the sediments. They concluded that processes (1) and (2) occur at all three MANOP nodule bearing sites and process (3) occurs only at site H. Chen & Owen (1989) used these results to interpret the factor analyses of geochemical data from nodules representing a broad area of the southeast Pacific Ocean. They concluded that nodule compositions are controlled by four factors: (1) suboxic diagenesis; (2) oxic diagenesis; (3) hydrogenous precipitation; and (4) hydrothermal precipitation. Three of these four factors are identical to those identified by Dymond *et al.* (1984) (Chen & Owen, 1989).

In the study by Chen & Owen (1989), they identified the hydrothermal nodules as being enriched in Fe but depleted in Mn, Co, Cu, and Ni. This composition agrees with the Fe-Si rich hydrothermal crusts and nodules identified in Survey Region B and the Fe-Si rich hydrothermal crusts studied by Toth (1980).

Both Dymond *et al.* (1984) and Chen & Owen (1989), however, misinterpreted the Mn-rich end-member composition of hydrothermal nodules. Dymond *et al.* (1984) stated that suboxic diagenesis results in accretion of material which is Mn-rich but depleted in other transition metals. They further stated that suboxic diagenesis results in an unstable todorokite which transforms to a 7Å phase (birnessite) upon dehydration. From their limited growth rate data for nodules from MANOP site H, they also concluded that suboxic accretion is the fastest of the three processes with rates at least 200mm/10<sup>6</sup>yr. The compositions of the suboxic diagenetic nodules described by Dymond *et al.* (1984) and by Chen & Owen (1989) are identical to both the Mn-rich hydrothermal crusts and nodules from Survey Region B and the Mn-rich crusts studied by Toth (1980). Although no growth rates have been determined for nodules that have been identified as being hydrothermal, rapid growth rates of greater than 100mm/Myr for hydrothermal crusts located near the EPR have been proposed by Manheim & Lane-Bostwick (1988), Toth (1980), and Moore & Vogt (1976).

#### 1.4.2.2.4 Variations with Depth

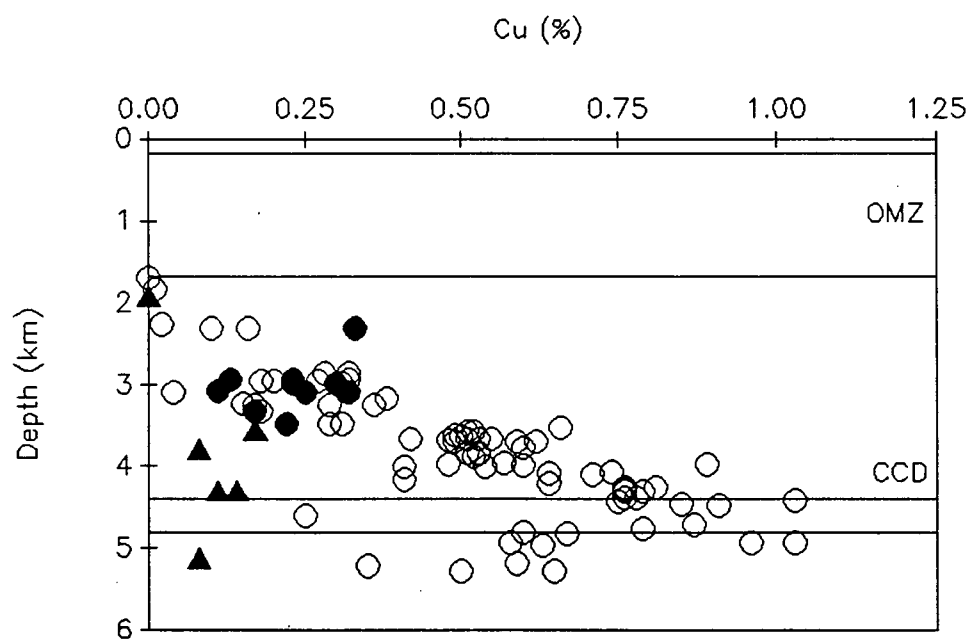
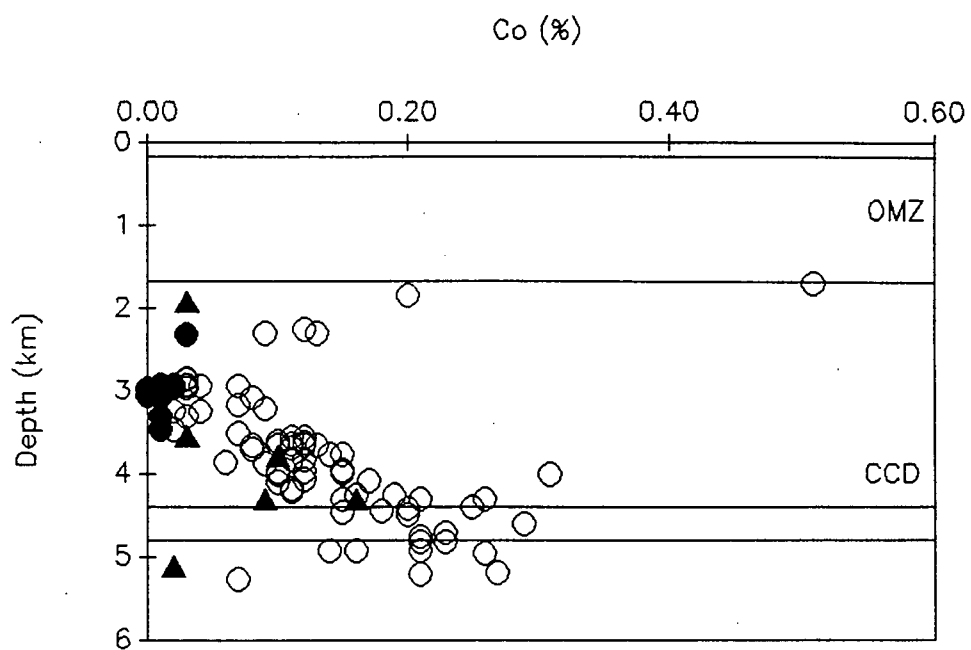
##### 1.4.2.2.4.1 Behaviour of Manganese and Iron

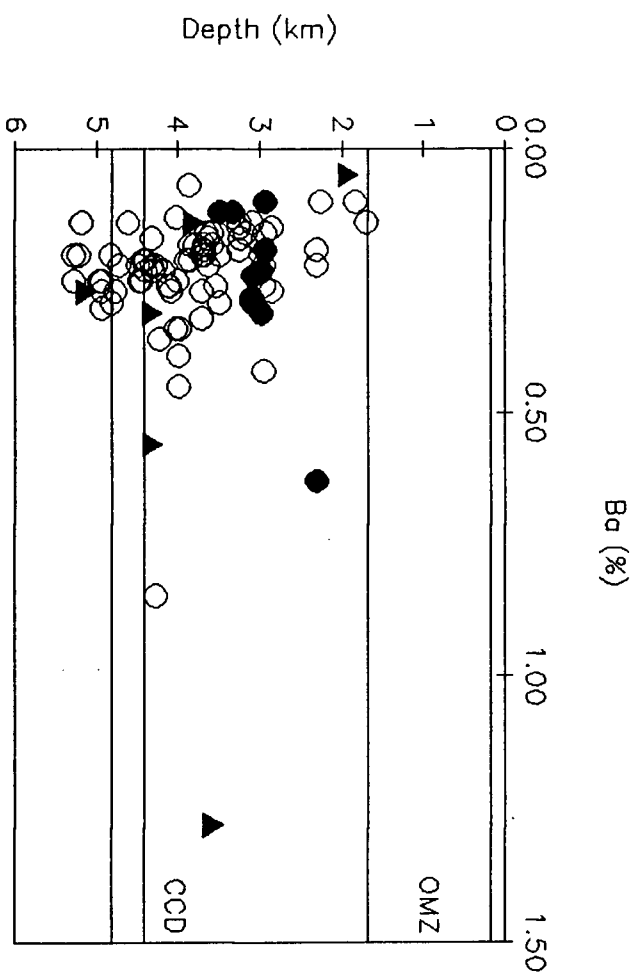
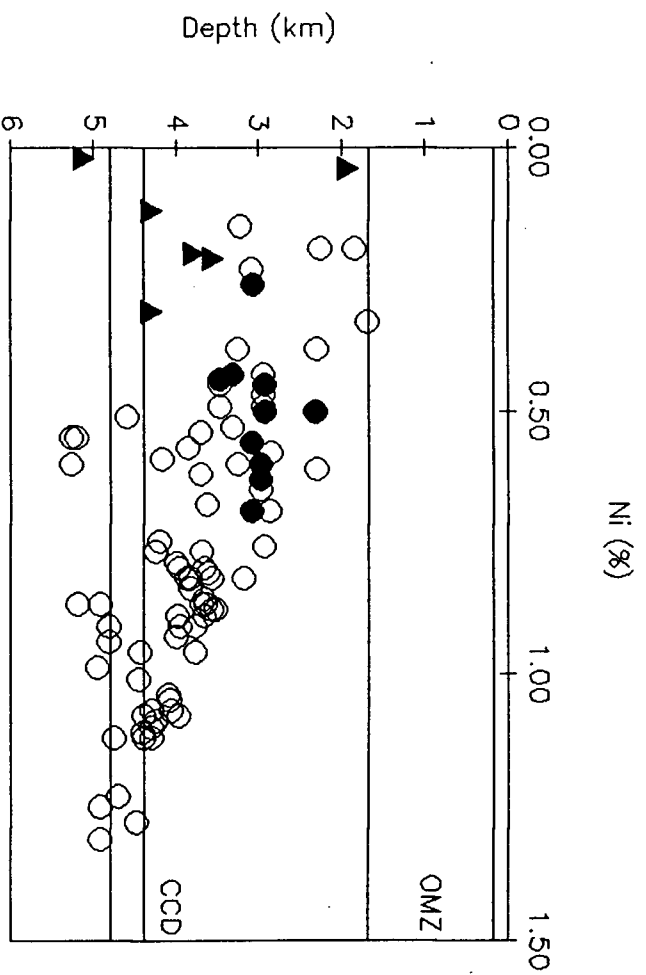
Unlike the nodules from Survey Region A, the composition of nodules from Survey Region B, appears to be related to water depth. Of those elements that show an association with Mn, Co, Cu, Ni, and Ba increase in concentration with increasing depth (Figure 1-37).

To understand the correlation between nodule composition and water depth, the source of constituent elements must be identified. Halbach & Puteanus (1984b) have proposed that for hydrogenetic crusts from the central Pacific Ocean which

Figure 1-37. The correlation between Mn and those elements that are associated with Mn and water depth. The open circles = hydrogenous and diagenetic nodules, the filled circles = Mn-enriched hydrothermal nodules, the filled triangles = Mn-depleted hydrothermal nodules.



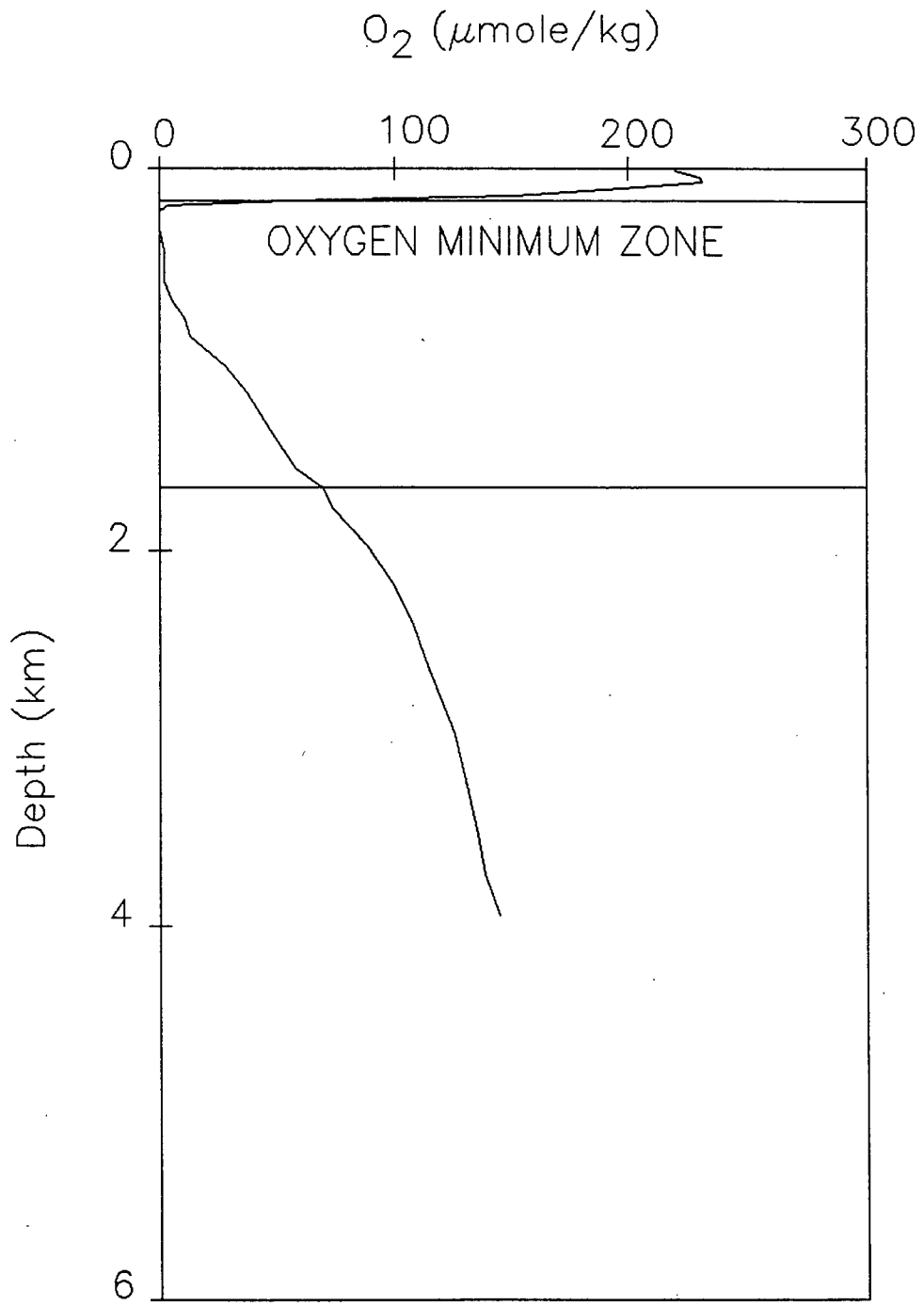




show a change in composition with depth, the main sources of Mn and its associated trace metals is colloidal Mn-hydroxide particles that are released in the water column from the dissolution of carbonate plankton skeletons and a further source of Mn and its associated trace metals supplied via the OMZ. Within the OMZ there is a high concentration of dissolved Mn as a result of the *in situ* decomposition of organic matter along with the insitu reduction of Mn-bearing solid phases (Klinkhammer & Bender, 1980; Landing & Bruland, 1980). This zone of maximum concentration of  $\text{Mn}^{2+}$  produces a flux of  $\text{Mn}^{2+}$  by diffusion and turbulent mixing into shallower and deeper waters which have an increased oxygen content. This causes oxidation of the  $\text{Mn}^{2+}$  and results in the formation of hydrated  $\text{MnO}_2$  particles which are incorporated into the hydrogenetic crusts (Halbach *et al.*, 1988). The extent of the OMZ in the eastern equatorial Pacific and the depletion of oxygen within this zone, are shown in Figure 1-38. Geosecs Station 343 is located within Survey Region B at 16°31.1'N and 122°59.3'W. Based on this profile at this site, the OMZ within Survey Region B lies at water depths of between 171 and 1675m; the minimum dissolved oxygen concentration is 0  $\mu\text{mole/kg}$ .

The metal concentrations in the nodules continue to increase below the CCD which is found between the water depths 4400 and 4800m (Berger *et al.*, 1976; Heath *et al.*, 1977; Piper *et al.*, 1979). The abyssal seafloor between the CCFZ lies below a zone of high biological productivity and is characterized by the presence of siliceous ooze with low sedimentation rates due to the erosional influence of the bottom waters. Biological production at the sea surface is considered to be the principal means of concentration of trace metals in the marine environment (Friedrich *et al.*, 1983). Trace metals are incorporated in the soft parts or tests of plankton, or perhaps are adsorbed to test surfaces (Lyle, 1978). After the organism dies, these metals are then transported to the seafloor where *in situ* dissolution is the principal mechanism making these metals available to the formation of manganese nodules

Figure 1-38. The profile of the O<sub>2</sub> concentration in seawater at Geosecs Station 343.



(Andrews *et al.*, 1983; Glasby & Thijessen, 1982b). As proposed by Stoffers *et al.* (1981), the enhanced supply of Ni, Cu, and Ba to the nodules in the equatorial high productivity zone is due to the dissolution of tests within the sediment column. Unlike Stoffers *et al.* (1981), significant correlations were found between the composition of nodules from Survey Region B and depth. When describing the regional setting of the abyssal seafloor between the CCFZ, it was stated that the CCD within the CCFZ ranges in depth from 4800m in the south to 4400m in the north (Berger *et al.*, 1976; Heath *et al.*, 1977; Piper *et al.*, 1979). The increase in concentrations of the elements Cu, Ni, and Ba with increasing depth can possibly be attributed to the biological productivity at the sea surface and the *in situ* dissolution at depth due to the CCD where diagenetic processes make these elements available for the formation of nodules. The increase in the concentrations of Co, Cu, Ni, and Ba in nodules with increasing depth below the CCD is possibly caused by the continued supply of these elements due to the dissolution of siliceous tests during early diagenesis (Halbach *et al.*, 1981b; Stoffers *et al.*, 1981).

#### 1.4.2.2.4.2 Behaviour of Cobalt

The positive linear correlation between Co and depth in nodules from Survey Region B, can also be explained by examining the regional bathymetry of the abyssal seafloor between the CCFZ. Subsidence of the cooling oceanic crust, formed at the EPR, has led to generally increasing regional water depths from the EPR to the west. The depth of the seafloor in Survey Region B is therefore an indicator of its distance from the EPR.

As proposed by Manheim & Lane-Bostwick (1988), the depletion of Co in Pacific crusts indicates the location and intensity of submarine hydrothermal discharge. They found that Co-enriched crusts are found where water masses are

most isolated from hydrothermal activity. In contrast, cobalt-depleted crusts coincide with known areas of hydrothermal activity. This same association between the depletion of Co and the location and intensity of hydrothermal discharge seems to apply to the nodules recovered from Survey Region B. Those nodules that are located close to the EPR occur in water depths of about 3000m (Figure 1-3). These nodules are found to have Co below 0.05 weight per cent (Figure 1-37). Those nodules located farthest away from the EPR occur in deeper water (Figure 1-3) and are enriched in Co (  $> 0.20$  weight percent) (Figure 1-37). This is the first time that the depletion of Co due to the hydrothermal influence of the EPR has been noted in oceanic ferromanganese nodules from the Eastern Equatorial Pacific.

## 1.5 REFERENCES

- Abbey, S., 1983. Studies in "standard samples" of silicate rocks and minerals 1969-1982. Geol. Surv. Can., Pap. 83-15, 114 pp.
- Andrews, J.E., 1971. Abyssal hills as evidence of transcurrent faulting on North Pacific Fracture Zones. Geol. Soc. Am. Bull., 82:463-470.
- Andrews, J.E., Craig, J.D., & Hardy, W.A., 1977. Investigations of the deep-sea floor by side-scan sonar techniques: Central Eastern Pacific. Deep-Sea Research, 24:975-986.
- Andrews, J.E., & Friedrich, G.H.W., 1979. Distribution patterns of manganese nodule deposits in the northeast equatorial Pacific. Mar. Min., 2(1-2):1-43.
- Andrews, J., Friedrich, G., Pautot, G., Plüger, W., Renard, V., Melguen, M., Cronan, D., Craig, J., Hoffert, M., Stoffers, P., Shearme, S., Thyssen, T., Glasby, G., LeNotre, N., & Saget, P., 1983. The Hawaii-Tahiti Transect: The oceanographic environment of manganese nodule deposits in the Central Pacific. Mar. Geol., 54:109-130.
- Aplin, A.C., & Cronan, D.S., 1985a. Ferromanganese oxide deposits from the central Pacific Ocean, I. Encrustations from the Line Islands Archipelago. Geochim. Cosmochim. Acta, 49:427-436.
- Aplin, A.C., & Cronan, D.S., 1985b. Ferromanganese oxide deposits from the central Pacific Ocean, II. Nodules and associated sediments. Geochim. Cosmochim. Acta, 49:437-451.
- Arrhenius, G., Cheung, K., Crane, S., Fisk, M., Frazer, J., Korkisch, J., Mellin, T., Nakao, S., Tsai, A., & Wolf, G., 1979. Counterions in marine manganates. La Genèse des Nodules du manganèse, Gif-Sur-Yvette, Colloques Internationaux, C.N.R.S. No. 289, pp. 333-356.
- Berger, W.H., Adeleck Jr., A.A., & Mayer, L.A., 1976. Distribution of carbonate in surface sediments of the Pacific Ocean. J. Geophys. Res., 81(15):2617-2627.
- Berner, R.A., 1973. Phosphate removal from sea water by adsorption on volcanogenic ferric oxides. Earth Planet. Sci. Lett., 18:77-86.
- Best, M.G., 1982. Igneous and Metamorphic Petrology. W.H. Freeman and Company, New York, 630 pp.
- Bischoff, J.L., Heath, G.R., & Leinen, M., 1979. Geochemistry of deep-sea sediments from the Pacific manganese nodule province: DOMES Site A, B, and C. In Marine Geology and Oceanography of the Pacific Manganese Nodule Province (ed. by J.L. Bischoff & D.Z. Piper), Plenum Press, N.Y., pp. 397-436.
- Bonatti, E., Kraemer, T., Rydell, H., 1972. Classification and genesis of submarine iron-manganese deposits. In Ferromanganese Deposits on the Ocean Floor (ed. by D.R. Horn), National Science Foundation, Washington, D.C., pp. 149-166.



- Boström, K., & Peterson, M.N.A., 1966. Precipitates from hydrothermal exhalations on the East Pacific Rise. *Econ. Geol.*, 61:1258-1265.
- Burns, R.G., 1965. Formation of cobalt (III) in the amorphous  $\text{FeOOH} \cdot n\text{H}_2\text{O}$  phase of manganese nodules. *Nature*, 203(4975):999.
- Burns, R.G., 1976. The uptake of cobalt into ferromanganese nodules, soils, and synthetic manganese (IV) oxides. *Geochim. Cosmochim. Acta*, 40:95-102.
- Burns, R.G., & Burns, V.M., 1977. Mineralogy. In *Marine Manganese Deposits* (ed. by G.P. Glasby), Elsevier Scientific Publishing Company, Amsterdam, pp. 185-248.
- Burns, R.G., & Burns, V.M., 1979. Manganese Oxides. In *Mineralogical Society of America Short Course Notes, Marine Minerals* (ed. by R.G. Burns), Vol. 6. Lithocrafters Inc., Chelsea, Michigan, pp. 1-46.
- Burns, R.G., Burns, V.M., & Stockman, H.M., 1983. A review of the todorokite-buserite problem: Implications to the mineralogy of marine manganese nodules. *Amer. Min.*, 68:972-980.
- Burns, R.G., Burns, V.M., & Stockman, H.W., 1985. The todorikite-buserite problem: Further considerations. *Amer. Min.*, 70:205-208.
- Burns, R.G., & Fuerstenau, D.W., 1966. Electron-probe determination of inter-element relationships in manganese nodules. *Amer. Min.*, 51:895-902.
- Callender, E., & Bowser, C.J., 1980. Manganese and copper geochemistry of interstitial fluids from manganese-nodule-rich pelagic sediments of the northeastern equatorial Pacific Ocean. *Amer. J. Sci.*, 280:1063-1069.
- Calvert, S.E., 1978. Geochemistry of oceanic ferromanganese deposits. *Phil. Trans. R. Soc. Lond. A.*, 290:43-73.
- Calvert, S.E., Cousens, B.L., & Soon, M.Y.S., 1985. An X-ray fluorescence spectrometric method for the determination of major and minor elements in ferromanganese nodules. *Chem. Geol.*, 51:9-18.
- Calvert, S.E., & Piper, D.Z., 1984. Geochemistry of ferromanganese nodules from DOMES Site A, Northern Equatorial Pacific: Multiple diagenetic metal sources in the deep sea. *Geochim. Cosmochim. Acta*, 48:1913-1928.
- Calvert, S.E., & Price, N.B., 1970. Composition of manganese nodules and manganese carbonates from Loch Fyne, Scotland. *Contrib. Mineral. Petrol.*, 29:215-233.
- Calvert, S.E., & Price, N.B., 1977a. Geochemical variation in ferromanganese nodules and associated sediments from the Pacific Ocean. *Mar. Chem.*, 5:43-74.
- Calvert, S.E., & Price, N.B., 1977b. Shallow water, continental margin deposits: Distribution and geochemistry. In *Marine Manganese Deposits* (ed. by G.P. Glasby), Elsevier, Amsterdam, pp. 45-86.

- Calvert, S.E., Price, N.B., Heath, G.R., & Moore, T.C. Jr., 1978. Relationship between ferromanganese nodule compositions and sedimentation in a small survey area of the equatorial Pacific. *J. Mar. Res.*, 36:161-183.
- Carpenter, R., & Wakeham, S., 1973. Mössbauer studies of marine and freshwater manganese nodules. *Chem. Geol.*, 11:109-116.
- Chase, T.E., Menard, H.W., & Mammerickx, J., 1970. Bathymetry of the North Pacific. Scripps Inst. Oceanogr. and Inst. Mar. Res., Tech. Rep. Ser. TR-14.
- Chen, J.C., & Owen, R.M., 1989. The hydrothermal component in ferromanganese nodules from the southeast Pacific Ocean. *Geochim. Cosmochim. Acta*, 53:1299-1305.
- Clague, D.A., 1981. Linear island and seamount chain, aseismic ridges and intraplate volcanism: results from the Deep-Sea-Drilling-Project. *Soc. Econ. Paleont. and Min., Spec. Publ.*, 32:7-22.
- Corliss, J.B., 1971. The origin of metal-bearing submarine hydrothermal solutions. *Jour. Geophys. Research.*, 76:8128-8138.
- Craig, J.D., 1979. The relationship between bathymetry and ferromanganese deposits in the north equatorial Pacific. *Mar. Geol.*, 29:165-186.
- Craig, J.D., & Andrews, J.E., 1978. A factor analysis study of seep sea ferromanganese deposits in the equatorial north Pacific Ocean. *Mar. Min.*, 1(4):305-326.
- Crerar, D.A., & Barnes, H.L., 1974. Deposition of deep-sea manganese nodules. *Geochim. Cosmochim. Acta*, 38:279-300.
- Cronan, D.S., 1967. The geochemistry of some manganese nodules and associated pelagic sediments. Ph.D. Thesis, Univ. of London, unpublished, 342 pp.
- Cronan, D.S., 1980. Manganese Nodules and Encrustations. *In* *Underwater Minerals*, Academic Press, pp. 61-169.
- Cronan, D.S., & Tooms, J.S., 1969. The geochemistry of manganese nodules and associated pelagic deposits from the Pacific and Indian Oceans. *Deep-Sea Research*, 16:335-359.
- Dillard, J.G., Crowther, D.L., & Murray, J.W., 1982. The oxidation states of cobalt and selected metals in Pacific ferromanganese nodules. *Geochim. Cosmochim. Acta*, 46:755-759.
- Dymond, J., Lyle M., Finney, B., Piper, D., Murphy, K., Conard, R., & Pisias, N., 1984. Ferromanganese nodules from MANOP sites H,S, and R - control of mineralogical and chemical composition by multiple accretionary processes. *Geochim. Cosmochim. Acta*, 48:931-949.
- Elderfield, H., & Greaves, M.J., 1981. Negative cerium anomalies in rare earth element patterns of oceanic ferromanganese nodules. *Earth Planet. Sci. Lett.*, 55:163-170.

- Exon, N.F., 1983. Manganese nodule deposits in the central Pacific Ocean and their variation with latitude. *Mar. Min.*, 4(1):79-107.
- Flanagan, F.J., & Gottfried, D., 1980. USGS rock standards, III. Manganese-nodule reference samples USGS-Nods-A-1 and USGS-Nods-P-1. *U.S. Geol. Surv., Prof. Pap.* 1155, 39 pp.
- Frank, D.J., Meylan, M.A., & Craig, J.D., 1976. Ferromanganese deposits of the Hawaiian Archipelago. *Hawaii Inst. of Geophysics, Report No. HIG-76-14*, 71 pp.
- Frazer, J.Z., & Fisk, M.B., 1981. Geological factors related to characteristics of sea-floor manganese nodule deposits. *Deep Sea Research*, 28A(12):1533-1551.
- Friedrich, G., Glasby, G.P., Thijssen, T., & Plüger, W.L., 1983. Morphological and geochemical characteristics of manganese nodules collected from three areas on an equatorial Pacific transect by R.V. SONNE. *Mar. Min.*, 4(2-3):167-253.
- Friedrich, G., & Plüger, W., 1974. Die verteilung von mangan, eisen, kobalt, nickel, kupfer und zink in manganknollen verschiedener felder (The distribution of manganese, iron, cobalt, nickel, copper and zinc in manganese nodules from various fields). *Meerestechnik* 5:203-206.
- Friedrich, G., Plüger, W., Kunzendorf, H., Roonwal, G., Wiechowski, A.S., Gürkan, A., Zuleta, J.R., & Krömer, E., 1977. Studies on the geochemistry and genetic interpretation of manganese nodule deposits. *Natural Resources and Development A Biannual Collection of Recent German Contributions Concerning the Exploration and Exploitation of Natural Resources*, Vol. 6, Laupp & Göbel, Tübingen, pp. 26-47.
- Gager, H.M., 1968. Mössbauer spectra of deep-sea iron-manganese nodules. *Nature*, 220:1021-1023.
- Gianone, C., da Cruz, F., & Douppnik, J.R., 1988. MS-DOS Kermit User Guide for the IBM PC Family, Compatibles, and Other MS-DOS Systems. unpublished, 100 pp.
- Glasby, G.P., 1972. The mineralogy of manganese nodules from a range of marine environments. *Mar. Geol.*, 13:57-72.
- Glasby, G.P., Friedrich, G., Thijssen, T., Plüger, W.L., Kunzendorf, H., Ghosh, A.K., & Roonwal, G.S., 1982. Distribution, morphology, and geochemistry of manganese nodules from the Valdivia 13/2 Area, equatorial north Pacific. *Pacific Science*, 36(2):241-263.
- Glasby, G.P., & Thijessen, T., 1982a. Control of the mineralogy and composition of marine manganese nodules by the supply of divalent transition metal ions. *N. Jb. Miner. Abh.*, 145:291-307.
- Glasby, G.P., & Thijessen, T., 1982b. The nature and composition of the acid-insoluble residue and hydrosate fraction of manganese nodules from selected areas in the equatorial and S.W. Pacific. *TMPM Tschermaks Min. Petr. Mitt.*, 30:205-225.

- Goldberg, E.D., 1954. Marine chemistry, I. Chemical scavengers of the sea. *J. Geol.*, 62:249-265.
- Gordon, D.C., & Gerard, R.D., 1970. North Pacific bottom potential temperature. *In* Geological Investigations of the North Pacific, *Geol. Soc. Am. Mem.*, 126:23-29.
- Halbach, P., Friedrich, G., & von Stackelberg, U., 1988. The Manganese Nodule Belt of the Pacific Ocean: Geological Environment, Nodule Formation, and Mining Aspects. Ferdinand Enke Verlag, Stuttgart, 254 pp.
- Halbach, P., Hebisch, U., & Scherhag, C., 1981a. Geochemical variations of ferromanganese nodules and crusts from different provinces of the Pacific Ocean and their genetic control. *Chem. Geol.*, 34:3-17.
- Halbach, P., & Manheim, F.T., 1984. Potential of cobalt and other metals in ferromanganese crusts on seamounts of the central Pacific basin. *Mar. Min.*, 4(4):319-336.
- Halbach, P., Manheim, F.T., & Otten, P., 1982. Co-rich ferromanganese deposits in the marginal seamount regions of the central Pacific Basin - results of the Midpac '81. *Erzmetall*, 35(9):447-453.
- Halbach, P., Marchig, V., & Scherhag, C., 1980. Regional variations in Mn, Ni, Cu, and Co, of ferromanganese nodules from a basin in the southeast Pacific. *Mar. Geol.*, 38:M1-M9.
- Halbach, P., & Özkara, M., 1979. Morphological and geochemical classification of deep-sea ferromanganese nodules and its genetical interpretation. *In* La genèse des nodules de manganèse, *Colloques Internationaux, C.N.R.S.* No 289, pp. 77-88.
- Halbach, P., & Puteanus, D., 1984a. Cobalt-rich ferromanganese crusts from central Pacific seamount regions - composition and formation. *In* Proceedings of the 27th International Geological Congress, Vol. 6, *Geology of Ocean Basins*, VNU Science Press, pp. 321-346.
- Halbach, P., & Puteanus, D., 1984b. The influence of the carbonate dissolution rate on the growth and composition of Co-rich ferromanganese crusts from central Pacific seamount areas. *Earth Plant. Sci. Lett.*, 68:73-87.
- Halbach, P., Puteanus, D., & Giovanoli, R., 1988. Transportation and Accumulation Processes. *In* The Manganese Nodule Belt of the Pacific Ocean. Geological Environment, Nodule Formation, and Mining Aspects (ed. by P. Halbach, G. Friedrich, U. von Stackelberg), Ferdinand Enke Verlag, Stuttgart, pp. 155-159.
- Halbach, P., Scherhag, C., Hebisch, U., & Marchig, V., 1981b. Geochemical and mineralogical control of different genetic types of deep-sea nodules from the Pacific Ocean. *Mineral. Deposita*, 16:59-84.

- Halbach, P., Segl, M., Puteanus, D., & Mangini, A., 1983. Co-fluxes and growth rates in ferromanganese deposits from central Pacific seamount areas. *Nature*, 304:716-719.
- Harvey, P.K., Taylor, D.M., Hendry, R.D., & Bancroft, F., 1973. An accurate fusion method for the analysis of rocks and chemically related materials by X-ray fluorescence spectrometry. *X-Ray Spectrom.*, 2:33-44.
- Heath, G.R., Moore Jr, T.C., & van Andel, T.H., 1977. Carbonate accumulation and dissolution in the equatorial Pacific during the past 45 million years. *In* The fate of fossil fuel CO<sub>2</sub> in the oceans (ed. by N.R. Anderson & A. Malahoff), *Marine Science*, Vol. 6, Plenum Press, pp. 627-639.
- Hein, J.R., Manheim, F.T., Schwab, W.C., Davis, A.S., Daniel, C.L., Bouse, R.M., Morgenson, L.A., Sliney, R.E., Clague, D., Tate, C.B., & Cacchione, D.A., 1985. Geological and Geochemical Data for Seamounts and Associated Ferromanganese Crusts in and Near the Hawaiian, Johnston Island, and Palmyra Island Exclusive Economic Zones. U.S. Dept. of the Interior Geological Survey, Open-File Report 85-292, 129 pp.
- Hein, J.R., Morgenson, L.A., Clague, D.A., Koski, R.A., 1987. Cobalt-Rich Ferromanganese Crusts from the Exclusive Economic Zone of the United States and Nodules from the Oceanin Pacific. *In* Geology and Resource Potential of the Continental Margin of Western North America and Adjacent Ocean Basins - Beaufort Sea to Baja California (ed. by D.W. Scholl, A. Grantz, & J.G. Vedder), Vol. 6, Circum-Pacific Council for Energy and Mineral Resources, Earth Science Series, Houston, Texas, pp. 753-771.
- Hein, J.R., Schulz, M.S., & Gein, L.M., in Press a. Central Pacific Cobalt-Rich Ferromanganeses Crusts: Historical Perspective and Regional Variability. *In* Geology and Offshore Mineral Resources of the Central Pacific Region (ed. by B. Keating, & B. Bolton), Circum-Pacific Council for Energy and Mineral Resources, Earth Science Series, Houston, Texas, 23 pp.
- Hein, J.L., Schulz, M.S., & Kang, J.K., in Press b. Insular and Submarine Ferromanganese Mineralization of the Tonga-Lau Region. *In* Geology of the Tonga-Lau Regions of the Southwest Pacific (ed. by P.F. Ballance, R.H. Herzer, & T.L. Vallier), Circum-Pacific Council for Energy and Mineral Resources, Earth Science Series, Houston, Texas, 46 pp.
- Hem, J.D., 1978. Redox processes at surfaces of manganese oxide and their effects on apueous metal ions. *Chem. Geol.*, 21:199-218.
- Herzenberg, C., & Riley, D.L., 1969. Interpretation of the mössbauer spectra of marine iron-manganese nodules. *Nature*, 224:259-260.
- Hurlbut Jr, C.S., & Klein, C., 1977. X-Ray Crystallography. *In* Manual of Mineralogy (after James D. Dana), John Wiley & Sons, New York, pp. 105-121.
- Johnston, C.E., & Glasby, G.P., 1969. Mössbauer effect determination of particle size in microcrystalline iron-manganese nodules. *Nature, Lond.*, 222:376-377.

- Jackson, E.D., & Schlanger, S.O., 1976. Regional syntheses, Line Islands Chain, Tuamotu Island Chain and Manihiki Plateau, Central Pacific Ocean. *Init. Rep. D.S.D.P.*, 33:915-928.
- Keller, G., & Barron, J.A., 1983. Paleooceanographic implications of Miocene deep-sea hiatuses. *Geol. Soc. Am. Bull.*, 94:590-613.
- Kennett, J., 1982. *Marine Geology*. Prentice-Hall Inc., Englewood Cliffs, N.J., 813 pp.
- Kennett, J.P., Honk, R.E., Andrews, P.B., Edward, R.R., Sostin, V.A., Hajos, M., Hampton, Mc., Jenkins, D.G., Margolis, S.V., Ovenshine, A.T., & Perch-Nielsen, K., 1975. Cenozoic paleo-oceanography in the southwest Pacific ocean, Antarctic glaciation, and the development of the circum Antarctic current. *Init. Reports of the D.S.D.P.*, 24:1155-1169.
- Klinkhammer, G.P., 1980. Early diagenesis in sediments from the eastern equatorial Pacific. II. Pore water metal results. *Earth Planet. Sci. Lett.*, 49:81-101.
- Klinkhammer, G.P., & Bender, M.L., 1980. The distribution of manganese in the Pacific Ocean. *Earth Plant. Sci. Lett.*, 49:81-101.
- Klinkhammer, G.P., Heggie, D.T., & Graham, D.W., 1982. Metal diagenesis in oxic marine sediments. *Earth Planet. Sci. Lett.*, 61:211-219.
- Krauskopf, K.B., 1957. Separation of manganese from iron in sedimentary processes. *Geochim. Cosmochim. Acta*, 12:61-84.
- Landing, W.M., & Bruland, K.W., 1980. Manganese in the North Pacific. *Earth Plant. Sci. Lett.*, 49:45-56.
- Lonsdale, P., Burns, V.M., & Fisk, M., 1980. Nodules of hydrothermal birnessite in the caldera of a young seamount. *Journ. Geol.*, 88:611-618.
- Luyendyk, B.P., 1970. Origin and history of abyssal hills in the northeastern Pacific Ocean. *Geol. Soc. Am.*, 81:2237-2260.
- Lyle, M., 1976. Estimation of hydrothermal manganese input to the oceans. *Geology*, 4(12):733-736.
- Lyle, M., 1978. The Formation and Growth of Ferromanganese Oxides on the Nazca Plate. Ph. D. Thesis, unpublished, 172 pp.
- Lyle, M., 1981. Formation and growth of ferromanganese oxides on the Nazca plate. *Geological Society of America, Memoir 154*, pp. 269-293.
- Lyle, M., Dymond, J., & Heath, G.R., 1977. Copper-nickel-enriched ferromanganese nodules and associated crusts from the Bauer Basin, northwest Nazca Plate. *Earth Planet. Sci. Lett.*, 35:55-64.
- Mangini, A., Halbach, P., Puteanus, D., & Segle, M., 1987. Chemistry and growth history of central Pacific Mn-crusts and their economic importance. In *Marine Minerals* (ed. by P.G. Teleki, M.R. Dobson, J.R. Moore, & U. von Stackelberg), D. Reidel Publishing Company, pp. 205-220.

- Manheim, F.T., 1986. Marine cobalt resources. *Science*, 232:600-608.
- Manheim, F.T., & Lane-Bostwick, C.M., 1988. Cobalt in ferromanganese crusts as a monitor of hydrothermal discharge on the Pacific sea floor. *Nature*, 335(1):59-62.
- Manheim, F.T., & Lane-Bostwick, C.M., 1989. Chemical composition of ferromanganese crusts in the world ocean: A review and comprehensive database. U.S. Dept. of the Interior Geological Survey, Open-File Report 89-020, 400 pp.
- Marchig, V., & Gundlach, H., 1979. Changes in chemical composition of some Pacific manganese nodules during their growth. *In* Marine Geology and Oceanography of the Pacific Manganese Nodule Province (ed. by J.L. Bischoff & D.Z. Piper), Plenum Press, N.Y., pp. 729-746.
- Margolis, S.V., & Burns, R.G., 1976. Pacific deep-sea manganese nodules: Their distribution, composition, and origin. *In* Annual Review of Earth and Planetary Sciences (ed. by F.A. Donath, F.G. Stehli, G.W. Wetherill), Vol. 4, Annual Reviews Inc., Palo Alto California, pp. 229-263.
- Meyer, K., 1977. Untersuchungen an sedimentkernen aus dem zentralen Pazifik SE von Hawaii von der "Valdivia" - Fahrt VA-13/1. BMFT - Forschungsbericht, M77-08:1-44.
- Melson, W.G., *et al.*, 1976. Chemical diversity of abyssal volcanic glasses erupted along Pacific, Atlantic, and Indian Ocean seafloor spreading centers. *In* The Geophysics of the Pacific Ocean Basin and its Margin (ed. by G.H. Sutton *et al.*), Washington, D.C., American Geophysical Union Monograph 19, pp. 351-367.
- Moore, J.G., 1965. Petrology of deep-sea basalt near Hawaii. *American Journal of Science*, 263:40-52.
- Moore, T.C., & Heath, G.R., 1966. Manganese nodules, topography and thickness of Quaternary sediments in the central Pacific. *Nature*, 212(5066):983-985.
- Moore, W.S., & Vogt, P.R., 1976. Hydrothermal manganese crusts from two sites near the Galapagos Spreading Axis. *Earth Planet. Sci. Lett.*, 29:349-356.
- Nishimura, A., 1981. Deep-sea sediments in the GH 79-1 Area: Their geological properties. Cruise Report 15, Geol. Surv. Jap., pp. 110-135.
- Norrish, K., & Hutton, J.T., 1969. An accurate X-ray spectrographic method for the analysis of a wide range of geological samples. *Geochim. Cosmochim. Acta*, 33:431-453.
- Piper, D.Z., Cook, H.E., & Gardner, J.V., 1979. Lithic and acoustic stratigraphy of the equatorial North Pacific: DOMES Sites A, B, and C. *In* Marine Geology and Oceanography of the Pacific Manganese Nodule Province (ed. by J.L. Bischoff & D.Z. Piper), Marine Science Vol. 9, Plenum Press, New York, pp. 309-348.

- Price, N.B., & Calvert, S.E., 1970. Compositional variation in Pacific Ocean ferromanganese nodules and its relationship to sediment accumulation rates. *Mar. Geol.*, 9:145-171.
- Raab, W., 1972. Physical and chemical features of Pacific deep sea manganese nodules and their implications to the genesis of nodules. *In* *Ferromanganese Deposits on the Ocean Floor* (ed. by D.R. Horn), National Science Foundation, Washington, D.C., pp. 31-50.
- Raab, W.J., & Meylan, M.A., 1977. Morphology. *In* *Marine Manganese Deposits* (ed. by G.P. Glasby), Elsevier Scientific Publishing Company, Amsterdam, pp. 109-146.
- Roonwal, G.S., & Friedrich, G.H., 1980. Chemical variation and element correlation in manganese nodules from a dredge haul in the central Pacific. *Indian Journal of Marine Sciences*, 9:235-239.
- Sevast'yanov, V.F., & Volkov, I.I., 1966. Chemical composition of iron-manganese concretions in Black Sea sediment. *Dokl. Akad. Nauk. SSSR*, 176:191-193. (Engl. Transl., 180-182).
- Siegel, M.D., 1981. Studies of the mineralogy, chemical composition, textures and distribution of manganese nodules at a site in the North Equatorial Pacific Ocean. Ph.D. dissertation, Harvard Univ., 274 pp.
- Skornyakova, N.S., 1964. Dispersed iron and manganese in Pacific Ocean sediments. *Intern. Geol. Rev.*, 7:2161-2174.
- Skornyakova, N.S., 1979. Zonal regularities in occurrence, morphology and chemistry of manganese nodules of the Pacific Ocean. *In* *Marine Geology and Oceanography of the Pacific Manganese Nodule Province* (ed. by J.L. Bischoff & D.Z. Piper), Plenum Press, N.Y., pp. 699-727.
- Snedecor, G.W., & Cochran, W.G., 1956. *Statistical Methods. Applied to experiments in agriculture and biology.* The Iowa State University Press, Ames, Iowa, U.S.A., pp. 42-44.
- Sorem, R.K., Reinhart, W.R., Fewkes, R.H., & McFarland, W.D., 1979. Occurrence and character of manganese nodules in DOMES Sites A, B, and C, east equatorial Pacific Ocean. *In* *Marine Geology and Oceanography of the Pacific Manganese Nodule Province* (ed. by J.L. Bischoff & D.Z. Piper), *Marine Science Vol. 9*, Plenum Press, N.Y., pp. 475-527.
- Stoffers, P., Glasby, G.P., Thijessen, T., Shrivastava, P.C., & Melguen, M., 1981. The geochemistry of coexisting manganese nodules, micronodules, sediments and pore waters from five areas in the equatorial and S.W. Pacific. *Chem. Erde*, 40:273-297.
- Theyer, F., 1977. Micropaleontological dating of DOMES project box cores from test area A and B. Tropical Pacific. *In* *Deep Ocean Environmental Study: Geology and Geochemistry of DOMES Sites A, B, and C, Equatorial North Pacific* (ed. by D.Z. Piper, *et al.*), U.S. Geol. Sur. Open-File Report 77-79, pp. 179-194.



- Toth, J.R., 1980. Deposition of submarine crusts rich in manganese and iron. *Geol. Soc. Amer. Bull.*, Part 1, 91:44-54.
- Turner, S., Siegel, M.D., & Buseck, P.R., 1982. Structural features of todorokite intergrowths in manganese nodules. *Nature*, 296:841-842.
- Usui, A., & Mita, N., 1987. Comparison of manganese nodules from the northeast equatorial Pacific (cruise SO 25) with nodules from the central Pacific basin. *Geol. Jb.*, D87:287-313.
- Usui, A., Moritani, T., (in press). Manganese nodule deposits in the central Pacific basin: Distribution, geochemistry, mineralogy, and genesis. *In* *Geology and Offshore Mineral Resources of the Central Pacific Basin* (ed. by B.H. Keating & B.R. Bolton), Circum-Pacific Council for Energy & Mineral Resources, Houston, Texas, 18 pp.
- van Andel, T.H., *et al.*, 1973. Initial Reports of the Deep Sea Drilling Project, Vol 16. Washington, D.C., U.S. Government Printing Office, 949 pp.
- van Andel, T.H., & Heath, G.R., 1973. Geological results, central equatorial Pacific West-East Rise. *Init. Rep. D.S.D.P.*, 16:937-949.
- van Andel, T.H., Heath, G.R., & Moore Jr, T.C., 1975. Cenozoic history and paleo-oceanography of the central equatorial Pacific. *Geol. Soc. Am. Memo*, 143, 134 pp.
- von Stackelberg, U., 1982. Influence of hiatuses and volcanic ash rains on the origin of manganese nodules of the equatorial north Pacific (Valdivia cruises VA-13/2 and VA-18). *Mar. Min.*, 3(3-4):297-314.
- von Stackelberg, U., 1988. Sediments. *In* *The Manganese Nodule Belt of the Pacific Ocean: Geological Environment, Nodule Formation, and Mining Aspects* (ed. by P. Halbach, G. Friedrich, & U. von Stackelberg), Ferdinand Enke Verlag Stuttgart, pp. 110-141.
- Winterhalter, B., 1966. Iron-manganese concretions from the Gulf of Bothnia and the Gulf of Finland. *Geotekn. Julk.*, 69:1-77.
- Winterhalter, B., & Siivola, J., 1967. An electron microprobe study of the distribution of iron, manganese and phosphorus in concretions from the Gulf of Bothnia. *C.R. Soc. Geol. Finl.*, 39:161-172.
- Zar, J.H., 1974. *Biostatistical Analysis*. Prentice-Hall, Inc., Englewood Cliffs, N.J., U.S.A., pp. 34, 103-105.

## 1.6 APPENDIX A

### **THE LOCATION OF CRUST AND NODULE SAMPLES FROM SURVEY REGION A**

# FERROMANGANESE CRUSTS

LAB NUMBER	CRUISE	NUMBER	LATITUDE		LONGITUDE		DEPTH (m)
			DEGREES	MINUTES	DEGREES	MINUTES	
	DODO	6	19	6.0 N	158	14.0 W	3400
	DODO	7	18	43.0 N	158	17.0 W	750
	DODO	8	18	21.0 N	158	27.0 W	1317
	DODO	9-1	18	18.0 N	161	46.0 W	3720
	DODO	9-2	18	18.0 N	161	46.0 W	3350
	DODO	13	18	47.0 N	162	3.0 W	3148
	DODO	14	19	22.0 N	162	19.0 W	4868
	MIDPAC	25-F1	19	7.0 N	169	44.0 W	1740
	MIDPAC	25-F2	19	7.0 N	169	44.0 W	1740
	STYX	2	19	35.0 N	168	52.5 W	1805
	7TOW	123	5	52.3 N	160	50.9 W	1604
	7TOW	129	9	19.0 N	163	16.9 W	1563
	7TOW	130	8	20.0 N	164	21.7 W	1519
	7TOW	133	12	4.2 N	165	50.3 W	1488
	7TOW	137	14	27.5 N	168	58.7 W	1750
	7TOW	142	18	8.1 N	169	4.0 W	2139
	7TOW	143	19	30.7 N	168	52.5 W	1805
	7TOW	144	21	32.1 N	167	55.8 W	1690

FERROMANGANESE NODULES

LAB NUMBER	CRUISE	NUMBER	LATITUDE		LONGITUDE		DEPTH (m)
			DEGREES	MINUTES	DEGREES	MINUTES	
82-MN-D-24	DODO	27P	9	0.0 N	169	0.0 W	5170
82-MN-D-25	DODO	27PG	9	0.0 N	169	0.0 W	5170
82-MN-D-26	DODO	31PG	9	11.0 N	168	48.0 W	5220
	DODO	11	18	47.0 N	162	3.0 W	4630
	DODO	12	18	38.0 N	162	8.0 W	5040
	DODO	15	19	21.0 N	162	10.0 W	5032
	DODO	15-3	19	21.0 N	162	10.0 W	5032
82-MN-S-41	STYX I	10FF	9	54.0 N	149	57.0 W	5304
82-MN-S-76	STYX	9FFGB	12	2.0 N	145	46.0 W	5330
82-MN-W-80	WAHINE	13FF-4	8	22.6 N	152	59.0 W	5127
82-MN-W-81	WAHINE	18FF-3	8	16.3 N	152	58.0 W	5133
82-MN-W-82	WAHINE	18FF-6	8	16.3 N	152	58.0 W	5023
82-MN-W-83	WAHINE	2P	11	51.0 N	152	57.0 W	5221
82-MN-W-86	WAHINE	2PG	11	51.0 N	152	57.0 W	5221
82-MN-W-87	WAHINE	4P	8	57.0 N	152	52.0 W	4839
82-MN-W-88	WAHINE	4PG	8	57.0 N	152	52.0 W	4839
82-MN-W-89	WAHINE	7PG	3	58.0 N	153	2.0 W	4992
83-MN-J-118	JYN V	14G	9	20.0 N	150	35.0 W	4813
83-MN-J-119	JYN V	15PG	8	2.0 N	149	54.0 W	5073
83-MN-J-120	JYN V	17PG	6	5.0 N	148	52.0 W	5036
83-MN-J-121	JYN V	29G	13	32.0 N	146	1.8 W	5285
83-MN-J-122	JYN V	31PG	11	55.0 N	144	54.0 W	5539
MN 32	SUMMA	44DB	19	58.7 N	166	5.0 W	4941
MN 33	SUMMA	51DB	6	51.4 N	166	51.5 W	4762
MN 34	SUMMA	52DB	6	49.6 N	167	1.2 W	4682
MN 35	SUMMA	53DB	6	47.0 N	166	53.0 W	4674
MN 36	SUMMA	57DB	7	48.0 N	159	19.0 W	5128
MN 37	SUMMA	59DB	8	5.7 N	153	54.9 W	5003
MN 38	SUMMA	60DB	8	5.9 N	152	36.2 W	5036
MN 39	SUMMA	63DB	8	16.4 N	150	59.6 W	4833
MN 40	SUMMA	65DB	8	44.4 N	147	31.9 W	5126

MN 41	SUMMA	66DB	8	43.6 N	147	35.4 W	5062
MN 42	SUMMA	68DB	8	34.5 N	147	46.7 W	5128
MN 43	SUMMA	69DB	8	57.9 N	146	40.1 W	5104
MN 44	SUMMA	70DB	8	57.3 N	145	48.4 W	5033
MN 45	SUMMA	72DB	8	58.8 N	145	6.6 W	4943
MN 46	SUMMA	74DB	9	39.4 N	146	19.9 W	5036
MN 47	SUMMA	79DB	11	7.9 N	148	4.3 W	5128
MN 48	SUMMA	80DB	10	58.7 N	148	19.5 W	5124
MN 49	SUMMA	83DB	11	1.1 N	148	29.9 W	5344
MN 50	SUMMA	84DB	11	56.0 N	146	26.9 W	5314
MN 51	SUMMA	85DB	11	48.2 N	148	39.7 W	5503
MN 52	SUMMA	86DB	12	1.4 N	149	18.0 W	5311
MN 53	SUMMA	87DB	11	58.2 N	150	18.5 W	5003
MN 54	SUMMA	88DB	11	58.2 N	150	18.5 W	5003
MN 55	SUMMA	89DB	11	29.2 N	149	11.0 W	5303
MN 56	SUMMA	90DB	11	30.8 N	148	34.7 W	5128
MN 86	SUMMA	158DB	7	49.8 N	154	49.3 W	4908
MN 89	RP80C75	47-12	9	3.5 N	151	11.1 W	5005
MN 90	RP80C75	47-13	9	2.3 N	151	11.2 W	5039
MN 91	RP80C75	50-29	8	43.8 N	150	18.7 W	5033
MN 92	RP80C75	50-30	8	41.1 N	150	15.1 W	4928
	PLDS	80-1	11	1.0 N	140	8.5 W	4500

## **1.7 APPENDIX B**

### **THE LOCATION OF CRUST AND NODULE SAMPLES FROM SURVEY REGION B**

FERROMANGANESE CRUSTS

LAB NUMBER	CRUISE	NUMBER	LATITUDE		LONGITUDE		DEPTH (m)
			DEGREES	MINUTES	DEGREES	MINUTES	
83-MN-B-106	BNFC	25P	10	22.5 N	108	38.4 W	2693
	CARR II	6	9	57.0 N	108	48.0 W	1228
	CERES	1	13	26.4 N	102	36.3 W	3424
	CERES	5	12	44.2 N	102	34.3 W	2700
	CERES	6	12	44.3 N	102	33.6 W	1950
	DPSOND	3	9	8.4 N	105	10.9 W	3240
	DPSOND	4	9	7.8 N	105	0.6 W	2957
	DPSOND	5	9	12.7 N	105	12.2 W	3124
	HENDSMT	D-1-3	25	15.0 N	119	40.0 W	64
	QBR	1	12	47.0 N	110	25.0 W	2550
	QBR	2	12	47.0 N	110	25.0 W	2550
	QBR	7(A)	10	22.0 N	108	23.0 W	3000
	QBR	7(B)	10	22.0 N	108	23.0 W	3000
	QBR	22	9	55.2 N	104	29.0 W	1680
	RISE III	3	8	49.5 N	103	55.0 W	2095
	RISE III	6	11	30.0 N	103	17.5 W	2703
	RISE III	7	11	31.0 N	103	13.0 W	2183
	RISE III	8	11	30.0 N	103	13.5 W	2450
	RISE III	13	12	32.0 N	103	17.0 W	2251
	SIQR	4	8	9.4 N	104	27.4 W	3325
	SOTW IX	32	14	5.3 N	110	48.9 W	3400
	TRIPOD	2	20	45.0 N	112	47.0 W	1711
	TRIPOD	3	21	18.0 N	112	42.0 W	2496
	TRIPOD	9	21	5.0 N	119	22.0 W	2984

FERROMANGANESE NODULES

LAB NUMBER	CRUISE	NUMBER	LATITUDE		LONGITUDE		DEPTH (m)
			DEGREES	MINUTES	DEGREES	MINUTES	
83-MN-A-90	AMPH	3P	15	4.0 N	125	5.0 W	4459
82-MN-B-4	BNFC	19	10	43.6 N	108	32.5 W	3172
82-MN-B-5	BNFC	54	11	51.6 N	110	0.1 W	3886
82-MN-B-6	BNFC	56	13	22.1 N	114	5.0 W	4105
83-MN-B-102	BNFC	5G	13	38.5 N	106	18.9 W	3220
83-MN-B-103	BNFC	14PG	10	42.0 N	109	6.0 W	5118
83-MN-B-104	BNFC	17P	11	10.6 N	109	36.3 W	3522
83-MN-B-105	BNFC	18PG	10	42.0 N	108	32.5 W	3551
83-MN-B-107	BNFC	58PG	13	32.1 N	114	20.7 W	4003
83-MN-B-109	BNFC	70FF	14	31.8 N	117	19.6 W	3988
83-MN-B-110	BNFC	71FF	14	31.9 N	117	19.0 W	3964
83-MN-B-111	BNFC	77FF	14	36.7 N	117	26.1 W	4087
83-MN-B-112	BNFC	81G	14	35.1 N	118	33.3 W	4169
83-MN-B-113	BNFC	84P	15	5.6 N	120	44.9 W	4207
83-MN-B-114	BNFC	86P	14	35.1 N	121	3.7 W	4295
	CARR II	9	10	39 N	108	45 W	5276
	CERES	9	13	0.0 N	100	50.0 W	2300
	CERES	11	12	14.9 N	100	31.4 W	2850
	CERES	10	12	57.7 N	100	53.9 W	3478
	CERES	13	12	34.0 N	100	22.2 W	3317
	CERES	14	12	1.4 N	101	35.6 W	3070
	CERES	15	11	26.1 N	101	37.4 W	2940
	CERES	16	12	4.4 N	101	34.5 W	3250
	CERES	17	12	3.0 N	101	33.9 W	1920
	CERES	18	11	57.4 N	101	37.2 W	2860
	CERES	19	11	16.0 N	101	3.9 W	2930
	CERES	20	11	14.3 N	101	7.6 W	2975
	CERES	21	10	52.3 N	101	31.6 W	3080
	DWBD	1	21	27.0 N	126	43.0 W	4300
83-MN-J-123	JYN V	46PG	13	24.0 N	136	11.0 W	4822
83-MN-J-124	JYN V	47PG	14	39.0 N	135	4.0 W	4813



83-MN-J-125	JYN V	48PG	15	54.0 N	133	57.0 W	4606
83-MN-J-126	JYN V	49PG	17	10.0 N	132	50.0 W	5188
83-MN-J-127	JYN V	50PG	18	16.0 N	131	46.0 W	5210
	MERO	29-52	9	56.4 N	137	48.1 W	4930
MN 1	SUMMA	2DB	14	58.2 N	116	13.7 W	3980
MN 2	SUMMA	3DB	14	26.3 N	119	9.1 W	4072
MN 3	SUMMA	4DB	14	12.4 N	118	52.5 W	3980
MN 4	SUMMA	5DB	13	54.3 N	120	48.8 W	4255
MN 5	SUMMA	6DB	13	40.4 N	122	18.4 W	4255
MN 6	SUMMA	7DB	14	14.8 N	123	42.1 W	4438
MN 7	SUMMA	8DB	15	6.0 N	125	10.0 W	4392
MN 8	SUMMA	9DB	15	7.9 N	125	7.0 W	4300
MN 9	SUMMA	10DB	15	9.0 N	125	8.5 W	4392
MN 10	SUMMA	12DB	15	8.9 N	125	9.7 W	4002
MN 11	SUMMA	13DB	15	2.6 N	125	8.3 W	4302
MN 12	SUMMA	16DB	13	15.4 N	126	48.0 W	4758
MN 13	SUMMA	17DB	13	8.5 N	128	36.1 W	4712
MN 15	SUMMA	20DB	20	55.8 N	113	57.1 W	3568
MN 16	SUMMA	21DB	20	54.5 N	113	57.5 W	3614
MN 17	SUMMA	22DB	20	57.3 N	113	57.5 W	3660
MN 18	SUMMA	23DB	20	56.6 N	113	55.9 W	3568
MN 19	SUMMA	24DB	20	52.9 N	113	58.1 W	3660
MN 20	SUMMA	25DB	20	57.1 N	113	59.3 W	3660
MN 21	SUMMA	26DB	20	56.1 N	113	58.3 W	3660
MN 22	SUMMA	27DB	20	56.3 N	113	58.3 W	3660
MN 24	SUMMA	29DB	20	58.3 N	113	59.5 W	3642
MN 25	SUMMA	30DB	20	54.8 N	113	58.2 W	3623
MN 26	SUMMA	31DB	20	57.8 N	113	56.0 W	3861
MN 27	SUMMA	32DB	20	55.0 N	113	55.9 W	3697
MN 28	SUMMA	33DB	20	57.0 N	113	57.6 W	3687
MN 29	SUMMA	36DB	19	36.5 N	115	18.3 W	3770
MN 30	SUMMA	37CC	19	39.8 N	115	18.3 W	3770
MN 31	SUMMA	41DB	12	31.8 N	122	27.5 W	4483
MN 93	RP80C75	58-61	15	20.6 N	125	26.8 W	4414
	QBR	8<C>	10	24.0 N	108	26.0 W	3700
	RISE III	19	14	43.0 N	102	33.5 W	2260
	RISE III	20	14	43.5 N	102	34.5 W	1843

	RISE III	24	13	1.3 N	100	49.0 W	2308
	RISE III	28	13	46.0 N	101	52.3 W	1693
82-MN-S-74	STYX	2FFGB	23	43.0 N	124	6.0 W	3787
82-MN-S-75	STYX	3FFGB	20	4.0 N	130	5.0 W	4959
	TRIPOD	4	20	45.0 N	114	27.0 W	3840

## 1.8 APPENDIX C

### **THE CONCENTRATIONS OF THE MAJOR ELEMENTS AND THE TODOROKITE/ $\delta\text{MnO}_2$ RATIOS FOR CRUST AND NODULE SAMPLES FROM SURVEY REGION A**

The abundance of each of the major elements present in the crusts and nodule samples are given as weight percents. The abundances of todorokite to  $\delta\text{MnO}_2$  is given as a ratio and therefore has no units.

FERROMANGANESE CRUSTS

LAB NUMBER	DODO 6 D-1	DODO 7 D-1	DODO 7 D-2	DODO 7 D-3	DODO 8 D-1	DODO 8 D-2	DODO 8 D-3	DODO 9-1 D-1	DODO 9-1 D-2	DODO 9-1 D-3	DODO 9-2 D-1
DEPTH (m)	3400	750	750	750	1317	1317	1317	3720	3720	3720	3350
Si	9.24	1.11	1.14	0.92	3.30	3.21	5.31	15.09	15.66	3.43	14.05
Ti	1.21	0.62	0.75	0.86	0.85	0.97	0.85	1.09	0.97	0.89	0.94
Al	2.09	0.86	0.20	0.15	0.94	0.72	1.92	5.73	5.60	0.42	5.67
Fe	15.46	5.95	8.71	10.03	11.93	12.15	11.83	10.13	9.96	17.12	10.59
Mn	9.13	21.56	18.71	20.91	17.85	17.38	14.52	5.92	5.15	15.03	5.17
Mg	1.98	2.04	1.01	1.11	1.02	0.97	0.98	1.39	1.21	0.81	1.19
Ca	2.35	8.46	8.21	4.64	2.42	2.02	3.63	2.52	4.15	1.88	5.15
Na	1.81	0.72	1.43	1.44	2.42	2.07	2.51	2.07	1.80	1.40	1.77
K	0.72	0.42	0.32	0.38	0.78	0.53	1.00	1.31	2.03	0.27	1.01
P	0.26	2.72	2.55	1.21	0.43	0.36	0.90	0.38	0.98	0.37	1.15
Co	0.18	0.39	0.41	0.61	0.45	0.63	0.28	0.17	0.15	0.37	0.12
Ni	0.11	1.23	0.48	0.49	0.36	0.35	0.31	0.08	0.07	0.17	0.05
Cu	0.01	0.22	0.05	0.04	0.09	0.06	0.11	0.05	0.05	0.02	0.02
Zn	0.03	0.11	0.04	0.04	0.04	0.04	0.05	0.02	0.02	0.04	0.03
Ba	0.09	0.21	0.16	0.14	0.19	0.77	0.40	0.09	0.08	0.14	0.08
TOD/DEL	0.00	0.74	0.00	0.00	0.09	0.00	0.09	0.00	0.00	0.00	0.00

LAB NUMBER	DODO 9-2 D-2	DODO 13 D-1	DODO 13 D-2	MP 25-F1	MP 25-F2	STYX 2 D-1	STYX 2 D-2	STYX 2 D-3	7TOW 123 D-1	7TOW 129 D-1	7TOW 129 D-2
DEPTH (m)	3350	3148	3148	1740	1740	1805	1805	1805	1604	1563	1563
Si	21.28	7.84	3.57	5.58	3.73	3.07	2.02	2.17	15.57	1.33	1.05
Ti	0.82	1.57	1.07	0.95	0.89	0.92	0.96	1.00	1.36	0.61	0.99
Al	8.97	2.34	0.69	1.66	1.07	0.58	0.21	0.24	5.15	0.40	0.17
Fe	6.47	16.04	16.31	13.22	12.43	13.41	12.31	12.94	8.38	7.71	11.72
Mn	1.71	10.60	15.43	14.31	17.76	18.00	20.16	19.30	1.02	17.52	20.80
Mg	1.43	1.21	0.90	1.02	1.28	1.00	0.88	0.91	4.95	1.19	1.10
Ca	4.83	1.99	1.80	2.75	2.25	2.05	2.11	2.07	10.69	9.90	2.32
Na	3.03	1.80	1.51	2.32	1.89	1.55	1.27	1.43	1.54	0.84	0.69
K	1.70	0.80	0.38	0.54	0.49	0.43	0.35	0.32	1.13	0.35	0.35
P	0.53	0.36	0.31	0.64	0.36	0.32	0.30	0.31	2.80	3.23	0.34
Co	0.03	0.24	0.38	0.50	0.78	0.60	0.82	0.78	0.06	0.52	0.87
Ni	0.01	0.20	0.20	0.23	0.33	0.31	0.36	0.32	0.06	0.60	0.42
Cu	0.00	0.11	0.08	0.03	0.03	0.02	0.04	0.02	0.00	0.06	0.05
Zn	0.01	0.05	0.04	0.03	0.04	0.03	0.03	0.03	0.04	0.07	0.05
Ba	0.05	0.15	0.16	0.11	0.10	0.13	0.12	0.13	0.05	0.17	0.17
TOD/DEL	0.00	0.02	0.00	0.00	0.00	0.00	0.00	0.00	0.00	0.14	0.01

LAB NUMBER	7TOW 129 D-3	7TOW 130	7TOW 133 D-1	7TOW 133 D-2	7TOW 137 D-1	7TOW 137 D-2	7TOW 137 D-3	7TOW 142 D-1	7TOW 143 D-1	7TOW 143 D-2	7TOW 144 D-1
DEPTH (m)	1563	1519	1488	1488	1750	1750	1750	2139	1805	1805	1690
Si	0.52	1.16	1.14	0.90	5.30	1.81	2.45	3.09	2.43	3.38	6.34
Ti	0.92	0.79	0.35	0.23	0.90	0.79	0.59	0.90	0.87	0.87	1.17
Al	0.01	0.14	0.53	0.47	1.64	0.38	0.67	0.66	0.56	0.63	1.61
Fe	10.32	10.22	5.26	4.00	11.81	10.85	7.59	12.76	11.71	13.27	14.42
Mn	22.47	23.76	18.76	9.79	12.97	15.59	13.39	17.19	17.47	17.90	13.67
Mg	1.00	1.17	1.59	1.28	1.07	0.90	0.79	0.85	1.04	1.05	1.15
Ca	2.67	2.29	14.34	24.88	7.12	9.18	13.80	2.78	4.65	2.00	1.92
Na	0.98	1.60	1.10	1.04	1.25	0.84	1.20	1.66	1.51	1.32	1.35
K	0.34	0.42	0.41	0.18	0.69	0.34	0.41	0.40	0.41	0.38	0.60
P	0.42	0.34	5.02	9.33	2.34	2.96	4.70	0.60	1.31	0.37	0.36
Co	0.98	0.92	0.34	0.31	0.44	0.47	0.42	0.64	0.50	0.64	0.43
Ni	0.46	0.63	0.82	0.58	0.32	0.37	0.34	0.31	0.39	0.36	0.25
Cu	0.30	0.02	0.08	0.04	0.06	0.04	0.05	0.04	0.09	0.04	0.02
Zn	0.07	0.06	0.08	0.07	0.05	0.04	0.03	0.03	0.05	0.04	0.04
Ba	0.17	0.17	0.43	0.32	0.28	0.24	0.12	0.16	0.21	0.13	0.13
TOD/DEL	0.00	0.00	0.43	0.52	0.03	0.06	0.00	0.00	0.00	0.00	0.00

LAB	7TOW	7TOW
NUMBER	144 D-2	144 D-3
DEPTH (m)	1690	1690
Si	4.52	7.53
Ti	1.08	0.65
Al	1.01	2.77
Fe	14.93	9.99
Mn	15.37	17.03
Mg	1.04	1.63
Ca	1.97	1.40
Na	1.17	1.79
K	0.43	0.83
P	0.37	0.17
Co	0.53	0.23
Ni	0.25	0.62
Cu	0.03	0.34
Zn	0.04	0.04
Ba	0.15	0.15
TOD/DEL	0.07	0.91

FERROMANGANESE NODULES

LAB	D	D	D	0000	0000	0000	0000	0000	0000	0000	0000
NUMBER	24	25	26	11 D-1	11 D-2	12-2 D-1	12-2 D-2	14-2 D-1	14-2 D-2	14-2 D-3	15 D-1
DEPTH (m)	5170	5170	5220	4630	4630	5040	5040	4868	4868	4868	5032
Si	7.45	4.09	7.63	8.32	8.89	8.23	7.59	2.30	6.42	2.73	6.16
Ti	0.67	1.03	0.65	1.20	0.88	1.09	1.31	1.03	1.16	0.99	1.13
Al	1.99	1.24	2.38	2.58	3.28	2.77	2.24	0.36	1.82	0.58	1.79
Fe	14.19	14.13	9.83	14.32	12.18	13.19	16.06	15.44	15.34	15.10	15.08
Mn	13.64	17.63	18.86	10.87	11.50	11.69	10.65	17.31	11.41	17.19	13.65
Mg	1.07	1.15	1.64	1.08	1.00	1.05	1.09	0.84	0.97	0.92	0.98
Ca	1.98	1.85	1.67	2.59	2.34	2.04	1.86	1.98	3.08	2.04	1.95
Na	1.65	1.74	1.03	2.67	1.75	2.66	2.51	1.32	1.38	1.31	1.49
K	1.06	0.49	0.78	0.83	0.82	0.99	0.84	0.32	0.75	0.39	0.68
P	0.34	0.26	0.17	0.57	0.41	0.34	0.33	0.29	0.84	0.31	0.32
Co	0.14	0.37	0.22	0.30	0.24	0.28	0.29	0.40	0.29	0.39	0.29
Ni	0.20	0.33	0.55	0.15	0.17	0.15	0.10	0.23	0.14	0.25	0.18
Cu	0.23	0.20	0.43	0.06	0.09	0.06	0.04	0.08	0.07	0.09	0.10
Zn	0.04	0.04	0.05	0.03	0.03	0.03	0.03	0.04	0.03	0.03	0.03
Ba	0.17	0.13	0.16	0.12	0.12	0.11	0.13	0.17	0.13	0.19	0.15
TOD/DEL	0.00	0.12	0.85	0.00	0.00	0.00	0.00	0.00	0.00	0.00	0.00



LAB NUMBER	DODD 15 D-2	DODD 15 D-3	DODD 15-3 D-1	DODD 15-3 D-2	DODD 15-3 D-3	S 41	S 76	W 80	W 81	W 82	W 83
DEPTH (m)	5032	5032	5032	5032	5032	5304	5330	5127	5133	5123	5221
Si	3.80	2.39	9.84	13.08	9.52	5.68	8.62	6.95	6.66	6.99	6.66
Ti	1.13	1.21	0.41	0.56	1.02	0.83	0.47	0.35	0.47	0.46	0.88
Al	0.95	0.57	3.46	5.22	3.50	1.75	3.06	2.49	2.50	2.52	2.27
Fe	13.46	12.13	6.78	7.78	10.63	10.80	6.83	5.05	6.84	6.53	10.15
Mn	18.24	18.04	7.84	9.49	11.69	18.67	19.94	24.14	22.50	24.54	18.30
Mg	1.07	0.96	0.85	1.31	1.35	1.45	1.86	1.98	2.03	2.17	1.61
Ca	1.93	2.03	10.44	1.76	2.88	1.64	1.59	1.55	1.61	1.58	1.99
Na	1.65	1.41	1.83	2.05	1.37	1.25	1.87	2.01	2.22	2.13	1.98
K	0.53	0.43	1.54	1.85	1.14	0.57	1.25	0.85	0.83	0.84	0.79
P	0.24	0.26	3.73	0.38	0.62	0.21	0.18	0.16	0.17	0.16	0.34
Co	0.39	0.53	0.15	0.14	0.25	0.27	0.23	0.14	0.18	0.19	0.28
Ni	0.28	0.33	0.18	0.25	0.23	0.56	0.88	1.04	0.99	1.07	0.58
Cu	0.07	0.06	0.09	0.15	0.12	0.30	0.67	1.02	0.76	0.91	0.34
Zn	0.04	0.03	0.02	0.03	0.03	0.04	0.07	0.09	0.08	0.09	0.05
Ba	0.15	0.16	0.08	0.09	0.12	0.15	0.10	0.23	0.16	0.15	0.17
TOD/DEL	0.00	0.00	0.00	0.00	0.00	0.59	0.95	1.48	1.00	0.52	0.45

LAB NUMBER	W 86	W 87	W 88	W 89	J 118	J 119	J 120	J 121	J 122	MN 32	MN 33
DEPTH (m)	5221	4839	4839	4992	4813	5073	5036	5285	5539	4941	4762
Si	6.12	6.34	5.34	19.26	8.47	4.33	5.06	10.14	8.19	14.37	4.87
Ti	0.91	0.72	0.74	0.39	0.51	0.42	0.69	0.34	0.64	1.24	0.83
Al	2.08	2.09	1.80	3.80	2.56	1.77	1.47	3.45	2.48	4.88	1.49
Fe	11.50	9.62	9.42	11.32	6.56	5.83	10.52	5.90	8.28	12.77	11.53
Mn	20.57	20.50	21.49	0.46	15.23	25.34	19.17	19.51	17.66	7.47	20.38
Mg	1.81	1.85	1.72	2.06	2.04	2.22	1.68	2.01	1.67	1.73	1.36
Ca	1.70	2.18	1.87	6.40	3.67	1.50	2.17	1.50	1.55	1.33	2.21
Na	1.23	1.61	1.91	1.46	3.10	4.48	2.82	4.44	2.98	2.44	0.77
K	0.66	0.74	0.69	2.06	0.86	0.92	0.58	1.58	1.10	1.49	0.52
P	0.23	0.19	0.18	1.88	0.18	0.15	0.32	0.17	0.20	0.17	0.20
Co	0.31	0.25	0.25	0.01	0.17	0.17	0.23	0.19	0.23	0.13	0.29
Ni	0.64	0.77	0.74	0.06	0.64	1.01	0.63	0.83	0.66	0.23	0.53
Cu	0.36	0.45	0.44	0.06	0.40	0.89	0.39	0.69	0.35	0.15	0.38
Zn	0.06	0.07	0.06	0.02	0.05	0.09	0.05	0.07	0.05	0.03	0.05
Ba	0.18	0.19	0.18	0.03	0.21	0.22	0.14	0.16	0.18	0.08	0.16
TOD/DEL	0.51	0.33	0.11	0.00	0.86	1.44	0.32	1.30	0.00	0.54	0.35

LAB NUMBER	MN 34	MN 35	MN 36	MN 37	MN 38	MN 39	MN 40	MN 41	MN 42	MN 43	MN 44
DEPTH (m)	4682	4674	5128	5003	5036	4833	5126	5062	5128	5104	5033
Si	4.84	5.57	6.76	7.42	7.55	6.38	5.28	5.40	16.44	4.79	6.83
Ti	0.85	0.70	0.39	0.38	0.72	0.44	0.36	0.37	0.35	0.37	0.26
Al	1.60	2.35	2.76	2.81	2.56	2.54	2.24	2.24	4.36	2.09	2.87
Fe	12.50	10.16	6.56	5.81	10.78	6.39	5.34	4.99	9.57	5.16	4.01
Mn	19.83	21.07	23.47	24.12	18.84	23.97	27.65	27.51	9.04	28.08	26.46
Mg	1.35	1.65	2.08	2.21	1.73	2.17	2.28	2.26	1.32	2.08	2.25
Ca	1.82	1.61	1.52	1.57	1.50	1.56	1.52	1.37	1.58	1.40	1.54
Na	0.96	1.62	1.30	0.71	0.71	0.71	0.38	0.65	3.14	0.80	0.82
K	0.53	0.73	0.72	0.77	0.90	0.81	0.71	0.75	1.15	0.73	0.73
P	0.22	0.19	0.14	0.14	0.20	0.15	0.13	0.13	0.16	0.14	0.14
Co	0.28	0.25	0.17	0.17	0.26	0.19	0.17	0.16	0.10	0.19	0.14
Ni	0.49	0.72	1.14	1.24	0.70	1.14	1.32	1.36	0.24	1.21	1.45
Cu	0.34	0.52	1.15	1.22	0.47	1.02	1.04	1.06	0.16	1.09	1.25
Zn	0.05	0.06	0.09	0.11	0.06	0.11	0.14	0.13	0.03	0.10	0.12
Ba	0.14	0.14	0.13	0.14	0.14	0.15	0.15	0.16	0.09	0.22	0.22
TOD/DEL	0.26	0.58	1.34	1.01	0.64	1.45	1.17	1.42	0.00	1.40	1.48

LAB NUMBER	MN 45	MN 46	MN 47	MN 48	MN 49	MN 50	MN 51	MN 52	MN 53	MN 54	MN 55
DEPTH (m)	4943	5036	5128	5124	5344	5314	5503	5311	5003	5003	5303
Si	5.57	7.65	6.09	6.63	5.29	6.09	6.92	7.33	9.18	6.70	5.84
Ti	0.42	0.37	0.38	0.39	0.34	0.41	0.40	0.42	0.33	0.32	0.45
Al	2.15	2.84	2.34	2.51	2.23	2.50	2.70	2.79	2.43	2.65	2.48
Fe	6.10	5.63	5.49	5.89	5.26	5.66	5.71	6.31	4.75	4.48	6.47
Mn	27.37	23.15	25.91	25.19	26.22	24.66	24.20	23.35	23.17	25.85	22.49
Mg	2.12	2.20	2.14	2.32	2.08	2.31	2.27	2.04	1.79	2.25	1.97
Ca	1.60	1.90	1.44	1.54	1.43	1.60	1.73	1.54	1.71	1.57	1.49
Na	0.13	0.89	0.45	0.80	0.64	0.45	0.51	0.65	2.04	0.59	0.60
K	0.70	0.82	0.70	0.74	0.68	0.76	0.80	0.84	0.74	0.75	0.66
P	0.15	0.27	0.12	0.15	0.12	0.14	0.20	0.17	0.12	0.14	0.15
Co	0.21	0.16	0.21	0.24	0.21	0.23	0.21	0.18	0.17	0.15	0.24
Ni	1.19	1.19	1.25	1.20	1.15	1.13	1.14	1.04	1.07	1.35	1.05
Cu	0.85	0.84	0.97	0.99	1.02	0.99	1.02	0.97	1.11	1.18	0.84
Zn	0.11	0.10	0.11	0.10	0.11	0.13	0.12	0.12	0.12	0.12	0.11
Ba	0.18	0.21	0.16	0.14	0.19	0.13	0.18	0.18	0.11	0.20	0.16
TOD/DEL	1.04	1.01	1.50	1.32	1.55	1.26	1.23	1.12	1.15	1.30	1.27

LAB NUMBER	MN 56	MN 86	MN 89	MN 90	MN 91	MN 92	PLDS 8 D-1
DEPTH (m)	5128	4908	5005	5039	5033	4928	4500
Si	5.12	10.54	5.60	6.08	12.82	5.72	8.25
Ti	0.32	0.54	0.26	0.26	0.53	0.86	0.39
Al	2.13	3.53	2.47	2.52	4.19	1.51	2.46
Fe	5.00	9.11	3.99	4.08	7.43	10.53	6.11
Mn	26.53	14.13	27.06	26.60	13.01	19.85	21.73
Mg	1.98	1.53	2.26	2.34	1.37	1.37	2.01
Ca	1.52	4.40	1.49	1.54	1.14	1.60	1.43
Na	0.61	1.47	0.55	1.71	0.88	0.91	1.78
K	0.63	0.74	0.70	0.80	2.15	0.59	1.24
P	0.13	1.19	0.13	0.15	0.18	0.18	0.18
Co	0.18	0.18	0.14	0.14	0.19	0.30	0.20
Ni	1.11	0.59	1.37	1.42	0.57	0.72	0.95
Cu	1.11	0.50	1.41	1.74	0.43	0.46	0.73
Zn	0.12	0.08	0.14	0.38	0.08	0.07	0.10
Ba	0.18	0.10	0.18	0.20	0.12	0.17	0.17
TOD/DEL	1.33	0.78	1.59	1.51	2.45	0.61	1.55

## 1.9 APPENDIX D

**THE CONCENTRATIONS OF THE MAJOR ELEMENTS AND  
THE TODOROKITE/ $\delta\text{MnO}_2$  RATIOS FOR CRUST AND  
NODULE SAMPLES FROM SURVEY REGION B**

The abundance of each of the major elements present in the crusts and nodule samples are given as weight percents. The abundances of todorokite to  $\delta\text{MnO}_2$  is given as a ratio and therefore has no units.

FERROMANGANESE CRUSTS

LAB NUMBER DEPTH (m)	B 106 2693	CARR 6 D-1 1228	CERS 1 D-1 3424	CERS 1 D-2 3424	CERS 1 D-3 3424	CERS 1 D-4 3424	CERS 5 D-1 2700	CERS 5 D-2 2700	CERS 5 D-3 2700	CERS 6 D-1 1950	DPSN 3 D-1 3240
Si	8.41	12.56	7.40	8.89	8.67	8.36	9.98	7.46	9.17	5.76	12.01
Ti	0.34	0.98	0.20	0.27	0.22	0.21	0.28	0.24	0.27	0.47	0.49
Al	2.06	4.30	1.68	2.35	2.11	1.92	2.28	1.71	2.12	1.41	3.39
Fe	15.23	8.30	17.54	16.06	17.25	17.30	19.36	18.51	18.54	16.54	13.16
Mn	8.78	11.79	11.30	11.82	10.57	11.40	7.88	10.36	8.56	13.26	11.31
Mg	1.07	2.05	1.09	1.38	0.92	1.12	0.99	1.08	1.13	1.02	2.01
Ca	7.67	2.51	1.38	1.76	1.35	1.37	1.48	1.48	1.63	2.08	2.90
Na	1.43	2.87	1.29	1.42	1.87	1.46	2.06	1.90	1.45	1.79	2.42
K	0.59	1.81	0.51	0.60	0.66	0.61	0.58	0.52	0.53	0.49	0.57
P	0.22	0.94	0.34	0.29	0.35	0.32	0.33	0.34	0.32	0.39	0.20
Co	0.10	0.00	0.03	0.03	0.03	0.03	0.04	0.05	0.05	0.16	0.04
Ni	0.17	0.00	0.23	0.33	0.19	0.26	0.10	0.18	0.12	0.18	0.26
Cu	0.19	0.00	0.10	0.17	0.09	0.13	0.04	0.07	0.05	0.04	0.14
Zn	0.05	0.02	0.05	0.05	0.04	0.05	0.05	0.06	0.05	0.04	0.04
Ba	0.19	0.13	0.12	0.12	0.13	0.12	0.14	0.14	0.13	0.14	0.21
TOD/DEL	0.24	2.82	0.14	0.65	0.09	0.33	0.00	0.13	0.16	0.00	1.17

LAB NUMBER	DPSN 3 D-1	DPSN 3 D-2	DPSN 3 D-2	DPSN 3 D-3	DPSN 3 D-3	DPSN 3 D-4	DPSN 4 D-1	DPSN 5 D-1	DPSN 5 D-2	DPSN 5 D-3	HEN SMT D-3
DEPTH (m)	3240	3240	3240	3240	3240	3240	2957	3124	3124	3124	64
Si	13.15	6.92	13.10	13.16	13.63	8.58	10.89	7.27	8.14	9.38	10.52
Ti	0.59	0.19	0.58	0.31	0.33	0.31	0.42	0.23	0.27	0.35	0.11
Al	3.75	1.68	3.85	4.59	4.49	2.34	2.88	1.86	2.04	2.17	0.88
Fe	11.56	15.08	13.10	10.96	12.70	13.21	15.06	14.90	16.50	13.79	12.67
Mn	10.14	14.42	8.70	9.03	7.33	14.89	10.12	13.32	12.02	14.37	19.72
Mg	2.27	1.04	2.04	3.32	3.11	1.50	1.64	1.11	1.12	1.81	2.18
Ca	3.80	1.72	3.58	4.69	4.18	2.24	2.68	1.87	1.81	2.38	0.68
Na	1.92	1.54	1.90	1.56	1.82	1.77	1.66	2.39	1.28	1.88	1.12
K	0.44	0.50	0.50	0.35	0.43	0.58	0.54	0.58	0.50	0.56	2.34
P	0.19	0.26	0.21	0.16	0.17	0.24	0.23	0.27	0.26	0.24	0.15
Co	0.02	0.04	0.04	0.03	0.04	0.03	0.03	0.04	0.04	0.03	0.06
Ni	0.27	0.35	0.19	0.22	0.17	0.34	0.23	0.30	0.24	0.29	0.20
Cu	0.14	0.16	0.10	0.08	0.09	0.21	0.10	0.13	0.12	0.15	0.01
Zn	0.04	0.06	0.03	0.04	0.04	0.05	0.05	0.05	0.05	0.06	0.02
Ba	0.13	0.19	0.15	0.10	0.13	0.23	0.15	0.16	0.18	0.23	0.65
TOD/DEL	0.86	0.42	0.63	0.51	0.46	1.04	0.51	0.17	0.63	1.17	0.41



LAB NUMBER	QBR 1 D-1	QBR 2 D-1	QBR 7 D-1	QBR 7(B) D-1	QBR 7(B) D-2	QBR 22 D-1	RISE 3 3 D-1	RISE 3 3 D-2	RISE 3 6 D-1	RISE 3 6 D-2	RISE 3 6 D-3
DEPTH (m)	2550	2550	3000	3000	3000	1680	2095	2095	2703	2703	2703
Si	12.78	11.36	10.95	12.68	20.64	1.25	0.03	0.00	13.83	8.45	8.58
Ti	0.71	0.70	0.84	0.30	1.37	0.04	0.04	0.02	0.41	0.23	0.22
Al	4.16	3.27	2.99	1.14	5.78	0.07	0.00	0.00	4.33	1.92	2.06
Fe	11.84	13.79	13.75	13.58	11.64	4.77	0.23	0.19	11.83	18.05	17.65
Mn	8.73	8.43	9.87	13.89	2.08	33.60	42.34	42.31	8.71	10.37	10.18
Mg	2.38	1.86	2.06	2.25	3.54	1.98	1.68	1.19	2.80	0.91	0.90
Ca	4.47	2.62	3.30	1.50	7.09	1.53	2.94	2.55	4.36	1.64	1.61
Na	1.59	1.97	2.51	1.59	2.32	2.31	2.08	3.88	2.48	1.54	1.85
K	0.46	0.95	0.41	1.72	0.32	0.90	0.72	0.50	0.45	0.50	0.53
P	0.18	0.23	0.22	0.10	0.12	0.12	0.02	0.02	0.20	0.35	0.36
Co	0.07	0.12	0.08	0.02	0.02	0.00	0.00	0.01	0.05	0.04	0.03
Ni	0.15	0.12	0.21	0.12	0.04	0.12	0.03	0.01	0.21	0.13	0.14
Cu	0.10	0.02	0.12	0.05	0.02	0.01	0.00	0.00	0.11	0.06	0.07
Zn	0.01	0.02	0.04	0.04	0.01	0.06	0.01	0.00	0.03	0.04	0.04
Ba	0.07	0.09	0.13	0.08	0.07	0.09	0.33	0.11	0.15	0.15	0.14
TOD/DEL	0.00	0.00	0.56	0.00	0.08	0.19	1.67	1.33	0.87	0.05	0.07

LAB NUMBER DEPTH (m)	RISE 3 7 D-1 2183	RISE 3 8 D-1 2450	RISE 3 13 D-1 2251	SIQR 4 D-1 3325	SIQR 4 D-2 3325	SIQR 4 D-3 3325	SIQR 4 D-4 3325	SOTW 9 32 D-1 3400	TRIPOD 2 D-1 1711	TRIPOD 2 D-2 1711	TRIPOD 3 D-1 2496
Si	5.37	11.32	8.67	7.61	6.83	6.90	6.68	22.79	3.67	3.16	10.66
Ti	0.29	0.37	0.42	0.29	0.27	0.25	0.27	0.81	0.45	0.48	0.32
Al	1.15	3.23	2.35	1.78	1.66	1.59	1.61	7.41	0.55	0.34	2.90
Fe	20.66	16.97	16.03	17.61	17.34	17.96	17.21	8.22	17.19	17.91	10.37
Mn	11.11	7.15	10.46	11.54	12.89	12.71	13.45	0.53	15.50	15.88	13.33
Mg	0.87	1.81	1.53	1.11	1.05	1.02	1.02	5.77	0.85	0.85	2.11
Ca	1.74	2.93	2.79	1.77	1.67	1.60	1.68	7.79	1.88	1.88	1.19
Na	1.13	1.56	1.43	1.35	1.43	1.23	1.02	1.91	2.44	2.54	1.64
K	0.39	0.50	0.53	0.48	0.48	0.47	0.48	0.19	0.52	0.42	0.99
P	0.41	0.30	0.33	0.27	0.29	0.27	0.28	0.05	0.50	0.50	0.17
Co	0.06	0.04	0.06	0.05	0.04	0.04	0.04	0.02	0.26	0.28	0.18
Ni	0.14	0.07	0.15	0.23	0.27	0.29	0.27	0.01	0.18	0.18	0.44
Cu	0.03	0.02	0.03	0.11	0.13	0.15	0.12	0.00	0.00	0.00	0.11
Zn	0.04	0.03	0.05	0.04	0.05	0.05	0.06	0.00	0.03	0.03	0.05
Ba	0.13	0.11	0.11	0.15	0.15	0.18	0.15	0.02	0.14	0.16	3.10
TOD/DEL	0.00	0.00	0.00	0.03	0.20	0.24	0.16	0.00	0.00	0.00	2.13

LAB NUMBER	TRIPOD 3 D-2	TRIPOD 9 D-1	TRIPOD 9 D-2
DEPTH (m)	2496	2984	2984
Si	7.60	19.42	8.93
Ti	0.42	1.58	0.77
Al	1.61	7.37	2.71
Fe	15.95	9.14	11.76
Mn	14.44	1.94	12.95
Mg	1.21	3.09	1.47
Ca	1.46	4.53	1.74
Na	1.33	2.58	1.83
K	0.62	1.48	0.92
P	0.32	0.25	0.20
Co	0.22	0.04	0.21
Ni	0.33	0.06	0.40
Cu	0.04	0.04	0.24
Zn	0.05	0.02	0.05
Ba	0.21	0.08	0.34
TOD/DEL	0.55	0.00	0.52

FERROMANGANESE NODULES

LAB NUMBER	A 90	B 4	B 5	B 6	B 102	B 103	B 104	B 105	B 107	B 109	B 110
DEPTH (m)	4459	3172	3886	4105	3220	5118	3522	3551	4003	3988	3964
Si	6.04	5.85	5.32	5.23	9.70	20.39	4.99	10.07	7.58	7.45	6.37
Ti	0.23	0.36	0.35	0.29	0.39	1.11	0.28	0.16	0.31	0.30	0.33
Al	1.95	1.77	1.75	1.81	2.28	4.15	1.54	2.76	2.72	2.50	2.18
Fe	4.60	11.21	8.90	6.97	14.85	11.10	7.24	5.11	6.91	6.64	7.77
Mn	26.79	21.14	22.14	25.36	12.54	1.12	23.81	4.91	21.83	24.05	23.16
Mg	1.97	1.43	1.58	1.77	1.07	1.99	1.40	1.23	2.11	1.97	1.81
Ca	1.47	2.08	1.88	1.54	3.72	0.83	1.59	13.04	1.36	1.46	1.57
Na	2.08	2.02	1.79	1.92	1.77	2.59	1.98	2.44	2.35	2.22	1.93
K	1.18	0.57	0.67	0.80	0.73	1.48	0.67	1.22	1.01	1.02	0.89
P	0.13	0.24	0.19	0.16	0.25	0.07	0.16	4.71	0.16	0.16	0.17
Co	0.15	0.07	0.09	0.10	0.09	0.02	0.07	0.03	0.10	0.15	0.15
Ni	1.01	0.82	0.82	1.04	0.15	0.02	0.88	0.21	0.93	0.89	0.91
Cu	0.85	0.38	0.52	0.71	0.15	0.08	0.66	0.17	0.54	0.60	0.57
Zn	0.16	0.09	0.10	0.10	0.04	0.02	0.12	0.04	0.09	0.09	0.08
Ba	0.25	0.16	0.21	0.26	0.17	0.27	0.26	1.28	0.34	0.25	0.34
TOD/DEL	1.43	0.57	0.88	1.21	0.45	0.00	0.95	0.00	1.12	1.07	0.94

LAB NUMBER	B 111	B 112	B 113	B 114	CARR 9 D-1	CARR 9 D-2	CERS 9 D-1	CERS 9 D-2	CERS 10 D-1	CERS 10 D-2	CERS 10 D-3
DEPTH (m)	4087	4169	4207	4295	5276	5276	2300	2300	3478	3478	3478
Si	5.85	13.72	11.00	6.67	6.48	7.22	7.24	14.46	4.73	6.21	6.74
Ti	0.30	0.25	0.21	0.30	0.60	0.49	0.36	0.47	0.15	0.17	0.19
Al	1.98	3.87	3.28	2.39	2.20	2.33	1.82	4.62	1.78	2.16	2.34
Fe	7.34	7.64	5.72	5.29	10.44	9.94	14.39	10.40	4.30	6.70	8.43
Mn	25.04	14.31	19.83	25.75	19.12	20.47	16.03	10.40	30.65	26.03	23.39
Mg	1.73	1.96	1.90	1.97	1.37	1.53	1.67	3.33	1.73	1.70	1.79
Ca	1.54	0.99	1.15	1.44	1.52	1.36	1.36	4.74	1.22	1.26	1.21
Na	2.39	2.03	2.30	1.60	1.88	1.91	1.55	1.58	1.55	2.23	1.84
K	0.89	1.89	1.54	1.07	0.71	0.79	0.58	0.50	0.74	0.75	0.84
P	0.17	0.13	0.13	0.13	0.22	0.19	0.25	0.12	0.12	0.16	0.18
Co	0.17	0.11	0.11	0.15	0.07	0.07	0.13	0.09	0.01	0.01	0.02
Ni	1.05	0.59	0.75	1.12	0.55	0.60	0.61	0.38	0.44	0.49	0.45
Cu	0.64	0.41	0.64	0.76	0.50	0.65	0.16	0.10	0.22	0.31	0.29
Zn	0.17	0.07	0.21	0.11	0.06	0.07	0.07	0.04	0.14	0.11	0.09
Ba	0.26	0.23	0.36	0.23	0.20	0.25	0.22	0.19	0.12	0.20	0.29
TOD/DEL	0.79	0.88	1.47	1.11	1.19	1.25	1.19	1.25	0.88	1.41	1.54

LAB NUMBER DEPTH (m)	CERS 11 D-1 2850	CERS 13 D-1 3317	CERS 13 D-2 3317	CERS 14 D-1 3070	CERS 15 D-1 2940	CERS 15 D-2 2940	CERS 15 D-3 2940	CERS 16 D-1 3250	CERS 16 D-2 3250	CERS 16 D-3 3250	CERS 17 D-1 1920
Si	6.45	4.65	6.51	2.23	7.61	9.26	9.68	5.90	8.35	6.60	26.84
Ti	0.20	0.16	0.22	0.09	0.22	0.20	0.22	0.19	0.17	0.19	0.13
Al	1.88	1.45	1.95	0.91	2.24	2.66	2.69	1.78	1.92	1.93	0.56
Fe	9.12	5.72	11.72	1.65	10.41	12.70	9.09	12.66	13.31	12.07	16.89
Mn	23.12	30.27	18.31	39.48	21.37	15.91	19.98	18.58	15.77	19.45	1.07
Mg	2.07	1.47	1.26	1.68	1.99	1.92	1.87	1.54	1.43	1.41	1.31
Ca	1.25	1.31	1.53	1.29	1.18	1.36	1.26	1.42	1.27	1.49	0.18
Na	0.70	1.87	1.61	2.15	1.52	1.92	1.40	1.60	1.58	1.84	0.53
K	0.78	0.59	0.56	0.82	0.77	0.72	0.80	0.56	0.77	0.57	1.63
P	0.17	0.13	0.23	0.07	0.17	0.17	0.15	0.23	0.21	0.23	0.10
Co	0.03	0.01	0.03	0.00	0.07	0.04	0.03	0.04	0.02	0.02	0.03
Ni	0.58	0.43	0.53	0.26	0.47	0.43	0.49	0.60	0.38	0.60	0.04
Cu	0.32	0.17	0.18	0.11	0.27	0.18	0.20	0.36	0.17	0.29	0.00
Zn	0.11	0.10	0.12	0.08	0.07	0.07	0.08	0.10	0.08	0.12	0.01
Ba	0.27	0.12	0.13	0.24	0.42	0.22	0.26	0.19	0.15	0.14	0.05
TOD/DEL	1.23	1.20	0.51	2.36	1.50	1.27	1.66	1.16	0.68	0.82	0.00

LAB NUMBER	CERS 18 D-1	CERS 19 D-1	CERS 19 D-2	CERS 19 D-3	CERS 20 D-1	CERS 20 D-2	CERS 20 D-3	CERS 21 D-1	CERS 21 D-2	CERS 21 D-3	DWBD 1-1
DEPTH (m)	2860	2930	2930	2930	2975	2975	2975	3080	3080	3080	4300
Si	6.16	4.56	3.24	5.42	6.02	4.14	4.60	5.24	4.58	2.38	14.42
Ti	0.18	0.15	0.13	0.21	0.21	0.14	0.17	0.34	0.17	0.09	0.55
Al	1.75	1.57	1.33	1.67	1.97	1.63	1.54	1.22	1.76	1.14	5.12
Fe	9.17	4.24	2.88	7.44	6.68	3.57	5.89	15.90	4.53	1.82	8.89
Mn	22.52	31.36	34.25	25.31	26.08	33.45	29.23	13.98	31.07	37.22	7.82
Mg	1.33	1.54	1.51	1.61	1.92	2.28	1.70	0.89	1.95	2.13	0.80
Ca	1.61	1.34	1.27	1.56	1.34	1.19	1.42	1.65	1.22	1.15	1.49
Na	1.99	2.59	2.93	1.94	1.02	1.27	1.60	1.58	1.45	1.37	2.82
K	0.63	0.62	0.71	0.67	0.69	0.83	0.77	0.46	0.76	0.84	2.40
P	0.20	0.11	0.10	0.17	0.14	0.10	0.13	0.32	0.13	0.08	0.23
Co	0.03	0.02	0.01	0.03	0.03	0.00	0.02	0.08	0.01	0.01	0.16
Ni	0.69	0.50	0.45	0.76	0.65	0.63	0.60	0.23	0.69	0.56	0.12
Cu	0.28	0.23	0.13	0.32	0.31	0.30	0.23	0.04	0.32	0.25	0.11
Zn	0.12	0.12	0.14	0.19	0.11	0.14	0.12	0.03	0.12	0.22	0.02
Ba	0.15	0.19	0.10	0.16	0.20	0.31	0.23	0.14	0.28	0.29	0.31
TOD/DEL	1.08	2.00	0.39	1.11	1.57	2.22	1.39	0.00	2.23	2.68	0.00

LAB	DWBD	J	J	J	J	J	MERO	MERO	MERO	MN	MN
NUMBER	1-2	123	124	125	126	127	2P-52-1	2P-52-2	2P-52-3	1	2
DEPTH (m)	4300	4822	4813	4606	5188	5210	4930	4930	4930	3980	4072
Si	27.51	10.42	6.10	7.65	6.90	11.92	4.37	10.65	7.05	5.58	5.03
Ti	0.26	0.33	0.45	0.66	0.52	0.41	0.25	0.38	0.21	0.21	0.26
Al	1.58	3.57	2.17	2.53	2.55	4.30	1.70	3.13	2.17	2.04	1.89
Fe	8.17	5.19	6.36	9.22	8.03	8.76	3.90	6.03	3.25	5.72	5.50
Mn	6.01	19.36	23.57	16.70	21.30	13.90	29.01	18.81	25.69	26.13	27.94
Mg	1.15	2.16	2.16	1.56	2.01	1.71	2.16	2.03	1.69	1.84	1.76
Ca	0.37	1.51	1.55	1.61	1.47	0.96	1.35	1.38	1.62	1.50	1.40
Na	0.84	1.57	2.58	3.99	1.99	2.54	1.48	1.92	2.02	1.31	0.98
K	0.98	1.40	1.15	1.45	0.88	1.96	0.90	1.11	0.85	0.70	0.71
P	0.06	0.18	0.20	0.23	0.17	0.17	0.13	0.19	0.12	0.14	0.14
Co	0.09	0.21	0.23	0.29	0.27	0.21	0.16	0.21	0.14	0.12	0.12
Ni	0.31	0.91	0.94	0.51	0.87	0.55	1.25	0.87	1.31	1.08	1.07
Cu	0.14	0.67	0.60	0.25	0.59	0.35	0.96	0.58	1.03	0.89	0.74
Zn	0.02	0.07	0.07	0.04	0.06	0.04	0.12	0.07	0.11	0.11	0.13
Ba	0.56	0.20	0.29	0.14	0.14	0.20	0.30	0.27	0.25	0.45	0.27
TOD/DEL	0.11	0.95	1.01	0.44	0.91	0.91	1.77	1.43	1.39	1.35	1.19



LAB NUMBER	MN 3	MN 4	MN 5	MN 6	MN 7	MN 8	MN 9	MN 10	MN 11	MN 12	MN 13
DEPTH (m)	3980	4255	4255	4438	4392	4300	4392	4002	4302	4758	4712
Si	12.20	8.04	10.01	6.78	6.63	6.42	5.50	5.34	5.99	7.56	5.00
Ti	0.25	0.28	0.23	0.37	0.32	0.35	0.29	0.61	0.32	0.37	0.29
Al	3.91	2.69	2.91	2.28	2.22	2.30	2.12	1.77	2.14	2.63	1.98
Fe	5.70	6.13	5.24	6.15	6.59	6.39	5.97	10.24	6.34	5.65	5.10
Mn	16.17	23.76	21.78	24.06	25.49	25.04	26.70	21.82	26.14	22.55	27.56
Mg	1.67	2.11	2.12	1.77	1.95	1.94	1.89	1.56	2.10	1.83	1.80
Ca	1.08	1.39	1.16	1.48	1.48	1.46	1.38	1.60	1.40	1.54	1.49
Na	2.38	0.67	1.77	2.11	1.52	0.76	0.79	0.93	0.75	0.71	0.67
K	2.01	1.06	1.38	0.99	0.95	0.89	0.67	0.58	0.77	0.87	0.61
P	0.13	0.14	0.16	0.15	0.16	0.14	0.13	0.20	0.14	0.15	0.13
Co	0.10	0.19	0.16	0.18	0.25	0.21	0.25	0.31	0.26	0.21	0.23
Ni	0.80	1.09	0.77	0.96	1.08	1.07	1.12	0.79	1.10	1.12	1.23
Cu	0.48	0.81	0.76	0.75	0.76	0.76	0.78	0.41	0.79	0.79	0.87
Zn	0.08	0.08	0.07	0.08	0.09	0.10	0.10	0.06	0.09	0.08	0.10
Ba	0.39	0.22	0.85	0.25	0.21	0.17	0.23	0.13	0.22	0.27	0.22
TOD/DEL	2.49	1.40	1.81	1.01	1.33	1.35	1.27	0.70	1.38	1.02	1.56

LAB NUMBER	MN 15	MN 16	MN 17	MN 18	MN 19	MN 20	MN 21	MN 22	MN 24	MN 25	MN 26
DEPTH (m)	3568	3614	3660	3568	3660	3660	3660	3660	3642	3623	3861
Si	6.08	6.67	7.12	6.70	7.10	6.12	7.20	6.62	6.42	7.24	3.64
Ti	0.25	0.26	0.21	0.26	0.24	0.25	0.25	0.28	0.26	0.28	0.11
Al	1.89	1.99	2.32	1.92	2.18	1.78	2.19	1.98	1.87	2.13	1.15
Fe	9.18	8.82	7.08	9.36	8.11	9.35	8.63	9.90	8.64	10.31	2.07
Mn	23.77	23.82	24.57	23.14	24.01	24.68	23.18	23.88	22.79	21.51	12.44
Mg	1.63	1.77	1.70	1.79	1.79	1.69	1.65	1.78	1.73	1.74	1.13
Ca	1.40	1.40	1.46	1.45	1.42	1.45	1.44	1.49	1.42	1.30	20.62
Na	0.82	0.65	0.87	0.79	0.51	1.35	0.87	0.85	0.94	0.87	1.19
K	0.73	0.80	0.82	0.82	0.81	0.73	0.78	0.77	0.76	0.83	0.41
P	0.17	0.18	0.15	0.19	0.17	0.18	0.17	0.19	0.17	0.19	8.13
Co	0.12	0.10	0.08	0.11	0.10	0.12	0.12	0.13	0.11	0.12	0.06
Ni	0.88	0.81	0.89	0.82	0.86	0.86	0.89	0.80	0.87	0.68	0.57
Cu	0.51	0.49	0.51	0.52	0.55	0.51	0.53	0.42	0.50	0.49	0.53
Zn	0.11	0.10	0.10	0.10	0.10	0.11	0.10	0.09	0.11	0.07	0.06
Ba	0.16	0.17	0.20	0.18	0.18	0.18	0.19	0.18	0.16	0.22	0.07
TOD/DEL	1.07	1.16	0.90	1.10	1.11	0.97	0.96	0.82	1.00	1.11	1.94

LAB NUMBER DEPTH (m)	MN 27 3697	MN 28 3687	MN 29 3770	MN 30 3770	MN 31 4483	MN 93 4414	QBR 8(C) D-1 3700	QBR 8(C) D-2 3700	RISE 3 19 D-1 2260	RISE 3 20 D-1 1843	RISE 3 24 D-1 2308
Si	6.51	6.28	6.68	6.27	5.24	5.89	7.42	6.64	8.72	9.06	4.21
Ti	0.26	0.24	0.28	0.22	0.32	0.23	0.46	0.50	0.56	0.69	0.12
Al	1.98	1.91	2.10	2.05	2.01	2.16	2.58	2.22	2.68	2.97	1.56
Fe	8.91	8.78	8.55	7.67	5.89	5.10	8.57	8.66	14.32	12.57	5.35
Mn	23.90	23.55	23.41	24.87	27.47	27.24	20.24	21.73	10.74	12.48	32.26
Mg	1.73	1.64	1.58	1.63	1.60	1.91	1.81	1.55	1.52	2.17	2.37
Ca	1.37	1.38	1.44	1.46	1.45	1.49	1.52	1.46	2.58	2.13	0.95
Na	0.94	0.85	0.99	1.25	0.67	0.93	1.85	2.88	1.69	1.51	1.76
K	0.80	0.73	0.75	0.80	0.62	0.86	0.77	0.76	0.59	0.81	1.00
P	0.19	0.18	0.17	0.16	0.13	0.14	0.18	0.18	0.31	0.27	0.13
Co	0.11	0.11	0.15	0.14	0.20	0.20	0.08	0.08	0.12	0.20	0.03
Ni	0.77	0.87	0.96	0.91	1.28	1.11	0.62	0.54	0.19	0.19	0.50
Cu	0.49	0.48	0.60	0.60	0.91	1.03	0.62	0.59	0.02	0.01	0.33
Zn	0.09	0.10	0.10	0.11	0.10	0.17	0.06	0.06	0.03	0.04	0.08
Ba	0.20	0.19	0.18	0.18	0.22	0.21	0.27	0.32	0.10	0.10	0.63
TOD/DEL	1.07	1.06	1.00	1.20	1.25	1.29	1.52	1.25	0.00	0.65	2.27

LAB	RISE 3	S	S	TRIPOD	TRIPOD
NUMBER	28 D-1	74	75	4 D-1	4 D-2
DEPTH (m)	1693	3787	4959	3840	3840
Si	3.53	18.93	7.22	6.01	5.82
Ti	0.65	0.43	0.38	0.27	0.21
Al	0.83	5.13	2.58	1.85	1.88
Fe	14.54	10.00	6.20	8.94	7.67
Mn	16.38	4.67	23.99	21.27	23.14
Mg	1.06	1.41	2.27	1.58	1.66
Ca	1.84	0.90	1.20	1.36	1.47
Na	1.61	2.72	1.63	1.55	2.09
K	0.39	2.97	1.17	0.84	0.96
P	0.41	0.18	0.12	0.19	0.16
Co	0.51	0.10	0.26	0.11	0.12
Ni	0.33	0.20	0.99	0.82	0.84
Cu	0.00	0.08	0.63	0.53	0.51
Zn	0.04	0.02	0.08	0.09	0.12
Ba	0.14	0.14	0.25	0.18	0.21
TOD/DEL	0.10	0.03	1.41	1.06	1.16

## **CHAPTER 2**

# **DEVELOPMENT OF A SELECTIVE SEQUENTIAL EXTRACTION SCHEME AND A DIFFERENTIAL X-RAY DIFFRACTION TECHNIQUE TO DETERMINE THE CHEMICAL PARTITIONING OF Mn, Fe, Cu, Ni, AND Co BETWEEN THE MANGANESE AND IRON OXIDE PHASE MINERALOGY IN FERROMANGANESE CRUSTS AND NODULES**

## 2.1 INTRODUCTION

### 2.1.1 REVIEW OF PREVIOUS WORK

#### 2.1.1.1 Selective Dissolution of Manganese and Iron Oxides in Soils and Sediments

Several reagents have been employed over the past several years for the selected removal of Fe or Mn oxides in soils and sediments, the most widely used being sodium dithionite. Deb (1949) found this reagent to be superior to several others in terms of the efficient removal of Fe oxides and less destructive effects on clay minerals. Different versions of the sodium-dithionite method have been published since then (Aguilera & Jackson, 1953; Mitchell & Mackenzie, 1954; Mehra & Jackson, 1960; Kilmer, 1960; Coffin, 1963; Holmgren, 1967). The major variations involved in this reduction step are: (1) pH and temperature of the reaction medium, (2) presence of chelating and buffering agents, (3) single or multiple treatments, (4) length of reaction, and (5) the form (solution vs. solid) and amounts of sodium-dithionite added. Another variation employs sodium dithionite for the reduction, sodium bicarbonate as a buffer, and sodium citrate as a chelating agent for ferrous and ferric iron. The citrate-dithionite-bicarbonate (CDB) method was developed by Mehra & Jackson (1960) and Coffin (1963).

Acid ammonium oxalate (Tamm's reagent) is another reagent that has been widely used in soil studies. Le Riche & Weir (1963) and de Endredy (1963) used ammonium oxalate for the extraction of free iron oxides in soils under ultraviolet irradiation. They found that both hematite and goethite were dissolved. The same procedure was carried out in darkness by McKeague & Day (1966) and by

McKeague *et al.* (1971). They found that the oxalate extraction dissolved much of the Fe from the amorphous oxides and very little from the crystalline oxides.

Potassium or sodium pyrophosphate has been suggested for the extraction of organically-complexed Fe (Aleksandrova, 1960; Bascomb, 1968). McKeague (1967) and McKeague *et al.* (1971) showed that sodium pyrophosphate is reasonably specific for the removal of organically-complexed Fe.

Oxalic acid has been used as an extractant in studies of soil weathering (Alminas & Mosier, 1976), and for studies of the classification and interpretation of the course of podsolization in soils (Ball & Beaumont, 1972). Gallagher & Walsh (1943) used boiling oxalic acid to dissolve weathering products for characterizing different soils.

On the basis of the differential response of Mn oxides and Fe oxides to chemical reduction and solution in an acid medium, Chao (1972) developed a method for the selective dissolution of Mn oxides from soils and sediments using acidified hydroxylamine hydrochloride. He found that the hydroxylamine solution was effective in dissolving Mn oxide minerals but did not dissolve Fe oxides.

#### 2.1.1.2 Selective Sequential Extraction Schemes for Soils and Sediments

Selective chemical extraction schemes are widely employed to obtain information about the "solid speciation" of metals in soils, sediments, and other natural particulate phases (Salomons & Förstner, 1983). In a sequential extraction scheme, each successive chemical treatment is more drastic than the previous one (Chao & Theobald, 1976). Several selective sequential extraction schemes have been proposed over the last several years. An example of some of these sequential extraction schemes can be found in Chao & Theobald (1976), Hoffman & Fletcher

(1979), Tipping *et al.* (1985). All of the extraction schemes have used chemical reduction as the initial step for removing Mn and Fe oxides (Oades, 1963). Most of the proposed schemes have used hydroxylamine hydrochloride in nitric acid to remove the Mn oxides and ammonium oxalate in oxalic acid to remove the Fe oxides.

### 2.1.1.3 Selective Dissolution of Manganese and Iron Oxides

#### in Crusts and Nodules

Selective dissolution studies of Mn and Fe oxides in marine ferromanganese crusts and nodules has not been as intense as for soils and sediments. The first attempts at the selective dissolution of Mn oxides in nodules were by Buser & Grütter (1956) and by Arrhenius & Korkish (1959). They showed that nodules contain a reduceable fraction of Mn oxides which can be separated by using a solution of hydroxylamine hydrochloride. Arrhenius (1963) then investigated selective dissolution in nodules by using hydrochloric acid and hydroxylamine hydrochloride. Chester & Hughes (1967) later confirmed the findings of Buser & Grütter (1956) and Arrhenius & Korkish (1959), and found that a combined acid-reducing solution of hydroxylamine hydrochloride in acetic acid will effectively dissolve almost all the iron and manganese oxide phases from nodules.

During the 1970's, interest in the selective extraction of Mn and Fe oxides in nodules was directed towards extractive metallurgy. Nodules are an oxidized ferromanganese matrix containing about 3% combined content of the highly valued metals cobalt, copper, and nickel. These metals are disseminated throughout the oxide phases as well as being a part of the matrix minerals. The valued metals are therefore not present in nodules as discrete minerals and cannot be concentrated by conventional methods. Most of the extractive metallurgical processes are based upon destruction of the manganese oxide crystal lattice to liberate the contained

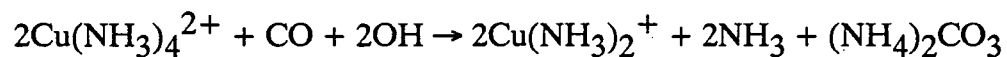
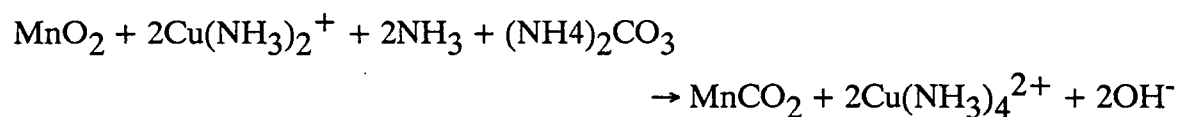


metals, usually by chemical reduction. Such hydrometallurgical processes can be classified according to those that solubilize the manganese, such as a hydrochloric acid leach or a sulphuric acid leach, and those that specifically dissolve only the highly valued metals, such as an ammonia leach process (Hubred, 1980).

The principal hydrometallurgical processes have evolved from the work of companies grouped together in four major consortia and they have been reviewed by Hubred (1980). The process used by Kennecott is a reductive ammonia leach. An ammonia leach is well suited to manganese nodules because the Co, Cu, and Ni all form soluble amine complexes with ammonia; but the iron, manganese, silica, and carbonates are nearly insoluble during the overall reaction. Manganese is reacted with carbon monoxide and precipitated as manganese carbonate:



Iron is not attacked, but Cu, Ni, and Co released during the matrix attack are solubilized by ammonia. The process is called the Curion process, because cuprous ion is a "catalyst" necessary for the reduction of the manganese:



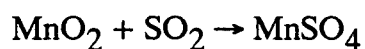
Nickel, copper, and cobalt are then recovered by fluid ion exchange. The metals are coextracted and then selectively stripped.

The Ocean Mining Associates have developed an acid-chloride leaching process, which is characterized by total dissolution of the manganese oxides. Manganese is reduced with hydrochloric acid:



All the other metals are solubilized as chloride complexes. Chlorine gas is generated as a by-product. Iron is removed from solution by anion exchange solvent extraction and copper by cation exchange. Increasing the pH allows for the removal of nickel and cobalt as hydroxides.

In the late 1970's and into the 1980's, the exploitive use of selective dissolution of Mn and Fe oxides from crusts and nodules diminished. Arrhenius *et al.*, (1979), Bowser *et al.* (1979), Takematsu (1979), and Bléry-Oustrière (1980), using a variety of chemical leaches have all examined the selective dissolution of Mn, Fe and associated metals from manganese nodules. These studies, however, were all carried out on a very limited number of deep-sea nodules. Several studies still explored extractive metallurgy. The use of a sulphuric acid leaching procedure under moderate conditions was proposed by Itoh *et al.* (1980) in the metallurgical processing of nodules by Japan, while Han & Fuerstenau (1980) examined a sulphur dioxide leaching procedure. The sulphuric acid leaching procedure was found to be the most effective and economical procedure for the extraction of Cu, Ni and Co from nodules without dissolving any Mn or Fe oxides. The sulphur dioxide leaching procedure, however, was found to be just as effective as hydroxylamine hydrochloride. Sulphur dioxide quickly attacks the Mn oxides and releases the metals:



Moorby & Cronan (1981) used several selective leaching procedures to extract the principal chemical phases from nodules. They proposed the following leaching procedure. An acidic acid leach which dissolves any calcium carbonate present and will attack absorbed ions. An hydroxylamine-hydrochloride in acidic acid leach dissolves the reducible Mn and Fe oxides and oxyhydroxides. Finally an hydrochloric acid leach which dissolves the iron oxyhydroxides which are not soluble in the hydroxalymine-hydrochloride. By using these progressively more vigorous chemical attacks, the principal phases of the nodules were selectively removed in sequential order (Moorby & Cronan, 1981). Although they proposed this selective sequential extraction scheme, each step of the leaching procedure was preformed on a new sample instead of sequentially removing each principal chemical phase from the same sample. This procedure can not be truely considered a selective sequential extraction scheme aimed at specifically removing the Mn oxyhydroxides first then removing the Fe oxyhydroxides from a crust or nodule.

Extractive metallurgy of crusts was first attempted by Haynes *et al.* (1987). They examined two hydrometallurgical processes. The first process is called the Cuprion Ammoniacal Leach Process involves a low-temperature hydrometallurgical reduction of manganese IV to manganese II by an aqueous ammonia solution containing an excess of cuprous ions. The metals are solubilized from the reduced crusts with a strong aqueous solution of ammonia and carbon dioxide at low temperature and pressure. The metal-bearing solution is treated to remove copper, followed by nickel recovery using liquid ion exchange methods. The cobalt can then be recovered by selective precipitation with hydrogen sulfide, pressure leached with sulphuric acid, and selective reduction with hydrogen to precipitate cobalt as a powder. The second process is called the High-Temperature and High-Pressure Sulphuric Acid Leach Process involves a sulphuric acid leaching of the crusts under

high temperature and pressure. Copper, nickel, and cobalt are dissolved while manganese and iron are not solubilized. After cooling, the metal-bearing sulfuric solution is treated similarly to the ammoniacal solution.

Murad & Schwertmann (1988) first attempted to identify the Fe oxide mineralogy of some deep-sea crusts by using a selective sequential extraction scheme. They selectively dissolved the Mn oxides using ammonium oxalate in the dark (Schwertmann, 1964). This method is widely used in soils studies and dissolves all  $\text{Mn}^{4+}$  oxides, but only the poorly crystalline  $\text{Fe}^{3+}$  oxides such as ferrihydrite and ferrihydrite. To concentrate the iron oxides, the samples were then treated to eight successive treatments with hydroxylamine hydrochloride. This treatment reduces the  $\text{Mn}^{4+}$  oxides and not the  $\text{Fe}^{3+}$  oxides. They concluded that the extraction of Mn oxides from the crusts using hydroxylamine-hydrochloride treatment causes the iron oxide mineralogy to change and recommended that this reagent not be used for the selective enrichment of iron oxides in deep-sea crusts.

Acharya *et al.* (1989) studied the ammonia leaching of ocean nodules using various reductants. The leaching of nodules with ammonia has several advantages. These are the non-dissolution of iron, and aluminosilicate and the selective dissolution of Cu, Ni, and Co. For the effective and rapid dissolution of Cu, Ni, and Co from Mn oxides, the presence of a reductant is necessary. The various reductants used by these authors include  $\text{FeSO}_4$ ,  $\text{MnSO}_4$ ,  $\text{H}_2\text{SO}_3$ ,  $\text{FeS}$ , and glucose. They concluded that most of the Cu, Ni, and Co could be leached using  $\text{FeSO}_4$ ,  $\text{MnSO}_4$ ,  $(\text{NH}_4)_2\text{SO}_3$ , and  $\text{FeS}$  as reductants. The complete chemical equations for the reductant processes can be found in Acharya *et al.* (1989).

#### 2.1.1.4 Differential X-Ray Diffraction

As in the case of ferromanganese crusts and nodules, the identification and quantitative determination of Fe oxides in soils by routine X-ray diffraction (XRD) procedures is often difficult or impossible. The reasons are similar to those plaguing the identification of Fe oxides in crusts and nodules: (1) the Fe oxides often make up only a small percentage of the sample and/or (2) as in the case of ferrihydrite, the Fe oxide peaks are so broad that they are difficult to recognize when peaks due to other mineral components are also present (Schulze, 1981).

Schulze (1981) first described a method for identifying the Fe phase mineralogy in soils. An XRD pattern of a sample containing Fe oxides can be considered as being made up of two components: (1) the pattern of the Fe oxide minerals and (2) the pattern of the other minerals present. If an X-ray pattern of a sample is obtained before any treatment and a second pattern is obtained for the sample after selective dissolution of all or part of the Fe oxides, this second pattern should be identical to the first, except that the peaks due to the components dissolved by the selective dissolution procedure will be absent. Subtraction of this pattern from the pattern of the untreated sample should therefore yield the pattern of the Fe oxides. This pattern is referred to as a differential X-ray diffraction pattern (DXRD). In some cases, this simple subtraction of the two patterns may be all that is necessary, but normally an additional step is needed.

Because of the removal of the Fe oxides, the remaining minerals are concentrated, and the mass adsorption coefficient of the sample may be changed. The result is that the XRD pattern from the treated sample generally has a *greater* overall intensity than that of the untreated sample. However, *relative* intensities within the two patterns should remain essentially the same. To subtract the two patterns from one another, the peaks common to both must have the same height or

intensity. To accomplish this, all of the points in the pattern from the treated sample must be multiplied by a factor that is less than unity, i.e., a scale factor. Subtraction of this scaled pattern from the pattern of the untreated sample then produces the correct differential diagram. The technique can be described as differential X-ray diffraction (DXRD) because the Fe oxide pattern obtained is the difference between the two XRD patterns.

This can be expressed mathematically as:

$$A_i - kB_i = C_i$$

where  $A_i$ ,  $B_i$ , and  $C_i$  are the number of counts at angle  $i$  in the untreated, treated, and subtracted spectra, respectively, and  $k$  is the scale factor.

In the method described by Schulze (1981), a scale factor is determined by trial and error. This approach relies on the assumption that the intensities of the silicate peaks are not affected by the selective dissolution treatment. Bryant *et al.* (1983) solved this problem by incorporating an internal standard, into the sample which is not affected by the dissolution treatment and therefore allows for an objective calculation of the scale factor  $k$ . The internal standard can also be used to correct for errors in alignment or sample positioning in the X-ray beam, so that the positions of Fe oxide peaks may be more accurately determined.

Bryant *et al.* (1983) selected an internal standard using the following criteria: (1) the shape and intensity of the diffraction peaks from the internal standard should not be affected by the dissolution treatment; (2) the material should have diffraction peaks within the range of spacings diagnostic for the iron minerals being studied; and (3) diffraction peaks from the internal standard should not overlap the broad diffraction peaks of the iron oxide minerals. Based on these criteria, they selected  $\alpha$ -alumina as an internal standard.

Since then DXRD has been used extensively in the study of Fe oxides in soils and sediments. Examples can be found in Cambell & Schwertmann (1984) and Brown & Wood (1985). The examination of Fe oxides in a lake environment was conducted by Schwertmann *et al.* (1987). To date the use of DXRD has not been attempted on marine crusts and nodules

## 2.1.2 STATEMENT OF PROBLEM

Although there exist numerous methods to extract Mn, Fe, Cu, Ni, and Co from crusts and nodules, all of the above mentioned methods are not selective sequential extraction schemes. Some of these methods may be economic for processing crusts and nodules to extract valuable metals; however, they do not take into consideration the relationship between these metals and the specific mineral phase in which they reside; while other methods do attempt to determine the principal chemical phases. A selective sequential extraction scheme must therefore be devised so as to discover which Mn and Fe oxide mineral phases are hosting the economically important metals Cu, Ni, and Co. In developing a selective sequential extraction scheme, two goals had to be attained. These goals are: (1) since crust and nodule samples are finite in size and numerous different analyses are to be performed on a single sample, a selective sequential extraction scheme should be developed which uses as small amount of sample as feasible; and (2) develop a selective sequential extraction scheme which is as time efficient as possible. Borrowing the methods used in the study of Mn and Fe oxides in the soils, a selective sequential extraction scheme was developed to determine the partitioning between Mn, Fe, Cu, Ni, and Co.

The application of DXRD in conjunction with the selective sequential extraction scheme allowed determination of the Mn and Fe oxide mineral phases

which are responsible for hosting Cu, Ni, and Co. In developing the DXRD procedure two other goals had to be attained. These are: (1) use as small amount of leached sample as possible, and (2) prepare the sample for XRD analysis so that it is recoverable.

## 2.2 ANALYTICAL METHODS AND RESULTS

### 2.2.1 EFFECTIVENESS OF SELECTED REAGENTS

#### 2.2.1.1 Reagents Used

A total of five reagents were tested to determine their effectiveness in the selective removal of Mn or Fe oxides in a laboratory standard ferromanganese crust. The following reagents were selected based in their reported ability to quickly and effectively remove Mn and Fe oxides:

- (1) 0.25M  $\text{NH}_2\text{OH}\cdot\text{HCl}$  in 0.25M  $\text{HCl}$  (Chao & Zhou, 1983),
- (2) 0.25M  $\text{NH}_2\text{OH}\cdot\text{HCl}$  in 0.25M  $\text{HAc}$  (Chao & Zhou, 1983),
- (3) 0.10M  $\text{NH}_2\text{OH}\cdot\text{HCl}$  in 0.01M  $\text{HNO}_3$  (Chao, & Sanzalone, 1973),
- (4) 0.175M Ammonium Oxalate in 0.10M Oxalic Acid  
(de Endredy, 1963; Chao & Zhou, 1983),
- (5) 1 part  $\text{H}_2\text{NNH}_2$ , 6 parts concentrated  $\text{NH}_4\text{OH}$ , and  
3 parts 0.30M Citric Acid in 7N  $\text{NH}_4\text{OH}$   
(Shen & Boyle, 1988).

The reagents numbered 1 to 4 are commonly used in soil studies to selectively remove either Mn or Fe oxyhydroxides from soil samples. Reagent number 5 is used in the reductive cleaning of corals to remove any oxide coatings. None of these



reagents has ever been used to selectively dissolve the Mn or Fe oxyhydroxides in crusts and nodules. A modification of reagent number 2 has been used by Chester & Hughes (1967) to remove almost all of the Mn and Fe oxides from nodules.

#### 2.2.1.2 Experimental Conditions

Each reagent was tested on a ferromanganese crust lab standard (DODO 14DZ). A crust was used to determine the effectiveness of each reagent since it contains high concentrations of both Mn and Fe as compared to a ferromanganese nodule. The composition of the crust lab standard is known quite accurately since it was used to determine the precision of the XRF (Table 2-1).

With the choice of so many reagents to use in the selective removal of Mn and Fe oxides, a series of experiments were developed to determine: (1) which reagents would be best suited for the selective removal of Mn and Fe oxides, and (2) what are the optimum conditions (i.e. sample to solution ratio and the duration of leaching) for the selected reagents to remove most or all of the targeted oxyhydroxide phases. To meet the above conditions, five samples of the laboratory standard crust were leached at consecutive times of  $\frac{1}{2}$ , 1, 2, 4, and 8 hours at a fixed sample to solution ratio. This experiment was then repeated for a different sample to solution ratio. The sample to solution ratios chosen for these experiments were 1:250, 2:250, 3:250, 4:250, and 5:250. Bearing in mind the first goal of developing a selective sequential extraction scheme, a sample to solution ratio of 5:250 used 1g of crust leached in 50mL of reagent. For a sample to solution ratio of 1:250, 0.2g of crust was leached in 50mL of reagent. The whole procedure was repeated for each of the different reagents.

The sample and reagent were measured into a 125mL Erlenmeyer flask and were allowed to equilibrate for the fixed times on an orbital shaker set at 85rpm.

Table 2-1. The mean composition of the laboratory standard crust DODO 14DZ.  
Mean concentrations are given as weight per cents.

Element	Replicate No.					Mean	S.D.	C.V. (%)
	1	2	3	4	5			
Si	9.46	6.24	6.10	5.22	5.25	6.45	1.75	27.13
Ti	1.13	1.17	1.17	1.17	1.15	1.16	0.02	1.72
Al	1.77	1.92	1.84	1.86	1.83	1.84	0.05	2.72
Fe	15.23	15.91	15.47	15.66	15.49	15.55	0.25	1.61
Mn	12.27	13.08	12.47	12.60	12.22	12.53	0.34	2.71
Ca	0.95	1.00	1.06	1.02	0.96	1.00	0.05	5.00
Na	1.55	1.72	1.36	1.65	1.54	1.56	0.14	8.97
K	0.76	0.76	0.76	0.73	0.74	0.75	0.01	1.33
P	0.65	0.68	0.67	0.68	0.65	0.67	0.02	2.99
Co	0.30	0.30	0.30	0.30	0.30	0.30	0.00	0.00
Ni	0.15	0.15	0.15	0.15	0.16	0.15	0.00	0.00
Cu	0.06	0.07	0.05	0.06	0.04	0.06	0.01	16.67
Zn	0.03	0.03	0.04	0.04	0.04	0.04	0.01	25.00
Ba	0.13	0.13	0.12	0.13	0.13	0.13	0.00	0.00

The solution was then transferred to a 50mL centrifuge tube and centrifuged for 20min at 3000rpm. The leachate was decanted into a 100mL volumetric flask. The residue was washed three times with reagent and centrifuged again for 20min. The wash solutions were combined with the leachate in the 100mL volumetric flask. The leachate was then made up to volume with further reagent and stored in an acid washed 125mL Nalgene® polyethylene bottles until it could be analysed for Mn, Fe, Cu, Ni, and Co. The residue was then washed and centrifuged three times with distilled deionized water and freeze dried.

Although only five reagents were selected to determine their effectiveness in the selective removal of Mn or Fe oxides, a total of six experiments using the reagents mentioned in the previous section were conducted. Two experiments were preformed using 0.175M Ammonium Oxalate in 0.10M Oxalic Acid (Tamm's Reagent). The first experiment using Tamm's reagent used a modification of the method described by McKeague & Day (1966) and by Chao & Zhou (1983). The same experimental procedure was followed as for all other reagents, except that the reagent and the sample were allowed to equilibrate in the dark. The 125mL Erlenmeyer flasks were wrapped with black electrician's tape and the orbital shaker was also covered with a black plastic sheet to ensure that no light would reach the samples. The samples were processed as before.

The second experiment used a modification of the photolytic method described by de Endredy (1963). A total of five samples each consisting of the laboratory standard crust and Tamm's reagent at one of the sample to solution ratios were measured into 125mL Erlenmeyer flasks. These were then placed at the base of a 450W, medium pressure Hanovia lamp on a heater/stirring plate and agitated for one hour with magnetic stirring beans. After one hour the samples were removed from the base of the Hanovia lamp and processed as before.

## 2.2.2 ANALYSIS OF LEACHATES

The concentrations of Mn, Fe, Cu, Ni, and Co in the leachates were determined by atomic adsorption spectrometry using a Perkin-Elmer 560® spectrometer with a four inch one slot burner head, lean air-acetylene flame, and single-element hollow cathode lamps. The instrument was operated under the conditions shown in Table 2-2.

### 2.2.2.1 Calibration

A series of five standards were used in the calibration of the atomic absorbtion spectrometer. Each standard was prepared by pipetting carefully measured amounts of Baker Analyzed Reagent® (1000ppm) Mn, Fe, Cu, Ni, and Co into a 50mL volumetric flask in a laminar flow hood using a digital Eppendorf® pipette. The elements were then diluted by making up to volume with the appropriate leaching reagent. A series of standards consisted of 0ppm, 2.5ppm, 5ppm, 7ppm, and 10ppm of each of the above elements. Since five different reagents were used in the selective extraction experiments, five sets of standards were prepared. Calibration curves for the elements Mn, Fe, Cu, Ni, and Co are shown in Figure 2-1. All calibration curves are linear over the concentration ranges used.

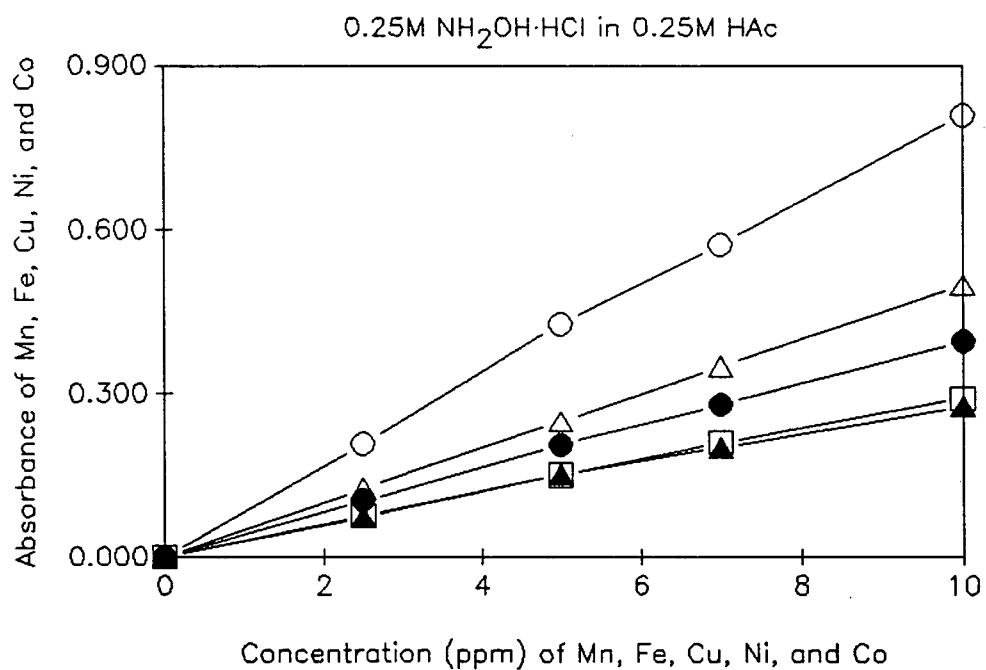
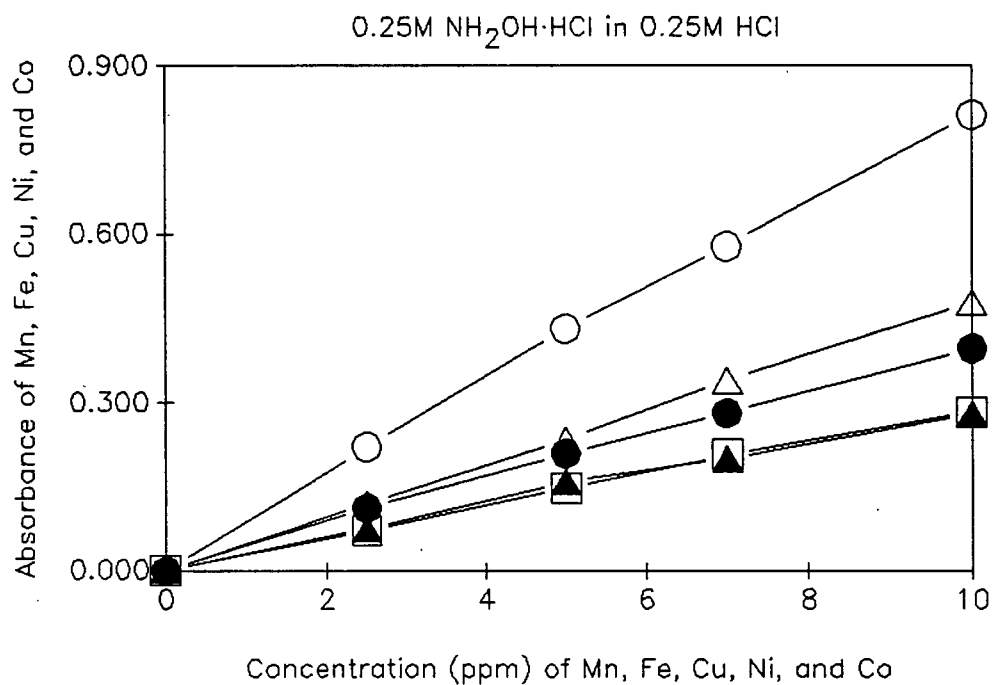
### 2.2.2.2 Sample Preparation

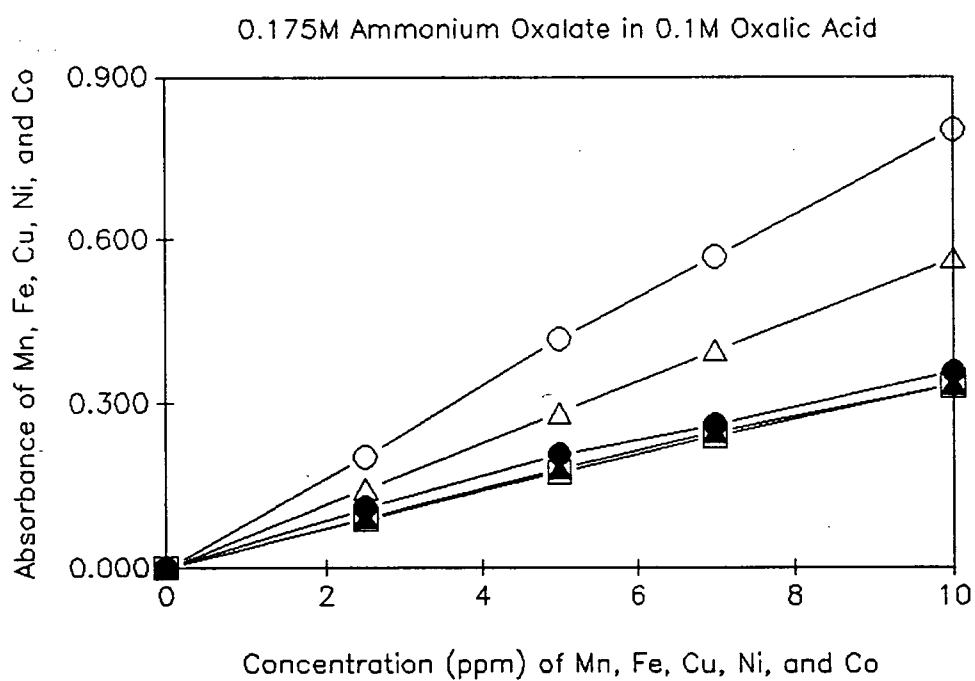
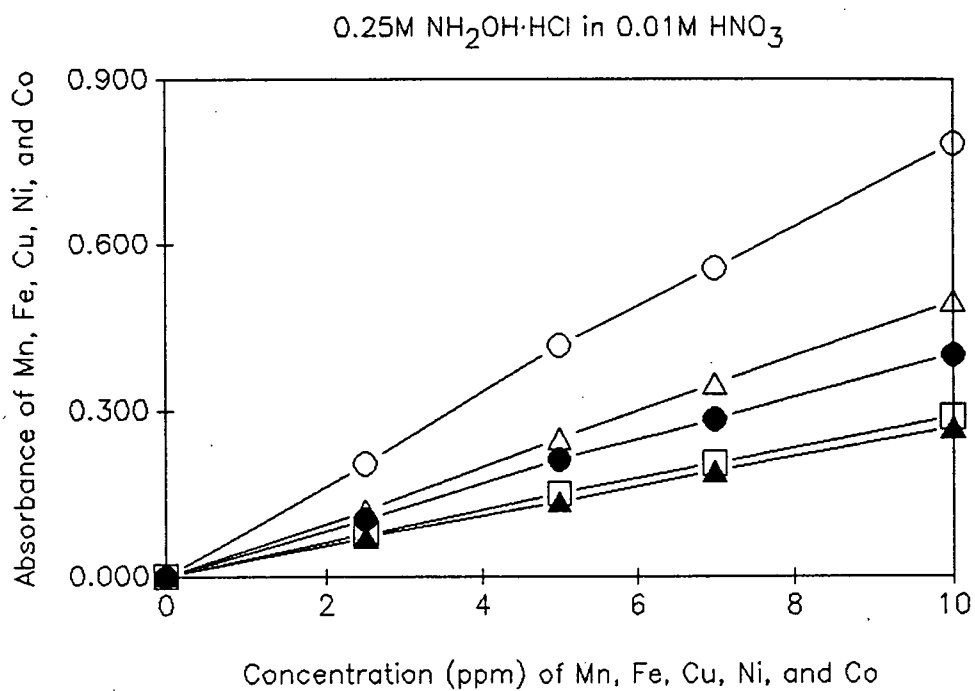
By measuring the absorbance of Mn, Fe, Cu, Ni, and Co in the leachates, the concentrations of these elements were found to exceed the range of concentrations of those in the standards. The leachate samples, therefore, had to be diluted so that the measured absorbance values of the elements of interest can be plotted onto the

Table 2-2. Instrumental setting for analysis of the five metals on the atomic absorption spectrophotometer.

Element	Wavelength (nm)	Lamp Current (mA)	Slit (nm)	Air Flow (L/min)	Fuel Flow (L/min)
Mn	279.5	15	0.2	19.5	0.6
Fe	248.3	15	0.2	19.5	0.6
Cu	324.8	7	0.2	19.5	0.6
Ni	232.0	15	0.2	19.5	0.6
Co	240.7	15	0.2	19.5	0.6

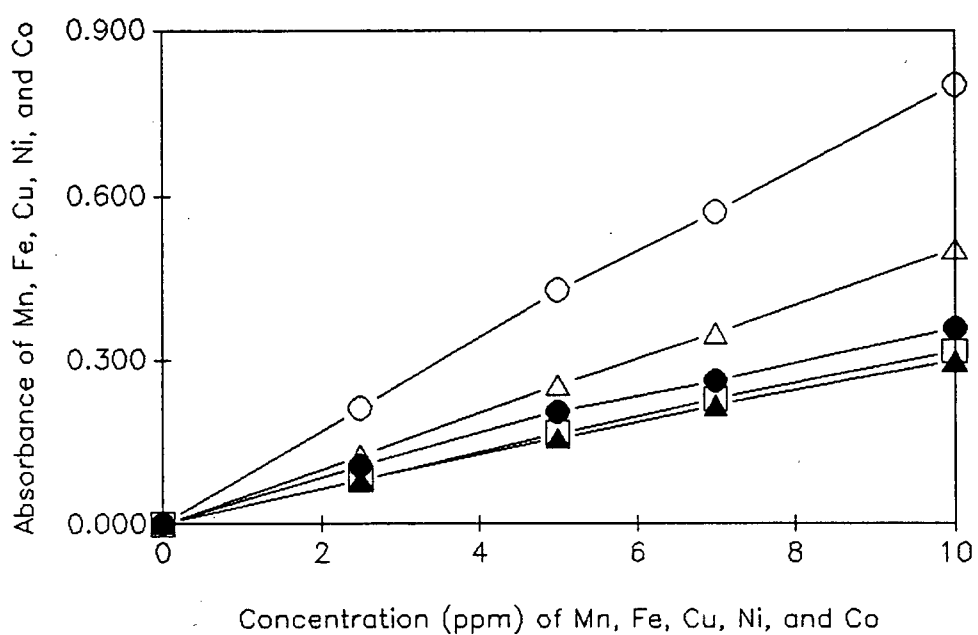
Figure 2-1. Calibration curves of the elements Mn, Fe, Cu, Ni, and Co in various reagents. The open circles = Mn, the filled circles = Fe, the open triangles = Cu, the filled triangles = Ni, the open squares = Co.







1 part Hydrazine, 6 parts concentrated  $\text{NH}_4\text{OH}$ , and  
3 parts 0.3M Citric Acid in 7N  $\text{NH}_4\text{OH}$



calibration lines. An aliquot of the leachate was diluted 500 times by measuring 10 $\mu$ L of leachate and 4.99mL of the same reagent used in the experiment into an acid washed 5mL test tube. The test tube was capped and shaken vigorously to ensure sample homogeneity. The concentration of Mn, Fe, Cu, Ni, and Co in the leachate was then determined by plotting their measured absorbance values onto calibration curves. The results of these analysis are given in Appendix A.

#### 2.2.2.3 Determining the Effectiveness of Each Reagent

The relative effectiveness of each reagent in selectively removing either Mn or Fe and the associated Cu, Ni, and Co from the laboratory standard crust are shown in Appendix B. The results show that none of the reagents tested removed 100% of the manganese or iron present in the crust. This may be due to the fact that some of the iron present in the laboratory standard crust may be associated with the manganese phase mineralogy and present as iron bearing aluminosilicates.

Two reagents were found to be most effective in developing a two stage sequential extraction scheme for crusts and nodules. First, using 0.1M  $\text{NH}_2\text{OH}\cdot\text{HCl}$  in 0.01M  $\text{HNO}_3$  as the leaching reagent, a sample to solution ratio of 3:250, and an extraction time of eight hours, was found to be the most effective in removing almost all of the manganese but only a minor amount of iron in the laboratory standard crust. Second, to selectively remove all of the iron, 0.175M Ammonium Oxalate in 0.1M Oxalic Acid, a sample to solution ratio of 1:250, and an extraction time of eight hours was found to be the most effective, however, this reagent also removed a large portion of the manganese as well. This is of little consequence since almost all of the manganese will have been previously removed in the first stage of the sequential selective extraction scheme. The effectiveness of these two reagents in selectively

removing Mn and Fe from the laboratory standard crust are indicated in Table 2-3 by the arrow-head.

### 2.2.3 DEVELOPMENT OF THE TWO STAGE LEACHING PROCEDURE

Using the results of the above leaching experiments, a two stage selective sequential extraction scheme was devised and tested on a laboratory standard crust and a nodule. Since both laboratory standards were used to determine the precision of the XRF, the concentrations of Mn, Fe, Cu, Ni, and Co in these laboratory standards is known quite precisely. The composition of the crust lab standard has been listed in Table 2-1 while the composition of the nodule lab standard is listed in Table 2-4. A total of eleven samples were subjected to the two stage selective sequential extraction scheme. Ten samples were replicates of the laboratory standard crust and one sample of the laboratory standard nodule. The ten replicates of the crust were analysed to determine the precision and accuracy of the method of analysis.

#### 2.2.3.1 First Stage of the Selective Sequential Extraction Scheme

One gram of sample and 83mL of reagent were sequentially measured into an acid washed 125mL Nalgene® polyethylene bottle and capped. The sample was then placed onto an orbital shaker set at 85rpm and allowed to equilibrate for eight hours, after which the residue and leachate were separated by centrifugation for 20min at 3000rpm. The leachate was decanted into a 100mL volumetric flask and the residue was washed three times with 0.1M  $\text{NH}_2\text{OH}\cdot\text{HCl}$  in 0.01M  $\text{HNO}_3$  and centrifuged

Table 2-3. The effectiveness of 0.25M  $\text{NH}_2\text{OH}\cdot\text{HCl}$  in 0.01M  $\text{HNO}_3$  and 0.175M Ammonium Oxalate in 0.1M Oxalic Acid. Results are listed as the per cent of Mn and Fe removed from the laboratory standard crust DODO14DZ.

0.25M  $\text{NH}_2\text{OH}\cdot\text{HCl}$  in 0.01M  $\text{HNO}_3$   
 Sample:Solution = 3:250

Time (hr)	Mn (Percent)	Fe
0.5	84.60	6.11
1.0	89.04	7.98
2.0	85.24	4.23
4.0	84.73	1.18
▶ 8.0	99.28	3.54

0.175M Ammonium Oxalate in 0.1M Oxalic Acid  
 Sample:Solution = 1:250

Time (hr)	Mn (Percent)	Fe
0.5	84.79	89.17
1.0	80.41	87.40
2.0	78.52	106.29
4.0	73.96	110.50
▶ 8.0	83.00	104.82



again for 20min at 3000rpm. Each wash was combined with the leachate, made up to volume with 0.1M  $\text{NH}_2\text{OH}\cdot\text{HCl}$  in 0.01M  $\text{HNO}_3$  and stored in an acid washed 125mL Nalgene® polyethylene bottle. The residue was washed three times with distilled deionized water, centrifuged for 20min at 3000rpm and freeze dried.

#### 2.2.3.2 Second Stage of the Selective Sequential Extraction

##### Scheme

Depending on how much residue remained after the first stage of the extraction scheme, an appropriate amount of 0.175M Ammonium Oxalate in 0.1M Oxalic Acid was added to the residue in the plastic bottle to maintain a sample to solution ratio of 1:250. The capped bottle was then shaken at 85rpm for eight hours in the dark. The residue was then separated from the leachate using the methods described above.

#### 2.2.3.3 Analysis of the Leachates

Analysis of the leachates from the two stage sequential selective extraction scheme were again carried out as described in section 2.2.2. The results from the two stage selective sequential extraction scheme are given in Table 2-5. Table 2-5a lists the weight per cent of Mn, Fe, Cu, Ni, and Co removed during the first stage of leaching. For the ten replicates of the laboratory standard crust, the average weight per cent of each element removed is given. The individual results will be later explained to determine the precision of the methods of analysis. Table 2-5b lists the weight per cent of Mn, Fe, Cu, Ni, and Co removed during the second stage of leaching. Again, for the ten replicates of the laboratory standard crust, the average weight per cent of each element removed is given. Some partitioning of Mn, Fe, Cu,

Table 2-5a. Concentrations of Mn, Fe, Cu, Ni, and Co in the leachates from the first stage of the two stage selective sequential extraction scheme. Results are given as weight per cents.

Sample	Element				
	Mn	Fe	Cu	Ni	Co
Crust	12.55	0.75	0.02	0.14	0.29
Nodule	27.50	0.63	1.03	0.87	0.14

Table 2-5b. Concentrations of Mn, Fe, Cu, Ni, and Co in the leachates from the second stage of the two stage selective sequential extraction scheme. Results are given as weight per cents and have been adjusted to be comparable to the first stage of leaching.

Sample	Element				
	Mn	Fe	Cu	Ni	Co
Crust	0.47	11.91	0.07	0.07	0.11
Nodule	0.32	2.50	0.44	0.55	0.15

Ni, and Co in the laboratory standard crust and nodule is evident from these results. For both the crust and nodule, the leachates from the first stage of leaching both contain a large concentration of Mn, with only minor amounts of Fe, while the leachates from the second stage of leaching contain a higher concentration of Fe with only minor amounts of Mn. The behaviour of Cu, Ni, and Co in the leachates from the two stages of the extraction scheme are distinctively different for the crust and nodule. For the crust, the leachates from the first stage contain higher concentrations of Ni and Co when compared to the leachates from the second stage, whereas Cu is higher in the second stage leachates. For the the nodule, the leachate from the first stage contains a higher concentration of Cu when compared to the leachate from the second stage. The same is observed for Ni except not to the same extreme. For Co, however, equal amounts of Co are extracted from both the first and second stage of leaching.

#### 2.2.3.4 Precision and Accuracy

The precision of the methods involved for determination of Mn, Fe, Cu, Ni, and Co was obtained by analysing ten replicates of the laboratory standard crust DODO 14DZ. Ten sub-samples from a well mixed bulk sample were subjected to the two stage selective sequential extraction scheme and analysed by atomic absorbtion spectrophotometer. The sample precision includes errors due to the inherent inhomogeneity of the samples, sample handling and weighing during the extraction procedures, and preparation of the leachates for analysis. In addition, one of the calibration standards, chosen randomly, was analyzed eight times in order to determine the instrumental precision of the atomic absorption spectrophotometer. The sample precision results are shown in Table 2-6. Table 2-6a lists the mean, standard deviation, and coefficient of variation (C.V.) for Mn, Fe, Cu, Ni, and Co



Table 2-6a. Precision of the method of analysis for the first stage of the two stage selective sequential extraction scheme. Replicate samples are from the laboratory standard crust DODO 14DZ. Concentrations are given as weight per cents.

Replicate	Element				
	Mn	Fe	Cu	Ni	Co
1-1	12.11	0.62	0.02	0.14	0.30
1-2	12.36	0.69	0.02	0.14	0.27
1-3	12.29	0.69	0.02	0.14	0.28
1-4	12.70	0.67	0.02	0.14	0.30
1-5	12.81	0.77	0.02	0.14	0.29
1-6	12.94	0.80	0.02	0.14	0.29
1-7	12.29	0.79	0.02	0.14	0.30
1-8	12.72	0.80	0.02	0.15	0.30
1-9	12.59	0.81	0.03	0.15	0.29
1-10	12.71	0.82	0.02	0.15	0.30
Mean	12.55	0.75	0.02	0.14	0.29
S.D.	0.27	0.07	0.00	0.00	0.01
C.V. (%)	2.15	9.33	0.00	0.00	3.45

Table 2-6b. Precision of the method of analysis for the second stage of the two stage selective sequential extraction scheme. Replicate samples are from the laboratory standard crust DODO 14DZ. Concentrations are given as weight per cents.

Replicate	Element				
	Mn	Fe	Cu	Ni	Co
2-1	0.46	12.00	0.07	0.06	0.11
2-2	0.46	12.10	0.07	0.09	0.10
2-3	0.49	11.40	0.09	0.09	0.11
2-4	0.45	12.00	0.07	0.11	0.10
2-5	0.48	12.20	0.07	0.05	0.17
2-6	0.48	12.00	0.06	0.08	0.12
2-7	0.47	12.40	0.07	0.05	0.09
2-8	0.48	12.40	0.07	0.06	0.10
2-9	0.49	12.70	0.05	0.06	0.10
2-10	0.48	12.90	0.07	0.08	0.07
Mean	0.47	11.91	0.07	0.07	0.11
S.D.	0.01	0.32	0.01	0.02	0.02
C.V. (%)	2.12	2.67	14.28	28.57	18.18

Table 2-6c. Precision of the Atomic Absorbtion Spectrometer as determined by the absorbances of the standard 5ppm.

First Stage of the Two Stage Extraction Scheme

Repeat Analysis	Element				
	Mn	Fe	Cu	Ni	Co
1	0.226	0.206	0.349	0.172	0.125
2	0.223	0.204	0.349	0.167	0.126
3	0.225	0.206	0.346	0.170	0.128
4	0.226	0.209	0.349	0.169	0.129
5	0.227	0.202	0.342	0.168	0.126
6	0.227	0.203	0.349	0.170	0.127
7	0.224	0.204	0.346	0.168	0.127
8	0.225	0.203	0.348	0.170	0.124
Mean	0.225	0.205	0.347	0.169	0.127
S.D.	0.001	0.002	0.002	0.001	0.002
C.V. (%)	0.44	0.97	0.57	0.59	1.57

Second Stage of the Two Stage Extraction Scheme

Repeat Analysis	Element				
	Mn	Fe	Cu	Ni	Co
1	0.255	0.294	0.195	0.067	0.072
2	0.256	0.295	0.190	0.068	0.068
3	0.257	0.299	0.190	0.067	0.069
4	0.259	0.298	0.193	0.068	0.071
5	0.258	0.298	0.191	0.067	0.067
6	0.261	0.295	0.194	0.068	0.072
7	0.259	0.297	0.194	0.067	0.073
8	0.259		0.197	0.067	0.070
Mean	0.258	0.297	0.193	0.067	0.070
S.D.	0.002	0.002	0.002	0.000	0.002
C.V. (%)	0.78	0.67	1.04	0.00	2.86

from the first stage of the two stage selective sequential extraction scheme. The sample precision for the first stage of leaching was found to vary from 0.00% (Cu and Ni) up to 9.33% (Fe) (C.V.). Table 2-6b lists the mean, standard deviation, and C.V. for Mn, Fe, Cu, Ni, and Co from the second stage of the two stage selective sequential extraction scheme. The sample precision for the second stage of leaching was found to vary from 2.12 (Mn) up to 28.57% (Ni) (C.V.). In most cases the C.V. for the second stage of leaching was found to be greater than for the first stage of leaching. Table 2-6c lists the instrumental precision when using each reagent to prepare the standards used to determine the concentrations of Mn, Fe, Cu, Ni, and Co in the leachates. When using 0.1M  $\text{NH}_2\text{OH}\cdot\text{HCl}$  in 0.01M  $\text{HNO}_3$  to prepare the standards for the atomic absorption spectrometer, the instrumental precision was found to vary between 0.44 (Mn) and 1.57% (Co) (C.V.). When using 0.175M Ammonium Oxalate in 0.1M Oxalic Acid to prepare the standards for the atomic absorption spectrometer, the instrumental precision was found to vary between 0.00 (Ni) and 2.86% (Co) (C.V.). The C.V. for the instrumental precision for both reagents was found to be far smaller than sample precision for both stages of the selective sequential extraction scheme.

The accuracy of the methods used to determine the concentrations of Mn, Fe, Cu, Ni, and Co in the leachates was checked by comparing the analytical results of the sum of the two stages of leaching to the known concentrations of these elements in the crust and nodule as determined by XRF (Table 2-7). Table 2-7 shows that the selective extractions remove all of the Mn, Cu, Ni, and Co from both crusts and nodules. The concentration of Fe is lower in the leachates because the XRF results include Fe in the aluminosilicate fraction.

Table 2-7. Comparison of the total amount of Mn, Fe, Cu, Ni, and Co removed from the laboratory standard crust and nodule by the two stage selective sequential extraction scheme compared to the XRF results used to determine precision of the XRF. Results are given as weight per cents.

Element	AA Results		XRF Results	
	Crust	Nodule	Crust	Nodule
Mn	13.02	27.82	12.53	28.26
Fe	12.66	3.13	15.55	5.36
Cu	0.09	1.47	0.06	1.37
Ni	0.21	1.42	0.15	1.43
Co	0.40	0.29	0.30	0.18

## 2.2.4 DEVELOPMENT OF DIFFERENTIAL X-RAY DIFFRACTION TECHNIQUE

The development of the DXRD procedure for the identification of manganese and iron oxyhydroxides in crusts and nodules was carried out in conjunction with the development of the two stage selective sequential extraction scheme. The same laboratory standard crust and nodule samples used in the two stage selective sequential extraction scheme were also used in the development of DXRD procedure. The development of the DXRD procedure was a simple process of modifying the existing XRD equipment to suit the specific needs required to produce a DXRD diffractogram.

### 2.2.4.1 Sample Preparation

As already pointed out, two goals had to be obtained during sample preparation for DXRD. These are: (1) to use as small amount of residue as possible, and (2) to prepare the sample for DXRD analysis so that it is recoverable. A small amount of residue was ground in a mortar and pestle and placed onto the centre of a ground quartz glass disc. The sample was then suspended with distilled deionized water mixed into a slurry with a clean stainless steel spatula and dried in a laminar flow hood. The ground quartz glass disc contributes less background noise to the XRD pattern as compared to a conventional glass disc. Suspension of the sample with distilled deionized water allows the sample to settle in a random orientation. The samples are dried in a laminar flow hood to prevent sample contamination; allow the sample to dry slowly; and to prevent desiccation cracks which result from the sample drying too quickly. The quartz glass disc and the dried sample was then placed into an aluminium XRD sample holder.

After analysis the sample is scraped off the quartz glass disc with a clean stainless steel spatula and mixed with the rest of the residue. The quartz glass disc is then cleaned in an ultra-sonic bath for five minutes, rinsed with isopropyl alcohol and allowed to dry.

#### 2.2.4.2 Experimental Conditions

The prepared samples were loaded into a Philips® PW 1775 sample changer to be analyzed by a Philips X-ray diffractometer powered by a Philips® PW 1729 constant potential generator. Diffraction data were obtained using Cu K $\alpha$  radiation (40kV, 20mA) and a Philips® PW 1050/70 vertical goniometer equipped with a diffracted beam graphite monochromator, an automated divergence slit, 0.1mm receiving slit, 1° scatter slit, and a gas proportional counter. Although identification of low intensity peaks is made difficult by the high background due to the fluorescent Mn and Fe radiation, Glasby (1972) found that an iron tube was only slightly superior to the copper tube. Work was therefore completed using a copper tube. The diffractometer was controlled by a Philips® PW 1710/00 diffraction control unit. Measurement and control parameters were set up in the PW 1710/00 microprocessor through a Zenith® Z-150 personal computer using MS-DOS Kermit version 2.31 (Gianone *et al.*, 1988).

The laboratory standard crust and nodule samples were step scanned from 5° to 71°2 $\theta$  in 0.01°2 $\theta$  increments, using a counting time of one second per increment. The number of counts measured at each 0.01°2 $\theta$  were therefore a measure of the intensity (counts/second) at each 0.01°2 $\theta$  increment. Instead of sending the intensity along with the degrees 2 $\theta$  to the ratemeter to produce a diffractogram, they were sent to the computer and stored in an ASCII file to be later processed. Thus, an

analog XRD diffractogram has been digitized which allows for the data to be further manipulated and used to produce a DXRD diffractogram by computer.

#### 2.2.4.3 Production of a DXRD Diffractogram

##### 2.2.4.3.1 Smoothing the Data

Superimposed upon and indistinguishable from the digitized XRD spectrum are random errors which regardless of their source, are characteristically described as noise. Before the digitized XRD spectrum can be plotted or used to produce a DXRD tracing, as much of the noise must be removed as possible without, at the same time, unduly degrading the underlying information (Savitzky & Golay, 1964). Following the computational methods described by Savitzky & Golay (1964), the removal of random noise from the XRD spectra involved the convolution methods of a moving average and that of least squares.

Savitzky & Golay (1964) wrote two computer programs, in FORTRAN, to perform the removal of random noise from a digitized spectra using the two convolution methods described above. These two subroutines have been combined into one program and translated into GW BASIC (Appendix C). The digitized XRD spectra stored in an ASCII file was subjected to a 17 point smoothing using this modified program. The new XRD spectra, devoid of excess noise, was stored in a new ASCII file and could now be plotted, by computer, to produce an XRD diffractogram or used to produce a DXRD diffractogram.

#### 2.2.4.3.2 Equation of DXRD Pattern

As previously discussed in greater detail, if an X-ray pattern of a sample is obtained before and after selective dissolution of all or part of the targeted mineral phases, the pattern obtained after selective dissolution should be identical to the one before, except that the peaks due to the components dissolved by the selective dissolution procedure will be absent. Subtraction of the treated pattern from the pattern of the untreated sample should therefore yield the pattern of the removed mineral phases. Because of the removal of the targeted mineral phases, the remaining minerals are concentrated, and the mass adsorption coefficient of the sample may be changed. The result is that the XRD pattern from the treated sample generally has a greater overall intensity than that of the untreated sample. However, relative intensities within the two patterns should remain essentially the same.

To subtract the two patterns from one another, the peaks common to both must have the same height or intensity. To accomplish this, all of the points in the pattern from the treated sample must be multiplied by a scale factor. Subtraction of this scaled pattern from the pattern of the untreated sample then produces the DXRD diffractogram. The most effective way of determining the scale factor is by using an internal standard as proposed by Bryant *et al.* (1983). The internal standard can also be used to correct for errors in alignment or sample positioning in the X-ray beam, so that the positions of the peaks of the removed mineral phases may be more accurately determined.

Since almost all crusts and nodules contain quartz, it is appropriate to use this mineral as an internal standard to determine the scale factor needed to subtract the treated XRD pattern from the untreated XRD pattern. The 3.34Å quartz peak is almost always present and can be easily identified in XRD patterns of crusts and nodules. This quartz peak meets the criteria for use as an internal standard as put



forward by Bryant *et al.* (1983): (1) the shape and intensity of the 3.34Å diffraction peak is not affected by the dissolution treatments; (2) the 3.34Å peak is within the range of d-spacings diagnostic for the manganese and iron minerals being studied; and (3) the 3.34Å diffraction peak for quartz does not overlap the broad diffraction peaks of the manganese and iron oxide minerals. The 3.34Å quartz peak was selected as the internal standard instead of the 3.18Å feldspar peak because feldspar is a group of minerals consisting of two solid solution series. The positive identification of a feldspar requires a knowledge not only of the chemical composition but also the structural state of the species (Hurlbut & Klein, 1977). Since several species of feldspar are present in crusts and nodules, the 3.18Å feldspar peak is broader and consists of a combination of several peaks due to the presence several species of feldspars. Quartz, on the other hand, has a constant composition with no solid solution effects; moreover the 3.34Å peak is narrower than the 3.18Å peak and consists of only one peak. This makes the 3.34Å quartz peak ideal for use as an internal standard.

Bryant *et al.* (1983) noted that their procedure for the selective dissolution of iron oxides in soils would also attack the silicates. They proposed that instead of using the silicates present in their samples as an internal standard, one should be added to the sample which is resistant to chemical attack. The same considerations were applied to the DXRD diffractograms of the laboratory standard crust and nodule produced during the two stage selective sequential extraction scheme. The quartz present in crusts and nodules is an adequate internal standard since the methods used in the two stage selective sequential extraction scheme are not as destructive as those of Bryant *et al.* (1983). Quartz is composed essentially of  $\text{SiO}_2$  and is therefore electrically neutral. Furthermore, low quartz, the most common polymorph of  $\text{SiO}_2$  found at the earth's surface, has the most compact structure of all the polymorphs of  $\text{SiO}_2$ . This is indicated by its low amount of crystal symmetry

(Hurlbut & Klein, 1977). This makes quartz essentially unreactive and immune to chemical attack during the leaching procedures of the two stage selective sequential extraction scheme.

To determine the value of the scale factor  $k$ , it must be remembered that the goal of subtracting the treated from the untreated XRD pattern is to remove the presence of the aluminosilicates and any other mineral phases not affected by the chemical dissolution. This goal is simple to achieve with the use of the 3.34Å quartz peak used as an internal standard and a simple modification of the equation of the DXRD pattern. To remove the presence of the aluminosilicates the following situation must exist.

$$A_i - kB_i = 0$$

It is now a simple procedure of dividing the intensity of the 3.34Å quartz peak from the untreated XRD pattern by the 3.34Å quartz peak from the treated XRD pattern.

$$A_i/B_i = k$$

The intensities of the treated XRD pattern ( $B_i$ ) must now be multiplied by the value of  $k$  and subtracted from the intensities of the untreated XRD pattern ( $A_i$ ) to produce the intensities of the DXRD pattern ( $C_i$ ). This was a simple procedure when both smoothed ASCII files for the untreated and treated XRD patterns are imported into LOTUS 123® and the repetitious calculations are performed by the program.

#### 2.2.4.3.3 Plotting the Tracing

The graphs of the untreated, treated, and DXRD diffractograms were initially plotted using LOTUS 123®. These graphs were then imported into LOTUS FREELANCE PLUS® where they were horizontally rotated to fill an entire page in landscape mode. An added advantage of using LOTUS FREELANCE PLUS® was the ability to label the identified peaks on the pattern before being printed. It is also worth noting that even though the data needed to produce the DXRD pattern are subjected to several computer manipulations and printed on a laser printer, the d-spacings of the DXRD pattern are not distorted.

#### 2.2.4.4 Description of the DXRD Results

Figures 2-2 and 2-3 show the XRD diffraction patterns of the laboratory standard crust and nodule, respectively, before being subjected to the two stage selective sequential extraction scheme. The predominant mineralogy of the untreated crust is  $\delta\text{MnO}_2$  with minor quartz and feldspar. The predominant mineralogy of the untreated nodule is todorokite and possibly some  $\delta\text{MnO}_2$  together with quartz and feldspar. Figures 2-4 and 2-5 show the XRD diffraction patterns of the crust and nodule after the first stage of the sequential extraction scheme. For the crust, there does not appear to be a significant change between the two diffraction patterns Figures 2-2 and 2-4. However, the difference between these two patterns becomes apparent when examining the DXRD pattern from these two XRD diffractograms (Figure 2-6), which shows that the manganese oxide mineral removed during the first stage of leaching is  $\delta\text{MnO}_2$ . Like the crust, there also does not appear to be a significant change in the XRD diffractograms after the first stage of leaching on the nodule. Again, the difference between Figures 2-3 and 2-5 become

Figure 2-2. The XRD diffraction pattern of the laboratory standard crust DODO 14 DZ.

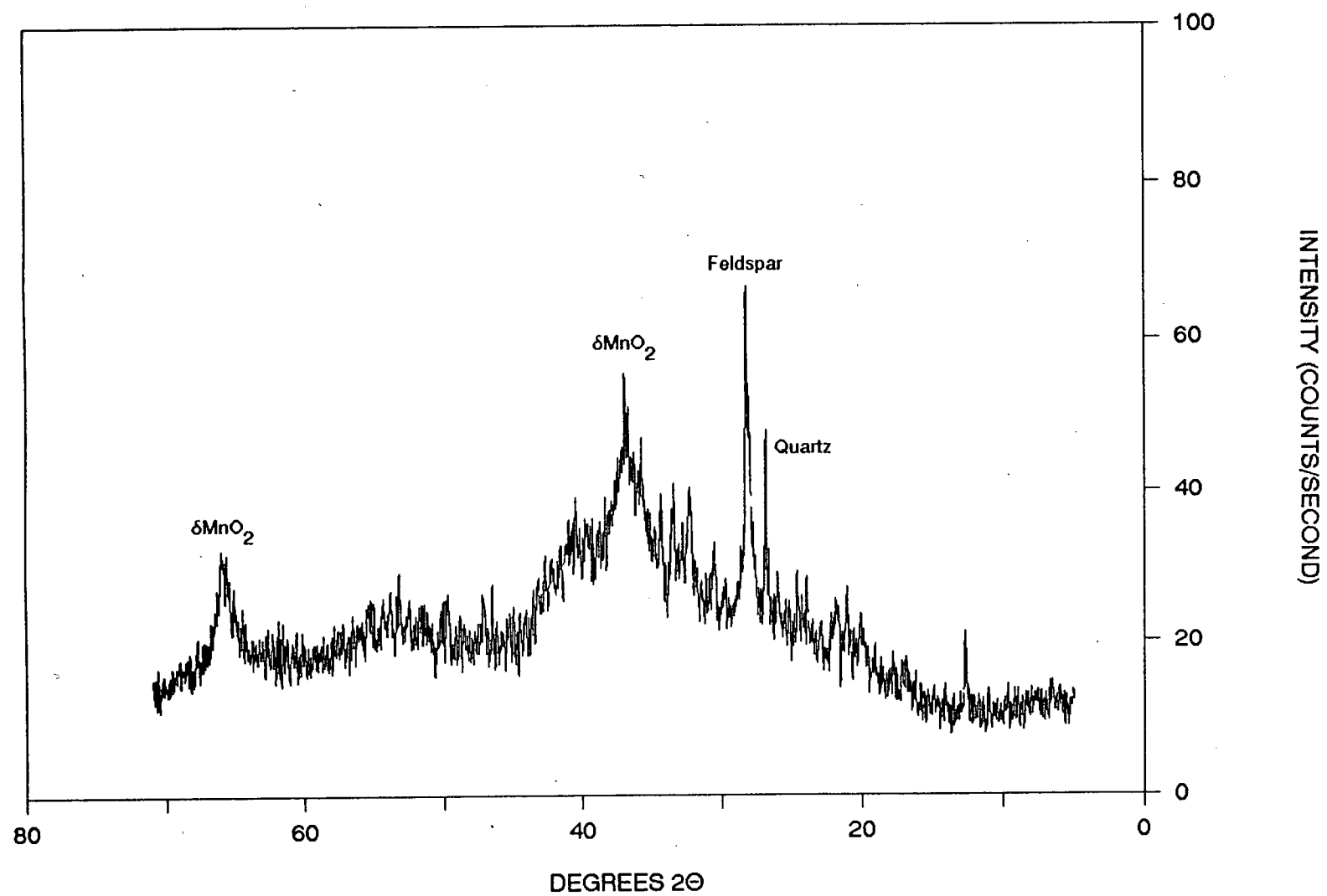


Figure 2-3. The XRD diffraction pattern of the laboratory standard nodule Mn 191 6-8.

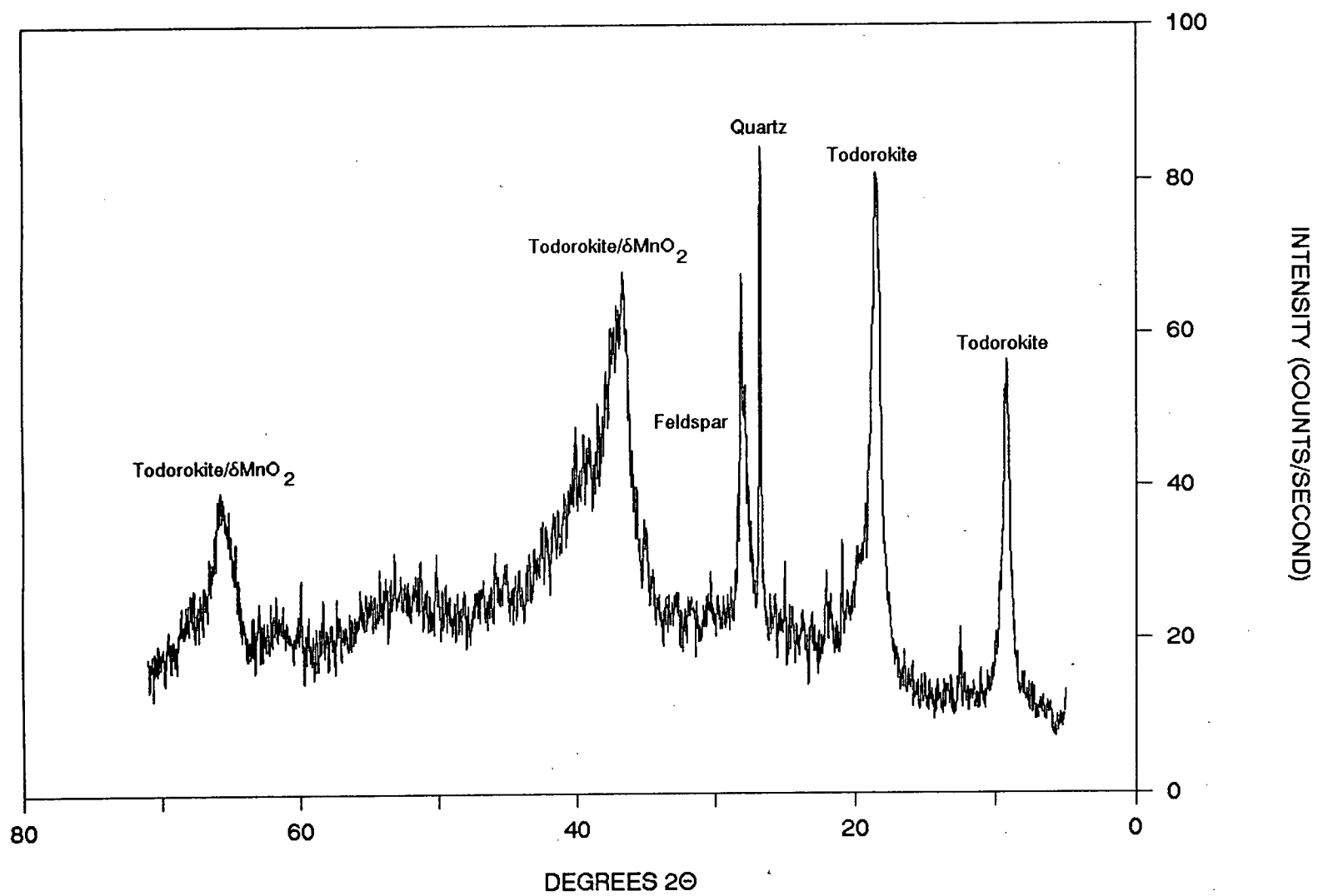


Figure 2-4. The XRD diffraction pattern of the laboratory standard crust DODO 14 DZ after the first stage of the sequential extraction scheme.



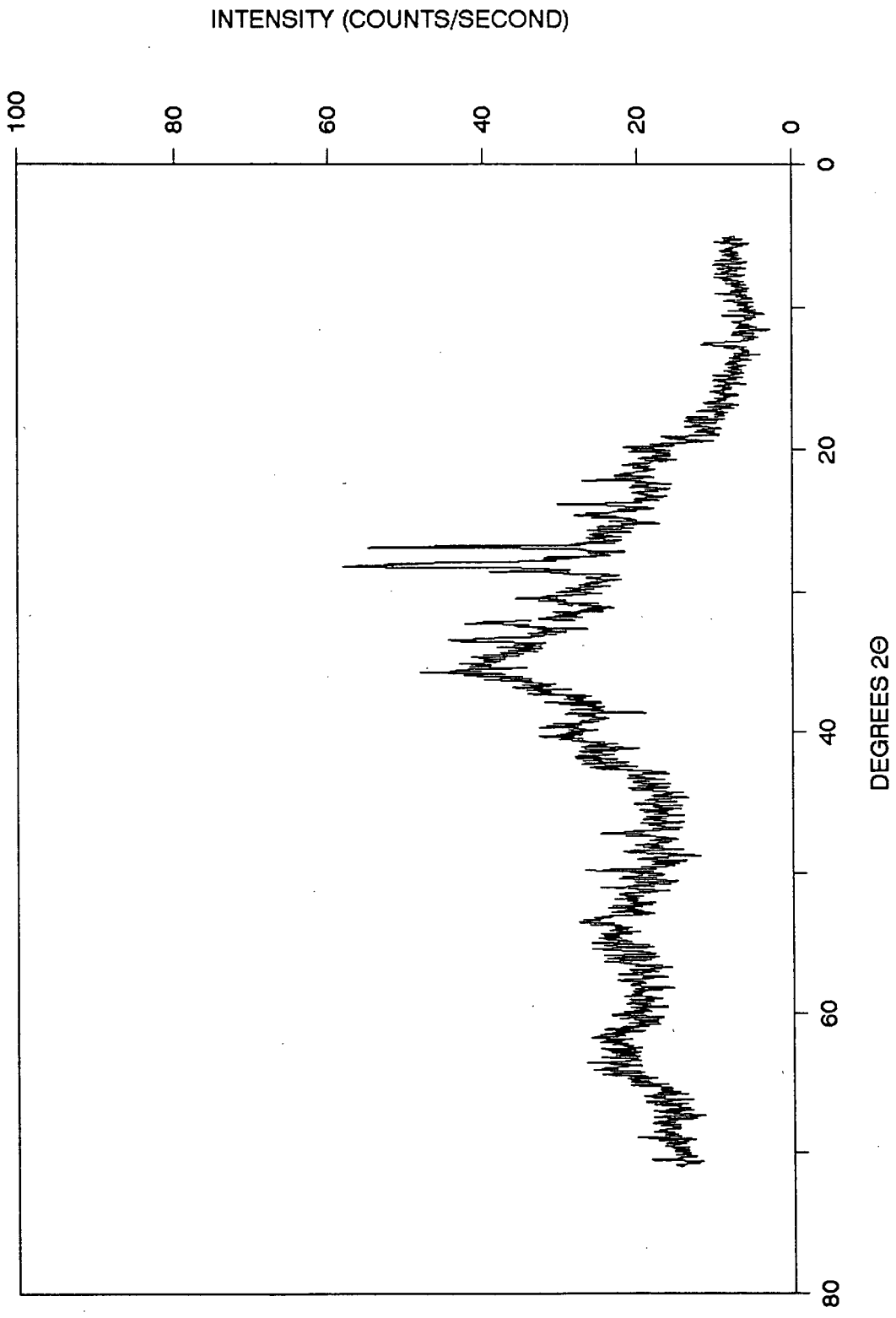


Figure 2-5. The XRD diffraction pattern of the laboratory standard nodule Mn 191 6-8 after the first stage of the sequential extraction scheme.

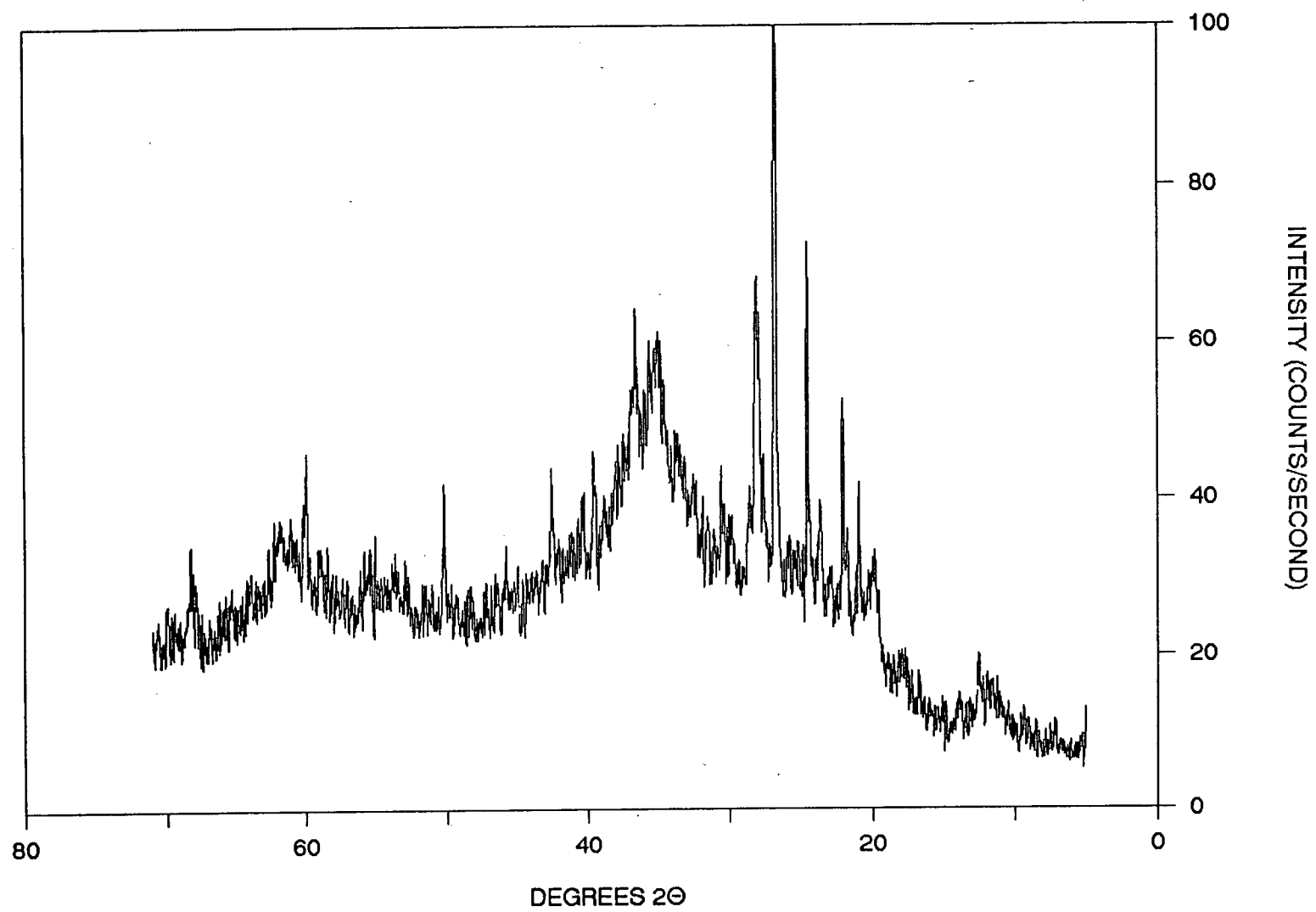
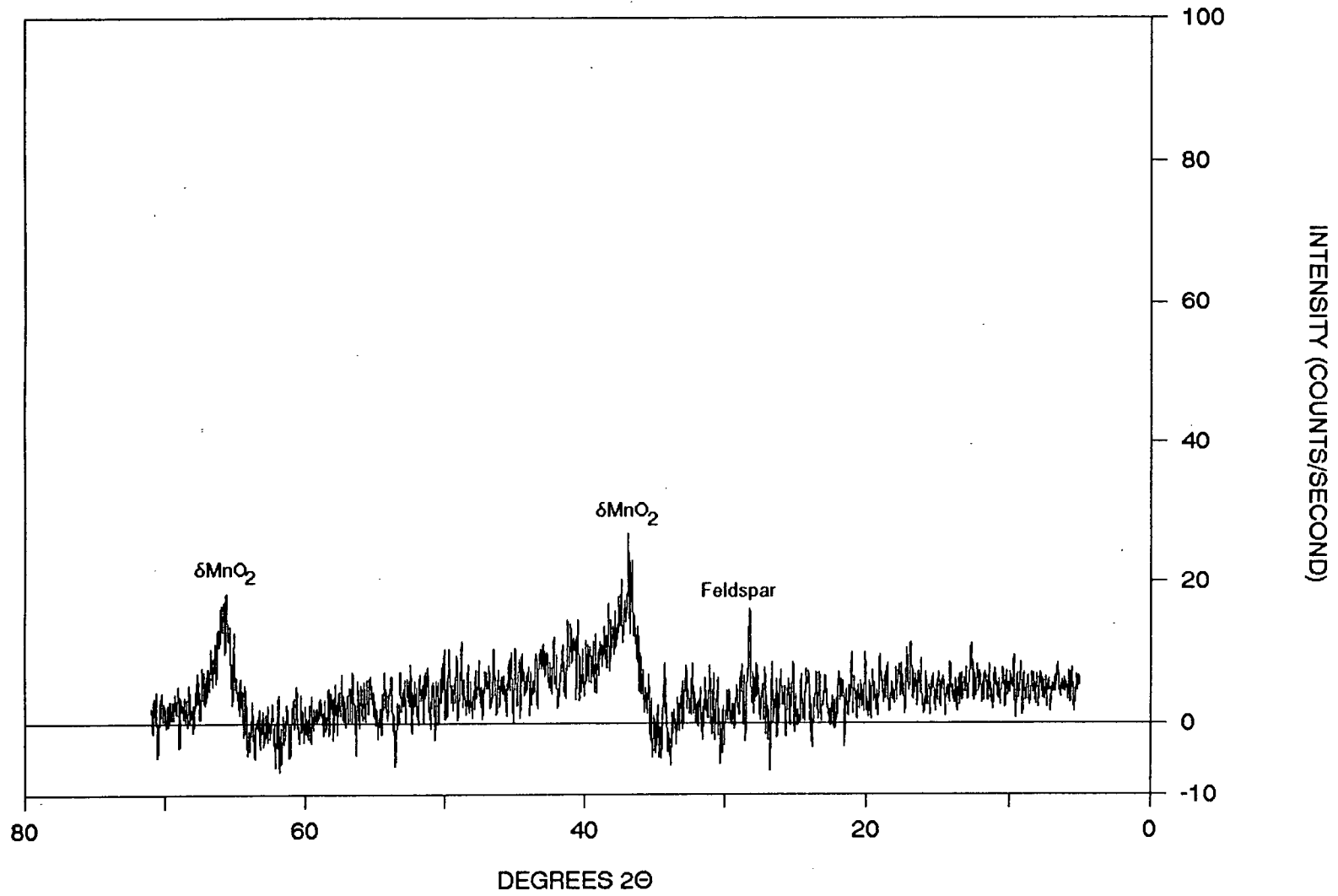


Figure 2-6. The DXRD pattern obtained after the first stage of leaching of the sequential extraction scheme on the laboratory standard crust DODO 14 DZ.



apparent in the DXRD pattern from these two XRD patterns (Figure 2-7), which shows that the manganese oxide mineral removed during the first stage of leaching is todorokite and  $\delta\text{MnO}_2$ . Present in both DXRD patterns for the crust and nodule is the  $3.18\text{\AA}$  peak of feldspar. The presence of this peak in both DXRD patterns is due to: (1) feldspar is partially dissolved by the  $0.1\text{M NH}_2\text{OH}\cdot\text{HCl}$  in  $0.01\text{M HNO}_3$  used in the first stage of the extraction scheme; (2) the  $3.18\text{\AA}$  peak for feldspar is broad due to the fact several feldspars are present in the crust and nodule; therefore, the subtraction of the scaled treated XRD diffractogram from the untreated XRD diffractogram will not totally remove the presence of this peak; and (3) due to the random orientation of the sample when it is prepared for X-ray diffraction the fortuitous orientation of the mineral crystallites will change the relative intensities of the diffraction peaks from one XRD diffractogram to another.

The XRD diffractograms of the crust and nodule after the second stage of leaching are shown in Figures 2-8 and 2-9, respectively. Subtraction of these XRD diffractograms from the XRD diffractograms obtained after the first stage of leaching will produce the DXRD patterns of the mineral phases removed during the second stage of leaching with  $0.175\text{M Ammonium Oxalate}$  in  $0.1\text{M Oxalic Acid}$ . The DXRD pattern for the crust shows the broad peaks of the poorly crystalline iron oxide ferrihydrite (Figure 2-10). The DXRD pattern for the nodule shows the broad peaks of another poorly crystalline iron oxide akaganéite (Figure 2-11). Also present in the DXRD pattern of the nodule is two narrow aluminosilicate peaks probably belonging to feldspar. These are present in the DXRD pattern of the nodule for the same reasons as the  $3.18\text{\AA}$  feldspar peak was present in both DXRD patterns of the crust and nodule from the first stage of leaching. Table 2-8 gives a comparison of the d-spacings of the two iron oxides identified in this study to those listed in the JCPDS card index.

Figure 2-7. The DXRD pattern obtained after the first stage of leaching of the sequential extraction scheme on the laboratory standard nodule Mn 191 6-8.

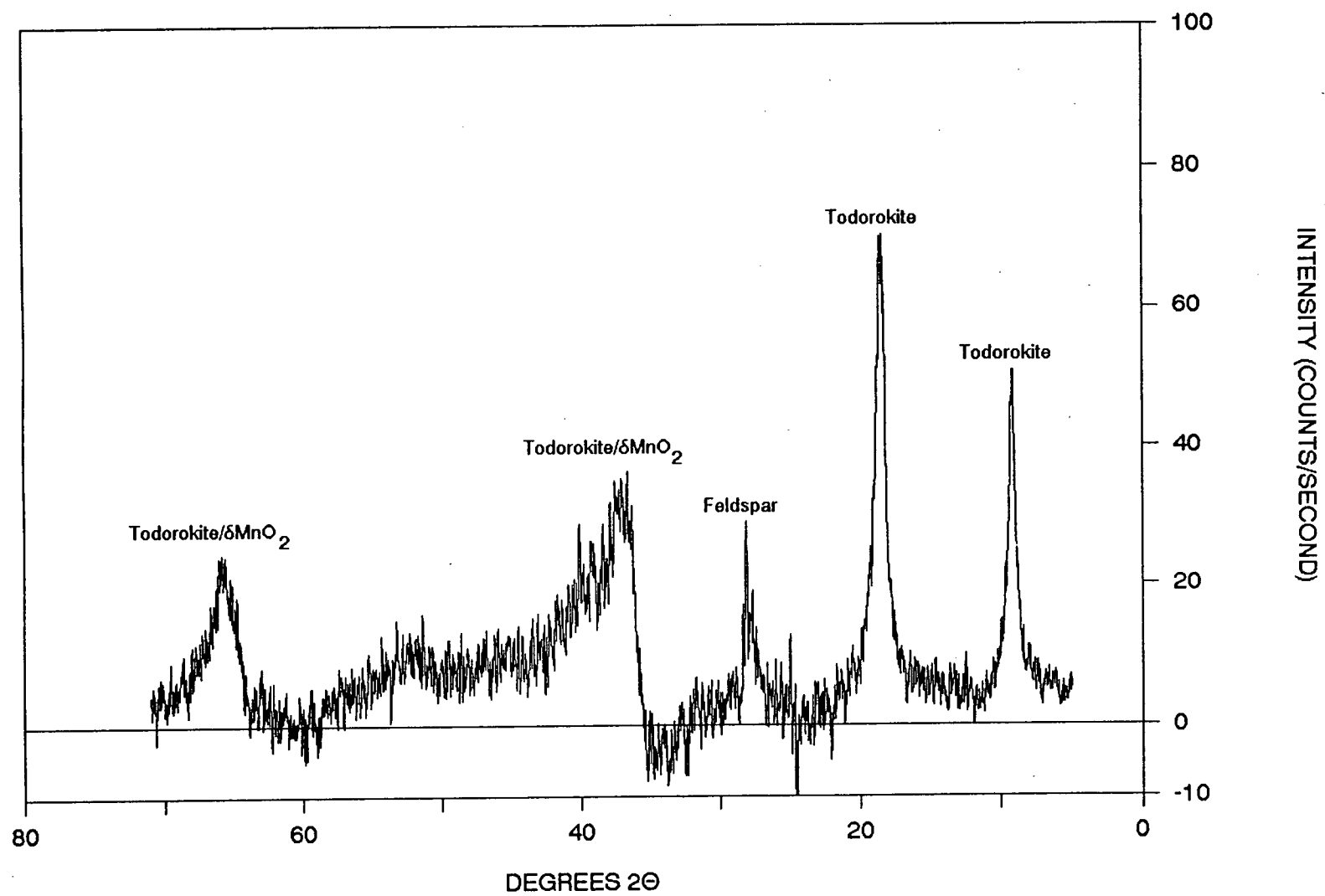




Figure 2-8. The XRD diffraction pattern of the laboratory standard crust DODO 14 DZ after the second stage of the sequential extraction scheme.

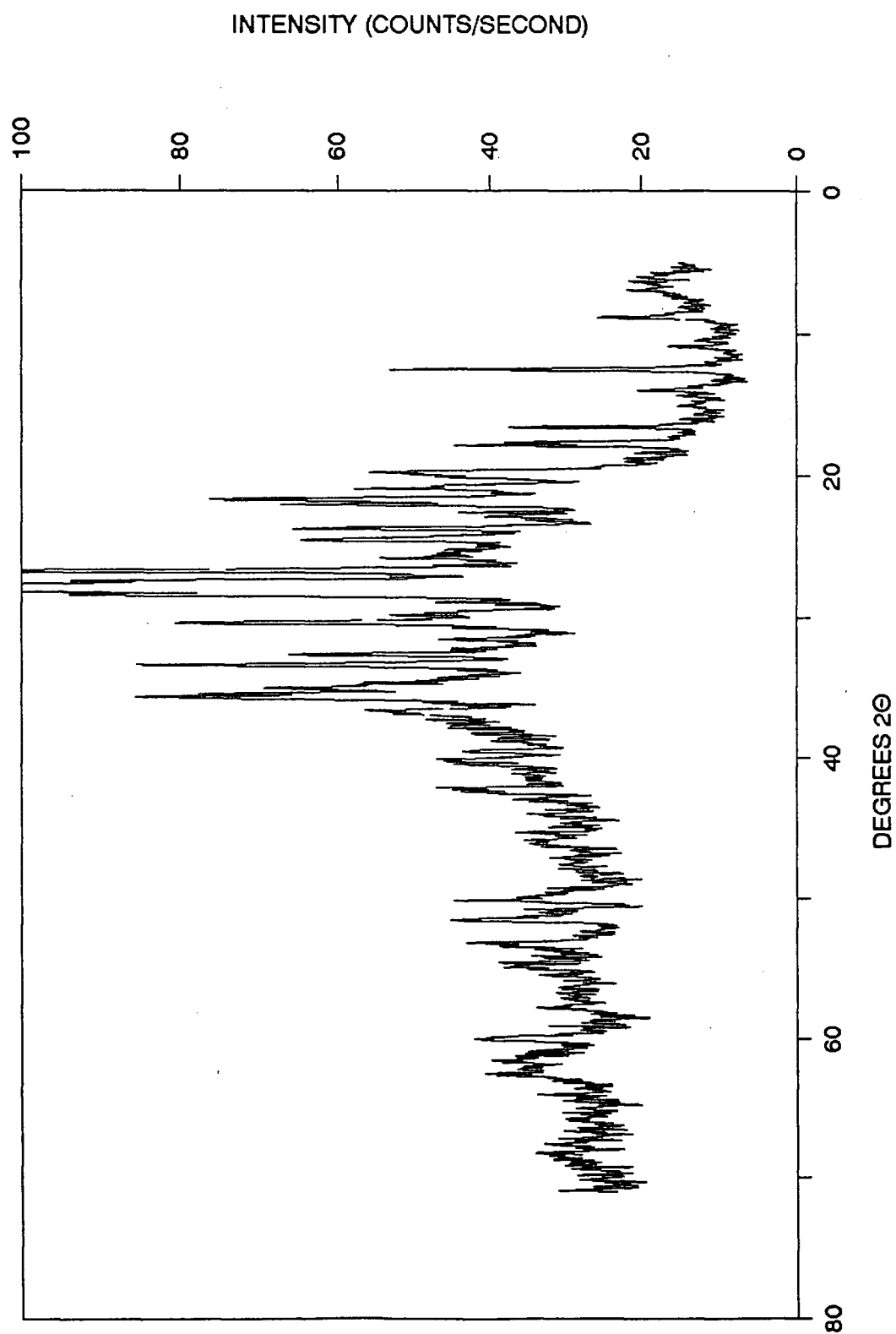


Figure 2-9. The XRD diffraction pattern of the laboratory standard nodule Mn 191 6-8 after the second stage of the sequential extraction scheme.

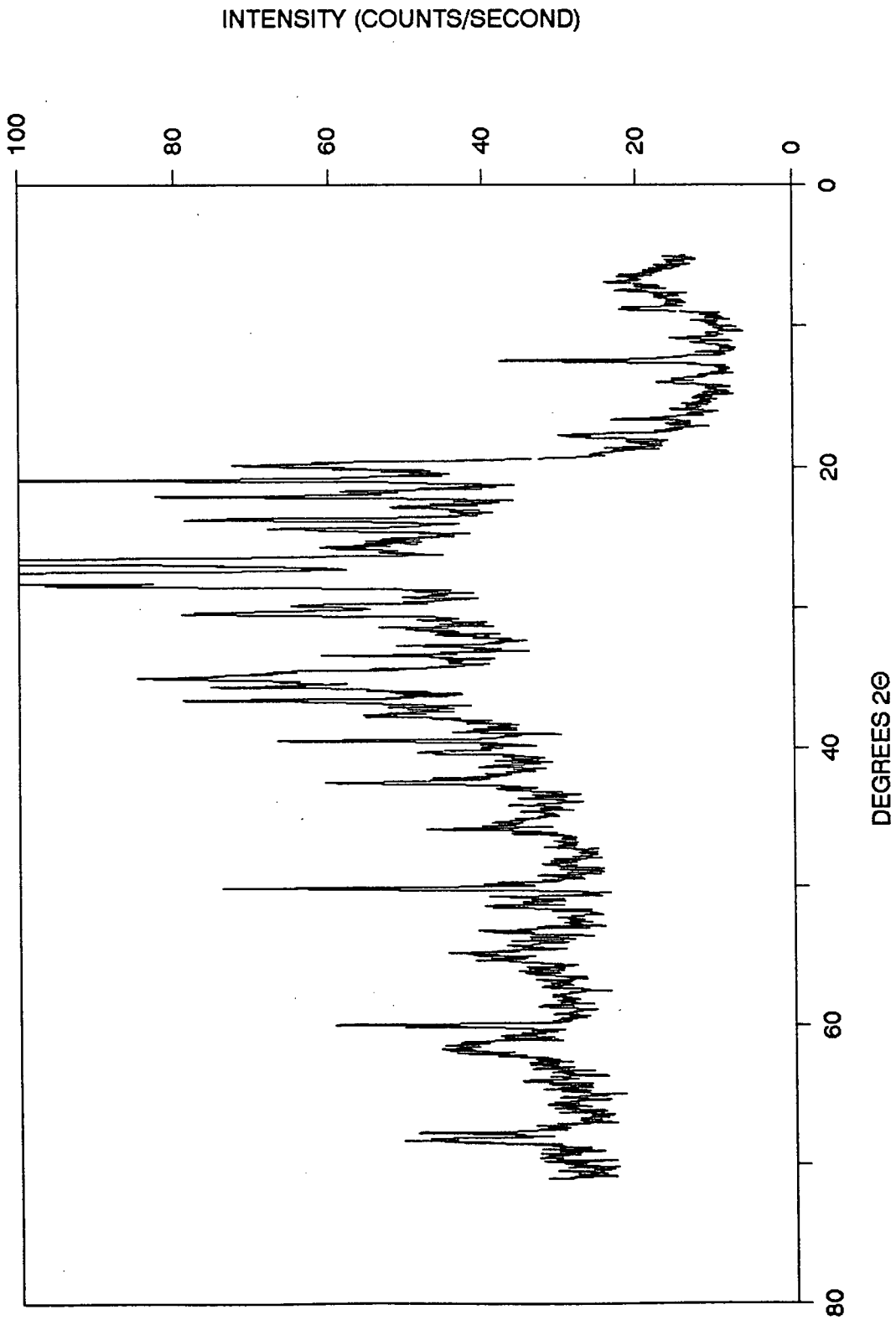


Figure 2-10. The DXRD pattern obtained after the second stage of leaching of the sequential extraction scheme on the laboratory standard crust DODO 14 DZ.

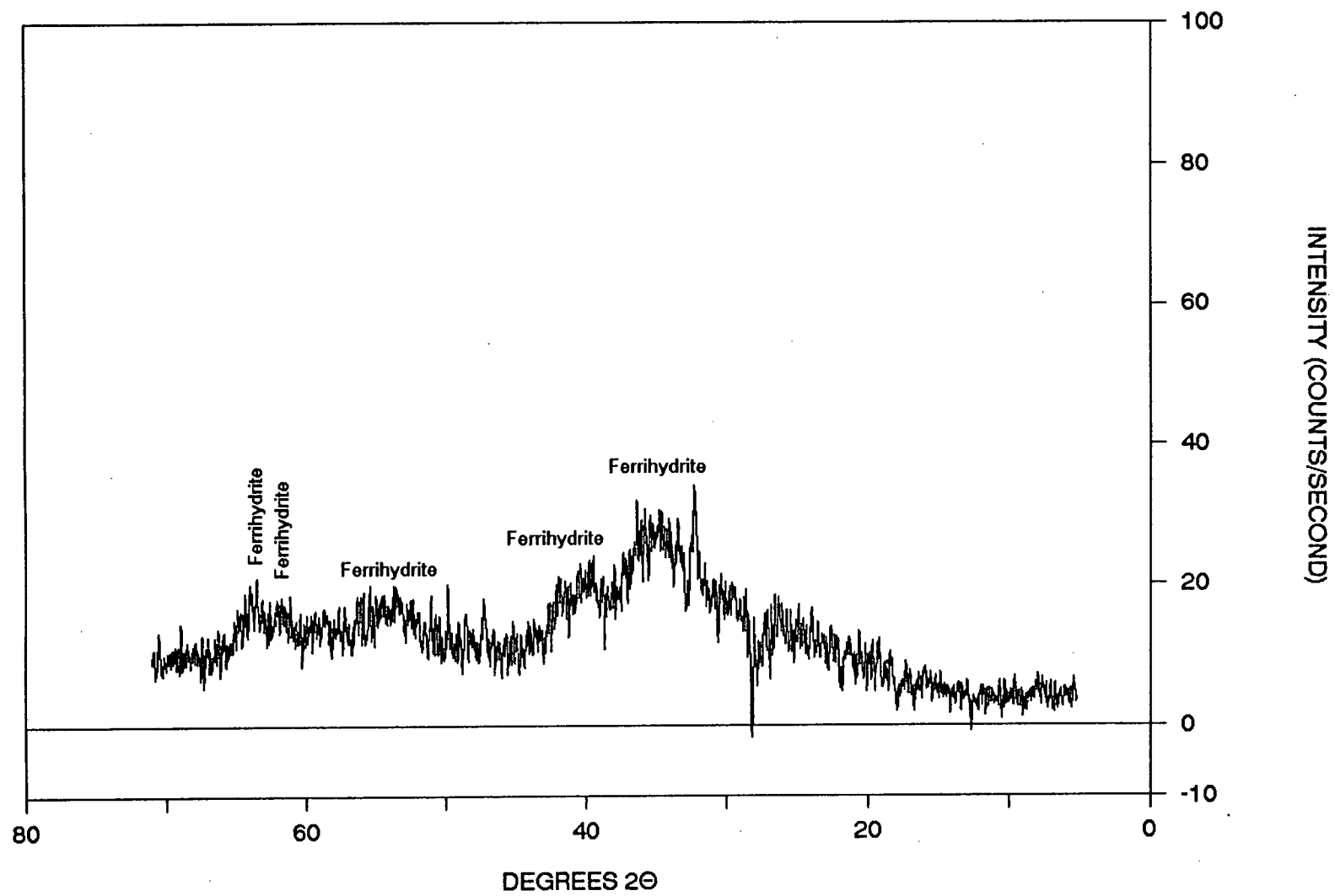


Figure 2-11. The DXRD pattern obtained after the second stage of leaching of the sequential extraction scheme on the laboratory standard nodule Mn 191 6-8.

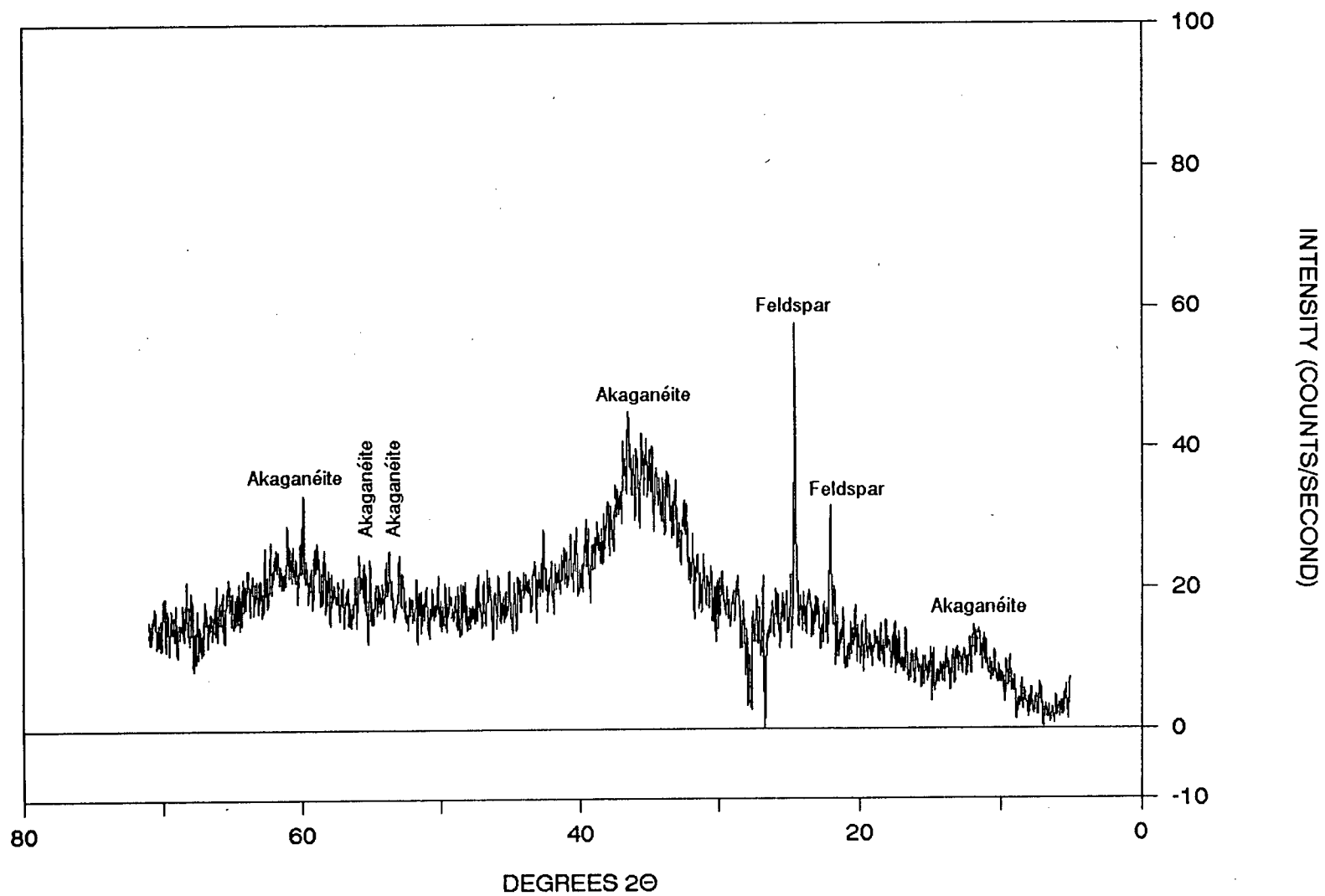




Table 2-8. Comparison of the d-spacings ( $\text{\AA}$ ) of the two iron oxides identified in this study to those listed in the JCPDS card index.

Ferrihydrite		Akaganéite	
This Study	JCPDS Card No. 29-713	This Study	JCPDS Card No. 13-157
2.52	2.50	7.49	7.40
2.25	2.21		5.25
1.96	1.96	3.65	3.70
1.70	1.72		3.311
1.50	1.51		2.616
1.46	1.48	2.51	2.543
			2.343
			2.285
			2.097
			2.064
			1.944
			1.854
			1.746
		1.71	1.719
		1.64	1.635
		1.51	1.515
			1.497
			1.480
			1.459
			1.438
			1.374

## 2.3 DISCUSSION AND CONCLUSIONS

In the crust samples, the majority of the Mn, Ni, and Co are associated with the manganese oxide mineral  $\delta\text{MnO}_2$ , while most of the Fe and Cu are probably associated in the iron oxide mineral ferrihydrite. Both  $\delta\text{MnO}_2$  and ferrihydrite consist of a randomly disordered array of octahedra of Mn and Fe, respectively. In the nodule sample, most of the Mn and Cu and half of the Ni and Co are associated with the manganese oxide mineral todorokite, while most of the Fe and the remaining Ni and Co are contained by the iron oxide mineral akaganéite. Both todorokite and akaganéite are characterized by their well ordered tunnel structures.

Most of the proposed selective sequential extraction schemes directed towards the study of manganese and iron oxides in soils have also used hydroxylamine hydrochloride in nitric acid to remove the Mn oxide minerals and ammonium oxalate in oxalic acid to remove the Fe oxide minerals. Murad & Schwertmann (1988) proposed that the extraction of manganese oxides from crusts and nodules by hydroxylamine hydrochloride causes an alteration in the iron oxide mineralogy. Hence, there is some doubt on the validity of the results from the DXRD patterns obtained after the second stage of the extraction procedure. Is the presence of ferrihydrite and akaganéite in the DXRD patterns an artifact due to changes in the iron oxide mineralogy caused by the chemical leaching with 0.10M  $\text{NH}_2\text{OH}\cdot\text{HCl}$  in 0.01M  $\text{HNO}_3$  during the first stage of the sequential extraction procedure, or are they truly oxyhydroxides originally present in the crust and nodule? Although it can not be proven conclusively that the two stage selective sequential extraction scheme proposed above does not significantly change the iron oxide mineralogy, several pieces of evidence suggests that the iron oxides identified in the DXRD patterns are the authentic iron mineral phases and not artifacts caused by the chemical leaching. Firstly, the observed iron oxides have DXRD patterns

characterized by broad peaks. If the chemical leaching with 0.10M  $\text{NH}_2\text{OH}\cdot\text{HCl}$  in 0.01M  $\text{HNO}_3$  changed the iron oxide mineralogy they most likely would invert to goethite which is the polymorph most other  $\text{FeOOH}$  phases revert to (Murray, 1979). Goethite was observed in the XRD patterns of the hydroxylamine-treated crusts studied by Murad & Schwertmann (1988). Secondly, although Murad & Schwertmann (1988) also identified feroxyhite in the XRD patterns of the hydroxylamine-treated crusts, they concluded that Mössbauer spectra of the untreated crusts indicates that most of the Fe is bound to a ferrihydrite-like phase that is intimately intergrown with the Mn oxides not feroxyhite. The presence of ferrihydrite was indeed identified in the crust sample studied here.

## 2.4 REFERENCES

- Acharya, S., Anand, S., Das, S.C., Das, R.P., & Jena, P.K., 1989. Ammonia leaching of ocean nodules using various reductants. *Erzmetall*, 42(2):66-73.
- Aguilera, N.H., & Jackson, M.L., 1953. Iron oxide removal from soils and clays. *Soil Sci. Soc. Amer. Proc.*, 17:359-364.
- Aleksandrova, L.N., 1960. The use of sodium pyrophosphate for isolating free humic substances and their organic-mineral compounds from soil. *Soviet Soil Sci.*, 2:190-197.
- Alminas, H.V., & Mosier, E.M., 1976. Oxalic-acid leaching of rocks, soils and stream-sediment samples as an anomaly-accentuation technique. *U.S. Geol. Surv. Open-File Rep.*, 76-275.
- Arrhenius, G.O., 1963. Pelagic Sediments. In *The Sea* (ed. by M.N. Hill), Vol. 3, Interscience, New York, N.Y., pp. 655-727.
- Arrhenius, G., Cheung, K., Crane, S., Fisk, M., Frazer, J., Korkisch, J., Mellin, T., Nakao, S., Tsai, A., & Wolf, G., 1979. Counterions in marine manganates. In *Sur la Genèse des Nodules du Manganèse, Gif-Sur-Yvette, Colloques Internationaux, C.N.R.S. No. 289*, pp. 333-356.
- Arrhenius, G.O., & Korkish, J., 1959. Uranium and thorium in marine minerals. 1st Internat. Ocean. Congr., Amer. Assoc. Advan. Sci., Preprints, 497 pp.
- Ball, D.J., & Beaumont, P., 1972. Vertical distribution of extractable iron and aluminium in soil profiles from a Brown Earth-Peaty Podsol association. *J. Soil Sci.*, 23:298-308.
- Bascomb, C.L., 1968. Distribution of pyrophosphate-extractable iron and organic carbon in soils of various groups. *Jour. Soil Sci.*, 19:251-268.
- Bléry-Oustrière, P., 1980. Contribution a l'étude mineralogique et géochimique des nodules polymétalliques du Pacifique Nord. Ph.D. thesis, Univ. of Paris, unpublished, 116 pp.
- Bowser, C.J., Mills, B.A., & Callender, E., 1979. Extractive chemistry of equatorial Pacific pelagic sediments and relationship to nodule forming processes. In *Marine Geology and Oceanography of the Pacific Manganese Nodule Province* (ed. by J.L. Bischoff & D.Z. Piper), Plenum Press, N.Y., pp. 587-619.
- Brown, G., & Wood, I.G., 1985. Estimation of iron oxides in soil clays by profile refinement combined with differential X-ray diffraction. *Clay Minerals*, 20:15-27.
- Bryant, R.B., Curi, N., Roth, C.B., & Franzmeir, D.P., 1983. Use of an internal standard with differential X-ray diffraction analysis for iron oxides. *Soil Sci. Soc. Amer. J.*, 47:168-173.
- Buser, W., & Grütter, A., 1956. Über die natur der manganknollen. *Schweiz. Miner. Petrogr. Mitt.*, 36:49-62.

- Cambell, A.S., & Schwertmann, U.S., 1984. Iron Oxide mineralogy of placic horizons. *Jour. of Soil Sci.*, 35:569-582.
- Chao, T.T., 1972. Selective dissolution of manganese oxides from soils and sediments with acidified hydroxylamine hydrochloride. *Soil Sci. Soc. Amer. Proc.*, 36:764-768.
- Chao, T.T., & Sanzolone, R.F., 1973. Atomic absorbtion spectrophotometric determination of microgram levels of Co, Ni, Cu, Pb, and Zn in soil and sediment extracts containing large amounts of Mn and Fe. *Journ. Res. U.S. Geol. Surv.*, 1(6):681-685.
- Chao, T.T., & Theobald Jr., P.K., 1976. The significance of secondary iron and manganese oxides in geochemical exploration. *Econ. Geol.*, 71:1560-1569.
- Chao, T.T., & Zhou, L., 1983. Extraction techniques for selective dissolution of amorphous iron oxides from soils and sediments. *Soil Sci. Soc. Amer. J.*, 47:225-232.
- Chester, R., & Hughes, M.J., 1967. A chemical technique for the separation of ferromanganese minerals, carbonate, minerals and adsorbed trace elements from pelagic sediments. *Chem. Geol.*, 2:249-262.
- Coffin, D.E., 1963. A method for the detrmination of free iron in soils and clays. *Canadian Jour. of Soil Sci.*, 43:7-17.
- de Endredy, A.S., 1963. Estimation of free iron oxides in soils and clays by a photolytic method. *Clay Minerals*, 5:218-226.
- Deb, B.C., 1949. The estimation of free iron oxides in soils and clays and their removal. *J. Soil Sci.*, 1:212-220.
- Gallagher, P.H., & Walsh, T., 1943. The solubility of soil components in oxalic acid as an index to the effects of weathering. *Royal Irish Acad. Proc.*, 498:1-26.
- Gianone, C., da Cruz, F., & Doupnik, J.R., 1988. MS-DOS Kermit User Guide for the IBM Family, Compatibles, and Other MS-DOS Systems. unpublished, 100 pp.
- Glasby, G.P., 1972. The mineralogy of manganese nodules from a range of marine environments. *Mar. Geol.*, 13:57-72.
- Han, K.N., & Fuerstenau, D.W., 1980. Extraction behavior of metal elements from deep-sea manganese nodules in reducing media. *Mar. Min.*, 2(3):155-169.
- Haynes, B.W., Magyar, M.J., & Goolay, F.E., 1987. Extractive metallurgy of ferromanganese crusts from the Necker Ridge Area, Hawaiian Exclusive Economic Zone. *Mar. Mining*, 6:23-36.
- Hoffman, S.J., & Fletcher, W.K., 1979. Selective sequential extraction of Cu, Zn, Fe, Mn, and Mo from soils and sediments. *Int. Geochem. Explor. Symp. Proc.*, 7:289-299.

- Holmgren, G.G.S., 1967. A rapid citrate-dithionite extractable iron procedure. *Soil Sci. Soc. Amer. Proc.*, 31:210-211.
- Hubred, G., 1980. Manganese nodule extractive metallurgy review 1973-1978. *Mar. Mining*, 2(3):191-212.
- Hurlbut Jr, C.S., & Klein, C., 1977. *Manual of Mineralogy* (after James D. Dana), John Wiley & Sons, New York, 532 pp.
- Itoh, H., Okuwaki, A., & Okabe, T., 1980. Processing of Pacific Ocean manganese nodules. 12th. Annual Offshore Technology Conference, Proceedings, Vol. 3, pp. 359-368.
- Kilmer, V.J., 1960. The estimation of free iron oxides in soils. *Soil Sci. Soc. Amer. Proc.*, 24:420-421.
- Le Riche, H.H. & Weir, A.H., 1963. A method of studying trace elements in soil fractions. *Jour. Soil Sci.*, 14:225-235.
- McKeague, J.A., 1967. An evaluation of 0.1M pyrophosphate and pyrophosphate-dithionite in comparison with oxalate as extractants of the accumulation products on Podzols and some other soils. *Canadian Jour. Soil Sci.*, 47:95-99.
- McKeague, J.A., Brydon, J.E., & Miles, N.M., 1971. Differentiation of forms of extractable iron and aluminium in soils. *Soil Sci. Soc. Amer. Proc.*, 35:33-38.
- McKeague, J.A., & Day, J.H., 1966. Dithionite and oxalate-extractable Fe and Al as aids in differentiating various classes of soils. *Canadian Jour. Soil Sci.*, 46:13-22.
- Mehra, O.P., & Jackson, M.L., 1960. Iron oxide removal from soils and clays by a dithionite-citrate system buffered with sodium bicarbonate. 7th Natl. Conf., on Clays and Clay Minerals, pp. 317-327.
- Mitchell, B.D., & Mackenzie, R.C., 1954. Removal of free-iron oxide from clays. *Soil Sci.*, 77:173-184.
- Moorby, S.A., & Cronan, D.S., 1981. The distribution of elements between co-existing phases in some marine ferromanganese-oxide deposits. *Geochim. Cosmochim. Acta*, 45:1855-1877.
- Murad, E., & Schwertmann, U., 1988. Iron oxide mineralogy of some deep-sea ferromanganese crusts. *Amer. Mineral.*, 73:1395-1400.
- Murray, J.W., 1979. Iron-oxides. In *Mineralogical Society of America Short Course Notes, Marine Minerals* (ed. by R.G. Burns), Vol. 6. LithoCrafters Inc., Chelsea, Michigan, pp. 47-98.
- Oades, J.M., 1963. The nature and distribution of iron compounds in soils. *Soils Fert.*, 26:69-80.
- Salomons, W., Förstner, U., 1983. "Metals in the Hydrocycle". Springer-Verlag, Berlin.

- Savitzky, A., & Golay, M.J., 1964. Smoothing and differentiation of data by simplified least squares procedures. *Anal. Chem.*, 36(8):1627-1639.
- Schulze, D.G., 1981. Identification of soil iron oxide minerals by differential X-ray diffraction. *Soil Sci. Soc. Amer. J.*, 45:437-440.
- Schwertmann, U., 1964. Differenzierung der eisenoxide des Bodens durch extraktion mit ammoniumoxalat-lösung. *Zeitschrift für Pflanzenernährung, Düngung und Bodenkunde*, 105:194-202.
- Schwertmann, U., Carlson, L., & Murad, E., 1987. Properties of iron oxides in two Finnish lakes in relation to the environment of their formation. *Clays and Clay Minerals*, 35(4):297-304.
- Shen, G.T., & Boyle, E.A., 1988. Determination of lead, cadmium and other trace metals in annually-banded corals. *Chem Geol.*, 67:47-62.
- Takematsu, N., 1979. The incorporation of minor transition metals into marine manganese nodules. *J. Oceanogr. Soc. Jpn.*, 35:191-198.
- Tipping, E., Hetherington, N.B., Hilton, J., Thompson, D.W., Bowls, E., & Taylor, J.H., 1985. Artifacts in the use of selective chemical extraction to determine distributions of metals between oxides of manganese and iron. *Anal. Chem.*, 57:1944-1946.

## 2.5 APPENDIX A

### **THE WEIGHT PERCENT Mn, Fe, Cu, Ni, AND Co IN THE LABORATORY STANDARD CRUST AS DETERMINED FROM THE LEACHATES**

The results in this Appendix are listed under the experimental order in which they were tested. The reagent used in each experiment are listed below.

Experiment 1: 0.25M  $\text{NH}_2\text{OH}\cdot\text{HCl}$  in 0.25M  $\text{HCl}$

Experiment 2: 0.25M  $\text{NH}_2\text{OH}\cdot\text{HCl}$  in 0.25M  $\text{HAc}$

Experiment 3: 0.1M  $\text{NH}_2\text{OH}\cdot\text{HCl}$  in 0.01M  $\text{HNO}_3$

Experiment 4: 0.175M Ammonium Oxalate in 0.1M Oxalic Acid (Dark Method)

Experiment 5: 0.175M Ammonium Oxalate in 0.1M Oxalic Acid  
(Photolytic Method)

Experiment 6: 1 part  $\text{H}_2\text{NNH}_2$ , 6 parts concentrated  $\text{NH}_4\text{OH}$ ,  
and 3 parts 0.3M Citric Acid in 7N  $\text{NH}_4\text{OH}$



EXPERIMENT NO.	TIME (hr)	Mn	Fe (Weight Percent)	Cu	Ni	Co
EXPERIMENT 1	0.5	12.66	10.43	0.09	0.21	0.29
Sample:Solution	1	13.93	10.25	0.09	0.21	0.28
1:250	2	15.12	12.59	0.09	0.21	0.29
	4	13.83	7.43	0.09	0.21	0.29
	8	14.51	6.79	0.08	0.20	0.30
EXPERIMENT 1	0.5	14.06	11.78	0.09	0.19	0.26
Sample:Solution	1	13.61	11.81	0.09	0.19	0.30
2:250	2	12.52	12.66	0.09	0.18	0.31
	4	12.76	13.61	0.09	0.18	0.31
	8	13.51	12.99	0.09	0.18	0.31
EXPERIMENT 1	0.5	12.32	13.54	0.08	0.17	0.25
Sample:Solution	1	13.58	11.91	0.09	0.18	0.24
3:250	2	12.69	12.71	0.09	0.18	0.24
	4	8.21	7.72	0.09	0.18	0.24
	8	12.79	13.31	0.09	0.17	0.24
EXPERIMENT 1	0.5	12.62	11.74	0.09	0.16	0.21
Sample:Solution	1	11.92	11.68	0.08	0.15	0.20
4:250	2	12.23	12.34	0.09	0.15	0.21
	4	12.45	11.94	0.09	0.15	0.21
	8	11.95	11.47	0.09	0.15	0.20
EXPERIMENT 1	0.5	11.69	10.89	0.07	0.13	0.18
Sample:Solution	1	12.41	11.42	0.08	0.13	0.18
5:250	2	12.07	11.54	0.08	0.14	0.17
	4	13.26	11.66	0.08	0.14	0.17
	8	12.95	11.89	0.08	0.14	0.17
EXPERIMENT 2	0.5	10.98	3.93	0.07	0.17	0.36
Sample:Solution	1	10.84	4.69	0.08	0.18	0.36
1:250	2	12.62	4.19	0.08	0.18	0.35
	4	11.16	5.12	0.08	0.18	0.35
	8	13.38	8.58	0.08	0.18	0.35
EXPERIMENT 2	0.5	12.13	5.67	0.07	0.15	0.29
Sample:Solution	1	11.98	7.31	0.07	0.15	0.30
2:250	2	11.53	8.78	0.07	0.15	0.30
	4	11.30	9.61	0.07	0.14	0.30
	8	12.14	9.88	0.08	0.15	0.29
	16	12.03	7.19	0.07	0.15	0.28
EXPERIMENT 2	0.5	11.07	4.91	0.06	0.15	0.25
Sample:Solution	1	11.24	5.85	0.06	0.16	0.25
3:250	2	11.93	7.28	0.06	0.16	0.24
	4	11.18	7.65	0.06	0.16	0.24
	8	11.22	7.65	0.06	0.16	0.24

EXPERIMENT 2	0.5	11.02	3.86	0.05	0.11	0.20
Sample:Solution	1	11.48	4.31	0.05	0.14	0.20
4:250	2	10.73	4.67	0.05	0.14	0.20
	4	10.68	5.03	0.05	0.15	0.20
	8	11.06	5.71	0.05	0.15	0.20
EXPERIMENT 2	0.5	10.76	4.19	0.04	0.14	0.17
Sample:Solution	1	11.37	3.99	0.04	0.14	0.17
5:250	2	11.03	4.03	0.04	0.13	0.17
	4	12.79	4.45	0.05	0.13	0.17
	8	12.09	5.02	0.05	0.13	0.17
EXPERIMENT 3	0.5	11.09	2.12	0.02	0.19	0.30
Sample:Solution	1	10.25	1.62	0.02	0.19	0.32
1:250	2	9.73	1.80	0.02	0.19	0.32
	4	10.79	0.17	0.03	0.20	0.33
	8	9.59	3.62	0.03	0.20	0.33
EXPERIMENT 3	0.5	10.19	2.09	0.01	0.16	0.24
Sample:Solution	1	9.81	1.92	0.01	0.16	0.27
2:250	2	10.35	2.81	0.00	0.17	0.26
	4	11.73	0.00	0.01	0.17	0.28
	8	10.35	3.71	0.02	0.17	0.27
EXPERIMENT 3	0.5	10.60	0.95	0.00	0.10	0.16
Sample:Solution	1	11.16	1.24	0.00	0.11	0.18
3:250	2	10.68	0.66	0.01	0.10	0.18
	4	10.62	0.18	0.01	0.10	0.18
	8	12.44	0.55	0.01	0.12	0.22
EXPERIMENT 3	0.5	9.56	0.49	0.00	0.07	0.08
Sample:Solution	1	10.08	0.06	0.00	0.09	0.11
4:250	2	9.61	0.06	0.00	0.09	0.10
	4	9.98	0.04	0.00	0.08	0.10
	8	10.25	0.06	0.01	0.09	0.15
EXPERIMENT 3	0.5	8.40	0.48	0.00	0.03	0.04
Sample:Solution	1	8.11	1.13	0.00	0.04	0.05
5:250	2	8.45	0.30	0.00	0.04	0.06
	4	9.48	0.66	0.00	0.04	0.07
	8	9.40	0.00	0.00	0.05	0.09
EXPERIMENT 4	0.5	10.63	13.95	0.06	0.20	0.35
Sample:Solution	1	10.08	13.60	0.06	0.18	0.38
1:250	2	9.84	16.53	0.07	0.21	0.37
	4	9.27	17.18	0.07	0.21	0.35
	8	10.40	16.30	0.06	0.20	0.34
EXPERIMENT 4	0.5	9.63	11.41	0.07	0.19	0.29
Sample:Solution	1	10.85	11.54	0.08	0.11	0.31
2:250	2	12.45	12.53	0.09	0.20	0.31
	4	11.00	10.71	0.08	0.20	0.32
	8	10.58	9.20	0.08	0.20	0.31

EXPERIMENT 4	0.5	8.86	8.76	0.07	0.14	0.24
Sample:Solution	1	9.87	8.30	0.07	0.15	0.25
3:250	2	10.05	13.10	0.07	0.16	0.27
	4	10.38	11.90	0.06	0.15	0.26
	8	10.24	11.39	0.08	0.16	0.28
EXPERIMENT 4	0.5	8.73	7.09	0.07	0.12	0.20
Sample:Solution	1	8.53	7.71	0.07	0.12	0.20
4:250	2	8.10	5.51	0.06	0.11	0.19
	4	8.28	5.72	0.07	0.11	0.19
	8	8.80	8.59	0.07	0.12	0.20
EXPERIMENT 4	0.5	6.60	4.54	0.05	0.11	0.18
Sample:Solution	1	6.87	3.87	0.04	0.11	0.18
5:250	2	6.38	4.36	0.05	0.11	0.18
	4	6.72	4.23	0.05	0.11	0.20
	8	6.83	6.21	0.05	0.11	0.20
EXPERIMENT 5	1	11.30	9.45	0.08	0.18	0.33
Sample:Solution						
1:250						
EXPERIMENT 5	1	9.91	9.02	0.08	0.16	0.32
Sample:Solution						
2:250						
EXPERIMENT 5	1	8.10	9.01	0.07	0.14	0.27
Sample:Solution						
3:250						
EXPERIMENT 5	1	7.28	5.98	0.07	0.12	0.21
Sample:Solution						
4:250						
EXPERIMENT 5	1	5.42	4.84	0.06	0.09	0.17
Sample:Solution						
5:250						
EXPERIMENT 6	0.5	1.98	0.00	0.08	0.16	0.22
Sample:Solution	1	6.48	1.43	0.08	0.18	0.23
1:250	2	5.93	0.00	0.07	0.14	0.22
	4	5.47	3.05	0.07	0.13	0.21
	8	7.20	0.00	0.07	0.15	0.22
EXPERIMENT 6	0.5	6.24	0.42	0.06	0.11	0.20
Sample:Solution	1	5.11	3.24	0.06	0.12	0.20
2:250	2	8.72	0.43	0.05	0.12	0.19
	4	10.05	2.92	0.06	0.12	0.20
	8	8.80	2.61	0.05	0.13	0.20

EXPERIMENT 6	0.5	9.36	2.88	0.05	0.10	0.19
Sample:Solution	1	9.66	4.03	0.05	0.11	0.19
3:250	2	9.92	4.46	0.05	0.12	0.18
	4	10.06	3.82	0.05	0.11	0.19
	8	10.15	3.18	0.04	0.10	0.19

EXPERIMENT 6	0.5	9.47	2.68	0.04	0.08	0.18
Sample:Solution	1	9.98	3.09	0.04	0.08	0.18
4:250	2	10.27	1.92	0.04	0.08	0.19
	4	9.57	2.68	0.05	0.07	0.19
	8	9.95.	2.46	0.05	0.08	0.19

EXPERIMENT 6	0.5	8.87	0.47	0.04	0.09	0.18
Sample:Solution	1	8.91	1.35	0.04	0.09	0.17
5:250	2	9.25	1.66	0.04	0.08	0.18
	4	9.54	1.89	0.04	0.08	0.18
	8	9.39	1.91	0.04	0.07	0.18

## 2.6 APPENDIX B

### **PERCENT Mn, Fe, Cu, Ni, AND Co REMOVED FROM THE LABORATORY STANDARD CRUST**

The results in this Appendix are listed under the experimental order in which they were tested. The reagent used in each experiment are listed below.

Experiment 1: 0.25M  $\text{NH}_2\text{OH}\cdot\text{HCl}$  in 0.25M  $\text{HCl}$

Experiment 2: 0.25M  $\text{NH}_2\text{OH}\cdot\text{HCl}$  in 0.25M  $\text{HAc}$

Experiment 3: 0.1M  $\text{NH}_2\text{OH}\cdot\text{HCl}$  in 0.01M  $\text{HNO}_3$

Experiment 4: 0.175M Ammonium Oxalate in 0.1M Oxalic Acid (Dark Method)

Experiment 5: 0.175M Ammonium Oxalate in 0.1M Oxalic Acid

(Photolytic Method)

Experiment 6: 1 part  $\text{H}_2\text{NNH}_2$ , 6 parts concentrated  $\text{NH}_4\text{OH}$ ,  
and 3 parts 0.3M Citric Acid in 7N  $\text{NH}_4\text{OH}$

EXPERIMENT NO.	TIME (hr)	Mn	Fe	Cu (Percent)	Ni	Co
EXPERIMENT 1	0.5	101.07	67.12	144.00	137.63	95.82
Sample:Solution	1	111.13	65.92	144.00	138.67	94.73
1:250	2	120.66	81.00	142.83	139.20	98.02
	4	110.29	47.75	142.00	137.63	96.92
	8	115.83	43.69	140.58	134.47	99.12
EXPERIMENT 1	0.5	112.19	75.77	148.08	126.13	85.75
Sample:Solution	1	108.59	75.93	143.83	123.77	101.67
2:250	2	99.94	81.42	142.96	119.82	103.49
	4	101.81	87.49	146.37	118.63	103.86
	8	107.80	83.56	154.92	119.02	104.41
EXPERIMENT 1	0.5	98.35	87.08	136.94	114.10	82.98
Sample:Solution	1	108.34	76.58	144.72	117.08	81.56
3:250	2	101.28	81.77	114.17	117.68	81.56
	4	65.50	49.62	150.81	117.38	81.56
	8	102.14	85.63	153.03	113.81	81.32
EXPERIMENT 1	0.5	100.71	75.52	142.81	104.09	68.71
Sample:Solution	1	95.12	75.08	138.10	103.20	68.09
4:250	2	97.57	79.38	142.25	102.98	68.80
	4	99.34	76.79	144.33	102.53	68.45
	8	95.41	73.79	146.00	97.85	68.00
EXPERIMENT 1	0.5	93.31	70.05	125.22	86.63	36.49
Sample:Solution	1	99.07	73.44	129.60	89.82	36.54
5:250	2	96.32	74.24	131.78	91.10	36.04
	4	105.85	75.00	135.55	90.73	36.13
	8	103.31	76.43	135.87	91.10	35.59
EXPERIMENT 2	0.5	87.59	25.24	125.75	114.40	118.67
Sample:Solution	1	86.52	30.19	129.83	119.60	119.82
1:250	2	100.72	27.00	127.08	120.33	117.53
	4	89.08	32.92	131.17	118.87	117.53
	8	106.74	55.14	138.00	117.37	118.28
EXPERIMENT 2	0.5	96.83	36.48	111.75	99.83	96.58
Sample:Solution	1	95.65	47.02	115.79	99.10	99.99
2:250	2	92.04	56.48	118.54	100.58	100.57
	4	90.18	61.82	121.92	96.87	99.23
	8	96.93	63.55	129.38	102.80	97.53
	16	96.05	46.29	125.33	100.58	94.67
EXPERIMENT 2	0.5	88.38	31.56	98.83	102.88	82.26
Sample:Solution	1	89.75	37.60	99.25	106.50	81.99
3:250	2	95.22	46.83	101.86	105.77	81.56
	4	89.22	49.23	104.47	105.29	81.32
	8	89.52	49.25	105.78	107.23	80.52

EXPERIMENT 2	0.5	87.99	24.80	81.94	76.25	66.91
Sample:Solution	1	91.58	27.77	85.52	96.20	66.31
4:250	2	85.64	30.06	86.19	94.38	66.20
	4	85.25	32.32	91.40	97.83	66.20
	8	88.27	36.73	90.08	98.93	66.61
EXPERIMENT 2	0.5	85.85	26.94	74.02	91.25	56.57
Sample:Solution	1	90.77	25.69	73.77	91.11	56.16
5:250	2	88.02	25.91	74.02	89.01	55.01
	4	102.10	28.64	80.32	89.61	55.67
	8	96.49	32.25	82.15	88.56	56.24
EXPERIMENT 3	0.5	88.52	13.65	40.33	125.07	101.58
Sample:Solution	1	81.77	10.45	35.00	129.80	107.82
1:250	2	77.61	11.58	37.67	125.07	106.35
	4	86.16	11.25	50.92	132.63	110.37
	8	76.59	23.30	52.25	132.63	110.00
EXPERIMENT 3	0.5	81.36	13.49	16.17	105.55	106.03
Sample:Solution	1	72.28	12.37	10.21	107.90	118.72
2:250	2	82.60	18.09	8.25	110.75	116.60
	4	93.57	0.00	23.46	114.07	122.62
	8	82.60	23.87	34.04	113.12	121.89
EXPERIMENT 3	0.5	84.60	6.11	3.83	65.58	80.88
Sample:Solution	1	89.04	7.98	6.36	72.99	92.09
3:250	2	85.24	4.23	11.05	68.88	89.15
	4	84.73	1.18	15.31	69.97	91.91
	8	99.28	3.54	15.31	80.69	109.38
EXPERIMENT 3	0.5	76.31	3.17	2.55	35.80	26.64
Sample:Solution	1	80.46	0.40	1.69	46.93	37.95
4:250	2	76.67	0.40	3.83	43.42	34.92
	4	79.61	0.24	5.11	39.51	34.18
	8	81.78	0.40	14.42	58.46	49.73
EXPERIMENT 3	0.5	67.07	3.12	4.43	21.63	13.21
Sample:Solution	1	64.75	7.30	1.42	25.79	17.68
5:250	2	67.46	1.96	3.68	25.96	19.47
	4	75.65	4.24	3.18	28.46	23.86
	8	75.02	0.00	5.45	33.31	29.67
EXPERIMENT 4	0.5	84.79	89.71	105.67	133.93	118.40
Sample:Solution	1	80.41	87.46	100.67	119.07	126.43
1:250	2	78.52	106.29	123.00	137.00	124.00
	4	73.96	110.50	120.50	137.00	117.60
	8	83.00	104.82	105.67	135.47	114.40
EXPERIMENT 4	0.5	76.88	73.36	125.08	125.09	127.04
Sample:Solution	1	86.64	74.23	130.00	128.17	139.33
2:250	2	99.40	80.58	148.75	134.87	136.13
	4	87.79	68.89	138.75	136.67	143.62
	8	84.40	59.16	133.75	135.60	137.20

EXPERIMENT 4	0.5	70.74	56.31	121.22	93.13	118.23
Sample:Solution	1	70.74	53.75	125.72	97.04	126.30
3:250	2	80.19	84.27	118.17	104.38	133.93
	4	82.85	76.56	128.78	102.42	132.58
	8	81.74	73.26	148.39	107.31	140.20
EXPERIMENT 4	0.5	69.67	45.65	111.29	82.68	66.07
Sample:Solution	1	68.04	49.56	111.29	82.68	65.39
4:250	2	64.64	35.41	106.75	76.82	64.28
	4	66.04	36.78	113.00	76.45	65.17
	8	70.27	55.29	113.00	80.85	65.39
EXPERIMENT 4	0.5	52.71	29.23	79.57	71.96	59.52
Sample:Solution	1	58.83	24.89	75.30	75.92	58.89
5:250	2	58.88	28.04	77.43	74.51	60.15
	4	53.66	27.23	79.13	74.51	66.68
	8	54.54	39.96	84.67	76.20	65.83
EXPERIMENT 5	1	90.18	60.77	141.00	117.60	108.53
Sample:Solution						
1:250						
EXPERIMENT 5	1	79.09	58.03	129.92	105.53	144.38
Sample:Solution						
2:250						
EXPERIMENT 5	1	64.64	57.93	120.56	91.60	133.55
Sample:Solution						
3:250						
EXPERIMENT 5	1	58.11	38.50	117.50	78.97	71.24
Sample:Solution						
4:250						
EXPERIMENT 5	1	43.25	31.12	105.03	62.61	58.47
Sample:Solution						
5:250						
EXPERIMENT 6	0.5	15.76	0.00	128.50	109.97	73.55
Sample:Solution	1	51.68	9.16	126.92	120.63	76.43
1:250	2	47.29	0.00	114.50	92.27	73.55
	4	43.69	19.61	120.75	85.90	70.65
	8	57.46	0.00	114.50	99.27	73.55
EXPERIMENT 6	0.5	49.77	2.73	106.29	73.68	88.73
Sample:Solution	1	40.79	20.82	103.17	81.70	88.73
2:250	2	69.62	2.75	92.29	80.37	86.18
	4	80.19	18.81	93.08	81.70	88.10
	8	70.23	16.80	89.17	84.37	88.10



EXPERIMENT 6	0.5	74.69	18.54	84.67	68.72	95.35
Sample:Solution	1	77.08	25.94	85.17	76.49	93.83
3:250	2	79.20	28.72	78.67	78.21	92.31
	4	80.33	24.59	76.64	72.18	93.33
	8	80.99	20.47	66.64	66.13	94.84

EXPERIMENT 6	0.5	75.61	17.24	74.00	53.48	60.83
Sample:Solution	1	79.71	19.86	72.88	51.54	61.34
4:250	2	81.95	12.34	68.00	50.89	62.61
	4	76.41	17.24	78.13	48.30	61.85
	8	79.41	15.84	79.25	50.89	61.85

EXPERIMENT 6	0.5	70.82	3.05	67.37	62.22	58.55
Sample:Solution	1	71.11	8.65	60.82	60.09	57.94
5:250	2	73.82	10.67	61.72	50.51	59.35
	4	76.09	12.19	64.68	51.04	60.15
	8	74.98	12.28	66.17	46.25	59.55

## 2.7 APPENDIX C

### **THE SAVITZKY & GOLAY (1964) SMOOTHING PROGRAM TRANSLATED INTO GW BASIC**

```

Total% = 15000
'$DYNAMIC
DIM D(Total%), Array%(Total%), SG%(34)
DIM B(Total%)
CLS
INPUT "file name (no extension) "; Filename$
OPEN Filename$ + ".prn" FOR INPUT AS #1
OPEN Filename$ + ".out" FOR OUTPUT AS #2
PRINT "Wait file crunching"
DO WHILE NOT EOF(1)
    Count = Count + 1
    INPUT #1, D(Count), Array%(Count)
LOOP
PRINT "Total count = "; Count
t1 = 1: t2 = Count
GOSUB smooth
GOSUB Outfile
END

smooth:
' Savitsky-Golay smoothing
INPUT "9, 17, or 23 point smooth...9,17,23 "; PR
IF PR = 0 THEN PR = 9
IF PR = 9 THEN
    PO = 1
    PT = 9: OF = 4
    RESTORE 5090
    FOR I = 1 TO PT
        READ SG%(I)
    NEXT I
END IF
IF PR = 17 THEN
    PO = 2
    PT = 17: OF = 8
    RESTORE 5100
    FOR I = 1 TO PT

```

```

        READ SG%(I)
    NEXT I
END IF
IF PR = 23 THEN
    PO = 3
    PT = 23: OF = 12
    RESTORE 5110
    FOR I = 1 TO PT
        READ SG%(I)
    NEXT I
END IF
CLS
LOCATE 1, 1: PRINT "wait, smoothing data"
FOR I = t1 TO t2
    B(I) = 0: DF% = 0
    FOR J = -OF TO OF
        IF NOT (I + J < 1 OR I + J > Count) THEN
            'put integer point into larger number class
            Cast = Array%(I + J)
            B(I) = B(I) + Cast * SG%(J + OF + 1)
            DF% = DF% + SG%(J + OF + 1)
        END IF
    NEXT J
    B(I) = B(I) / DF%
    'PRINT Array%(I), B(I)
NEXT I
RETURN

Outfile:
FOR I = t1 TO t2
    'PRINT USING "###.##"; D(I), B(I)
    PRINT #2, USING "###.##"; D(I), B(I)
NEXT I
RETURN

```

' quadratic,cubic

5090 DATA -21,14,39,54,59,54,39,14,-21: ' 9 point

5100 DATA -21,-6,7,18,27,34,39,42,43,42,39,34,27,18,7,-6,-21: ' 17 point

5110 DATA -42,-21,-2,15,30,43,54,63,70,75,78,79,78,75,70,63,54,43,30,15,-2,-21,-42: '23 point

## **CHAPTER 3**

# **THE APPLICATION OF THE SELECTIVE SEQUENTIAL EXTRACTION SCHEME AND THE DIFFERENTIAL X-RAY DIFFRACTION TECHNIQUE TO A SMALL POPULATION OF CRUSTS AND NODULES FROM THE NORTHEAST EQUATORIAL PACIFIC OCEAN**

### 3.1 INTRODUCTION

#### 3.1.1 PREVIEW

In Chapter 1, a large population of crusts and nodules from the northeastern equatorial Pacific Ocean were analysed for their major element composition. From the major element compositions, different groups of crusts and nodules could be identified by their distinctive compositions and inter-element correlations. The distinctive compositions were related to the environment of formation while the inter-element correlations were related to the mineralogy identified from a bulk powdered sample. In Chapter 2, a two stage selective sequential extraction scheme as well as a DXRD technique was developed for selectively removing and identifying first the manganese and then the iron oxyhydroxides present in crusts and nodules. The concentrations of Mn, Fe, Cu, Ni, and Co associated with the manganese phase(s) and the iron phase(s) could then be determined. The selective sequential extraction scheme and the DXRD technique were developed on laboratory standard crust and nodule samples to determine the precision and accuracy of the methods of analysis. In this chapter the two stage selective sequential extraction scheme and the DXRD technique will be used on a small number of samples selected from the large population of crusts and nodules studied in Chapter 1.

#### 3.1.2 STATEMENT OF THE PROBLEM

Although Chapter 1 showed that inter-element correlations existed between Mn and Fe and other elements in crusts and nodules, only the correlations with Mn could be attributed to manganese oxide phase(s) identified in a bulk powdered sample. Examination of the compositional data showed that inter-element

correlations with Fe did exist, but how those elements associated with Fe were hosted within the crusts and nodules remained unknown. The application of the two stage selective sequential extraction scheme and the DXRD technique on a small population of crusts and nodules from the northeastern equatorial Pacific Ocean was studied for two purposes: (1) to separate the manganese oxides from the iron oxyhydroxides and to identify the iron oxyhydroxide phase(s) present in crusts and nodules; and (2) to identify the partitioning of the Cu, Ni, and Co concentrations between the manganese and iron oxides in crusts and nodules.

### 3.2 SELECTION OF SAMPLES

In Chapter 1 a large number of crusts and nodules from the northeast equatorial Pacific Ocean were divided into two study areas and the crusts and nodules from each study area could be classified into different groups based on their distinctive compositions. To achieve the two purposes set out in this chapter, two samples from each group of crusts and nodules from the two study areas was selected for analysis. The Fe-rich hydrothermal crusts from Survey Region B were not analyzed because such crusts contain little or no manganese so there is no manganese oxide(s) present in these samples, amorphous hydrated iron oxides and silica are the dominant iron- and silica rich mineral phase present and these crusts contain low concentrations of Cu, Ni and Co. Because the manganese phase mineralogy does not exist and the iron phase mineralogy has already been identified and is found to contain little or no Cu, Ni, and Co, there is no need to study Fe-rich hydrothermal crusts from Survey Region B. The location and depth of the samples selected for analysis in this chapter are listed in Table 3-1. Table 3-1a lists the samples selected from Survey Region A while Table 3-1b lists the samples selected from Survey Region B.



Table 3-1a. Location and depth of crust and nodule samples selected from Survey Region A for analysis. The location and depth of these samples are also shown in Figure 1-2 in Chapter 1.

Sample	Latitude		Longitude		Depth (m)
	Degrees	Minutes	Degrees	Minutes	
Hydrogenetic Crusts					
7TOW 130 D-FRAG	8	20.0 N	164	21.7 W	1519
7TOW 142 D-1	18	8.1 N	169	4.0 W	2139
Hydrogenous Nodules					
DODO 12-2 D-1	18	38.0 N	162	8.0 W	5040
DODO 14-2 D-2	19	22.0 N	162	19.0 W	4868
Diagenetic Nodules					
Mn 39	8	16.4 N	150	59.6 W	4833
Mn 56	11	30.8 N	148	34.7 W	5128

Table 3-1b. Location and depth of crust and nodule samples selected from Survey Region B for analysis. The location and depth of these samples are also shown in Figure 1-3 in Chapter 1.

Sample	Latitude		Longitude		Depth (m)
	Degrees	Minutes	Degrees	Minutes	
Hydrogenetic Crusts					
Henderson Smt	25	15.0 N	119	40.0 W	64
RISE III 28 D-1	13	46.0 N	101	52.3 W	1693
Mn-rich Hydrothermal Crusts					
QBR 22 D-1	9	55.2 N	104	29.0 W	1680
RISE III 3 D-1	8	49.5 N	103	55.0 W	2095
Hydrogenous and Diagenetic Nodules					
B 104	11	10.6 N	109	36.3 W	3522
B 114	14	35.1 N	121	3.7 W	4295
Mn-rich Hydrothermal Nodules					
CERS 20 D-2	11	14.3 N	101	7.6 W	2975
CERS 21 D-3	10	52.3 N	101	31.6 W	3080
Fe-rich Hydrothermal Nodules					
DWBD 1-2	21	27.0 N	126	43.0 W	4300
S 74	23	43.0 N	124	6.0 W	3787

### 3.3 ANALYTICAL METHODS

A complete description of the XRF analysis has been given in Chapter 1 while a complete description of the selective sequential extraction scheme, and the differential X-ray diffraction technique has been given in Chapter 2.

### 3.4 RESULTS

#### 3.4.1 BACKGROUND GEOCHEMISTRY AND MINERALOGY

A complete discussion about the major element composition and its relation to the mineralogy of crusts and nodules from Northeast Pacific Ocean is given in Chapter 1. In this section only a brief review about the behaviour of Mn, Fe, Cu, Ni, and Co will be provided. The major element composition of the untreated crust and nodule samples are listed in Table 3-2. Table 3-2a gives the major element composition of those crusts and nodule samples from Survey Region A while Table 3-2b gives the major element composition of those crusts and nodule samples from Survey Region B. The mineralogy of the untreated samples selected for the selective sequential extraction scheme and differential X-ray diffraction technique is also described.

Table 3-2a. The major element composition of the bulk crust and nodule samples selected from Survey Region A. Results are listed as weight per cent.

Element	Samples		Hydrogenetic Crusts	
	7TOW	7TOW		
	130	142 D-1		
Si	1.16	3.09		
Ti	0.79	0.90		
Al	0.14	0.66		
Fe	10.22	12.76		
Mn	23.76	17.19		
Mg	1.17	0.85		
Ca	2.29	2.78		
Na	1.60	1.66		
K	0.42	0.40		
P	0.34	0.60		
Co	0.92	0.64		
Ni	0.63	0.31		
Cu	0.02	0.04		
Zn	0.06	0.03		
Ba	0.17	0.16		

Element	Samples		Diagenetic Nodules	
	Hydrogenous Nodules		Mn 39 Mn 56	
	DODO	DODO		
	12-2 D-1	14-2 D-2		
Si	8.23	6.42	6.38	5.12
Ti	1.09	1.16	0.44	0.32
Al	2.77	1.82	2.54	2.13
Fe	13.19	15.34	6.39	5.00
Mn	11.69	11.41	23.97	26.53
Mg	1.05	0.97	2.17	1.98
Ca	2.04	3.08	1.56	1.52
Na	2.66	1.38	0.71	0.61
K	0.99	0.75	0.81	0.63
P	0.34	0.84	0.15	0.13
Co	0.28	0.29	0.19	0.18
Ni	0.15	0.14	1.14	1.11
Cu	0.06	0.07	1.02	1.11
Zn	0.03	0.03	0.11	0.12
Ba	0.11	0.13	0.15	0.18

Table 3-2b. The major element composition of the bulk crust and nodule samples selected from Survey Region B. Results are listed as weight per cent.

Element	Samples		Mn-rich	
	Hydrogenetic Crusts		Hydrothermal Crusts	
	HEN SMT	RISE III 28 D-1	QBR 22 D-1	RISE III 3 D-1
Si	10.52	3.53	1.25	0.03
Ti	0.11	0.65	0.04	0.04
Al	0.88	0.83	0.07	0.00
Fe	12.67	14.54	4.77	0.23
Mn	19.72	16.38	33.60	42.34
Mg	2.18	1.06	1.98	1.68
Ca	0.68	1.84	1.53	2.94
Na	1.12	1.61	2.31	2.08
K	2.34	0.39	0.90	0.72
P	0.15	0.41	0.12	0.02
Co	0.06	0.51	0.00	0.00
Ni	0.20	0.33	0.12	0.03
Cu	0.01	0.00	0.01	0.00
Zn	0.02	0.04	0.06	0.01
Ba	0.65	0.14	0.09	0.33

Element	Samples		Mn-rich		Fe-rich	
	Hydrogenous and Diagenetic Nodules		Hydrothermal Nodules		Hydrothermal Nodules	
	B 104	B 114	CERS 20 D-2	CERS 21 D-3	DWBD 1-2	S 74
Si	4.99	6.67	4.14	2.38	27.51	18.93
Ti	0.28	0.30	0.14	0.09	0.26	0.43
Al	1.54	2.39	1.63	1.14	1.58	5.13
Fe	7.24	5.29	3.57	1.82	8.17	10.00
Mn	23.81	25.75	33.45	37.22	6.01	4.67
Mg	1.40	1.97	2.28	2.13	1.15	1.41
Ca	1.59	1.44	1.19	1.15	0.37	0.90
Na	1.98	1.60	1.27	1.37	0.84	2.72
K	0.67	1.07	0.83	0.84	0.98	2.97
P	0.16	0.13	0.10	0.08	0.06	0.18
Co	0.07	0.15	0.00	0.01	0.09	0.10
Ni	0.88	1.12	0.63	0.56	0.31	0.20
Cu	0.66	0.76	0.30	0.25	0.14	0.08
Zn	0.12	0.11	0.14	0.22	0.02	0.02
Ba	0.26	0.23	0.31	0.29	0.56	0.14

### 3.4.1.1 Survey Region A

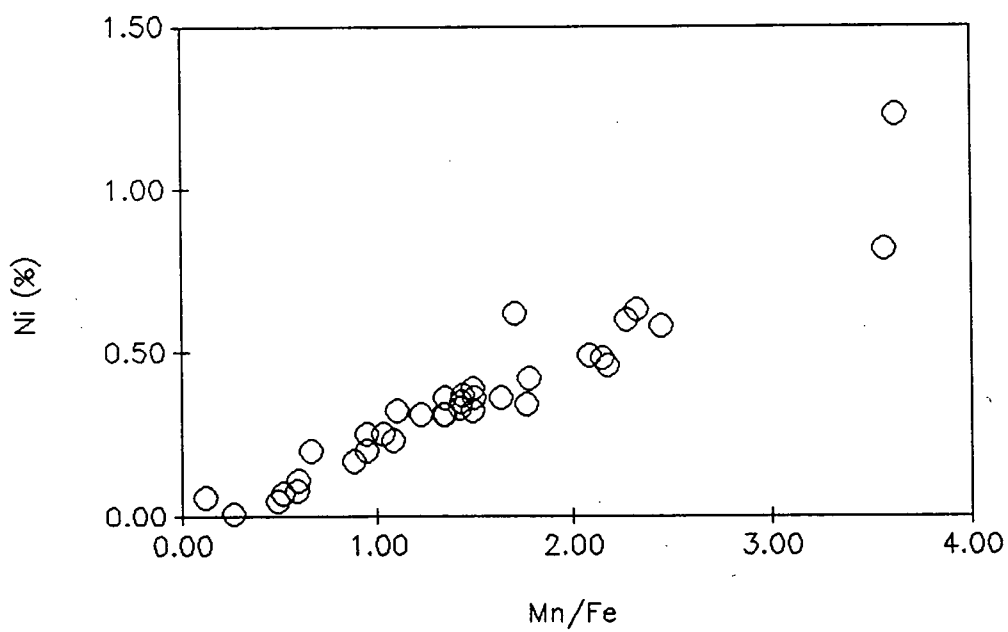
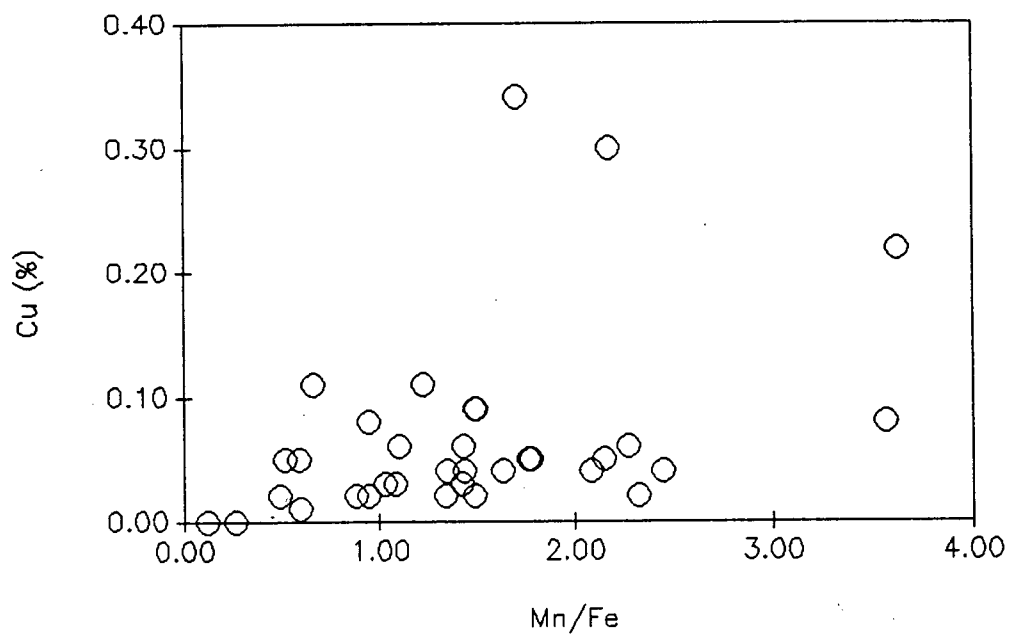
#### 3.4.1.1.1 Crusts

To examine the regional compositional variations with respect to Mn and Fe, the effects of the dilutant aluminosilicates and carbonate fluorapatite material must be removed (Calvert, 1978). Price & Calvert (1970) solved the problem by using element ratios instead of absolute abundances of elements to represent geochemical variations. Using the elemental ratio of Mn/Fe, the association of the major elements with either of the major oxide phases will become more apparent. Elements correlated with the manganese phase mineralogy will show a positive linear correlation with the Mn/Fe ratio. For Cu, Ni and Co, only Ni and Co show a strong correlation with Mn while Cu shows a very weak correlation (Figure 3-1). The XRD patterns of the hydrogenetic crusts selected for analysis shows that the dominant oxide phase present in these crusts is  $\delta\text{MnO}_2$  (Figure 3-2).

#### 3.4.1.1.2 Nodules

Although not the first, Halbach & Özkara (1979) used the Mn/Fe ratio as a criterion for distinguishing between different types of nodules from a small study area located within Survey Region A. They decided that nodules with an Mn/Fe ratio less than 2.5 were hydrogenous in origin while nodules with an Mn/Fe ratio above 2.5 were diagenetic in origin. Nodules from Survey Region A can also be divided into these two groups and show a marked compositional distinction between them. As shown in Figure 3-3, hydrogenous nodules are depleted in Mn, Cu, and Ni compared to the diagenetic nodules which are enriched in these elements.

Figure 3-1. The association of Cu, Ni with Mn/Fe in hydrogenetic crusts from Survey Region A.





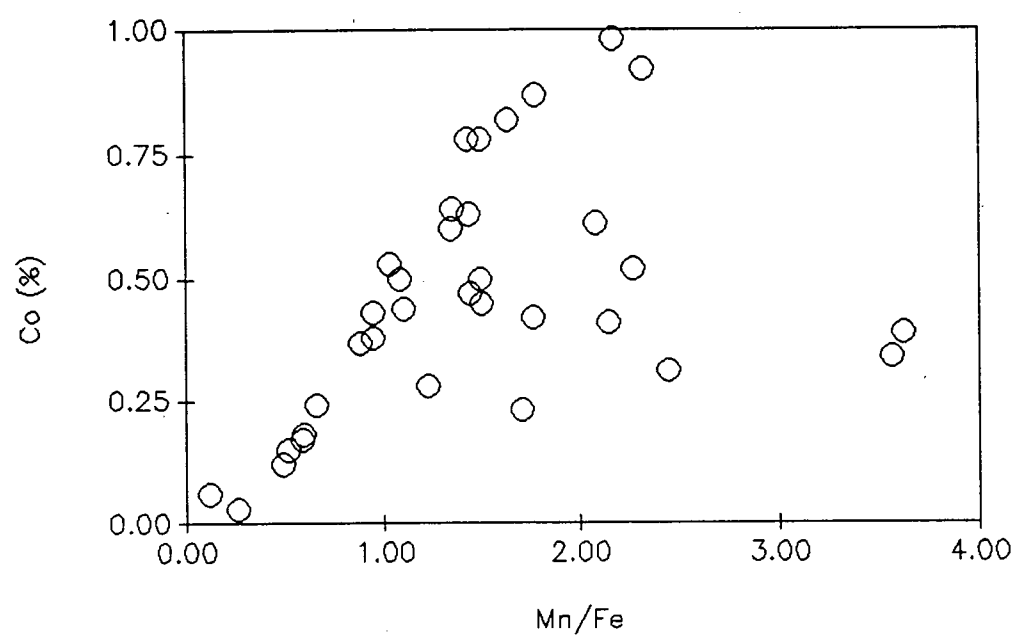
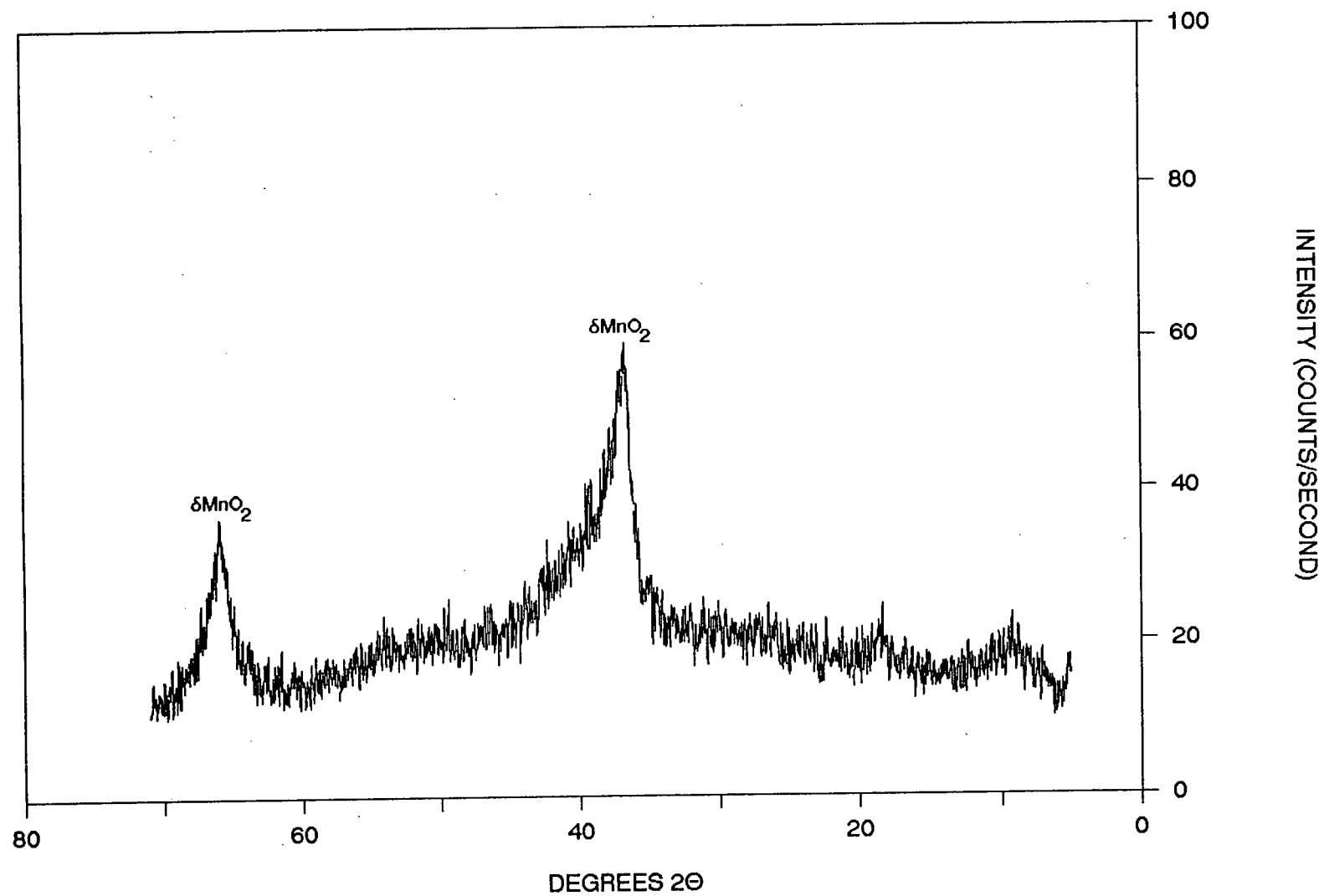


Figure 3-2. The XRD patterns of hydrogenetic crusts selected for the two stage selective sequential extraction scheme.

# 7TOW 130 D-FRAG



## 7TOW 142 D-1

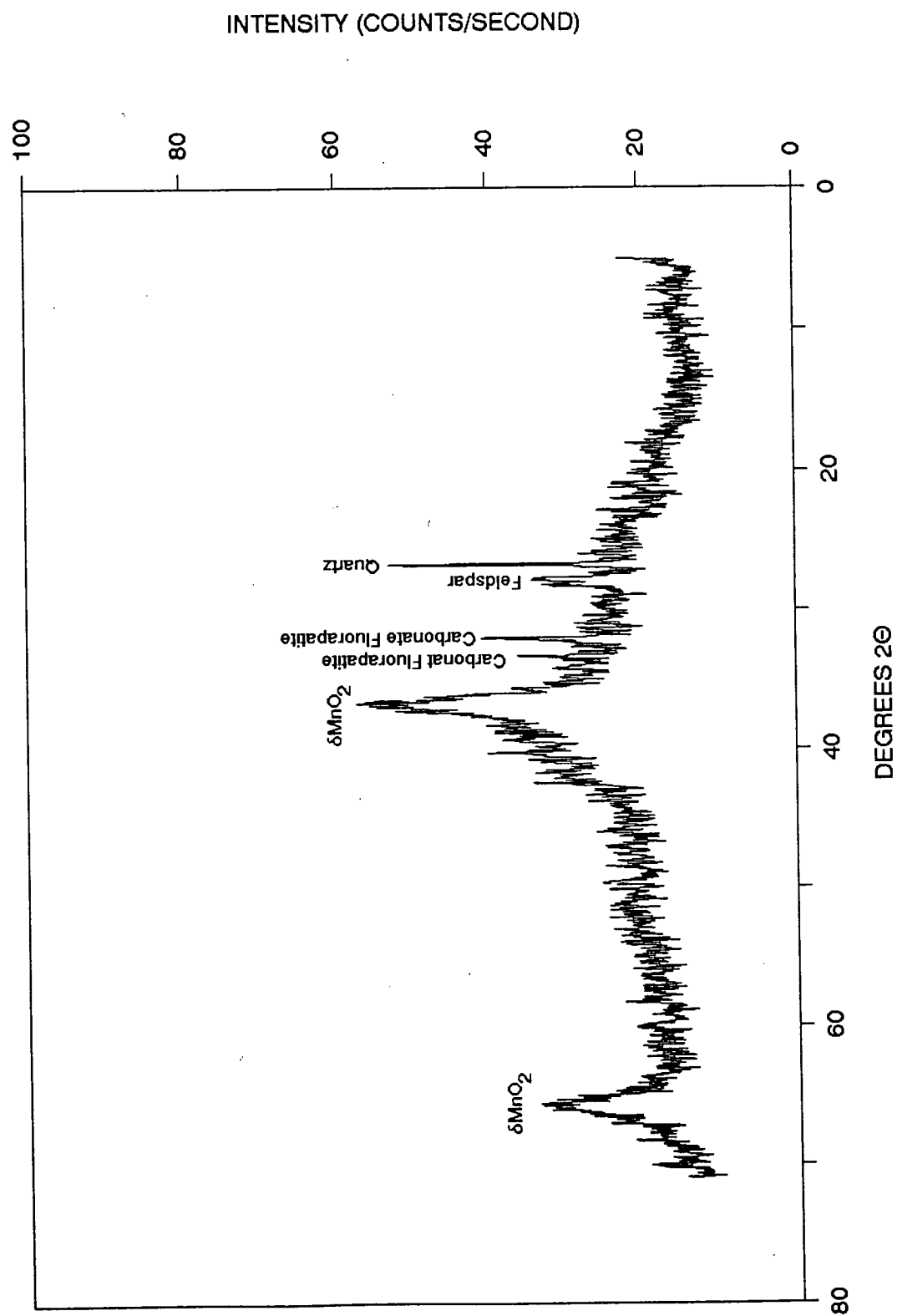
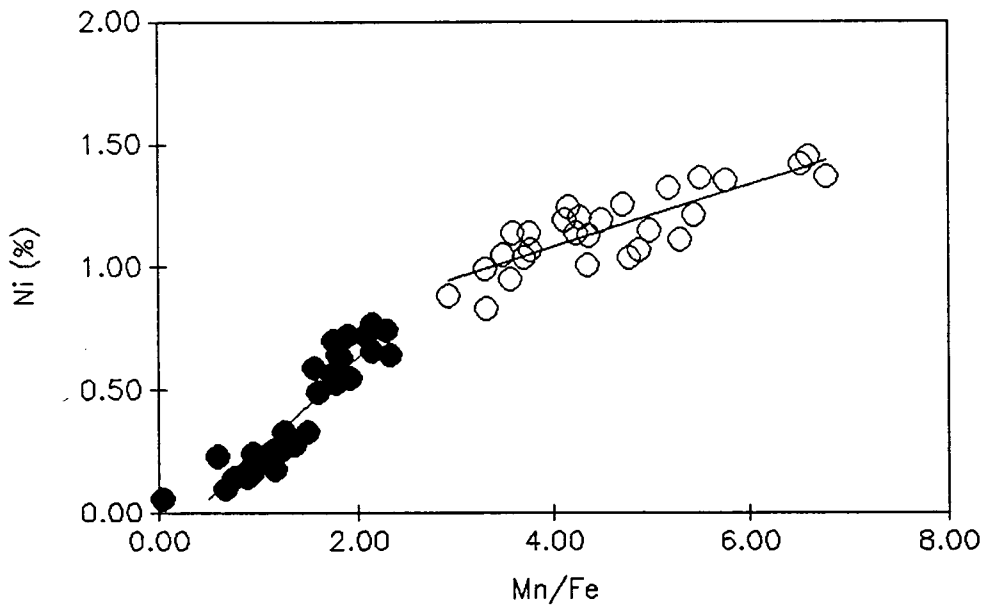
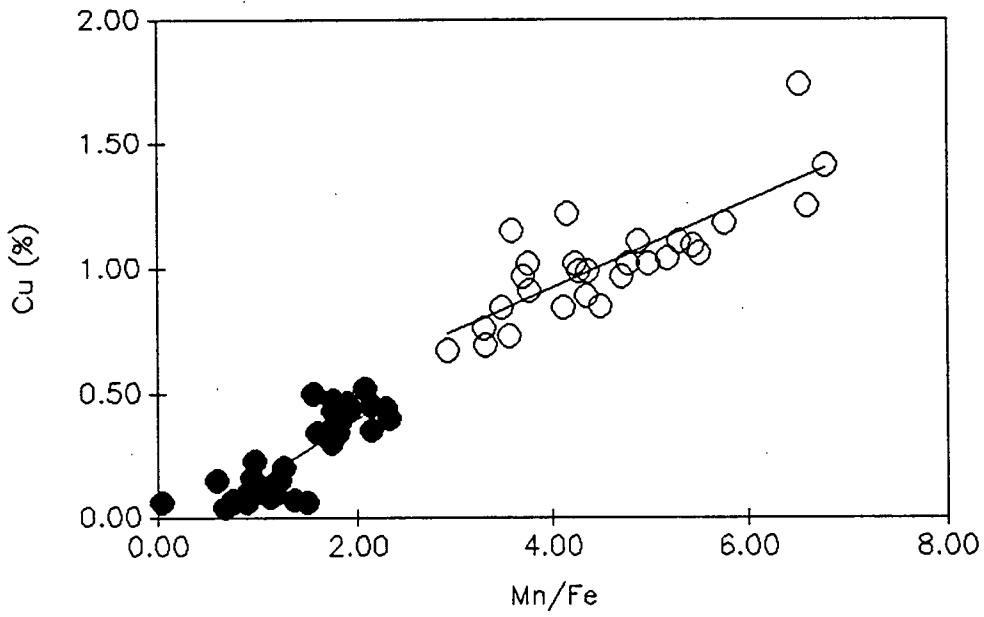


Figure 3-3. The association of Cu, Ni with Mn/Fe. The open circles = diagenetic nodules, the filled circles = hydrogenous nodules.



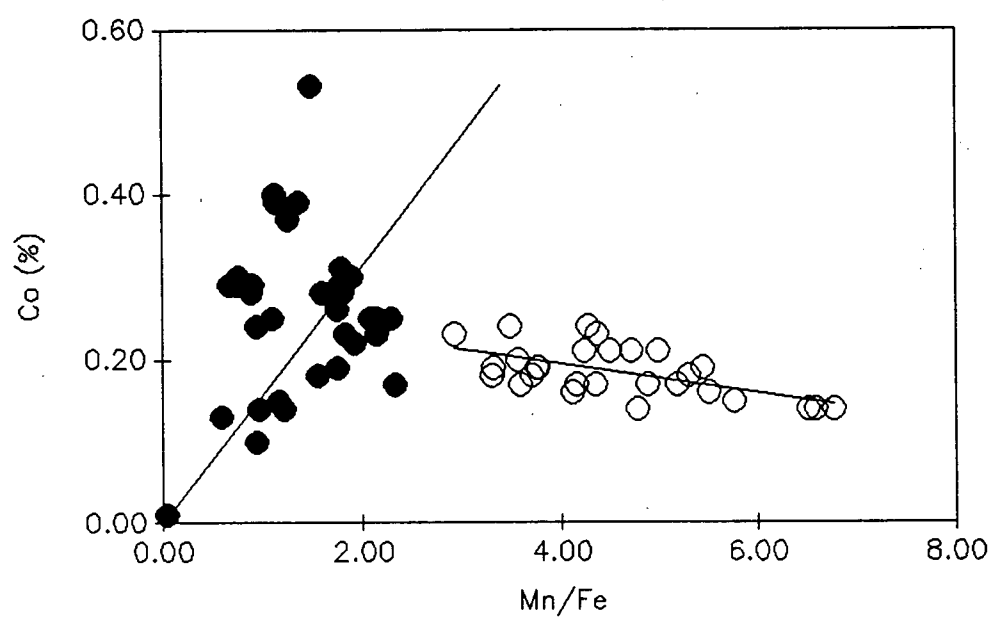
It is interesting to note in Figure 3-3 that there is a sharp break in slope of a first order regression line drawn through the hydrogenous nodules compared to one drawn through the diagenetic nodules. For Cu and Ni, the slope of the regression line for the hydrogenous nodules is greater than that of the diagenetic nodules. A non-linear correlation between Ni and Cu versus the Mn/Fe ratio has also been observed by Halbach *et al.* (1981b) in nodules from the Northeast Pacific nodule belt and by Usui & Mita (1987) in nodules from the three survey areas of SONNE Cruise SO-25 in the Northeast equatorial Pacific. Halbach *et al.* (1981b) concluded that their non-linear regressions describe the natural saturation of divalent cations in the lattice of todorokite. The decrease in the slope of the first order regression lines from the hydrogenous nodules to the diagenetic nodules recovered from Survey Region A can therefore be attributed to the saturation of the todorokite crystal lattice by manganese and associated divalent cations.

Cobalt shows a complex association with Mn and Fe, which is unlike that of Cu and Ni (Figure 3-4). In hydrogenous nodules, Co is positively correlated with Mn, whereas in diagenetic nodules Co is positively correlated with Fe. The complex association of Co with the manganese and iron oxide phases have been previously observed by Cronan & Tooms (1969), Price & Calvert (1970) and by Halbach *et al.* (1983).

Price & Calvert (1970) suggested that this observed complex behavior of Co in nodules is due to  $\text{Co}^{3+}$  substituting for  $\text{Mn}^{4+}$  in nodules containing  $\delta\text{MnO}_2$  as well as  $\text{Fe}^{3+}$  in the iron oxyhydroxide phases. Cobalt (III) ( $d^6$ ) is stable when in the low spin state with octahedral coordination and has an ionic radius almost identical to that of  $\text{Fe}^{3+}$  or  $\text{Mn}^{4+}$ . Cobalt (III) will therefore preferentially substitute for both  $\text{Fe}^{3+}$  in the  $\text{FeOOH} \cdot n\text{H}_2\text{O}$  phase (Burns, 1965) and  $\text{Mn}^{4+}$  in the  $\delta\text{MnO}_2$  phase (Glasby & Thijessen, 1982a; Halbach *et al.*, 1981a). Cobalt (III) will also substitute for  $\text{Mn}^{4+}$  in the "ceilings" of todorokite (Burns, 1976).

Figure 3-4. The complex association of Co with Mn/Fe. The open circles = diagenetic nodules, the filled circles = hydrogenous nodules.





The XRD patterns of the hydrogenous nodules selected for analysis shows that the dominant oxide phase present in these nodules is  $\delta\text{MnO}_2$  (Figure 3-5) while the diagenetic nodules selected for analysis shows that the dominant oxide phases present these nodules is both todorokite and  $\delta\text{MnO}_2$  (Figure 3-6). Since hydrogenous nodules contain both  $\delta\text{MnO}_2$ , this would explain the positive association of Co with Mn. Diagenetic nodules, on the other hand, contain mostly todorokite. Although the substitution of  $\text{Co}^{3+}$  for  $\text{Mn}^{4+}$  in the "ceilings" of todorokite probably occurs, the substitution of  $\text{Co}^{3+}$  for  $\text{Fe}^{3+}$  in the  $\text{FeOOH} \times n\text{H}_2\text{O}$  phase appears to be more dominant as seen by the correlation of Co with Fe in these nodules.

### 3.4.1.2 Survey Region B

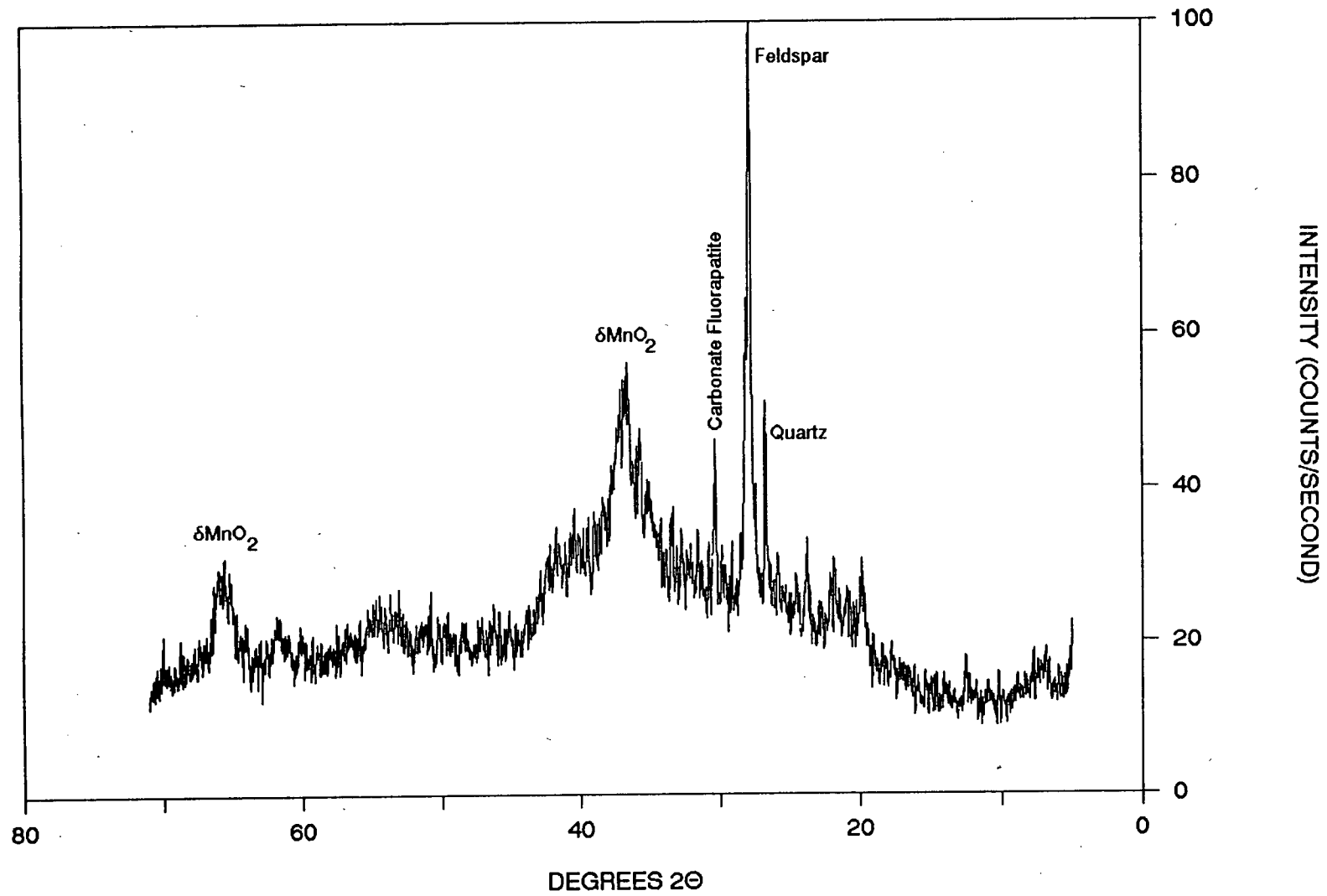
#### 3.4.1.2.1 Crusts

Crusts from Survey Region B have an extremely wide range Mn/Fe ratios ( $0.06 \leq \text{Mn/Fe} \leq 222.68$ ). Consequently, there is a high degree of fractionation of these two elements in the crusts from this region.

The concentrations of Mn indicate that there are three distinct groups of crusts within Survey Region B. The largest group of crusts within Survey Region B have Mn concentrations ranging from 7 to 20 weight per cent. This group of hydrogenetic crusts show a strong positive linear correlations with Mn to Co, Cu, and Ni (Figure 3-7). The XRD patterns of the two hydrogenetic crusts selected for analysis are not consistent as to the dominant oxide phases present in these crusts (Figure 3-8). If the two hydrogenetic crusts selected for analysis are representative of hydrogenetic crusts from this region, then the dominant oxide phases that can be present are birnessite, todorokite, and  $\delta\text{MnO}_2$ .

Figure 3-5. The XRD patterns of hydrogenous nodules selected for the two stage selective sequential extraction scheme.

# DODO 12-2 D-1



# DODO 14-2 D-2

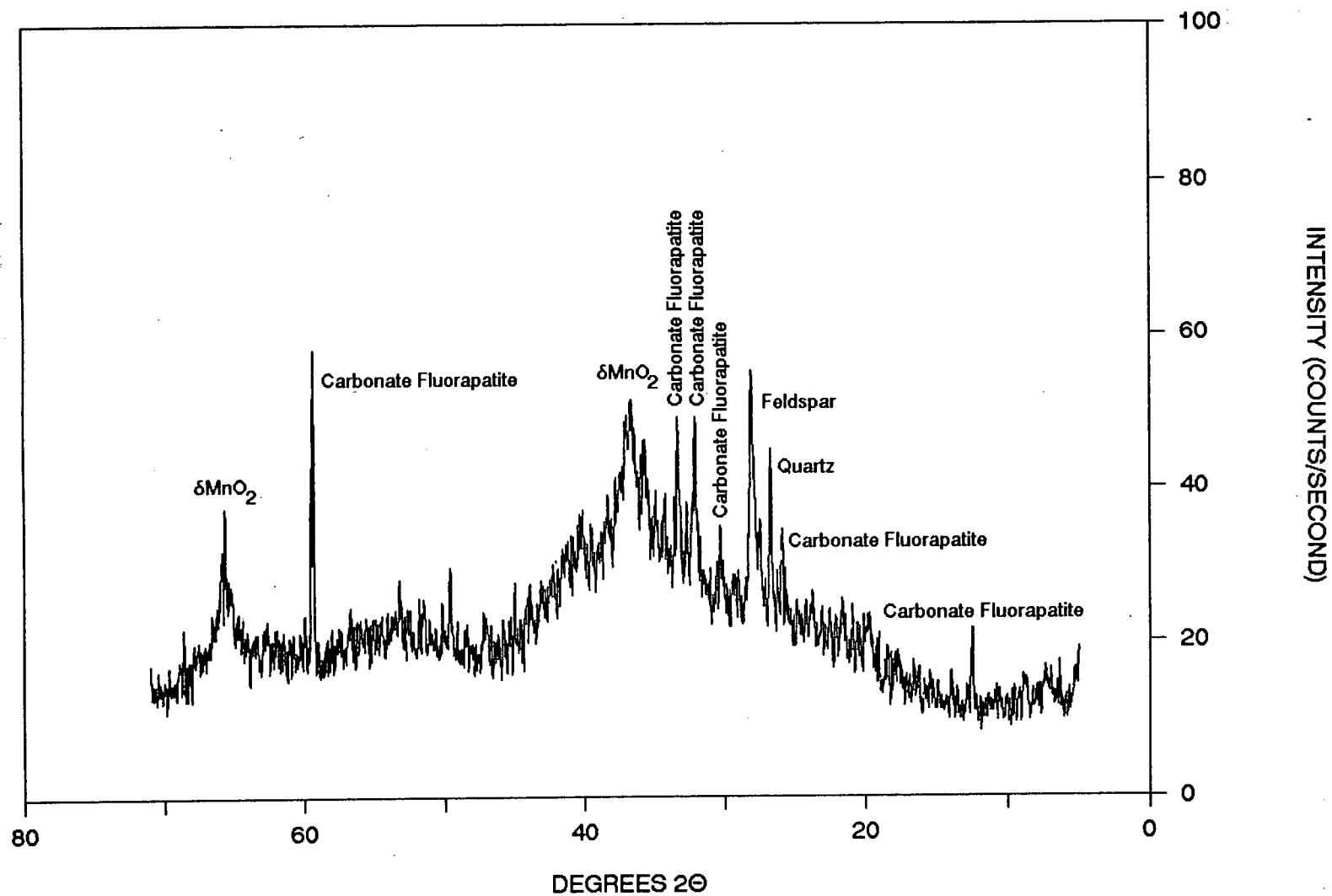
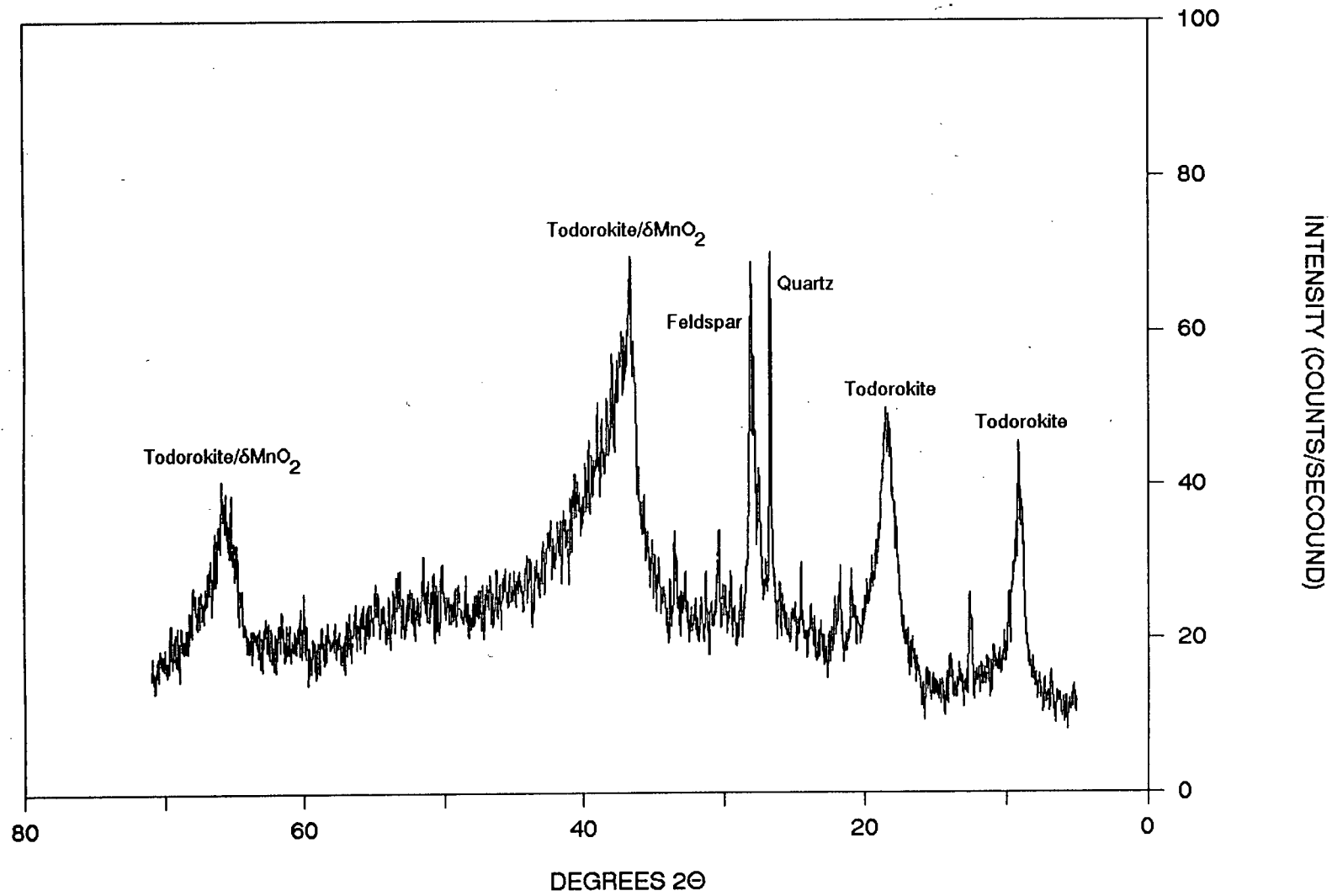


Figure 3-6. The XRD patterns of diagenetic nodules selected for the two stage selective sequential extraction scheme.

# MN 39



# MN 56

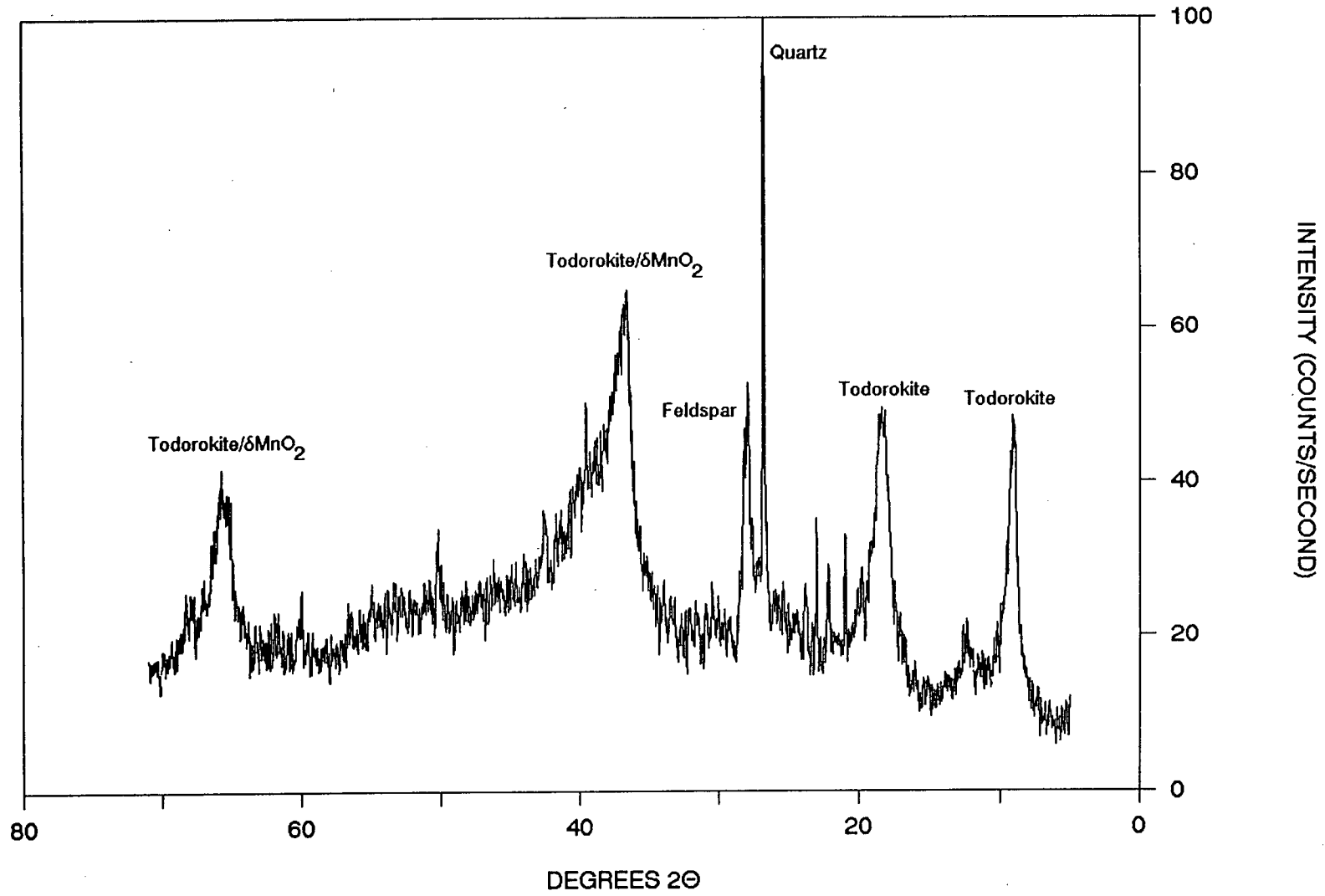
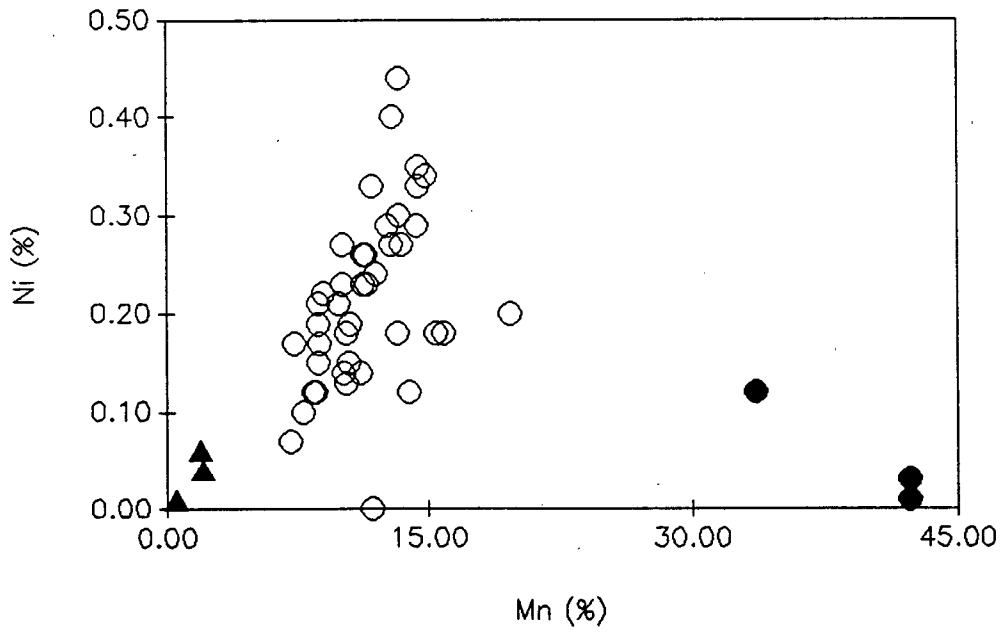
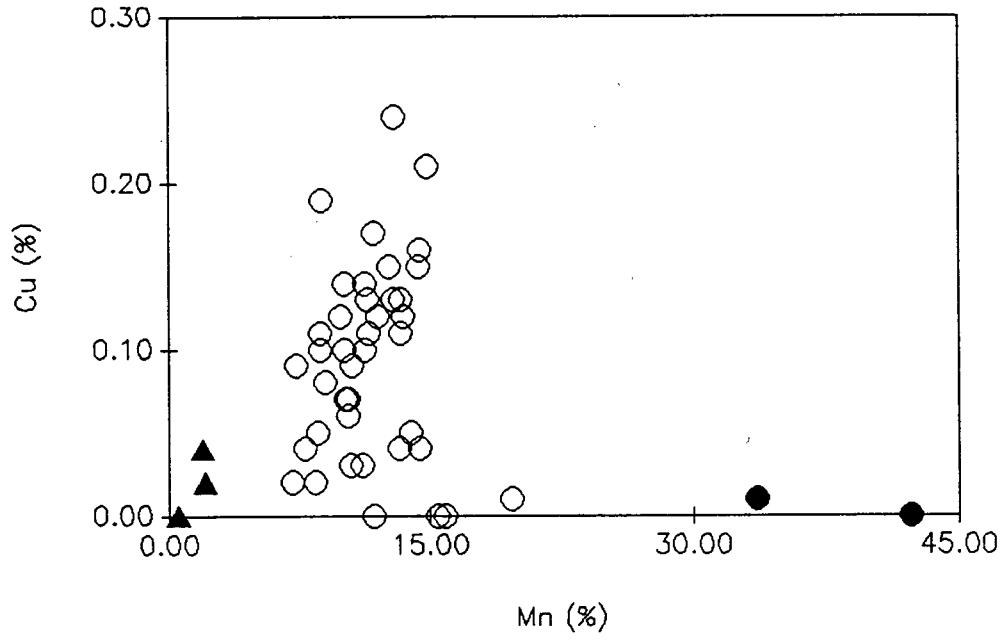




Figure 3-7. The relationship between Mn with Cu, Ni, and Co. The open circles = hydrogenetic crusts, the filled circles = Mn-enriched hydrothermal crusts, the filled triangles = Mn-depleted hydrothermal crusts.



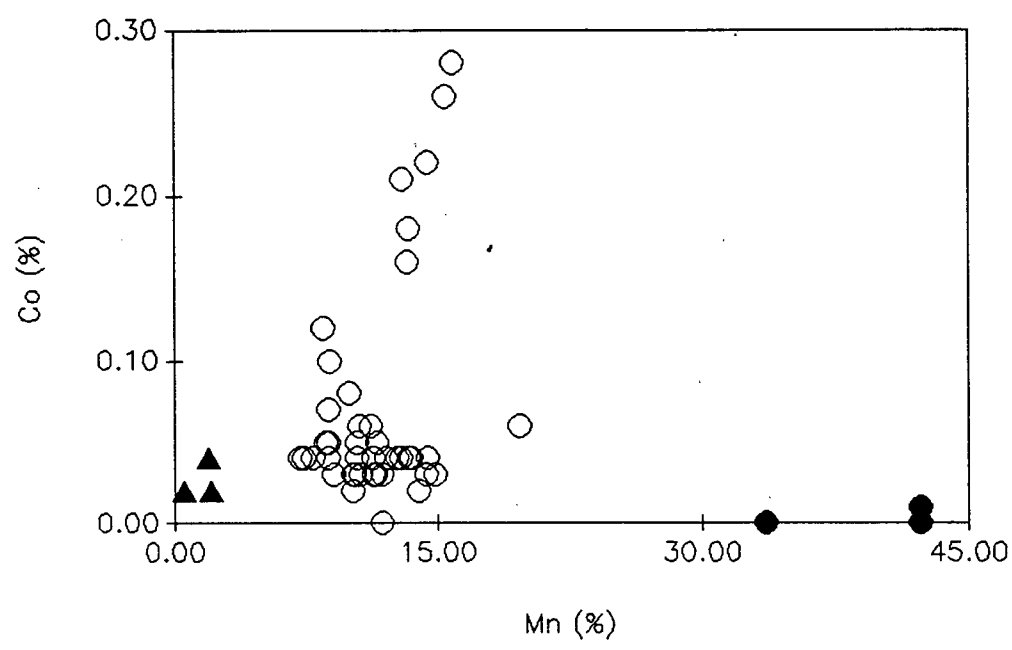
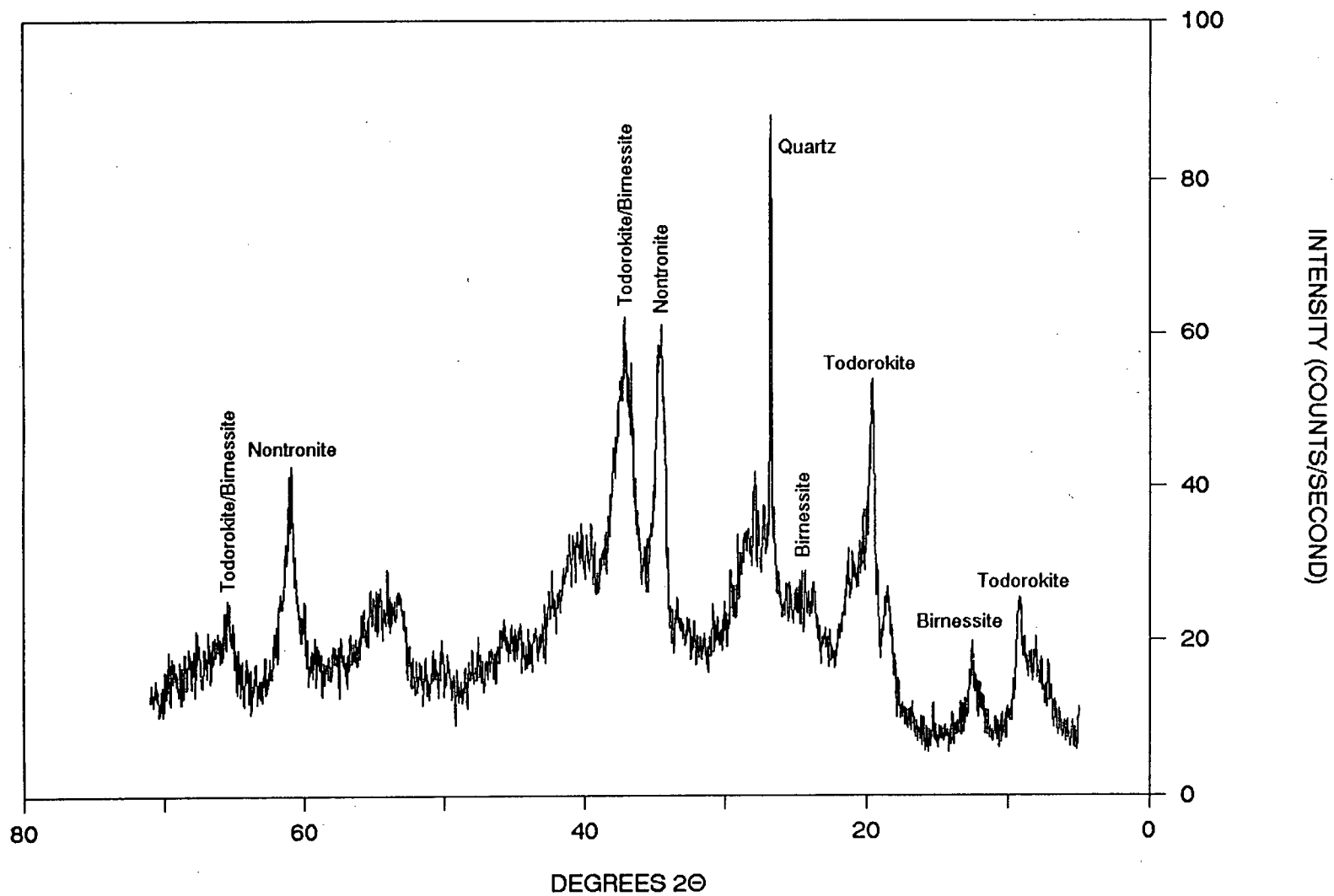
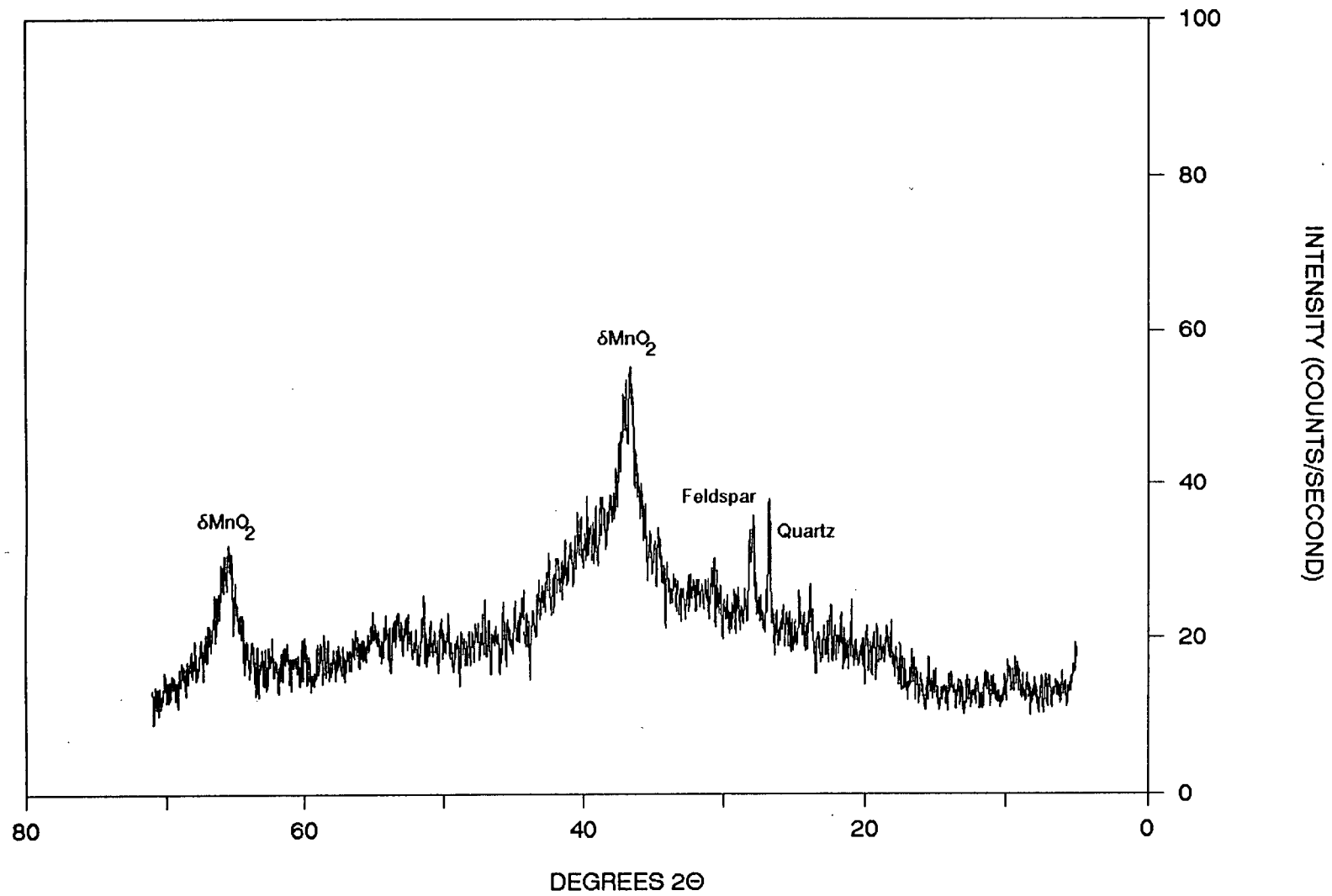


Figure 3-8. The XRD patterns of hydrogenetic crusts selected for the two stage selective sequential extraction scheme.

# Henderson Seamount



# RISE III 28 D-1



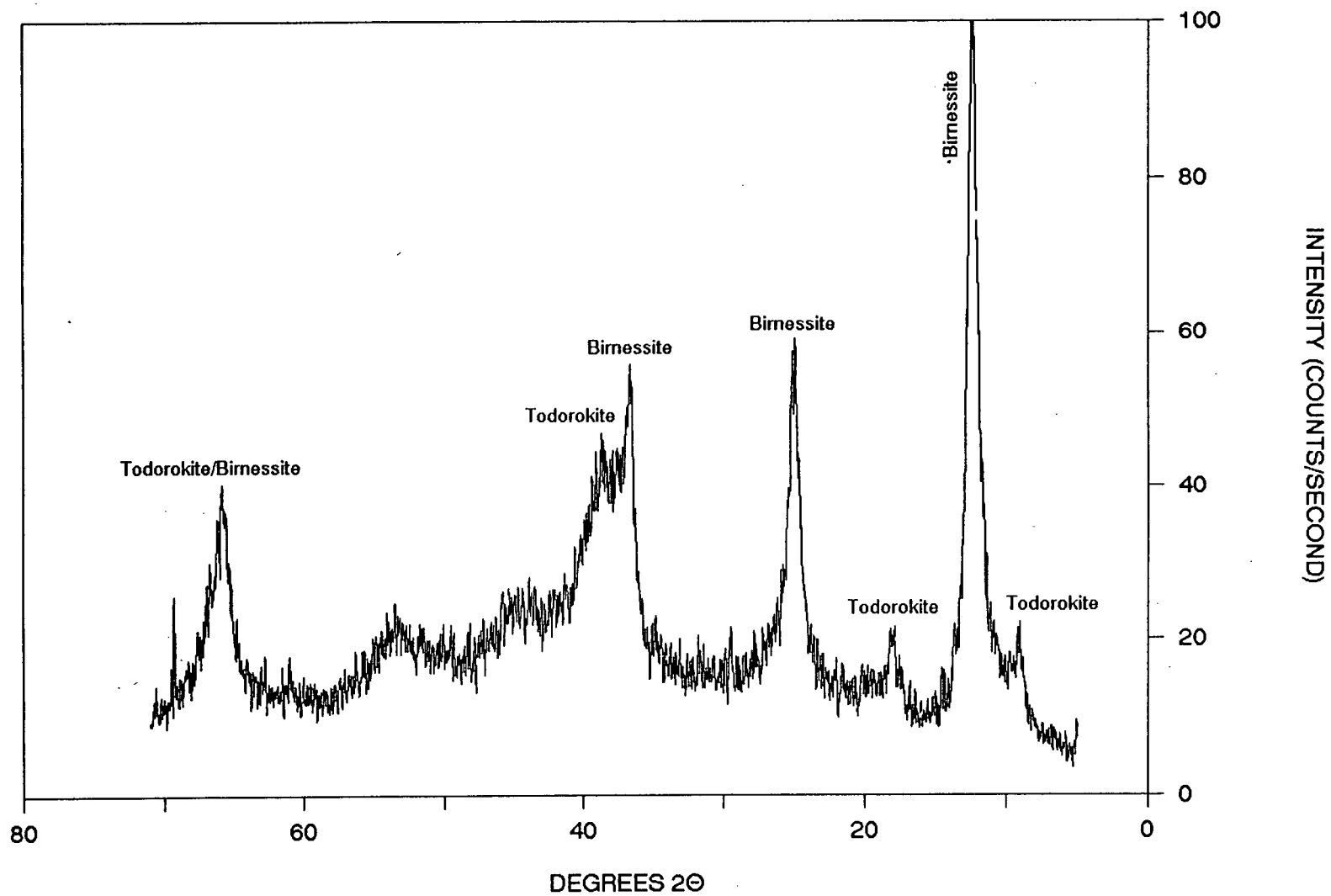
Because of the different geochemical behavior of Fe and Mn, fractionation of the two elements is common in hydrothermal solutions (Lyle, 1981). This results in the formation of two distinct end member deposits: (1) Mn-enriched hydrothermal crusts, characterized by Mn concentrations above 30 weight per cent and generally very low Cu, Ni and Co contents with well-crystallized birnessite and todorokite (Figure 3-9), and (2) Mn-depleted hydrothermal crusts, characterized by Mn concentrations below 3 weight per cent also with very low Cu, Ni, and Co contents but are iron- and silica-rich and composed of amorphous hydrated iron oxides and silica, (Figure 3-10). The fractionation of Fe and Mn occurs as a result of the lower solubility of iron species as both Fe and Mn undergo oxidation (Krauskopf, 1957) by mixing of the reduced hydrothermal fluid with oxygenated bottom water. The geochemical association of Si with Fe may result from coprecipitation or adsorption of dissolved  $\text{SiO}_2$  onto hydrated iron-oxide colloids. The low content of minor elements in these deposits results from: (1) the low concentrations of these elements relative to Fe and Mn in hydrothermal solutions, and (2) the rapid deposition of the deposits which minimizes adsorption of elements from seawater (Toth, 1980).

In hydrogenetic crusts from this region, Co also shows an association with Fe, which is unlike that Cu and Ni (Figure 3-11). In the Mn-rich and Mn-depleted hydrothermal crusts, Co is so depleted the correlation with Fe is not observed. Price & Calvert (1970) suggested that this observed complex behavior of Co is due to  $\text{Co}^{3+}$  substituting for  $\text{Mn}^{4+}$  in  $\delta\text{MnO}_2$  as well as  $\text{Fe}^{3+}$  in the iron oxyhydroxide phases. Cobalt (III) ( $d^6$ ) is stable when in the low spin state with octahedral coordination and has an ionic radius almost identical to that of  $\text{Fe}^{3+}$  or  $\text{Mn}^{4+}$ . Cobalt (III) will therefore preferentially substitute for both  $\text{Fe}^{3+}$  in the  $\text{FeOOH} \times n\text{H}_2\text{O}$  phase (Burns, 1965) and  $\text{Mn}^{4+}$  in the  $\delta\text{MnO}_2$  phase (Glasby & Thijssen, 1982a; Halbach *et al.*, 1981a). Cobalt (III) will also substitute for  $\text{Mn}^{4+}$  in the "ceilings" of todorokite (Burns, 1976). Since hydrogenetic crusts contain

Figure 3-9. The XRD patterns of Mn-enriched hydrothermal crusts selected for the two stage selective sequential extraction scheme.



# QBR 22 D-1



# RISE III 3 D-1

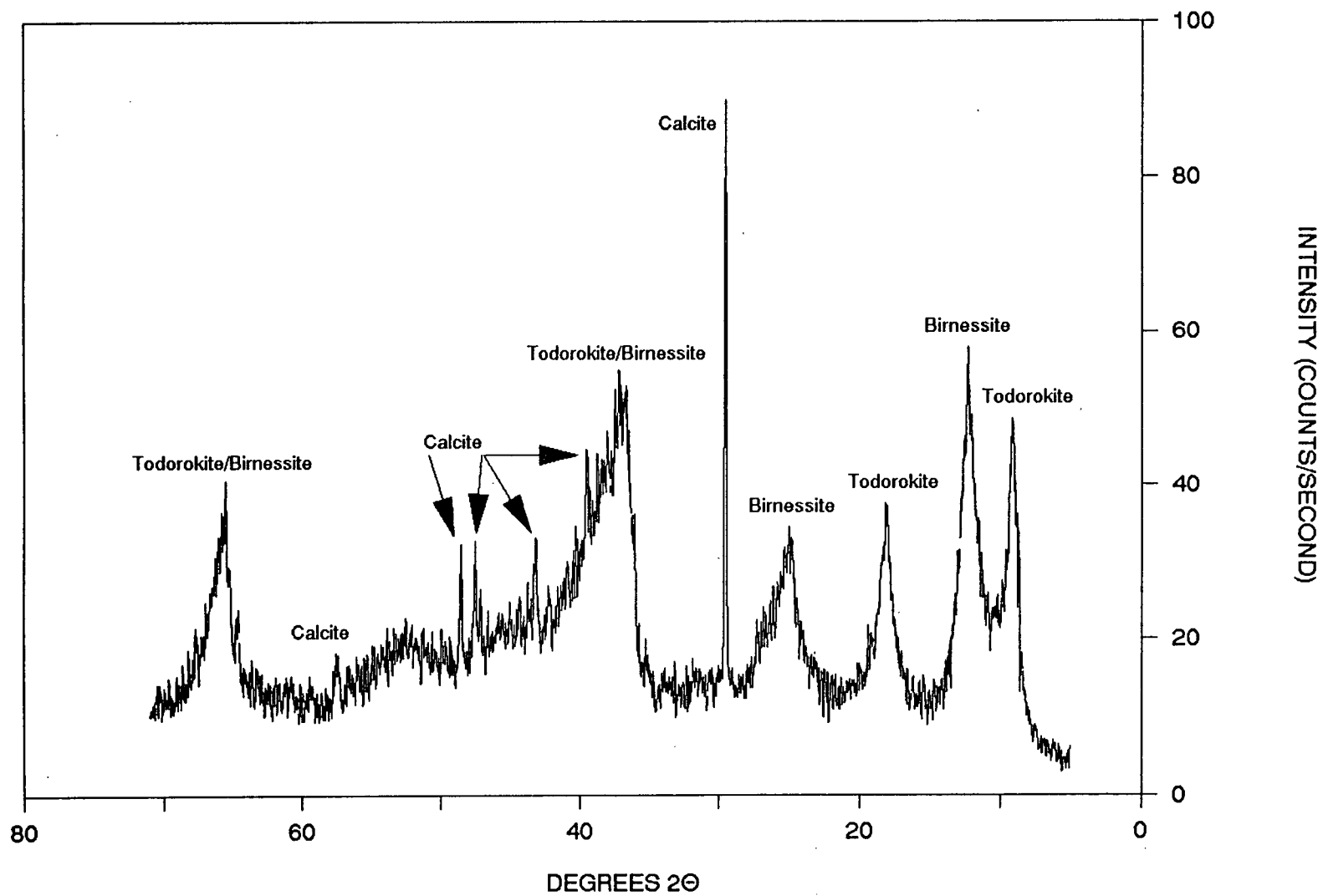


Figure 3-10. The XRD pattern of a Mn-depleted hydrothermal crust enriched in Fe and Si.

# SOTW 9 32 D-1

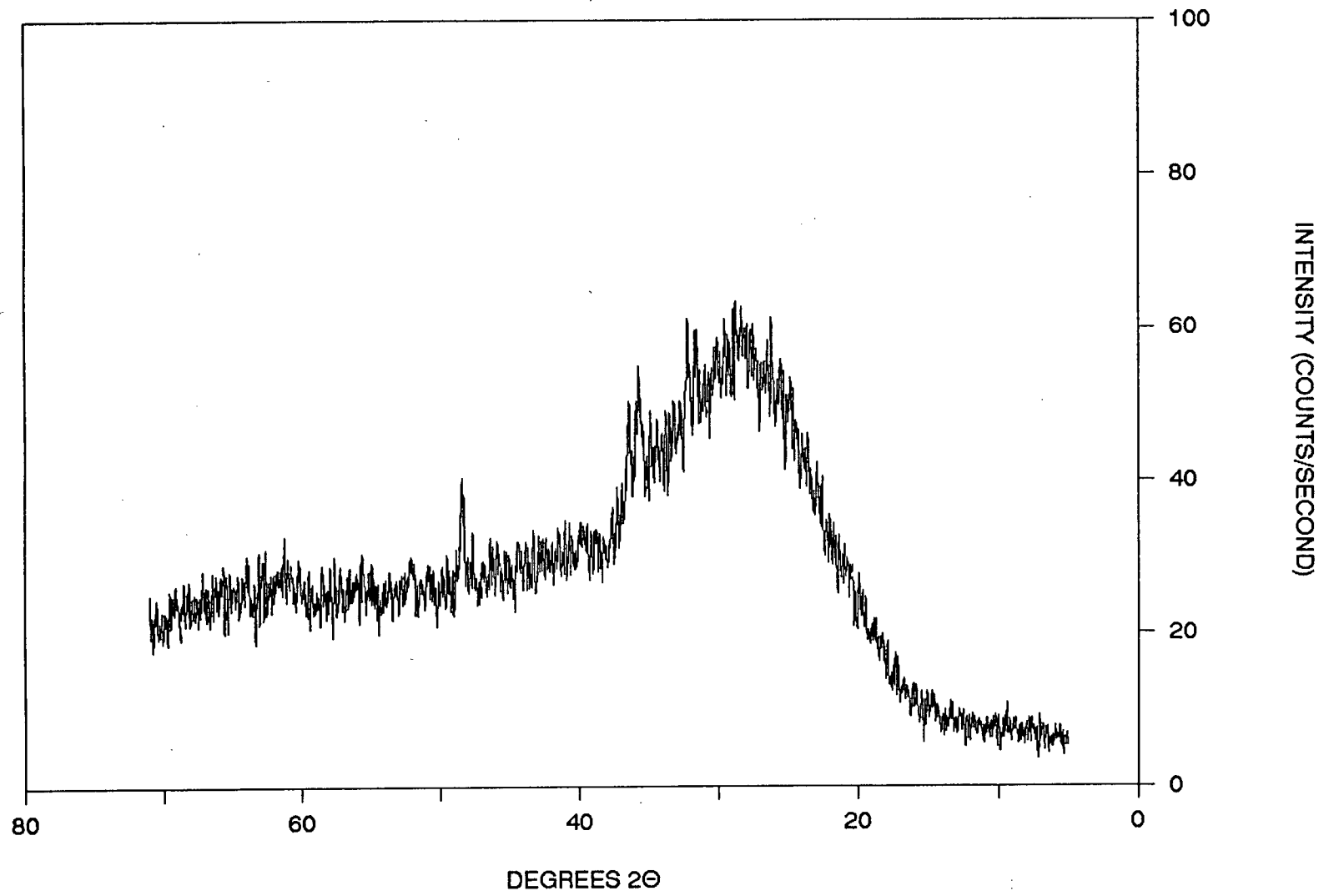
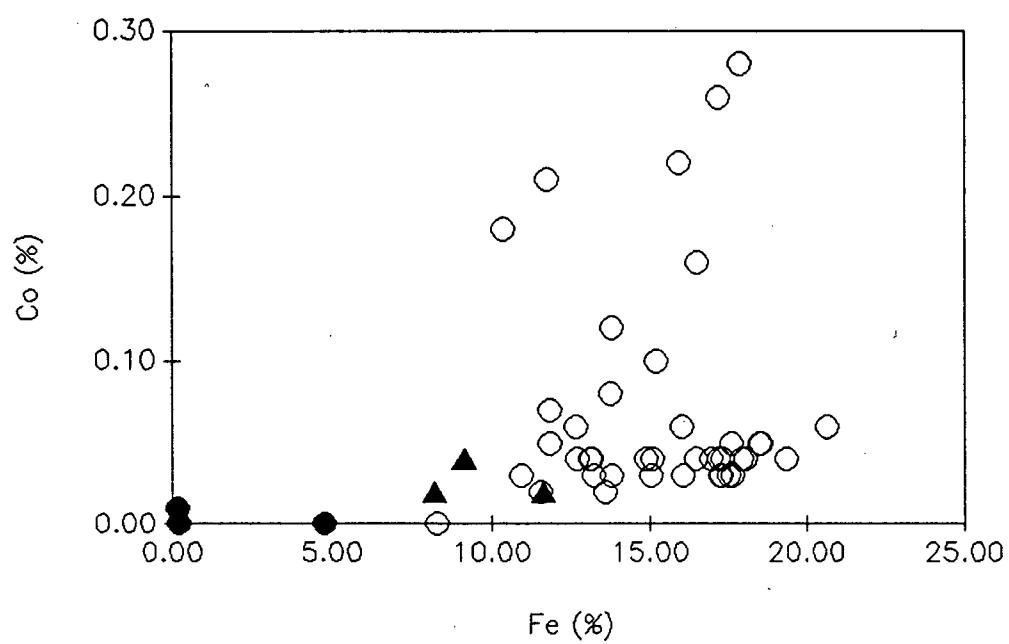


Figure 3-11. The relationship between Fe and Co. The open circles = hydrogenetic crusts, the filled circles = Mn-enriched hydrothermal crusts, the filled triangles = Mn-depleted hydrothermal crusts.



$\text{FeOOH} \times n\text{H}_2\text{O}$ ,  $\delta\text{MnO}_2$ , and todorokite, this would explain the positive association of Co with Mn and Co with Fe.

#### 3.4.1.2.2 Nodules

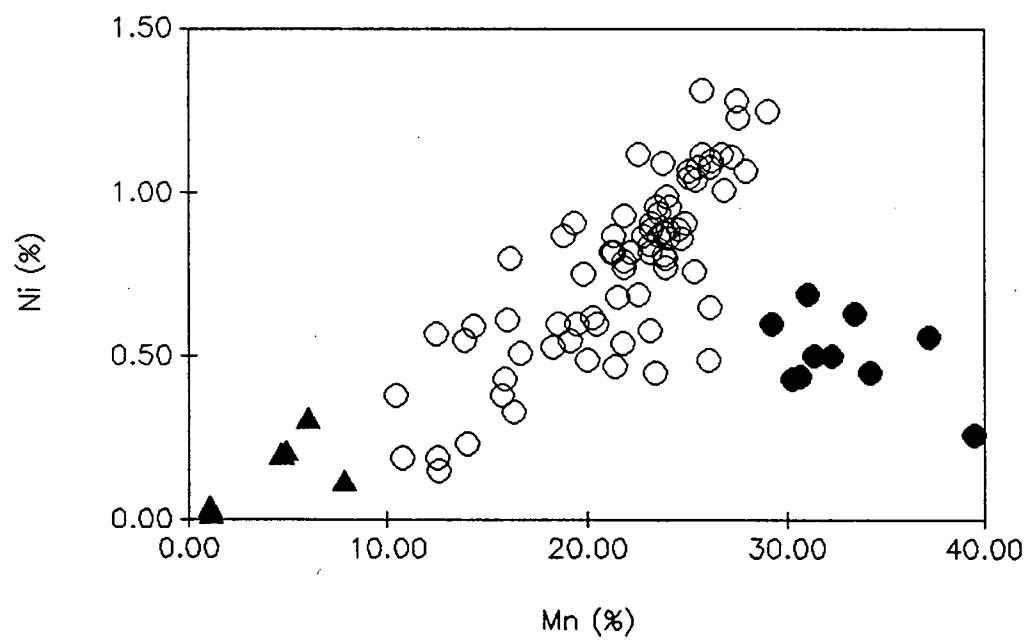
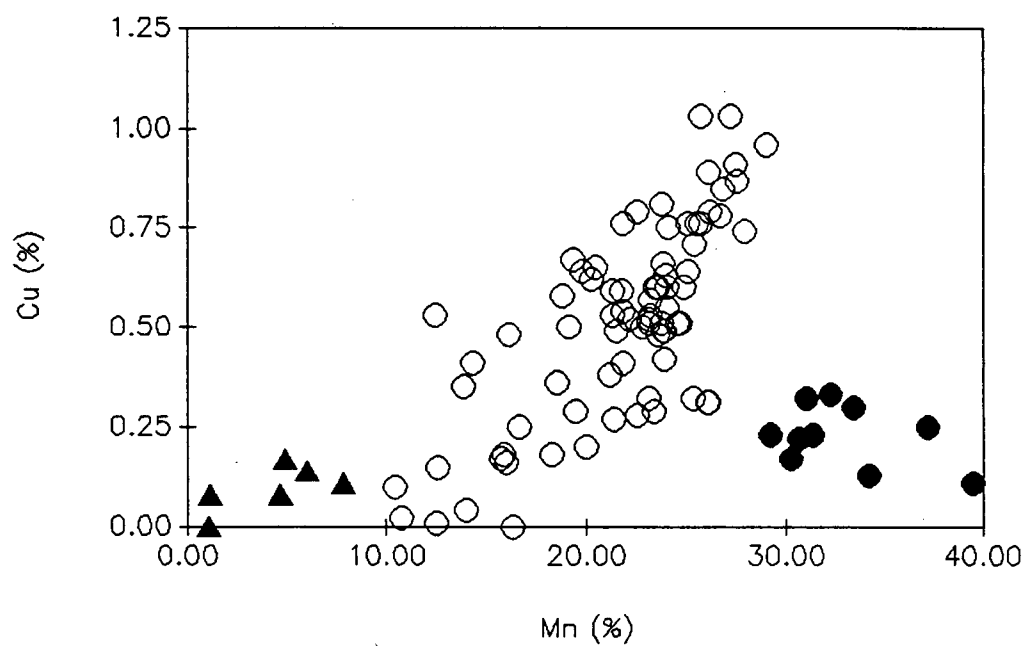
The Mn/Fe ratios for nodules from Survey Region B are found to vary from 0.63 up to 23.93. Although the Mn/Fe ratios for the nodules is not as extreme as for the crusts ( $0.06 \leq \text{Mn/Fe} \leq 222.68$ ), the concentrations of Cu, Ni, and Co will be considered with respect to Mn concentrations.

The relationship of Mn with Cu, Ni, and Co indicate that three distinct groups of nodules can be distinguished within Survey Region B. The largest group of nodules has Mn concentrations ranging from 10 to 30 weight per cent, Mn/Fe ratios between 0.75 and 7.70, and show strong positive linear correlations between Mn and Cu, Ni, and Co (Figure 3-12). Unlike nodules from Survey Region A, this group of nodules does not show a distinct division between hydrogenous nodules ( $\text{Mn/Fe} < 2.5$ ) and diagenetic nodules ( $\text{Mn/Fe} > 2.5$ ). Although the range of Mn/Fe ratios shows that these two types of nodules are present, the two groups do not show the same variation in interelement correlations as seen in Survey Region A. For identification purposes, this large group of nodules will be called hydrogenous nodules. The XRD patterns of the hydrogenous nodules selected for analysis shows that the dominant oxide phase present in these nodules is todorokite and  $\delta\text{MnO}_2$  along with minor amounts of birnessite (Figure 3-13).

The two remaining groups of nodules are characterized by their distinctively different concentrations of Mn. One group is highly enriched in Mn ( $> 30$  weight per cent) and has low concentrations of Cu, Ni, and Co compared with the hydrogenous group. XRD analysis shows that well-crystallized todorokite, together with minor birnessite, is present (Figure 3-14). The second group of nodules is

Figure 3-12. The relationship between Mn with Cu, Ni, and Co. The open circles = hydrogenous and diagenetic nodules, the filled circles = Mn-enriched hydrothermal nodules, the filled triangles = Mn-depleted hydrothermal nodules.





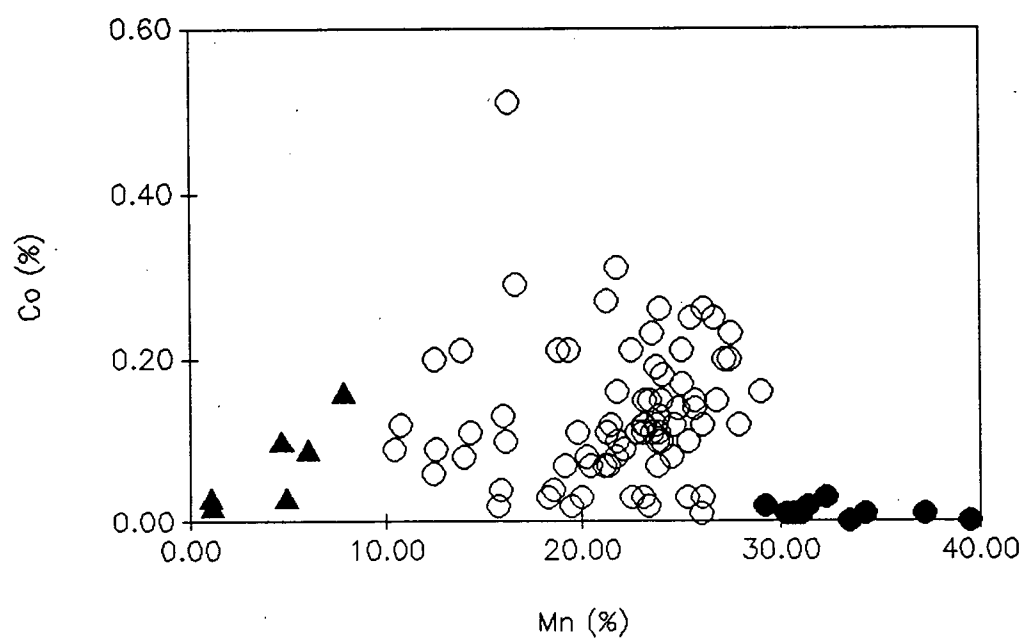
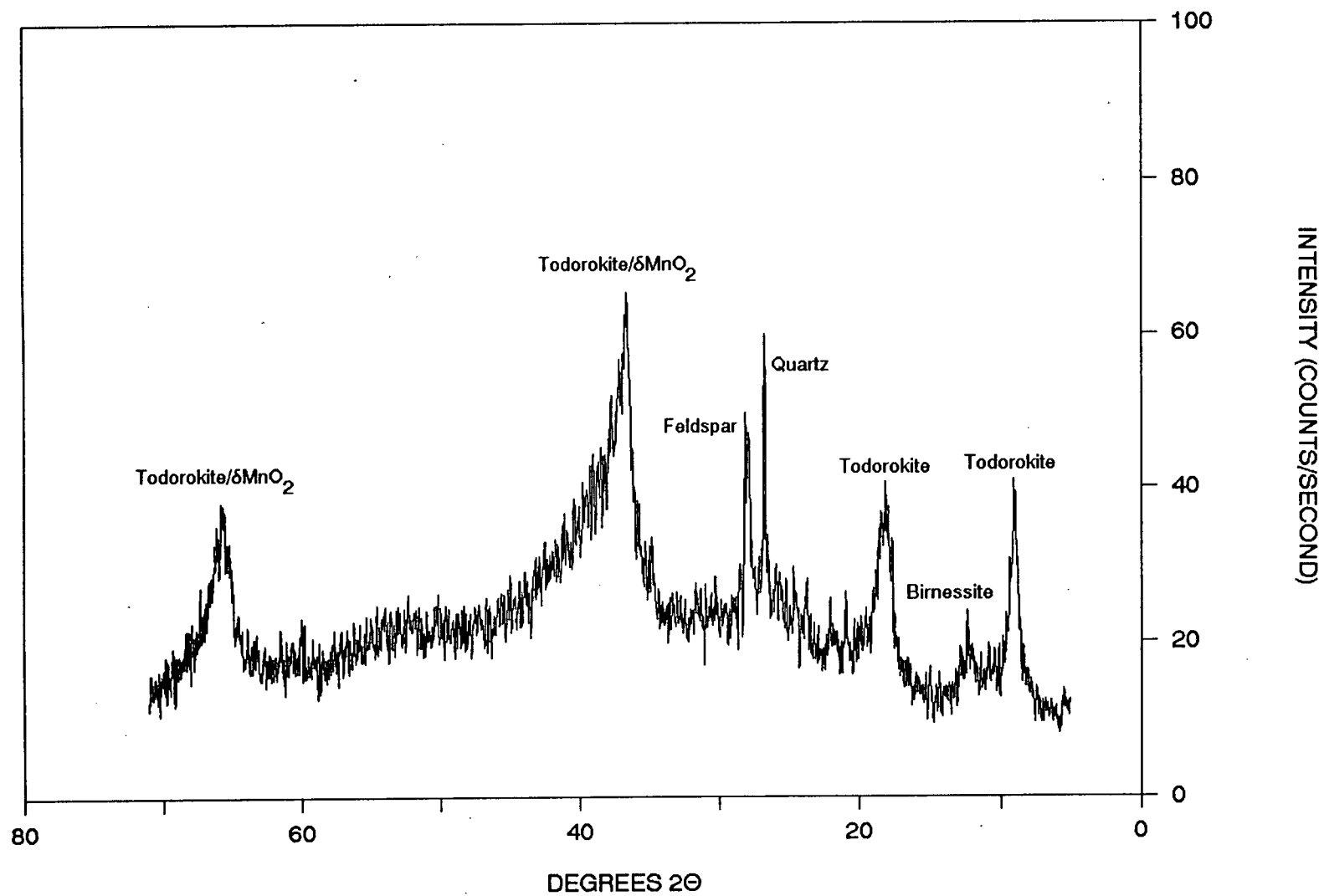


Figure 3-13. The XRD patterns of the hydrogenous and diagenetic nodules selected for the two stage selective sequential extraction scheme.

# B 104



# B 114

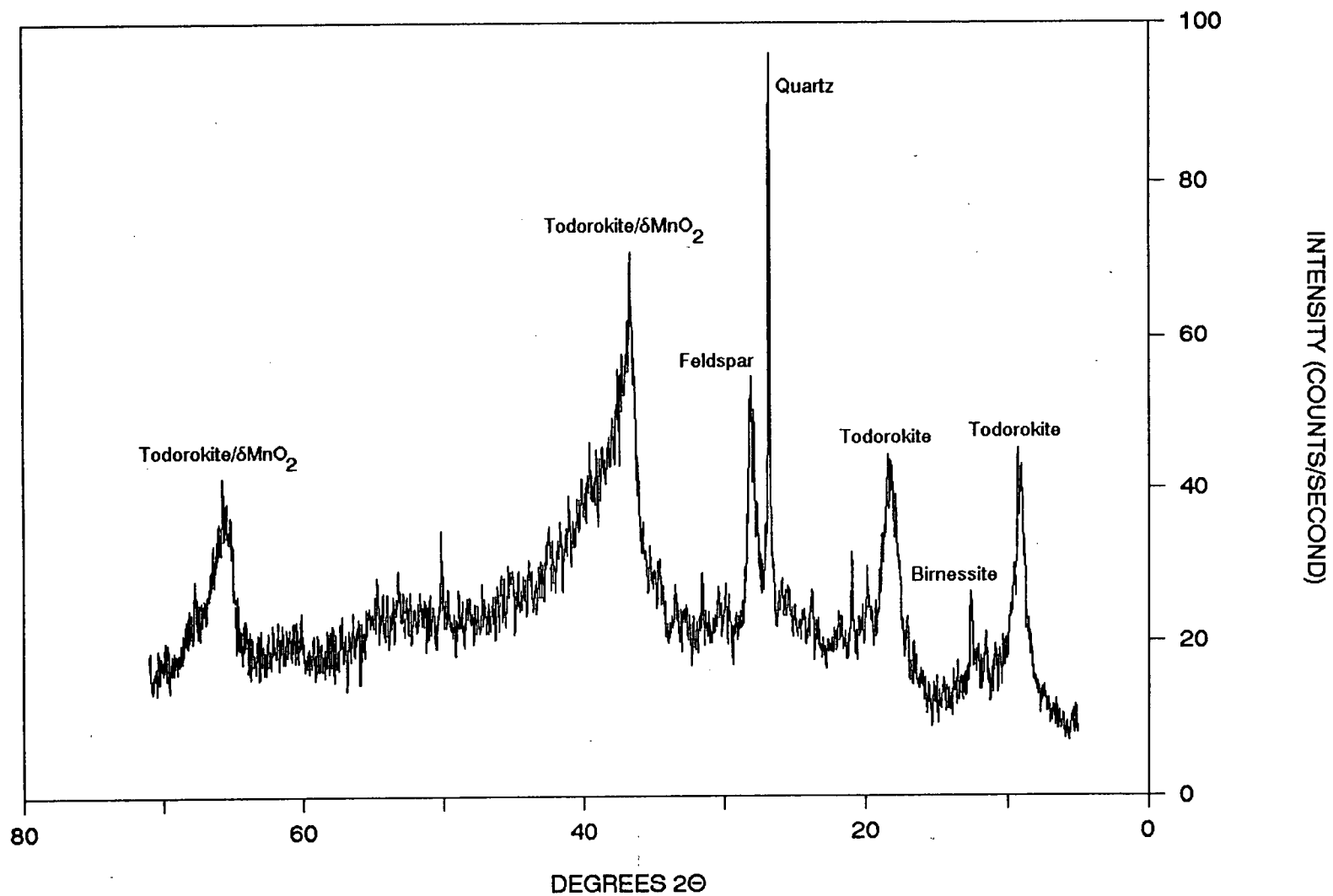
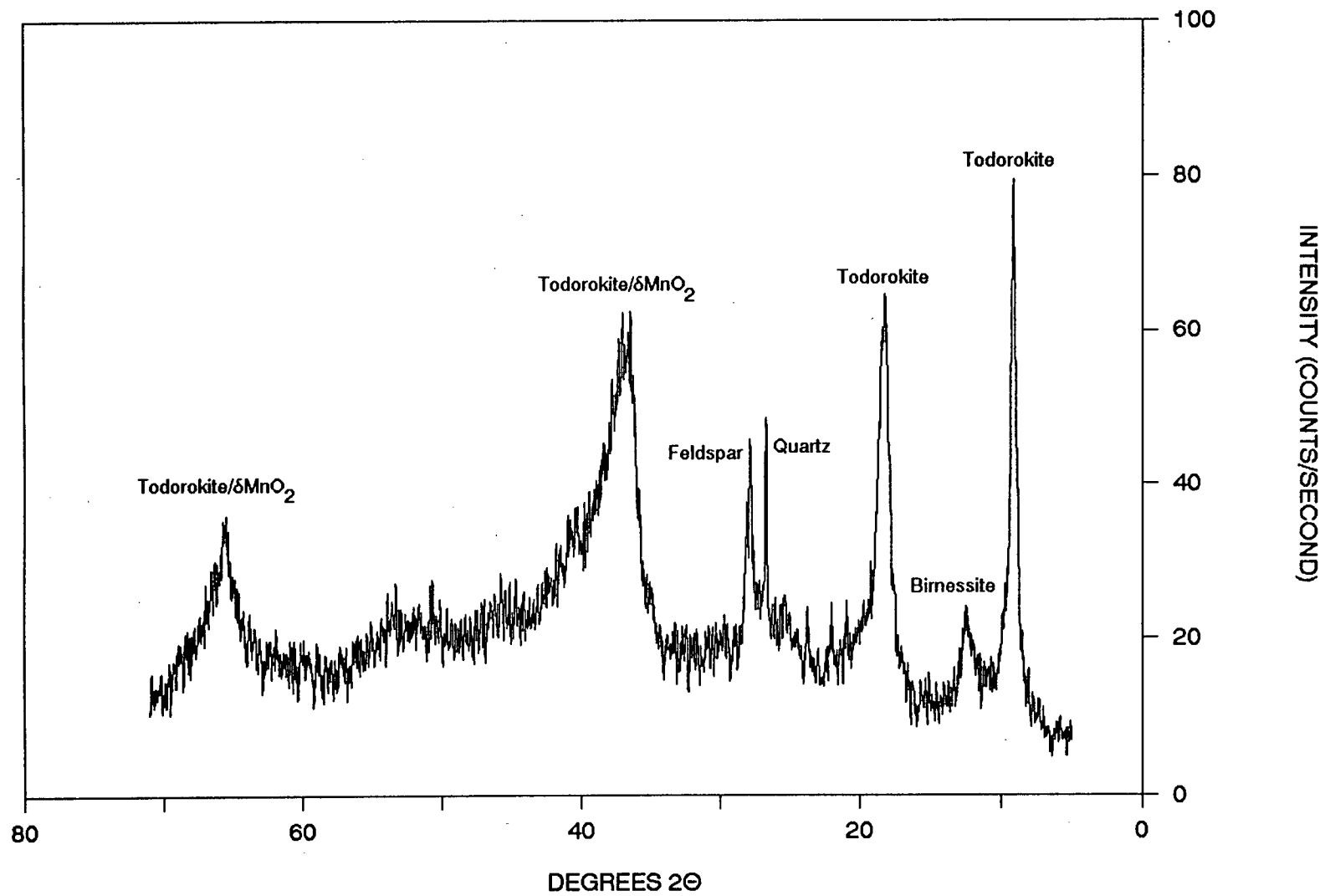
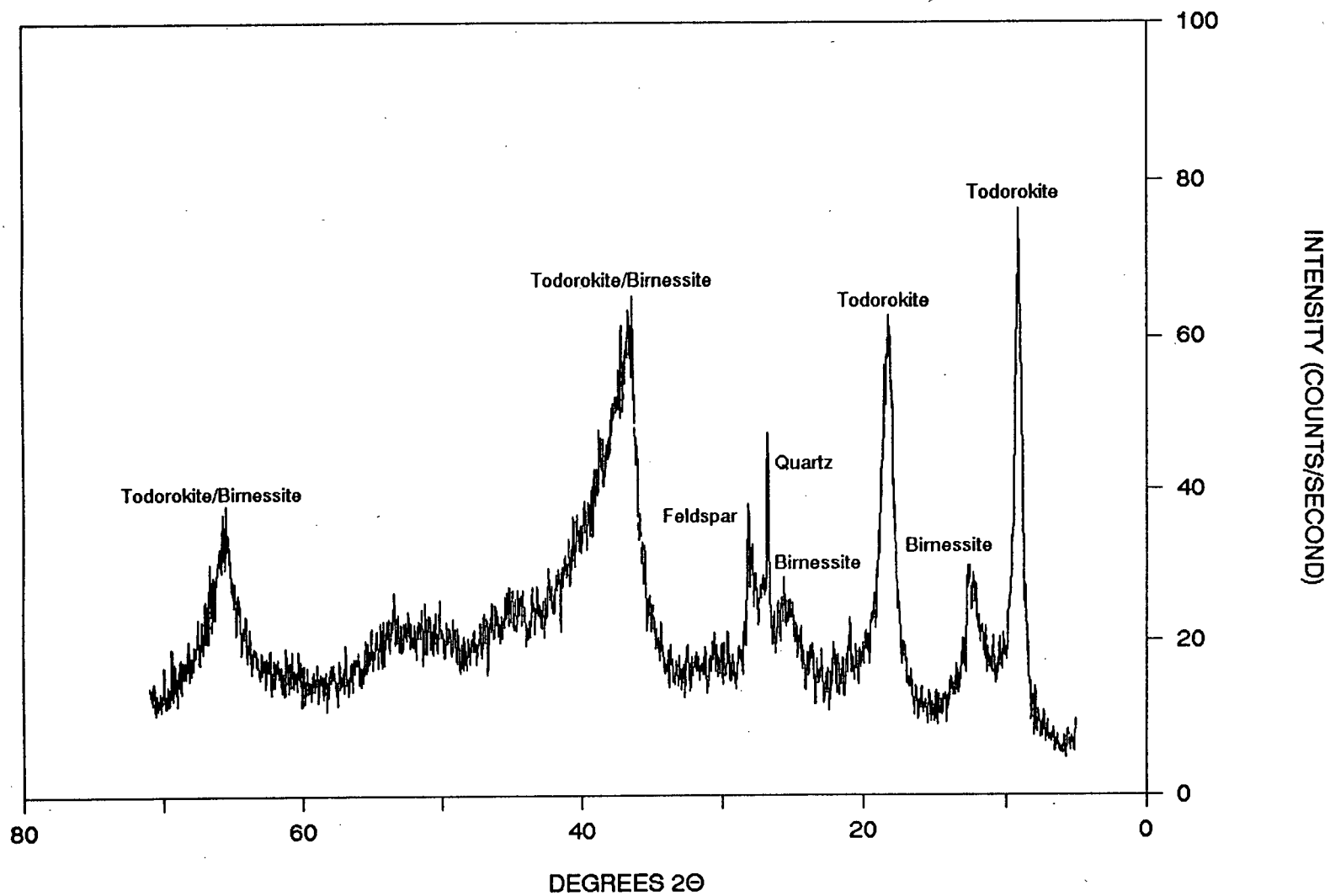


Figure 3-14. The XRD patterns of the Mn-enriched hydrothermal nodules selected for the two stage selective sequential extraction scheme.

# CERS 20 D-2



# CERS 21 D-3





depleted in Mn ( < 10 weight per cent) but are iron- and silica-rich and composed of nontronite (Figure 3-15). This group also has low concentrations of Cu, Ni, Co.

### 3.4.2 SELECTIVE SEQUENTIAL EXTRACTION AND DXRD

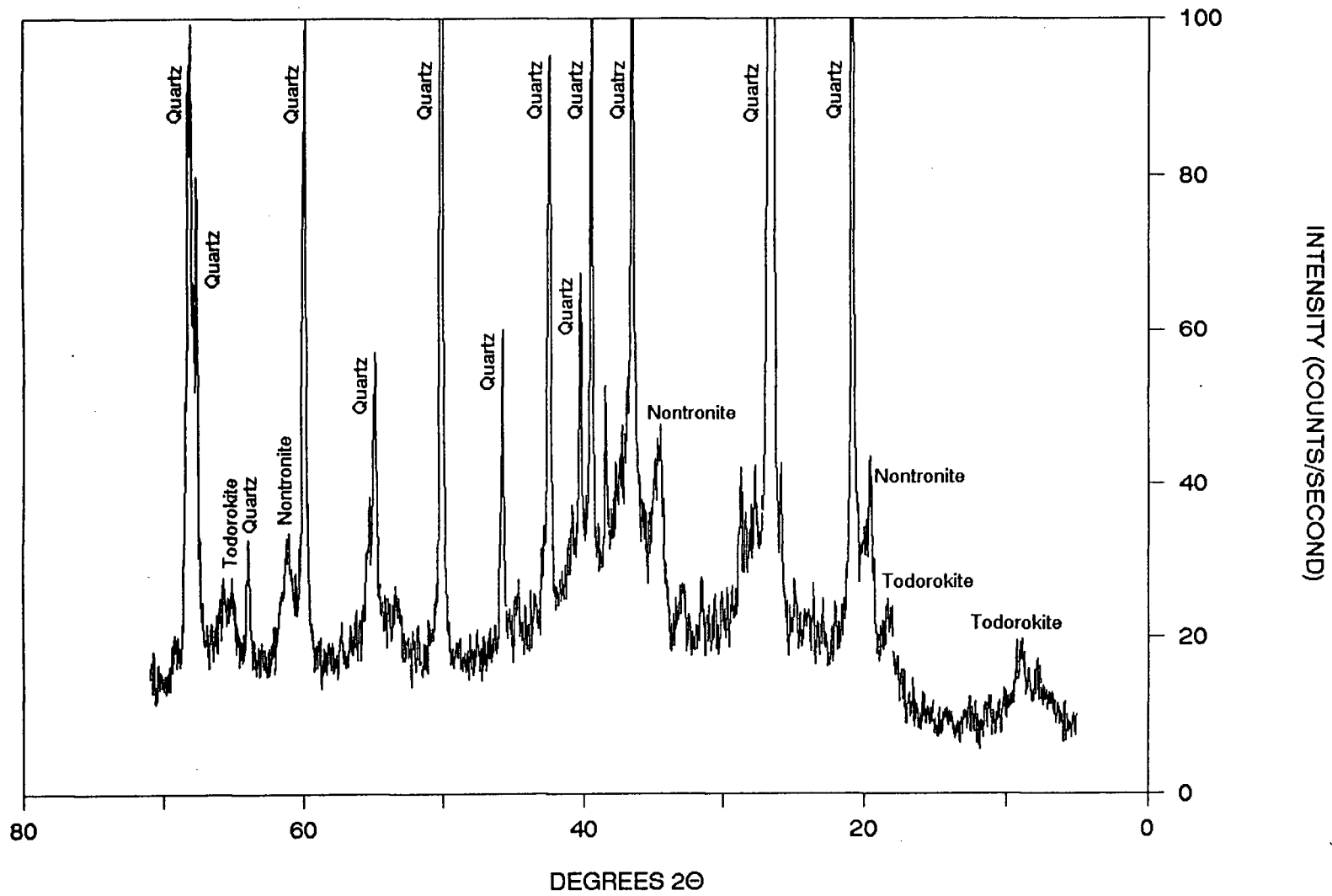
#### 3.4.2.1 Survey Region A

In order to better understand the partitioning of Mn, Fe, Cu, Ni, and Co between the manganese and iron oxide phase(s) identified in the crusts and nodules selected from Survey Region A, the results from the two stage selective sequential extraction scheme and the DXRD technique will be considered together. The weight per cent of Mn, Fe, Cu, Ni, and Co in the leachates from the first stage of the selective sequential extraction scheme are listed in Table 3-3a. These results represent the concentrations of Mn, Fe, Cu, Ni, and Co present in the manganese oxides of the crusts and nodules. The mineral phase(s) removed during the first stage of leaching and identified by DXRD are listed in Table 3-3b.

The weight per cent of Mn, Fe, Cu, Ni, and Co in the leachates from the second stage of the selective sequential extraction scheme are listed in Table 3-4a. These results represent the concentrations of Mn, Fe, Cu, Ni, and Co present in the iron oxides of the crusts and nodules. The mineral phase(s) removed during the second stage of leaching and identified by DXRD are listed in Table 3-4b.

**Figure 3-15.** The XRD patterns of the Mn-depleted hydrothermal nodules selected for the two stage selective sequential extraction scheme.

# DWBD 1-2



S 74

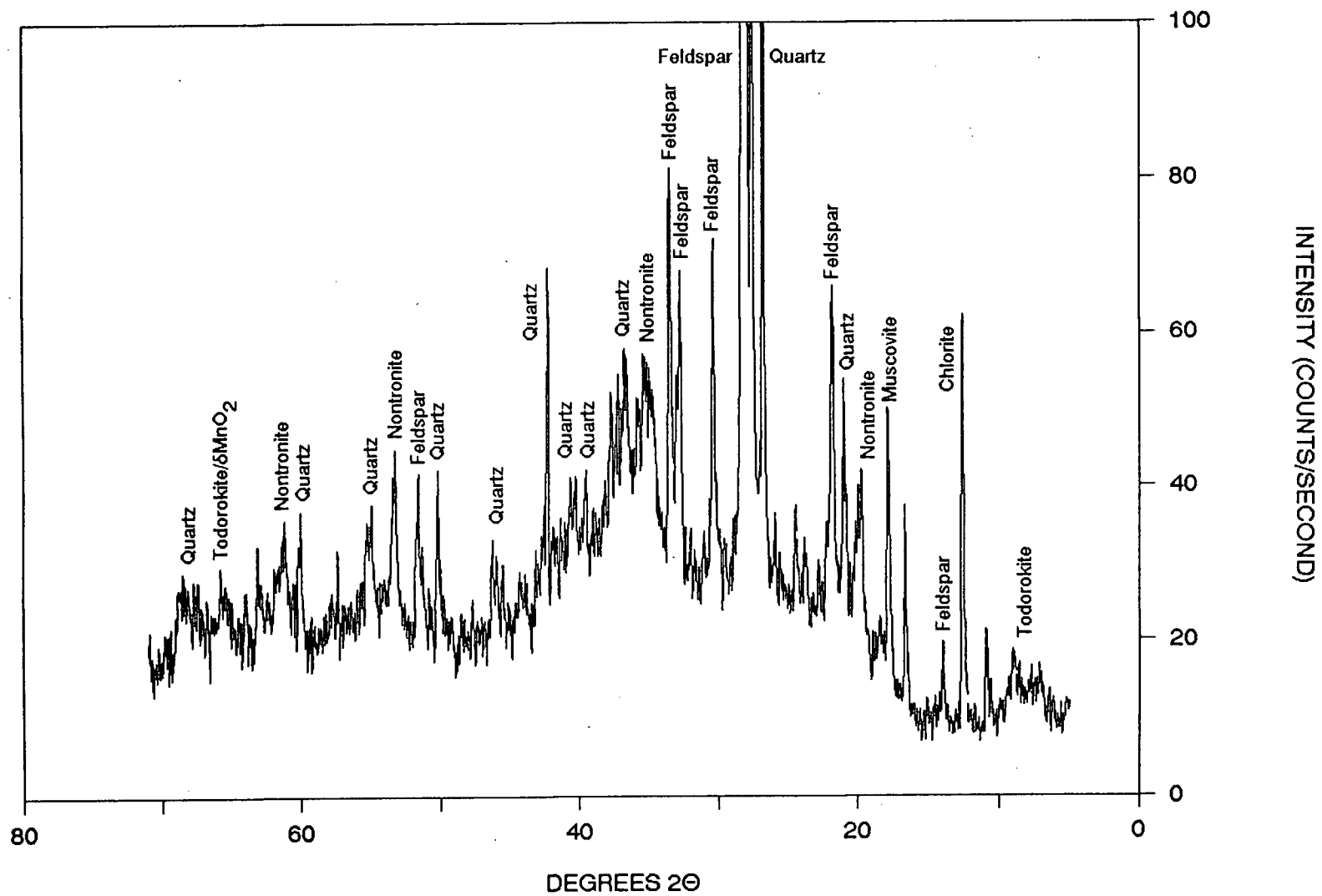


Table 3-3a. The concentrations of Mn, Fe, Cu, Ni, and Co in the leachates from the first stage of leaching samples from Survey Region A. Results are listed as weight per cent.

Element	Samples			
	Hydrogenetic Crusts			
	7TOW 130	7TOW 142	D-1	
Fe	0.23	0.56		
Mn	21.79	17.55		
Co	0.30	0.55		
Ni	0.15	0.21		
Cu	0.01	0.01		

Element	Samples			
	Hydrogenous Nodules		Diagenetic Nodules	
	DODO 12-2	DODO D-1	DODO 14-2	Mn 39 Mn 56 D-2
Fe	1.00	0.74	0.43	0.41
Mn	11.83	11.64	22.04	24.53
Co	0.36	0.33	0.12	0.12
Ni	0.16	0.14	0.56	0.58
Cu	0.04	0.02	0.31	0.42

Table 3-3b. The mineral phase(s) removed during the first stage of the selective sequential extraction scheme and identified by DXRD.

Sample	Mineral Phase(s) Identified by DXRD
Hydrogenetic Crusts	
7TOW 130 D-FRAG	$\delta\text{MnO}_2$
7TOW 142 D-1	$\delta\text{MnO}_2$
Hydrogenous Nodules	
DODO 12-2 D-1	$\delta\text{MnO}_2$
DODO 14-2 D-2	$\delta\text{MnO}_2$
Diagenetic Nodules	
Mn 39	Todorokite/ $\delta\text{MnO}_2$
Mn 56	Todorokite/ $\delta\text{MnO}_2$

Table 3-4a. The concentrations of Mn, Fe, Cu, Ni, and Co in the leachates from the second stage of leaching for samples from Survey Region A. Results are listed as weight per cent.

Element	Samples			
	Hydrogenetic Crusts			
	7TOW 130	7TOW 142	D-1	
Fe	8.79	9.70		
Mn	0.83	0.38		
Co	0.55	0.10		
Ni	0.49	0.09		
Cu	0.04	0.06		

Element	Samples			
	Hydrogenous Nodules		Diagenetic Nodules	
	DODO 12-2	DODO D-1	DODO 14-2	Mn 39 Mn 56 D-2
Fe	8.10	10.00	2.30	1.70
Mn	0.41	0.48	0.44	1.01
Co	0.02	0.02	0.06	0.07
Ni	0.01	0.02	0.41	0.52
Cu	0.05	0.07	0.54	0.52

Table 3-4b. The mineral phase(s) removed during the second stage of the selective sequential extraction scheme and identified by DXRD.

Sample	Mineral Phase(s) Identified by DXRD
Hydrogenetic Crusts	
7TOW 130 D-FRAG	Ferrihydrite
7TOW 142 D-1	Ferrihydrite
Hydrogenous Nodules	
DODO 12-2 D-1	Ferrihydrite
DODO 14-2 D-2	Ferrihydrite
Diagenetic Nodules	
Mn 39	Ferrihydrite
Mn 56	Ferrihydrite

### 3.4.2.1.1 First Stage of the Selective Sequential Extraction

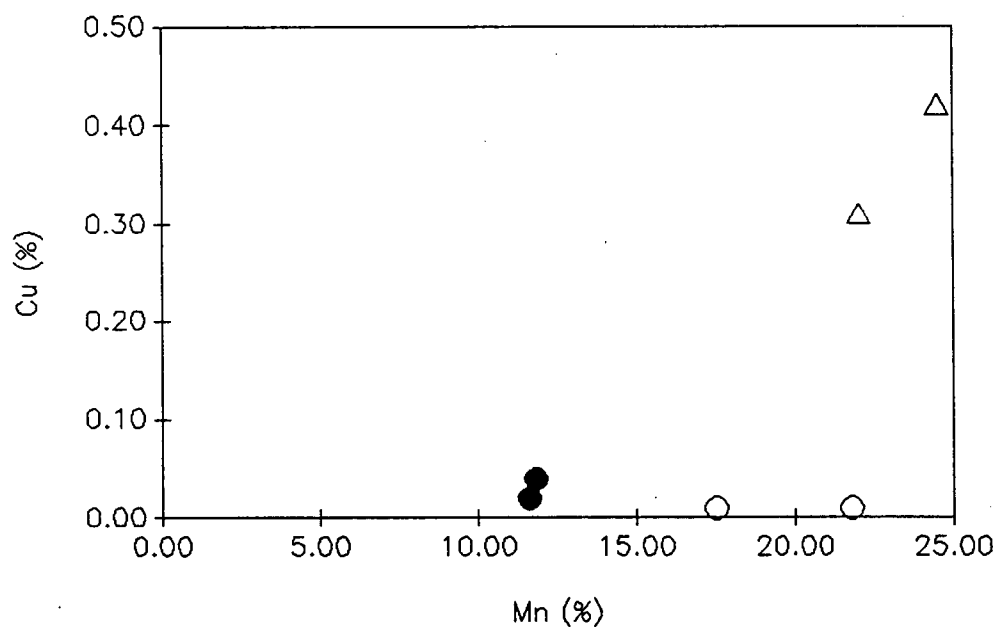
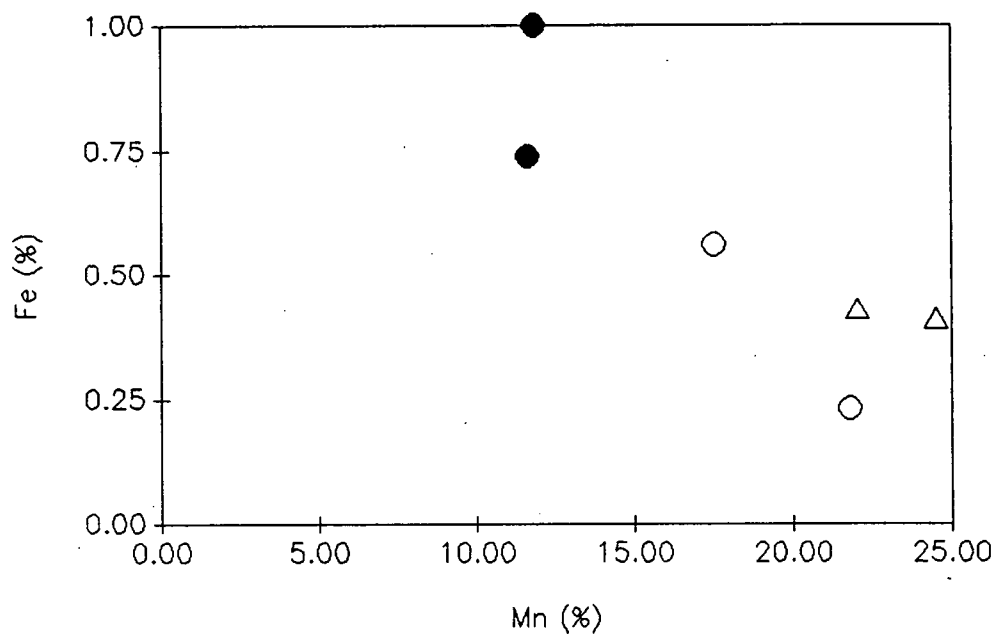
#### Scheme and DXRD

Since the manganese oxides are removed during the first stage of the selective sequential extraction scheme, plotting the concentrations of Fe, Cu, Ni, and Co against the concentration of Mn will give a better indication of the association of these elements to Mn and the manganese oxide phase(s) in the crust and nodule samples. The results from the first stage of the sequential extraction scheme indicates that the manganese oxides present in hydrogenetic crusts and hydrogenous nodules contain similar concentrations of Cu, Ni, and Co (Figure 3-16). The manganese oxide phase present in hydrogenetic crusts and hydrogenous nodules is  $\delta\text{MnO}_2$  (Figure 3-17, 3-18), which has very low concentrations of Cu and Ni but relatively high concentrations of Co. The  $\delta\text{MnO}_2$  in the hydrogenous nodules are found to contain a lower concentration of Mn and a higher concentration of Fe than the  $\delta\text{MnO}_2$  in hydrogenetic crusts.

The diagenetic nodules are found to contain similar concentrations of Fe, consistently higher concentrations of Mn, Cu, and Ni, and the lowest concentration of Co compared to the hydrogenetic crusts and the hydrogenous nodules. The results from DXRD indicate that todorokite and possibly a minor amount of  $\delta\text{MnO}_2$  is present in the diagenetic nodules and is responsible for these observed compositional trends (Figure 3-19).

Figure 3-16. The weight per cent of Mn, Fe, Cu, Ni, and Co associated with the manganese phase mineralogy which was removed during the first stage of the selective extraction scheme. The open circles = hydrogenetic crusts, the filled circles = hydrogenous nodules, the open triangles = diagenetic nodules.





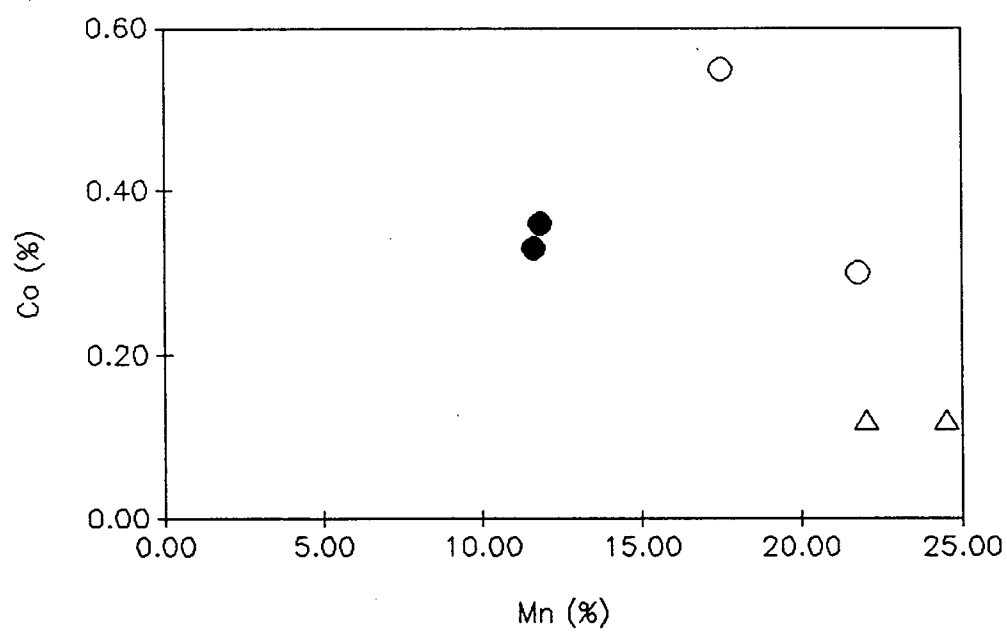
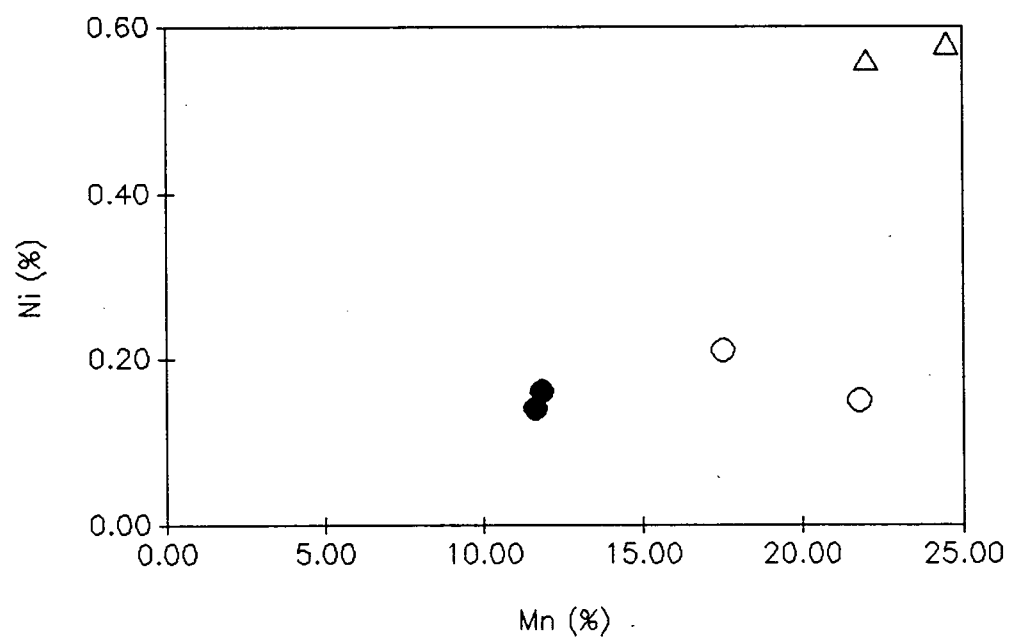
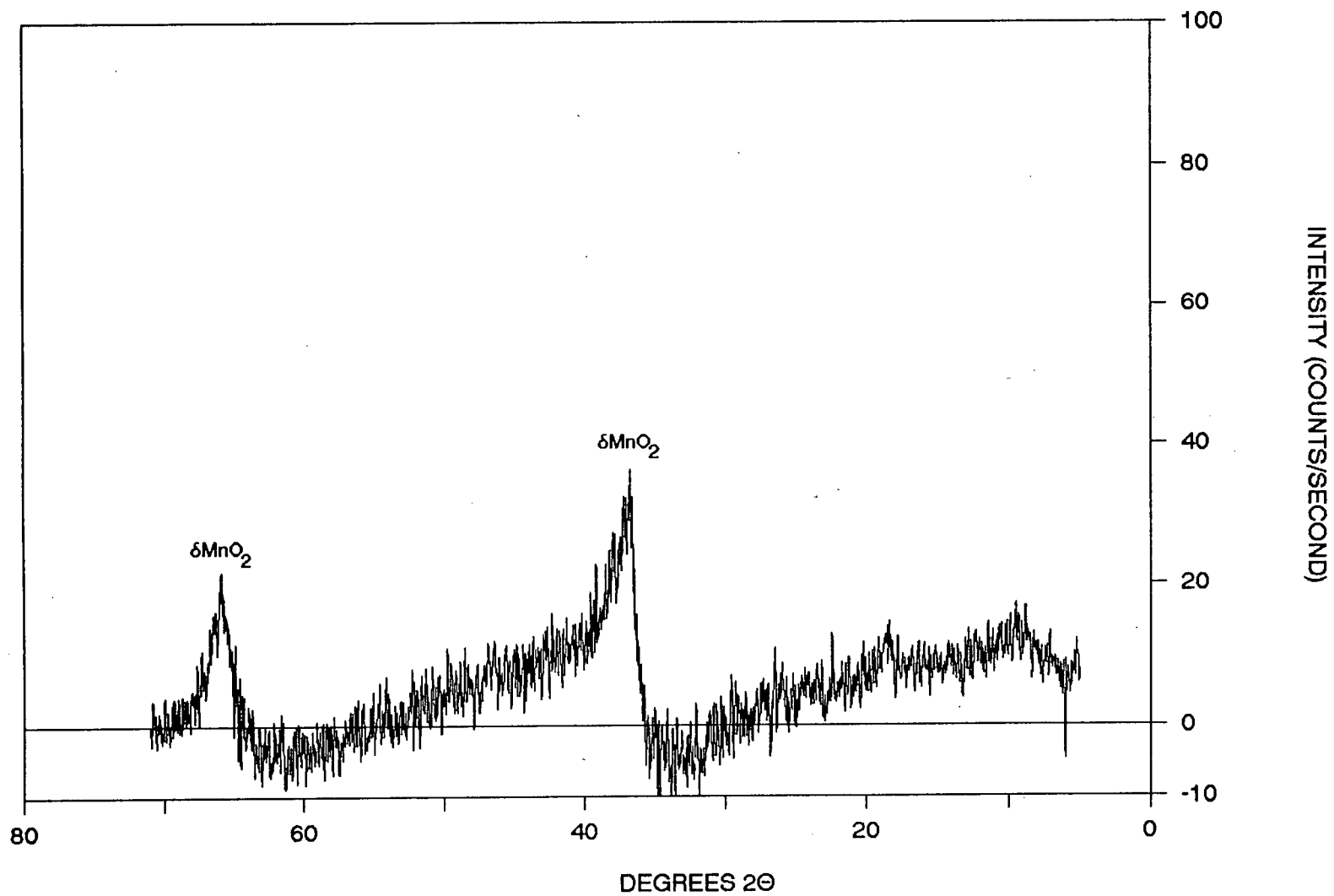


Figure 3-17. The DXRD pattern obtained after the first stage of leaching of the sequential extraction scheme on the hydrogenetic crusts.

# 7TOW 130 D-FRAG



# 7TOW 142 D-1

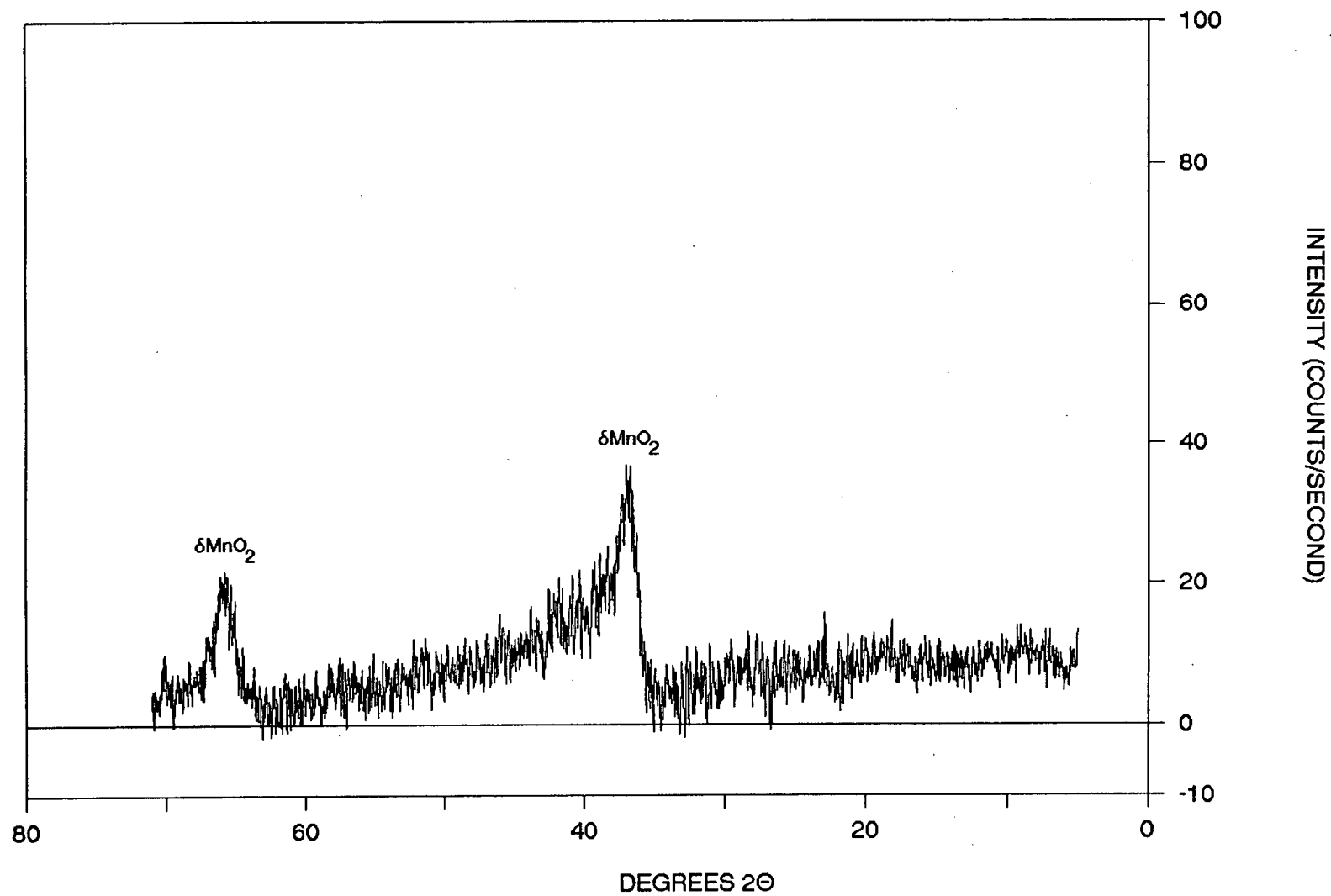
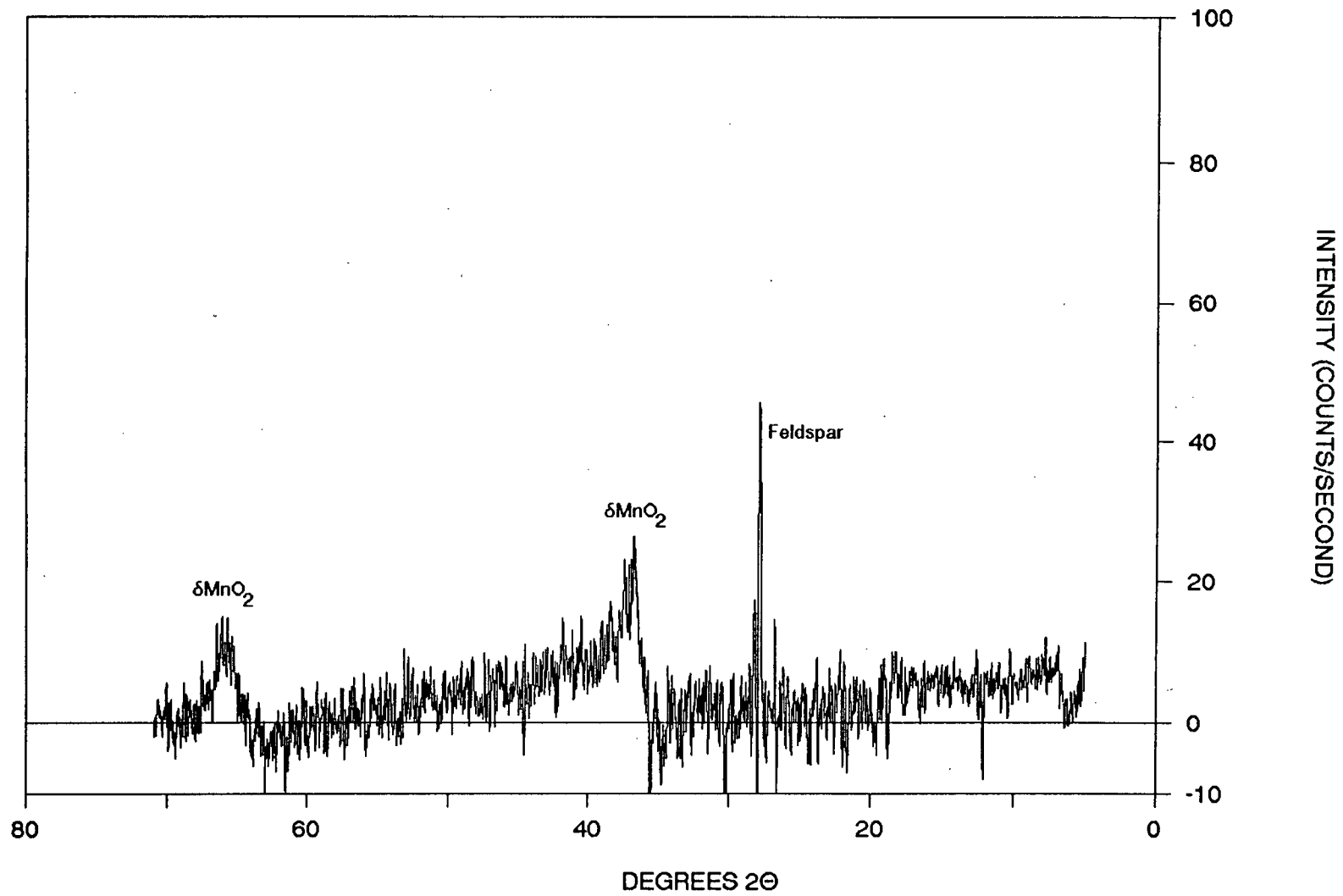


Figure 3-18. The DXRD pattern obtained after the first stage of leaching of the sequential extraction scheme on the hydrogenous nodules.

# DODO 12-2 D-1



# DODO 14-2 D-2

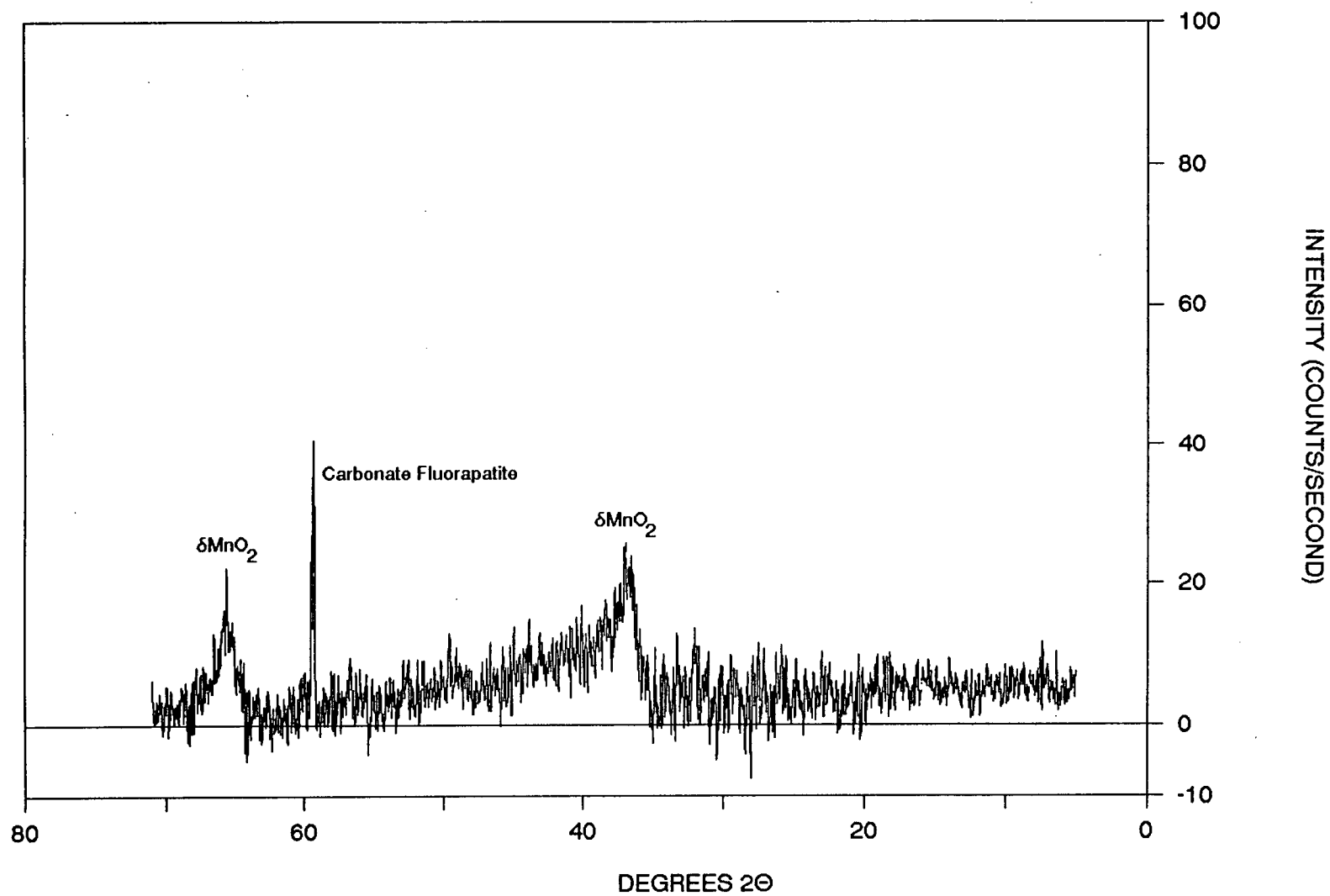
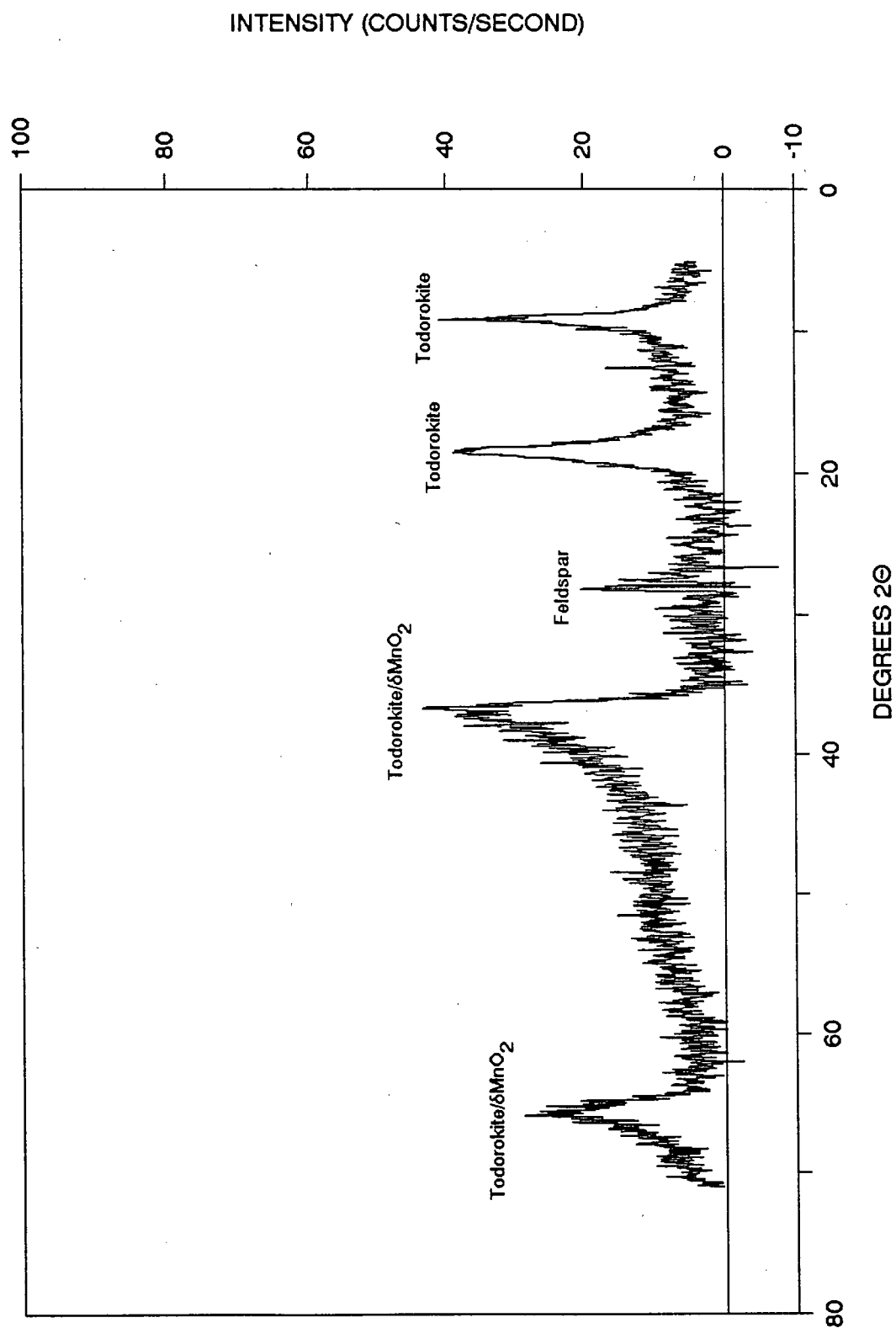


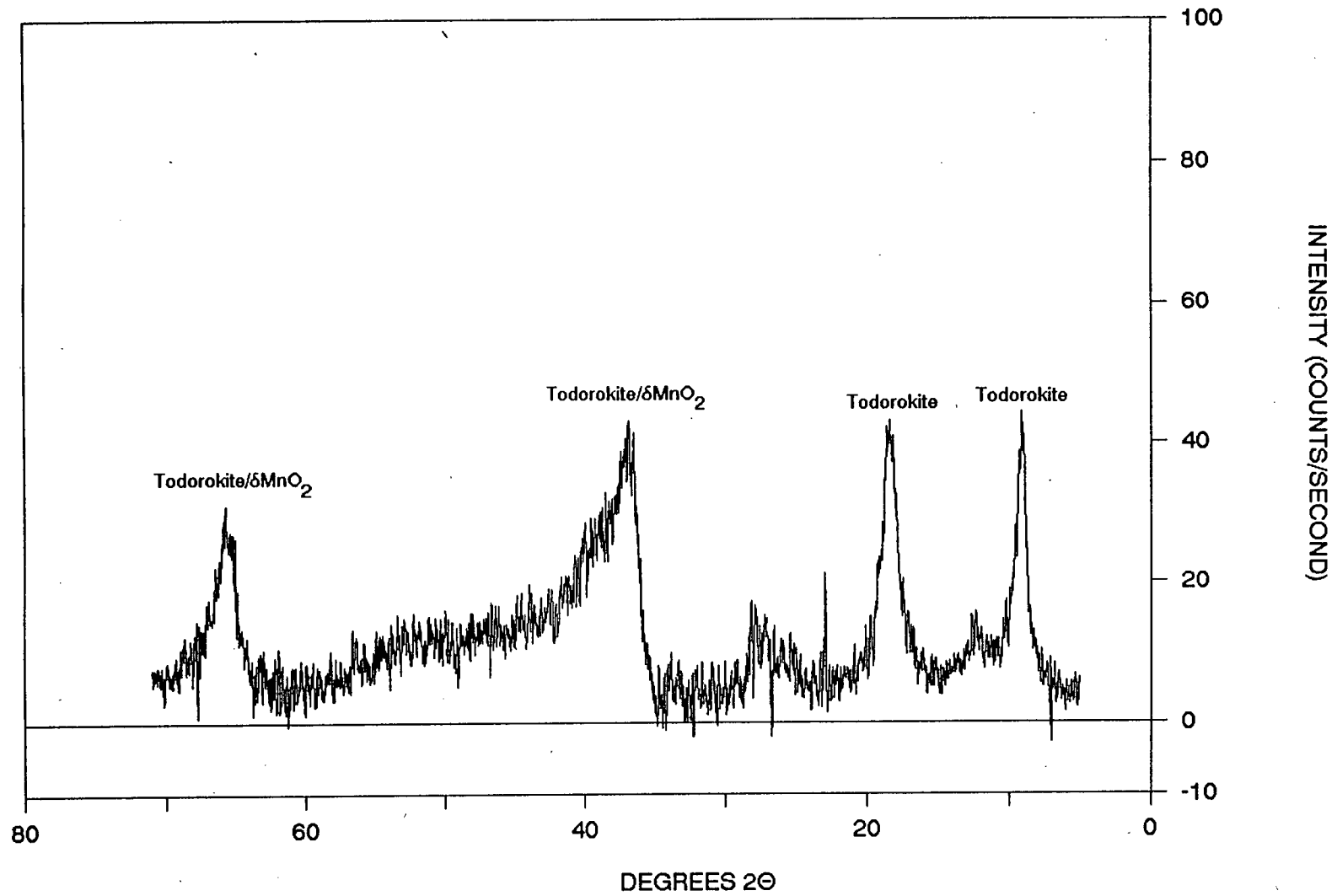


Figure 3-19. The DXRD pattern obtained after the first stage of leaching of the sequential extraction scheme on the diagenetic nodules.

# Mn 39



# Mn 56

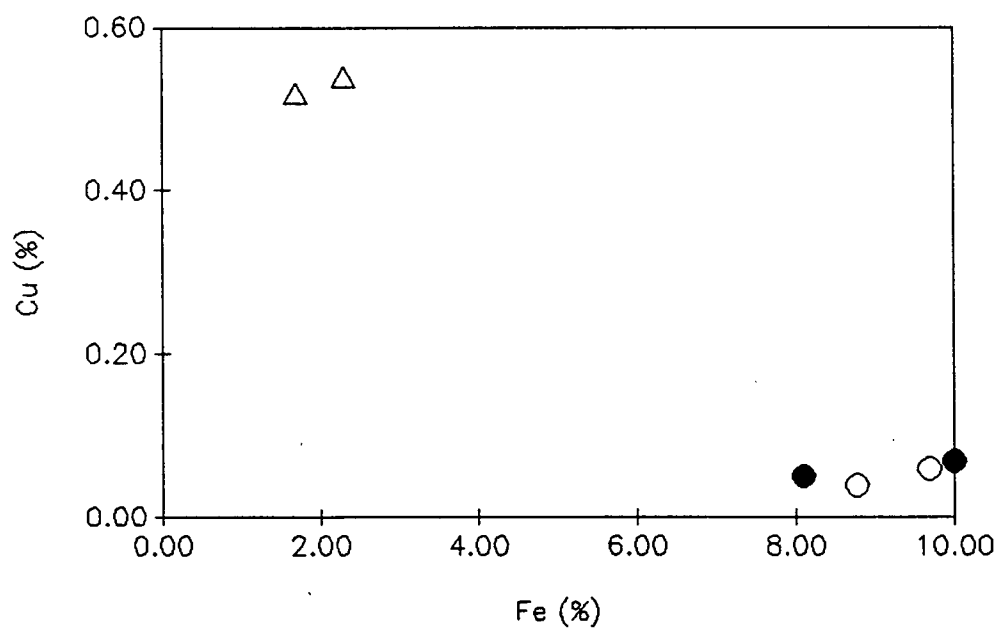
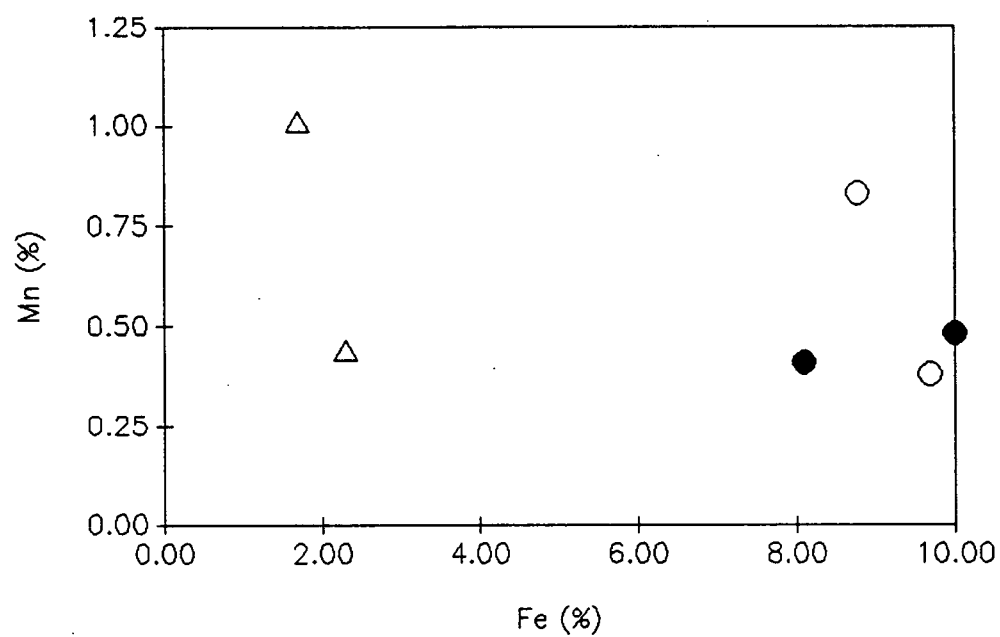


### 3.4.2.1.2 Second Stage of the Selective Sequential

#### Extraction Scheme and DXRD

Since the iron oxides are removed during the second stage of the selective sequential extraction scheme, plotting the concentrations of Mn, Cu, Ni, and Co against the concentration of Fe will give a better indication of the association of Mn, Cu, Ni, and Co to Fe and the iron oxide phase(s) in the selected crusts and nodules. The results from the second stage of the sequential extraction scheme indicate that the iron oxide present in crust and nodule samples from this region show considerable variations in Fe, Cu, Ni, and Co concentrations (Figure 3-20). DXRD identified the iron oxide present in hydrogenetic crusts, hydrogenous nodules and diagenetic nodules as ferrihydrite which is shown in Figures 3-21, 3-22, and 3-23 respectively. The ferrihydrite present in all three groups of crusts and nodules contains relatively consistent concentrations of Mn, while the ferrihydrite in both hydrogenetic crusts and hydrogenous nodules contains higher concentrations of Fe. In the hydrogenetic crusts, the ferrihydrite has a low concentration of Cu and displays a wide range in Ni and Co concentrations while in the hydrogenous nodules, the ferrihydrite also has a low Cu, Ni, and Co concentrations compared to the hydrogenetic crusts and diagenetic nodules. In the diagenetic nodules, the ferrihydrite contains consistently higher concentrations of Cu and Ni than that present in the hydrogenous nodules and the hydrogenetic crusts but low concentrations of Co similar to the hydrogenous nodules.

Figure 3-20. The weight per cent of Mn, Fe, Cu, Ni, and Co associated with the iron phase mineralogy which was removed during the second stage of the selective extraction scheme. The open circles = hydrogenetic crusts, the filled circles = hydrogenous nodules, the open triangles = diagenetic nodules.



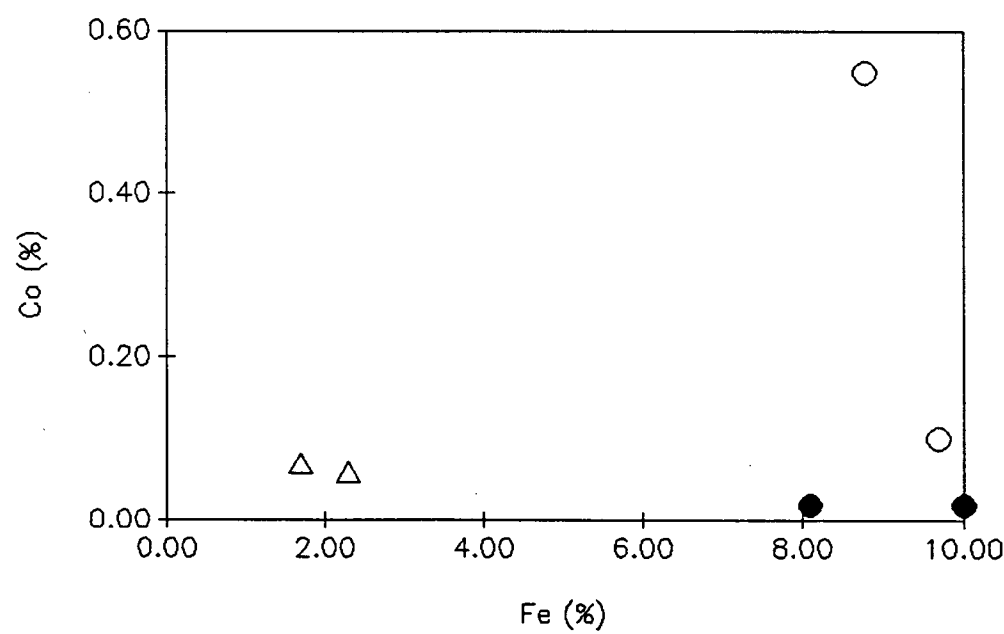
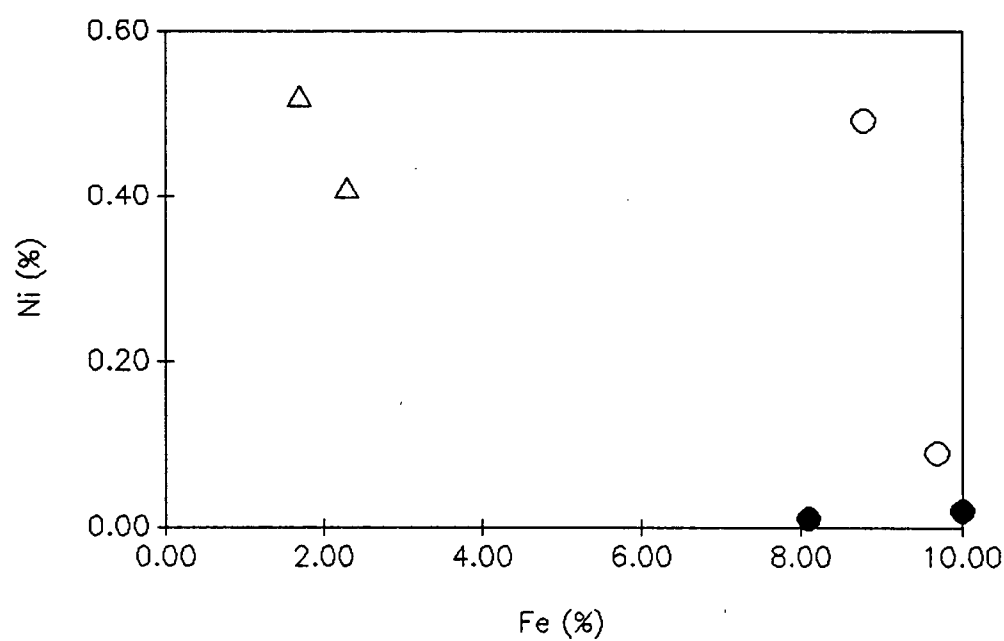
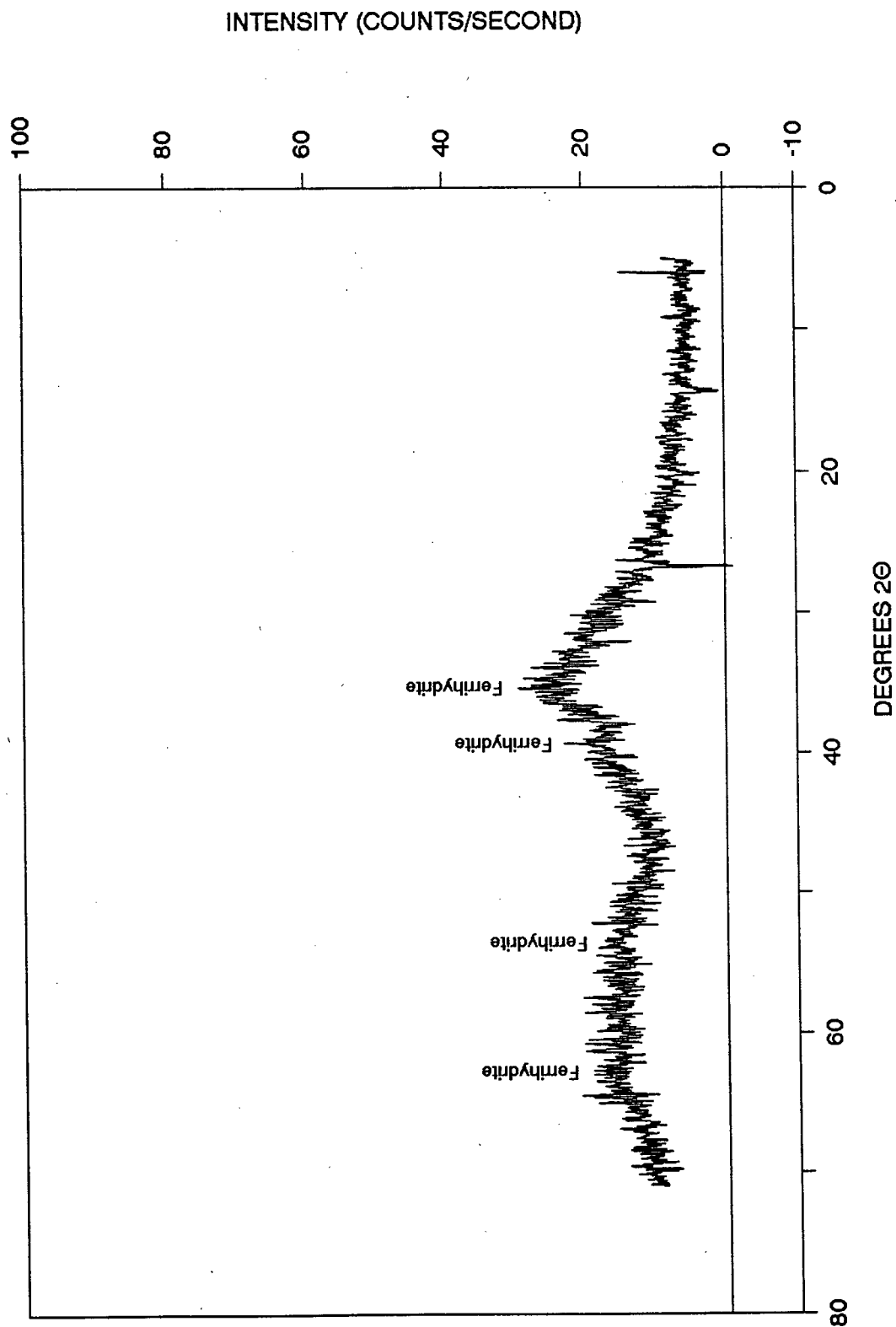


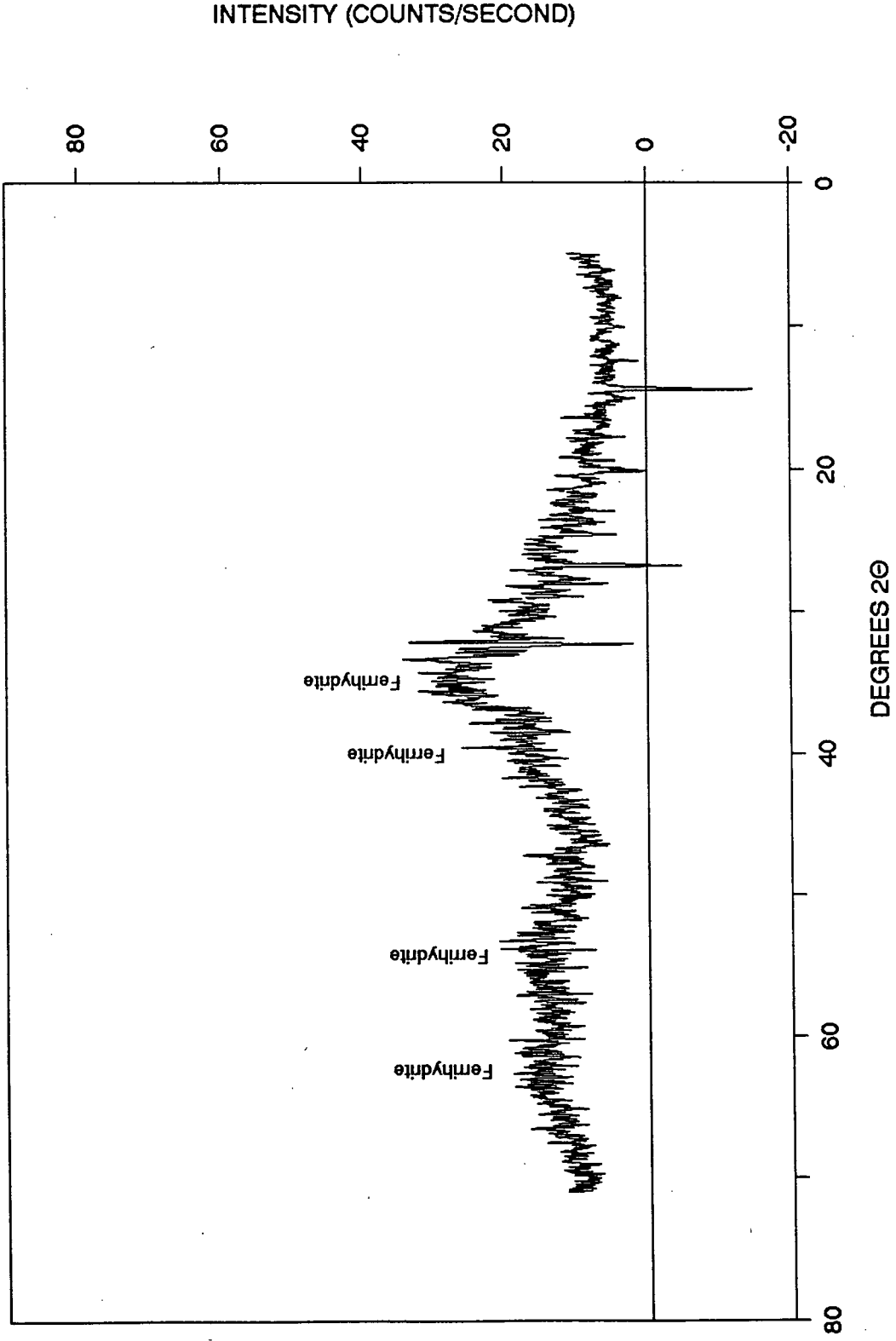
Figure 3-21. The DXRD pattern obtained after the second stage of leaching of the sequential extraction scheme on the hydrogenetic crusts.



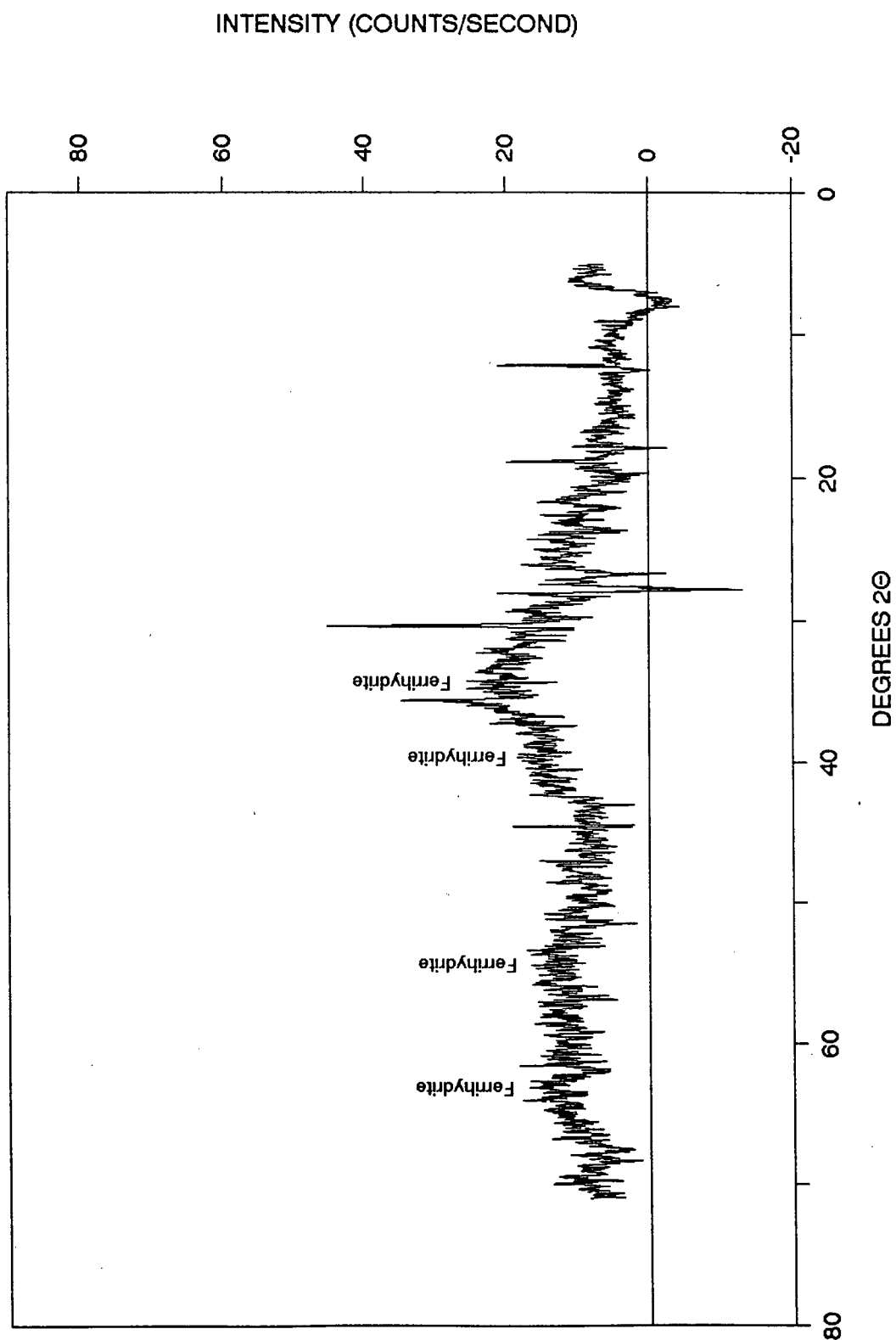
# 7TOW 130 D-FRAG



# 7TOW 142 D-1



**Figure 3-22.** The DXRD pattern obtained after the second stage of leaching of the sequential extraction scheme on the hydrogenous nodules.

**DODO 12-2 D-1**

# DODO 14-2 D-2

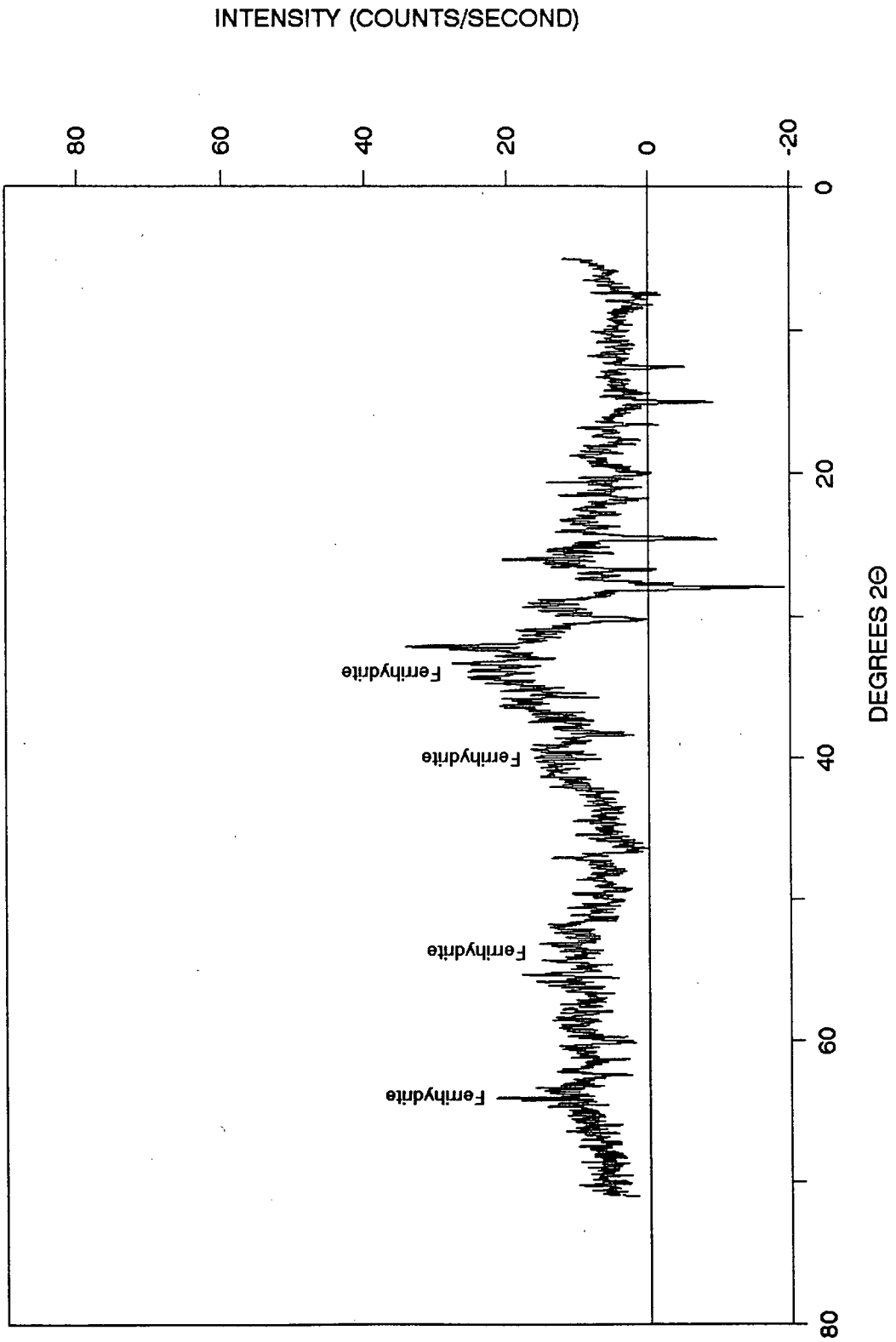
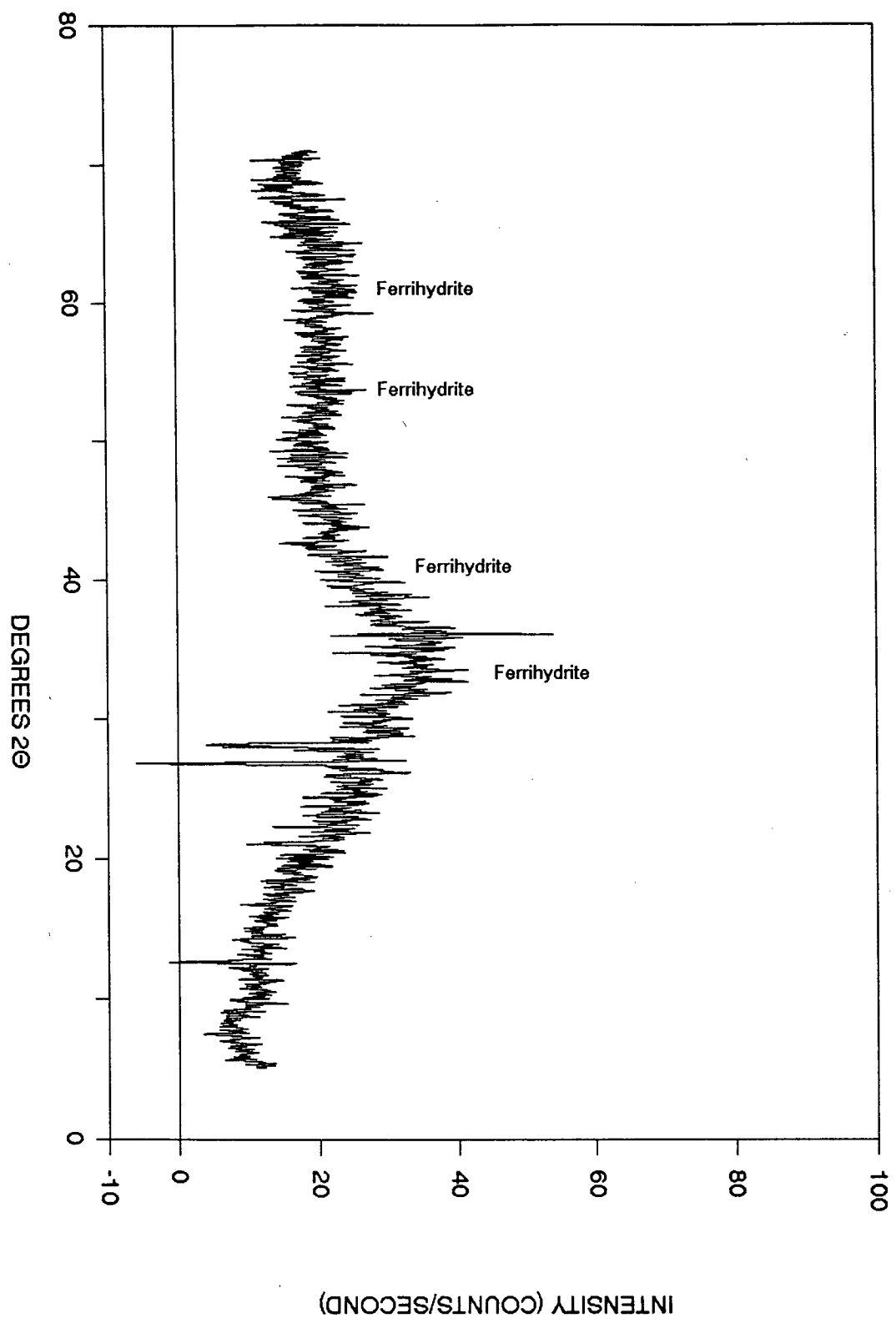
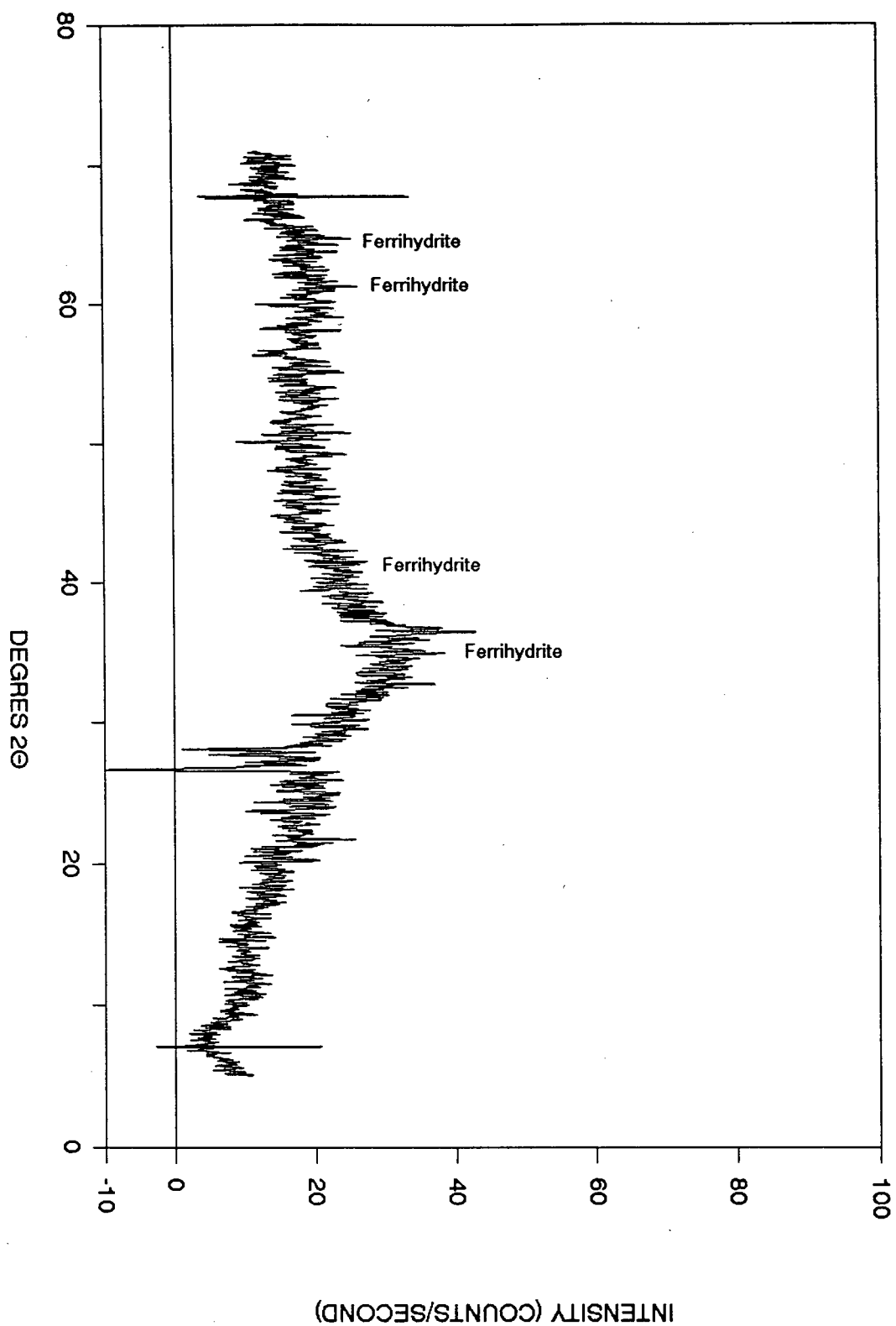


Figure 3-23. The DXRD pattern obtained after the second stage of leaching of the sequential extraction scheme on the diagenetic nodules.

# Mn 39



# Mn 56





### 3.4.2.2 Survey Region B

In order to better understand the partitioning of Mn, Fe, Cu, Ni, and Co between the manganese and iron oxide phase(s) identified in the crusts and nodules selected from Survey Region B, the results from the two stage selective sequential extraction scheme and the DXRD technique will be considered together. The weight per cent of Mn, Fe, Cu, Ni, and Co in the leachates from the first stage of the selective sequential extraction scheme are listed in Table 3-5a. These results represent the concentrations of Mn, Fe, Cu, Ni, and Co present in the manganese oxides of the crusts and nodules. The mineral phase(s) removed during the first stage of leaching and identified by DXRD are listed in Table 3-5b.

The weight per cent of Mn, Fe, Cu, Ni, and Co in the leachates from the second stage of the selective sequential extraction scheme are listed in Table 3-6a. These results represent the concentrations of Mn, Fe, Cu, Ni, and Co present in the iron oxides of the crusts and nodules. The mineral phase(s) removed during the second stage of leaching and identified by DXRD are listed in Table 3-6b.

#### 3.4.2.2.1 First Stage of the Selective Sequential Extraction

##### Scheme and DXRD

The results from the first stage of the sequential extraction scheme indicate that the manganese oxides present in the crust and nodule samples from this region show considerable variation in their concentrations of Mn, Fe, Cu, Ni, and Co (Figure 3-24). The manganese oxide phase mineralogy of the hydrogenetic crusts showed the most variation of all the different groups of crusts and nodules selected from this region (Figure 3-25). Despite this the concentrations of Mn, Fe, Cu, and Ni were relatively consistent in the  $\delta\text{MnO}_2$ , todorokite, and birnessite present. In the

Table 3-5a. The concentrations of Mn, Fe, Cu, Ni and Co in the leachates from the first stage of leaching for samples from Survey Region B. Results are listed as weight per cent.

Element	Samples Hydrogenetic Crusts		Mn-rich Hydrothermal Crusts	
	HEN SMT	RISE III 28 D-1	QBR 22 D-1	RISE III 3 D-1
Fe	0.40	0.75	0.05	0.00
Mn	19.24	16.12	22.78	24.65
Co	0.07	0.40	0.00	0.00
Ni	0.21	0.23	0.03	0.02
Cu	0.02	0.00	0.00	0.00

Element	Samples Hydrogenous and Diagenetic Nodules		Mn-rich Hydrothermal Nodules		Fe-rich Hydrothermal Nodules	
	B 104	B 114	CERS 20 D-2	CERS 21 D-3	DWBD 1-2	S 74
Fe	0.18	0.15	0.31	0.10	1.21	1.13
Mn	21.29	21.66	23.47	25.40	5.48	4.42
Co	0.03	0.05	0.00	0.00	0.11	0.12
Ni	0.38	0.38	0.09	0.20	0.37	0.20
Cu	0.16	0.20	0.05	0.06	0.12	0.06

Table 3-5b. The mineral phase(s) removed during the first stage of the selective sequential extraction scheme and identified by DXRD.

Sample	Mineral Phase(s) Identified by DXRD
<b>Hydrogenetic Crusts</b>	
Henderson Smt	Todorokite/Birnessite
RISE III 28 D-1	$\delta\text{MnO}_2$
<b>Mn-rich Hydrothermal Crusts</b>	
QBR 22 D-1	Birnessite/minor amounts of Todorokite
RISE III 3 D-1	Todorokite/Birnessite
<b>Hydrogenous and Diagenetic Nodules</b>	
B 104	Todorokite/minor amounts of Birnessite
B 114	Todorokite/minor amounts of Birnessite
<b>Mn-rich Hydrothermal Nodules</b>	
CERS 20 D-2	Todorokite/minor amounts of Birnessite
CERS 21 D-3	Todorokite/minor amounts of Birnessite
<b>Fe-rich Hydrothermal Nodules</b>	
DWBD 1-2	Todorokite/ $\delta\text{MnO}_2$
S 74	Todorokite/ $\delta\text{MnO}_2$

Table 3-6a. The concentrations of Mn, Fe, Cu, Ni and Co in the leachates from the second stage of leaching for samples from Survey Region B. Results are listed as weight per cent.

Element	Samples		Mn-rich	
	Hydrogenetic Crusts		Hydrothermal Crusts	
	HEN SMT	RISE III 28 D-1	QBR 22 D-1	RISE III 3 D-1
Fe	1.20	11.40	2.60	0.00
Mn	0.11	0.52	9.29	14.79
Co	0.00	0.10	0.00	0.00
Ni	0.00	0.10	0.05	0.00
Cu	0.01	0.03	0.02	0.00

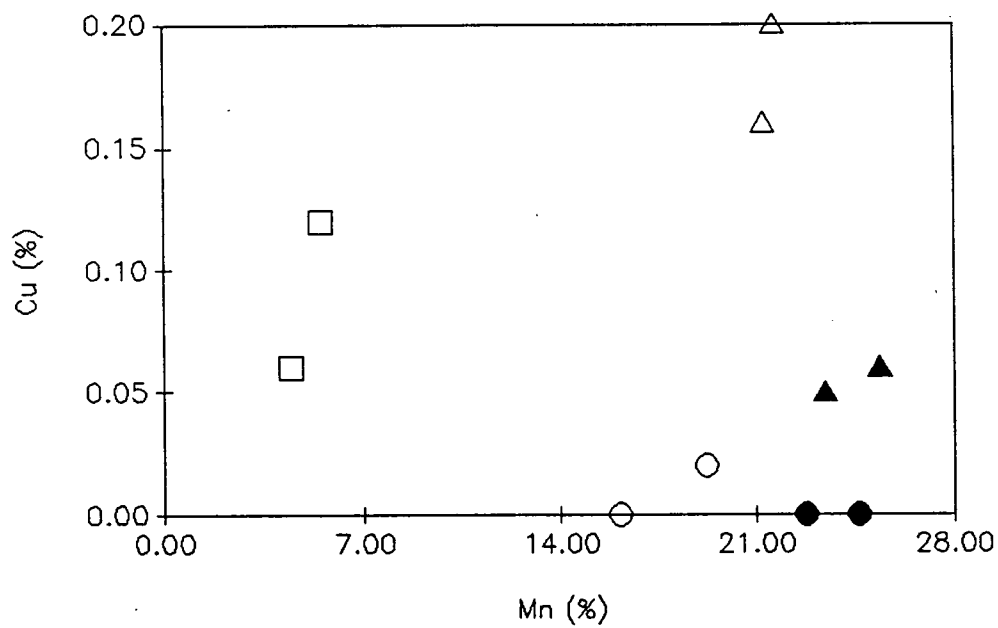
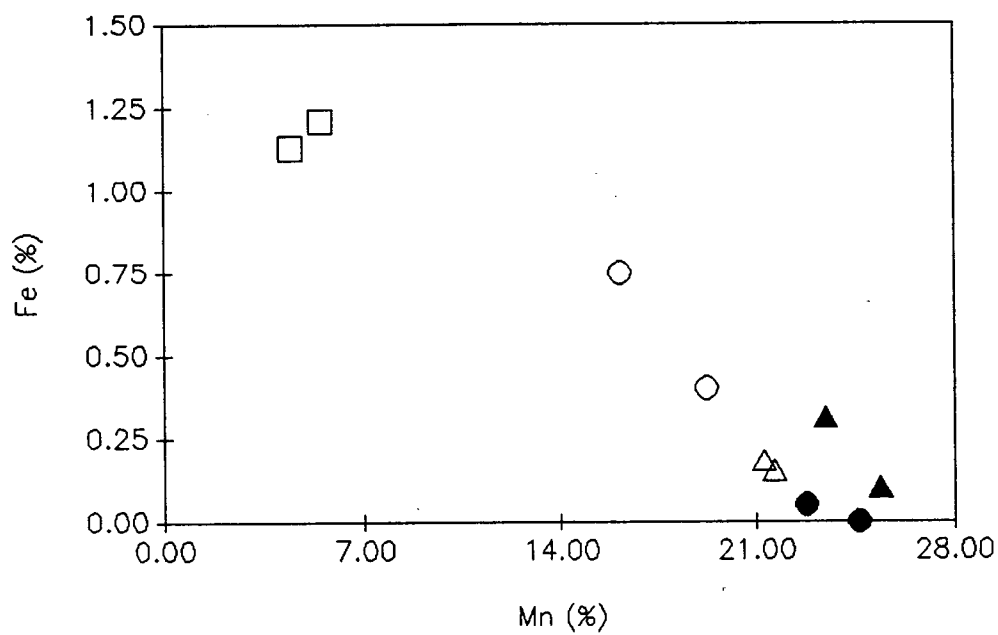
  

Element	Samples		Mn-rich		Fe-rich	
	Hydrogenous and Diagenetic Nodules		Hydrothermal Nodules		Hydrothermal Nodules	
	B 104	B 114	CERS 20 D-2	CERS 21 D-3	DWBD 1-2	S 74
Fe	4.30	3.20	1.50	0.70	1.50	3.40
Mn	1.15	1.58	5.69	8.79	0.04	0.10
Co	0.03	0.11	0.01	0.00	0.00	0.00
Ni	0.50	0.98	0.47	0.38	0.00	0.00
Cu	0.43	0.64	0.21	0.21	0.03	0.02

Table 3-6b. The mineral phase(s) removed during the second stage of the selective sequential extraction scheme and identified by DXRD.

Sample	Mineral Phase(s) Identified by DXRD
<b>Hydrogenetic Crusts</b>	
Henderson Smt	Ferrihydrite
RISE III 28 D-1	Ferrihydrite
<b>Mn-rich Hydrothermal Crusts</b>	
QBR 22 D-1	Haussmanite
RISE III 3 D-1	Haussmanite
<b>Hydrogenous and Diagenetic Nodules</b>	
B 104	Ferrihydrite
B 114	Ferrihydrite
<b>Mn-rich Hydrothermal Nodules</b>	
CERS 20 D-2	Akaganéite
CERS 21 D-3	Haussmanite
<b>Fe-rich Hydrothermal Nodules</b>	
DWBD 1-2	Ferrihydrite
S 74	Ferrihydrite

Figure 3-24. The weight per cent of Mn, Fe, Cu, Ni, and Co associated with the manganese phase mineralogy which was removed during the first stage of the selective extraction scheme. The open circles = hydrogenetic crusts, the filled circles = Mn-enriched hydrothermal crusts, the open triangles = hydrogenous and diagenetic nodules, the filled triangles = Mn-enriched hydrothermal nodules, the open squares = Mn depleted hydrothermal nodules.



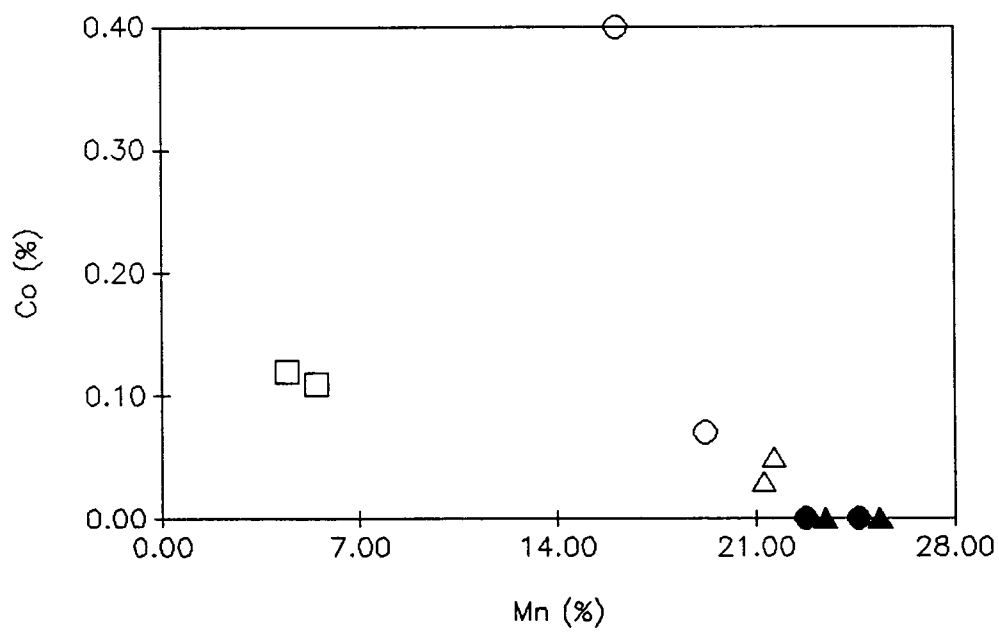
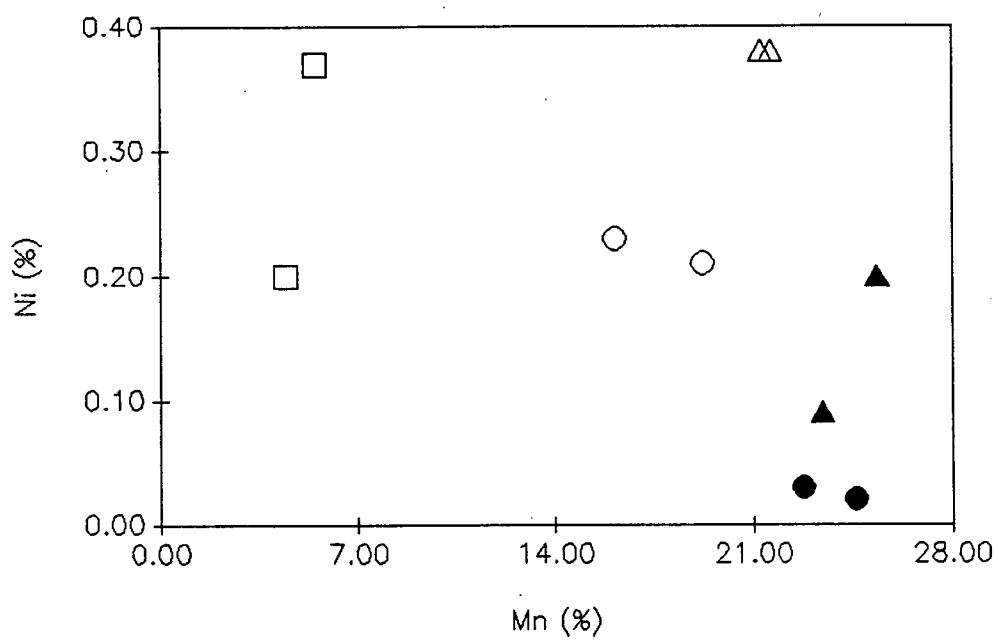
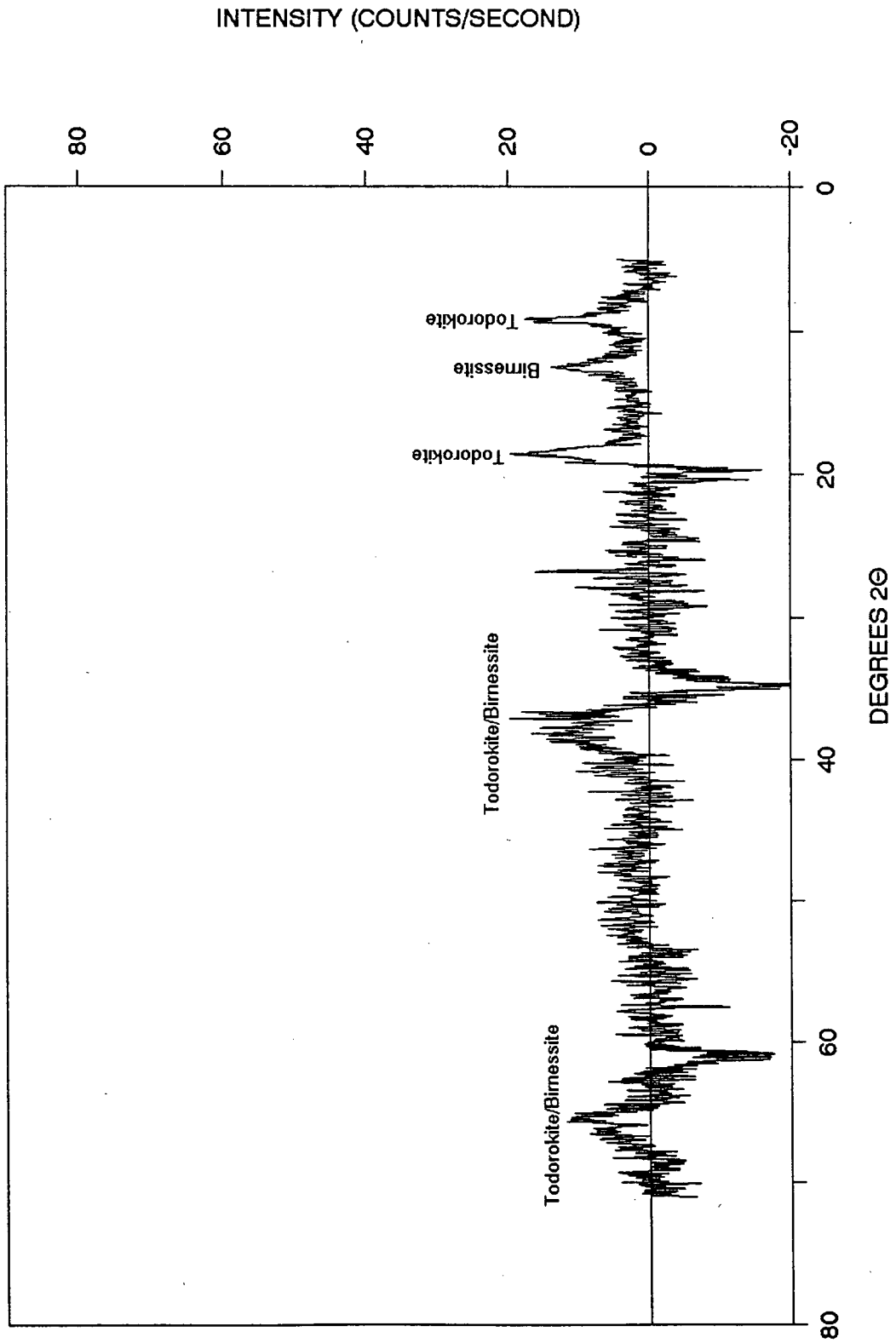


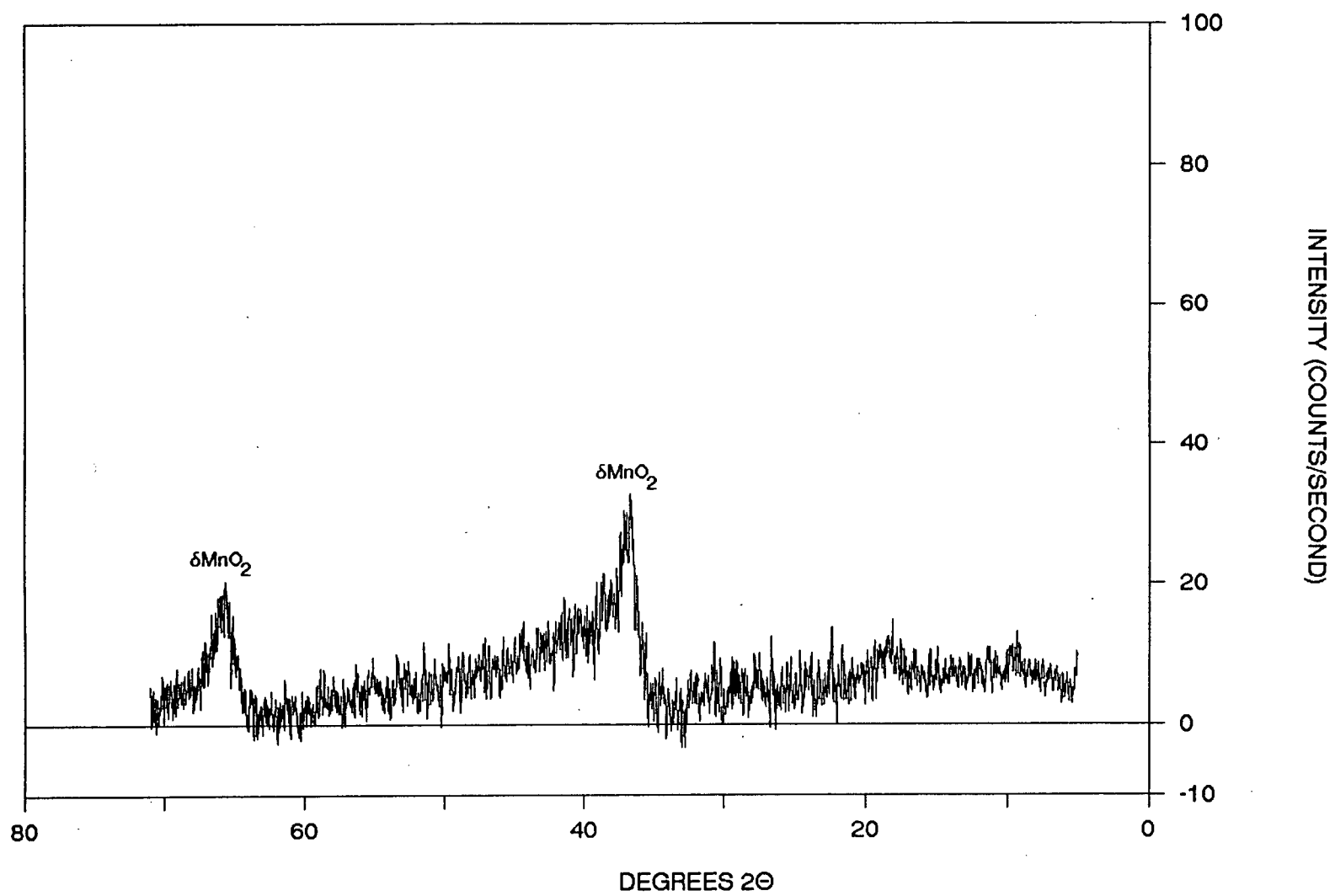


Figure 3-25. The DXRD pattern obtained after the first stage of leaching of the sequential extraction scheme on the hydrogenetic crusts.

# Henderson Seamount



# RISE III 28 D-2



hydrogenetic crusts, the Mn-bearing minerals contained moderate amounts of Fe and Ni and were depleted in Cu. Only Co showed a preferential enrichment in the  $\delta\text{MnO}_2$  bearing hydrogenetic crust and was depleted in the todorokite/birnessite bearing hydrogenetic crust. In the Mn-rich hydrothermal crusts and nodules, todorokite and birnessite were identified by DXRD (Figure 3-26 and 3-27). Both crusts and nodules were depleted in their concentrations of Fe, Cu, Ni, and Co but were enriched in Mn. It is interesting to note, however, that the Mn-rich hydrothermal nodules did contain slightly higher concentrations of Fe, Cu, and Ni compared to the Mn-rich hydrothermal crusts. In the Fe-rich hydrothermal nodules, todorokite and  $\delta\text{MnO}_2$  were identified by DXRD (Figure 3-28) and these samples were found to contain high concentrations of Fe, moderate concentrations of Cu, and Ni, and low concentrations of Mn and Co. In the hydrogenous and diagenetic nodules, todorokite and birnessite were identified by DXRD (Figure 3-29). These phases were found to contain low concentrations of Fe and Co and the highest concentrations of Mn, Cu, and Ni compared to the other samples.

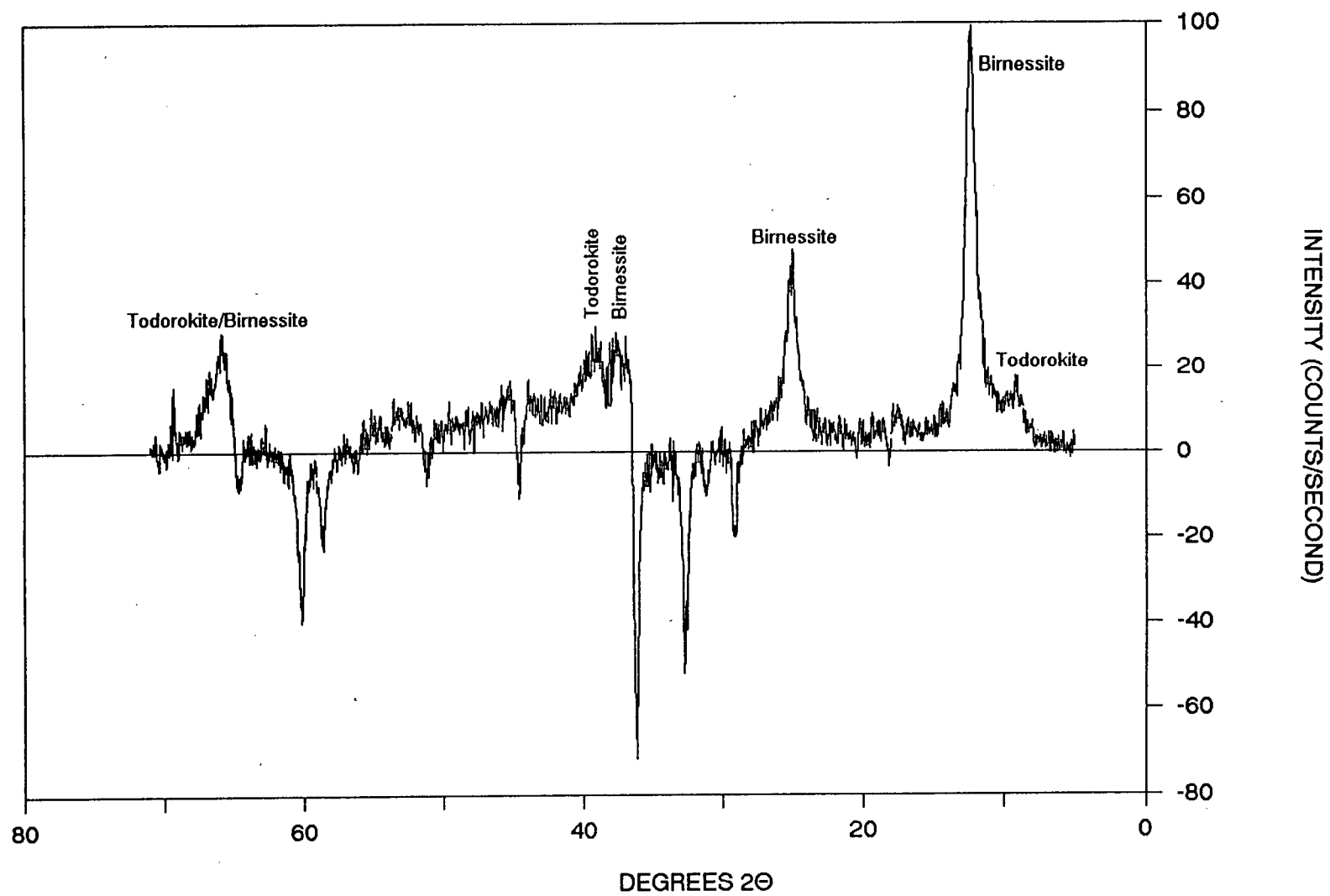
#### 3.4.2.2.2 Second Stage of the Selective Sequential

##### Extraction Scheme and DXRD

The results from the second stage of the sequential extraction scheme indicate that the oxyhydroxide phases removed during the the second stage of leaching are relatively depleted in Mn, Fe, Cu, Ni, and Co (Figure 3-30). DXRD results shows that the oxyhydroxide phases were identified as several oxides of iron and one oxide of manganese. Hydrogenetic crusts were found to be contain ferrihydrite (Figure 3-31), while the Mn-rich hydrothermal crusts were found to contain the manganese oxide hausmannite (Figure 3-32). Like the hydrogenetic crusts, the hydrogenous and diagenetic nodules were also found to contain ferrihydrite (Figure 3-33). The two

Figure 3-26. The DXRD pattern obtained after the first stage of leaching of the sequential extraction scheme on the Mn-enriched hydrothermal crusts.

# QBR 22 D-1



# RISE III 3 D-1

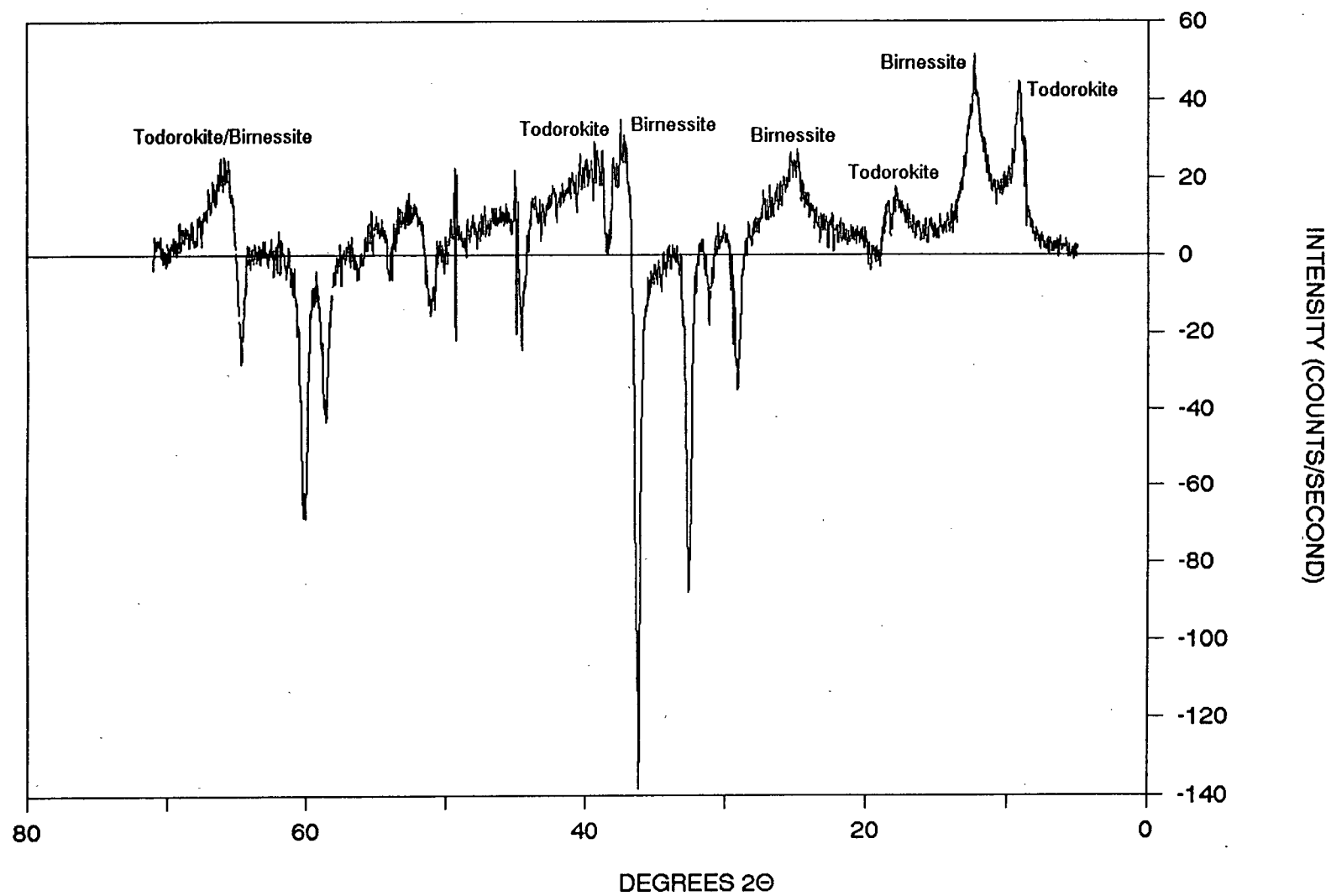
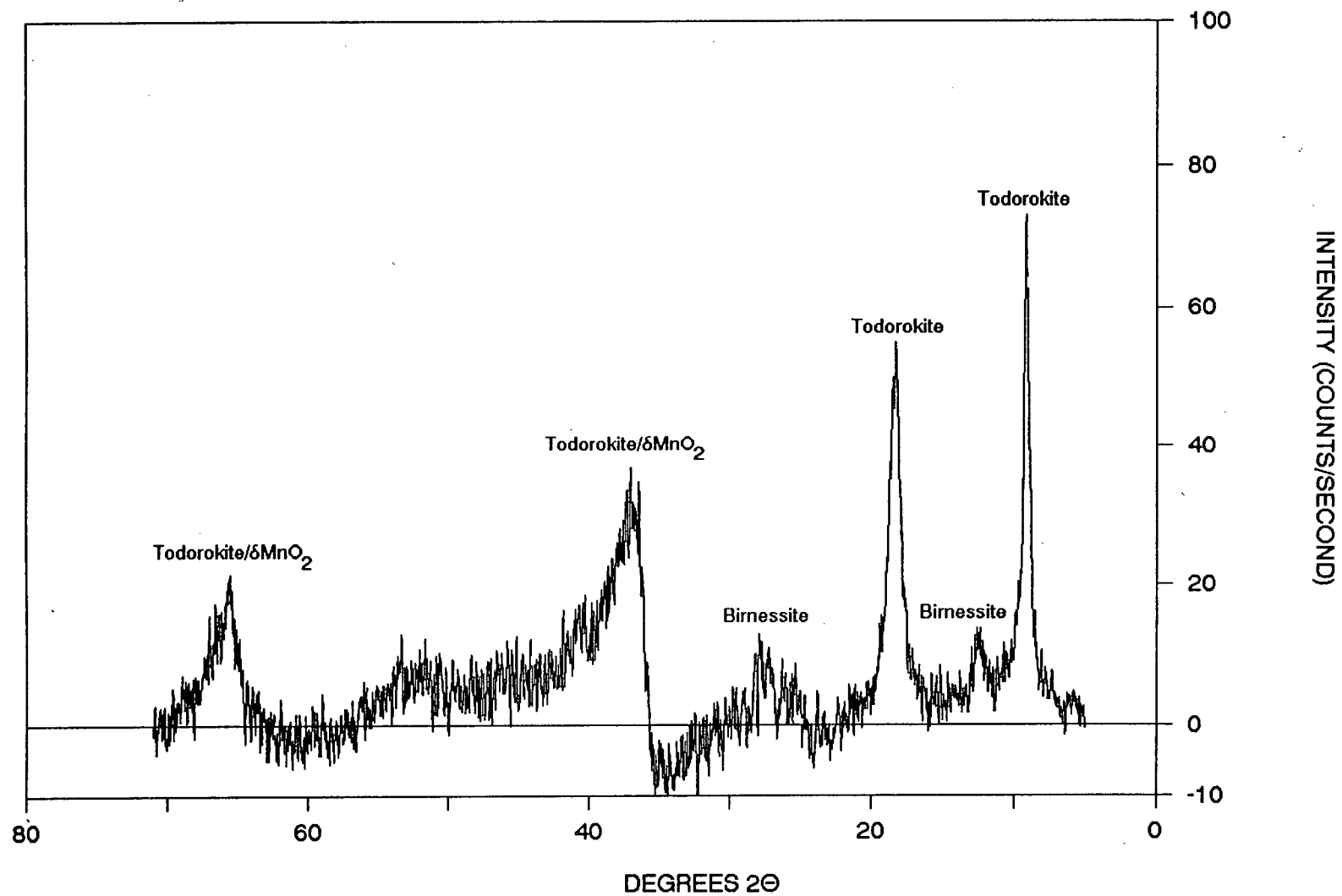


Figure 3-27. The DXRD pattern obtained after the first stage of leaching of the sequential extraction scheme on the Mn-enriched hydrothermal nodules.



# CERS 20 D-2



# CERS 21 D-3

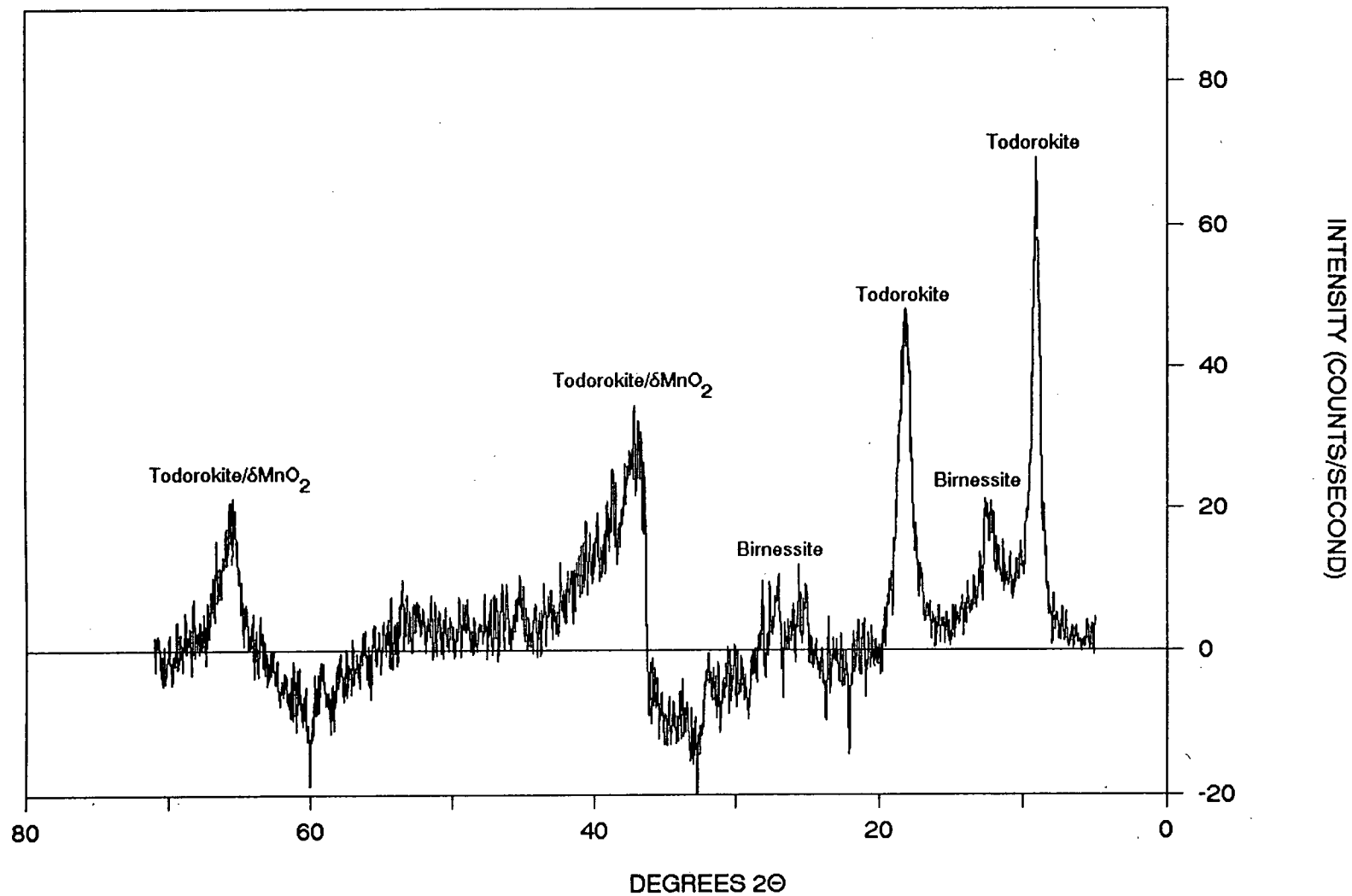
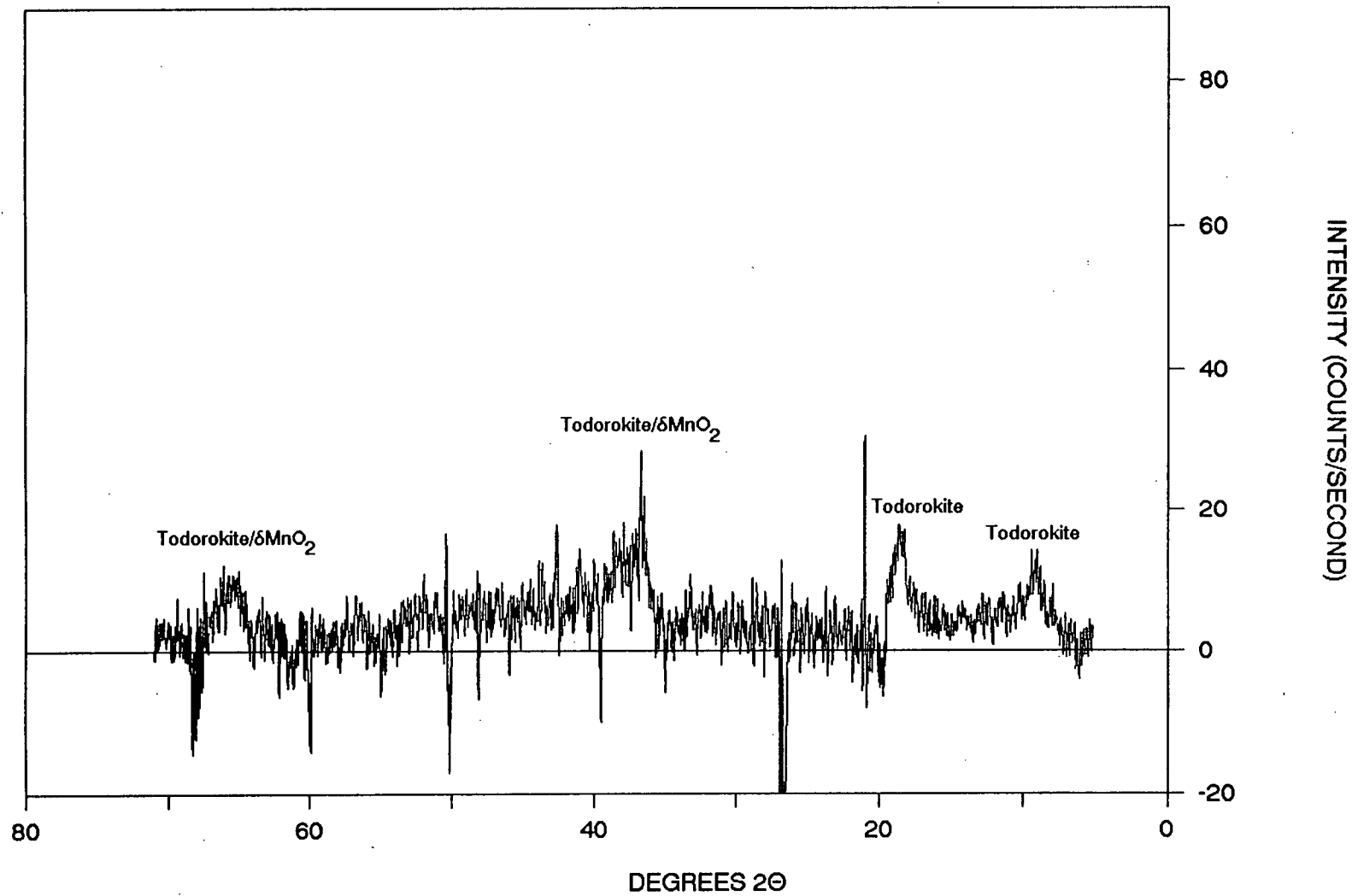
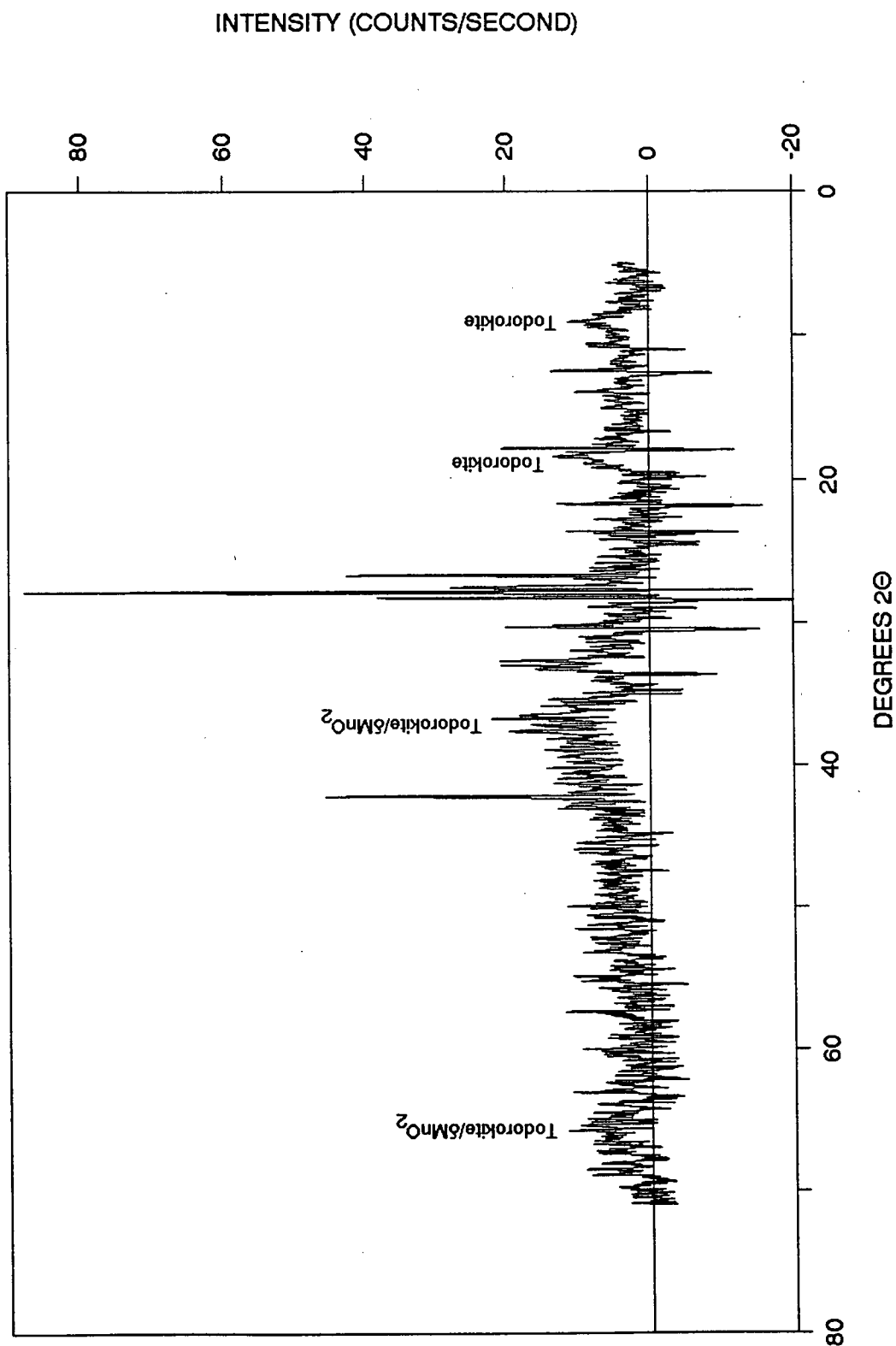


Figure 3-28. The DXRD pattern obtained after the first stage of leaching of the sequential extraction scheme on the Mn-depleted hydrothermal nodules.

# DWBD 1-2

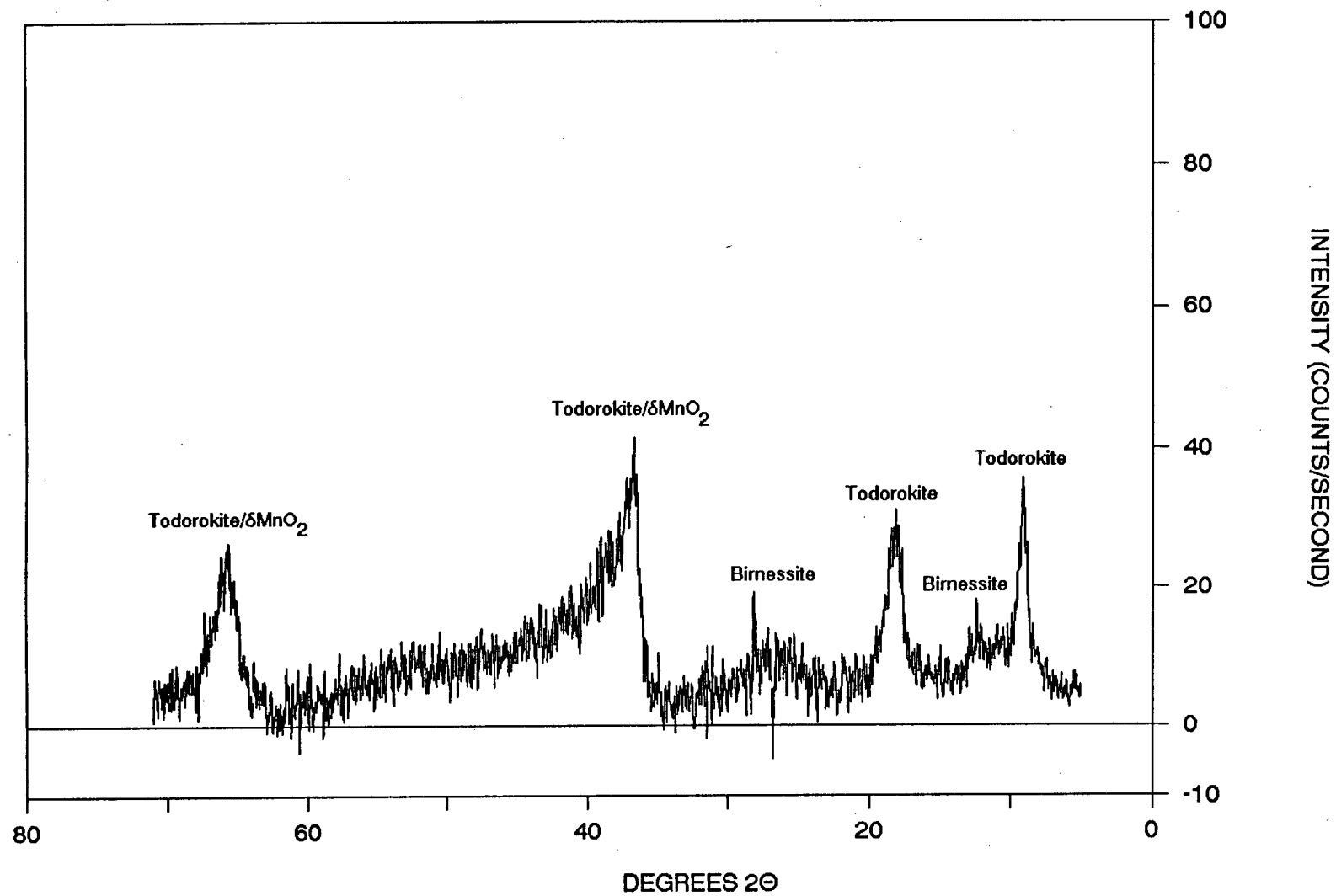


S 74



**Figure 3-29.** The DXRD pattern obtained after the first stage of leaching of the sequential extraction scheme on the hydrogenous and diagenetic nodules.

# B 104



# B 114

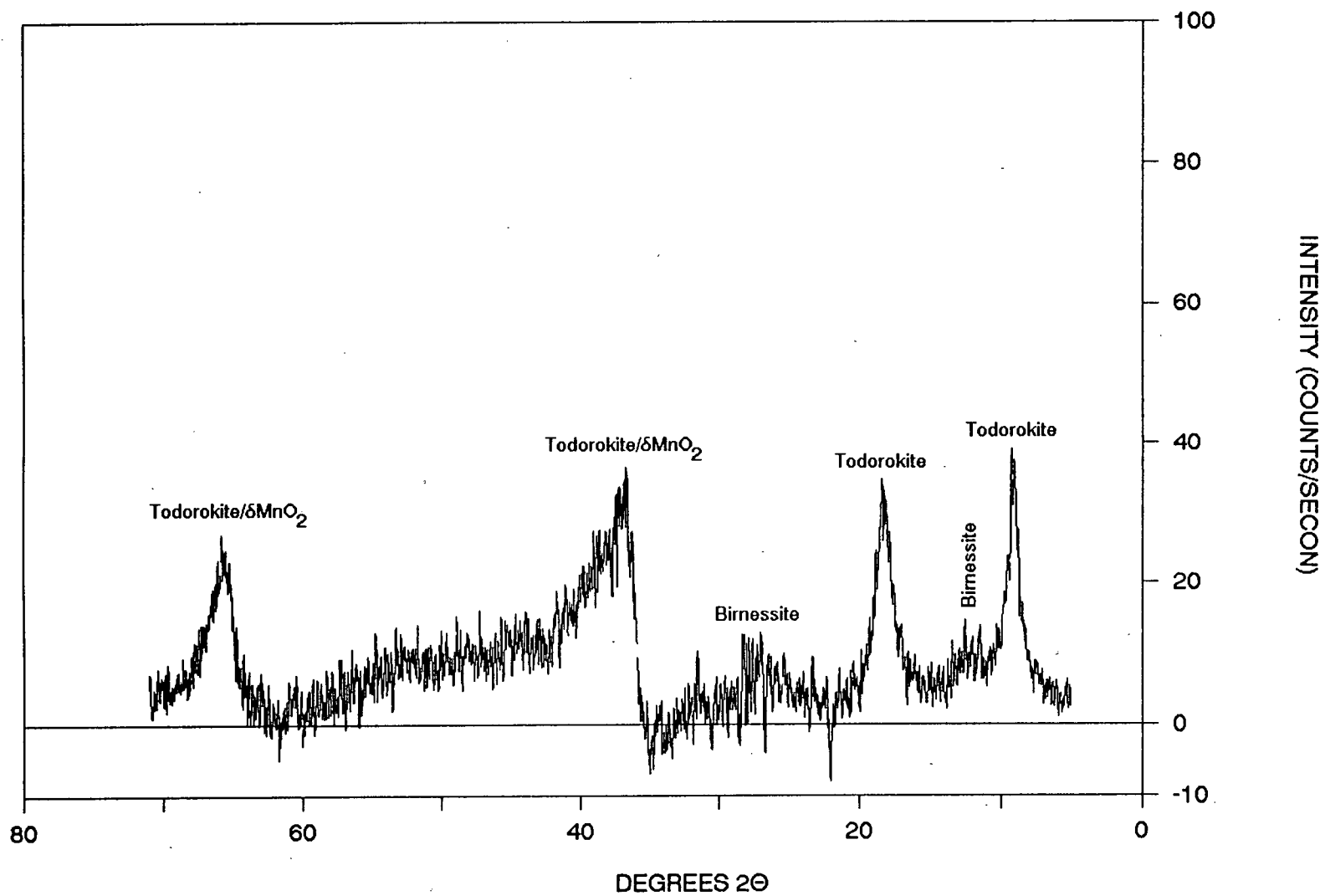
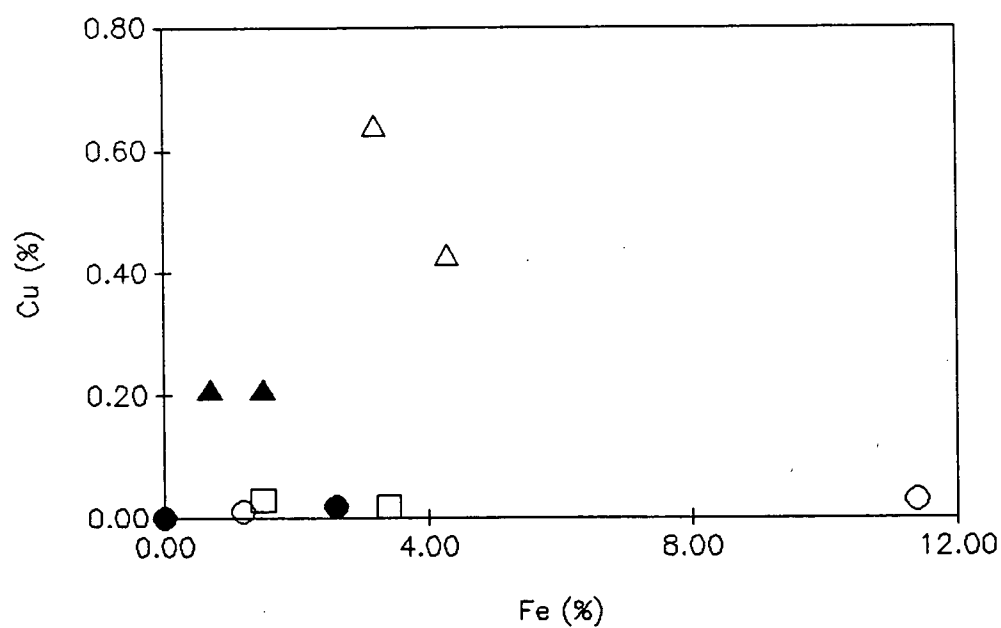
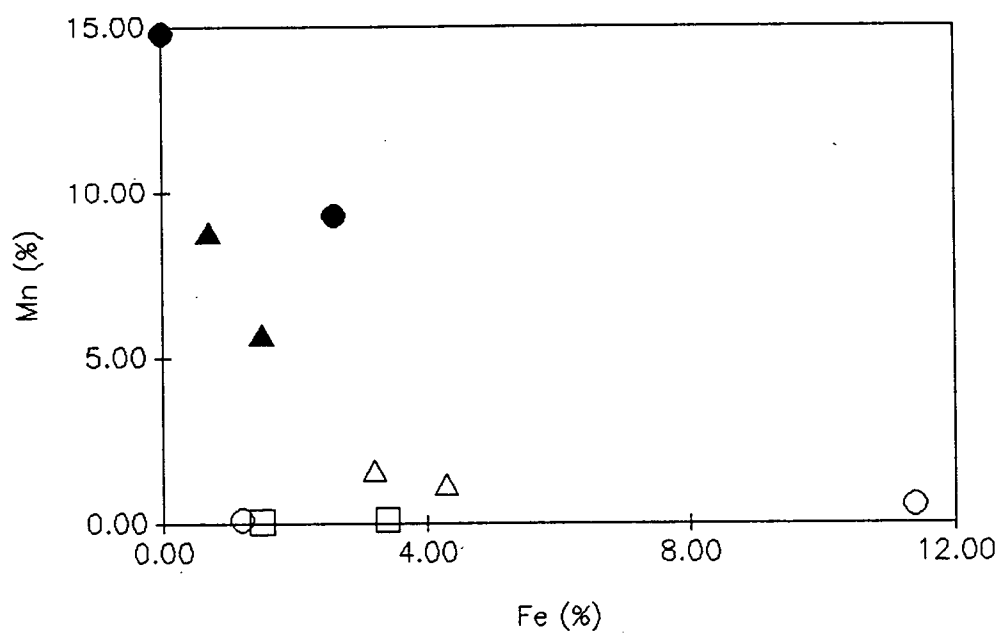




Figure 3-30. The weight per cent of Mn, Fe, Cu, Ni, and Co associated with the iron phase mineralogy which was removed during the second stage of the selective extraction scheme. The open circles = hydrogenetic crusts, the filled circles = Mn-enriched hydrothermal crusts, the open triangles = hydrogenous and diagenetic nodules, the filled triangles = Mn-enriched hydrothermal nodules, the open squares = Mn depleted hydrothermal nodules.



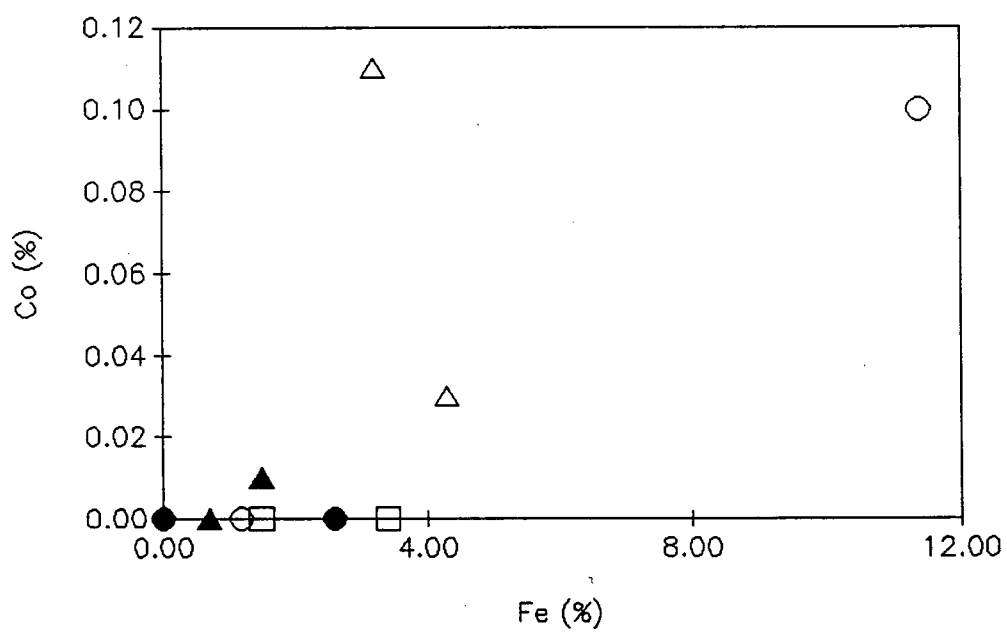
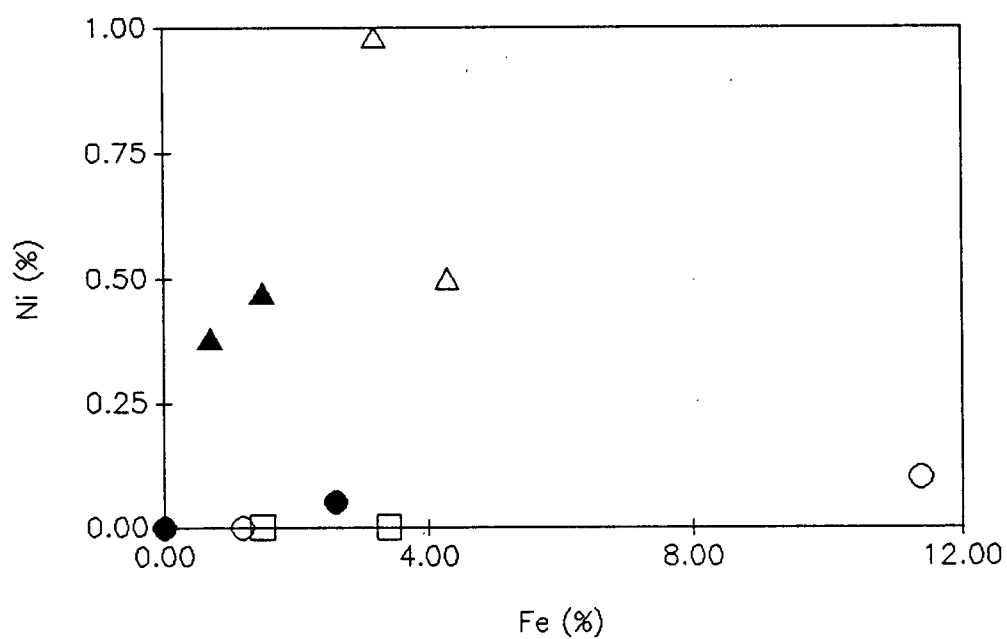
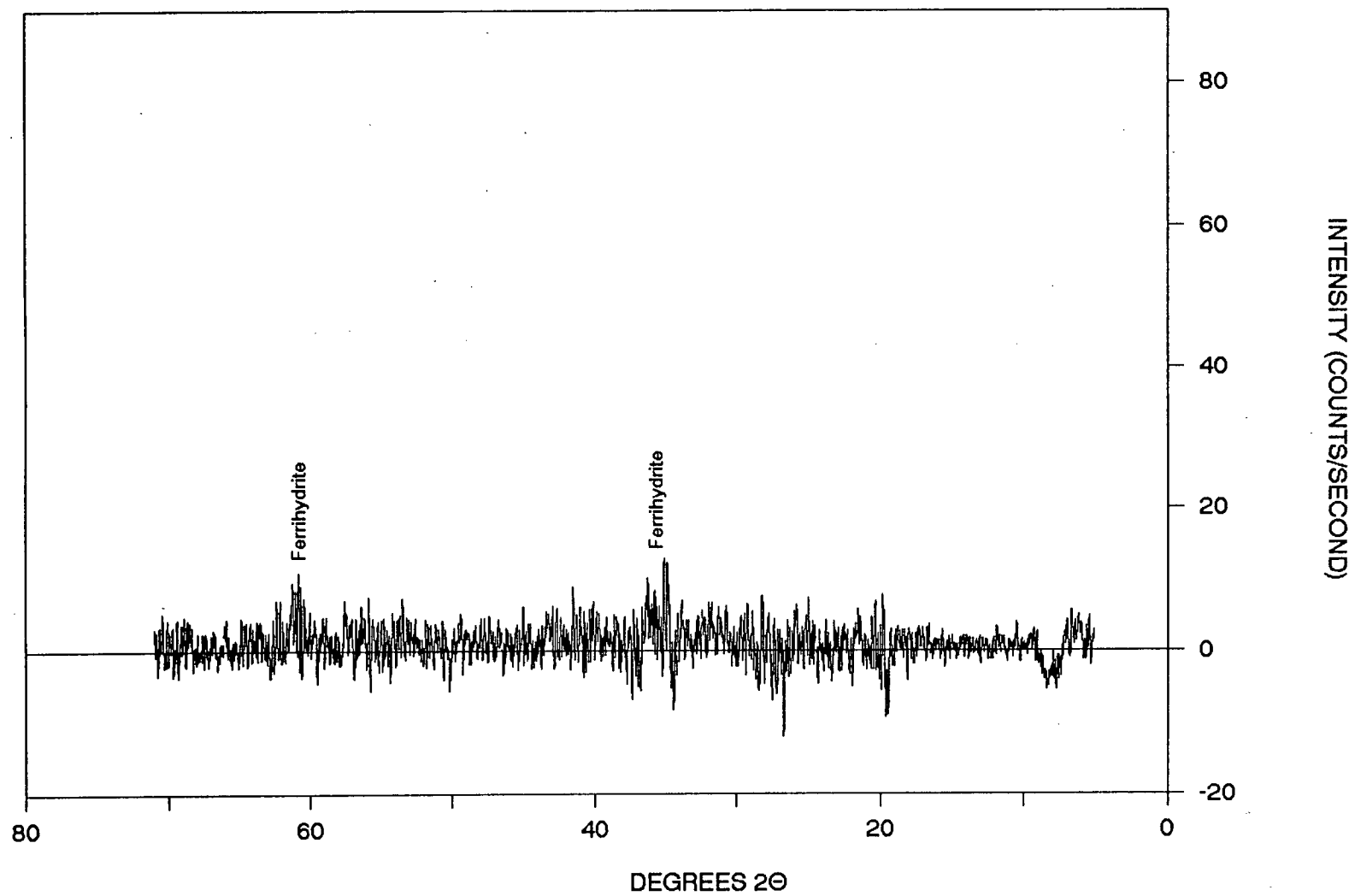


Figure 3-31. The DXRD pattern obtained after the second stage of leaching of the sequential extraction scheme on the hydrogenetic crusts.

# Henderson Seamount



# RISE III 28 D-1

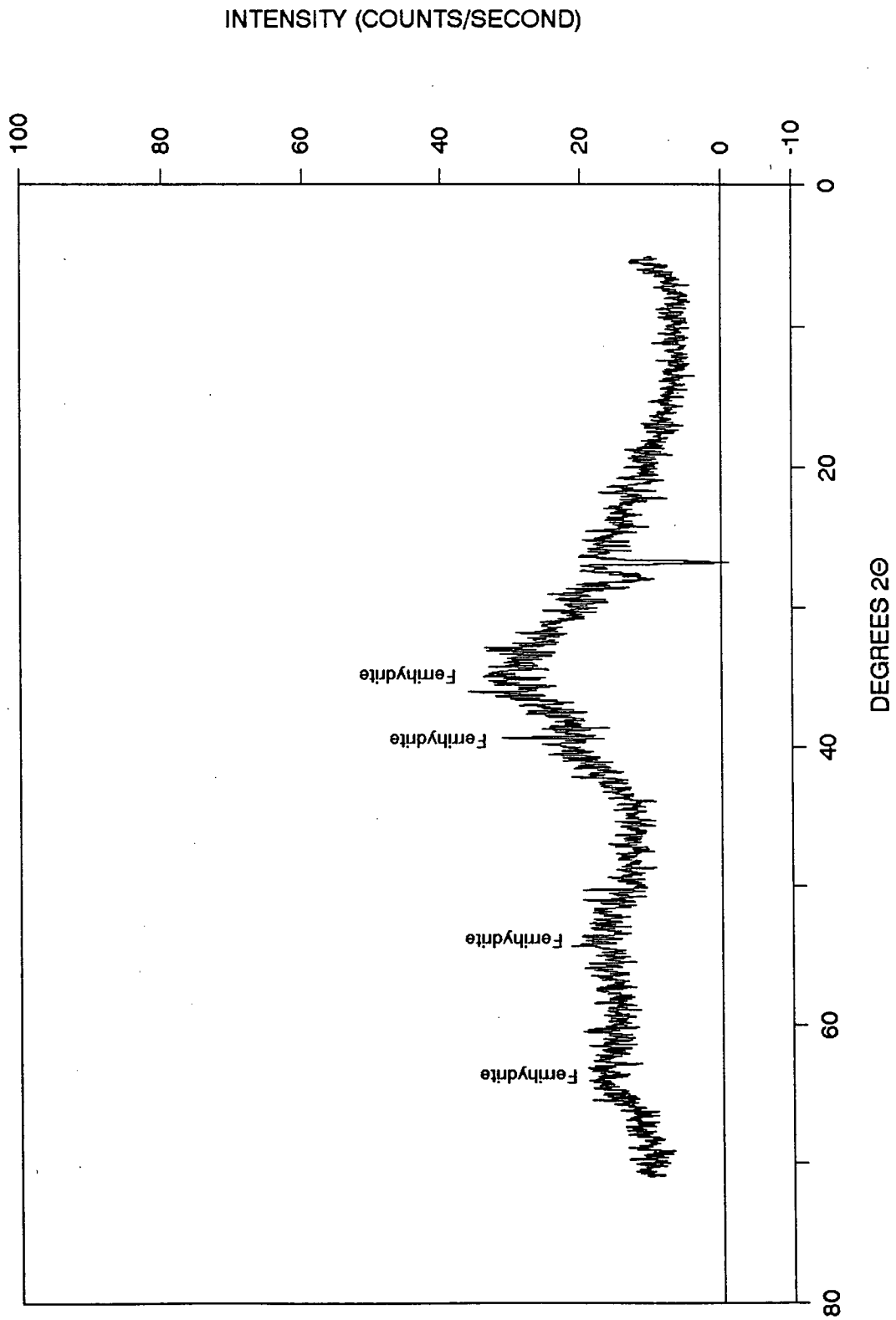
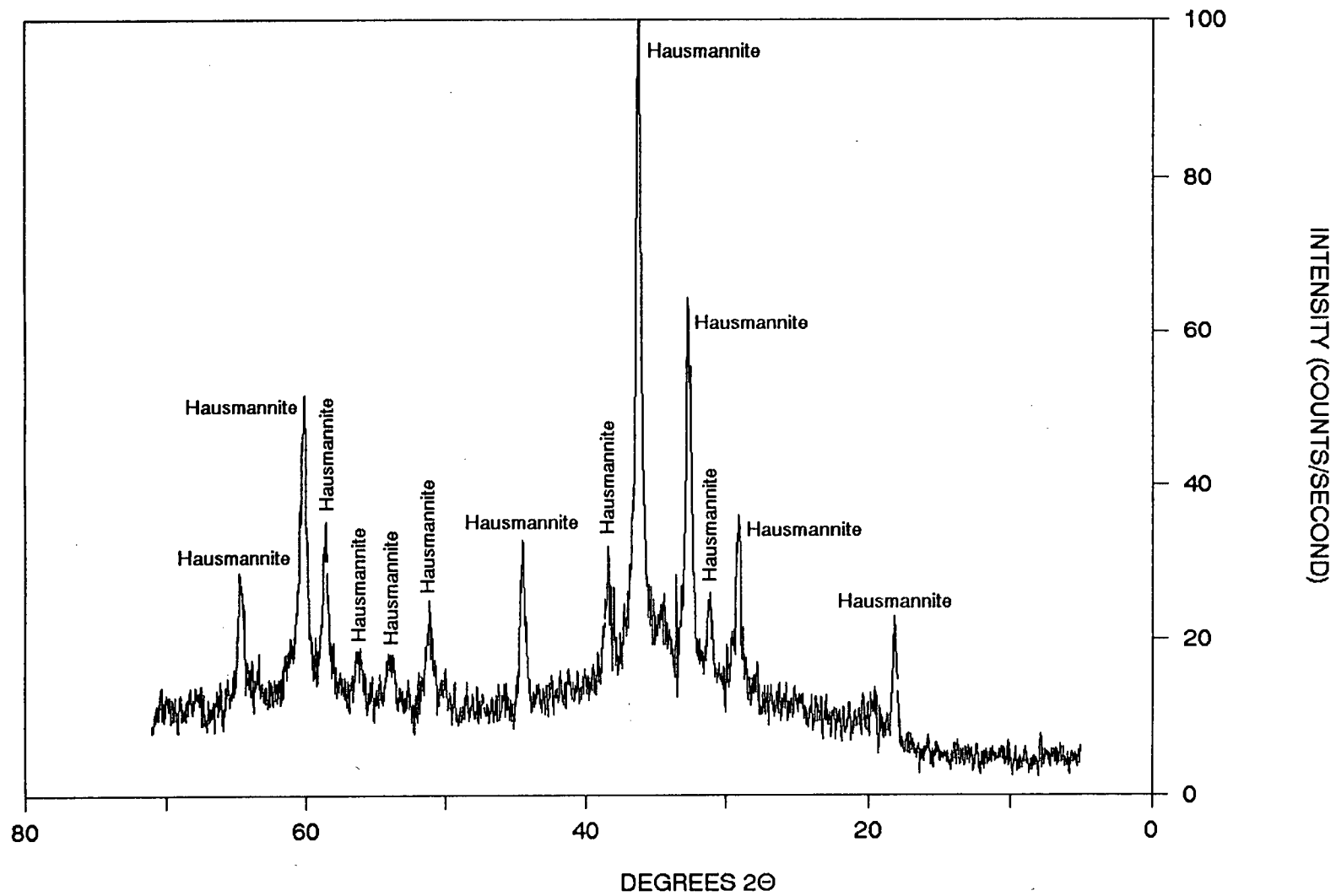


Figure 3-32. The DXRD pattern obtained after the second stage of leaching of the sequential extraction scheme on the Mn-enriched hydrothermal crusts.

# QBR 22 D-1





# RISE III 3 D-1

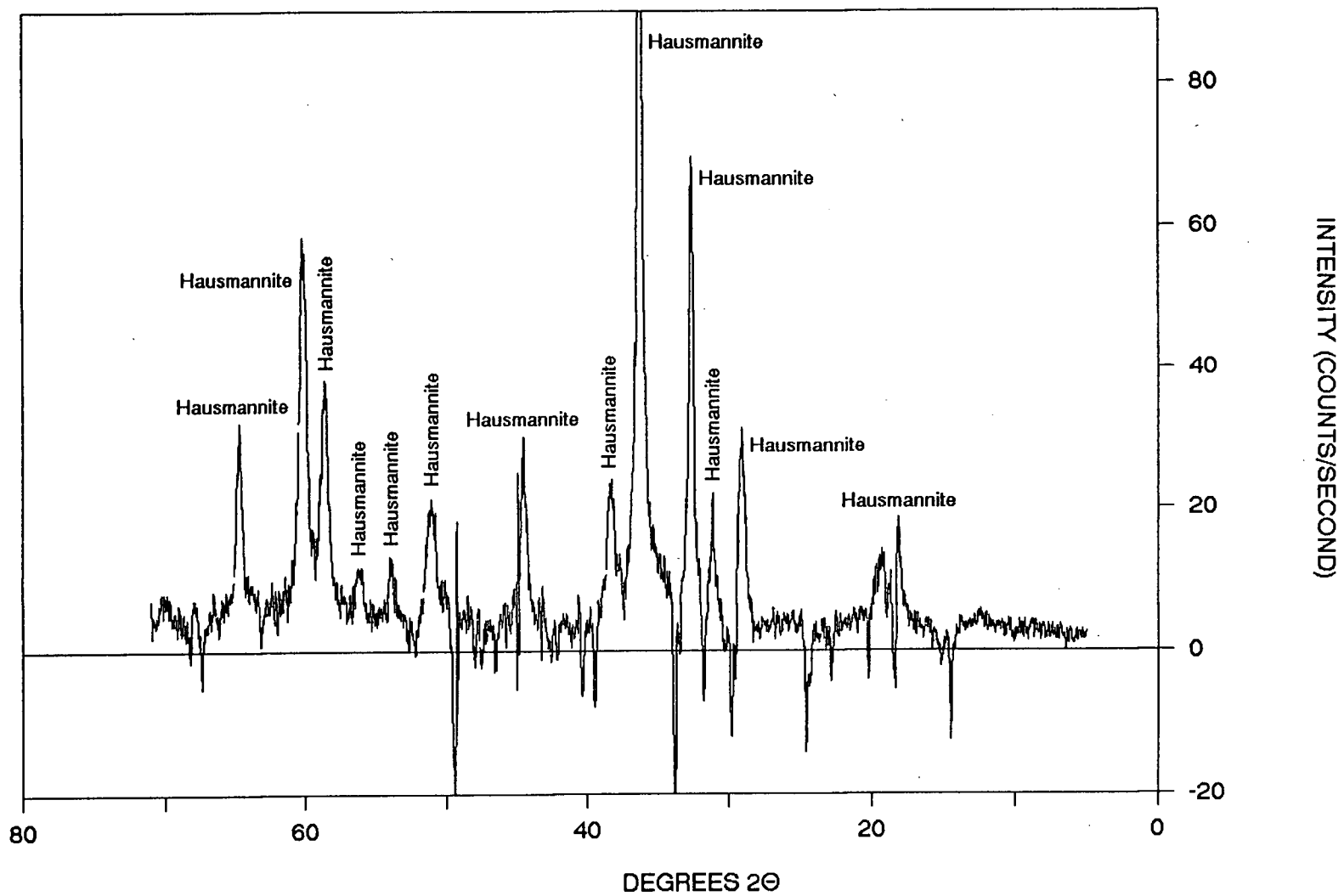
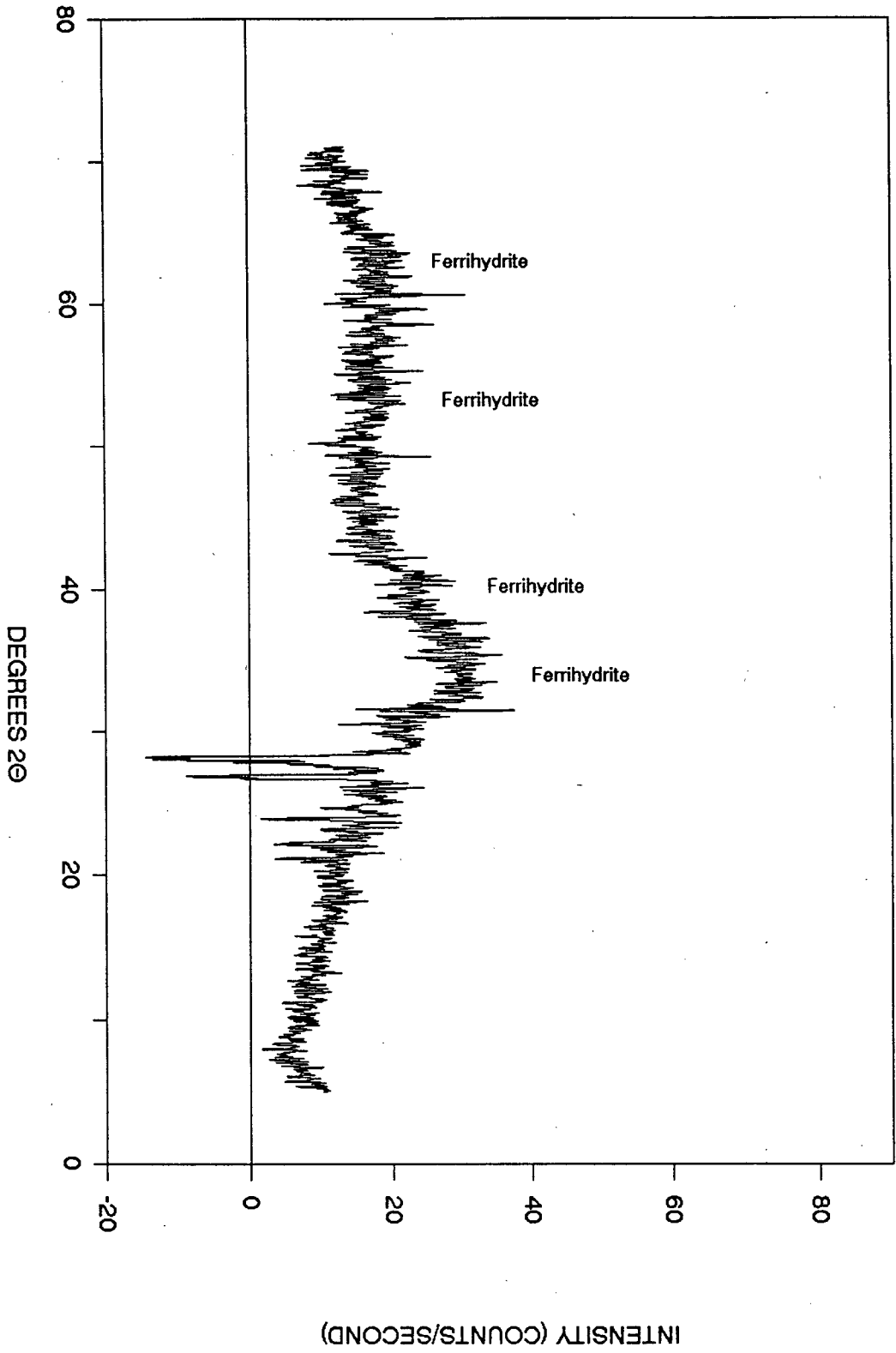
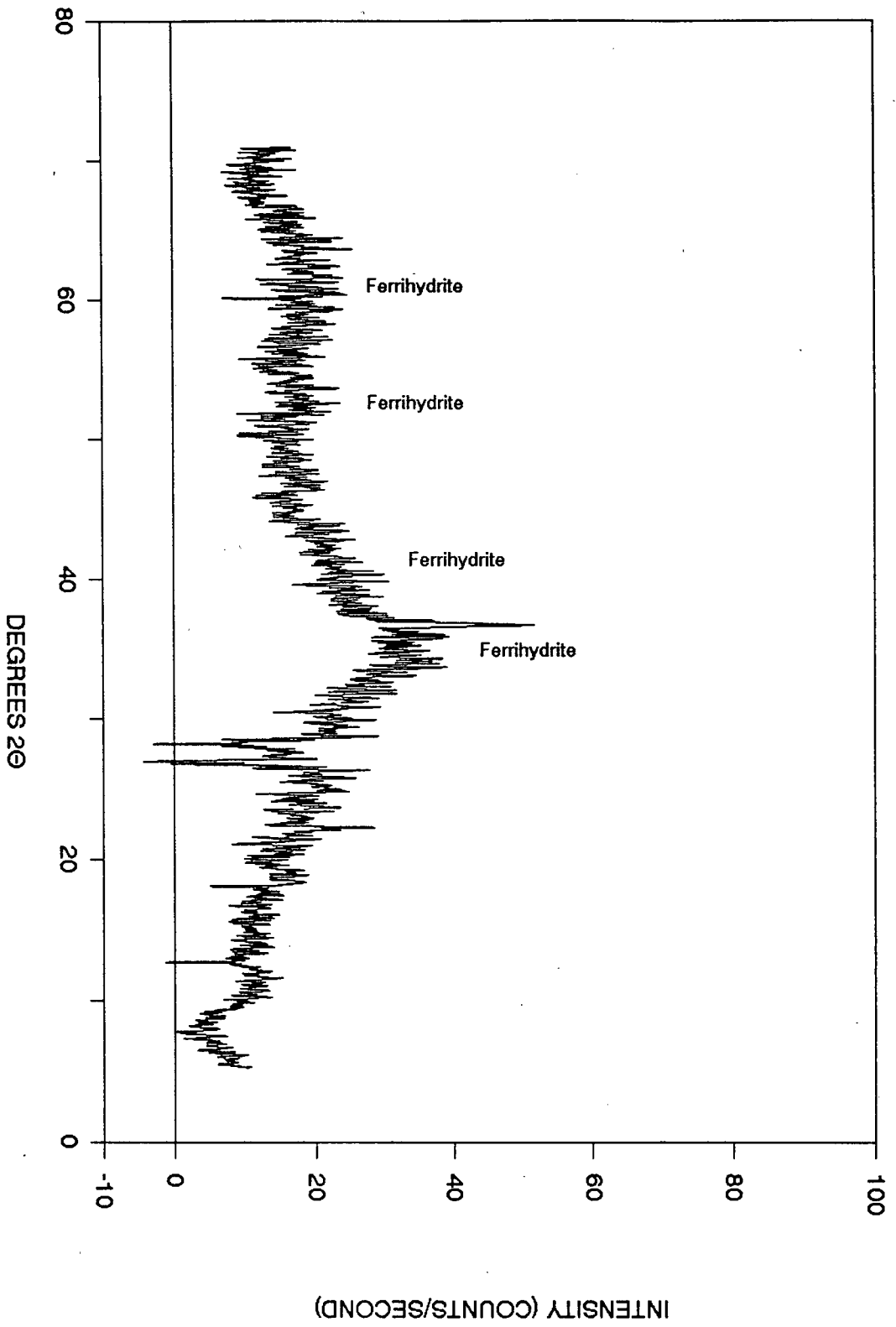


Figure 3-33. The DXRD pattern obtained after the second stage of leaching of the sequential extraction scheme on the hydrogenous and diagenetic nodules

**B 104**



**B 114**



groups of hydrothermal nodules displayed the most varied oxyhydroxide phase mineralogy of all the crust and nodule samples from this region. Mn-rich hydrothermal nodules were found to contain hausmannite and akaganéite (Figure 3-34) while the Fe-rich hydrothermal nodules were found to contain ferrihydrite (Figure 3-35).

The ferrihydrite identified in the crust and nodule samples shows a considerable variation in composition. In the hydrogenetic crusts, the ferrihydrite is found to have low concentrations of Mn, Cu, and Ni but has a wide range in Fe and Co concentrations, while in the hydrogenous and diagenetic nodules, the ferrihydrite is found to have the highest Cu, Ni, and Co concentrations but low concentrations of Mn and Fe. In the Mn-rich hydrothermal crusts and nodules, hausmannite and akaganéite is found to contain low concentrations of Fe, Cu, Ni, and Co but have the highest concentrations of Mn. It should be pointed out that the hausmannite present in the Mn-rich hydrothermal crusts has consistently higher concentrations of Mn and consistently lower concentrations of Cu, Ni, and Co compared with the hausmannite and akaganéite present in the Mn-rich hydrothermal nodules.

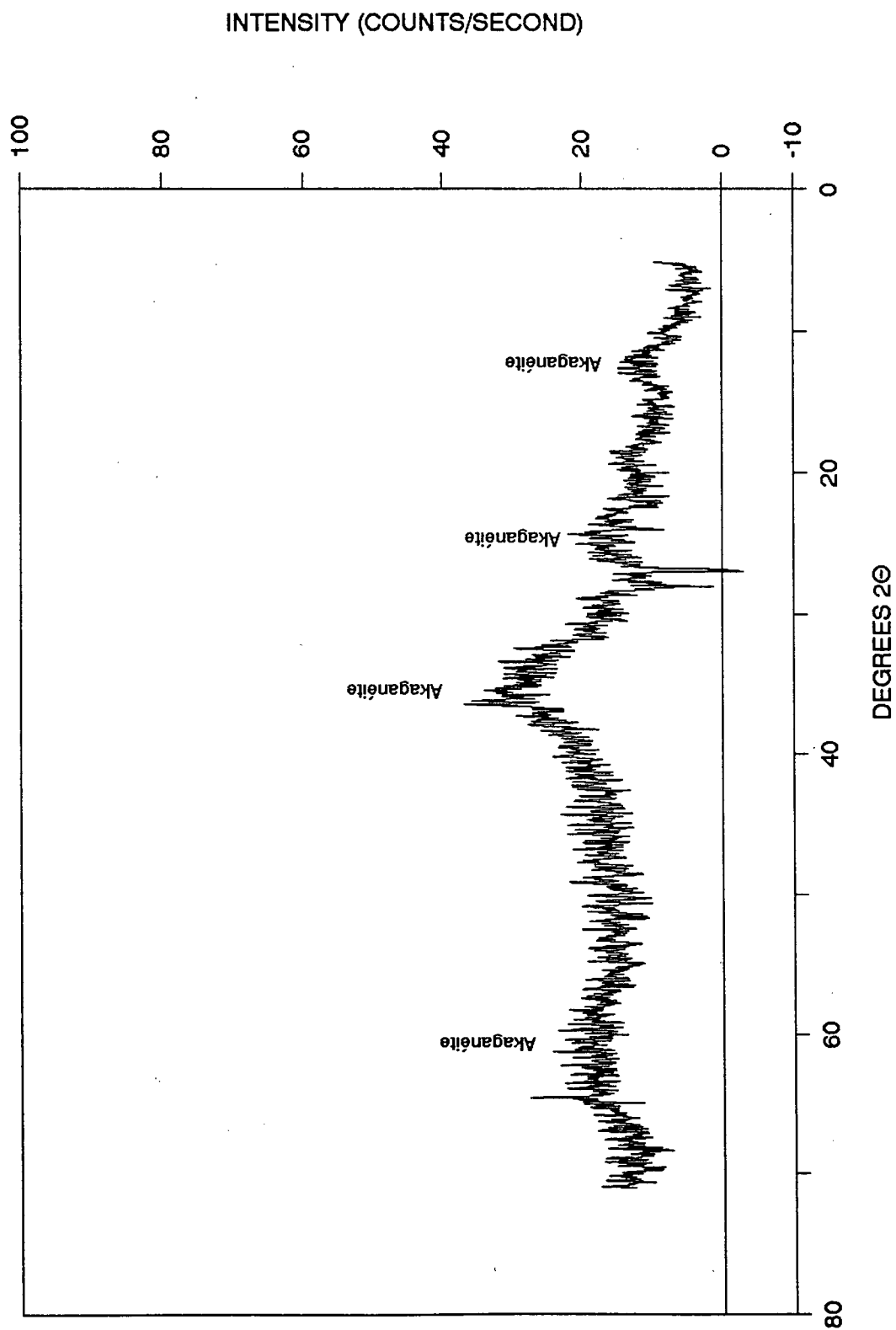
### 3.5 DISCUSSION

#### 3.5.1 MANGANESE OXIDES IDENTIFIED IN CRUSTS AND NODULES

The marine manganese oxide phases in crusts and nodules are often metastable, intimately intergrown with other materials, and poorly crystalline. The crystallography of manganese oxides found in the marine environment is characterized by numerous structural defects, essential vacancies in the crystal lattice which may or may not be ordered, domain intergrowths, extensive solid solution, and cation exchange properties. These phenomena not only lead to nonstoichiometry

Figure 3-34. The DXRD pattern obtained after the second stage of leaching of the sequential extraction scheme on the Mn-enriched hydrothermal nodules.

## CERS 20 D-2



# CERS 21 D-3

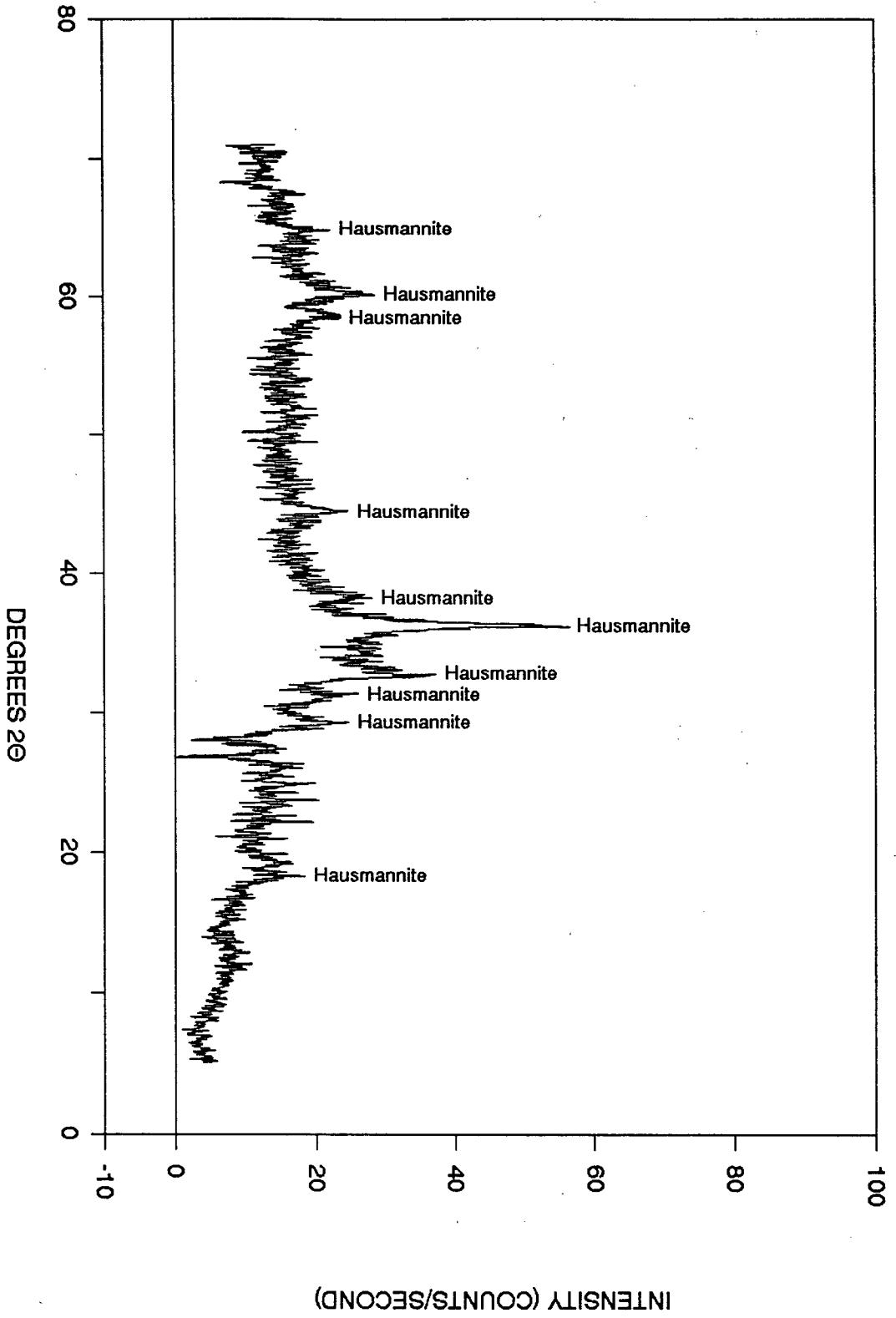
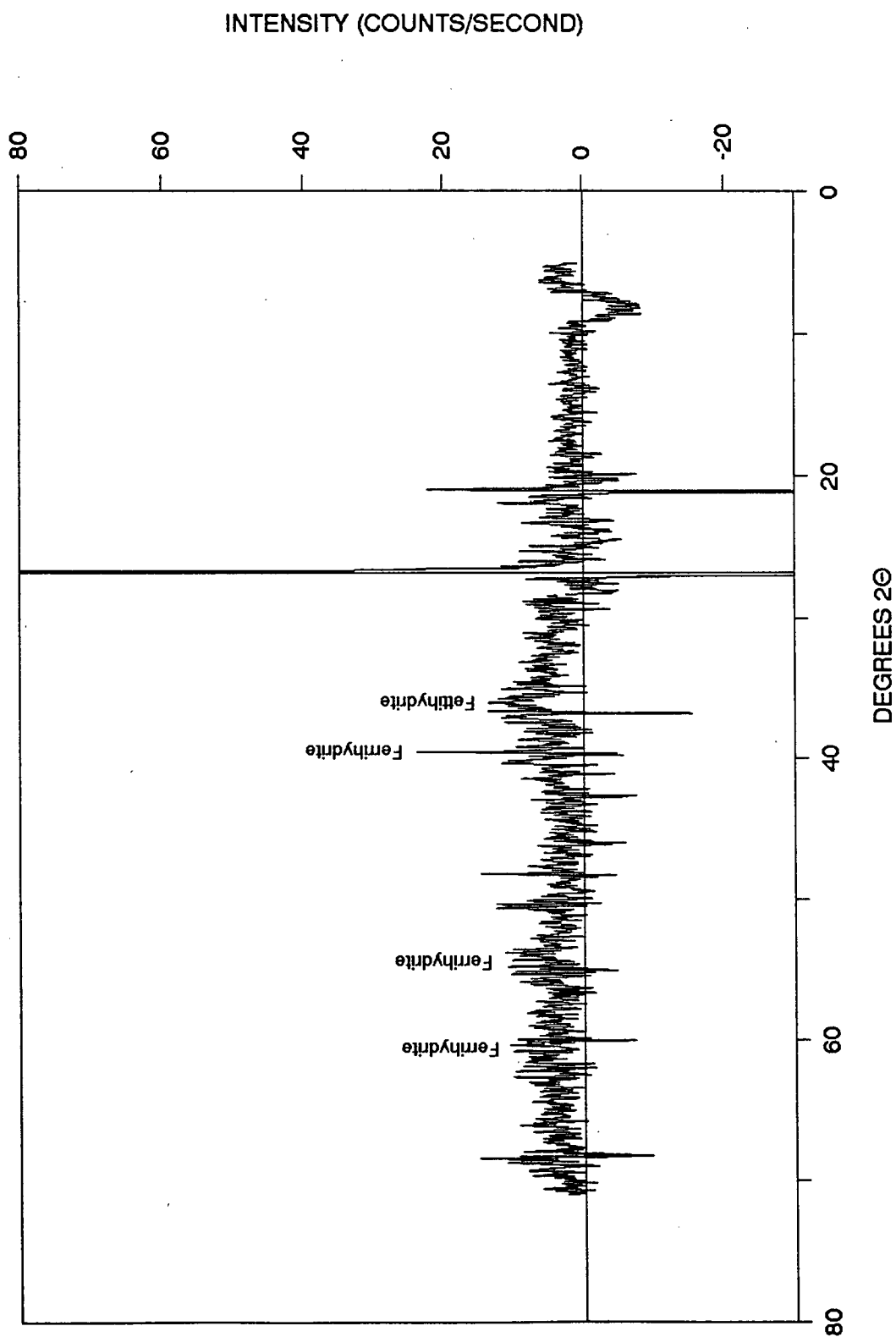
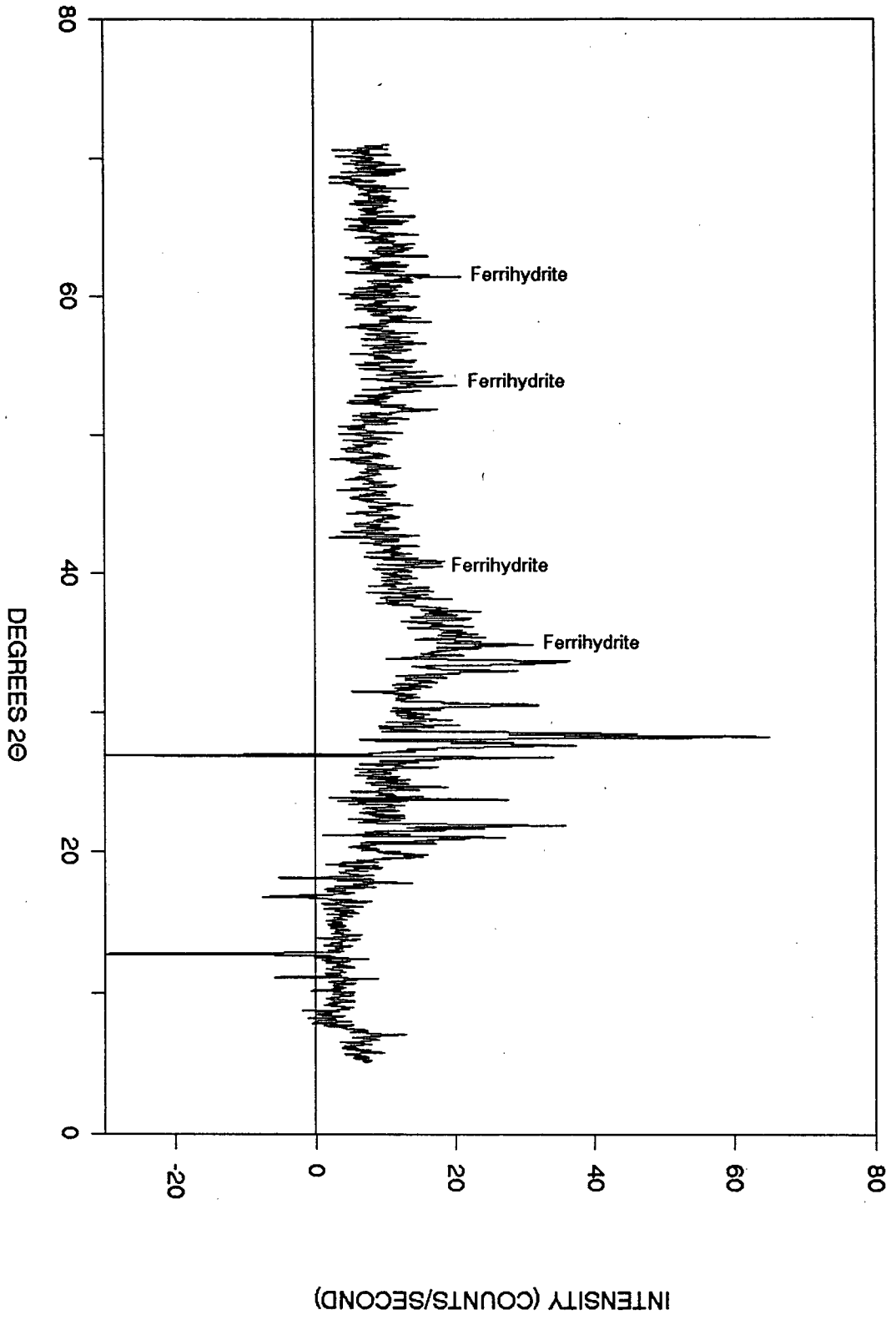




Figure 3-35. The DXRD pattern obtained after the second stage of leaching of the sequential extraction scheme on the Mn-depleted hydrothermal nodules.

**DWBD 1-2**

S 74



but detract from internal periodic long-range ordering. This makes crystal structure determination difficult and as a result has led to confusion over classification and nomenclature (Burns & Burns, 1979). Much confusion still exists about the nomenclature and structure of these minerals (Burns & Burns, 1977). Those manganese-bearing minerals that have been identified by DXRD in the crust and nodule samples selected for this study will be described.

#### 3.5.1.1 Todorokite

The marine 10Å-manganate group was first described by Buser (1959) and was termed "10Å manganite" on the basis of the similarities in X-ray diffraction patterns with synthetic 10Å "manganite". The 10Å-manganate minerals in deep-sea nodules have also been referred to as todorokite which was originally reported from a non-marine environment (Yoshimura, 1934). This dual nomenclature pervaded the literature during the 1960's (Burns & Burns, 1977) despite the complaints by Burns & Fuerstenau (1966) that the term "10Å manganite" led to confusion with the mineral manganite ( $\gamma\text{Mn}^{3+}\text{OOH}$ ).

Turner & Buseck (1981) showed by lattice images, obtained by high resolution transmission electron microscopy (HRTEM), that known todorokites from terrestrial deposits have well-ordered tunnel structures. The tunnel widths vary randomly between three and seven octahedral units. Turner *et al.* (1982) and Siegel & Turner (1983) then reported the same type of tunnel structure in a 10Å-manganate from a marine ferromanganese nodule. Todorokite is a tecktomanganate possessing a tunnel structure running parallel to the b-axis. The tunnels are composed of "walls" of triple chains of edge-shared  $[\text{MnO}_6]$  octahedra containing  $\text{Mn}^{4+}$  ions in the M1 positions and  $\text{Mn}^{2+}$  in the M2 positions. "Floors" and "ceilings" of these tunnels consist of edge-shared  $[\text{MnO}_6]$  octahedra, most commonly

three octahedra wide with  $\text{Mn}^{4+}$  ions in the M3 and M4 positions (Figure 3-36) (Burns *et al.*, 1983). These predominant  $[3 \times 3]$  tunnels are often intergrown with other tunnels ranging in dimensions from  $[3 \times 2]$  to  $[3 \times 8]$  and higher (Burns *et al.*, 1985). The very wide tunnels, obtaining dimensions of  $[3 \times 8]$  and higher, tend towards the  $[3 \times \infty]$  layered structure postulated for buserite (Burns *et al.*, 1983).

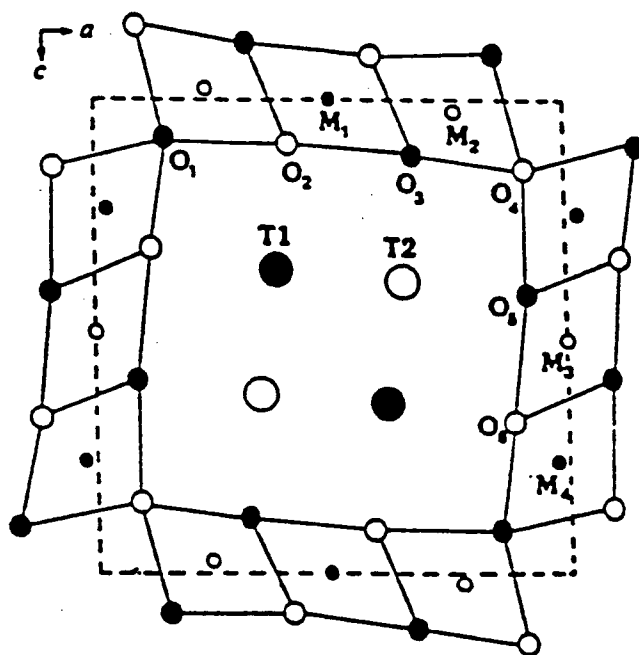
In the "ceilings" of the todorokite tunnels are cation vacancies within the bands of edge-shared  $[\text{Mn}^{4+}\text{O}_6]$  octahedra which become more prevalent with wider "ceiling" dimensions. These cation vacancies not only nucleate faults, kinks, and twinning observed in the HRTEM micrographs of todorokite fibers (Turner *et al.*, 1982), but they also influence the crystal chemistry and site occupancy of the tunnels. As a result, three types of atomic substitution contribute to the crystal chemistry of todorokite. First, substitution of  $\text{Mn}^{4+}$  cations by anions of smaller ionic radii in the "ceilings" such as low spin  $\text{Co}^{3+}$  ions (Burns, 1976). Secondly, substitution of divalent  $\text{Mn}^{2+}$  ions in the "walls" by  $\text{Mg}^{2+}$ ,  $\text{Ni}^{2+}$ ,  $\text{Cu}^{2+}$ ,  $\text{Zn}^{2+}$ , and other cations. Third, constituents of the tunnels (T1 and T2 positions) consist of large cations such as  $\text{K}^+$ ,  $\text{Ba}^{2+}$ ,  $\text{Ag}^+$ ,  $\text{Ca}^{2+}$ ,  $\text{Pb}^{2+}$ ,  $\text{Na}^+$ , and  $\text{H}_2\text{O}$  molecules (Burns *et al.*, 1983).

### 3.5.1.2 Birnessite

Another manganese oxide phase found in marine manganese crusts and nodules is birnessite. This manganese-bearing mineral phase is commonly confused with phillipsite and clay mineral groups, by X-ray diffraction, because all have d-spacings around  $7\text{\AA}$  (Burns & Burns, 1979).

It has been postulated that birnessite is a phyllomanganate similar in structure to the phyllomangnaate buserite (Chukhrov *et al.*, 1987). Birnessite is a double-layered compound consisting of sheets of water molecules and hydroxyl groups

Figure 3-36. The crystal structure of todorokite (Turner *et al.*, 1982).



- ● Manganese
- ● Oxygen
- ● Tunnel cations or water molecules

located between layers of edge-shared  $[\text{MnO}_6]$  octahedra separated by about  $7\text{\AA}$  along the c-axis. One out of every six octahedral sites in the layer of the linked  $[\text{MnO}_6]$  octahedra is unoccupied and  $\text{Mn}^{2+}$  ions are considered to lie above and below these vacancies. These low valence manganese ions are coordinated to oxygens in both the  $[\text{MnO}_6]$  layer and the  $(\text{H}_2\text{O}, \text{OH}^-)$  sheet (Figure 3-37) (Burns & Burns, 1977). Birnessite formation will occur in areas where the local conditions are moderately oxidizing and the supply of  $10\text{\AA}$  stabilizing cations is low. Toth (1980) proposed that well-crystallized birnessite would be observed in hydrothermal crusts and nodules because of the low concentrations of Co, Ni, Cu, Pb, and Ba relative to Fe and Mn in the hydrothermal solutions and because of the rapid deposition of these deposits which minimizes adsorption of elements from sea-water. Birnessite has been identified in hydrothermal crusts and nodules studied by Toth (1980) Lonsdale et al. (1980) and in the DXRD patterns obtained after the first stage of leaching on the hydrothermal crusts and nodules examined in this study.

### 3.5.1.3 $\delta\text{MnO}_2$

Under strongly oxidizing conditions, like those found on exposed rock surfaces in the ocean, the  $\text{Mn}^{2+}$  no longer exists in the  $\text{Mn}^{2+}(\text{OH})_2 \times 2\text{H}_2\text{O}$  layers to bind successive  $[\text{Mn}^{4+}\text{O}_6]$  layers together as it does in todorokite and birnessite; instead, the layers of linked  $[\text{Mn}^{4+}\text{O}_6]$  octahedra are randomly oriented and constitute the  $\delta\text{MnO}_2$  phase which does not give basal X-ray reflections (Figure 3-38) (Burns & Burns, 1979). Furthermore, it has been suggested that the poorly crystalline  $\delta\text{MnO}_2$  and not the more ordered birnessite plays an essential role in the nucleation and authigenesis of nodules through its ability to form epitaxial intergrowths with an isostructural iron (III) oxyhydroxide phase ( $\text{FeOOH} \times n\text{H}_2\text{O}$ ) (Burns & Burns, 1975).



Figure 3-37. The crystal structure of birnessite (Giovanoli & Brüttsch, 1979).

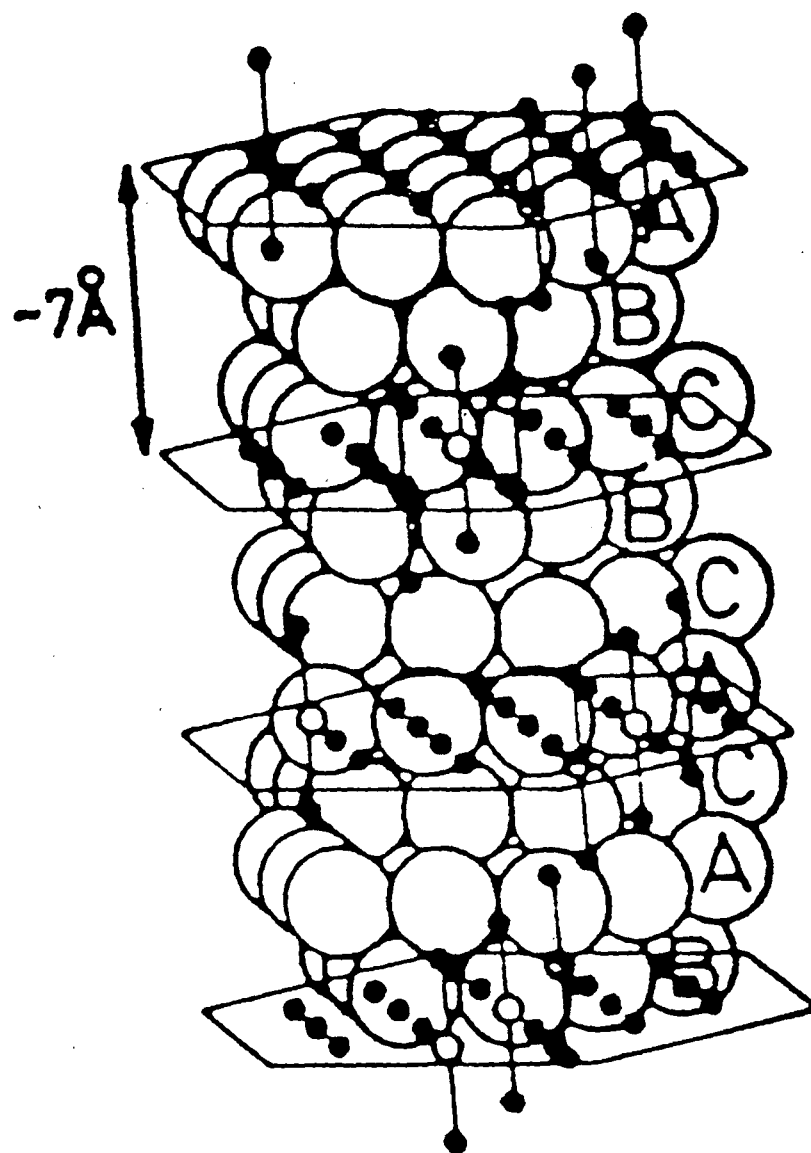
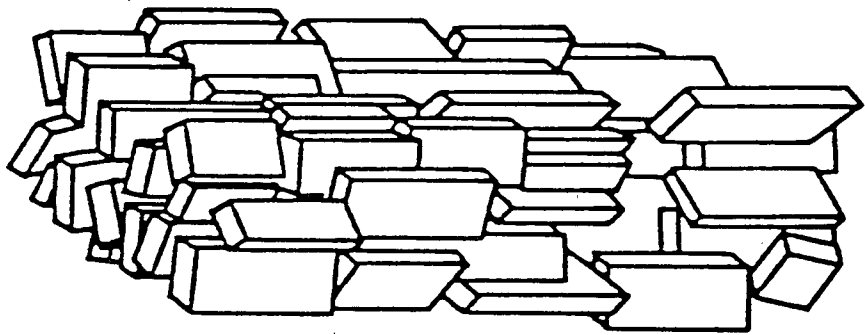


Figure 3-38. The crystal structure of  $\delta\text{MnO}_2$  (modified from Giovanoli *et al.*, 1965).

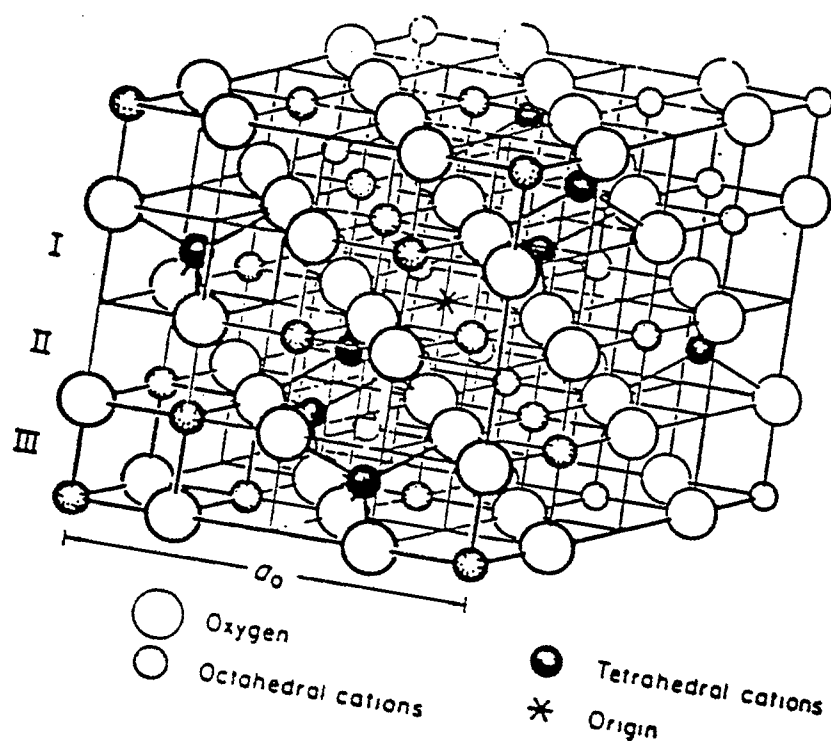


Burns & Burns (1977) regarded  $\delta\text{MnO}_2$  to be structurally-disordered birnessite. Since  $\delta\text{MnO}_2$  is characterized by a very high specific surface area and by significant Co concentrations,  $\delta\text{MnO}_2$  is regarded as a separate Mn-bearing mineral phase in the marine environment (Burns & Burns, 1979). The  $\delta\text{MnO}_2$  identified in the DXRD patterns obtained after the first stage of leaching on the crust and nodule samples in the present study contained the highest concentrations of Co compared to the concentrations of this element measured in the other Mn phase mineralogy (todorkite, birnessite, and hausmannite) and the Fe phase mineralogy (akaganéite and ferrihydrite) which was identified by DXRD.

#### 3.5.1.4 Hausmannite

The crystal structure of hausmannite is defined as a distorted spinel structure (Bricker, 1965; Giovanoli, 1985). The spinel crystal structure is characterized by a unit cell which is face-centred cubic and contains 32 oxygen ions, which forms a nearly cubic close-packed framework as viewed along the cubic diagonals [111] and manganese cations which occupy some of the interstices within the oxygen framework (Figure 3-39). By convention, there is a set of compatible tetrahedral and octahedral sites which divalent and trivalent manganese cations can occupy. These are defined as 16d (octahedral) and 8a (tetrahedral) vacancies. In a distorted spinel structure, 1/9 of the metal cation sites of the spinel structure are vacant. These vacant sites are distributed in one of two ways, either randomly distributed throughout the tetrahedral (8a) and octahedral (16d) sites or confined only to the octahedral (16d) sites. The crystal structure is not exactly that of a spinel structure because the vacancies are ordered along a particular [100] axis, the repeat distance being three times the cubic cell edge. The crystal structure is, therefore, tetragonal due to the vacancy superlattice.

Figure 3-39. The crystal structure of hausmannite (Murray, 1979).



Hausmannite has never been identified in marine manganese nodules (Burns & Burns, 1977; Murray & Dillard, 1979). von Heimendahl *et al.* (1976) did, however, identify hydrohausmannite in a nodule from the eastern equatorial Pacific. Evidence for the possible origin of hausmannite in marine manganese crusts and nodules is provided by the experimental work of Bricker (1965). Bricker (1965) was able to form synthetic hausmannite at 25°C and one atmospheric pressure. It was found that with the proper control of Eh and pH hausmannite could be preserved indefinitely. Suitable Eh and pH values were 0.5 and 6.5, respectively. Except for the low pH, the laboratory solutions were similar in temperature, acidity, and redox potential to fluids in bottom sediments in an open circulation marine environment (Krumbein & Garrels, 1952). Given this evidence, hausmannite could indeed form on the sea floor, given the requisite chemical constituents (Sorem & Gunn, 1967).

### 3.5.2 IRON OXIDES IDENTIFIED IN CRUSTS AND NODULES

The iron-bearing phases in crusts and nodules have usually been described as being cryptocrystalline or amorphous hydrated iron oxides (Glasby, 1972; Crerar & Barns, 1974). Mössbauer spectroscopic studies by Herzenberg & Riley (1969), Gager (1968), Johnson & Glasby (1969), and Carpenter & Wakeman (1973) have also led to the suggestion that the iron-bearing phase can be regarded as an amorphous ferric hydroxide or oxide-hydroxide gel ( $\text{FeOOH} \times \text{H}_2\text{O}$ ) with a particle size less than 200Å. Various authors have reported several crystalline iron-bearing phases in crusts and nodules. These phases are: goethite (Buser, 1959), akaganéite (Johnston & Glasby, 1978), lepidocrocite (Glasby, 1972), feroxyhyte (Chukhrov *et al.*, 1976), maghemite (von Heimendahl *et al.*, 1976), and ferrihydrite (Murad & Schwertmann, 1988).



The lack of any definitive understanding of the iron phase mineralogy of crusts and nodules stems from two factors: (1) the fine grain size (cryptocrystallinity) of the iron oxide/oxyhydroxide minerals; and (2) the fact that the iron is present in the octahedrally coordinated, high spin ferric state. As a result of the fine grain size, X-ray diffraction patterns have rarely been recorded for these mineral phases. Because of the symmetry of the  $d^5$  electron shell in the ferric ion, it has not yet proved possible to identify definitively the major ferric oxide/oxyhydroxide minerals present in crusts and nodules using mössbauer spectroscopy.

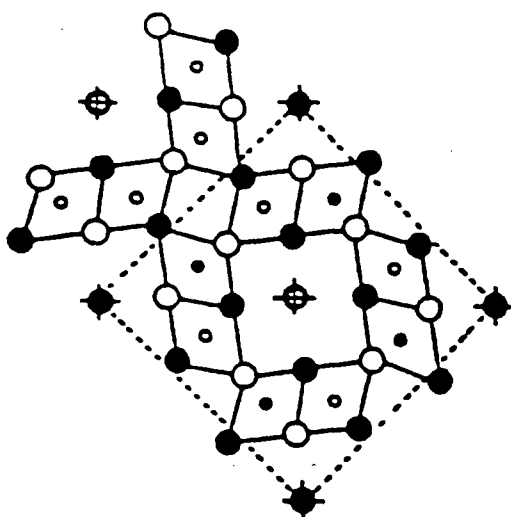
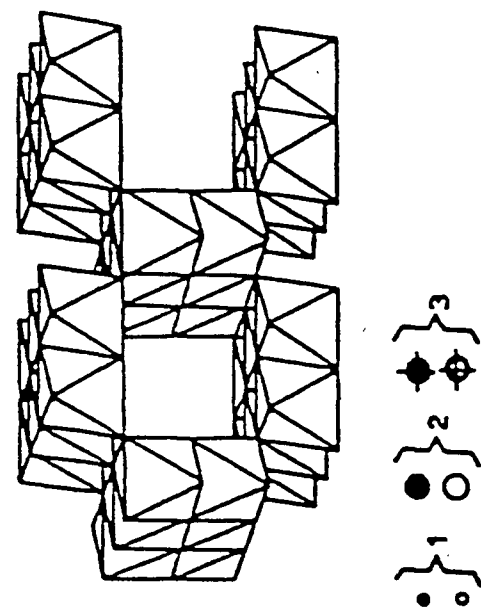
The mineralogy and crystallography of the iron-bearing minerals that have been identified in crusts and nodules has been reviewed by Burns & Burns (1977) and by Murray (1979). Those iron-bearing minerals that have been identified by DXRD in the crust and nodule samples selected for this study will be described.

#### 3.5.2.1 Akaganéite

Akaganéite ( $\beta\text{FeOOH}$ ) is characterized by tunnels that run parallel to the  $c$ -axis. In many respects akaganéite is similar in structure to the manganese mineral todorokite (Burn & Burn, 1979).  $[\text{FeO}_6]$  octahedra share edges and form double chains along the  $c$ -axis. The octahedra of the double chains share corners with adjacent double chains to form a three-dimensional framework with a body-centred trigonal unit cell (Figure 3-40). The tunnels accommodate  $\text{H}_2\text{O}$ , and  $\text{OH}^-$ ,  $\text{Cl}^-$ ,  $\text{F}^-$ ,  $\text{SO}_4^{2-}$ , and  $\text{NO}_3^-$  ions. These large ions (especially  $\text{Cl}^-$ ) are essential for the formation of this tunnelled structure (Ellis et al., 1976).

The first reported occurrence of akaganéite in marine nodules was by Goncharov *et al.* (1973). The presence of this mineral in marine nodules was discounted by Burns & Burns (1977). Since then the presence of akaganéite in

Figure 3-40. The crystal structure of akaganéite. 1 = Mn, 2 = oxygen, 3 = Ba, K, Pb, Na, or H<sub>2</sub>O (Murray, 1979).



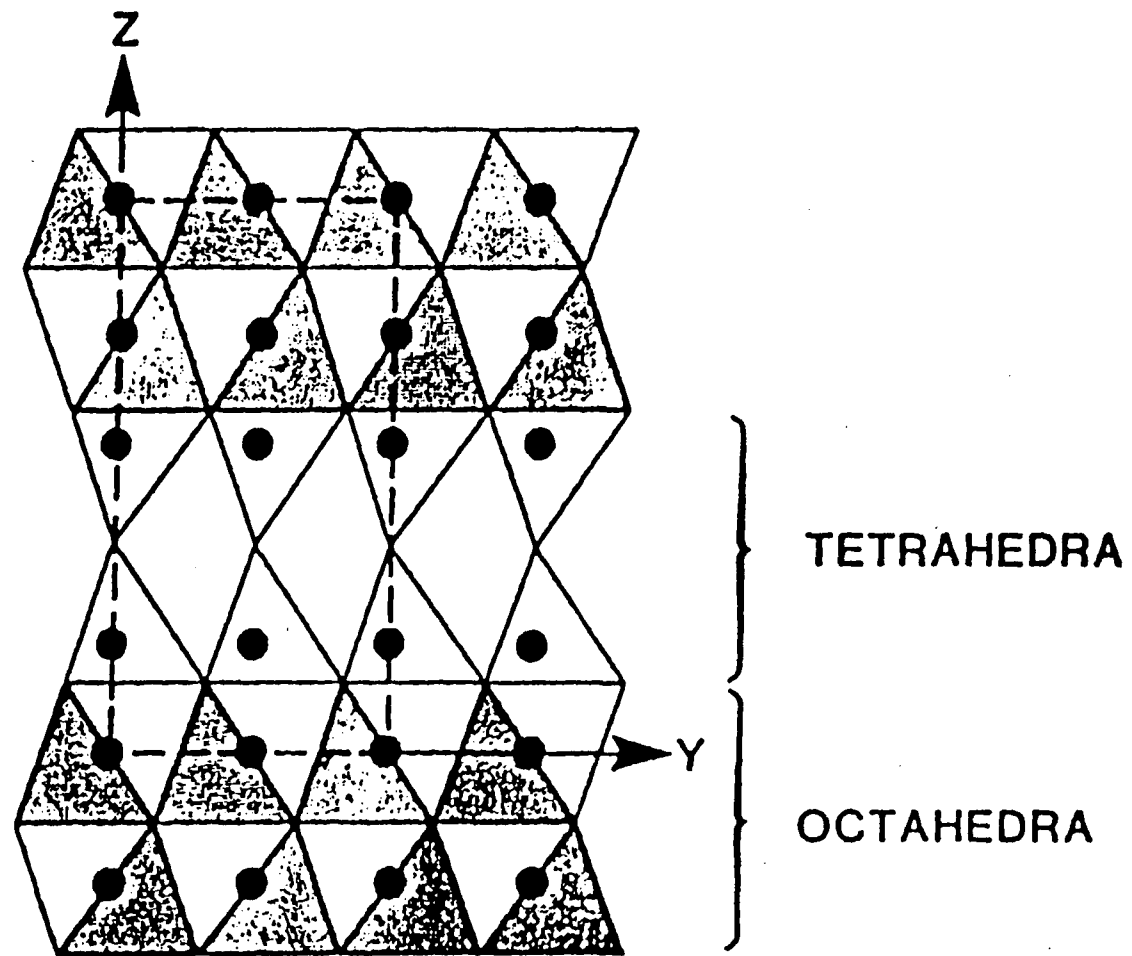
marine crusts and nodules has been reported by Johnston & Glasby (1978), Thijs *et al.* (1981), and in one Mn-rich hydrothermal crust in this study.

### 3.5.2.2 Ferrihydrite

The name ferrihydrite was first proposed for the mineral of composition  $5\text{Fe}_2\text{O}_3 \cdot 9\text{H}_2\text{O}$  by Chukhrov *et al.* (1973). The name was later accepted by the International Mineralogical Association. Eggleton & Fitzpatrick (1988) proposed that the ferrihydrite structure is based on the double-hexagonal close-packing of oxygens in an ABAC sequence. Two sheets of octahedrally coordinated iron are connected by two sheets of mixed tetrahedral and octahedral iron in the ratio 5 tetrahedral: 2 octahedral. This arrangement is similar to that of the spinels. Along the 3-fold axes of spinel, planes of oxygens in cubic close packing alternately host all octahedral iron or mixed tetrahedral and octahedral iron (Figure 3-41).

Eggleton & Fitzpatrick (1988) observed the probable presence of tetrahedrally coordinated  $\text{Fe}^{3+}$  in ferrihydrite and hypothesized that tetrahedral Si may substitute for the tetrahedral  $\text{Fe}^{3+}$ . Vempati *et al.* (in press) provided further evidence, through photoelectron spectroscopy, that tetrahedrally coordinated  $\text{Fe}^{3+}$  does exist in ferrihydrite and of tetrahedrally coordinated Si in Si-containing ferrihydrite having Si/Fe molar ratios greater than 0.10. Vempati & Loeppert (1989) studied the effect of structural and adsorbed Si in prohibiting synthetic ferrihydrite to transform into goethite and/or hematite. They noted that synthetic ferrihydrite with Si/Fe molar ratios greater than 0.10 did not transform to goethite and/or hematite. They concluded that in natural systems ferrihydrite containing adsorbed and/or coprecipitated silicate is probably influenced by the Si concentration, mechanism of silicate bonding, pH, and temperature. Siliceous ferrihydrite (Si/Fe molar ratios  $\geq 0.10$ ), formed during the coprecipitation of Fe oxides with silicate, would probably be

Figure 3-41. The crystal structure of ferrihydrite (modified from Eggleton & Fitzpatrick, 1988).



stable for extended periods of time at  $\text{pH} \geq 7$ , even at elevated temperatures. This evidence supports the fact that the ferrihydrite identified in the DXRD patterns obtained after the second stage of leaching on the crusts and nodule samples in the present study is an authentic iron oxide and not an artifact caused by the chemical leaching. This evidence is further supported the conclusions made by Murad & Schwertmann (1988) that Fe is bound to a ferrihydrite like phase that is intimately intergrown with the Mn oxides in crusts and nodules.

## 3.7 REFERENCES

- Bricker, O., 1965. Some stability relations in the system  $\text{Mn-O}_2\text{-H}_2\text{O}$  at  $25^\circ$  and one atmosphere total pressure. *American Mineralogist*, 50:1269-1354.
- Burns, R.G., 1965. Formation of cobalt (III) in the amorphous  $\text{FeOOH}\cdot n\text{H}_2\text{O}$  phase of manganese nodules. *Nature*, 203(4975):999.
- Burns, R.G., 1976. The uptake of cobalt into ferromanganese nodules, soils, and synthetic manganese (IV) oxides. *Geochim. Cosmochim. Acta*, 40:95-102.
- Burns, R.G., & Burns, V.M., 1975. Mechanism for nucleation and growth of manganese nodules. *Nature*, 255:130-131.
- Burns, R.G., & Burns, V.M., 1977. Mineralogy. In *Marine Manganese Deposits* (ed. by G.P. Glasby). Elsevier Scientific Publishing Company, Amsterdam, pp.185-248.
- Burns, R.G., & Burns, V.M., 1979. Manganese Oxides. In *Mineralogical Society of America Short Course Notes, Marine Minerals* (ed. by R.G. Burns), Vol. 6. LithoCrafters Inc., Chelsea, Michigan, pp. 1-46.
- Burns, R.G., Burns, V.M., & Stockman, H.M., 1983. A review of the todorokite-buserite problem: Implications to the mineralogy of marine manganese nodules. *American Mineralogist*, 68:972-980.
- Burns, R.G., Burns, V.M., & Stockman, H.M., 1985. The todorokite-buserite problem: Further considerations. *American Mineralogist*, 70:205-208.
- Burns, R.G., & Fuerstenau, D.W., 1966. Electron-probe determination of inter-element relationships in manganese nodules. *American Mineralogist*, 51:895-902.
- Buser, W., 1959. The nature of the iron and manganese compounds in manganese nodules. In *Scanning Electron Microscopy*, Vol. 1, SEM Inc., AMF O'Hare, IL 60666, U.S.A., pp. 245-252.
- Calvert, S.E., 1978. Geochemistry of oceanic ferromanganese deposits. *Phil. Trans. R. Soc. Lond. A.*, 290:43-73.
- Carpenter, R., & Wakeman, S., 1973. Mössbauer studies of marine and fresh water manganese nodules. *Chem. Geol.*, 11:109-116.
- Chukhrov, F.V., Drits, V.A., & Gorshkov, A.I., 1987. Structural transformations of manganese oxides in ocean nodules. *Internat. Geol. Rev.*, 29:110-121.
- Chukhrov, F.V., Zvyagin, B.B., Gorshkov, A.I., Yermilova, L.P., & Balashova, V.V., 1973. Ferrihydrite. *Internat. Geol. Rev.*, 16(10):1131-1143.
- Chukhrov, F.V., Zvyagin, B.B., Yermilova, L.P., & Gorshkov, A.I., 1976. Mineralogical criteria in the origin of marine iron-manganese nodules. *Mineral. Deposita*, 11:24-32.



- Crerar, D.A., & Barnes, H.L., 1974. Deposition of deep-sea manganese nodules. *Geochim. Cosmochim. Acta*, 38:279-300.
- Cronan, D.S., & Tooms, J.S., 1969. The geochemistry of manganese nodules and associated pelagic deposits from the Pacific and Indian Oceans. *Deep-Sea Research*, 16:335-359.
- Eggleton, R.A., & Fitzpatrick, R.W., 1988. New data and a revised structural model for ferrihydrite. *Clay and Clay Minerals*, 36(2):111-124.
- Ellis, J., Giovanoli, R., & Stumm, W., 1976. Anion exchange properties of  $\beta$ -FeOOH. *Chimia*, 30(3):194-197.
- Flanagan, F.J., & Gottfried, D., 1980. USGS rock standards, III. Manganese-nodule reference samples USGS-Nods-A-1 and USGS-Nods-P-1. U.S. Geol. Surv., Prof. Pap. 1155, 39 pp.
- Gager, H.M., 1968. Mössbauer spectra of deep-sea iron-manganese nodules. *Nature*, 220:1021-1023.
- Giovanoli, R., 1985. Layer structures and tunnel structures in manganates. *Chemie der Erde*, 44(3):227-244.
- Giovanoli, R., & Brütsch, R., 1979. Ueber die oxydhydroxide des Mn(IV) mit schichtengitter. 5. Mitteilung: Stochiometrie, austauschverhalten und die role bei der bildung von tiefsee-mangankon-kretionen. *Chimia*, 34(10):372-376.
- Giovanoli, R., Oswald, H.R., & Feitknecht, W., 1965. Étude des hydroxides de zinc cristallins instable par microscopie et microdiffraction electroniques et par diffraction des rayons X. *J. Microscopie*, 4(6):711-724.
- Glasby, G.P., 1972. The mineralogy of manganese nodules from a range of marine environments. *Mar. Geol.*, 13:57-72.
- Glasby, G.P., & Thijessen, T., 1982a. Control of the mineralogy and composition of marine manganese nodules by the supply of divalent transition metal ions. *N. Jb. Miner. Abh.*, 145:291-307.
- Goncharov, G.N., Kalyamin, A.V., & Lur'e, B.G., 1973. Iron-manganese concretions from the Pacific Ocean studied by a nuclear  $\gamma$ -resonance method. *Dokl. Akad. Nauk. S.S.S.R.*, 212:720-723.
- Halbach, P., Hebisch, U., Scherhag, C., 1981a. Geochemical variations of ferromanganese nodules and crusts from different provinces of the Pacific Ocean and their genetic control. *Chem. Geol.*, 34:3-17.
- Halbach, P., & Özkara, M., 1979. Morphological and geochemical classification of deep-sea ferromanganese nodules and its genetical interpretation. In *La genèse des nodules de manganèse*, Colloques Internationaux, C.N.R.S. No. 289, pp. 77-88.

- Halbach, P., Scherhag, C., Hebisch, U., & Marchig, V., 1981b. Geochemical and mineralogical control of different genetic types of deep-sea nodules from the Pacific Ocean. *Mineral. Deposita*, 16:59-84.
- Halbach, P., Segl, M., Puteanus, D., & Mangini, A., 1983. Co-fluxes and growth rates in ferromanganese deposits from central Pacific seamount areas. *Nature*, 304:716-719.
- Herzenberg, C.L., & Riley, D.L., 1969. Interpretation of the mössbauer spectra of marine iron-manganese nodules. *Nature*, 224:259-260.
- Johnson, C.E., & Glasby, G.P., 1969. Mössbauer affect determination of partical size in microcrystalline iron-manganese nodules. *Nature*, 222:376-377.
- Johnston, J.H., & Glasby, G.P., 1978. The secondary iron oxihydroxide mineralogy of some deep-sea and fossil manganese nodules: A mössbauer and X-ray study. *Geochim. Jour.*, 12:153-164.
- Krauskopf, K.P., 1957. Separation of manganese from iron in sedimentary processes. *Geochim. Cosmochim. Acta*, 12:61-84.
- Krumbein, W.C., & Garrels, R.M., 1952. Origin and classification of chemical sediments in terms of pH and oxidation-reduction potential. *Jour. Geol.*, 60:1-33.
- Lonsdale, P., Burns, V.M., & Fisk, M., 1980. Nodules of hydrothermal birnessite in the caldera of a young seamount. *Journ. Geol.*, 88:611-618.
- Lyle, M., 1981. Formation and growth of ferromanganese oxides on the Nazca plate. *Geol. Soc. of Amer. Mem.*, 154, pp. 269-293.
- Murad, E., & Schwertmann, U., 1988. Iron oxide mineralogy of some deep-sea ferromanganese crusts. *American Mineralogist*, 73:1395-1400.
- Murray, J.W., 1979. Iron Oxides. In *Mineralogical Society of America Short Course Notes, Marine Minerals* (ed. by R.G. Burns), Vol. 6. LithoCrafters Inc., Chelsea, Michigan, pp. 47-98.
- Murray, J.W., & Dillard, J.G., 1979. The oxidation of cobalt (II) adsorbed on manganese dioxide. *Geochim. Cosmochim. Acta*, 43:781-787.
- Price, N.B., & Calvert, S.E., 1970. Compositional variation in Pacific Ocean ferromanganese nodules and its relationship to sediment accumulation rates. *Mar. Geol.*, 9:145-171.
- Siegel, M.D., & Turner, S., 1983. Crystalline todorokite association with biogenic debris in manganese nodules. *Science*, 219:172-174.
- Sorem, R.K., & Gunn, D.W., 1967. Mineralogy of manganese deposits, Olympic Peninsula, Washington. *Econ. Geol.*, 62:22-56.
- Thijs, A., De Roy, G., Vansant, E.F., Glasby, G.P., & Thijssen, T., 1981. Mössbauer effect studies of iron in manganese nodules and associated marine sediments in five areas in the equatorial and S.W. Pacific. *Geochem. Jour.*, 15:25-37.

- Toth, J.R., 1980. Deposition of submarine crusts rich in manganese and iron. *Geol. Soc. of Amer. Bull.*, Part 1, 91:44-54.
- Turner, S., & Buseck, P.R., 1981. Todorokite: A new family of naturally occurring manganese oxides. *Science*, 212(29):1624-1626.
- Turner, S., Siegel, M.D., & Buseck, P.R., 1982. Structural features of todorokite intergrowths in manganese nodules. *Nature*, 296:841-842.
- Usui, A., & Mita, N., 1987. Comparison of manganese nodules from the northeast equatorial Pacific (cruise SO 25) with nodules from the central Pacific basin. *Geol. Jb.*, D87:287-313.
- Vempati, R.K., Loeppert, R.H., 1989. Influence of structural and adsorbed Si on the transformation of synthetic ferrihydrite. *Clays and Clay Minerals*, 37(3):273-279.
- Vempati, R.K., Loeppert, R.H., & Cocke, D.L., in press. Mineralogy and reactivity of Si-ferrihydrite. *Solid State Ionics*.
- von Heimandahl, M., Hubred, G.L., Fuerstenau, D.W., & Thomas, G., 1976. A transmission electron microscope study of deep-sea manganese nodules. *Deep-Sea Research*, 23:69-79.
- Yoshimura, T., 1934. Todorokite, a new manganese mineral from the Todoroki Mine, Hokkaido, Japan. *J. Fac. Sci., Hokkaido Univ. Sapporo, Ser. 4*, 2:289-297.

## **CHAPTER 4**

### **SUMMARY OF PRINCIPAL RESULTS**

## 4.1 RESULTS FROM CHAPTER 1

### 4.1.1 REGIONAL VARIATIONS IN THE GEOCHEMISTRY OF CRUSTS AND NODULES

#### 4.1.1.1 Survey Region A

Using the elemental ratio of Mn/Fe, the association of the major elements with either of the major oxide phases in the crusts from Survey Region A became more apparent. Elements correlated with the manganese phase mineralogy show a positive linear correlation with the Mn/Fe ratio. In the present case, these include Ba, Ni, Zn, and Co. Elements associated with the unidentified iron phase mineralogy show a negative correlation with the Mn/Fe ratio; these elements include Ti and Na. Hein *et al.* (in press a) identified the same correlations in crusts from the central Pacific. They noted however that the degree of the correlations vary from area to area.

Crusts derive most of their metal content from dissolved and particulate matter in ambient bottom water, in proportions modified by the variable scavenging efficiency of the manganese and iron oxide phase mineralogy for susceptible ions (Manheim & Lane-Bostwick, 1988). This model is supported by the striking resemblance between the crust/seawater trace metal enrichment sequence and laboratory determined oxide-trace metal selectivity sequences (Aplin & Cronan, 1985). Cobalt along with Ba, Ni, and Zn are fixed by lattice substitution for  $\text{Mn}^{4+}$  in the  $\text{MnO}_2$  or by coprecipitation of  $\text{CoO}_2$  with manganese oxide (Hem, 1978). The reason that Co is enriched in  $\delta\text{MnO}_2$  to a greater degree than are Ni, Zn, and Ba is because  $\text{Co}^{2+}$  is oxidized to  $\text{Co}^{3+}$  on the surface of the  $\text{MnO}_2$ . Cobalt (III) is less

soluble and therefore more stable in the marine environment (Goldberg, 1954; Dillard *et al.*, 1982; Halbach *et al.*, 1983; Aplin & Cronan, 1985).

Not only does there exist interelement associations in crusts from this region, but for crusts from the Hawaiian Archipelago there also exists a correlation between the major element contents and water depth. Manganese and those minor metals that are correlated with manganese (Zn, Ba, Co, Ni, and Cu) all show a decrease in concentration with increasing water depth, while those elements that show a correlation with iron (Na, and Ti) all show an increase in concentration with increasing water depth.

To understand the correlation between crust geochemistry and water depth, the source of constituent elements must be identified. Halbach & Puteanus (1984) have proposed that the main Fe source for hydrogenetic crusts of this region is colloidal Fe-hydroxide particles that are released in the water column from the dissolution of carbonate plankton skeletons. On the other hand, the source of Mn to hydrogenetic crusts evidently cannot be derived solely from this same source. They concluded that a further source of Mn enrichment following carbonate dissolution is necessary, and this is supplied via the Oxygen Minimum Zone (OMZ).

The extent of the OMZ in the central equatorial Pacific lies at water depths of between 503 and 2296m, and the minimum dissolved oxygen concentration is  $26\mu\text{mole/kg}$ . Within the OMZ there is a high concentration of dissolved Mn as a result of the *in situ* decomposition of organic matter along with the *in situ* reduction of Mn-bearing solid phases (Klinkhammer & Bender, 1980; Landing & Bruland, 1980). This zone of maximum concentration of  $\text{Mn}^{2+}$  produces a flux of  $\text{Mn}^{2+}$  by diffusion and turbulent mixing into shallower and deeper waters which have an increased oxygen content. This causes oxidation of the  $\text{Mn}^{2+}$  and results in the formation of hydrated  $\text{MnO}_2$  particles which are incorporated into the crusts (Halbach *et al.*, 1988). As noted by Halbach *et al.* (1983), an increasing supply of Fe

and its associated trace metals from the dissolution of calcite skeletons has a diluting effect on the concentration of Mn and its associated trace metals, that is the concentration of Mn and its associated trace metals should decrease with increasing water depth down to the CCD. This trend has also been observed by Halbach *et al.* (1983), Aplin & Cronan, (1985), and by Hein *et al.* (in press b).

Although  $\delta\text{MnO}_2$  is the most common manganese mineral present, todorokite also occurs in low abundances. The relative abundances of todorokite and  $\delta\text{MnO}_2$  in crusts from this region also appear to show a variation with water depth. Todorokite is more abundant in crusts located within the OMZ. As discussed by Glasby (1972), the redox potential in the environment of formation of ferromanganese deposits controls the manganese phase mineralogy. The depletion of oxygen in the OMZ to values of around  $26\mu\text{mole/kg}$  results in an environment with a lower redox potential. These lower redox potentials combined with the high  $\text{Mn}^{2+}$  concentrations will result in manganese oxyhydroxides being precipitated as todorokite, where the  $\text{Mn}^{2+}(\text{OH})_2 \times 2\text{H}_2\text{O}$  layers bind successive  $[\text{Mn}^{4+}\text{O}_6]$  octahedra together. Below the OMZ, oxygen is more plentiful, this results in higher redox potentials, and combined with the low concentration of  $\text{Mn}^{2+}$  the layers of linked  $[\text{Mn}^{4+}\text{O}_6]$  octahedra are randomly oriented and constitute the  $\delta\text{MnO}_2$  phase (Burns & Burns, 1979).

Although there appears to be a general correlation between crust geochemistry and water depth for crusts from the Hawaiian Archipelago, crusts from the Line Island Archipelago show a very wide range in composition over a very small range in water depth. This variability is related to location; the concentrations of Mn, Ni, Zn, Cu, Co, and Ba decrease from the Equator towards the northwest along the Line Island Archipelago, while the concentrations of Fe, Ti, and Na increase with distance away from the Equator in the same direction.

This variation in the regional geochemistry of crusts from the Line Island Archipelago has also been observed by Halbach *et al.* (1982) and by Halbach & Puteanus (1984). They proposed that although this correlation is not well understood, the processes likely to control these regional trends include deep and intermediate-depth current systems, biological productivity, differences in the position of the CCD, and the degree of depletion of oxygen in and the vertical extent of the OMZ zone.

Although not the first, Halbach & Özkara (1979) used the Mn/Fe ratio as a criterion for distinguishing between different types of nodules. They suggested that nodules with an Mn/Fe ratio less than 2.5 were predominantly hydrogenous in origin, while nodules with an Mn/Fe ratio above 2.5 were mainly diagenetic in origin. Nodules from Survey Region A can also be divided into these two groups, and there is a marked compositional distinction between them. Hydrogenous nodules are depleted in Mn, Cu, Ni, Zn, Mg, and Ba compared to the diagenetic nodules whereas hydrogenous nodules are enriched in Fe and Ti compared to the diagenetic nodules. It can therefore be stated that the abundances of Cu, Ni, Zn, Mg, and Ba are correlated with Mn and that the abundance of Ti is correlated with Fe.

Apart from Co and Zn, there is a non-linear correlation between those elements that are associated with Mn. The slope of the regression line for the hydrogenous nodules is greater than that of the diagenetic nodules. A non-linear correlation between Ni and Cu versus the Mn/Fe ratio has also been observed by Halbach *et al.* (1981b) in nodules from the Northeast Pacific nodule belt and by Usui & Mita (1987) in nodules from the three survey areas of SONNE Cruise SO-25 in the Northeast equatorial Pacific. Halbach *et al.* (1981b) concluded that their non-linear regressions describe the natural saturation of divalent cations in the lattice of todorokite. The decrease in the slope of the first order regression lines from the hydrogenous nodules to the diagenetic nodules recovered from Survey Region A can



therefore be attributed to the saturation of the todorokite crystal lattice by manganese and associated divalent cations. The relationship between Zn and Mn/Fe does not show the same behaviour as the other elements associated with manganese. The reason for this is probably because of the low concentration of zinc in the nodules from this region compared to the other elements. Zinc, therefore, does not become saturated in the todorokite lattice structure.

The Cu/Ni ratio shows a strong positive correlation with the Mn/Fe ratio. Hydrogenous nodules are found to have generally lower Cu/Ni ratios when compared to diagenetic nodules. This relationship has also been observed by Raab (1972), Calvert & Price (1977), and Calvert *et al.* (1978). The reason for this correlation can be explained by examining the behaviour of Cu and Ni during diagenesis. Work on the trace metal geochemistry of pelagic sediment pore waters by Klinkhammer (1980), Callender & Bowser (1980), and by Klinkhammer *et al.* (1982) has shown that Cu and Ni behave quite differently during diagenesis in marine sediments. During diagenesis, Ni follows Mn, apparently being taken up by solid Mn phases close to the sediment surface and is released to the pore water along with Mn at depth. In contrast, Cu is released to the pore water very close to the sediment surface where it can diffuse both into the bottom water and into the sediment. These different behaviours are consistent with the Cu-enrichment in the most markedly diagenetic nodules at Survey Region A.

It has already been shown that the abundance of Ti is correlated with the presence of Fe. When Ti is plotted against Mn/Fe there is a sharp break in the slope of the first order regression line drawn through the hydrogenous nodules compared to one drawn through the diagenetic nodules, the slope for the hydrogenous nodules being greater than that for the diagenetic nodules. Since Ti is correlated with Fe, this change in the slope of the first order regression lines is the inverse of that displayed by those elements (except Co and Zn) that correlate with Mn. Just like the

saturation of the todorokite crystal lattice with Mn and its associated divalent cations, the change in the slopes of the first order regression lines from the hydrogenous nodules to the diagenetic nodules can be interpreted as the saturation of the crystal lattice of the unidentified iron oxyhydroxide with Ti.

Cobalt shows a complex association with Mn and Fe, which is unlike that of the other minor elements. In hydrogenous nodules, Co is positively correlated with Mn, whereas in diagenetic nodules Co is positively correlated with Fe. The complex association of Co with the manganese and iron oxide phases have been previously observed by Cronan & Tooms (1969), Price & Calvert (1970) and by Halbach *et al.* (1983). Price & Calvert (1970) suggested that this observed complex behaviour of Co in nodules is due to  $\text{Co}^{3+}$  substituting for  $\text{Mn}^{4+}$  in nodules containing  $\delta\text{MnO}_2$  as well as  $\text{Fe}^{3+}$  in the iron oxyhydroxide phases. Cobalt (III) ( $d^6$ ) is stable when in the low spin state with octahedral coordination and has an ionic radius almost identical to that of  $\text{Fe}^{3+}$  or  $\text{Mn}^{4+}$ . Cobalt (III) will therefore preferentially substitute for both  $\text{Fe}^{3+}$  in the  $\text{FeOOH} \times n\text{H}_2\text{O}$  phase (Burns, 1965) and  $\text{Mn}^{4+}$  in the  $\delta\text{MnO}_2$  phase (Glasby & Thijessen, 1982; Halbach *et al.*, 1981a). As noted previously,  $\text{Co}^{3+}$  will also substitute for  $\text{Mn}^{4+}$  in the "ceilings" of todorokite (Burns, 1976). Since hydrogenous nodules contain both  $\delta\text{MnO}_2$  and todorokite, this would explain the positive association of Co with Mn. Diagenetic nodules, on the other hand, contain mostly todorokite. Although the substitution of  $\text{Co}^{3+}$  for  $\text{Mn}^{4+}$  in the "ceilings" of todorokite probably occurs, the substitution of  $\text{Co}^{3+}$  for  $\text{Fe}^{3+}$  in the  $\text{FeOOH} \times n\text{H}_2\text{O}$  phase appears to be more dominant as seen by the correlation of Co with Fe in these nodules.

#### 4.1.1.2 Survey Region B

Two groups of crusts with distinct end-member compositions and mineralogy were identified in the crusts from Survey Region B. One group of crusts was found to be enriched in Mn and depleted in Fe and Si. The Mn-rich mineral phase was identified to be todorokite and birnessite. The second group of crusts was found to be enriched in Fe and Si and depleted in Mn. The Fe-Si rich mineral phase was identified as amorphous hydrated iron oxides and silica. Both groups of hydrothermal crusts were depleted in Co, Cu, and Ni. Because of the different geochemical behaviours of Fe and Mn, fractionation of the two elements is common in hydrothermal solutions (Lyle, 1981). This results in the formation of two distinct end member deposits: (1) Manganese-rich well-crystallized birnessite and todorokite crusts with generally very low trace metal content, and (2) Iron- and silica-rich crusts composed of iron-rich nontronite or amorphous hydrated iron oxides and silica, also with very low trace metal contents. The fractionation of Fe and Mn occurs as a result of the lower solubility of iron species as both Fe and Mn undergo oxidation (Krauskopf, 1957) by mixing of the reduced hydrothermal fluid with oxygenated bottom water. The association of Si with Fe may result from coprecipitation or adsorption of dissolved  $\text{SiO}_2$  onto hydrated iron-oxide colloids during this process. The low content of minor elements in these deposits results from: (1) the low concentrations of these elements relative to Fe and Mn in hydrothermal solutions, and (2) the rapid deposition of the deposits which minimizes adsorption of elements from seawater (Toth, 1980).

Unlike crusts, nodules do not form by the direct precipitation of hydrothermal fluids; however, two groups of nodules from Survey Region B showed identical trends in composition and mineralogy to those shown by the two groups of hydrothermal crusts. One group of hydrothermal nodules was found to be enriched

in Mn and depleted in Fe and Si. The Mn-rich mineral phase was identified as todorokite and birnessite. The second group of hydrothermal nodules was found to be enriched in Fe and Si and depleted in Mn. The Fe-Si rich mineral phase was identified as iron-rich nontronite. Both groups of hydrothermal nodules were depleted in Co, Cu, and Ni.

The two types of hydrothermal nodules with these distinct end-member compositions and mineralogies have also been identified by Dymond *et al.* (1984) and by Chen & Owen (1989) in nodules from the eastern equatorial Pacific. Dymond *et al.* (1984) proposed that the chemical composition of nodules from the three MANOP sites can be accounted for in a qualitative way by variable contributions of distinct accretionary processes. They proposed that these accretionary modes are: (1) hydrogenous, the direct precipitation or accumulation of colloidal metal oxides from seawater; (2) oxic diagenesis, the variety of ferromanganese accretion processes occurring in oxic sediments; and (3) suboxic diagenesis, the reduction of  $\text{Mn}^{4+}$  by oxidation of organic matter in the sediments. They concluded that processes (1) and (2) occurred at all three MANOP sites and process (3) occurs only at site H, the hemipelagic site. Chen & Owen (1989) used these results to interpret the factor analysis of geochemical data from nodules representing a broad area of the southeast Pacific Ocean. They concluded that nodule compositions are controlled by four processes. Three of the four processes are discussed by Dymond *et al.* (1984) while the fourth process is hydrothermal precipitation.

Chen & Owen (1989) identified hydrothermal nodules as those enriched in Fe but depleted in Mn, Co, Cu, and Ni. These are the same criteria used by Toth (1980) and correspond with the Fe-Si rich hydrothermal crusts and nodules identified in Survey Region B in this thesis. Both Dymond *et al.* (1984) and Chen & Owen (1989), however, misidentified the Mn-rich hydrothermal nodules. Dymond *et al.* (1984) stated that suboxic diagenesis results in the accretion of material which is Mn-rich but

depleted in other transition metals. They further stated that suboxic diagenesis results in an unstable todorokite that transforms to a  $7\text{\AA}$  phase (birnessite) upon dehydration. From their limited growth rate data for nodules from MANOP site H, they also concluded that suboxic accretion is the fastest of the three processes with rates of at least  $200\text{mm}/10^6\text{yr}$ . The compositions of the suboxic diagenetic nodules described by Dymond *et al.* (1984) and by Chen & Owen (1989) are identical in composition and mineralogy to both the Mn-rich hydrothermal crusts and nodules from Survey Region B and the Mn-rich crusts studied by Toth (1980). Although no growth rates have been determined for nodules that have been identified as being hydrothermal, rapid growth rates of greater than  $100\text{mm}/\text{Myr}$  for hydrothermal crusts located near the EPR have been proposed by Manheim & Lane-Bostwick (1988), Toth (1980), and Moore & Vogt (1976).

The composition of the nodules from Survey Region B also indicates that there is a negative correlation between the concentration of Co in nodules from Survey Region B and their proximity to the hydrothermal discharge from the EPR. As proposed by Manheim & Lane-Bostwick (1988), the depletion of Co in Pacific crusts corresponds to the location and intensity of submarine hydrothermal discharge. They found that Co-enriched crusts are found where water masses are most isolated from hydrothermal activity. In contrast, cobalt-depleted crusts coincide with known areas of hydrothermal activity. This same association between the depletion of Co and the location and intensity of hydrothermal discharge seems to apply to the nodules recovered from Survey Region B. Those nodules that are located close to the EPR in water depths of about 3000m and have Co concentrations below 0.05 weight per cent. Those nodules located farthest away from the EPR in deeper water are enriched in Co ( $> 0.20$  weight per cent). This is the first time that the depletion of Co due to the hydrothermal influence of the EPR

has been noted in oceanic ferromanganese nodules from the Eastern Equatorial Pacific.

## 4.2 RESULTS FROM CHAPTER 2

### 4.2.1 SELECTIVE SEQUENTIAL EXTRACTION SCHEME

A two stage selective sequential extraction scheme was developed to first remove the manganese then the iron phase mineralogy in marine crusts and nodules. For the first stage of the selective sequential extraction scheme, one gram of sample and 83mL of reagent were sequentially measured into an acid washed 125mL Nalgene® polyethylene bottle and capped. The sample was then placed onto an orbital shaker set at 85rpm and allowed to equilibrate for eight hours, after which the residue and leachate were separated by centrifugation for 20min at 3000rpm. The leachate was decanted into a 100mL volumetric flask and the residue was washed three times with 0.1M  $\text{NH}_2\text{OH}\cdot\text{HCl}$  in 0.01M  $\text{HNO}_3$  and centrifuged again for 20min at 3000rpm. Each wash was combined with the leachate, made up to volume with 0.1M  $\text{NH}_2\text{OH}\cdot\text{HCl}$  in 0.01M  $\text{HNO}_3$  and stored in an acid washed 125mL Nalgene® polyethylene bottle. The residue was washed three times with distilled deionized water, centrifuged for 20min at 3000rpm and freeze dried.

Depending on how much residue remained after the first stage of the extraction scheme, an appropriate amount of 0.175M Ammonium Oxalate in 0.1M Oxalic Acid was added to the residue in the plastic bottle to maintain a sample to solution ratio of 1:250 for the second stage of the selective sequential extraction scheme. The capped bottle was then shaken at 85rpm for eight hours in the dark. The residue was then separated from the leachate using the methods described above.

The concentrations of Mn, Fe, Cu, Ni, and Co in the leachates were determined by atomic adsorption spectrometry using a Perkin-Elmer 560® spectrometer. The concentrations of Mn, Fe, Cu, Ni, and Co in the leachate was then determined by plotting their measured absorbance values onto the calibration curves.

Some partitioning of Mn, Fe, Cu, Ni, and Co in the laboratory standard crust and nodule is evident from the results of the selective sequential extraction scheme. For both the laboratory standard crust and nodule, the leachates from the first stage of leaching both contain a large concentration of Mn, with only minor amounts of Fe, while the leachates from the second stage of leaching contain a higher concentration of Fe with only minor amounts of Mn. The behaviour of Cu, Ni, and Co in the leachates from the two stages of the extraction scheme are distinctively different for the laboratory standard crust and nodule. For the crust, the leachates from the first stage contain higher concentrations of Ni and Co when compared to the leachates from the second stage, whereas Cu is higher in the second stage leachates. For the the nodule, the leachate from the first stage contains a higher concentration of Cu when compared to the leachate from the second stage. The same is observed for Ni except not to the same extreme. For Co, however, equal amounts of Co are extracted from both the first and second stage of leaching.

The sample precision for the first stage of leaching was found to vary from 0.00% (Cu and Ni) up to 9.33% (Fe) (C.V.). The sample precision for the second stage of leaching was found to vary from 2.12 (Mn) up to 28.57% (Ni) (C.V.). In most cases the C.V. for the second stage of leaching was found to be greater than for the first stage of leaching. When using 0.1M  $\text{NH}_2\text{OH}\cdot\text{HCl}$  in 0.01M  $\text{HNO}_3$  to prepare the standards for the atomic absorbtion spectrometer, the instrumental precision was found to vary between 0.44 (Mn) and 1.57% (Co) (C.V.). When using 0.175M Ammonium Oxalate in 0.1M Oxalic Acid to prepare the standards for the

atomic absorption spectrometer, the instrumental precision was found to vary between 0.00 (Ni) and 2.86% (Co) (C.V.). The C.V. for the instrumental precision for both reagents was found to be far smaller than sample precision for both stages of the selective sequential extraction scheme.

The accuracy of the methods used to determine the concentrations of Mn, Fe, Cu, Ni, and Co in the leachates was checked by comparing the analytical results of the sum of the two stages of leaching to the known concentrations of these elements in the crust and nodule as determined by XRF. The selective extractions remove all of the Mn, Cu, Ni, and Co from both crusts and nodules. The concentration of Fe is lower in the leachates because the XRF results include Fe in the aluminosilicate fraction.

#### 4.2.2 DIFFERENTIAL X-RAY DIFFRACTION TECHNIQUE

A differential X-ray diffraction technique was also developed to identify the manganese and iron phase mineralogy in marine crusts and nodules removed during the selective sequential extraction scheme. Samples were analyzed by a Philips® X-ray diffractometer. The samples were step scanned from  $5^\circ$  to  $71^\circ 2\theta$  in  $0.01^\circ 2\theta$  increments, using a counting time of one second per increment. The number of counts measured at each  $0.01^\circ 2\theta$  were therefore a measure of the intensity (counts/second) at each  $0.01^\circ 2\theta$  increment. Instead of sending the intensity along with the degrees  $2\theta$  to the ratemeter to produce a diffractogram, they were sent to the computer and stored in an ASCII file. The digitized XRD spectra, stored in an ASCII file, was subjected to a 17 point smoothing using a computer program written by Savitzky & Golay (1964). The new XRD spectra, devoid of excess noise, was stored in a new ASCII file.



Because of the removal of the targeted mineral phases, the remaining minerals are concentrated, and the mass adsorption coefficient of the sample may be changed. The result is that the XRD pattern from the treated sample generally has a greater overall intensity than that of the untreated sample. However, relative intensities within the two patterns should remain essentially the same. To subtract the XRD pattern of the treated sample from the XRD of the untreated sample, the peaks common to both must have the same height or intensity. To accomplish this, all of the points in the pattern from the treated sample must be multiplied by a scale factor. Subtraction of this scaled pattern from the pattern of the untreated sample then produces the DXRD diffractogram. This can be expressed mathematically as:

$$A_i - kB_i = C_i$$

where  $A_i$ ,  $B_i$ , and  $C_i$  are the number of counts at angle  $i$  in the untreated, treated, and subtracted spectra, respectively, and  $k$  is the scale factor.

The most effective way of determining the scale factor is by using an internal standard as proposed by Bryant *et al.* (1983). The internal standard can also be used to correct for errors in alignment or sample positioning in the X-ray beam, so that the positions of the peaks of the removed mineral phases may be more accurately determined. Since almost all crusts and nodules contain quartz, it is appropriate to use this mineral as an internal standard.

To determine the value of the scale factor  $k$ , it must be remembered that the goal of subtracting the treated from the untreated XRD pattern is to remove the presence of the aluminosilicates and any other mineral phases not affected by the chemical dissolution. To remove the presence of the aluminosilicates the following situation must exist.

$$A_i - kB_i = 0$$

It is now a simple procedure of dividing the intensity of the 3.34Å quartz peak from the untreated XRD pattern by the 3.34Å quartz peak from the treated XRD pattern.

$$A_i/B_i = k$$

The intensities of the treated XRD pattern ( $B_i$ ) must now be multiplied by the value of  $k$  and subtracted from the intensities of the untreated XRD pattern ( $A_i$ ) to produce the intensities of the DXRD pattern ( $C_i$ ). This was a simple procedure when both smoothed ASCII files for the untreated and treated XRD patterns are imported into LOTUS 123® and the repetitious calculations are preformed by the program.

The graphs of the untreated, treated, and DXRD diffractograms were initially plotted by using LOTUS 123®. These graphs were then imported into LOTUS FREELANCE PLUS® where they were horizontally rotated to fill an entire page in landscape mode. An added advantage of using LOTUS FREELANCE PLUS® was the ability to lable the identified peaks on the pattern before being printed. It is also worth noting that even though the data needed to produce the DXRD pattern is subjected to several computer manipulations and printed on a laser printer, the d-spacings of the DXRD pattern are not distorted.

For the laboratory standard crust, the DXRD pattern obtained after the first stage of leaching show that the manganese oxide present is  $\delta\text{MnO}_2$  while the DXRD pattern for the laboratory standard nodule show that the manganese oxide present is todorokite and  $\delta\text{MnO}_2$ . The DXRD pattern obtained after the second stage of leaching show that the iron oxide present in the laboratory standard crust is ferrihydrite while the DXRD pattern for the laboratory standard nodule show that

the iron oxide present is akaganéite. In the laboratory standard crust the majority of the Mn, Ni, and Co are associated with the manganese oxide mineral  $\delta\text{MnO}_2$ , while most of the Fe and Cu are associated in the iron oxide mineral ferrihydrite. Both  $\delta\text{MnO}_2$  and ferrihydrite consist of a randomly disordered array of octahedra of Mn and Fe, respectively. In the laboratory standard nodule most of the Mn and Cu and half of the Ni and Co are associated with the manganese oxide minerals todorokite and  $\delta\text{MnO}_2$ , while most of the Fe and the remaining Ni and Co are contained by the iron oxide mineral akaganéite. Both todorokite and akaganéite are characterized by their well ordered tunnel structures.

Most of the proposed selective sequential extraction schemes directed towards the study of manganese and iron oxides in soils have also used hydroxylamine hydrochloride in nitric acid to remove the Mn oxide minerals and ammonium oxalate in oxalic acid to remove the Fe oxide minerals. Murad & Schwertmann (1988) proposed that the extraction of manganese oxides from crusts and nodules by hydroxylamine hydrochloride causes an alteration in the iron oxide mineralogy. Hence, there is some doubt on the validity of the results from the DXRD patterns obtained after the second stage of the extraction procedure. Although it can not be proven conclusively that the two stage selective sequential extraction scheme proposed above does not significantly change the iron oxide mineralogy, several pieces of evidence suggests that the iron oxides identified in the DXRD patterns are authentic iron mineral phases and not artifacts caused by the chemical leaching. Firstly, the observed iron oxides have DXRD patterns characterized by broad peaks. If the chemical leaching with 0.10M  $\text{NH}_2\text{OH}\cdot\text{HCl}$  in 0.01M  $\text{HNO}_3$  changed the iron oxide mineralogy they most likely would invert to goethite which is the polymorph most other  $\text{FeOOH}$  phases revert to (Murray, 1979). Goethite was observed in the XRD patterns of the hydroxylamine-treated crusts studied by Murad & Schwertmann (1988). Secondly, although Murad &

Schwertmann (1988) also identified feroxyhite in the XRD patterns of the hydroxylamine-treated crusts, they concluded that Mössbauer spectra of the untreated crusts indicates that most of the Fe is bound to a ferrihydrite-like phase that is intimately intergrown with the Mn oxides not feroxyhite. The presence of ferrihydrite was indeed identified in the crust sample studied here.

#### 4.3 RESULTS FROM CHAPTER 3

The selective sequential extraction scheme and differential X-ray diffraction technique were applied to a small population of crusts and nodules from the two Survey Regions in order to identify the manganese and iron phase mineralogies and their compositions. While the Mn-phase mineralogy of crusts and nodules is easily identified and reasonably well understood, the iron-bearing phases in crusts and nodules have usually been described as being cryptocrystalline or amorphous hydrated iron oxides (Glasby, 1972; Crerar & Barns, 1974). Mössbauer spectroscopic studies by Herzenberg & Riley (1969), Gager (1968), Johnson & Glasby (1969), and Carpenter & Wakeman (1973) have also led to the suggestion that the iron-bearing phase can be regarded as a amorphous ferric hydroxide or oxide-hydroxide gel ( $\text{FeOOH} \times \text{H}_2\text{O}$ ) with a particle size less than  $200\text{\AA}$ .

The DXRD patterns from the second stage of leaching on the crusts and nodules showed that the iron phase mineralogy in marine crusts and nodules is either akaganéite or ferrihydrite. The first reported presence of akaganéite in marine nodules was by Goncharov *et al.* (1973), although the presence of this mineral in marine nodules was discounted by Burns & Burns (1977). Since then the presence of akaganéite in marine crusts and nodules has been reported by Johnston & Glasby (1978) and by Thijs *et al.* (1981). This phase was identified in one Mn-rich hydrothermal crust in this study.

An experimental study by Vempati & Loeppert (1989) showed that in natural systems ferrihydrite, containing adsorbed and/or coprecipitated silicate, is probably influenced by the Si concentration, mechanism of silicate bonding, pH, and temperature of the environment of formation. Siliceous ferrihydrite formed during the coprecipitation of Fe oxides with silicate, would probably be stable for extended periods of time at  $\text{pH} \geq 7$ , even at elevated temperatures (Vempati & Loeppert, 1989). This result is significant since the average pH of sea water is 8 as reported by Glasby (1972), Burns (1965), and Defant (1961). This evidence supports the identification of ferrihydrite identified in the DXRD patterns obtained after the second stage of leaching on the crusts and nodule samples in the present study as an authentic iron oxide and not an artifact caused by the chemical leaching. This evidence is further supported the by mössbauer spectroscopic studies on untreated crusts and nodules by Murad & Schwertmann (1988). They concluded that Fe is bound to a ferrihydrite like phase that is intimately intergrown with the Mn oxides in crusts and nodules.

The DXRD patterns from the second stage of leaching on the Mn-rich hydrothermal crusts and nodules, from Survey Region B, identified the manganese-bearing mineral hausmannite. Hausmannite has never been identified in marine manganese nodules (Burns & Burns, 1977; Murray & Dillard, 1979). von Heimendahl *et al.* (1976) did, however, identify hydrohausmannite in a nodule from the eastern equatorial Pacific. Evidence for the possible origin of hausmannite in marine manganese crusts and nodules is provided by the experimental work of Bricker (1965). Bricker (1965) was able to form synthetic hausmannite at 25°C and one atmospheric pressure. It was found that with the proper control of Eh and pH (+0.5mV and 6.5 respectively) hausmannite could be preserved indefinitely. Except for the low pH, the laboratory solutions used by Bricker (1965) were similar in temperature and redox potential to fluids in bottom sediments in an open circulation

marine environment (Kumbein & Garrels, 1952). Given this evidence, hausmannite could indeed form on the sea floor, given the requisite chemical constituents (Sorem & Gunn, 1967).

## 4.4 REFERENCES

- Aplin, A.C., & Cronan, D.S., 1985. Ferromanganese oxide deposits from the central Pacific Ocean, I. Encrustations from the Line Islands Archipelago. *Geochim. Cosmochim. Acta*, 49:427-436.
- Bricker, O., 1965. Some stability relations in the system  $Mn-O_2-H_2O$  at 25° and one atmosphere total pressure. *American Mineralogist*, 50:1269-1354.
- Bryant, R.B., Curi, N., Roth, C.B., & Franzmeir, D.P., 1983. Use of an internal standard with differential X-ray diffraction analysis for iron oxides. *Soil Sci. Soc. Amer. J.*, 47:168-173.
- Burns, R.G., 1965. Formation of cobalt (III) in the amorphous  $FeOOH \cdot nH_2O$  phase of manganese nodules. *Nature*, 203(4975):999.
- Burns, R.G., 1976. The uptake of cobalt into ferromanganese nodules, soils, and synthetic manganese (IV) oxides. *Geochim. Cosmochim. Acta*, 40:95-102.
- Burns, R.G., & Burns, V.M., 1977. Mineralogy. In *Marine Manganese Deposits* (ed. by G.P. Glasby). Elsevier Scientific Publishing Company, Amsterdam, pp.185-248.
- Burns, R.G., & Burns, V.M., 1979. Manganese Oxides. In *Mineralogical Society of America Short Course Notes, Marine Minerals* (ed. by R.G. Burns), Vol. 6. Lithocrafters Inc., Chelsea, Michigan, pp. 1-46.
- Callender, E., & Bowser, C.J., 1980. Manganese and copper geochemistry of interstitial fluids from manganese-nodule-rich pelagic sediments of the northeastern equatorial Pacific Ocean. *Amer. J. Sci.*, 280:1063-1069.
- Calvert, S.E., & Price, N.B., 1977. Geochemical variation in ferromanganese nodules and associated sediments from the Pacific Ocean. *Mar. Chem.*, 5:43-74.
- Calvert, S.E., Price, N.B., Heath, G.R., & Moore, T.C. Jr., 1978. Relationship between ferromanganese nodule compositions and sedimentation in a small survey area of the equatorial Pacific. *J. Mar. Res.*, 36:161-183.
- Carpenter, R., & Wakeman, S., 1973. Mössbauer studies of marine and fresh water manganese nodules. *Chem. Geol.*, 11:109-116.
- Chen, J.C., & Owen, R.M., 1989. The hydrothermal component in ferromanganese nodules from the southeast Pacific Ocean. *Geochim. Cosmochim. Acta*, 53:1299-1305.
- Crerar, D.A., & Barnes, H.L., 1974. Deposition of deep-sea manganese nodules. *Geochim. Cosmochim. Acta*, 38:279-300.
- Cronan, D.S., & Tooms, J.S., 1969. The geochemistry of manganese nodules and associated pelagic deposits from the Pacific and Indian Oceans. *Deep-Sea Research*, 16:335-359.

- Dillard, J.G., Crowther, D.L., & Murray, J.W., 1982. The oxidation states of cobalt and selected metals in Pacific ferromanganese nodules. *Geochim. Cosmochim. Acta*, 46:755-759.
- Dymond, J., Lyle M., Finney, B., Piper, D., Murphy, K., Conard, R., & Pisias, N., 1984. Ferromanganese nodules from MANOP sites H, S, and R - control of mineralogical and chemical composition by multiple accretionary processes. *Geochim. Cosmochim. Acta*, 48:931-949.
- Gager, H.M., 1968. Mössbauer spectra of deep-sea iron-manganese nodules. *Nature*, 220:1021-1023.
- Glasby, G.P., 1972. The mineralogy of manganese nodules from a range of marine environments. *Mar. Geol.*, 13:57-72.
- Glasby, G.P., & Thijessen, T., 1982. Control of the mineralogy and composition of marine manganese nodules by the supply of divalent transition metal ions. *N. Jb. Miner. Abh.*, 145:291-307.
- Goldberg, E.D., 1954. Marine chemistry, I. Chemical scavengers of the sea. *J. Geol.*, 62:249-265.
- Goncharov, G.N., Kalyamin, A.V., & Lur'e, B.G., 1973. Iron-manganese concretions from the Pacific Ocean studied by a nuclear  $\gamma$ -resonance method. *Dokl. Akad. Nauk. S.S.S.R.*, 212:720-723.
- Halbach, P., Friedrich, G., & von Stackelberg, U., 1988. The Manganese Nodule Belt of the Pacific Ocean: Geological Environment, Nodule Formation, and Mining Aspects. Ferdinand Enke Verlag, Stuttgart, 254 pp.
- Halbach, P., Hebisch, U., & Scherhag, C., 1981a. Geochemical variations of ferromanganese nodules and crusts from different provinces of the Pacific Ocean and their genetic control. *Chem. Geol.*, 34:3-17.
- Halbach, P., Manheim, F.T., & Otten, P., 1982. Co-rich ferromanganese deposits in the marginal seamount regions of the central Pacific Basin - results of the Midpac '81. *Erzmetall*, 35(9):447-453.
- Halbach, P., & Özkara, M., 1979. Morphological and geochemical classification of deep-sea ferromanganese nodules and its genetical interpretation. In *La genèse des nœuds de manganèse*, Colloques Internationaux, C.N.R.S. No 289, pp. 77-88.
- Halbach, P., & Puteanus, D., 1984. The influence of the carbonate dissolution rate on the growth and composition of Co-rich ferromanganese crusts from central Pacific seamount areas. *Earth Plant. Sci. Lett.*, 68:73-87.
- Halbach, P., Scherhag, C., Hebisch, U., & Marchig, V., 1981b. Geochemical and mineralogical control of different genetic types of deep-sea nodules from the Pacific Ocean. *Mineral. Deposita*, 16:59-84.
- Halbach, P., Segl, M., Puteanus, D., & Mangini, A., 1983. Co-fluxes and growth rates in ferromanganese deposits from central Pacific seamount areas. *Nature*, 304:716-719.



- Hein, J.R., Schulz, M.S., & Gein, L.M., in Press a. Central Pacific Cobalt-Rich Ferromanganeses Crusts: Historical Perspective and Regional Variability. *In* Geology and Offshore Mineral Resources of the Central Pacific Region (ed. by B. Keating, & B. Bolton), Circum-Pacific Council for Energy and Mineral Resources, Earth Science Series, Houston, Texas, 23 pp.
- Hein, J.L., Schulz, M.S., & Kang, J.K., in Press b. Insular and Submarine Ferromanganese Mineralization of the Tonga-Lau Region. *In* Geology of the Tonga-Lau Regions of the Southwest Pacific (ed. by P.F. Ballance, R.H. Herzer, & T.L. Vallier), Circum-Pacific Council for Energy and Mineral Resources, Earth Science Series, Houston, Texas, 46 pp.
- Hem, J.D., 1978. Redox processes at surfaces of manganese oxide and their effects on aqueous metal ions. *Chem. Geol.*, 21:199-218.
- Herzenberg, C.L., & Riley, D.L., 1969. Interpretation of the Mössbauer spectra of marine iron-manganese nodules. *Nature*, 224:259-260.
- Johnson, C.E., & Glasby, G.P., 1969. Mössbauer effect determination of particle size in microcrystalline iron-manganese nodules. *Nature*, 222:376-377.
- Johnston, J.H., & Glasby, G.P., 1978. The secondary iron oxyhydroxide mineralogy of some deep-sea and fossil manganese nodules: A Mössbauer and X-ray study. *Geochim. Jour.*, 12:153-164.
- Klinkhammer, G.P., 1980. Early diagenesis in sediments from the eastern equatorial Pacific. II. Pore water metal results. *Earth Planet. Sci. Lett.*, 49:81-101.
- Klinkhammer, G.P., & Bender, M.L., 1980. The distribution of manganese in the Pacific Ocean. *Earth Planet. Sci. Lett.*, 49:81-101.
- Klinkhammer, G.P., Heggie, D.T., & Graham, D.W., 1982. Metal diagenesis in oxic marine sediments. *Earth Planet. Sci. Lett.*, 61:211-219.
- Krauskopf, K.B., 1957. Separation of manganese from iron in sedimentary processes. *Geochim. Cosmochim. Acta*, 12:61-84.
- Kumbein, W.C., & Garrels, R.M., 1952. Origin and classification of chemical sediments in terms of pH and oxidation-reduction potential. *Jour. Geol.*, 60:1-33.
- Landing, W.M., & Bruland, K.W., 1980. Manganese in the North Pacific. *Earth Planet. Sci. Lett.*, 49:45-56.
- Lyle, M., 1981. Formation and growth of ferromanganese oxides on the Nazca plate. *Geological Society of America, Memoir 154*, pp. 269-293.
- Manheim, F.T., & Lane-Bostwick, C.M., 1988. Cobalt in ferromanganese crusts as a monitor of hydrothermal discharge on the Pacific sea floor. *Nature*, 335(1):59-62.
- Moore, W.S., & Vogt, P.R., 1976. Hydrothermal manganese crusts from two sites near the Galapagos Spreading Axis. *Earth Planet. Sci. Lett.*, 29:349-356.

- Murad, E., & Schwertmann, U., 1988. Iron oxide mineralogy of some deep-sea ferromanganese crusts. *American Mineralogist*, 73:1395-1400.
- Murray, J.W., 1979. Iron-oxides. In *Mineralogical Society of America Short Course Notes, Marine Minerals* (ed. by R.G. Burns), Vol. 6. LithoCrafters Inc., Chelsea, Michigan, pp. 47-98.
- Murray, J.W., & Dillard, J.G., 1979. The oxidation of cobalt (II) adsorbed on manganese dioxide. *Geochim. Cosmochim. Acta*, 43:781-787.
- Price, N.B., & Calvert, S.E., 1970. Compositional variation in Pacific Ocean ferromanganese nodules and its relationship to sediment accumulation rates. *Mar. Geol.*, 9:145-171.
- Raab, W., 1972. Physical and chemical features of Pacific deep sea manganese nodules and their implications to the genesis of nodules. In *Ferromanganese Deposits on the Ocean Floor* (ed. by D.R. Horn), National Science Foundation, Washington, D.C., pp. 31-50.
- Savitzky, A., & Golay, M.J., 1964. Smoothing and differentiation of data by simplified least squares procedures. *Anal. Chem.*, 36(8):1627-1639.
- Sorem, R.K., & Gunn, D.W., 1967. Mineralogy of manganese deposits, Olympic Peninsula, Washington. *Econ. Geol.*, 62:22-56.
- Thijs, A., De Roy, G., Vansant, E.F., Glasby, G.P., & Thijssen, T., 1981. Mössbauer effect studies of iron in manganese nodules and associated marine sediments in five areas in the equatorial and S.W. Pacific. *Geochem. Jour.*, 15:25-37.
- Toth, J.R., 1980. Deposition of submarine crusts rich in manganese and iron. *Geol. Soc. Amer. Bull.*, Part 1, 91:44-54.
- Usui, A., & Mita, N., 1987. Comparison of manganese nodules from the northeast equatorial Pacific (cruise SO 25) with nodules from the central Pacific basin. *Geol. Jb.*, D87:287-313.
- Vempati, R.K., Loeppert, R.H., 1989. Influence of structural and adsorbed Si on the transformation of synthetic ferrihydrite. *Clays and Clay Minerals*, 37(3):273-279.
- von Heimandahl, M., Hurbred, G.L., Fuerstenau, D.W., & Thomas, G., 1976. A transmission electron microscope study of deep-sea manganese nodules. *Deep-Sea Research*, 23:69-79.